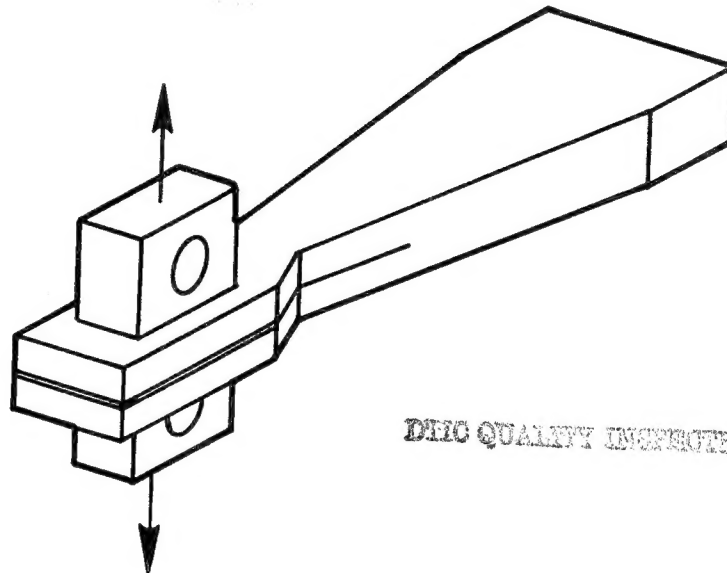


NASA Conference Publication 2334

Tough Composite Materials



19960307 015

DEPARTMENT OF DEFENSE
PLASTICS TECHNICAL EVALUATION CENTER
ARRADCOM, BOYER, N. J. 07001

*Proceedings of a workshop held at
NASA Langley Research Center
Hampton, Virginia
May 24-26, 1983*

DISTRIBUTION STATEMENT A

Approved for public release;
Distribution Unlimited

NASA

11/25/83
41653
41674

Add 438884-438905

NASA Conference Publication 2334

Tough Composite Materials

Compiled by
Louis F. Vosteen
Norman J. Johnston
and Louis A. Teichman
Langley Research Center

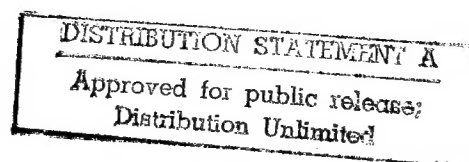
Proceedings of a workshop sponsored by
NASA Langley Research Center
Hampton, Virginia, and held in
Hampton, Virginia
May 24-26, 1983

NASA

National Aeronautics
and Space Administration

**Scientific and Technical
Information Branch**

1984



PREFACE

This publication is a compilation of papers and working group summaries presented at the Tough Composite Materials Workshop held at NASA Langley Research Center, Hampton, Virginia, May 24-26, 1983. Presentations were made by selected speakers conducting research aimed at improving composite material performance and improving our understanding of composite material behavior. The papers were divided into three sessions:

- Session I: Composite Fracture Toughness and Impact Characterization
- Session II: Constituent Properties and Interrelationships
- Session III: Matrix Synthesis and Characterization

The workshop also provided a forum for more in-depth discussions through separate panel meetings on the three disciplinary areas listed above. A summary of these discussions, including conclusions and selected recommendations, is included in this publication.

The long-range goal of NASA's composites program is to exploit the full weight reduction potential of composite materials for structural applications in commercial transports. In order to achieve this goal, the design strain capability of composites must be significantly increased. Today this design strain capability is in the neighborhood of 0.004, which permits significant weight savings in secondary structure and stiffness-critical control surfaces. But, to achieve a 30- to 40-percent weight savings in wing and fuselage structure, this design strain capability must be increased to 0.006 to 0.008. NASA sponsors and conducts a vigorous research program to accomplish this goal. New concepts, approaches, and ideas are constantly being reviewed and considered for support. One purpose of the workshop format was to solicit from the technical community an assessment of the adequacy of the current program and help focus attention on appropriate areas for future research.

Use of trade names or names of manufacturers in this report does not constitute an official endorsement of such products or manufacturers, either expressed or implied, by the National Aeronautics and Space Administration.

Louis F. Vosteen, Workshop Coordinator

Index all papers

CONTENTS

PREFACE iii

SESSION I: COMPOSITE FRACTURE TOUGHNESS AND IMPACT CHARACTERIZATION

CHARACTERIZATION OF INTERLAMINAR CRACK GROWTH IN COMPOSITES
WITH THE DOUBLE CANTILEVER BEAM SPECIMEN 47254 . . . (3)
Donald L. Hunston

CHARACTERIZING DELAMINATION RESISTANCE OF TOUGHENED RESIN COMPOSITES 47255 . (17)
T. Kevin O'Brien

COMPOSITE MATERIALS CHARACTERIZATION AND DEVELOPMENT AT AFWL . . 47256 . . (33)
C. E. Browning

EFFECT OF IMPACT DAMAGE AND OPEN HOLES ON THE COMPRESSION STRENGTH
OF TOUGH RESIN/HIGH STRAIN FIBER LAMINATES 47257 . . (61)
Jerry G. Williams

EFFECTS OF CONSTITUENT PROPERTIES ON COMPRESSION FAILURE MECHANISMS 47258 . (81)
H. Thomas Hahn

THE EFFECT OF MATRIX AND FIBER PROPERTIES ON IMPACT RESISTANCE . . 47259 . . (99)
Wolf Elber

SESSION II: CONSTITUENT PROPERTIES AND INTERRELATIONSHIPS

FUNDAMENTAL STUDIES OF COMPOSITE TOUGHNESS 47260 . . (125)
Kenneth J. Bowles

INVESTIGATION OF TOUGHENED NEAT RESINS AND THEIR RELATIONS TO
ADVANCED COMPOSITE MECHANICAL PROPERTIES 47261 . . (137)
R. S. Zimmerman

CONSTITUENT PROPERTY - COMPOSITE PROPERTY RELATIONSHIPS IN
THERMOSET MATRICES 47262 . . (159)
J. Diamant and R. J. Moulton

THE EFFECT OF CROSS-LINK DENSITY ON THE TOUGHENING MECHANISM OF
ELASTOMER-MODIFIED EPOXIES 47263 . . (173)
R. A. Pearson and A. F. Yee

FREE VOLUME CONSIDERATIONS IN THERMOPLASTIC AND THERMOSETTING RESINS 47264 . . (195)
Robert F. Landel, A. Gupta, J. Moacanin, D. Hong, F. D. Tsay, S. Chen,
S. Chung, R. Fedors, and M. Cigmecioğlu

THE CHEMICAL NATURE OF THE FIBER/RESIN INTERFACE IN COMPOSITE MATERIALS 47265 (209)
R. Judd Diefendorf

COMPOSITE PROPERTY DEPENDENCE ON THE FIBER, MATRIX, AND THE INTERPHASE 47266 . (227)
Lawrence T. Drzal

NEWER CARBON FIBERS AND THEIR PROPERTIES . . .	47267	245
Roger Bacon		

SESSION III: MATRIX SYNTHESIS AND CHARACTERIZATION

DEVELOPMENT OF A HETEROGENEOUS LAMINATING RESIN . . .	47268	261
Rex Gosnell		
MODIFIED EPOXY COMPOSITES . . .	47269	273
W. J. Gilwee		
MORPHOLOGY AND DYNAMIC MECHANICAL PROPERTIES OF DIGLYCIDYL ETHER OF BISPHENOL-A TOUGHENED WITH CARBOXYL-TERMINATED BUTADIENE-ACRYLONITRILE . . .		285
Su-Don Hong, Shirley Y. Chung, Robert F. Fedors, Jovan Moacanin, and Amitava Gupta		
MATRIX RESIN CHARACTERIZATION IN CURED GRAPHITE COMPOSITES USING DIFFUSE REFLECTANCE-FTIR . . .	47270	295
Philip R. Young and A. C. Chang		
SOLVENT RESISTANT THERMOPLASTIC COMPOSITE MATRICES . . .	47272	317
P. M. Hergenrother, B. J. Jensen, and S. J. Havens		
THERMOPLASTIC/MELT-PROCESSABLE POLYIMIDES . . .	47273	337
T. L. St. Clair and H. D. Burks		
ALIPHATIC-AROMATIC HETEROCYCLICS AS POTENTIAL THERMOPLASTICS FOR COMPOSITE MATRICES . . .	47274	357
Chad B. Delano and Charles J. Kiskiras		

WORKING GROUP SUMMARIES

SESSION I: COMPOSITE FRACTURE TOUGHNESS AND IMPACT CHARACTERIZATION . . .	381
T. K. O'Brien, Chairman	
SESSION II: CONSTITUENT PROPERTIES AND INTERRELATIONSHIPS . . .	385
R. F. Landel, Chairman	
SESSION III: MATRIX SYNTHESIS AND CHARACTERIZATION . . .	389
P. M. Hergenrother, Chairman	

SESSION I

COMPOSITE FRACTURE TOUGHNESS AND IMPACT CHARACTERIZATION

CHAIRMAN: T. K. O'BRIEN

PROJECT OBJECTIVES

Since delamination is considered to be a major failure mechanism in composites, there is a need and desire to develop test methods that assess the resistance of various composite materials to the growth of interlaminar cracks. In response to this need our program is examining the double cantilever beam (DCB) specimen. The program has two objectives (Figure 1). The first is to explore the DCB as a quantitative test method. This involves both a review of the results of other workers in this field and the completion of experiments in areas where additional work is required. The second objective is to investigate the micromechanics of failure for composites with tough matrix resins from certain generic types of polymeric systems: brittle thermosets, toughened thermosets, and tough thermoplastics. From this information it is hoped that a better picture of toughening in composites can be formulated.

EXPLORE DCB SPECIMEN AS A QUANTITATIVE TEST METHOD

INVESTIGATE MICROMECHANICS OF FAILURE WITH TOUGH MATRIX RESINS

Figure 1

CHARACTERIZATION OF INTERLAMINAR CRACK GROWTH
IN COMPOSITES WITH THE DOUBLE CANTILEVER BEAM SPECIMEN

Donald L. Hunston
National Bureau of Standards
Polymers Division
Washington, D.C.

COOPERATING PROGRAMS

The project is part of a larger effort involving a number of groups (Figure 2). Our work which focuses on the DCB specimen and an examination of failure mechanisms is coordinated with programs at NASA studying the edge delamination specimen and developing specialized materials. Through this combination, data on a variety of loading geometries and materials can be obtained. To assist in the analyses of the test methods, a cooperative project under the direction of Prof. S. S. Wang at the University of Illinois is developing stress analyses for the various specimen geometries using realistic constitutive equations. Finally, there is close coordination with industry including Bill Bascom at Hercules and Rich Moulton at Hexcel who are supplying commercial and model materials for study.

DELAMINATION PROGRAM:

NBS: DCB

FAILURE MECHANICS

NASA: EDGE DELAMINATION

SPECIALIZED MATERIALS

UNIV. OF ILL.: STRESS ANALYSIS

INDUSTRIES: COMMERCIAL & MODEL MATERIALS

Figure 2

APPROACH

The approach in this program is to examine in a systematic way all of the variables that could affect the DCB test. These variables, listed in Figure 3, are relatively obvious although the inclusion of analysis method deserves some comment. A number of different procedures are being used by various groups to evaluate a fracture energy from their DCB results. In the ideal case of a linear elastic material the analysis method should make no difference. With the tougher matrix resins, however, some deviations from ideal behavior can occur and thus the analysis method may make a difference. Consequently, this is being examined. The variables listed in Figure 3 are divided into 4 groups to indicate the approximate order in which they are being addressed. There are however strong interactions between these parameters and thus they cannot be entirely separated. The recent work on the effects of specimen geometry and lay-up will be covered in forthcoming publications. The purpose of this paper will be to focus on preliminary results in two other areas: the effects of temperature and loading rate for woven composites, and the effects of matrix toughening in woven and unidirectional composites.

VARIABLES

LAY-UP	(I)
DIMENSIONS & SHAPE	(II)
● TEMPERATURE & LOADING RATE	(II)
● MATRIX MATERIAL & FIBER TYPE	(III)
FIBER VOLUME FRACTION	(III)
ENVIRONMENT (HUMIDITY)	(IV)

ANALYSIS METHOD (I)

COMPLIANCE MEASUREMENT

AREA MEASUREMENT

COMPLIANCE MEASUREMENT WITH NON-LINEAR
BENDING

TAPERED BEAM WITH BENDING MODULUS

OTHER

Figure 3

SPECIMENS

The tests are examining the failure behavior of both the composite and bulk samples of the various resins. The bulk (or neat) tests are conducted with standard compact tension specimens. The composite specimens under examination are the simple double cantilever beam (DCB) and the width tapered DCB (see Figure 4) with various degrees of taper. The untapered DCB may have an advantage in being more easily addressed in a stress analysis. The tapered DCB may have a potential advantage in that the crack grows at a constant load thus simplifying the data analysis. Both woven reinforcement and unidirectional specimens are being fabricated with the 0 fiber direction defined to be down the length of the specimen. A wide range of specimens are being examined but the results reported here involve 12 ply woven reinforcement composites and 0_{24} unidirectional composites.

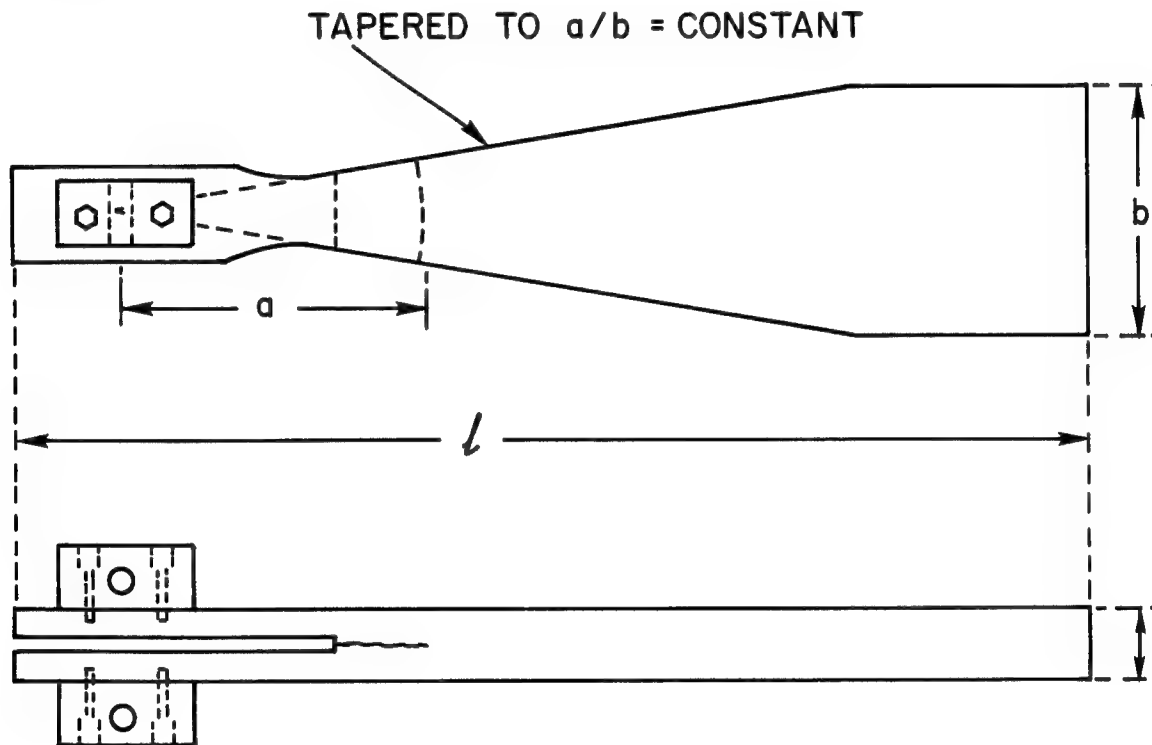


Figure 4

BULK RESIN RATE AND TEMPERATURE EFFECTS

The first topic to be examined here is the effects of temperature and loading rate (i.e., cross head speed of test machine). The motivation for the interest in these effects can be illustrated in Figure 5 which shows the fracture data for bulk samples of a model rubber-modified epoxy. With an unmodified epoxy the fracture energy for both bulk and composite specimens shows relatively small variations with moderate changes in temperature and loading rate. For tough materials, like the modified epoxy, however, the sensitivity of bulk samples to these variables is very large. In Figure 5, for example, the fracture energies vary by more than an order of magnitude depending on test conditions. In light of this behavior, there is a need to examine the effects of these parameters on the fracture properties of composites made with tough resins.

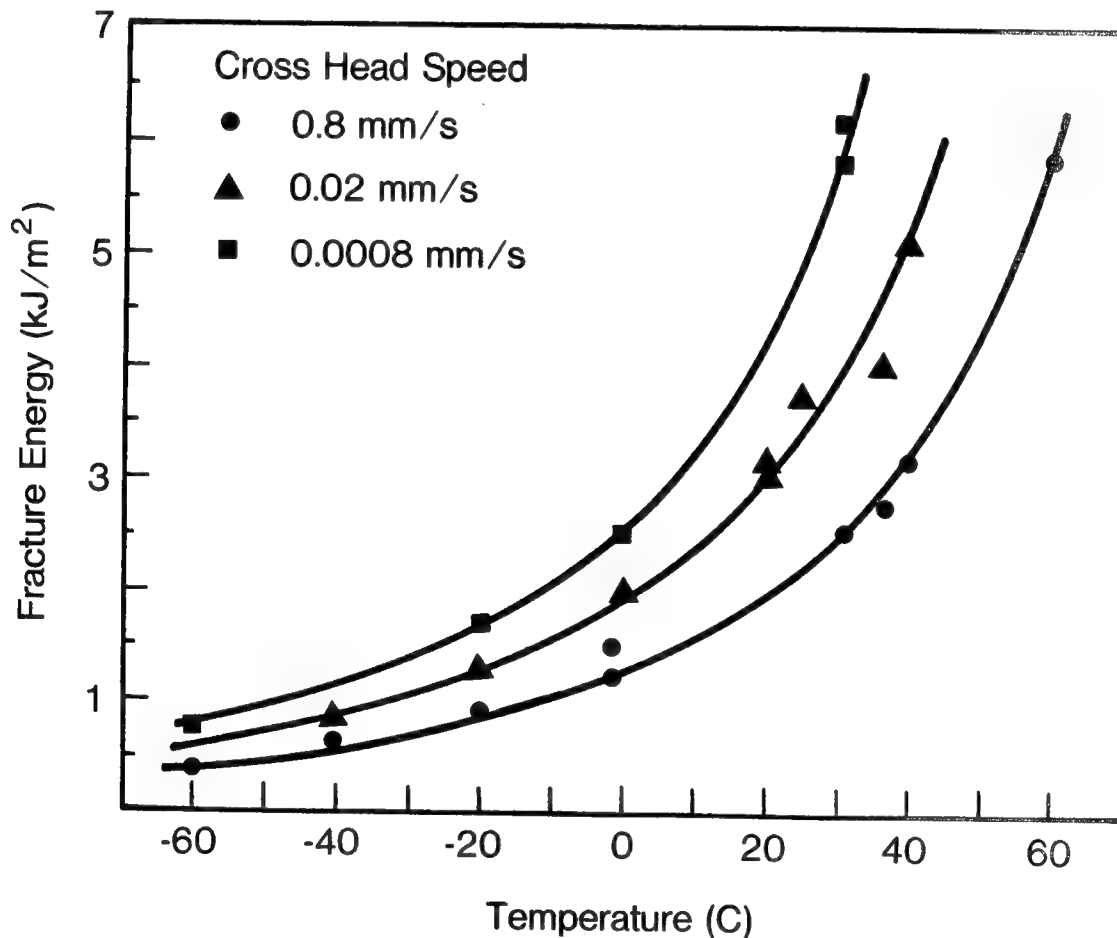


Figure 5

WOVEN COMPOSITE RATE AND TEMPERATURE EFFECTS

It has been shown that improving the fracture energy of the resin itself by 25 fold will increase the interlaminar fracture energy as measured by the DCB of a woven composite by 4 to 8 fold. This difference has been explained by noting that the high toughness of the resin is associated with a large crack tip deformation zone. In the composite, however, the deformation zone is restricted by the presence of the fibers. Consequently, there may be a potential for deformation in the matrix that is not utilized. If the temperature is lowered or the loading rate is increased, perhaps this reserve can be called upon. Such a hypothesis might suggest that composites fabricated with a tough resin might show less dependence on rate and temperature than the resin itself. Figure 6 gives some preliminary results for woven reinforcement composites made with a rubber-modified epoxy (2 fold improvement in composite fracture energy relative to the unmodified epoxy). The results show relatively little rate and temperature dependence over the range of conditions tested. Additional studies are now under way to examine these trends in more detail, particularly with unidirectional composites.

Temperature	Fracture Energy (kJ/m ²) at indicated		
	Cross-Head Speed (mm/sec)		
°C	0.0008	0.04	0.8
40	1.7	1.8	1.8
24	1.7	1.7	1.9
0	1.7	1.9	2.0
-25	1.9	2.1	2.4

Figure 6

BULK VS COMPOSITE FRACTURE

The second area of interest in this paper is the effects of varying the matrix resin toughness on the interlaminar fracture energy. Figure 7 shows baseline data on bulk specimens and woven and unidirectional composites all made with a model epoxy. The two unidirectional composites differ only in that one was fabricated by Hexcel and the other by NASA Langley. Note first the relative values for the bulk samples and the Hexcel composite. The interlaminar fracture energy is slightly higher than that for the resin indicating a rough transfer from the resin to the composite with some enhancement of toughness in the composite through additional mechanisms. Both fiber breakage and crack bifurcation were observed in the composite fracture surfaces. The woven composite exhibits significant data scatter but the fracture energy is clearly higher than that of the resin or the Hexcel composite. The crack propagation in the woven composite was stick slip with initiation and arrest at the crossover points in the weave. Consequently, one possible explanation for the enhanced toughness may be the addition of crack pinning as an added toughening mechanism. Compare now the NASA and Hexcel composites. The NASA samples clearly give a higher fracture energy.

ELASTOMER CONCENTRATION	FRACTURE ENERGY (KJ/M ²)			
	NEAT	WOVEN	O ₂₄ (HEXCEL)	O ₂₄ (NASA)
0%	0.23	0.6-1.3 ^A	0.37	0.77

^ANUMBERS INDICATE RANGE OF VALUES FOR 10 SPECIMENS.

Figure 7

FIBER NESTING AND BRIDGING

This comparison illustrates the importance of factors other than matrix type in determining interlaminar fracture behavior. The NASA and Hexcel samples were not fabricated with the same procedure and this produced differences in the fiber distribution. As a result the NASA materials exhibited substantially more nesting and fiber bridging. In nesting, the fibers from different plies mix together so the crack can not follow a planar surface between plies. If viewed from the end of the specimen, the crack front is not linear because it must go around the interpenetrating fibers (Figure 8). Fiber bridging is a related effect. When nesting is present, the crack front may not completely separate all the fibers on one side of the crack from those on the other. These unseparated fibers can then span across the crack behind the crack tip as shown in Figure 8. From the results in this work and other similar studies elsewhere, it appears that excessive fiber nesting and bridging in a specimen will cause an elevation in the measured interlaminar fracture energy.

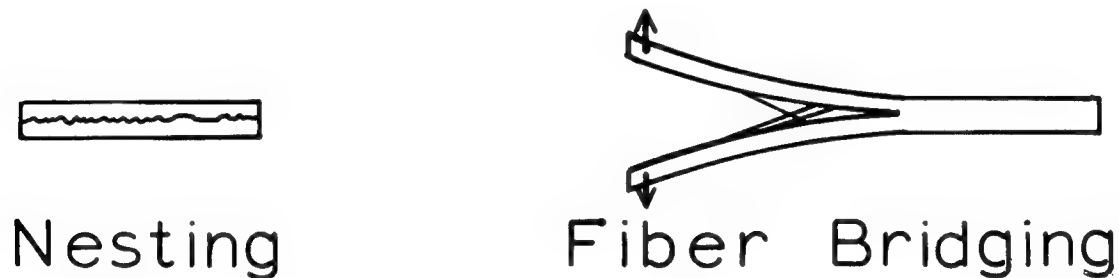


Figure 8

DATA WITH TOUGH MATRICES

Turn now to the effect of toughening the matrix resin. Figure 9 confirms the previous results, which found that an improvement of 25 fold in the resin fracture energy gives a 4 to 8 fold improvement in woven composite results. With unidirectional composites the improvement was expected to be much less because there are no resin rich areas equivalent to those at the cross-over points in the weave in woven composites. Surprisingly, however, the improvement in the unidirectional specimens, 2.5 to 5 fold, was almost as large as that found for woven composites. Moreover, the additional toughening mechanisms (nesting, fiber bridging, crack pinning, etc.) that were suggested in the unmodified epoxy results appear to be present in the toughened composite as well but perhaps to a lesser degree.

ELASTOMER CONCENTRATION	FRACTURE ENERGY (KJ/M ²)			
	NEAT	WOVEN	O ₂₄ (HEXCEL)	O ₂₄ (NASA)
0%	0.23	0.6-1.3 ^A	0.37	0.77
13.5%	5.8	3.6-4.6 ^A	1.6-2.0 ^B	1.9-2.3 ^B

^ANUMBERS INDICATE RANGE OF VALUES FOR 10 SPECIMENS.

^BLOWER NUMBER CORRESPONDS TO FIRST INDICATION OF CRACK GROWTH,
HIGHER NUMBER STEADY CRACK GROWTH AT 0.02 CM/S.

Figure 9

LOADING CURVES FOR BRITTLE AND TOUGH COMPOSITES

In the unidirectional composites the DCB test measures the strain energy release rate corresponding to relatively steady crack growth. With the brittle materials the first indication of crack growth in the composite occurs at about the same strain energy release rate as the steady growth. Figure 10 shows an example of the loading curves for such a composite with the tapered DCB specimen. When tough matrix resins are used, the first indication of crack growth occurs at a somewhat lower strain energy release rate than that corresponding to steady growth. This behavior can be seen either by observing the crack or by noting deviation from linearity in the load-displacement curves (Figure 10). As a result, for the tougher matrix resin composites, two fracture energies are given: an onset and a steady growth value. The onset number however may be somewhat subjective since its exact value may depend on how closely the data are examined. Nevertheless, the difference between the onset and steady growth values provides a measure of the magnitude of the effect.

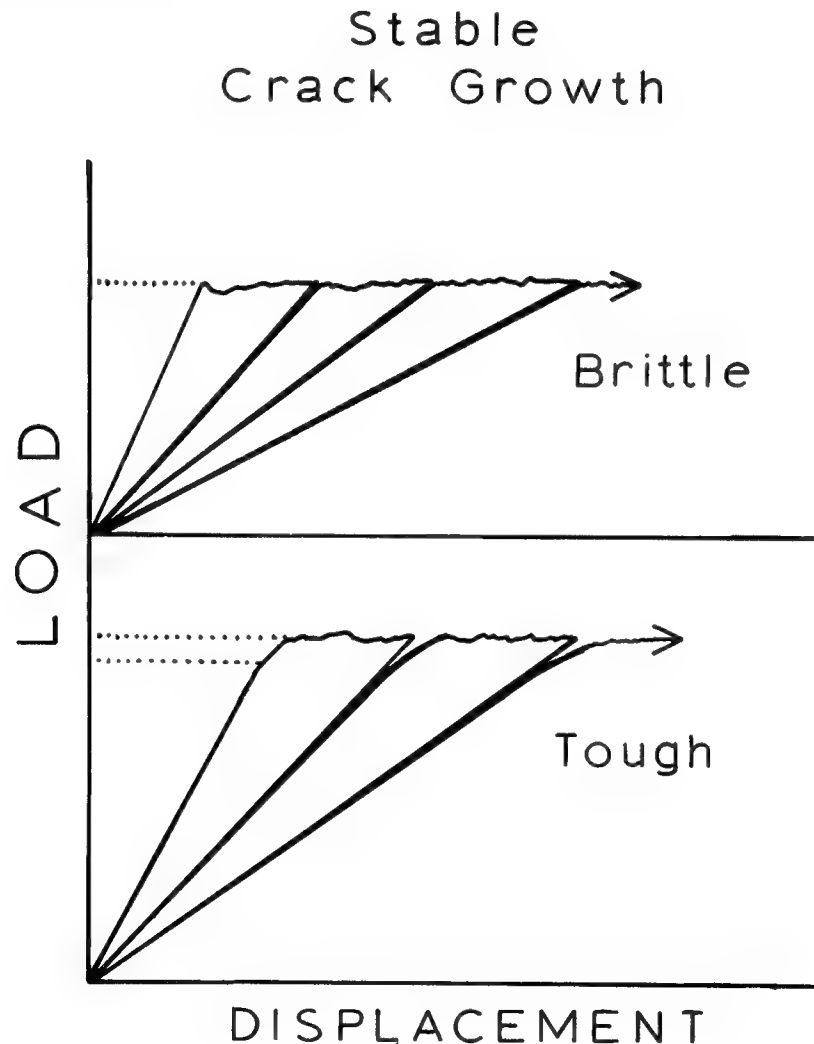


Figure 10

MATRIX VS COMPOSITE FRACTURE ENERGY

The results in Figure 9 show that a 25 fold improvement in resin fracture energy gives only a 4 fold improvement in composite interlaminar fracture energy. Since toughening of the resin usually degrades other desirable properties, it is of interest to see if a 10 fold improvement in resin fracture energy would still produce a 4 fold improvement in the composite. Figure 11 shows the results for the Hexcel materials in Figure 9 plus an intermediate toughness resin (8% rubber) also fabricated by Hexcel (\square). The results clearly indicate that an intermediate toughness resin produces an intermediate toughness composite. These limited data suggest that each 4 J/m² increase in resin fracture energy gives about 1 J/m² improvement in interlaminar fracture energy. Thus there is a trade-off between interlaminar toughness and other properties. Also shown on this graph are results for polysulfone (Δ) and polyetherimide (\diamond). Although the results are preliminary, these materials seem to follow the same general trend as the modified epoxies. The fracture surface of the polyetherimide exhibited significantly more interfacial failure than the other samples and thus inferior bonding may explain why this composite appears to fall somewhat below the general trend.

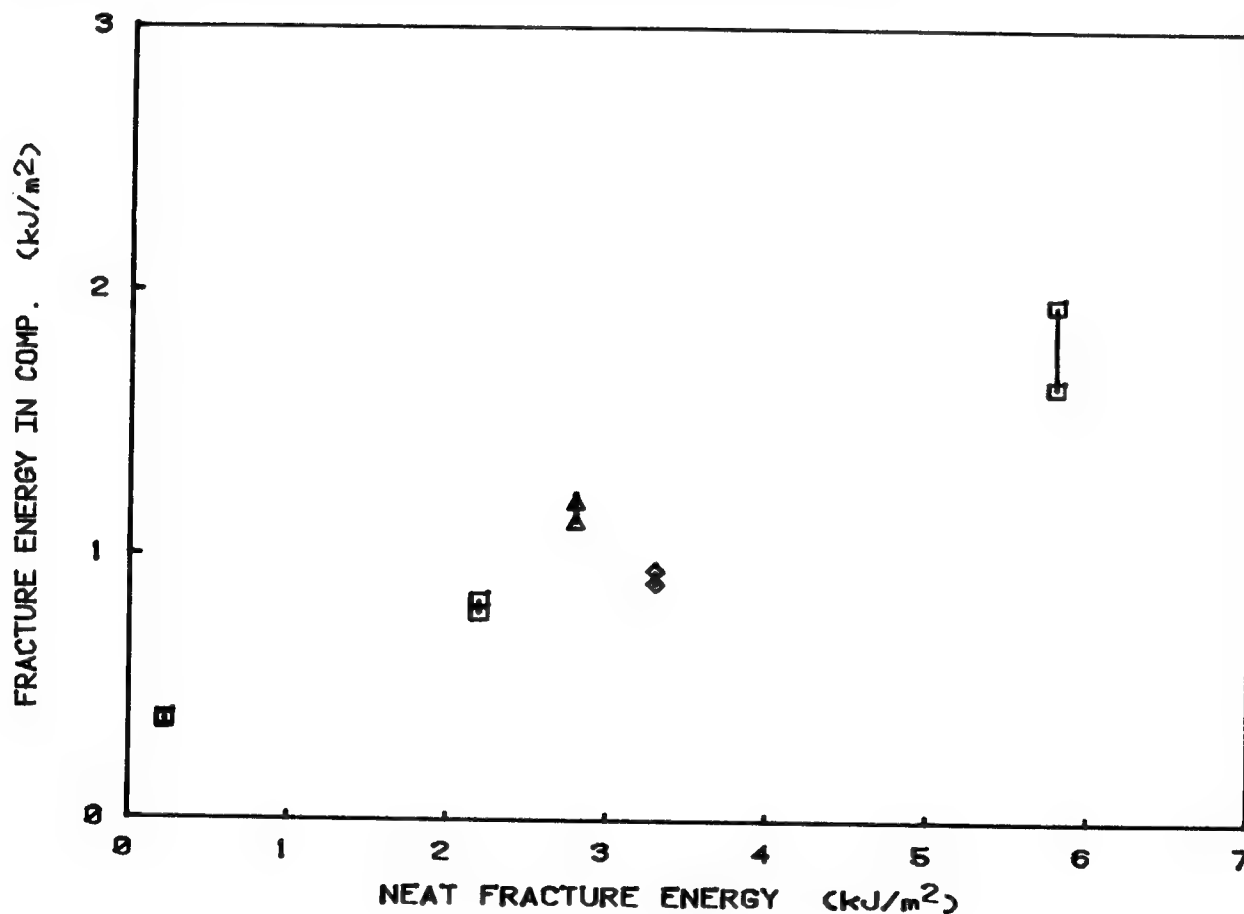


Figure 11

FUTURE PLANS

Future plans in this program (Figure 12) involve completing the study of phase I and II parameters. In addition the effects of matrix toughness will be included since a tough matrix may affect the results of experiments examining these variables. For example, preliminary experiments have suggested that with tougher matrix resins it is desirable to have stiffer specimens to minimize the effects of non-linear bending and deviation from linear elastic behavior in the resin. With regard to rate and temperature effects, the major focus will be on unidirectional composites since the behavior shown in Figure 10 suggests these variables may be important in this case. Thermoplastic matrix resins are of particular interest here since even the behavior in bulk has not been studied in detail. Finally, the implications of these studies in terms of the analysis method will be given attention because the test can only be as good as the approximations and assumptions involved in the fracture energy calculation, and with tough matrices more uncertainty is now present in this regard.

VARIABLES

LAY-UP	(I)
<u>DIMENSIONS & SHAPE</u>	(II)
<u>TEMPERATURE & LOADING RATE</u>	(II)
<u>MATRIX MATERIAL & FIBER TYPE</u>	(III)
FIBER VOLUME FRACTION	(III)
ENVIRONMENT (HUMIDITY)	(IV)

ANALYSIS METHOD (I)

COMPLIANCE MEASUREMENT
AREA MEASUREMENT
COMPLIANCE MEASUREMENT WITH NON-LINEAR
BENDING
TAPERED BEAM WITH BENDING MODULUS
OTHER

Figure 12

CHARACTERIZING DELAMINATION RESISTANCE OF TOUGHENED RESIN COMPOSITES

T. Kevin O'Brien
Structures Laboratory
U.S. Army Research and Technology Laboratories (AVRADCOM)
NASA Langley Research Center
Hampton, Virginia

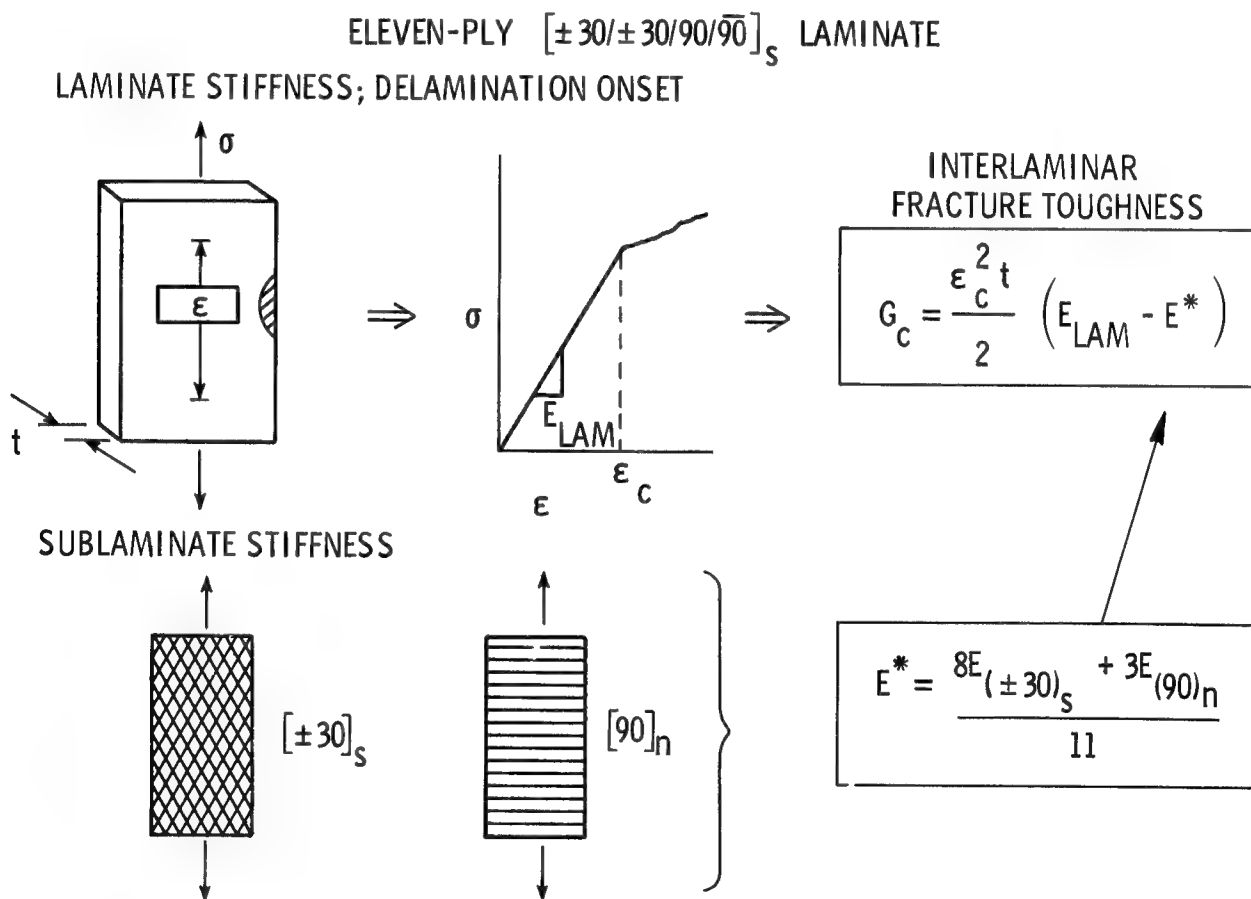
INTRODUCTION

One major obstacle to the efficient application of advanced composite materials in large primary aircraft structures is the tendency for these materials to delaminate. Because delamination may adversely influence stiffness, strength, and fatigue life, composites with toughened matrix resins are currently being developed to improve delamination resistance. However, whereas the fracture toughness of new resins can be measured in the bulk, no sound relationships yet exist to relate bulk fracture to delamination resistance in the composite. Therefore, investigators have measured the interlaminar fracture toughness of the composite in order to screen new toughened matrix resins for improved delamination resistance.

Interlaminar fracture can occur under a mixture of mode I (interlaminar tension or peel) and mode II (interlaminar shear). These modes are usually mixed in practice; hence the term "mixed-mode fracture." Of the specimens used to measure interlaminar fracture toughness, the double-cantilever-beam specimen delaminates under mode I only, whereas the edge delamination test specimen delaminates under a mixed mode. The purpose of this investigation was to determine the influence of mixed-mode fracture on interlaminar fracture toughness for "brittle" and "tough" matrices subjected to both static and cyclic loads, using the edge delamination test.

EDGE-DELAMINATION TENSION TEST MEASURES INTERLAMINAR FRACTURE TOUGHNESS

A simple test has been developed for measuring the interlaminar fracture toughness of composites made with toughened matrix resins (ref. 1). The test involves measuring the stiffness, E_{LAM} , and nominal strain at onset of delamination, ϵ_c , during a tension test of an 11-ply $[\pm 30/\pm 30/90/90]_S$ laminate (fig. 1). These quantities, along with the measured thickness t , are substituted into a closed-form equation for the strain energy release rate, G , for edge delamination growth in an unnotched laminate (ref. 2). The E^* term in the equation is the stiffness of the $[\pm 30/\pm 30/90/90]_S$ laminate if the 30/90 interfaces were completely delaminated. It can be calculated from the simple rule of mixtures equation shown in figure 1 by substituting the laminate stiffness measured during tension tests of $[\pm 30]_S$ and $[90]_N$ laminates. The critical value of G_c at delamination onset is a measure of the interlaminar fracture toughness of the composite. This edge delamination test is being used by Boeing, Douglas, and Lockheed under the NASA ACEE (Aircraft Energy Efficiency) key technologies contracts to screen toughened resin composites for improved delamination resistance (ref. 3).



INTERLAMINAR FRACTURE TOUGHNESS OF GRAPHITE COMPOSITES

Figure 2 illustrates how the edge delamination test (EDT) can rank the relative delamination resistance of graphite composites with different matrix resins. Results are shown for four matrices, ranging from a very brittle 350°F cure epoxy to a tougher thermoplastic, and from 250°F cure epoxy to a very tough "rubber-toughened" epoxy. Also shown in figure 2 are double-cantilever-beam (DCB) measurements for the same composites. Results indicate that either test will yield a qualitative ranking of improvements in delamination resistance. However, the G_{Ic} and G_c values differ because the DCB test involves only interlaminar tension, whereas the edge delamination test involves a combination of interlaminar tension and shear.

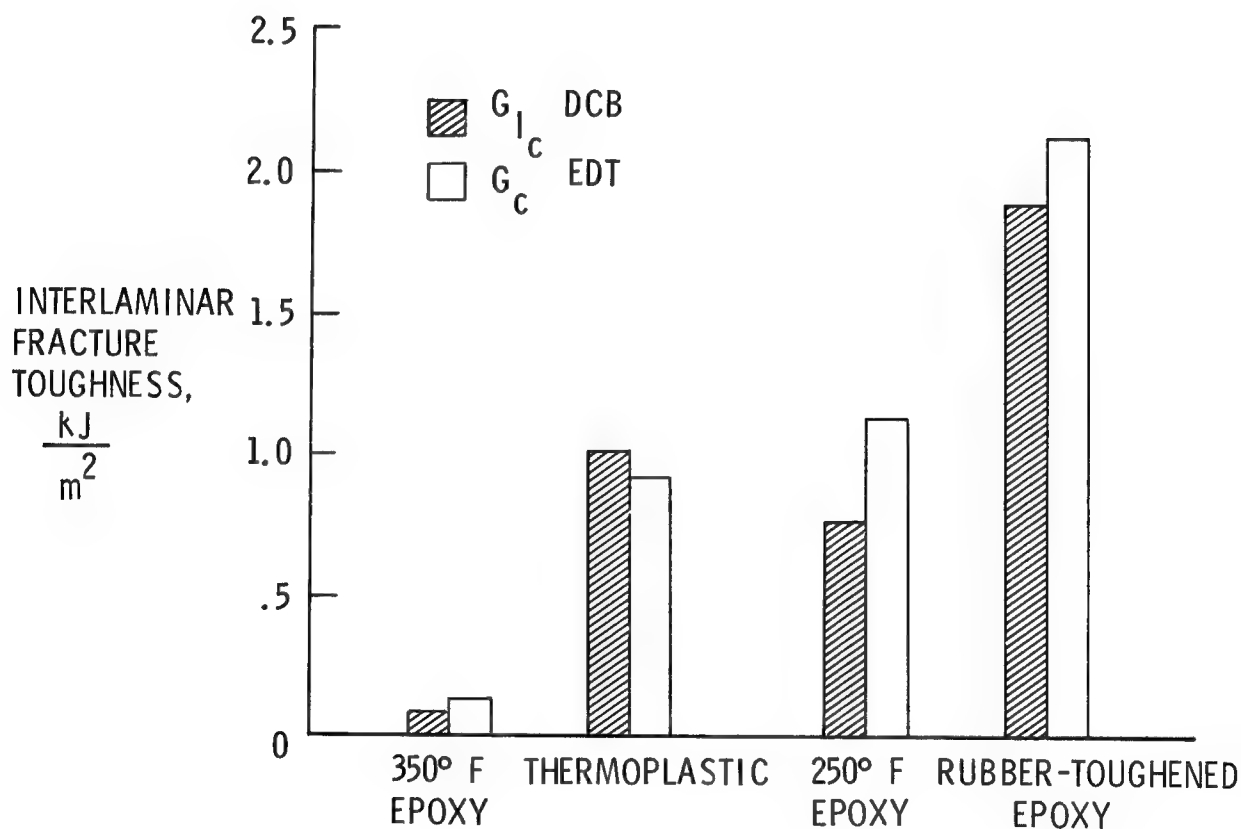


Figure 2

MIXED-MODE STRAIN ENERGY RELEASE RATES DETERMINED

A quasi-three-dimensional finite-element analysis (ref. 4) was performed to determine the relative crack-opening (mode I) and shear (mode II) contributions of the $[\pm 30/\pm 30/90/\overline{90}]_s$ edge delamination specimen (ref. 1). Delaminations were modeled in the $-30/90$ interfaces where they were observed to occur in experiments. Figure 3 indicates that the total G represented by G_I plus G_{II} reaches a value prescribed by the closed-form equation derived from laminated-plate theory and the rule of mixtures. Furthermore, like the total G , the G_I and G_{II} components are also independent of delamination size.

$[\pm 30/\pm 30/90/\overline{90}]_s$ LAMINATE

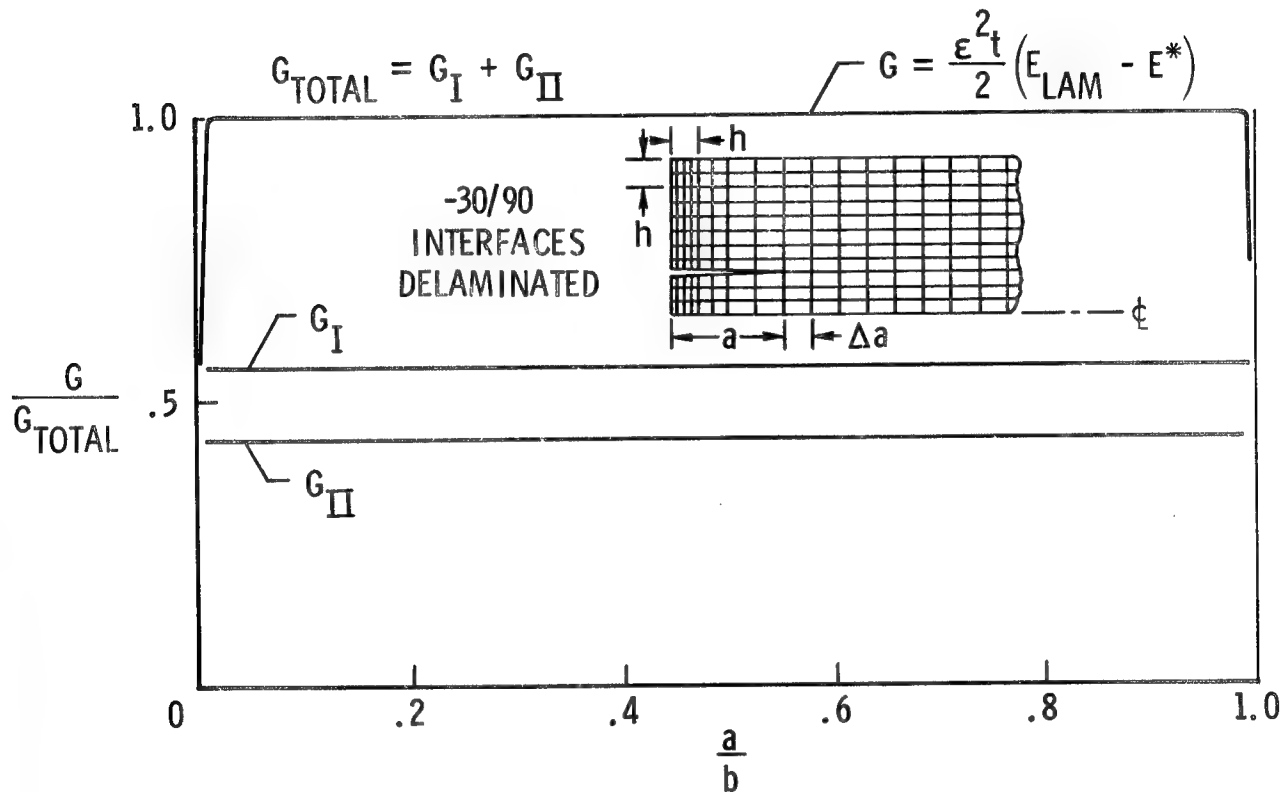


Figure 3

INTERLAMINAR FRACTURE TOUGHNESS OF GRAPHITE COMPOSITES MEASURED

Figure 4 shows results (ref. 1) of pure crack-opening (mode I) double-cantilever-beam tests and edge delamination tension tests for a relatively brittle 350°F cure epoxy (5208), a tougher 250°F cure epoxy (H205), and a still tougher rubber-toughened 250°F cure epoxy (F185). Results indicate that for the brittle epoxy, even in the mixed-mode test, only the crack-opening fracture mode contributes to delamination. However, for the tougher 250°F cure epoxy and its rubber-toughened version, both the crack-opening and shear fracture modes contribute to delamination. Hence, although both tests indicate relative improvements among materials, one test alone is not sufficient to quantify interlaminar fracture toughness.

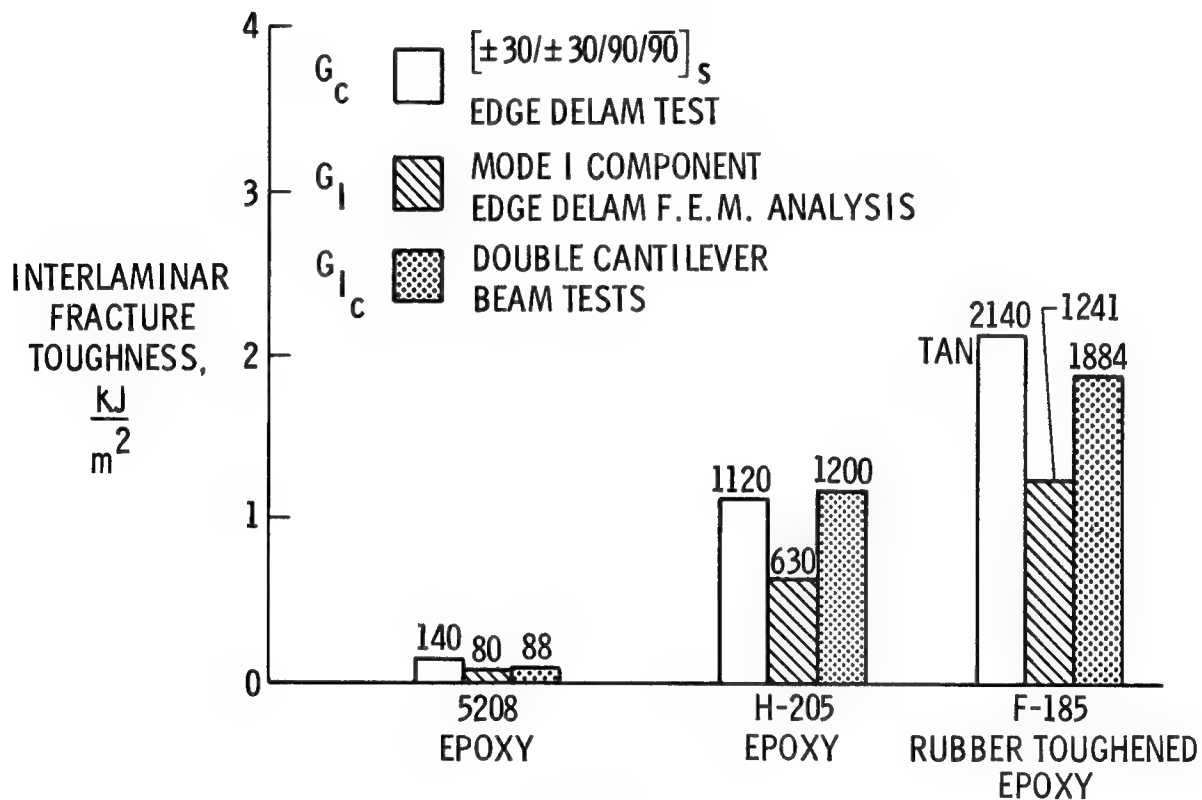


Figure 4

VARIATION IN DELAMINATION ONSET STRAINS WITH LAYUP

A parametric study was conducted (ref. 5) to optimize layups for the edge delamination test. Two families of layups were considered. The first, $[\pm\theta/\overline{90}]_S$, contained only angle plies and 90° plies. The second, $[\pm\theta/0/\overline{90}]_S$, contained angle plies, 0° plies, and 90° plies. Figure 5 shows the critical strain at delamination onset, ϵ_c , assuming a G_C of 0.15 kJ/m^2 , required to create an edge delamination in the two layup families. As shown in figure 5, the lowest ϵ_c occurs for θ in the vicinity of 30° and 35° for the $[\pm\theta/\overline{90}]_S$ and $[\pm\theta/0/\overline{90}]_S$ families, respectively. Hence, the $[\pm 30/\overline{90}]_S$ family and the $[\pm 35/0/\overline{90}]_S$ families appear to be good candidates for the edge delamination test.

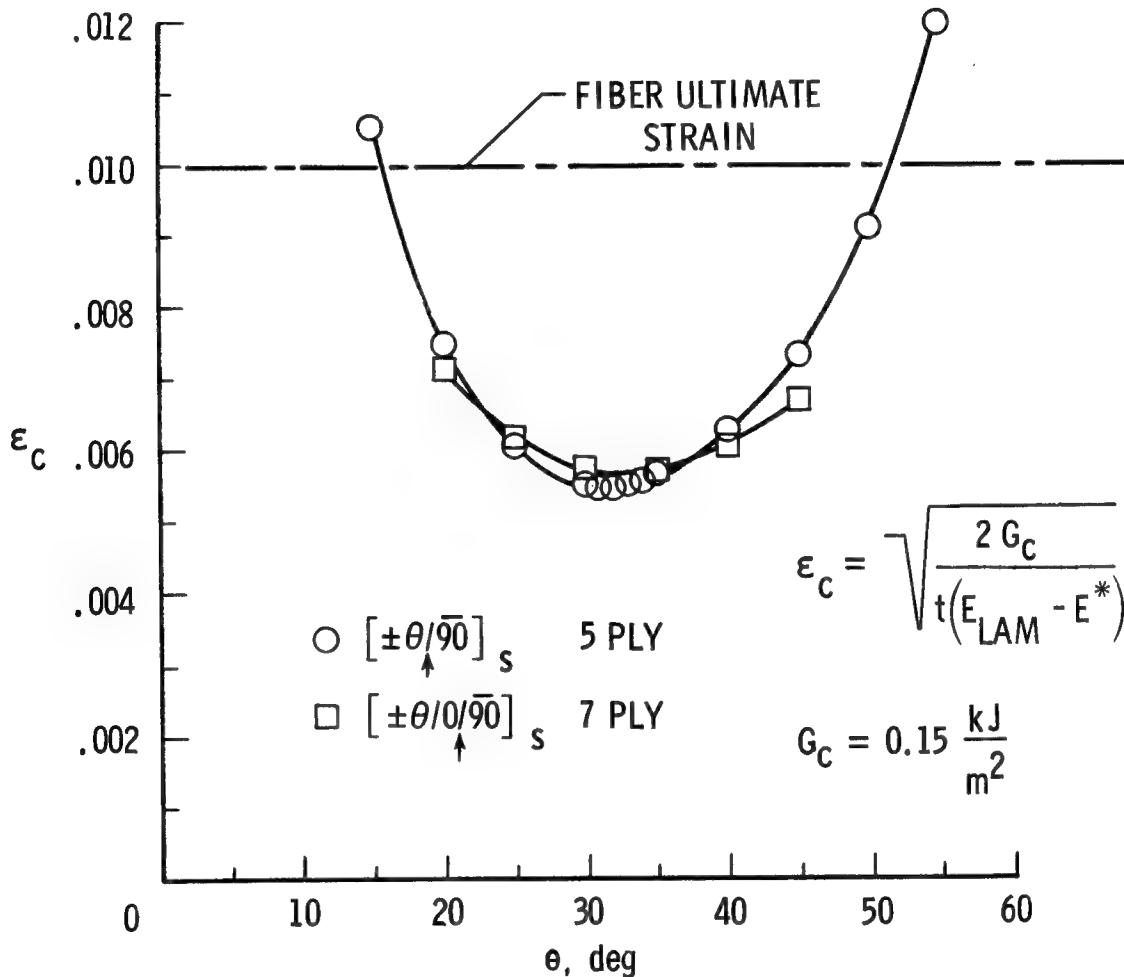


Figure 5

EFFECT OF STACKING SEQUENCE ON MIXED FRACTURE MODES

A finite-element analysis was performed in reference 5 to determine the crack-opening mode, G_I , and interlaminar shear mode, G_{II} , components of the total strain energy release rate, G , for the optimized layups of the edge delamination test. Three permutations of the $[\pm 35/0/90]_s$ layup family were analyzed. They were $[\pm 35/0/90]_s$, $[+35/0/-35/90]_s$, and $[0/\pm 35/90]_s$. All three layups had the same total G for a given nominal strain ϵ , but each had very different percentages of G_I and G_{II} . Figure 6 shows results for the $[\pm 35/0/90]_s$ family, as well as results for a similar quasi-isotropic family and for the original $[\pm 30/\pm 30/90/\overline{90}]_s$ layup. In all cases the delamination is modeled between the 90° ply and the adjacent plies. For the $[\pm \theta/0/90]_s$ layups, the G_I percentages range from very high to intermediate to very low when the 0° plies are either next to the interior 90° ply, between the $+\theta^\circ$ and $-\theta^\circ$ plies, or on the outside, respectively. Hence, the three permutations of the $[\pm 35/0/90]_s$ layup may be useful for evaluating the fracture mode dependence of composites with different matrices.

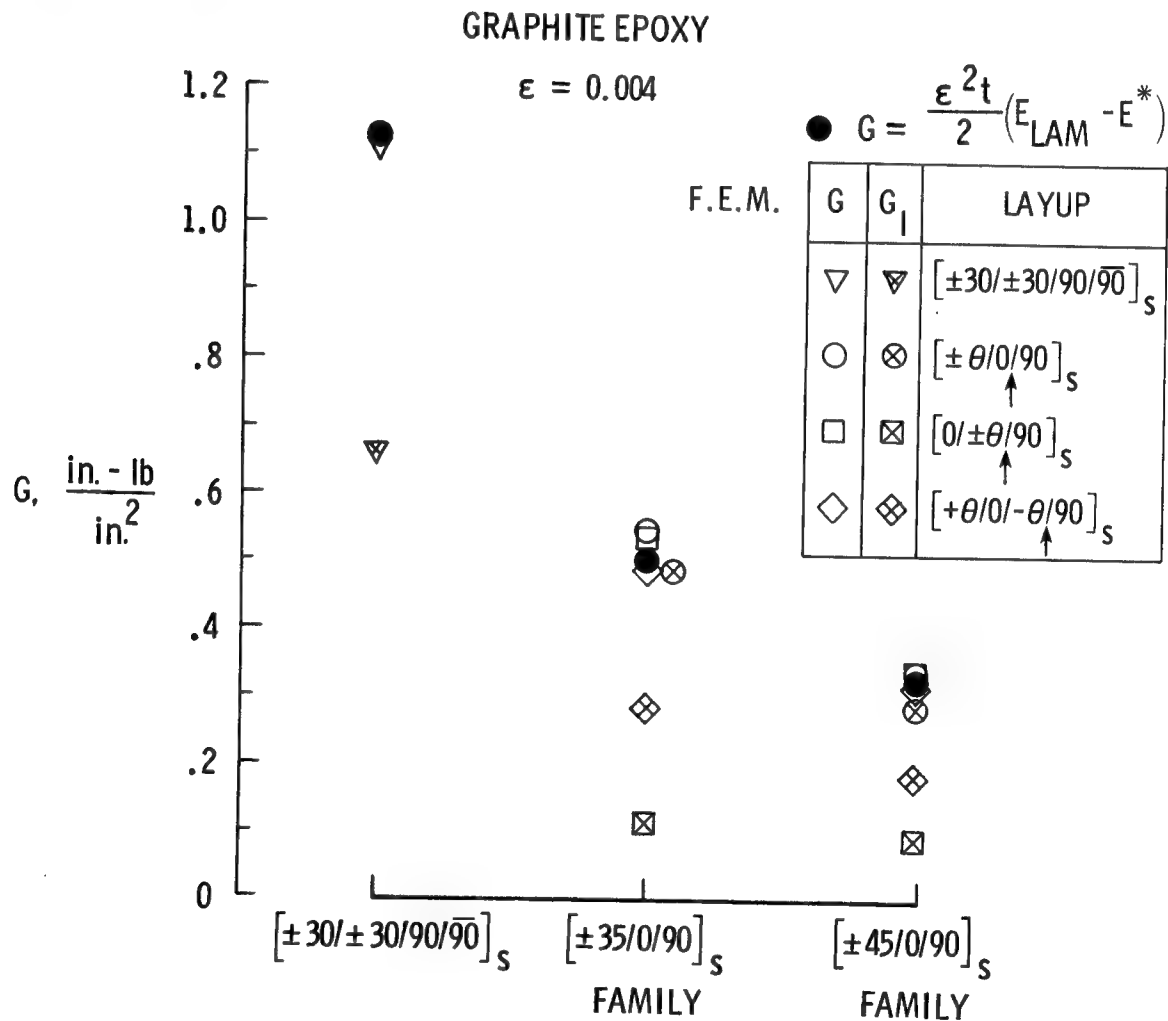


Figure 6

INFLUENCE OF MATERIAL PROPERTIES ON G_I PERCENTAGE

A parametric study was performed, using finite-element analyses, to determine the influence of material properties on the G_I and G_{II} components for all of the EDT layups. The results are shown in figure 7 for the $[\pm 35/0/90]_S$, $[+35/0/-35/90]_S$, $[0/\pm 35/90]_S$, and $[\pm 30/\pm 30/90/\bar{90}]_S$ layups made with several materials that have widely differing lamina properties. The G_I percentages are essentially constant for a given layup, independent of material properties. This material independence eliminates the need to run finite-element analyses for each new material evaluated. Hence, tests conducted on high G_I $[\pm 35/0/90]_S$, intermediate G_I $[\pm 30/\pm 30/90/\bar{90}]_S$ or $[+35/0/-35/90]_S$, and low G_I $[0/\pm 35/90]_S$ laminates may be used to quantify the interlaminar fracture mode dependence of various composite materials.

	LAMINA PROPERTIES OF GRAPHITE COMPOSITES				G_I PERCENTAGE			
	E_{11} , GPa	E_{22} , GPa	G_{12} , GPa	ν_{12}	$[\pm 35/0/90]_S$	$[+35/0-35/90]_S$	$[0/\pm 35/90]_S$	$[\pm 30/\pm 30/90/\bar{90}]_S$
T300/5208	134	10.2	5.5	0.30	90%	58%	22%	57%
C6000/H205	124	8.4	5.3	0.33	88%	59%	25%	57%
C6000/F185	119	6.2	2.6	0.34	90%	61%	23%	58%

Figure 7

INTERLAMINAR FRACTURE TOUGHNESS OF GRAPHITE COMPOSITES

Figure 8 shows mean values of G_c and their G_I components measured using three EDT layups (ref. 6) for graphite composites reinforced with brittle (5208 and 2220-1) and tough (H205 and F185) resin matrices. Also shown in figure 8 are G_{Ic} values measured from DCB tests on graphite composites made with the same resin matrices. All four tests (DCB and the three EDT layups) show improvements in interlaminar fracture toughness for the tougher resin composites (H205 and F185) compared to the brittle resin composites (5208 and 2220-1). Delamination onset occurred in the mixed-mode EDT test of the 5208 composite when the G_I component reached G_{Ic} as measured by the DCB test. Furthermore, although G_c measurements of the two 2220-1 EDT layups differed, delamination occurred at identical low values of G_I . Therefore, it appears that only the interlaminar tension, G_I , fracture mode contributes to delamination in brittle resin composites subjected to mixed-mode loading. However, this was not true for the tougher H205 and F185 specimens, where interlaminar shear did contribute to delamination. For the three EDT layups with widely different G_I percentages, delamination occurred when G_I was below G_{Ic} as measured by DCB tests (fig. 8). However, the total G_c mean values for each layup were different. The apparent G_c was increasing with decreasing G_I percentage. Hence, the interlaminar shear was only partially responsible for delamination.

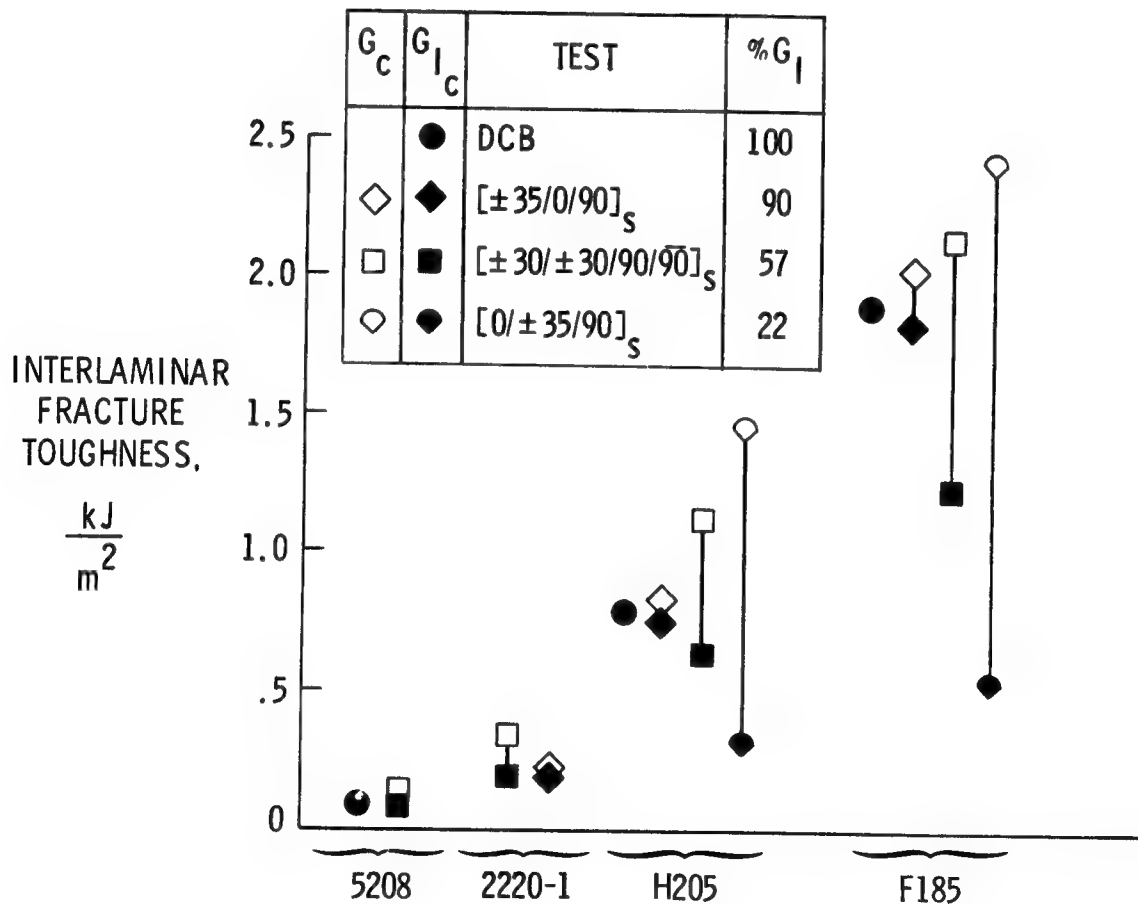


Figure 8

DELAMINATION FAILURE CRITERIA AS A FUNCTION OF MIXED-MODE PERCENTAGE FOR GRAPHITE/EPOXY COMPOSITES

The observations in figure 8 demonstrated the need for delamination failure criteria that would reflect the observed fracture mode dependence. Figure 9 shows a plot of average interlaminar fracture toughness as a function of G_I percentage for the four materials tested. For the brittle resin matrix composites (5208 and 2220-1), the interlaminar fracture toughness is simply a single value of G_{Ic} , independent of the G_I percentage. However, for the tougher resin matrix composites (H205 and F185) the interlaminar shear also contributes to delamination; therefore, a more appropriate failure criterion for these materials is a linear decrease in G_c with increasing G_I percentage. Hence, if the G_I percentage of a particular delamination failure in a structure made from these materials can be determined, then the appropriate G_c may be chosen from figure 9 to predict delamination extension.

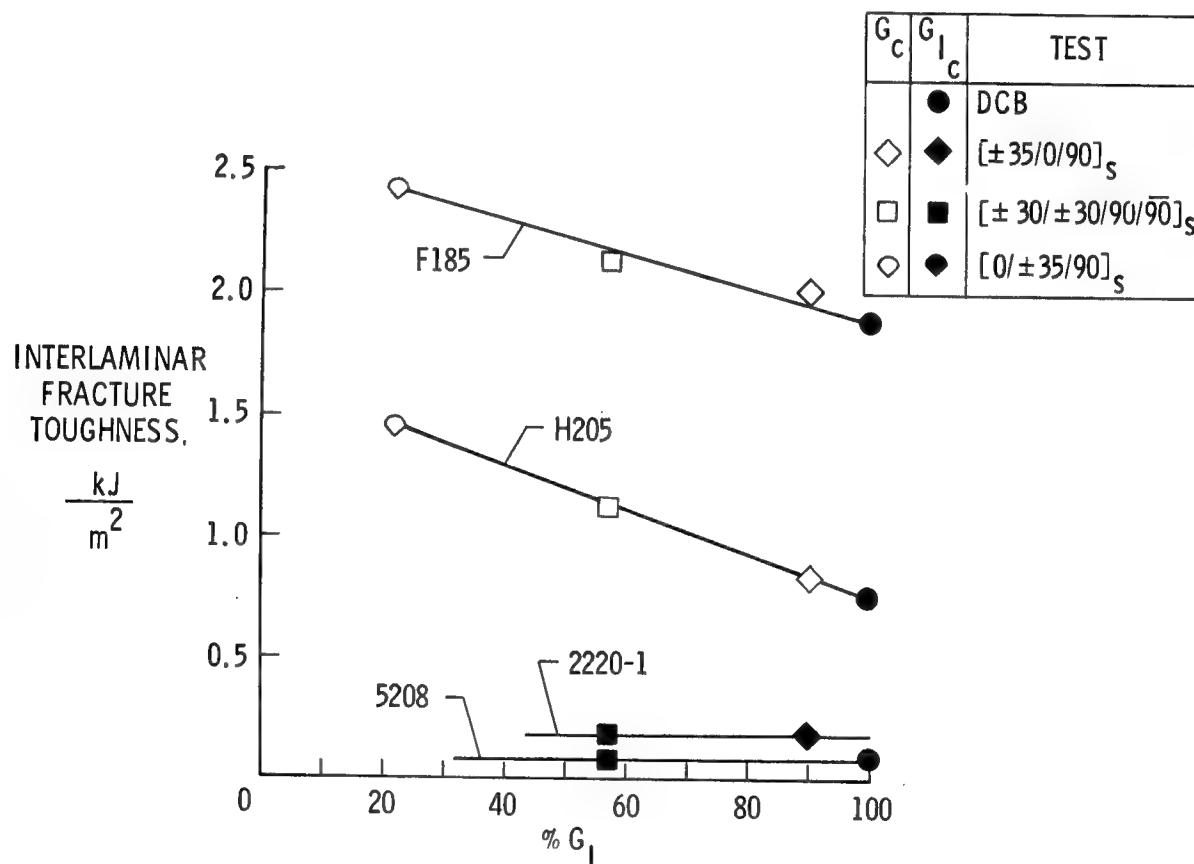


Figure 9

CHARACTERIZING DELAMINATION RESISTANCE IN FATIGUE WITH THE EDGE DELAMINATION TEST

Cyclic loading may cause extensive delamination in graphite composites, even for laminates that do not delaminate under static loads. Therefore, it is necessary to characterize delamination resistance in fatigue as well as in static loading. To this end, various EDT layups made with different resin matrices were cycled to strain levels below the delamination onset strain measured in the static tests (fig. 10). Delaminations formed at these lower cyclic strains after a certain number of cycles, N . Strain energy release rate (G) values, calculated from maximum cyclic strains and plotted as a function of the number of cycles to delamination onset, dropped sharply and then reached a plateau tantamount to a threshold for delamination onset in fatigue.

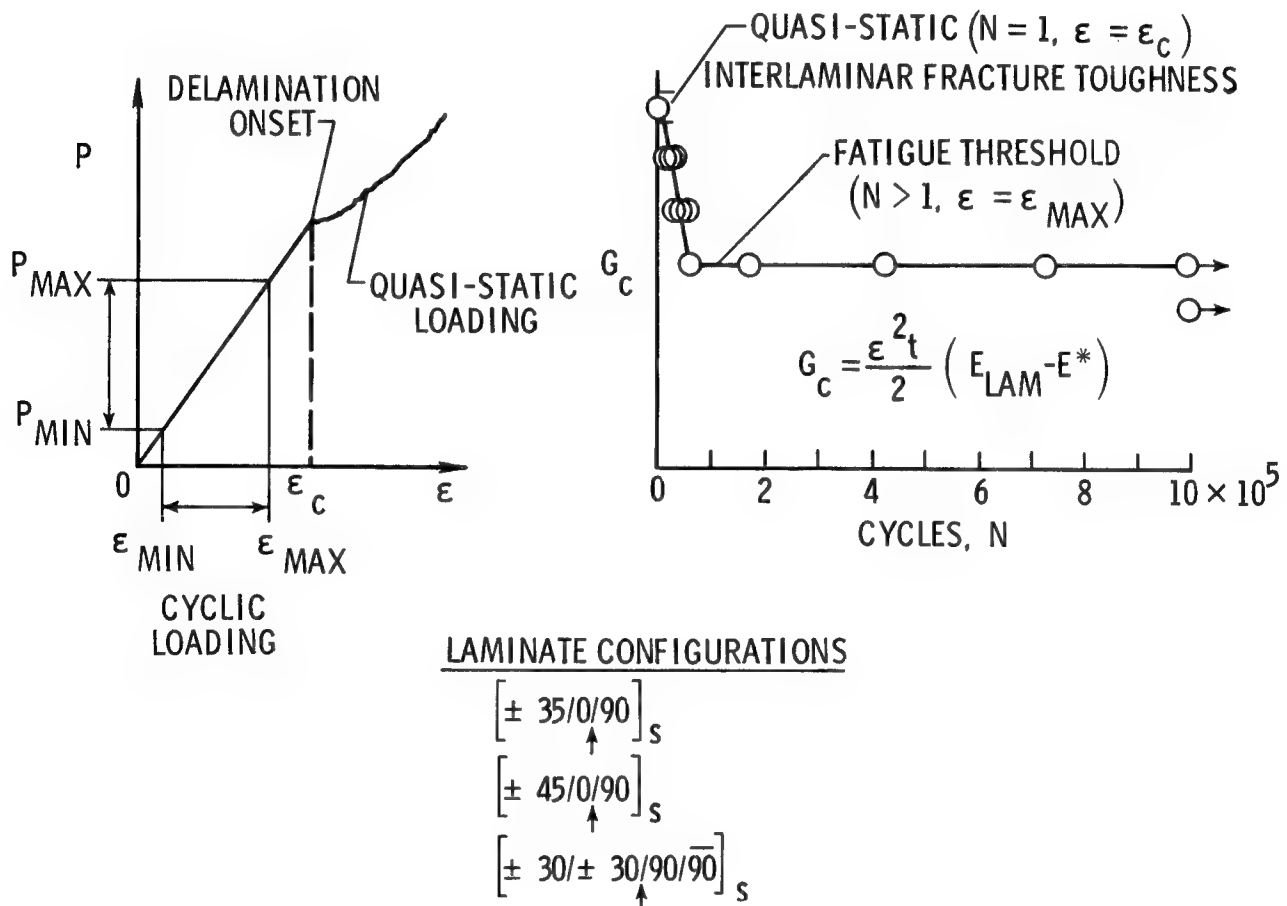


Figure 10

G_C AS A FUNCTION OF FATIGUE CYCLES

Figure 11 summarizes results of static and fatigue tests for $[\pm 45/0/90]_S$ T300/5208 laminates and for $[\pm 35/0/90]_S$ and $[0/\pm 35/90]_S$ C6000/H205 laminates using the technique outlined in figure 10. The total G is identical for the $[\pm 35/0/90]_S$ and $[0/\pm 35/90]_S$ laminates, but the G_I percentages are different, as shown in figure 7. For static tests, the G_C for these two layups is different; however, the G_C thresholds under cyclic loading for the two layups are nearly identical. Hence, the total G appears to govern the delamination threshold for fatigue. Furthermore, comparison of the 5208 matrix composite to the H205 matrix composite shows a significant improvement in the static G_C , yet the magnitude of this improvement for the G_C threshold in fatigue is much less. A series of mixed-mode static and cyclic tests like these may be needed to evaluate toughened resin composites subjected to cyclic loads.

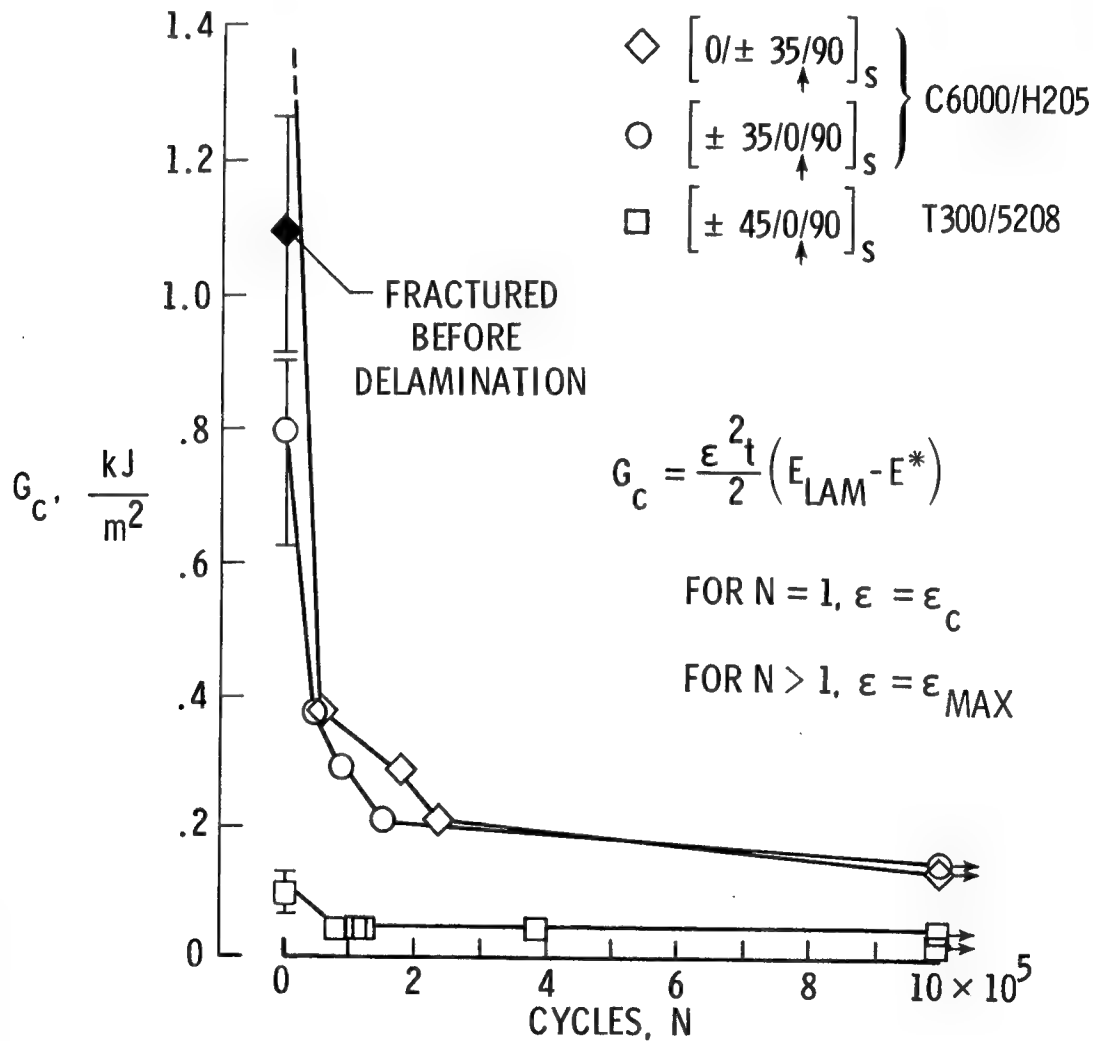


Figure 11

EDGE DELAMINATION TEST SPECIMEN SIZE OPTIMIZATION

As new matrix resins are developed, they must be evaluated for improved toughness. Ideally, this should be done on very small specimens because often only limited quantities of experimental resins are available. For this reason, a study was undertaken to miniaturize the edge delamination test. The configuration shown in figure 12 appears to be an optimal compromise between material and testing constraints. The G_c results from this specimen are identical to those measured on the larger coupons.

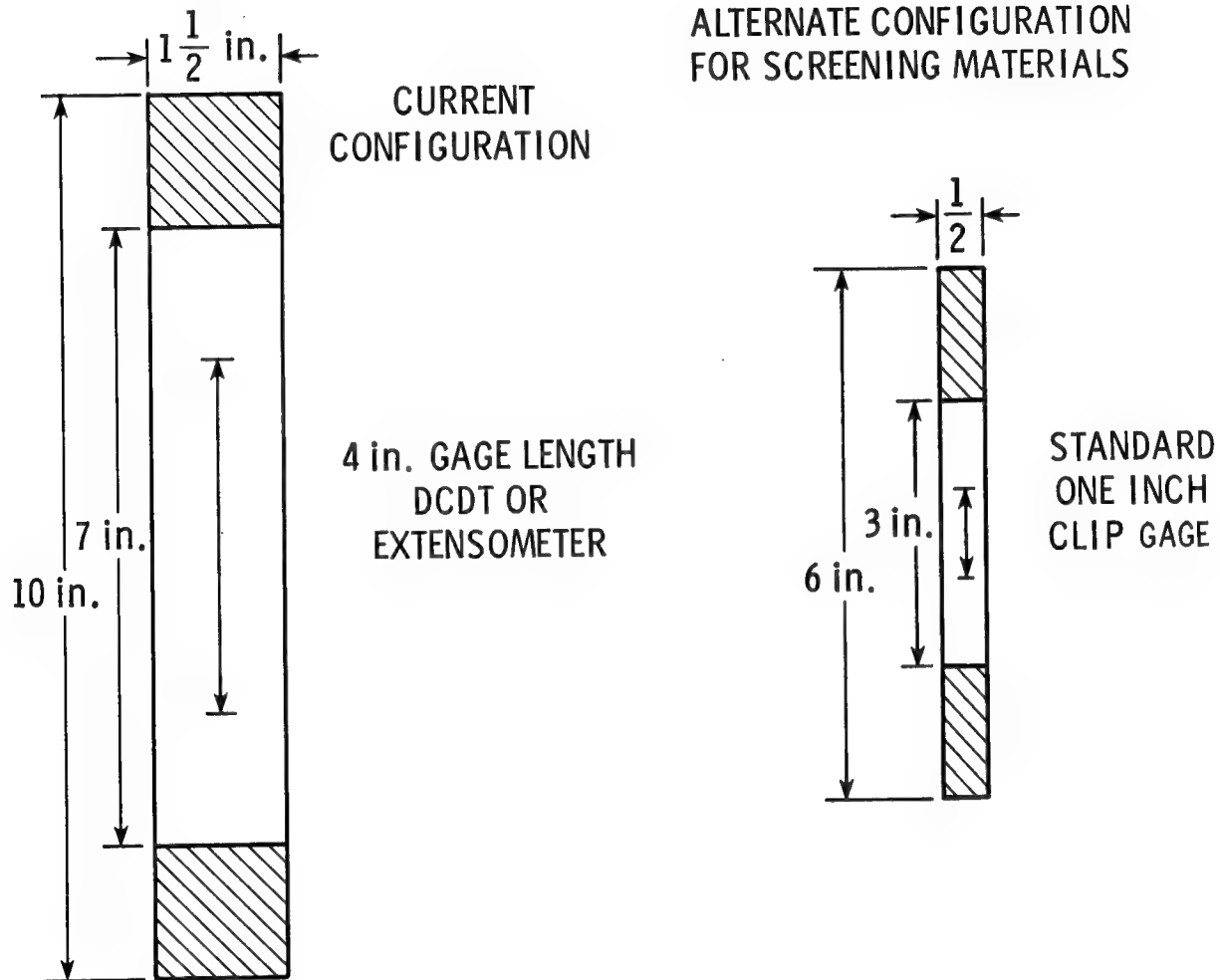


Figure 12

SUMMARY

A study was conducted to characterize the delamination resistance of toughened resin composites. Both the edge delamination test (EDT) and the double-cantilever-beam (DCB) test provided a useful ranking of improvements in delamination resistance between brittle and tough resin composites. Several layups were designed for the edge delamination test to cover a wide range of mixed-mode conditions. The DCB and the various layups of the EDT were then used to characterize the interlaminar fracture behavior of brittle and toughened resin composites subjected to both static and cyclic loading.

REFERENCES

1. O'Brien, T. K.; Johnston, N. J.; Morris, D. H.; and Simonds, R. A.: A Simple Test for the Interlaminar Fracture Toughness of Composites. SAMPE Journal, vol. 18, no. 4, 1982, pp. 8-15.
2. O'Brien, T. K.: Characterization of Delamination Onset and Growth in a Composite Laminate. Damage in Composite Materials, K. L. Reifsnider, ed., ASTM STP 775, American Society for Testing and Materials, 1982, pp. 140-167. (Also NASA TM-81940, January 1981)
3. Standard Tests for Toughened Resin Composites. NASA RP-1092, 1982. (Revised July 1983)
4. Raju, I. S.; and Crews, J. H., Jr.: Interlaminar Stress Singularities at a Straight Free Edge in Composite Laminates. Journal of Computers and Structures, vol. 14, no. 1-2, 1981, pp. 21-28.
5. O'Brien, T. K.: Mixed-Mode Strain Energy Release Rate Effects on Edge Delamination of Composites. NASA TM-85492, January 1983. (To appear in Effects of Defects in Composite Materials, D. J. Wilkins, ed., ASTM STP 836, 1984)
6. O'Brien, T. K.; Johnston, N. J.; Morris, D. H.; and Simonds, R. A.: Determination of Interlaminar Fracture Toughness and Fracture Mode Dependence of Composites Using the Edge Delamination Test. Proceedings of the International Conference on Testing, Evaluation, and Quality Control of Composites, TEQC83, T. Feest, ed., Butterworth Scientific Ltd., Kent, England, 1983, pp. 223-232.

COMPOSITE MATERIALS CHARACTERIZATION AND
DEVELOPMENT AT AFWAL

C. E. Browning
Air Force Wright Aeronautical Laboratories
Wright-Patterson Air Force Base, Ohio

The first subject area to be discussed is Composite Characterization for Matrix Dominated Failure Modes. The objective of this work is to develop test methodology for characterizing matrix dominated failure modes, emphasizing the two major issues of matrix cracking and delamination under static loading. Also of major importance is establishing the relationship of the composite properties to the matrix properties.

OBJECTIVE - TO DERIVE TEST METHODOLOGY FOR CHARACTERIZING
MATRIX DOMINATED COMPOSITE FAILURE MODES WITH EMPHASIS ON -

- MATRIX CRACKING
- DELAMINATION UNDER STATIC LOADING
- RELATING COMPOSITE PROPERTIES TO MATRIX
RESIN PROPERTIES

The major characterization methodologies which are applicable to the characterization of matrix dominated composite failure modes are underlined below. Strength characterization entails a detailed stress analysis with a failure criterion to predict and measure experimentally the onset of matrix cracking and delamination. Fracture mechanics characterization entails the application of classical techniques of linear elastic fracture mechanics. We have actively worked all of the areas shown below except for impact characterization.

STRENGTH CHARACTERIZATION

● NEAT RESIN

- TENSILE STRESS - STRAIN RESPONSE
- SHEAR STRESS - STRAIN BEHAVIOR

● COMPOSITE

- TRANSVERSE TENSION
- LAMINATE IN-SITU TRANSVERSE PLY FAILURE
- INPLANE SHEAR
- INTERLAMINAR SHEAR
- COMPRESSION STRENGTH

FRACTURE MECHANICS CHARACTERIZATION

● NEAT RESIN

- CENTER-NOTCH TEST
- EDGE-NOTCH TEST
- COMPACT TENSION TEST

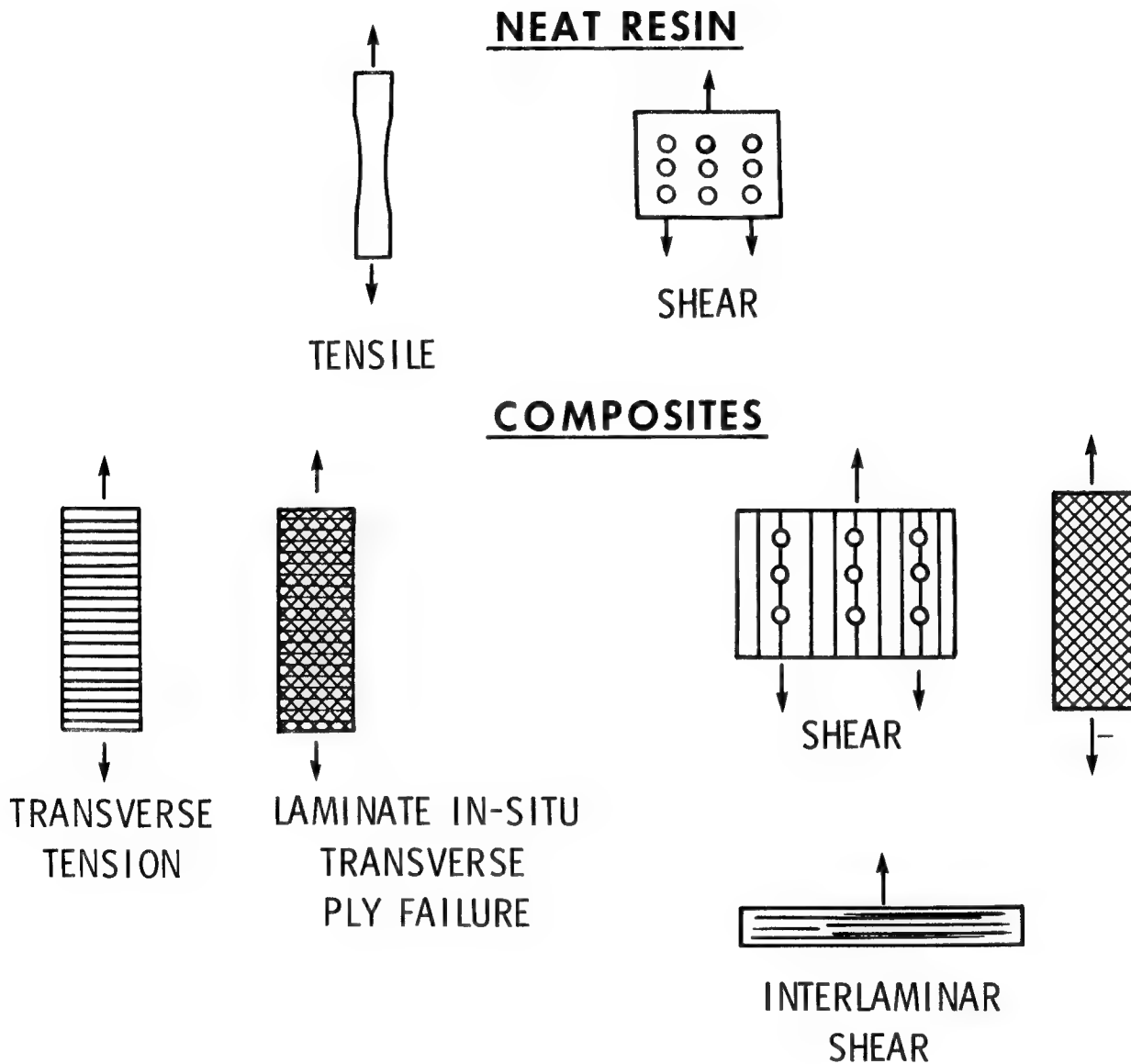
● COMPOSITE

- DOUBLE CANTILEVER BEAM TEST
- TRANSVERSE CENTER-NOTCH TEST
- FREE-EDGE DELAMINATION TEST

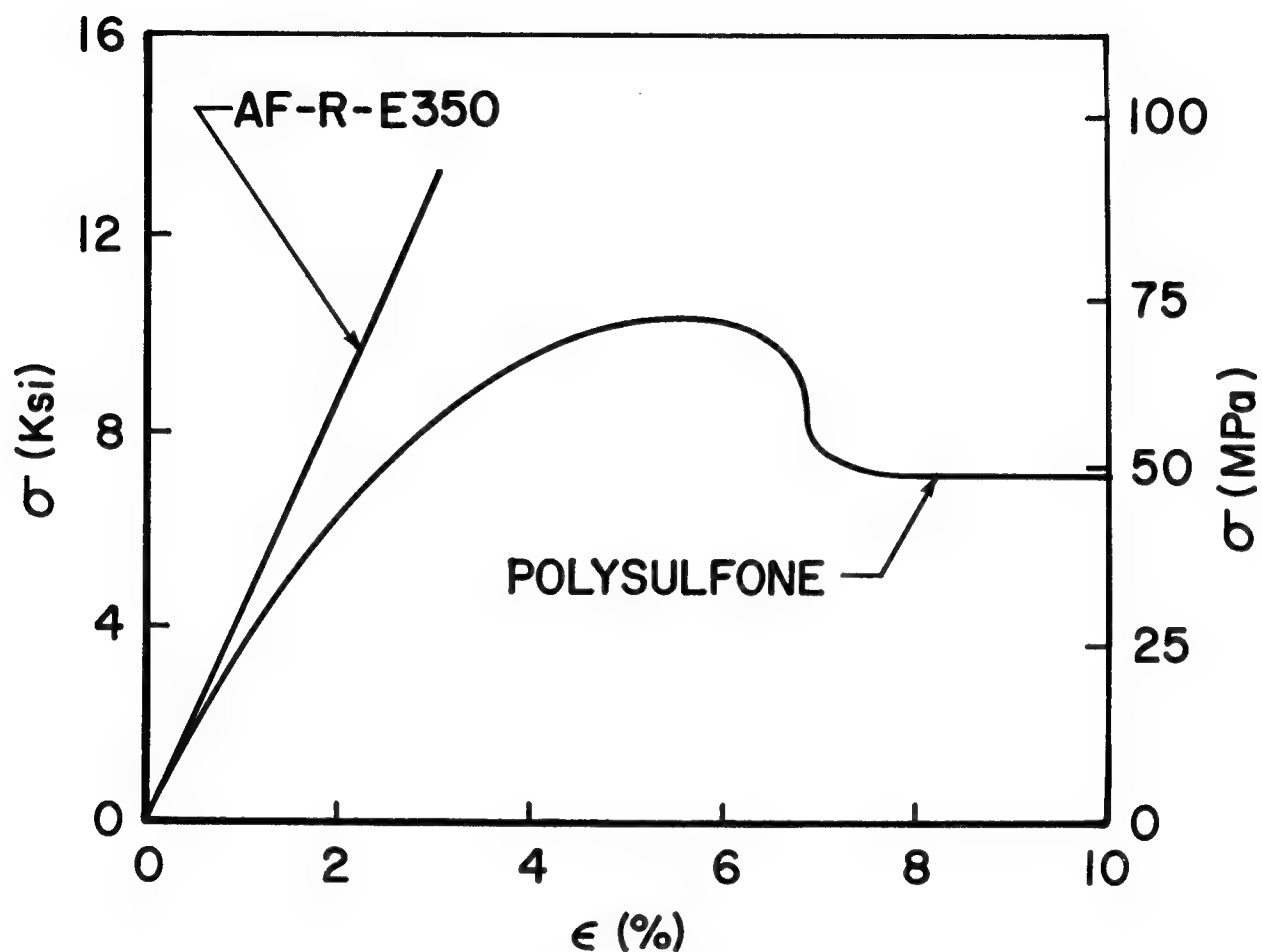
IMPACT CHARACTERIZATION

FRACTOGRAPHY

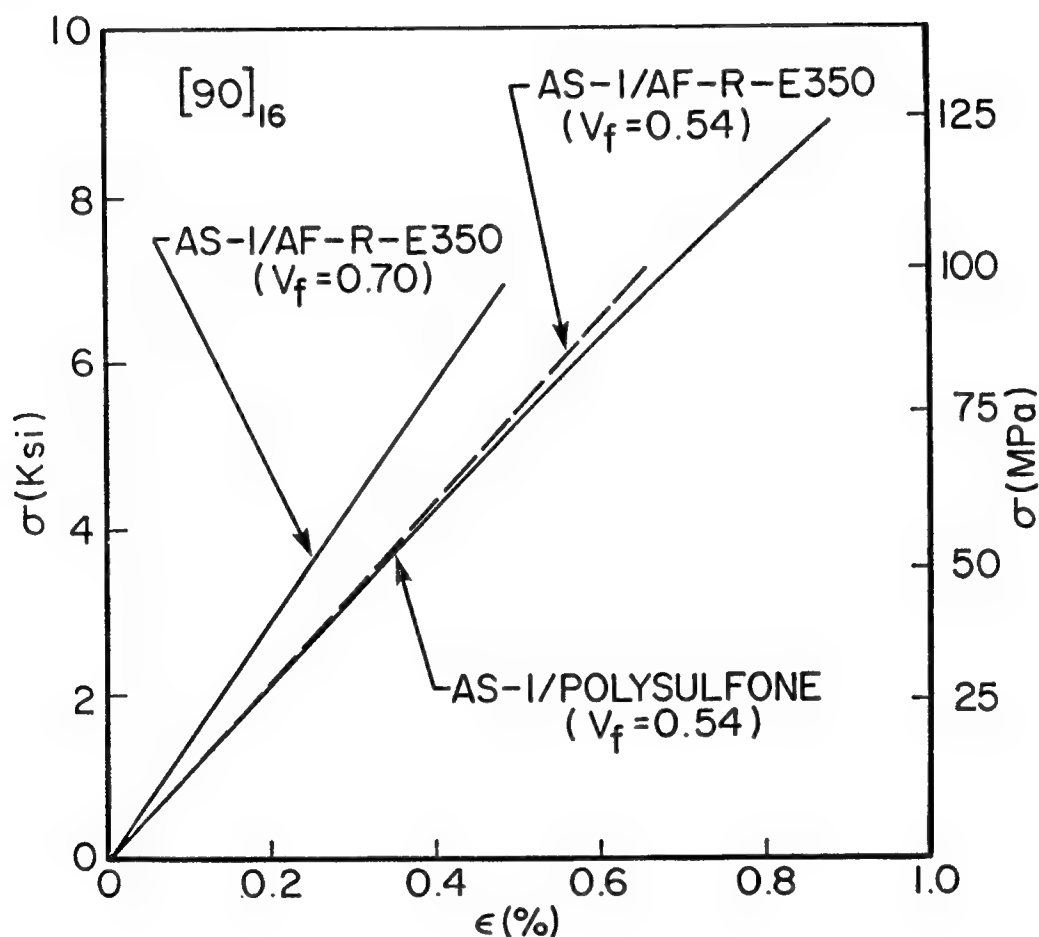
With respect to strength characterization, the tests shown below have been investigated. The tests from this group to be discussed include neat resin tensile, composite transverse tension, laminate in-situ transverse ply failure, and composite interlaminar shear.



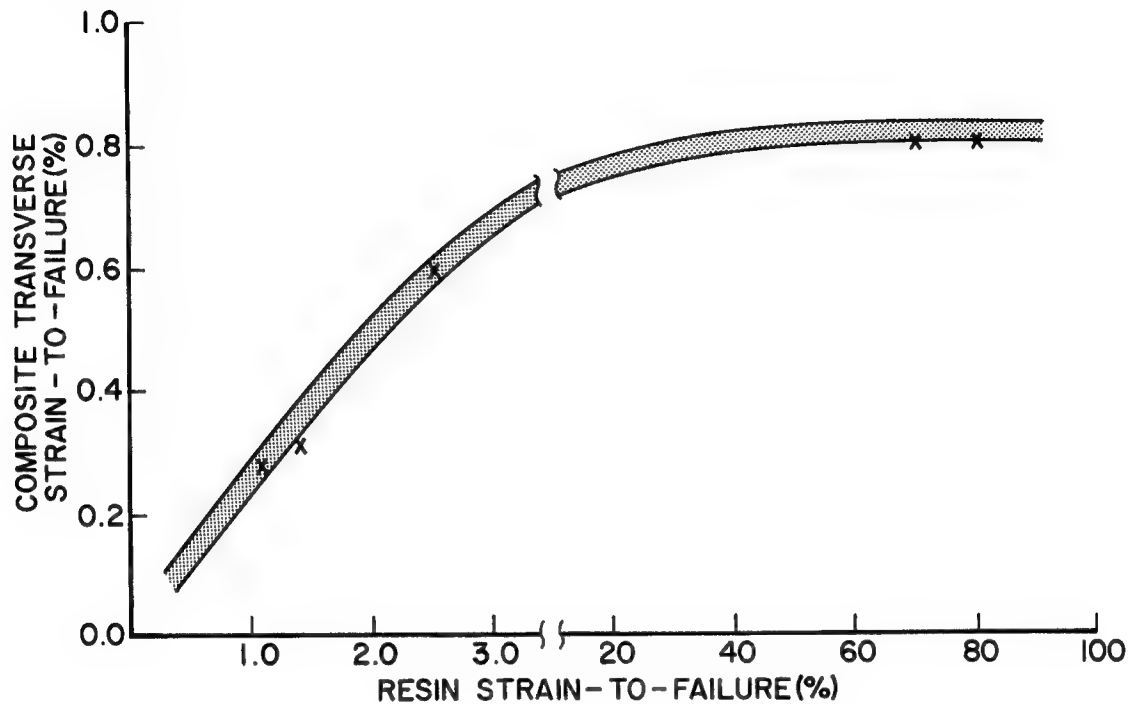
Neat resin tensile results are illustrated below. AF-R-E350 is a 350°F epoxy used in-house at the Materials Lab (ML). It contains MY-720 and DDS. This system typifies a brittle resin. Polysulfone is a thermoplastic that typifies a ductile resin. Typical stress strain responses are shown. The polysulfone curve actually continues to higher strain levels than shown.



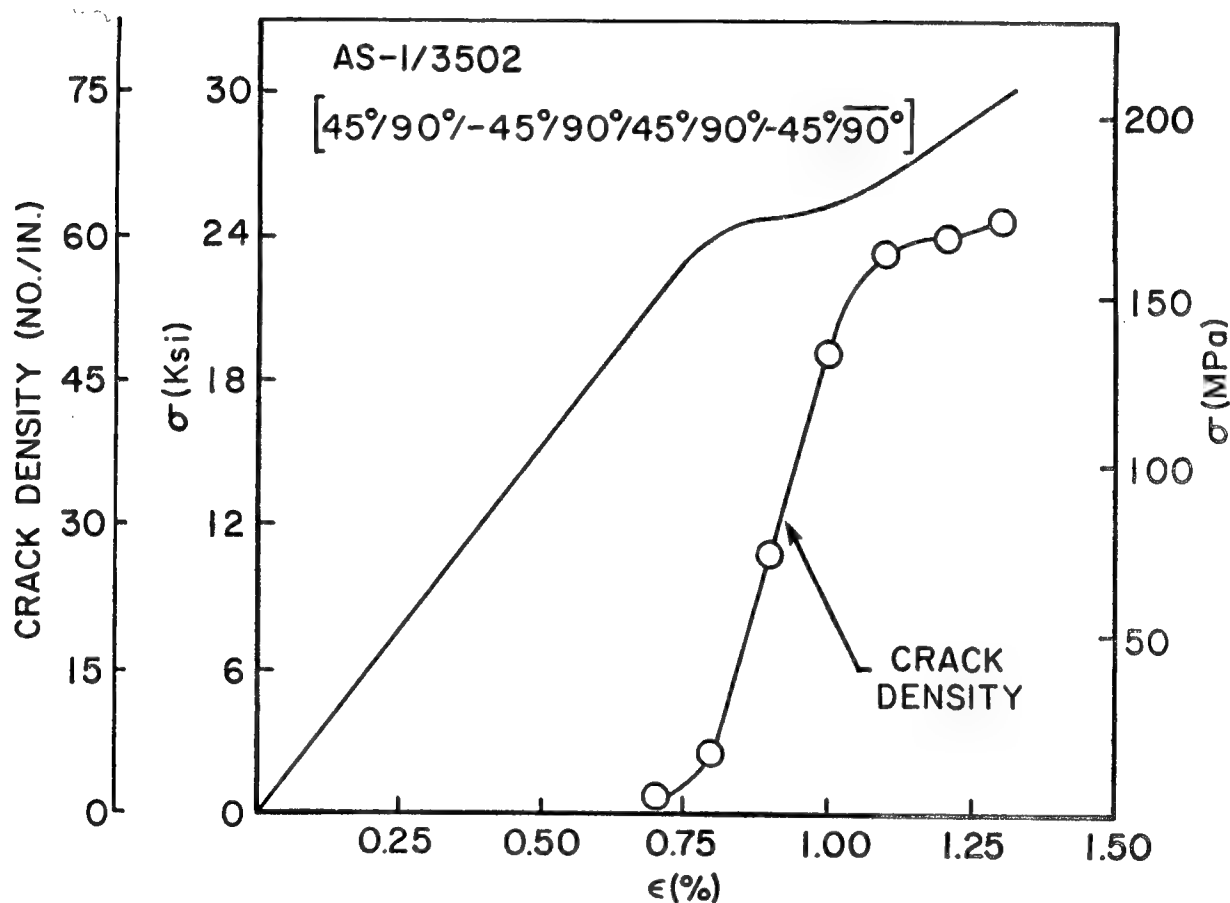
Composite transverse tension results are shown below for AF-R-E350 with AS-1 fiber at two fiber volume levels and polysulfone with AS-1 fiber. In many cases transverse tension is the limiting basis for design purposes. If the transverse ply failure is the limiting failure criterion, the transverse ply in a laminate will determine its strength. The data in the chart was normalized for fiber volume. It is important to normalize the transverse data as well as the unidirectional data. This was done by calculating strain concentration factors and using the Halpin-Tsai equations to extrapolate the epoxy to a fiber volume of 54%. This doesn't affect the stress but does change the strain as shown. Comparing the stress-strain curves for equivalent fiber volume shows that the strain-to-failure for the polysulfone/AS-1 composite vs. the epoxy/AS-1 is not in proportion to the neat resin data.



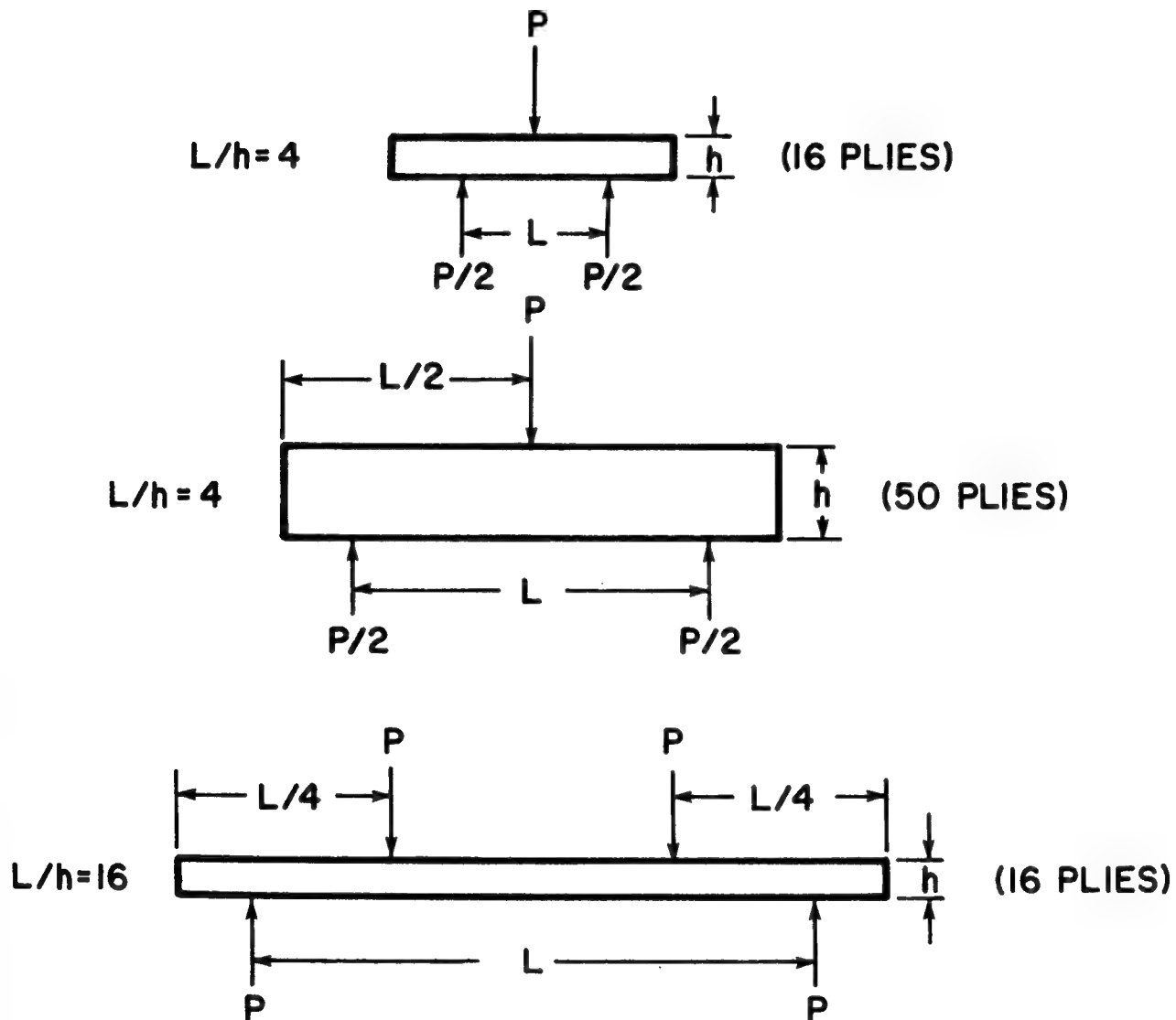
This chart shows that there may be a limiting value of composite strain-to-failure irrespective of neat resin properties. In the very ductile matrices, yielding of the neat resin during tensile testing leads to "necking" in the specimen at high strain levels. In the composite, due to the presence of the fibers, this necking is prevented, resulting in the resin being under a biaxial state of stress. Biaxial stress-strain behavior of a neat resin may be a better indicator of resin performance in the composite than uniaxial behavior.



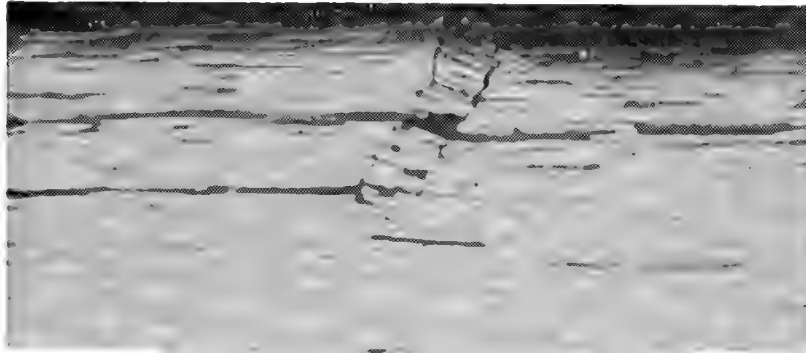
While a 90° tensile test gives useful information with respect to the transverse strain capability of a material, a multi-directional laminate containing 90° plies may be a more realistic approach to measuring and defining in-situ first-ply failure. A 90° tensile test provides initial transverse ply failure information only, while a multi-directional laminate containing multiple 90° plies allows one to observe multiple cracks in multiple transverse plies to assess their total effect on laminate mechanical behavior. Other plies in a multi-directional laminate can increase 90° ply failure strain due to constraints, resistance to crack growth, etc. This phenomenon is illustrated below for a $(\pm 45/90)$ laminate. Specimen edges are polished. Cracks in 90° plies are counted as a function of tensile testing. The knee in the stress-strain curve corresponds to the increase in crack density.



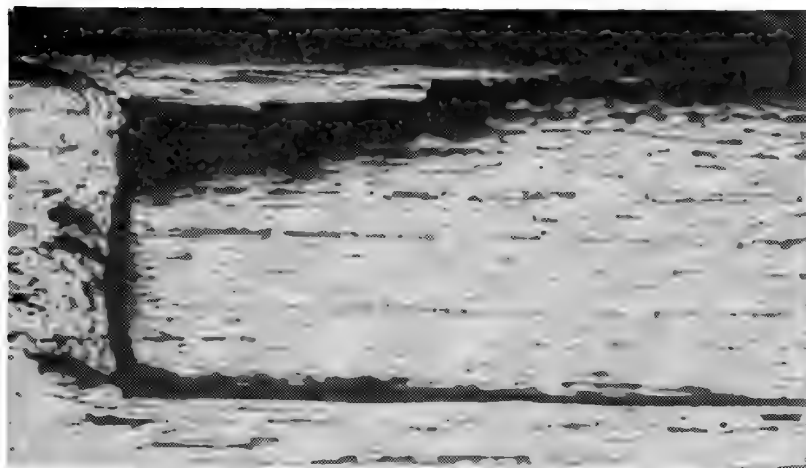
Another type of strength characterization test is an interlaminar (I-L) beam test. Three types of I-L beam tests investigated at the NL are shown below. The top one is the conventional short-beam shear specimen tested in 3-point loading with a span-to-depth ratio (L/h) of 4. Because this specimen rarely produces a shear failure, the other two coupons were investigated. One alternative is a thick (50 plies) beam tested in 3-point bending. This specimen consistently gives shear failures; however, its thickness creates undesirable processing and material problems. A better alternative is the four-point shear test shown at the bottom. This specimen consistently gives shear failures.



Shown below are photomicrographs of failed specimens representative of the three specimens on the previous figure. They provide additional insight into the complexity of beam failure modes. The failed 16-ply, 3-point beam specimen typically shows localized buckling adjacent to the top loading pin (compression surface). In the case of the 50-ply, 3-point beam, a vertical crack occurs under the top loading pin. This crack eventually leads to a horizontal shear failure. The 16-ply, 4-point beam specimen (bottom figure) also exhibits a vertical crack initially under the top loading pin. This crack eventually creates a horizontal shear crack.



16-PLY, 3-POINT BEAM

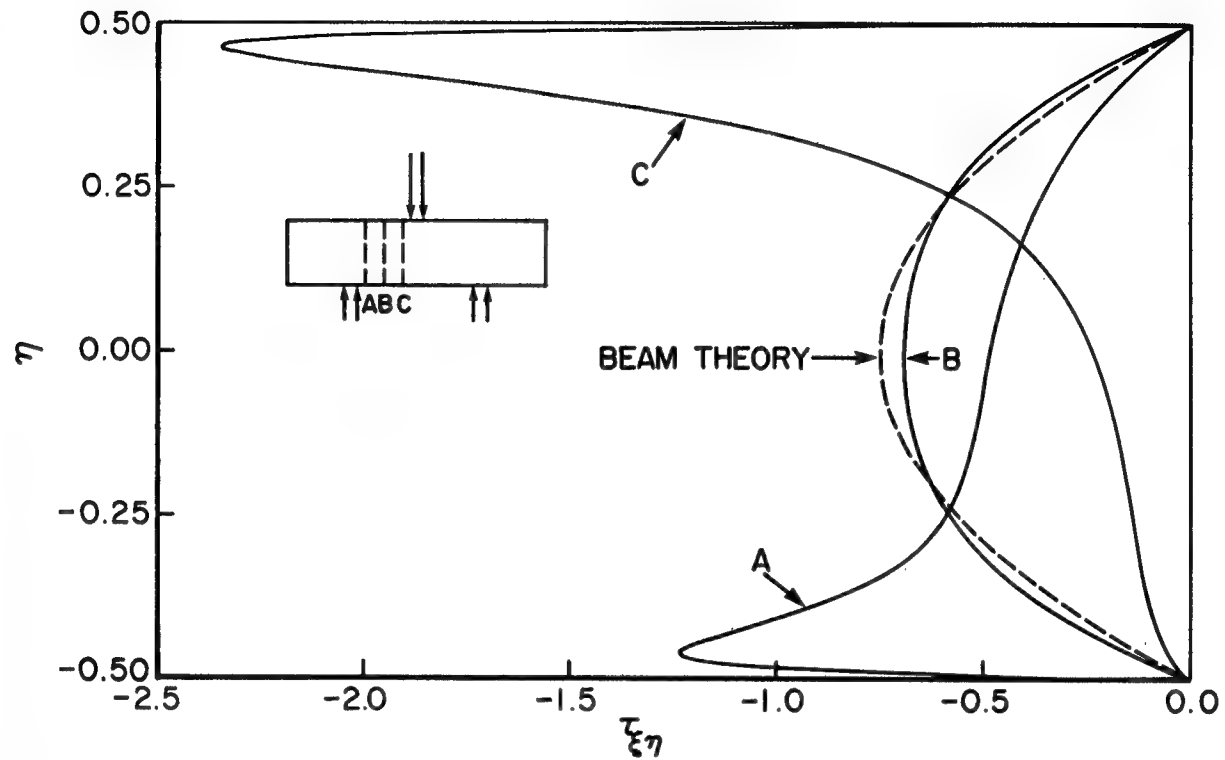


50-PLY, 3-POINT BEAM

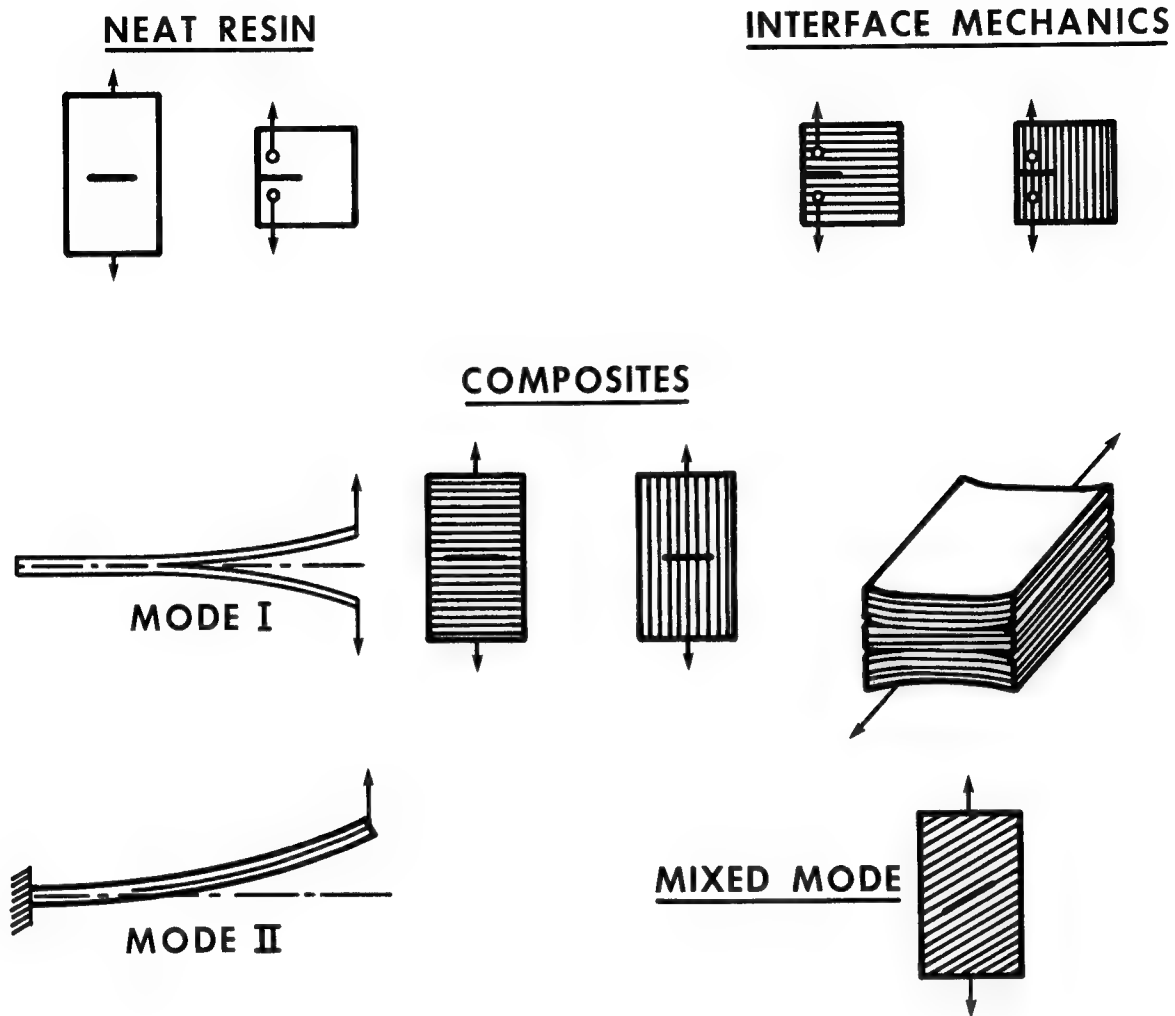


16-PLY, 4-POINT BEAM

The beam failures occur in regions where the stress distribution is very complex. The shear stress distribution at three different regions of a 16-ply beam are shown below. Classical beam theory is obtained only over a limited segment of the beam. Otherwise there will be a very complex stress distribution with high stress concentrations under the loading pins. Complex failure modes and complex stress distributions make I-beam specimens very difficult to interpret. The usefulness of I-beam tests are of questionable value.

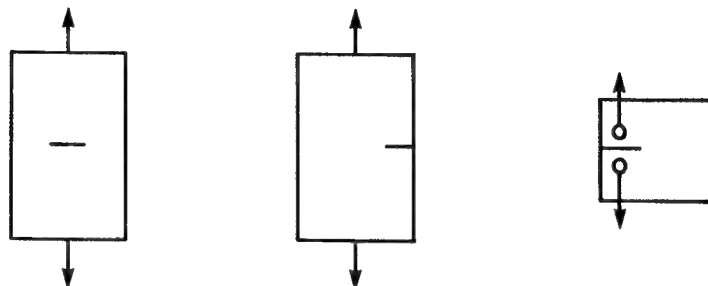


The next major area of characterization is Fracture Mechanics of Composites. The test methods shown below have been investigated. With respect to composites, major emphasis has been on interlaminar fracture mechanics. This seems to be a natural approach to treating delamination.



With respect to neat resin fracture toughness characterization, the three configurations shown below have been investigated with both dull and sharp cracks. The results show that the compact tension specimen on the right provided the best data with respect to resin vs. composite properties for the cases of the two epoxies. A major discrepancy exists with the polysulfone which may be due to the effective size of the plastic zone at the crack tip.

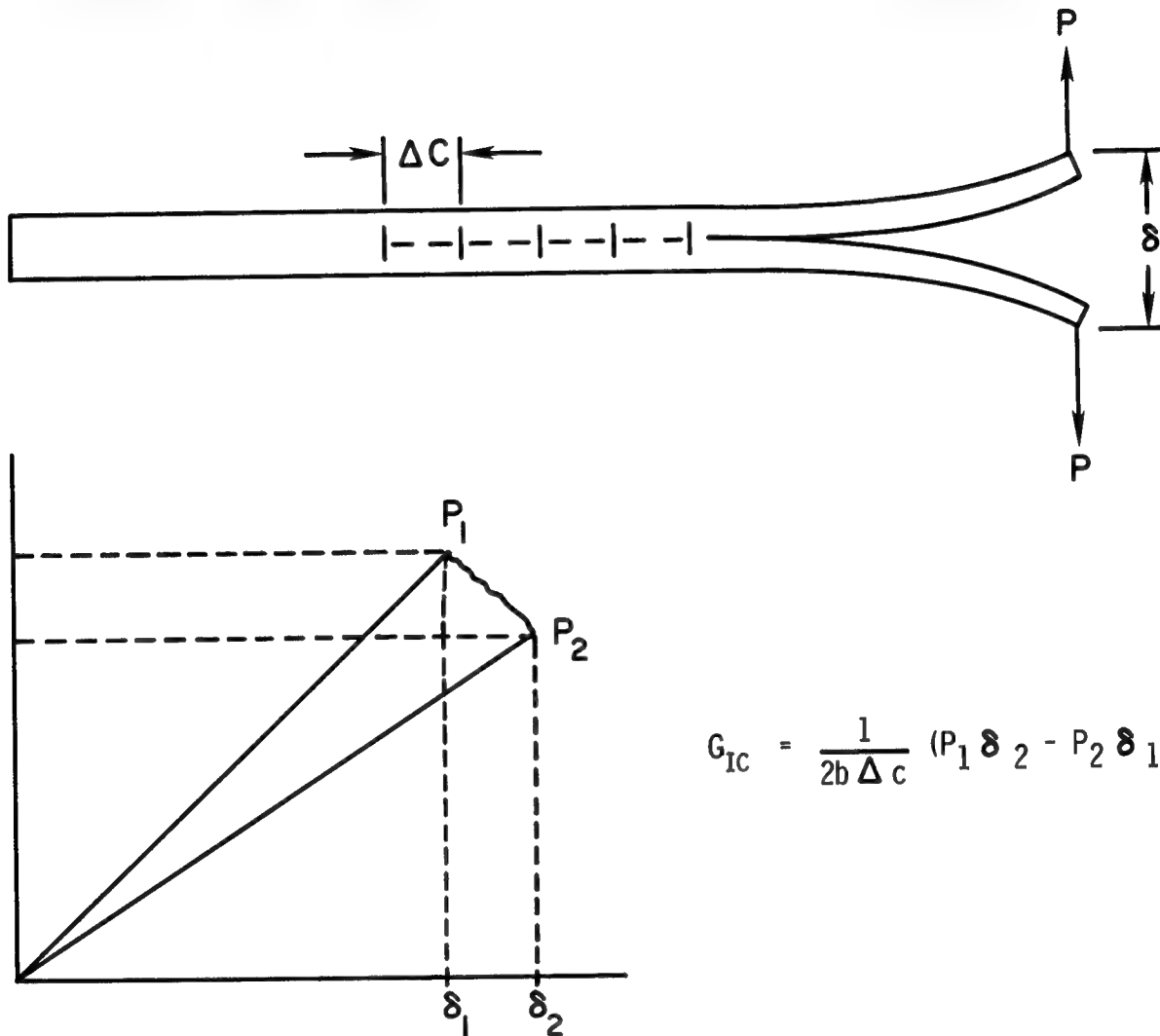
G_{Ic} , in-lb/in² (10^{-2} J/cm²)



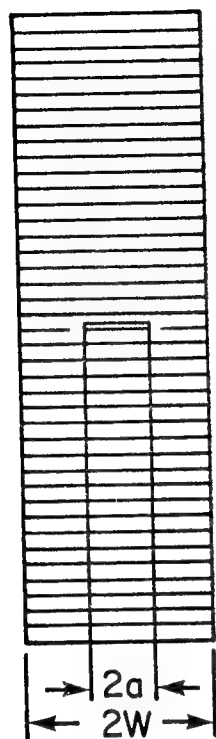
MATERIAL	DULL CRACK	SHARP CRACK	DULL CRACK	SHARP CRACK	DULL CRACK	SHARP CRACK	COMPOSITE DCB
BRITTLE EPOXY	6.5 (11.4)	-	4.1 (7.2)	0.5 (0.9)	-	0.8 (1.4)	0.8 (1.4)
DUCTILE EPOXY	12.1 (21.3)	-	-	-	24.0 (42.2)	0.6 (1.1)	0.8 (1.4)
POLYSULFONE	11.7 (20.6)	-	11.0 (19.4)	28.0 (49.3)	32.0 (56.3)	15 (26.4)	3.7 (6.5)

Most of our characterization work has been with composites. The principal technique used is the double cantilever beam (DCB) test shown below. The DCB coupon is straight-sided, 9-in. long, 1-in. wide, 24 plies, 0°, with a starter crack. Tests are run over ½-in. increments. Data reduction is by the area method. Test data will be shown in a subsequent chart.

MODE I TEST FOR INTERLAMINAR TOUGHNESS



A potential alternative to the DCB test is the transverse center-notch (CN) test. This specimen uses three crack sizes with three specimen widths. Results show it to be a reasonable alternative. Data will be shown in subsequent chart.



DATA REDUCTION

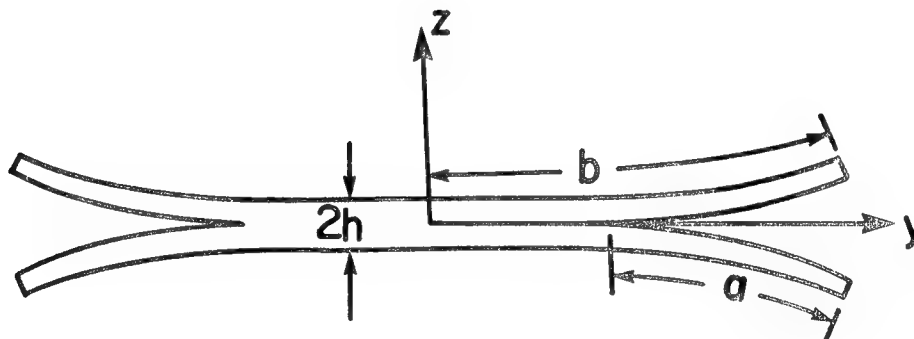
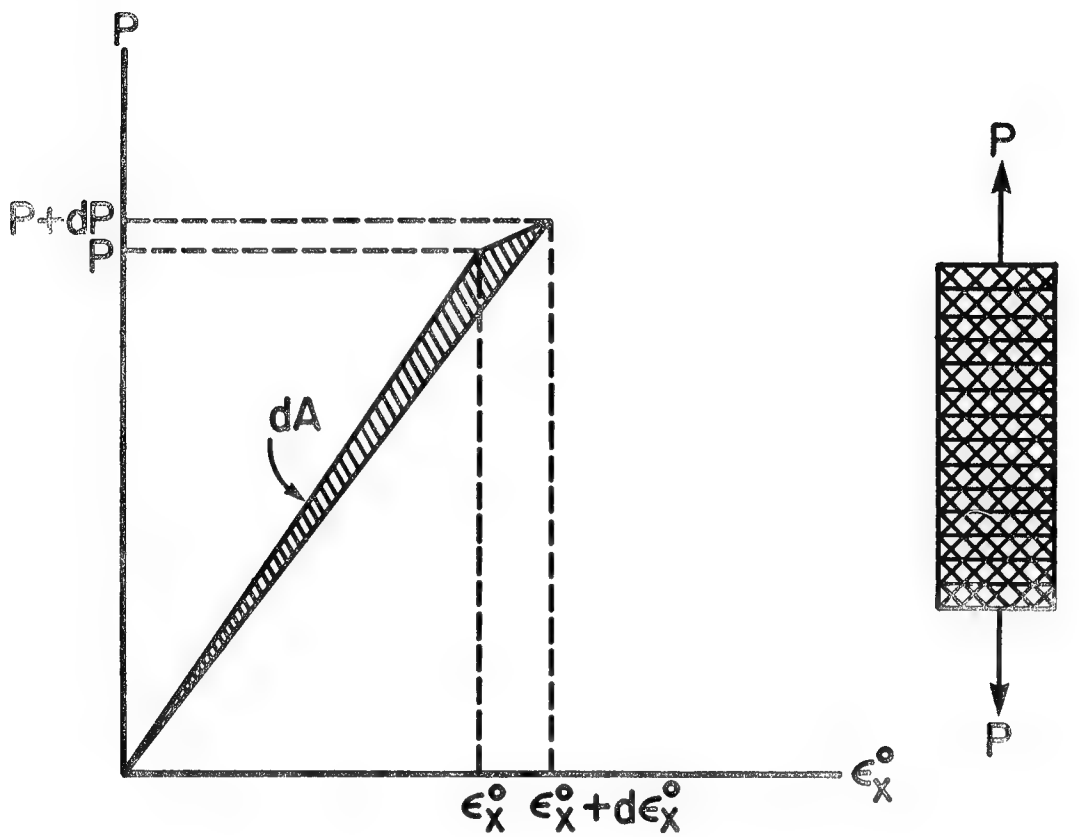
$$\sigma_n^{\infty} = \sigma_n [1 + 0.128(a/w) - 0.288(a/w)^2 + 1.53(a/w)^3]$$

$$K_{IC} = \sigma_n^{\infty} \sqrt{\pi(a+a_0)}$$

$$a_0 = \frac{1}{n} \sum_{i=1}^N \left[\frac{a_i}{\left(\frac{\sigma_0}{\sigma_n^{\infty}} \right) - 1} \right]$$

$$G_{IC} = K_{IC}^2 \sqrt{\left(\frac{1}{E_L E_T} \right) \left[\sqrt{\frac{E_L}{E_T}} + \frac{E_L}{E_T G_{LT}} (E_T - 2\nu_{LT} G_{LT}) \right]}$$

Another important test is the free edge delamination (ED) test. The stacking sequence is chosen such that delamination is induced along the straight-sided free edge under tension loading. The test discriminates between brittle and ductile resins and is an aid in screening matrix resins for toughness.



$$G_{IC} = h\epsilon_c^2 (E_I - E_I^*)$$

This table summarizes the results of Mode I delamination tests for the methods previously discussed as a function of several materials variables. The data shows that the DCB test is the preferred tool for characterizing interlaminar Mode I energy release rates.

G_{Ic} in lb/in ² (10 ⁻² J/cm ²)				
MATERIAL	V_f	DCB	90° CN	ED
AS-1/AF-R-E350	0.70	.752 (1.31)	1.32 (2.31)	1.11 (1.94)
AS-1/3502	0.70	.801 (1.40)	.881 (1.54)	1.53 (2.67)
AS-1/POLYSULFONE	0.54	3.74 (6.55)	---	---
AS-1/ATQ	0.55	2.10 (3.68)	---	.170 (.298)
AS-1/3502 (90° ₂ /0° ₈ /90° ₂) _s	0.70	1.60 (2.80)	---	---
XAS/PEEK (APC-1)	0.55	8.00 (14.08)	---	8.00 (14.08)

The edge delamination coupon is very useful for screening resins. Data is shown below for a series of materials of different degrees of brittleness/ductility. The ratio of the delamination stress to the ultimate stress shows that the test can discriminate between matrix resins.

COMPOSITE EDGE DELAMINATION (+30₂ / -30₂ / 90₂)_s

MATERIAL	σ_{DEL} (KSI)	σ_{ULT} (KSI)
AF-R-E350/AS-1	30.0	35.5
V378A/T-300	21.0	24.0
ATQ/AS-4	9.0	25.0
PS/AS-1	NO DELAM	46.0
PEEK/XAS	NO DELAM	60.0

Important summary points are shown below.

- RESIN TENSILE/COMPOSITE TRANSVERSE TENSION ARE USEFUL STRENGTH TESTS
- INPLANE SHEAR LESS INFORMATIVE
- LAMINATE TEST FOR INTERROGATING IN-SITU TRANSVERSE STRENGTH SHOULD BE UTILIZED
- SHORT BEAM SHEAR TEST SHOULD BE DELETED
- COMPACT TENSION IS A VIABLE RESIN FRACTURE TEST. ATTENTION MUST BE GIVEN TO SPECIMEN GEOMETRY / MATERIALS CHARACTERISTICS
- DOUBLE CANTILEVER BEAM TEST IS VIABLE MODE I - INTERLAMINAR FRACTURE TEST. SHOULD BE RESTRICTED TO 0^0 LAMINATES AT THE PRESENT TIME. ATTENTION MUST BE GIVEN TO SPECIMEN GEOMETRY / MATERIALS CHARACTERISTICS.
- FREE-EDGE DELAMINATION TENSILE TEST IS A POTENTIAL USEFUL ALTERNATIVE TO THE DOUBLE CANTILEVER BEAM TEST. IS ALSO USEFUL AS AN INTERLAMINAR TENSILE STRENGTH TEST FOR MATRIX SCREENING.

Areas of particular interest for future work are summarized below.

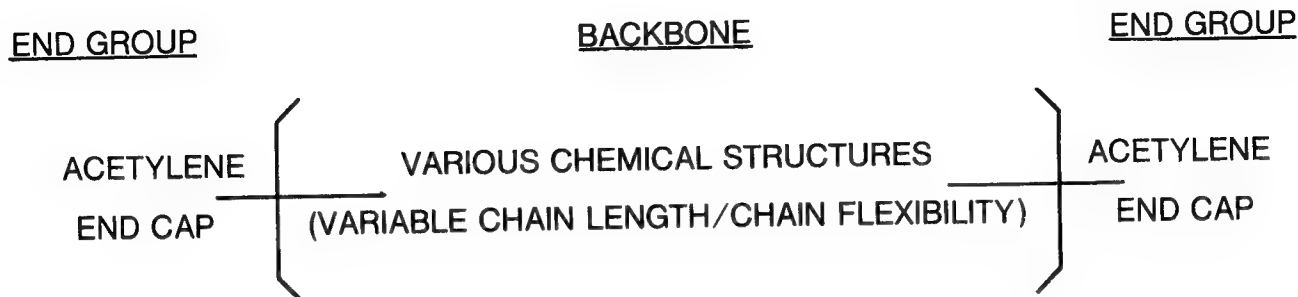
- RELATIONSHIP BETWEEN MATRIX STRESS-STRAIN RESPONSE AND UNIDIRECTIONAL TRANSVERSE TENSION AND INPLANE SHEAR
- MATRIX STRESS-STRAIN RESPONSE UNDER BIAXIAL LOADING
- BETTER UNDERSTANDING OF SHEAR AS A FAILURE MODE
- MECHANISM OF IN-SITU TRANSVERSE PLY FAILURE - RELATIONSHIP TO MATRIX PROPERTIES
- VIABLE MODE II AND MIXED MODE INTERLAMINAR FRACTURE TESTS

The next major discussion topic is Composite Materials Development at the ML. In so far as the investment of resources is concerned, the major areas of interest are those shown.

MAJOR AREAS OF INTEREST:

- 350-450⁰F USE/EPOXY-REPLACEMENT TYPE
 - ACETYLENE-TERMINATED (AT) RESINS
 - BISMALEIMIDE (BMI) RESINS
- THERMOPLASTICS
 - PEEK
 - REACTIVE PLASTICIZER CONCEPTS
- FAILURE RESISTANT COMPOSITE CONCEPTS
 - LAMINATE CONSTRUCTION

An important resin technology is that of acetylene terminated (AT) resins. A variety of acetylene end-capped resins are attainable by tailoring the backbone structure. A range of properties, including use temperature, are attainable. Backbone structures possible include imides, sulfone, bis-phenols, etc.



USE TEMPERATURE

LONG TERM

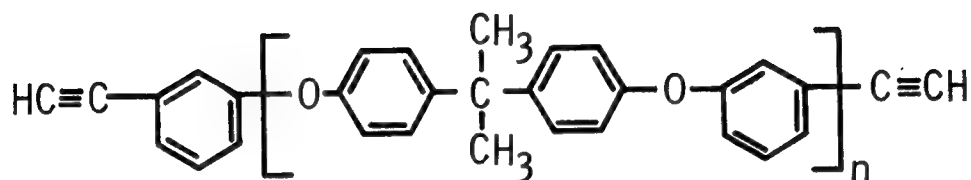
250 - 550°F

SHORT TERM

600 - 650°F

A specific example of an AT resin with high potential is the ATBA resin. It possess the outstanding attributes listed. In addition this resin possess excellent retention of hot/wet properties with low moisture uptake.

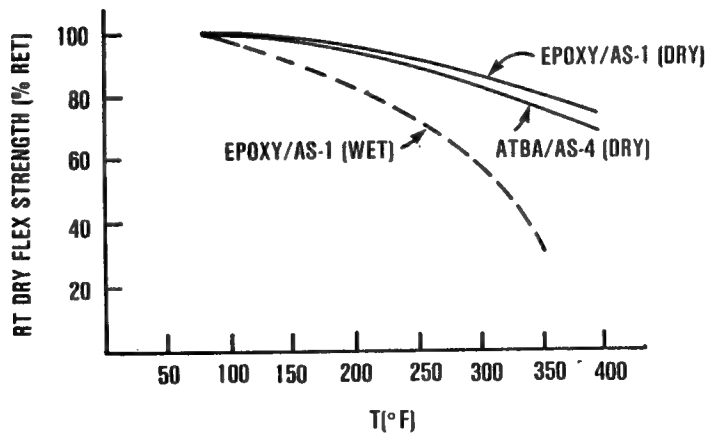
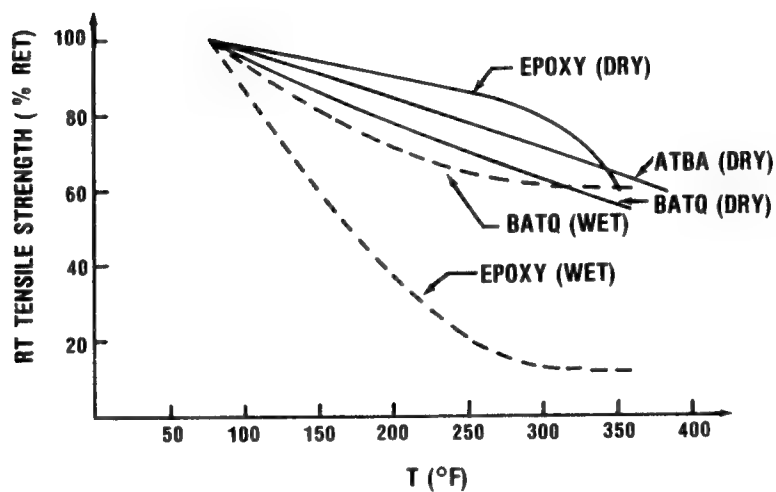
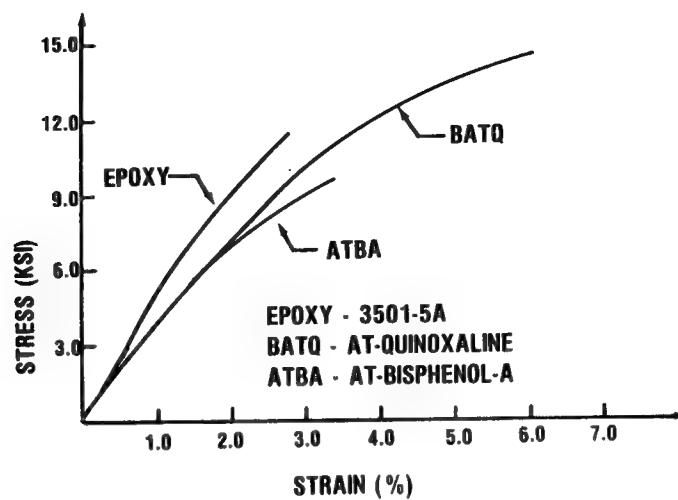
ACETYLENE-TERMINATED BISPHENOL A



HANDLING/PROCESSING CHARACTERISTICS:

- SINGLE COMPONENT
- LONG SHELF-LIFE /OUT-TIME
- EPOXY-LIKE PROCESSING
 - HOT-MELT
 - TACK /DRAPE
 - AUTOCLAVE CURE-400⁰F /100 PSI /NO BAG
 - POSTCURE - 482⁰F

The performance of AT resins, an AT-bisphenol A and an AT-quinoxaline, are shown versus performance of typical epoxy systems.



Another matrix resin technology of major importance is that of bismaleimides (BMI's). Areas to be addressed are shown in the chart.

AREAS OF ACTIVITY:

- IMPROVED PREPREG DEVELOPMENT (CONTRACT - FY 83)
 - PREPREG HANDLEABILITY
 - TOUGHNESS
- STRUCTURE - PROPERTY - PROCESSING RELATIONSHIPS
(IN-HOUSE - FY 83)
- PROCESSING SCIENCE/QUALITY ASSURANCE (CONTRACT - FY 85)

Another major materials technology area is that of thermoplastics. Thermoplastics offer significant advantages over contemporary materials in two key areas - damage tolerance and processing. Major areas of activity are summarized below.

AREAS OF ACTIVITY:

- TECHNOLOGY DEVELOPMENT
 - TP COMPOSITE TECHNOLOGY DEVELOPMENT (CONTRACT - FY 83)
 - IMPROVED TP COMPOSITE MATERIAL FORMS/PROCESS DEVELOPMENT (CONTRACT - FY 84)
- MANUFACTURING METHODS FOR TP COMPOSITES (CONTRACT - FY 85)
- PROCESSING SCIENCE/QUALITY ASSURANCE (CONTRACT - FY 85)
- MORPHOLOGY (IN-HOUSE - FY 83)
- REACTIVE PLASTICIZER CONCEPTS DEVELOPMENT (IN-HOUSE - FY 83)

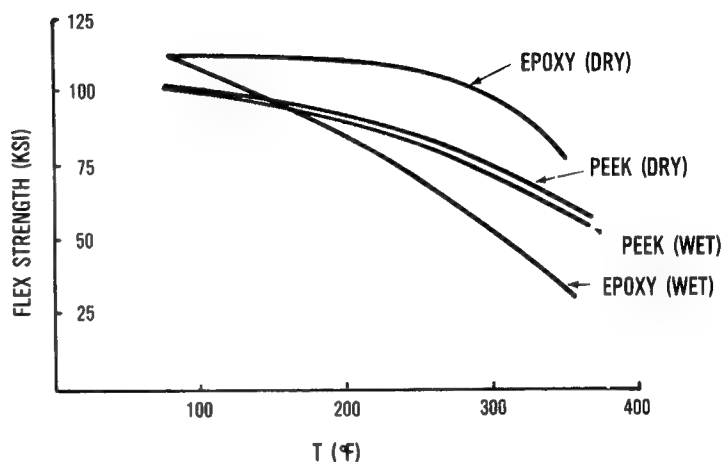
A considerable amount of work has been done on a semi-crystalline thermoplastic for advanced composites - polyetheretherketone (PEEK) from ICI. The results shown below provide the impetus to fully exploit the benefits thermoplastics have to offer.

POLYETHERETHERKETONE (PEEK)

CHEMICAL RESISTANCE*

CHEMICAL	t	EFFECT
MIL-H-56066	1 WK	NONE
SKYDROL	1 WK	NONE
JP-4	1 WK	NONE
DICHLORO METHANE	1 WK	NONE
MEK	1 WK	NONE
ACETONE	1 WK	NONE
T-5351 AL ³	1 WK	NONE

*STRESSED 1000 PSI



- IMPROVED TOUGHNESS (G_{1C} 11.4 VS 1.4 LBS/IN)
- INDEFINITE RT SHELF LIFE
- REDUCED QA COSTS
- REDUCED SCRAPPAGE
- LOWER COST FABRICATION

EFFECT OF IMPACT DAMAGE AND OPEN HOLES ON THE
COMPRESSION STRENGTH OF TOUGH RESIN/HIGH
STRAIN FIBER LAMINATES

Jerry G. Williams
NASA Langley Research Center
Hampton, Virginia

INTRODUCTION

Past experience has shown that structural damage and design-based inclusions such as cutouts can significantly reduce the strength of graphite-epoxy laminates (ref. 1). One composite mechanics research activity at the Langley Research Center is to assess and improve the performance of composite structures damaged by impact or containing local discontinuities such as cutouts. Reductions in strength are common to both tension and compression loaded laminates; however, the problem associated with compression performance has been found to be the most elusive to solve. Compression failure involves both shear crippling and delamination modes. Small-scale coupon tests have not yet been developed to adequately predict damaged-laminate compression performance reductions. Two plate specimen configurations, however, have been developed by NASA (ref. 2) to help define the severity of the compression strength reduction problem and to assess the relative merit of proposed toughened material systems. These two test configurations, one involving impact damage and the other open hole specimens, are shown in figure 1. The test technique for impact specimens involves damaging the plate at selected energies, measuring the size of damage by ultrasonic C-scan techniques and measuring the residual strength in a compression load test. Open-hole specimen compression tests are conducted for several different hole diameters and the failure strain and load and mode of failure recorded. The plate specimen used in these tests is designed with length, width, thickness and laminate stiffness to ensure that overall plate buckling is not responsible for initiating failure.

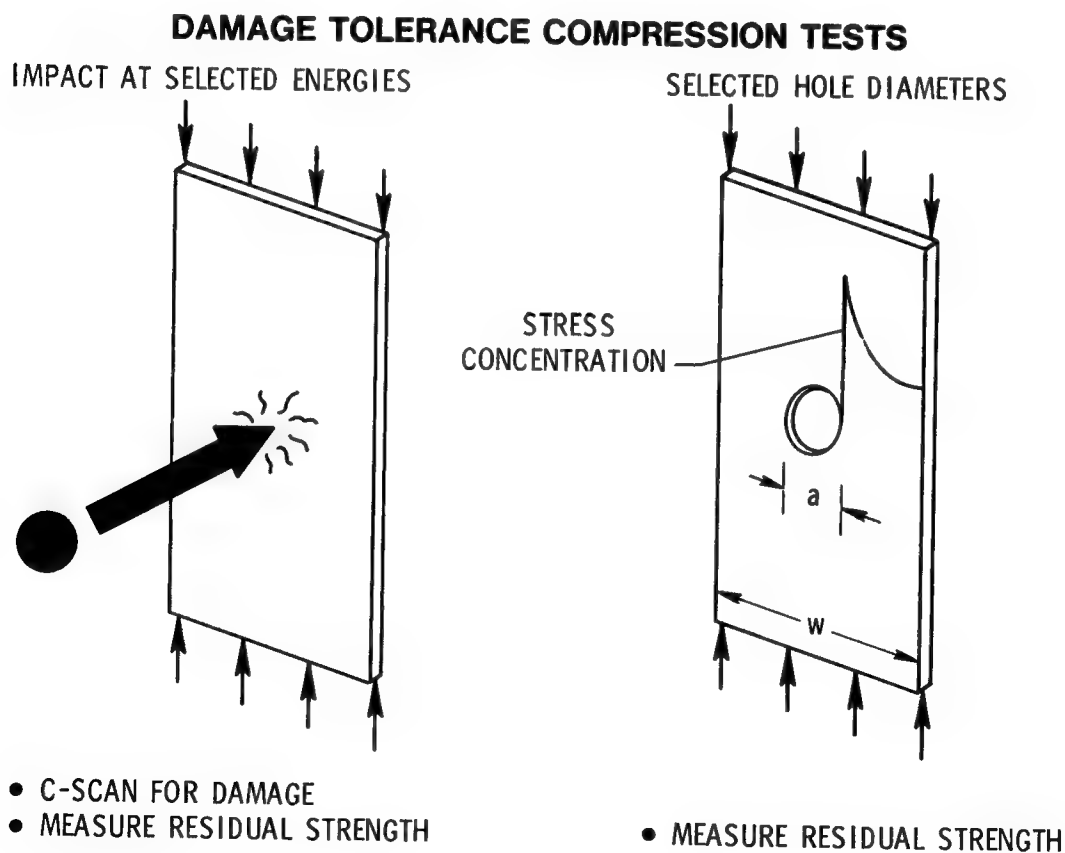


Figure 1

TEST SPECIMENS AND FIXTURE

In the current investigation, several new graphite-epoxy material systems proposed for improved damage tolerance and listed in figure 2 were studied. Material parameters included both tough resin formulations and high strain fibers. Material suppliers included Narmco (T300 fiber and 5208 resin), American Cyanamid (BP907 resin), and Hercules (AS4 and AS6 fibers and 3502, 2220-1, and 2220-3 resin). Ultimate tensile strains for these fibers are approximately: 1.2% - T300, 1.4% - AS4 and 1.8% - AS6. The T300/5208 material is used as a baseline and T300/BP907 was identified in past studies as exhibiting improved damage tolerance characteristics (ref. 3). All tests were conducted at room temperature and therefore do not address the reduction in strength of resin materials such as BP907 caused by moisture and elevated temperatures. Quasi-isotropic laminate specimens approximately 0.25 inches thick and 10 inches long by 5 inches wide were tested in the fixture shown in figure 2. The fixture imposed nearly clamped boundary conditions on the loaded ends and simple support boundary conditions on the lateral edges. Two sets of strain gages mounted back-to-back were used to measure the axial strain.

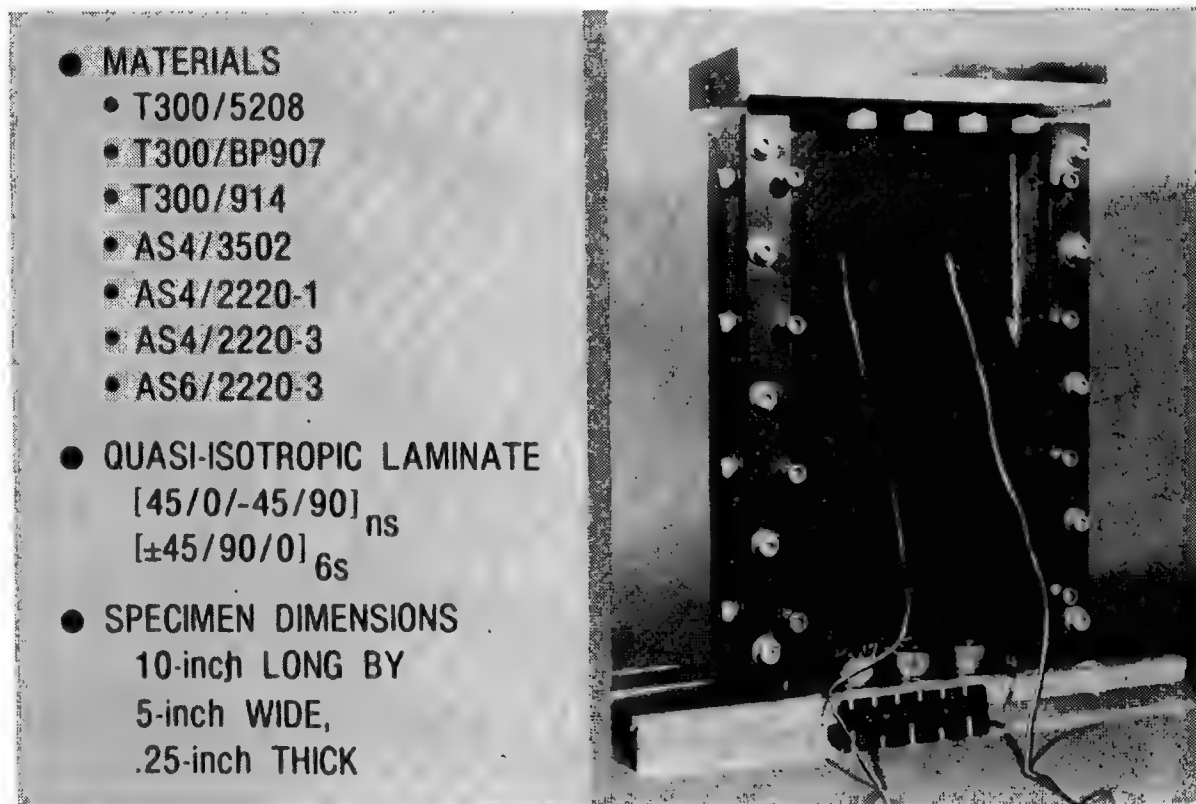


Figure 2

LAMINATE DAMAGE FOLLOWING IMPACT

An illustration of the influence the resin material has on the size and extent of damage in a graphite-epoxy laminate resulting from projectile impact is shown in figure 3. The damage following impact by a 1/2-inch diameter aluminum sphere at approximately 13 ft-lb of energy is shown on the top row for a brittle behavior resin and on the bottom row for a toughened resin system. The orthotropic laminate is approximately 0.25 inch thick. Less damage is observed for the tough resin material by visual observation of surface damage, by ultrasonic C-scan inspection and by microscopic inspection of a cross-section through the impact damage zone. This demonstration shows, therefore, that it is possible to tailor the matrix material properties to reduce the size of damage following projectile impact.

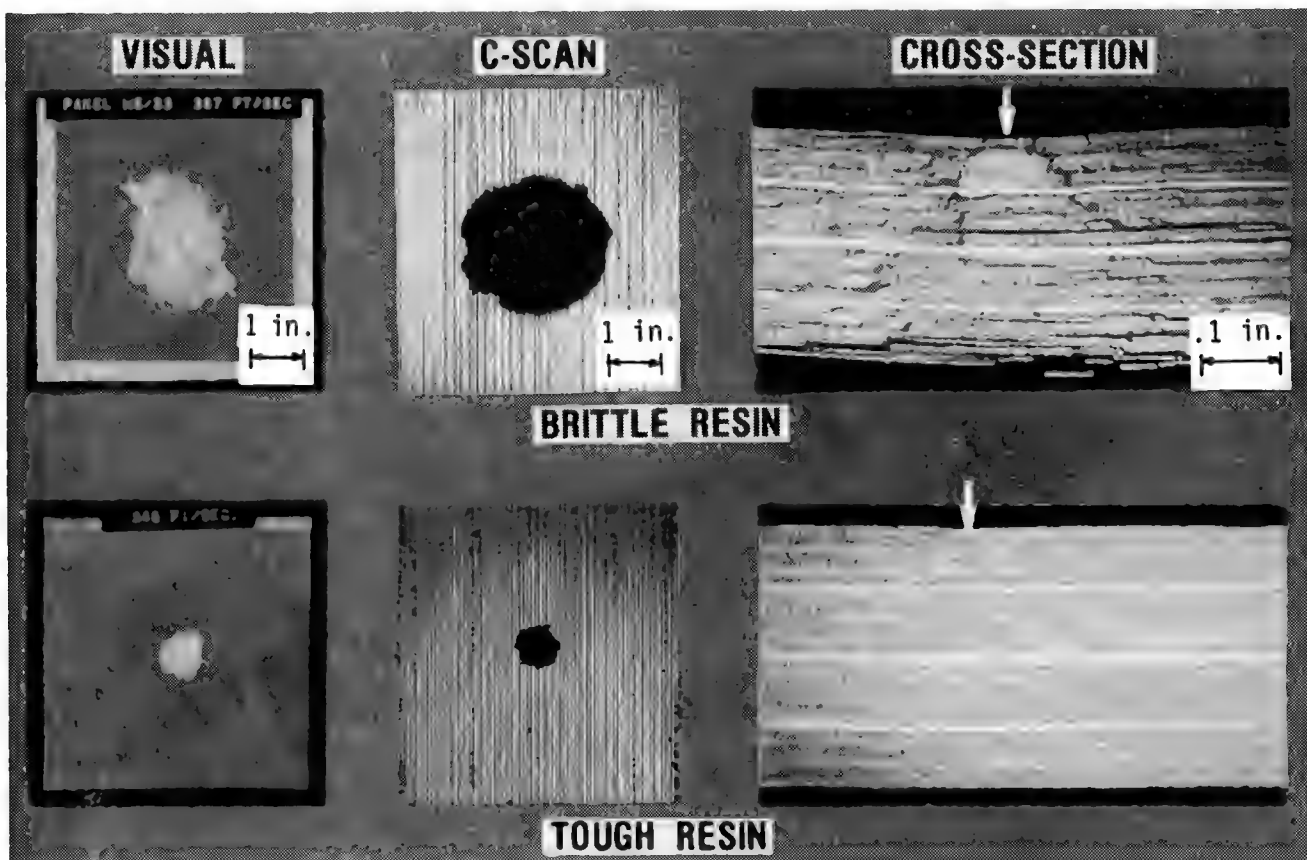


Figure 3

EFFECT OF IMPACT ENERGY ON DAMAGE SIZE

A plot of the damage area measured using ultrasonic C-scan signatures for several material systems is presented in figure 4 as a function of the projectile impact velocity and energy. The threshold energy at which damage can first be detected varies for the materials studied; however, all are in the range of three to five ft-lb. The largest damage size was measured for the T300/914 material. One variable for this material that differed from the other materials was that a thicker prepreg tape was used, resulting in approximately half as many plies for the 0.25-inch thick laminate. The effect of lamina thickness is not established. The results of several of the materials fall within a relatively narrow band for the energies studied. There appears to be a divergence of the results, however, at the upper energy levels, a trend which merits further study.

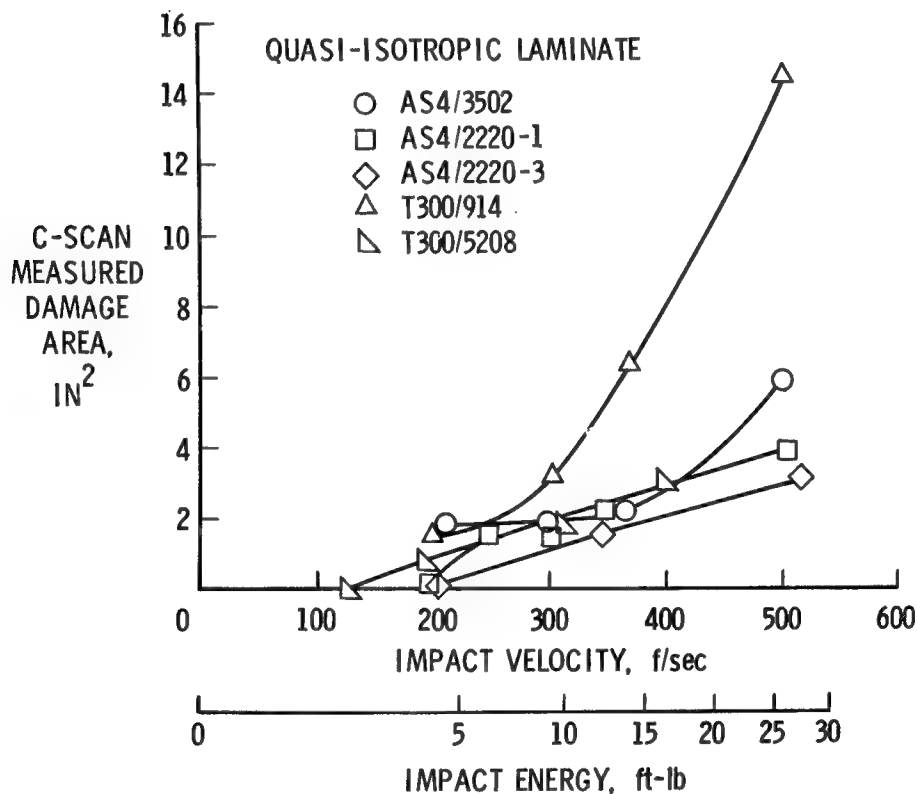


Figure 4

IMPACT INITIATED COMPRESSION FAILURE MODES

Experimental studies have shown that the failure of damaged composite laminates loaded in compression involves two primary failure mechanisms: delamination and transverse shear (ref. 4). These two failure mechanisms are illustrated in figure 5 for a brittle resin laminate and for a damage-tolerant tough resin laminate. The photographs on the right of the figure show cross-sections of failure regions which are typical for these two classes of material. The brittle resin laminate shows considerable evidence of delamination whereas the tough resin laminate cross-section is characterized by a through-the-thickness shear band which is approximately 0.07 inch wide. Closer inspection reveals, however, that both specimens actually exhibit both delamination and transverse shear failure mechanisms. The transverse shear failure mode for the brittle resin laminate develops in only a few plies before delamination occurs, while the transverse shear mode for tough resin laminates is several plies thick before it is interrupted by delamination caused by wedges of failed material prying apart the plies. Tough resin formulations improve damage tolerance by suppressing the delamination mode of failure, permitting failure to occur at the next higher energy mode involving transverse shear.

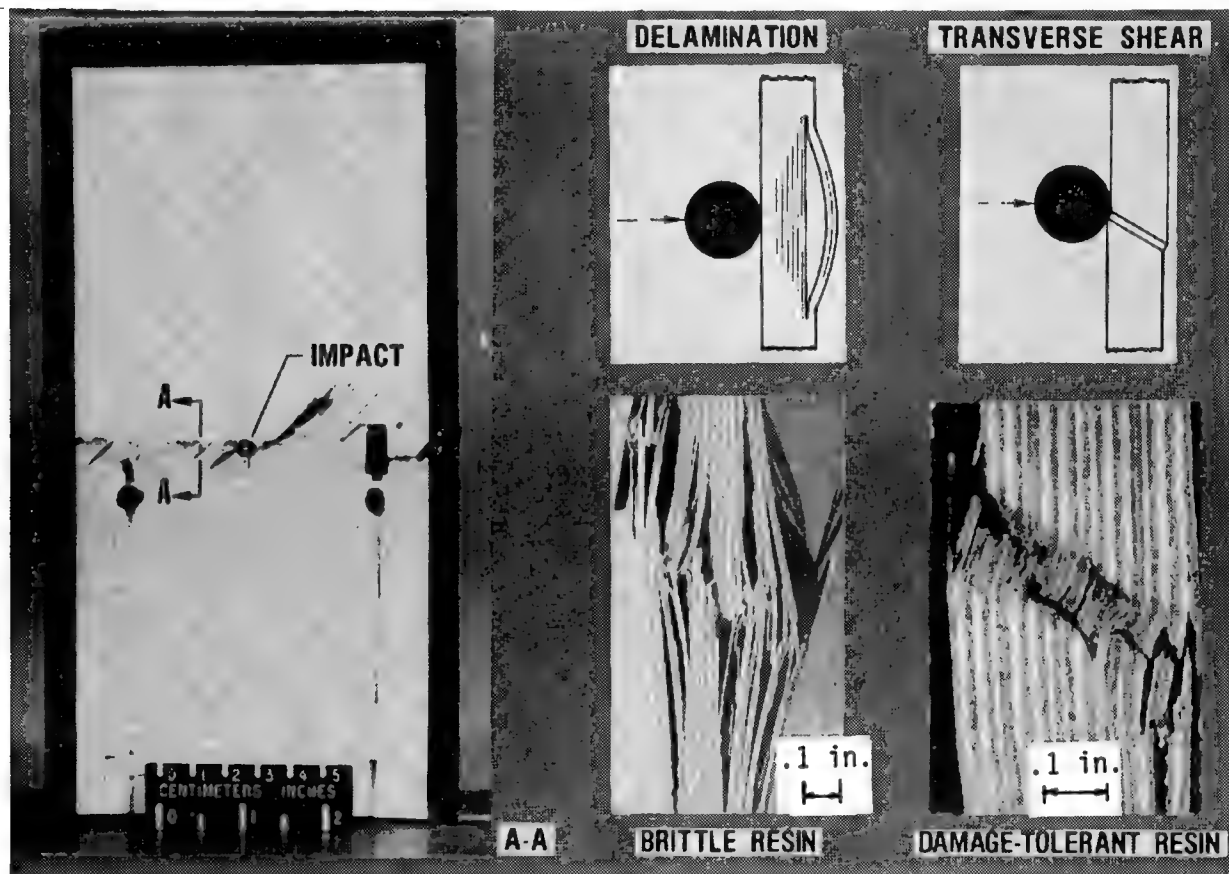


Figure 5

PROPAGATION OF IMPACT INDUCED DELAMINATION

The sequence of events which occurs when a brittle resin is damaged by impact and subsequently loaded in compression to failure is shown in figure 6. The moire fringe photographs show the local out-of-plane deformations of the laminate in the impact damaged region. Photographs presented left to right correspond to increasing load up to ultimate at which damage propagates from the center of the panel to the two lateral edges. Sublaminates caused by impact-induced delaminations have reduced bending stiffnesses compared to the undamaged laminate and, if sufficiently large, buckle at significantly lower loads than the overall plate buckles. These local buckles represented by the moire fringe contours cause high stresses in the resin at the delamination boundary. When the buckle is sufficiently advanced, these stresses cause fracture of the resin and the damage propagates.

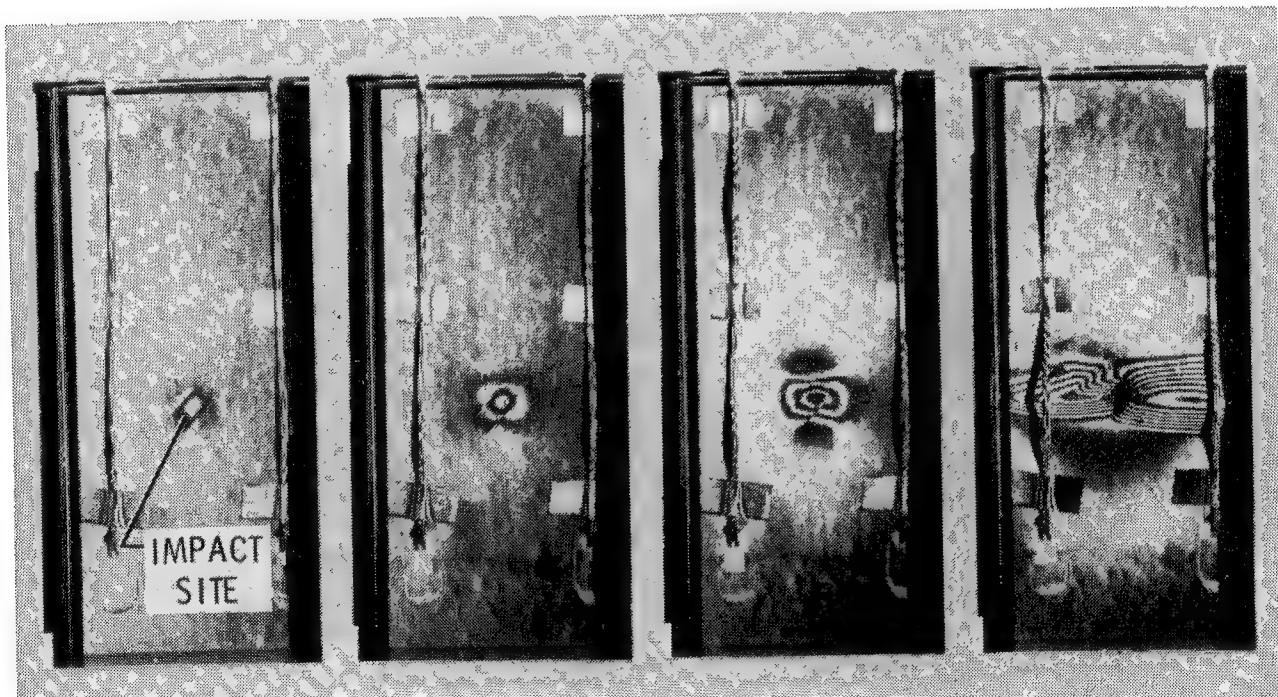


Figure 6

SHEAR CRIPPLING FAILURE MODE

The shear crippling mode of failure occurs not only at the macroscopic scale as illustrated in figure 5 but also on the microscopic scale involving individual graphite fibers as illustrated in figure 7. This tough resin orthotropic laminate was damaged by impact and loaded until the damage began to propagate across the panel. The damage propagation arrested; the load was removed and a cross-section was taken through the damaged region. Shown on the right of figure 7 is a photomicrograph of four of the interior plies [$45/0_2/-45$] of the 48-ply laminate. Graphite fibers in the zero degree plies (aligned coincident with the applied load) failed by shear crippling while fibers oriented at 45 degrees were undamaged. The model proposed to explain this phenomenon is that the strain concentration in zero-degree plies located in the damage zone and the reduced support to the fibers due to matrix fracture cause the graphite fibers to microbuckle. Fracture of the fiber occurs when the axial plus postbuckling bending strains reach a critical value.

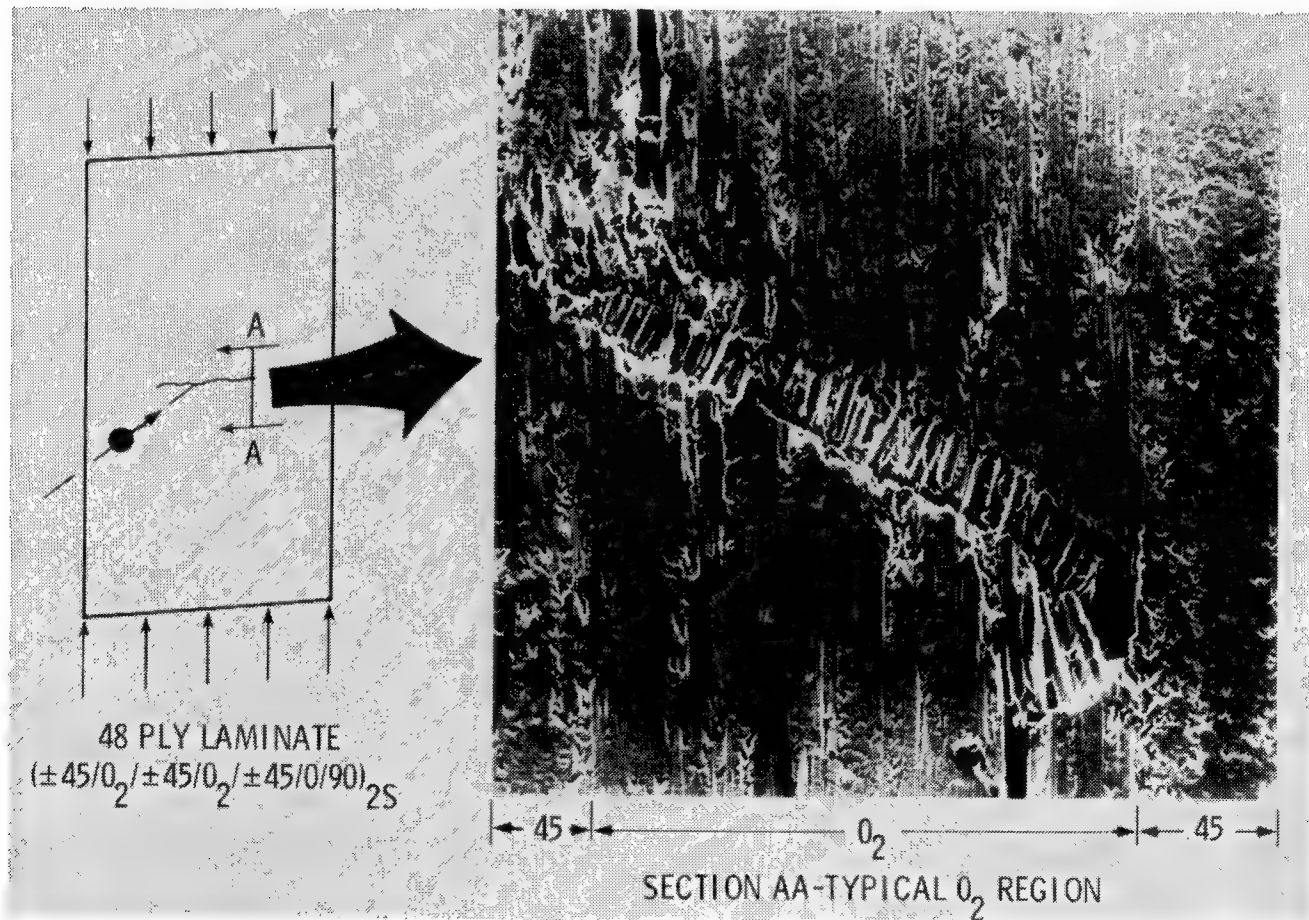


Figure 7

FAILURE OF OPEN-HOLE SPECIMEN LOADED IN COMPRESSION

A series of photographs showing the initiation and propagation of delamination for an open hole specimen loaded in compression is shown in figure 8. At 95.2% of the ultimate load, moire fringe photographs show no evidence of delamination around the hole boundary. At 95.4%, local fringes appear and grow in size with increasing load as can be seen comparing the photographs at 95.9% and 98.1% of ultimate. Ultimate failure occurs when damage propagates completely across the reduced section of the plate. One might conclude based on this evidence that the initiating failure mode for open hole specimens is delamination; however, as will be shown in the next figure, microscopic shear crippling occurs in the vicinity of the hole boundary in advance of delamination.

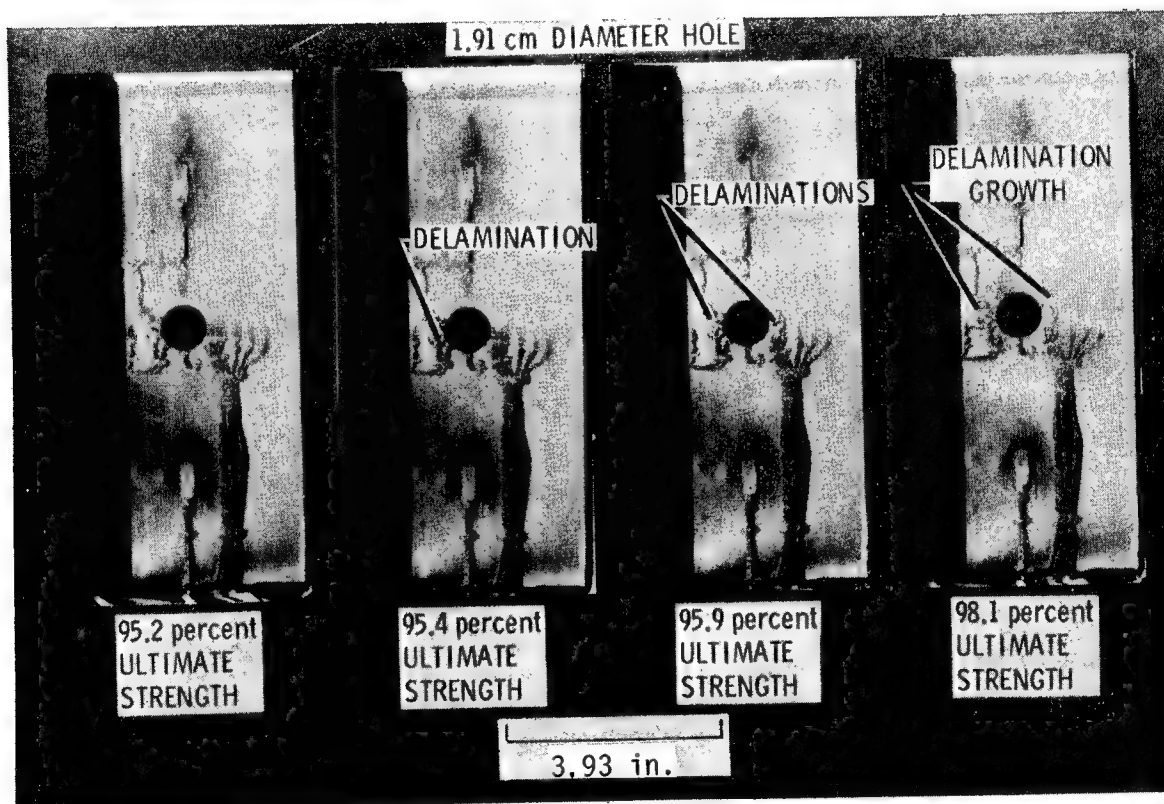


Figure 8

SHEAR CRIPPLING INITIATES OPEN-HOLE SPECIMEN FAILURE

Another specimen similar to the one shown in figure 8 was loaded to a load level just prior to the initiation of delamination (approximately 92% of ultimate) and unloaded. A small block of material adjacent to the hole boundary was cut from the specimen and surface material sanded away to expose an interior 0-degree layer. Scanning electron photomicrographs of this region are shown on the right of figure 9. Damage is the same failure of individual graphite fibers by shear crippling which was shown earlier in figure 7 for the compression failure of impact-damaged laminates. The higher magnification photomicrograph shows the failed fiber length to diameter ratio to be approximately four. The proposed failure model is the same as proposed earlier, i.e., graphite fibers microbuckle in the high strain concentration region adjacent to the hole and fail in the post-buckled state.

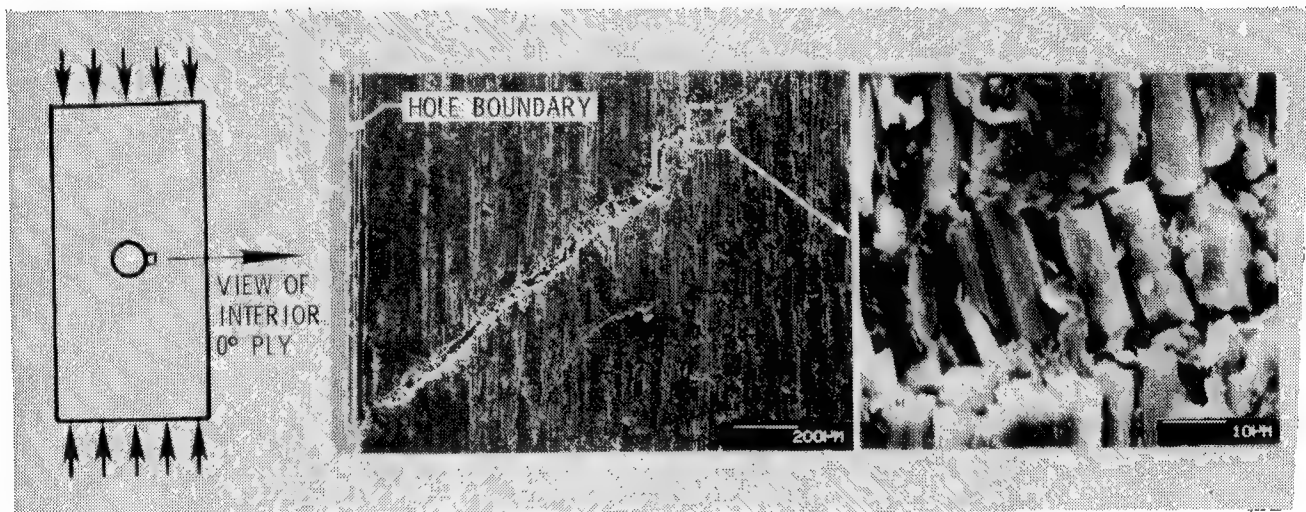


Figure 9

IMPACT-DAMAGE FAILURE THRESHOLD CURVE

The effect of impact damage on the failure strain of a compression loaded graphite-epoxy laminate constructed with a brittle-behavior resin material is presented in figure 10 (ref. 4). Filled circular symbols represent specimens which failed catastrophically when loaded to the indicated strain level and impacted by a 1/2-inch diameter aluminum sphere at the indicated velocities. Open circular symbols represent specimens which may have been damaged by impact, but the damage was contained with little loss of load. A narrow band separates open and closed symbols and a failure threshold curve has been drawn through the band, thus separating the graph into two zones. Impact conditions above and to the right of the curve result in specimen failure while the laminate survived the less severe conditions below and to the left of the curve. A severe reduction in strength occurs for impacts in the 165 to 250 ft/sec range and at 330 ft/sec the failure threshold strain is reduced to approximately 0.0028.

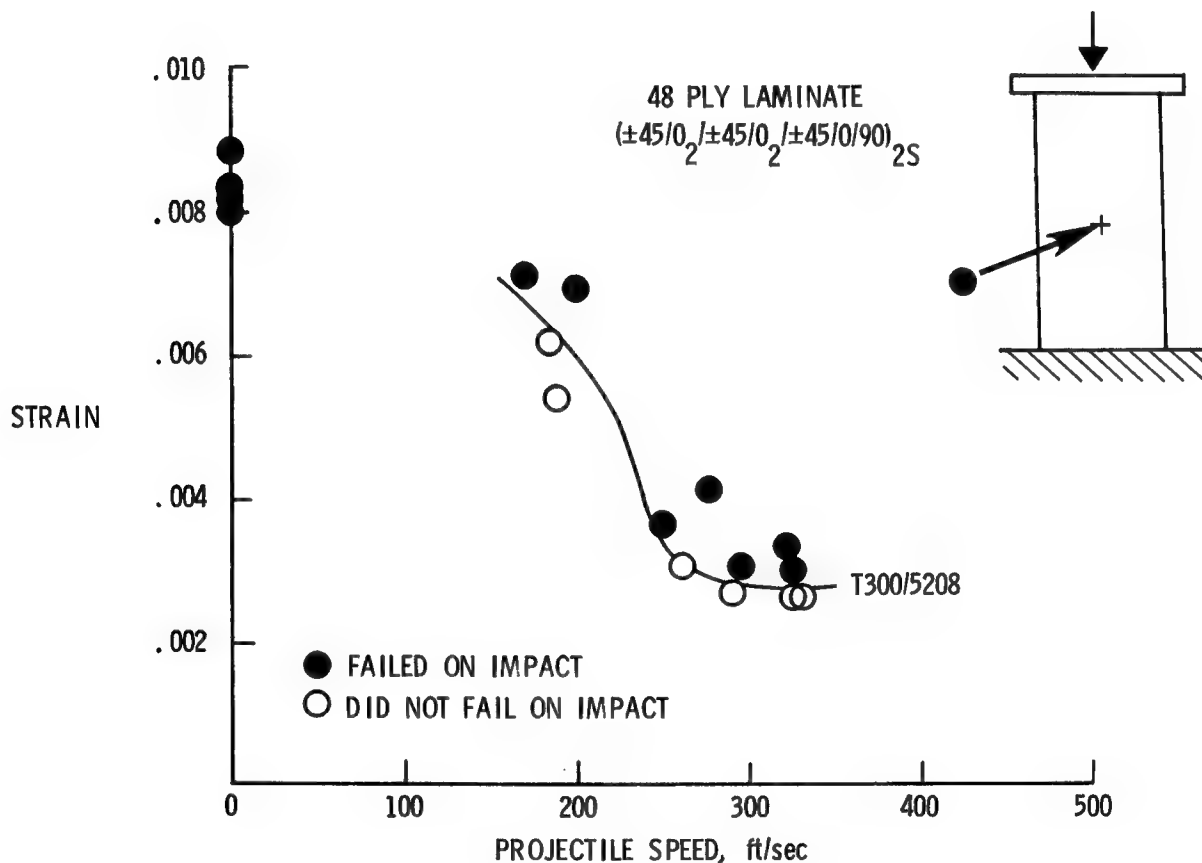


Figure 10

TOUGH RESIN IMPROVES LAMINATE DAMAGE TOLERANCE

Failure threshold curves for a 48-ply orthotropic graphite-epoxy laminate constructed using two different resin systems are shown in figure 11 (ref. 4). For the test conditions studied, the tough BP907 resin system shows substantial improvement relative to the brittle 5208 resin system. Similar improvements have also been observed for a 5208 resin laminate when it was reinforced by through-the-thickness stitching. The explanation for this improvement is that both the tough resin system and stitching suppress the delamination mode of failure. The delamination mode of failure has been studied using fracture toughness tests such as the double cantilever beam. Improved compression strength after impact has been correlated with fracture toughness measurements for material systems with widely varying fracture toughness properties such as the materials compared in figure 11. As shown in figure 7, however, shear crippling is also involved in the failure of impact-damaged laminates and fracture toughness tests do not address this mode of failure.

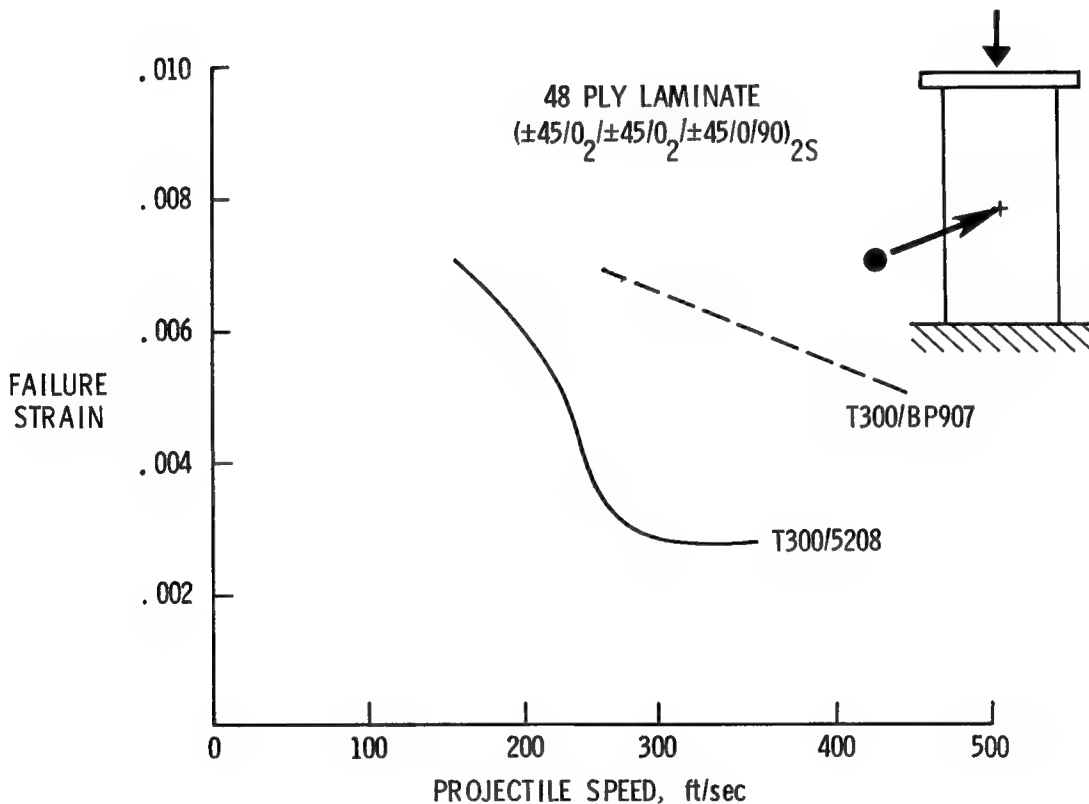


Figure 11

EFFECT OF SIZE OF IMPACT DAMAGE ON FAILURE STRAIN

A need exists for a comparison method which the composite structure designer can use to assess the effect of various impact conditions and material systems on structural strength. Trends for test data in which increasing strength losses were observed to occur with increasing impact damage size suggested the parameters used in the graph presented in figure 12. The failure strain for several different material systems constructed in a quasi-isotropic laminate is plotted as a function of the width of damage resulting from impact. The damage width was determined from ultrasonic C-scan photographs and is normalized by the specimen width (5 inches). For these laminates and impact conditions, the size of damage appears to be a parameter that reduces the test data for all four materials to a common curve. A two-parameter curve asymptotic to $a/w = .24$ has been drawn through the data. A large reduction in strength occurs around $a/w = .24$ and the failure strain for $a/w < .24$ is governed by conditions other than impact such as plate buckling. Additional study is required to assess the generalization of this data to other impact conditions and laminates.

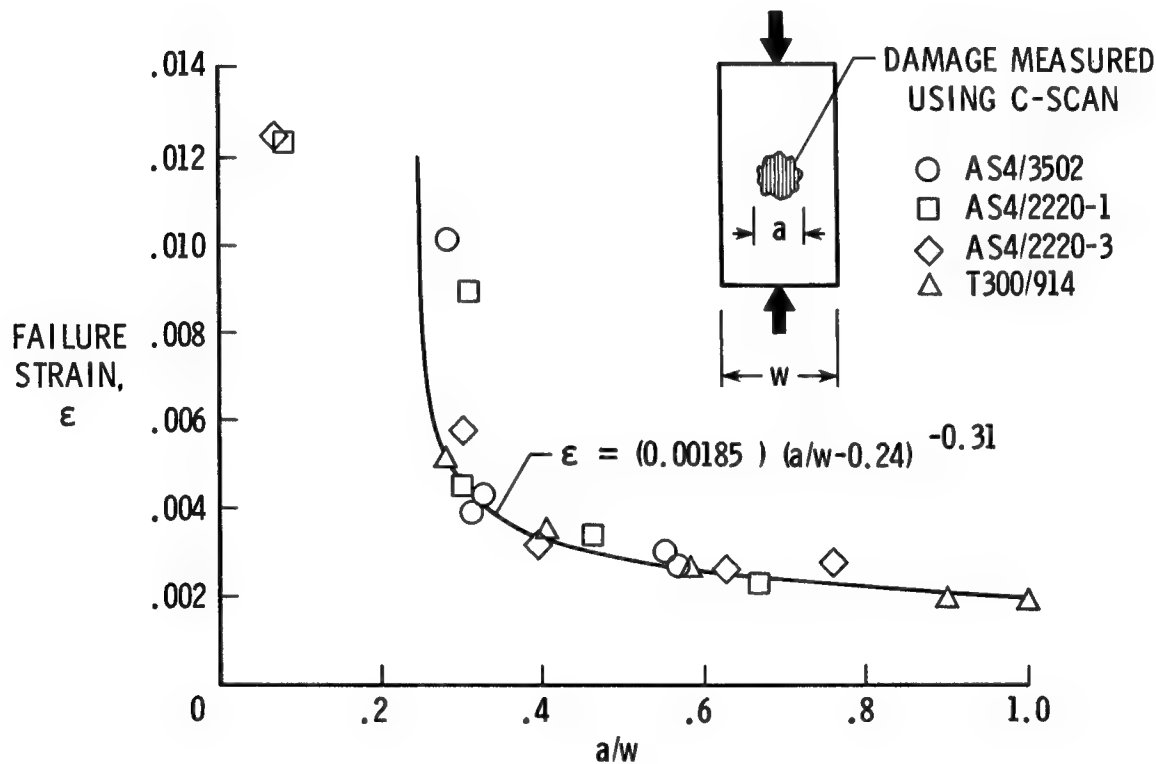


Figure 12

OPEN-HOLE COMPRESSION SPECIMENS

A series of 5-inch-wide and 10-inch-long quasi-isotropic specimens with selected centrally located holes were tested for several different material systems. Photographs of some of these specimens are presented in figure 13.

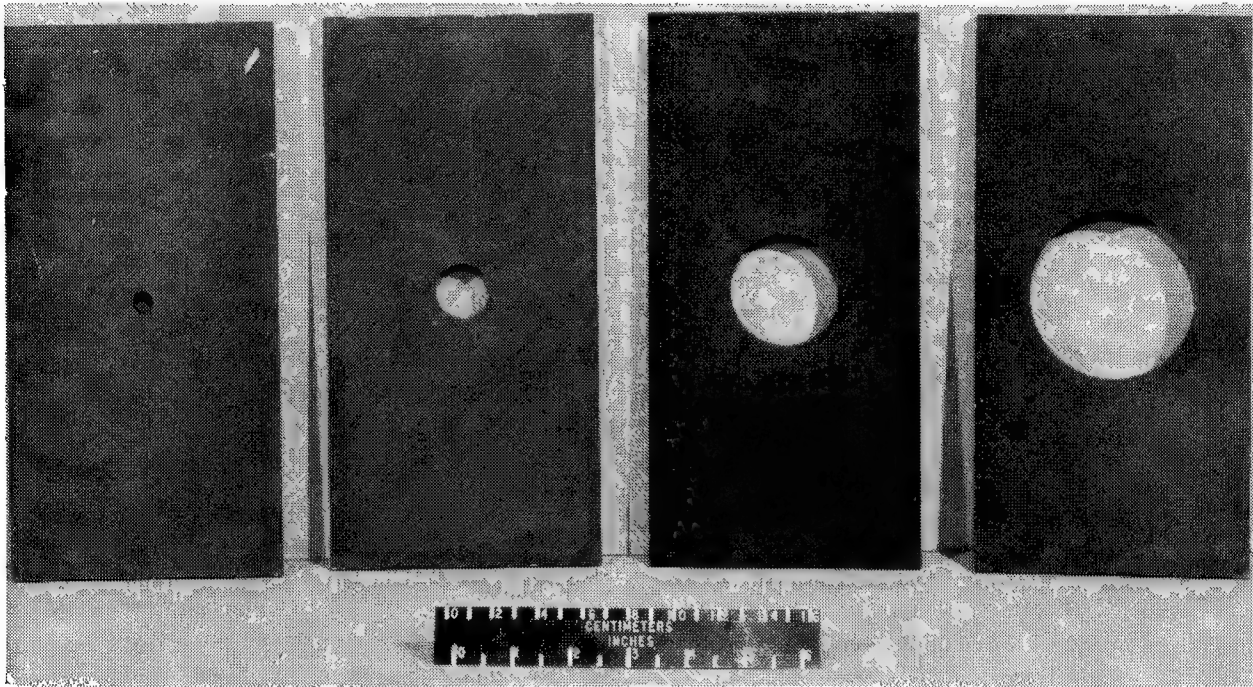


Figure 13

STRESS-STRAIN RESPONSE FOR OPEN-HOLE SPECIMENS

The stress-strain response up to failure for AS4/2220-3 quasi-isotropic 5-inch-wide specimens with selected a/w hole sizes is presented in figure 14. Strain data is taken from strain gages located near one end of the specimen. For large holes, the stress-strain response deviates from the no-hole ($a/w = 0$) curve. For purposes of data comparison, the failure strain for open-hole specimens reported in subsequent figures is the strain which the no-hole specimen carried at the same stress that the open-hole specimens carried at failure.

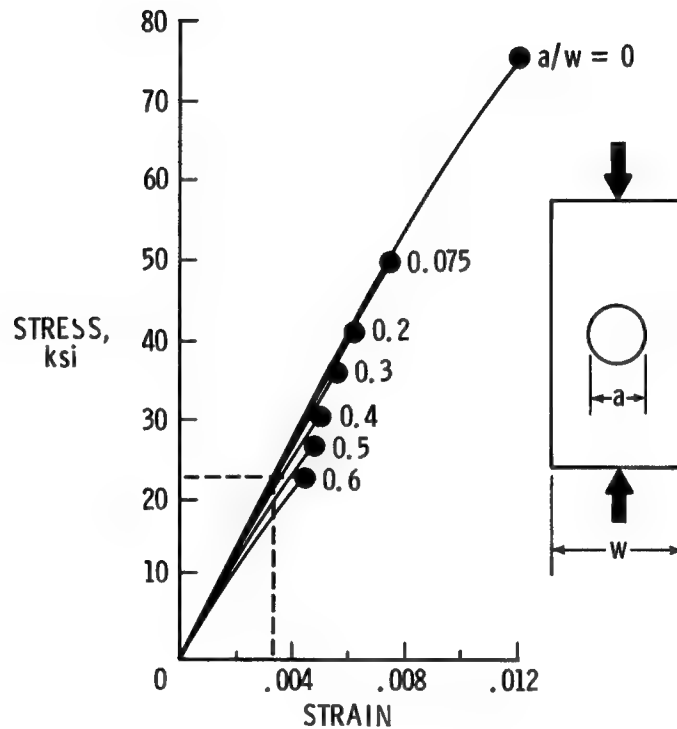


Figure 14

EFFECT OF CIRCULAR HOLES ON COMPRESSION STRENGTH

A comparison of the reduction in strength for a brittle (T300/5208) and tough (T300/BP907) resin system laminate is presented in figure 15 as a function of the hole diameter "a" normalized by the specimen width "w" (ref. 4). The curve faired through the data is a failure prediction base on the point-stress failure criterion proposed by Whitney and Nuismer (ref. 5). The curve is bounded on the top by a net-area notch-insensitive curve and on the bottom by a notch-sensitive curve in which failure is assumed to occur when the stress at the hole edge reaches the critical value for an unnotched specimen. The different resin formulations appear to have had no effect on the failure strain for these two orthotropic laminates. The explanation for this apparent paradox in which the tough resin improved the strength of impact damaged specimens (fig. 11) but not open-hole specimens involves understanding the governing failure mechanisms. For impact damage, tough resins improved the performance by suppressing the delamination mode of failure. For open hole specimens, as shown in figure 9, the failure initiation mechanism involves fiber microbuckling and shear crippling of highly stressed material adjacent to the hole. Fiber microbuckling is governed by the stiffness properties of the matrix and fiber and by other factors such as the integrity of the matrix-to-fiber bond. Similar strength reductions for these two material systems with holes occur since the same fiber was used in both laminates and because the two resin systems have similar initial elastic modulus properties.

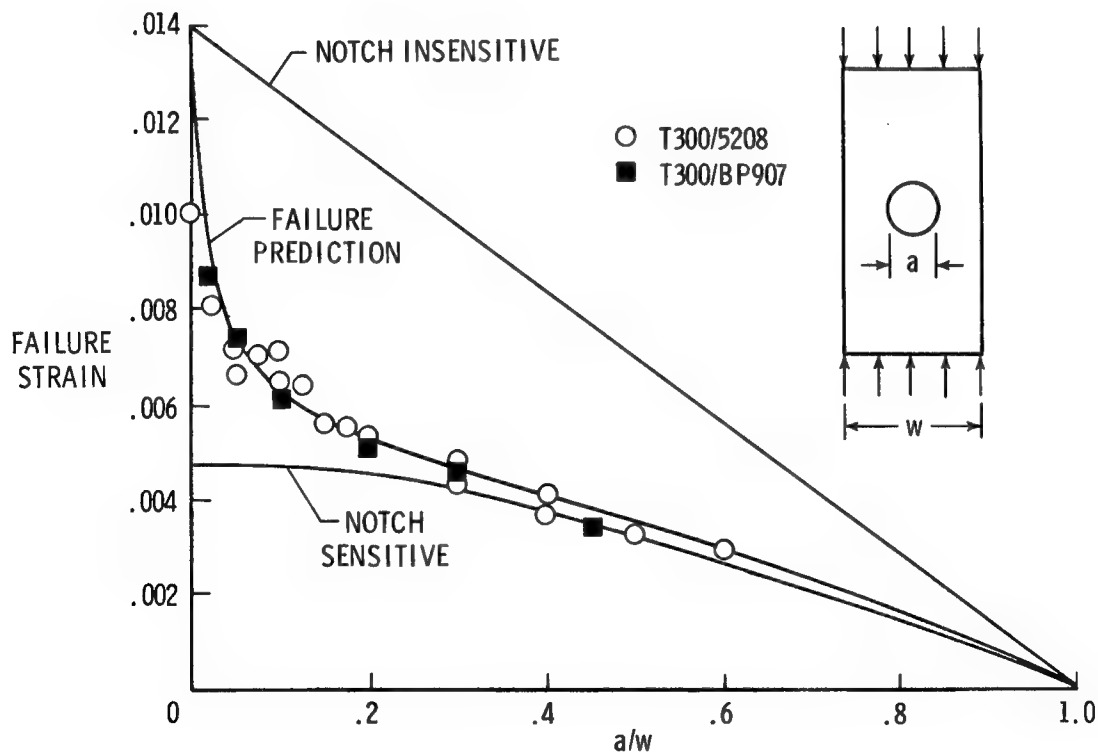


Figure 15

EFFECT OF HIGH STRAIN FIBER ON FAILURE STRAIN OF OPEN-HOLE SPECIMENS

The influence of hole size " a/w " on the failure strain of several quasi-isotropic laminates constructed with selected resin systems and two graphite fiber materials is presented in figure 16. The two theoretical failure curves are point stress failure predictions with the indicated characteristic parameters. The lower theoretical curve is taken from reference 6 and represents the best fit to date for T300/5208 graphite-epoxy. The data appear to group according to fiber reinforcement type with the AS4 fiber laminates exhibiting higher failure strain than T300 fiber laminates. The ultimate tension strains for T300 and AS4 are approximately 0.012 and 0.015, respectively. Recall from figure 15 that laminates with two different resin systems and the same fiber had identical strengths. If, as hypothesized, high bending strains in a buckled fiber initiate local failure, then one might expect a higher tension strain fiber to exhibit a higher laminate strength as was observed in this series of tests. Several material and structural properties govern fiber microbuckling and failure including the fiber extensional and bending stiffness and strength and the stiffness and strength properties of the matrix. Theoretically, a high shear modulus property of the resin should also increase the strain at which microbuckling would occur. All of the factors which affect microbuckling and compression strength need to be better understood in order to better tailor material and laminate properties for optimum performance.

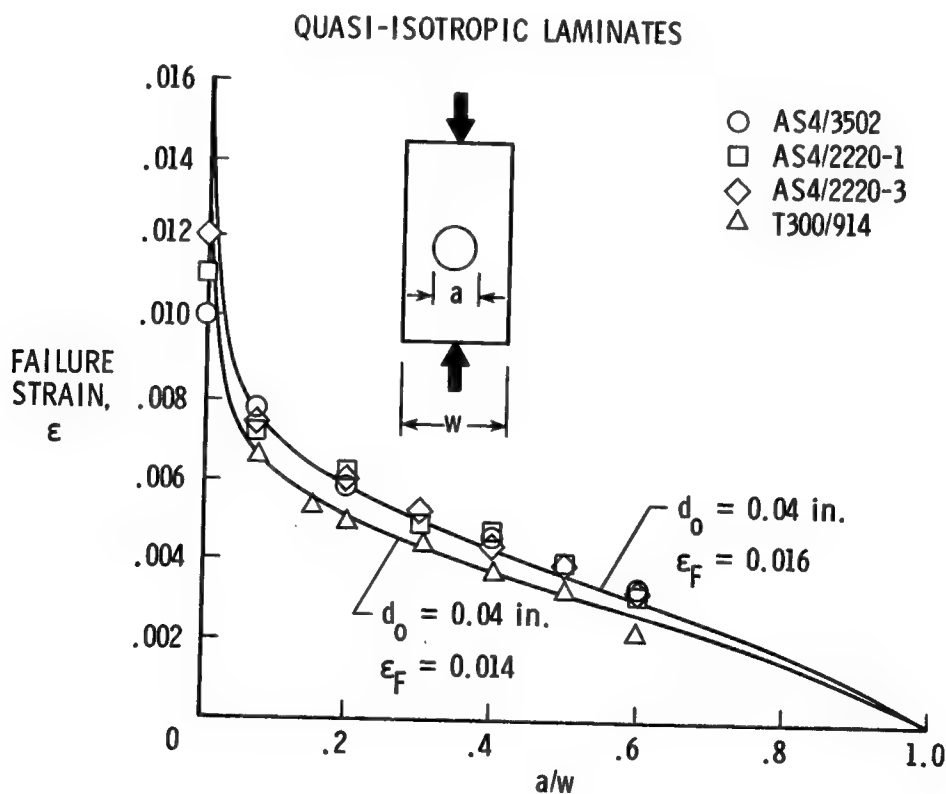


Figure 16

OPEN-HOLE VERSUS IMPACT STRENGTH REDUCTION

Designers of composite structures must address the effects of both holes and impact on design allowables and are interested in the range of conditions in which each factor governs structural performance. A comparison is made in figure 17 of the effect of these two types of local discontinuities. The open hole curves are taken from figure 16 for AS4 and T300 fiber laminates and the impact curve is taken from figure 12 in which the damage size was determined from C-scan measurements. The open hole causes the greatest reduction in strength for $a/w < .3$ ($w = 5$ inches) and impact damage causes the greatest reduction for $a/w > .3$. Additional curves need to be defined for other plate widths and laminates to establish the generality for design purposes of these findings.

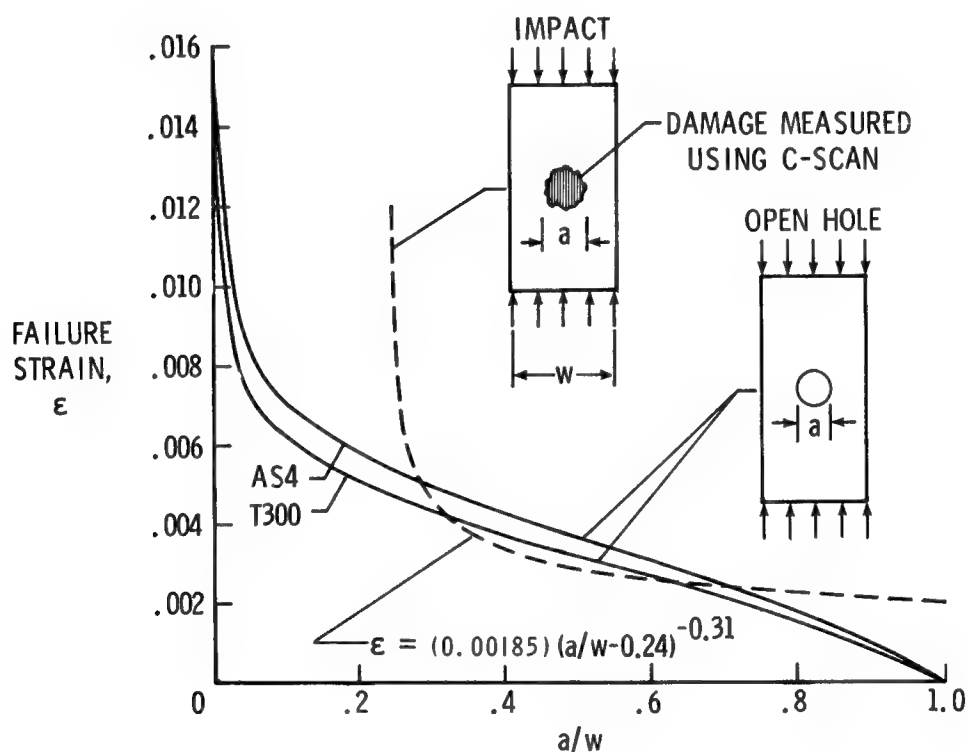


Figure 17

CONCLUSIONS

1. Tough resin system can reduce the size of the damage zone caused by impact.
2. Delamination and shear crippling are two fundamental mechanisms involved in the compression failure of graphite-epoxy laminates.
3. Tough resins (compared to brittle resins) can improve the compression strength of impact-damaged laminates by suppressing the delamination mode of failure.
4. Tough resins do not provide similar improvement in the performance of laminates with open holes where shear crippling is the dominant failure mechanism.
5. Several graphite-epoxy material systems were found to exhibit common strength reductions for equal size impact damage.
6. Higher strain fiber provided increase in failure strain of open hole specimens.

REFERENCES

1. Starnes, James H., Jr.; Rhodes, Marvin D.; and Williams, Jerry G.: Effect of Impact Damage and Holes on the Compressive Strength of a Graphite-Epoxy Laminate. ASTM STP 696, pp. 145-171, 1979.
2. Standard Tests for Toughening Resin Composites. NASA RP-1092, July 1983.
3. Williams, Jerry G.; and Rhodes, Marvin D.: Effect of Resin on the Impact-Damage Tolerance of Graphite-Epoxy Laminates. ASTM STP 787, pp. 450-480, 1983.
4. Starnes, James H., Jr.; and Williams, Jerry G.: Failure Characteristics of Graphite-Epoxy Structural Components Loaded in Compression. Mechanics of Composite Materials - Recent Advances. Hashin and Herakovich, Editors, Pergamon Press, 1983.
5. Whitney, J. M.; and Nuismer, R. J.: Stress Fracture Criteria for Laminated Composites Containing Stress Concentrations. Journal of Composite Materials, Vol. 8, July 1974, pp. 253-265.
6. Rhodes, Marvin D.; Mikulas, Martin M., Jr.; and McGowan, Paul E.: Effect of Orthotropic Properties and Panel Width on the Compression Strength of Graphite-Epoxy Laminates With Holes. AIAA Paper 82-0749 presented at AIAA/ASME/ASCE/AHS 23rd Structures, Structural Dynamics and Materials Conference. May 10-12, 1982.

EFFECTS OF CONSTITUENT PROPERTIES ON
COMPRESSION FAILURE MECHANISMS

H. Thomas Hahn
Washington University
St. Louis, Missouri

INTRODUCTION

Recent work by Williams and Rhodes [1] has shown that higher impact resistance can be obtained for composites by using a tough resin because a tough resin can absorb more energy and localize the impact damage. However, a tough resin usually cannot be obtained without a sacrifice on modulus, and the lower modulus may lead to a lower compressive strength for composites. Therefore, a judicious selection of resin should be based on a balanced evaluation of both impact resistance and compressive strength. Although the subject of compression failure of composites has been frequently addressed in the literature, how constituent phases contribute to the overall compression strength still needs to be elucidated. Thus, the objectives of the present work are to delineate compression failure mechanisms in unidirectional composites and to identify material parameters that control compressive strength. With this enhanced understanding, laminate behavior can finally be predicted from lamina behavior.

BACKGROUND

- Higher impact resistance requires tougher resin
- Tougher resin may reduce compressive strength

OBJECTIVES

- Delineate compression failure mechanisms
- Identify material parameters that need improvement
- Correlate lamina behavior with laminate behavior

APPROACH

Compression failure mechanisms are studied at three different levels of material construction. The first level is a fiber bundle embedded in epoxy. Using this type of specimens, one can monitor the sequence of failure of the fiber bundle because the bundle is well contained within the epoxy. Also, the failure modes of fibers themselves can be studied at this level. The second level is unidirectional laminas loaded in the fiber direction. A comparison between the results from these two levels will help us understand the influence on compressive strength of the internal structure of composites. Multidirectional laminates, reserved for the last level, are used to assess the effects of off-axis plies and interfaces between plies. Different combinations of fibers and matrices are used because one failure mechanism operating in one material system may be suppressed in another material system. The present paper is concerned with the behavior of fiber bundle specimens only. The work on unidirectional and multidirectional laminates is still in progress. The IITRI compression fixture was used with a gage length of 13 mm. Specimens varied from 4 to 6.5 mm in thickness while being held at the same width of 13 mm. An Instron testing machine was used at a cross-head speed of 1.3 mm/min. During testing the fiber bundle was monitored for failure through a microscope at magnifications up to 50X. Since the fiber bundle occupied a small fraction of the specimen volume, the bundle failure did not lead to the specimen failure. Thus the bundle failure could be contained and monitored.

APPROACH

- Study compression failure of
Fiber bundle in epoxy
Unidirectional lamina
Laminate
- Different fibers and matrices

EXPERIMENTAL PROCEDURE

- 4 - 6.5 x 6.4 x 13 mm
- IITRI compression fixture
- 1.3 mm/min.
- Fiber failure monitored through a
microscope at up to 50X magnification

MATRIX AND FIBER PROPERTIES

Representative matrix and fiber properties are listed in the tables below. Two different epoxies were used: Epon 828 with curing agent Z and Epon 815 with curing agent V140. The former epoxy is more brittle than the latter, but even the former is rather ductile compared with Narmco 5208, for example. The four different fibers used are listed in the order of decreasing tensile failure strain. In the table, WY is a high-strain graphite fiber and P75S is a high-modulus pitch fiber, both manufactured by Union Carbide. The glass fiber bundle contained about 200 filaments whereas the graphite fiber bundles had about 3000 filaments each. The matrix properties were measured but the fiber properties were taken from manufacturers' data sheets.

MATRIX PROPERTIES

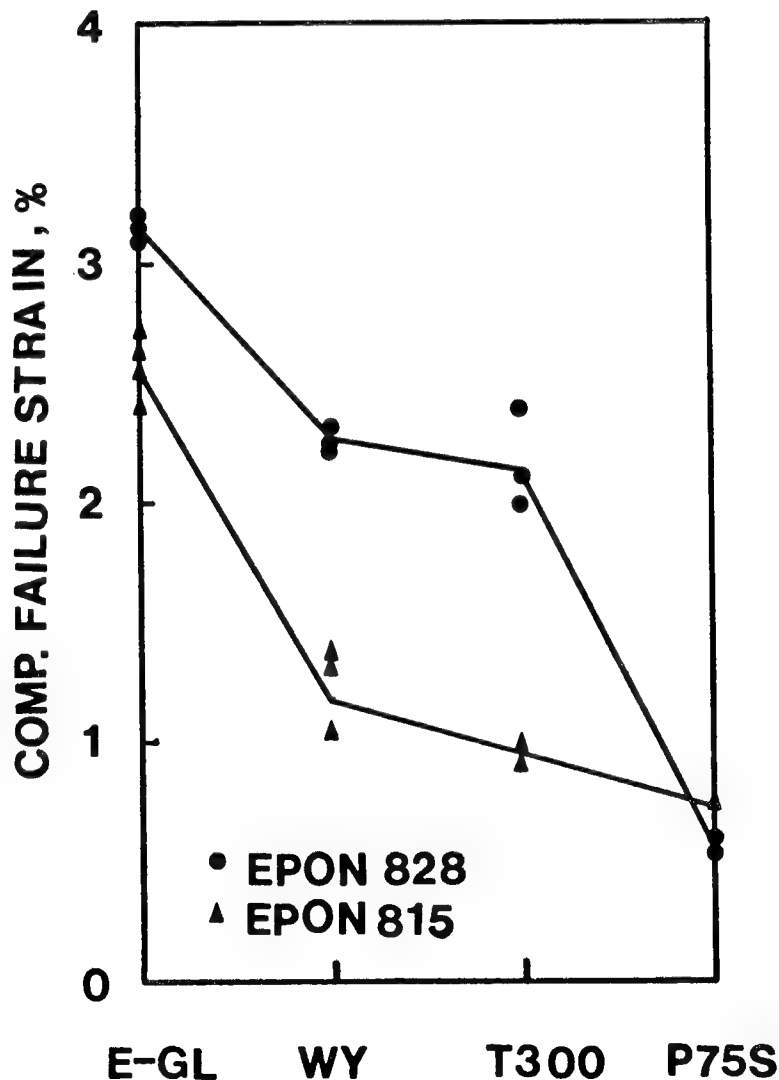
Epoxy	Modulus, GPa	Ultimate tensile stress, MPa	Tensile failure strain, %
Epon 828/Z (80/20)	3.45	85.4	9
Epon 815/V140 (60/40)	2.13	45.5	14

FIBER PROPERTIES

Fiber	Diameter, μm	Cross-sectional area of bundle, mm^2	Modulus, GPa	Tensile failure strain, %
E-G1	13.5	2.9×10^{-2}	72.35	4.8
WY-0224	5.1	9.16×10^{-2}	230.00	1.83
T300	7.0	11.61×10^{-2}	234.00	1.34
P75S	9.7	14.84×10^{-2}	517.00	0.40

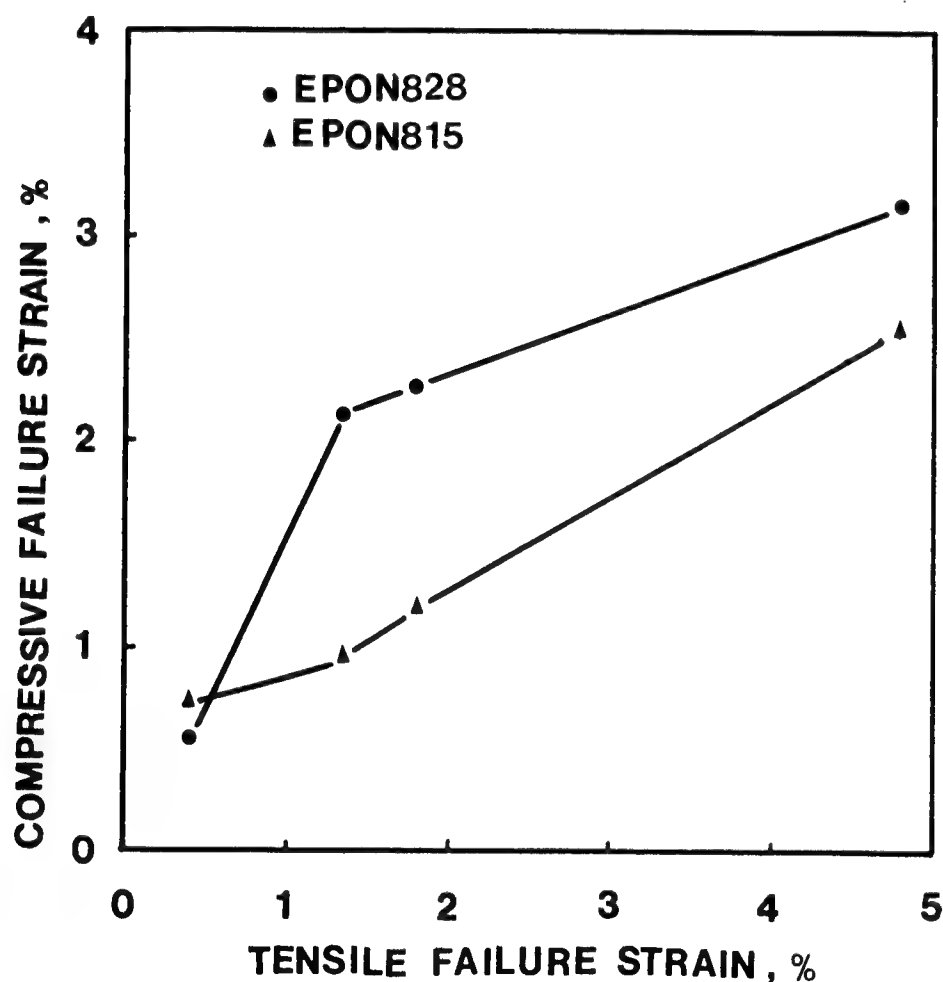
COMPRESSIVE FAILURE STRAINS OF FIBER BUNDLES

E-glass fiber bundle has the highest compressive failure strain while P75S has the lowest. The high-strain graphite fiber is slightly stronger than T300. As expected from the buckling theory, the stiffer epoxy yields higher failure strains. However, the difference disappears for the high-modulus graphite P75S. The reason is that P75S fibers under compression fail in shear while the other fibers fail in buckling. Failure of P75S fiber was quite difficult to detect because the filaments failed individually on a plane about 45° to the loading. The failure was quite gradual, spreading over the entire length of the filament. Therefore, there was no sudden release of energy as in the other fibers. The data for P75S fiber should be taken as an estimate based on the best ability to detect failure. Note also that the strains were calculated from the failure stresses under the assumption of linear behavior.



A CORRELATION BETWEEN COMPRESSION AND TENSION FAILURE STRAINS

Compressive failure strain increases with tensile failure strain. P75S graphite fiber has almost equal strength in both tension and compression. In the absence of buckling, T300 and WY fibers will be stronger in compression than in tension. E-glass fiber bundle buckles in compression before reaching a strain equal in magnitude to its tensile failure strain. Both T300 and WY fibers have almost the same modulus. Yet, T300 fiber is slightly weaker than WY fiber although the former is larger in diameter. Thus the same mechanism that controls tensile failure seems to affect buckling. For example, the same defect may become detrimental in compression as well as in tension. However, the defect sensitivity in buckling would be less than in tension because the superiority of WY fiber over T300 fiber is more pronounced in tension than in compression.



ANALYTICAL PREDICTIONS

Buckling of a fiber in an infinite matrix has been analyzed by several investigators [2,3]. An approximate equation for buckling strain can be derived by using the virtual work principle under the assumption that the matrix support of the fiber is proportional to the matrix modulus and the buckling pattern is sinusoidal. The predicted buckling strain is proportional to the square root of the matrix-to-fiber modulus ratio E_m/E_f . Further, the buckling wave length is inversely proportional to the fourth root of E_m/E_f . On the other hand, theories [4] on microbuckling of fibers in composites indicate that the buckling strain for extension mode, i.e., out-of-phase buckling, is proportional to the square root of the modulus ratio, as in the single-fiber case. However, the buckling strain for shear mode is predicted to be proportional to the modulus ratio itself. Thus, it is of interest to find out which theory can describe the experimental data obtained.

BUCKLING OF A FIBER IN MATRIX

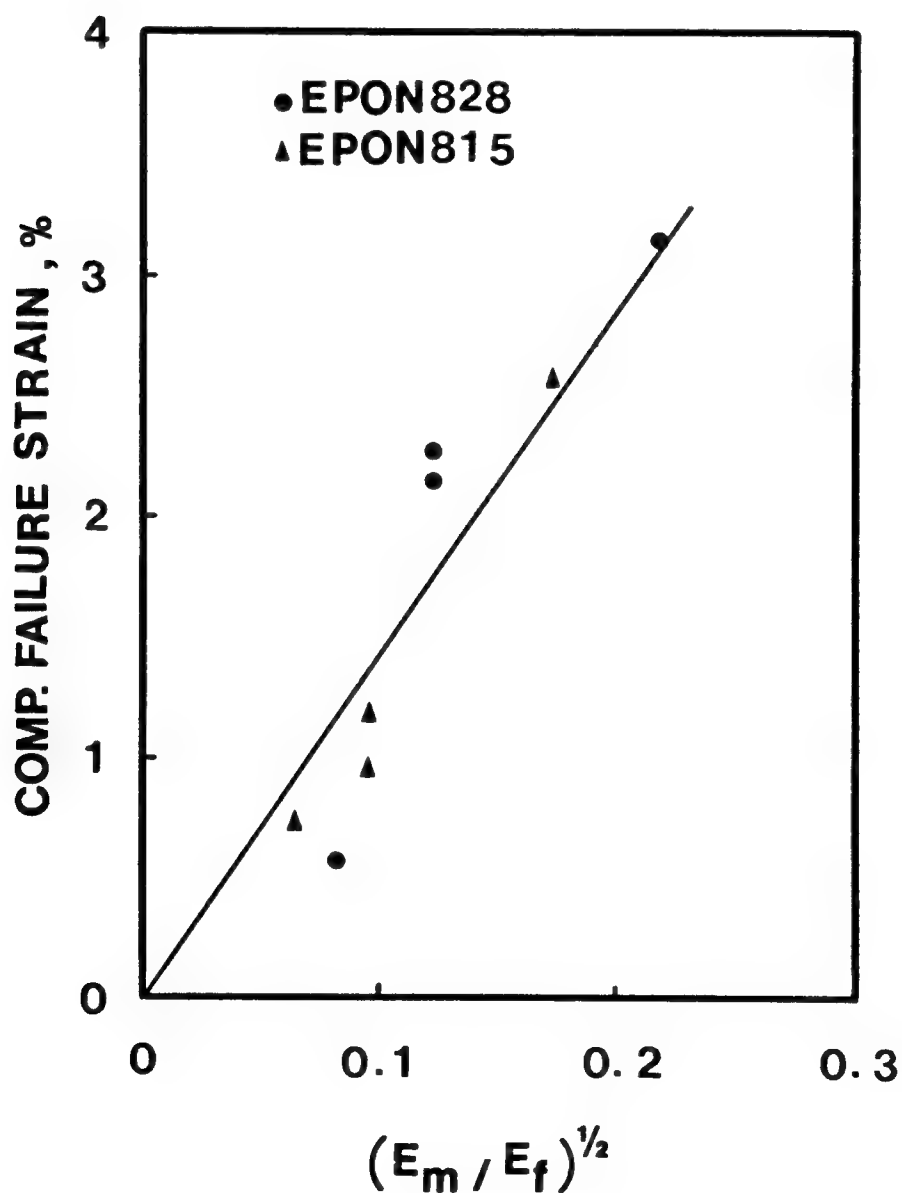
- Sadowsky, Pu and Hussain, 1967 (ref. 2)
Lanir and Fung, 1972 (ref. 3)
- Virtual work principle
- Matrix support proportional to modulus
- Buckling strain
$$\epsilon \propto (E_m/E_f)^{1/2}$$
- Buckling wave length
$$\delta \propto (E_m/E_f)^{-1/4}$$

BUCKLING OF COMPOSITE

- Rosen, 1965 (ref. 4) and others
- Extension mode
$$\epsilon \propto (E_m/E_f)^{1/2}$$
- Shear mode
$$\epsilon \propto E_m/E_f$$

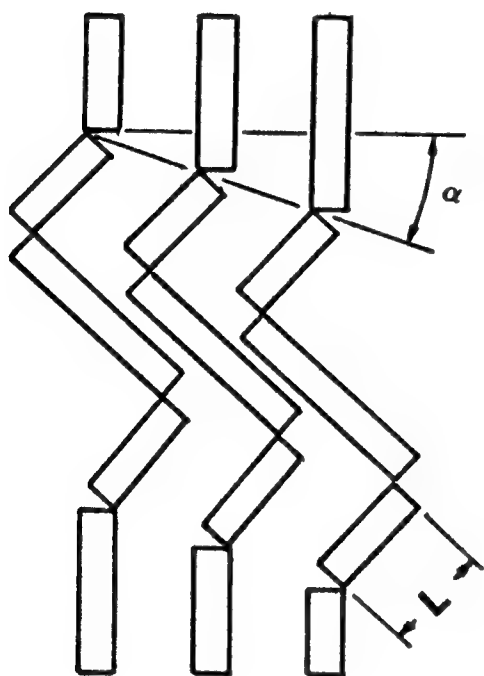
DEPENDENCE OF COMPRESSIVE FAILURE STRAIN ON MODULUS RATIO

Compressive failure strain is seen to be fairly proportional to the square root of the matrix-to-fiber modulus ratio. Even the high-modulus graphite fiber seems to follow the trend although its failure is not due to buckling. As will be shown in the following micrographs, the buckling of fiber bundles was in a characteristic shear mode. For microbuckling in composites, analysis predicts a linear relationship between the buckling strain and the shear modulus ratio. Therefore, the prediction equations for composites are not applicable to the present fiber bundles. However, the equation for buckling of a fiber in matrix correctly predicts the trend. It is thus possible that buckling of the bundle is triggered by buckling of a single fiber and hence the buckling strain is proportional to $(E_m/E_f)^{1/2}$.



MODE OF BUCKLING FAILURE

A schematic diagram describing a bundle failed in buckling is shown below. Also shown is a shear failure of a fiber. The three parameters that deserve special attention are the segment length L , the buckling boundary angle α , and the orientation of fiber fracture surface. If buckling mode is sinusoidal, L is likely to be one fourth of wave length. Also, if fiber fails as a result of buckling, its fracture surface will be normal to the fiber axis. Failure due to shear, on the other hand, will be associated with a slanted fracture surface. The buckling boundary angle, also called the crimp boundary angle, is generally less than 45° . All the foregoing parameters were examined on the failed specimens.



BUCKLING FAILURE



SHEAR FAILURE

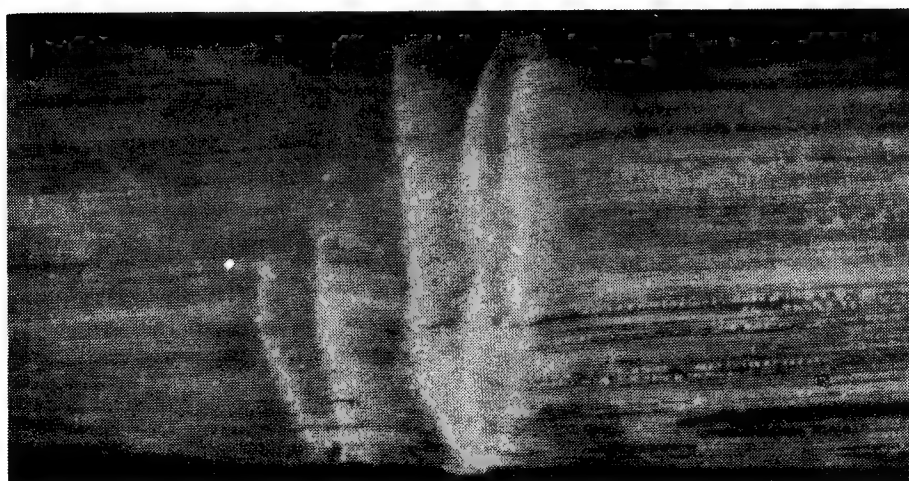
BUCKLING FAILURE OF E-GLASS FIBER BUNDLE

The top figure shows buckling of E-glass bundle in a weak epoxy over its entire length. Too much solvent was inadvertently added to the epoxy during formulation and, as a result, was much more brittle and softer than expected. Buckling of the fiber bundle in this epoxy was quite gradual, starting at a very low load, and occurred uniformly over the entire length. The elliptical spots on the bundle are cracks growing into the matrix almost normal to the plane of the photograph. These cracks were generated by the tensile stress between fibers as a result of buckling. Note also that fibers are bent but have not broken yet. Buckling of the bundle in a well formulated Epon 815 is catastrophic and much more localized, as seen in the lower figure. Buckling occurs without warning and leads immediately to breakage of the fibers. Fiber break is seen to progress from one edge of the bundle to the other. The buckling failure of the E-glass bundle in the brittle Epon 828 is also quite localized, as seen in the figures on the next page. Although the bundle has an elliptical cross section, it can buckle in the plane of the larger dimension as well. The buckled region is out of focus because of the out-of-plane movement of the filaments. Macroscopically, no distinction could be detected between failures in Epon 815 and Epon 828.

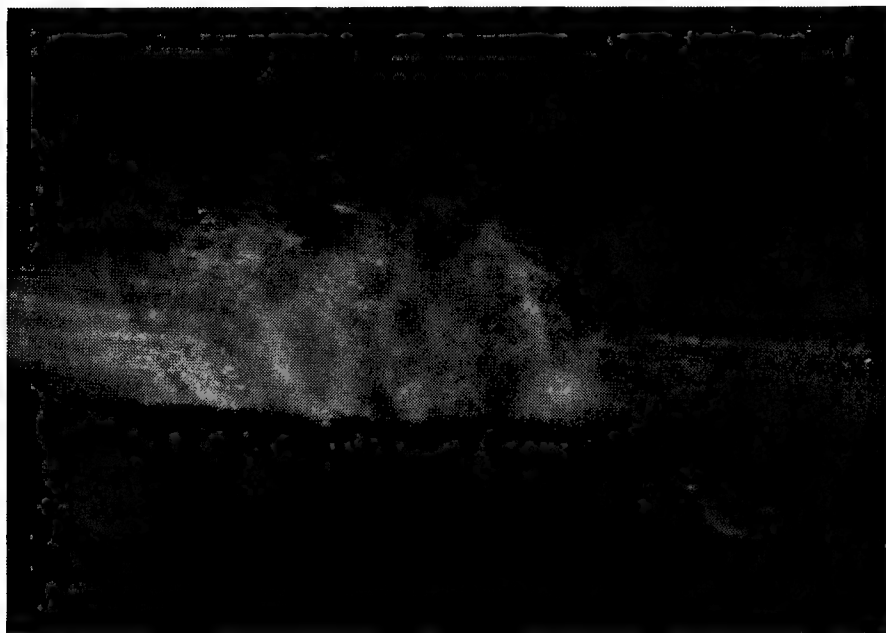
UNIFORM BUCKLING AND MATRIX CRACKING, E-GLASS IN WEAK EPOXY



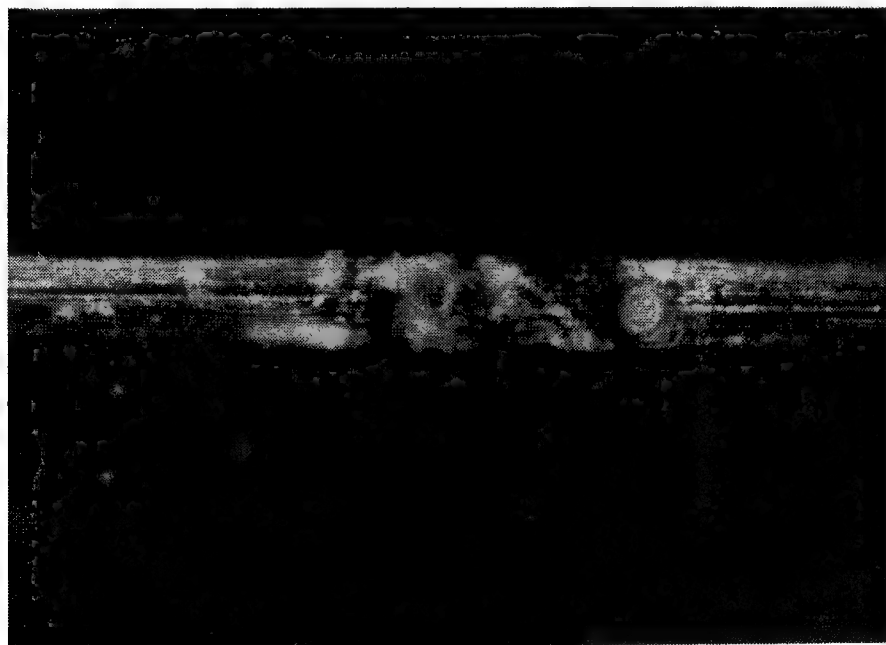
LOCAL BUCKLING OF E-GLASS BUNDLE IN EPON 815



LOCAL BUCKLING OF E-GLASS BUNDLE IN EPON 828: FRONT VIEW



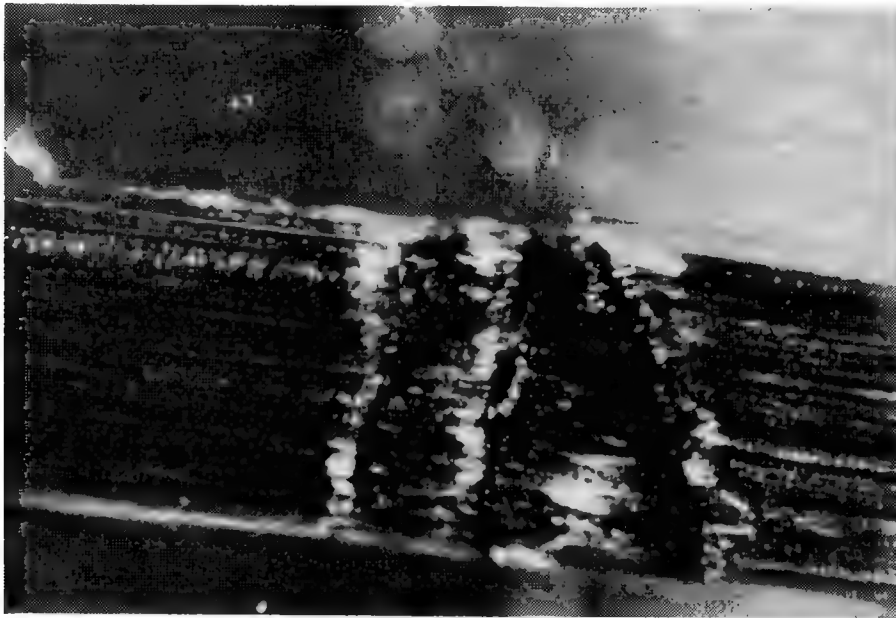
LOCAL BUCKLING OF E-GLASS BUNDLE IN EPON 828: SIDE VIEW



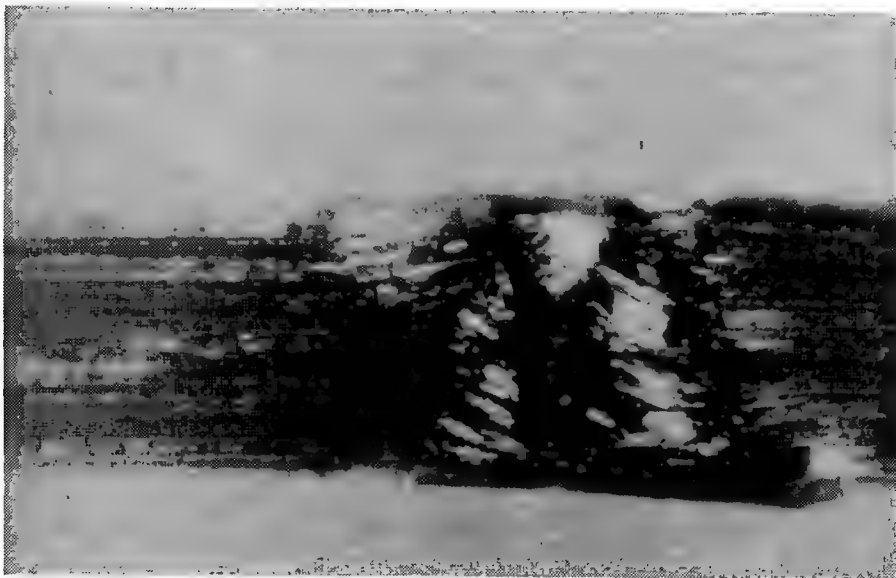
BUCKLING FAILURE OF GRAPHITE FIBER BUNDLES

The buckling failure of the T300 graphite fiber bundle in Epon 815 is similar to that of the E-glass fiber bundle in Epon 828. However, the buckling zone of the T300 bundle in Epon 828 is much narrower. Also, there is very little indication of buckling failure for the bundle in Epon 828. Rather, only a thin dark line indicates failure of the bundle. The high-strain WY graphite fiber behaves similarly to T300: the buckling failure is quite localized and the buckling zone in Epon 282 is smaller than in Epon 815.

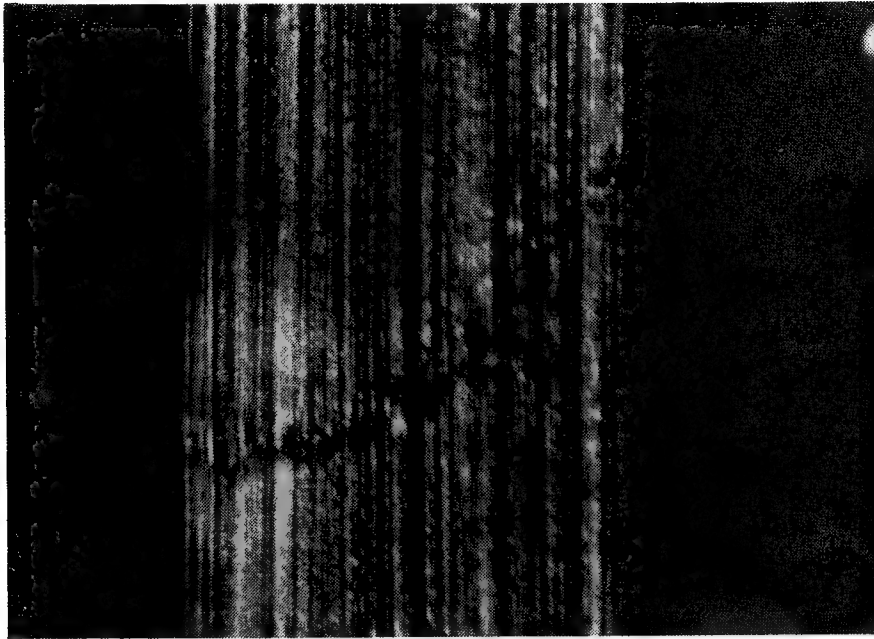
LOCAL BUCKLING OF T300 GRAPHITE BUNDLE IN EPON 815: FRONT VIEW



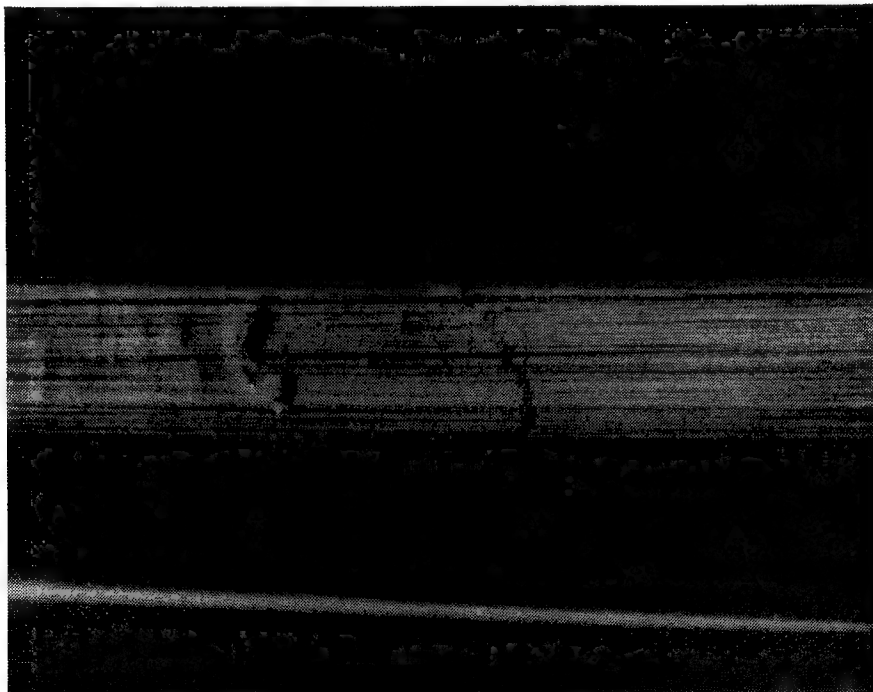
LOCAL BUCKLING OF T300 GRAPHITE BUNDLE IN EPON 815: SIDE VIEW



LOCAL BUCKLING OF T300 GRAPHITE BUNDLE IN EPON 828: FRONT VIEW



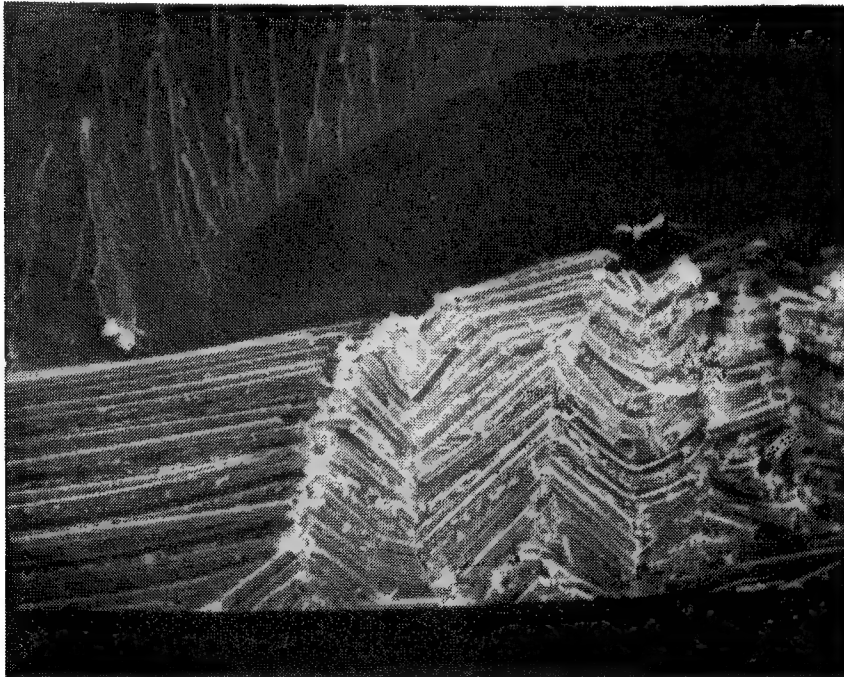
LOCAL BUCKLING OF T300 GRAPHITE BUNDLE IN EPON 828: SIDE VIEW



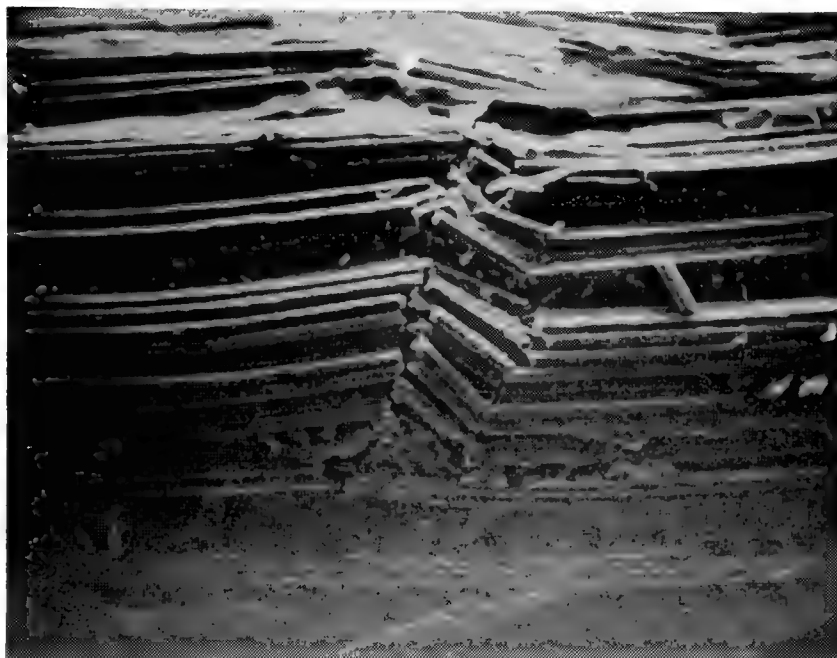
SEM MICROGRAPHS OF BUNDLES

After compression tests, one specimen from each group was cracked open through the bundle. The scanning electron micrograph of the E-glass bundle clearly shows a buckling-induced failure. The buckling is over the distance of several wavelengths. The rotation of broken fiber segments is clearly seen. The failure mode in Epon 815 was similar to the one shown below. The T300 graphite bundle shows more localized buckling failure than the E-glass bundle, as seen in the upper figure on the next page. As in tension, buckling will occur first at the weakest point. If fiber failure does not follow immediately, buckling may spread along the fiber axis. Since graphite fibers have lower tensile failure strain than glass fibers, the former are more likely to fail immediately after buckling. This may explain why fewer waves are involved in the buckling failure of graphite bundles. The failure mode of WY fiber observed in SEM micrographs was similar to that of T300 fiber. Note in the figures that the filaments on the left side of the fiber breaks remain bent. The high-modulus P75S fiber failed in shear without buckling, as seen in the lower figure on the next page. Even after failure the filaments remained straight without rotation or curvature. The figure shows a slanted fracture surface. Whereas the buckling failure of the other fibers was at a few isolated sites along the fiber length, the shear failure was quite uniformly distributed over the entire length. In other words, failure of P75S fiber was more like the multiple fracture frequently observed in tension of a fiber embedded in epoxy.

SCANNING ELECTRON MICROGRAPH OF E-GLASS BUNDLE IN EPON 828



SCANNING ELECTRON MICROGRAPH OF T300 GRAPHITE BUNDLE IN EPON 815

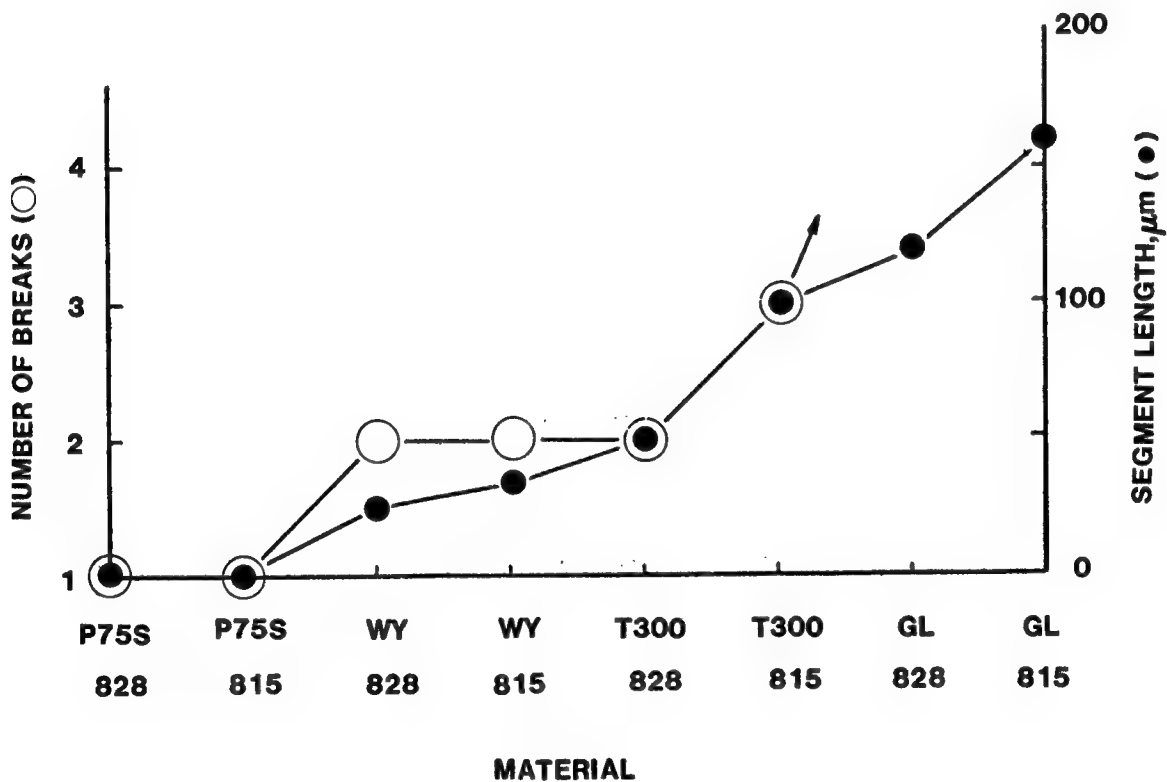


SCANNING ELECTRON MICROGRAPH OF P75S GRAPHITE BUNDLE IN EPON 828



GEOMETRIC DESCRIPTION OF BUNDLE FAILURE

The number of fiber breaks and segment lengths in a typical failure zone is shown in the figure. The geometrical details of the failure zone vary much more than could be described by average numbers alone. Yet, the data in the figure indicate a certain trend. As was seen earlier, the failure zone of P75S fiber is a single, slanted fracture surface. Failure of WY fiber in both epoxies and T300 fiber in Epon 828 is characterized by double breaks in each filament. The number of breaks increases to three for T300 in Epon 815. E-glass bundles exhibit more than three breaks in each filament regardless of the epoxy type. The length of each broken segment also increases with the number of breaks. Discounting the direct role of the internal structure of fiber, we can infer from the figure that an increase in the number of breaks as well as in the segment length is associated with a lower modulus and higher compression failure strain.



CONCLUSIONS

The use of a fiber bundle embedded in matrix can provide much needed information on compression failure mechanisms because failure of the bundle is well contained and can be monitored during testing. The method can clearly distinguish between buckling-induced failure and shear-induced failure. The present study indicates that WY and T300 graphite fibers and E-glass fiber fail in buckling while the high-modulus P75S graphite fiber fails in shear. Buckling-induced failure becomes more evident with low-modulus fiber in softer epoxy. Further specific conclusions are described below.

- Uniform buckling and matrix cracking in weak epoxy
- Buckling in plane of fibers
- Localized buckling in stiffer epoxy
- Higher buckling strain for E-g1 than for graphite fibers
- Debonding after buckling
- Buckling strain increasing with tensile failure strain
- Fiber break at buckling except in weak epoxy
- Buckling strain proportional to $(E_m/E_f)^{1/2}$
- P75S fiber - No buckling, gradual compression failure, no buckling even after compression failure
- Failure more violent at higher strain
- Number of breaks in each filament highest for E-g1 and lowest for high-modulus graphite
- Segment length longest in E-g1/Epon 815, and longer in Epon 828 than in Epon 815

REFERENCES

1. Williams, J. G. and Rhodes, M. D.: The Effect of Resin on the Impact Damage Tolerance of Graphite-Epoxy Laminates. NASA TM-83213, October 1981.
2. Sadowsky, M. A., Pu, S. L. and Hussain, M. A.: Buckling of Microfibers. J. Appl. Mech., Vol. 34, 1967, pp. 1011-1016.
3. Lanir, Y. and Fung, Y. C. B.: Fiber Composite Columns under Compression. J. Composite Materials, Vol. 6, 1972, pp. 387-401.
4. Rosen, B. W.: Mechanics of Composite Strengthening. Fibre Composite Materials, American Society for Metals, 1965, pp. 37-75.

THE EFFECT OF MATRIX AND FIBER PROPERTIES ON IMPACT RESISTANCE

Wolf Elber
NASA Langley Research Center
Hampton, Virginia

INTRODUCTION

Studies of impact damage in composites are aimed partly at evaluating the performance of structures with impact damage, and partly at establishing which basic material properties affect the impact resistance. Impact studies can be divided into three areas: impact dynamics, damage mechanics, and effects studies. Many of the studies in industry are in the last area. They seek to find residual compressive strengths after impact.

In our research effort we are concentrating on the other areas: impact dynamics and damage mechanics. The purpose of these studies (fig. 1) is to improve testing techniques and to identify the basic material properties which control impact damage. As a result, we expect to contribute to the criteria for selection or development of more impact-resistant matrix resins.

OBJECTIVES

- * *Isolate basic material properties dominating the impact damage response of composite laminates.*
- * *Show that matrix improvements alone cannot solve all problems (and that some tests are insensitive to matrix properties.)*
- * *Show that fiber ultimate strain dominates the penetration phase.*
- * *Show that for best impact resistance both fibers and matrix must be improved.*
- * *Warn of the danger of unsafe failure modes for overly tough or strong matrix resins.*

Figure 1

FAILURE MODES IN THIN LAMINATES (I)

For thin laminates bonded over a circular aperture in a flat plate, the most severe damage from impact is usually observed on the back face. The specimen shown in figure 2 was a quasi-isotropic 8-ply plate of T300/5208. The low peel strength of the matrix resin results in extensive internal delamination and splitting, as well as peeling of the back face.



Figure 2

FAILURE MODES IN THIN LAMINATES (II)

For a tougher material (fig. 3) such as C6000/HX205, less peeling of the back face fibers is observed, and a cross-shaped transverse crack pattern accompanies the delamination.

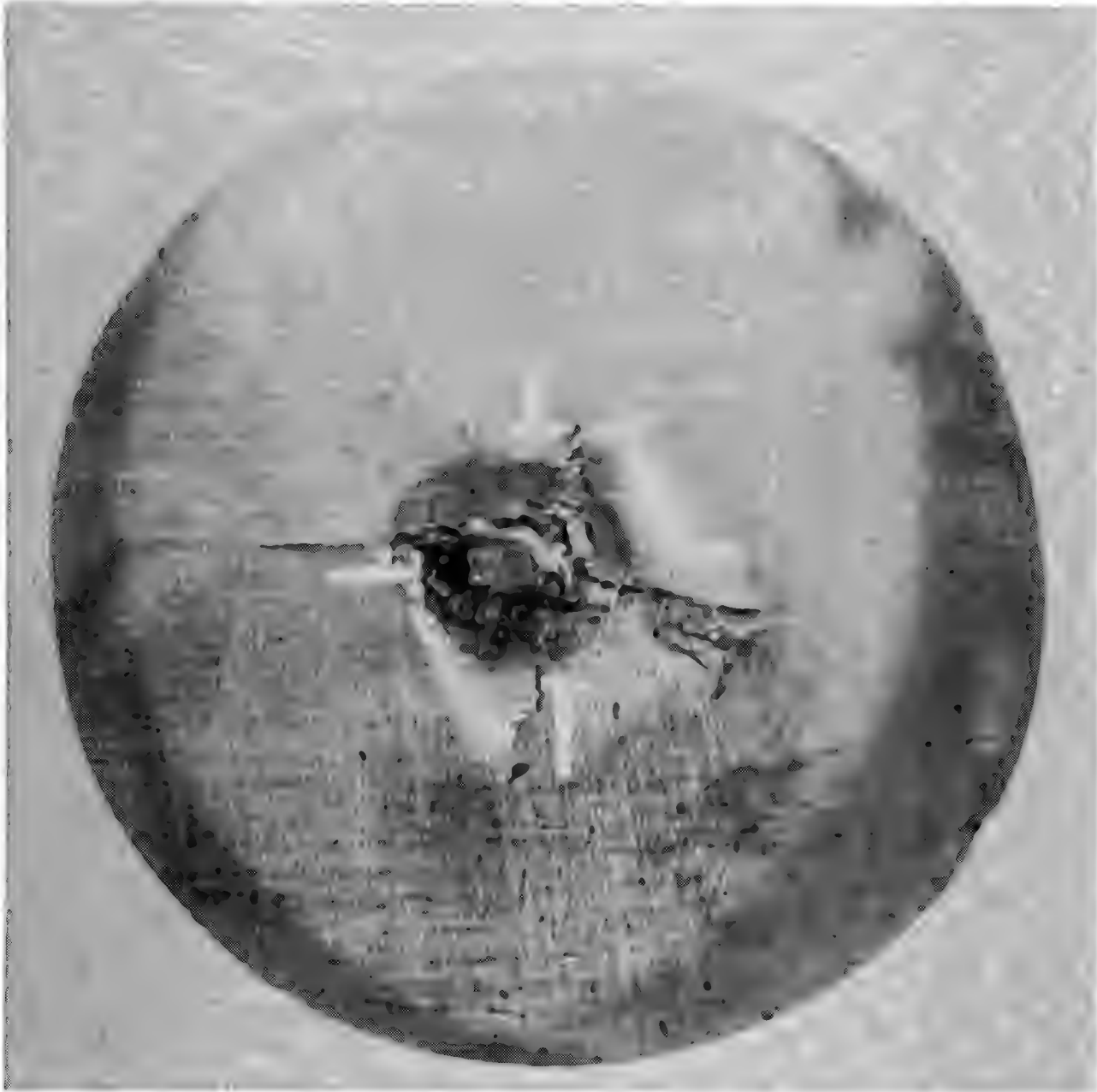


Figure 3

FAILURE MODES IN THIN LAMINATES (III)

For a thermoplastic resin such as polysulfone in C6000/P1700, the toughness and strength of the resin are so high that virtually no delamination occurs. Instead, a crossed pair of through-the-thickness cracks develops, allowing the impactor to penetrate the laminate by folding out the resulting leaves between the cracks. In the specimen shown in figure 4, one of these leaves broke during the penetration process.

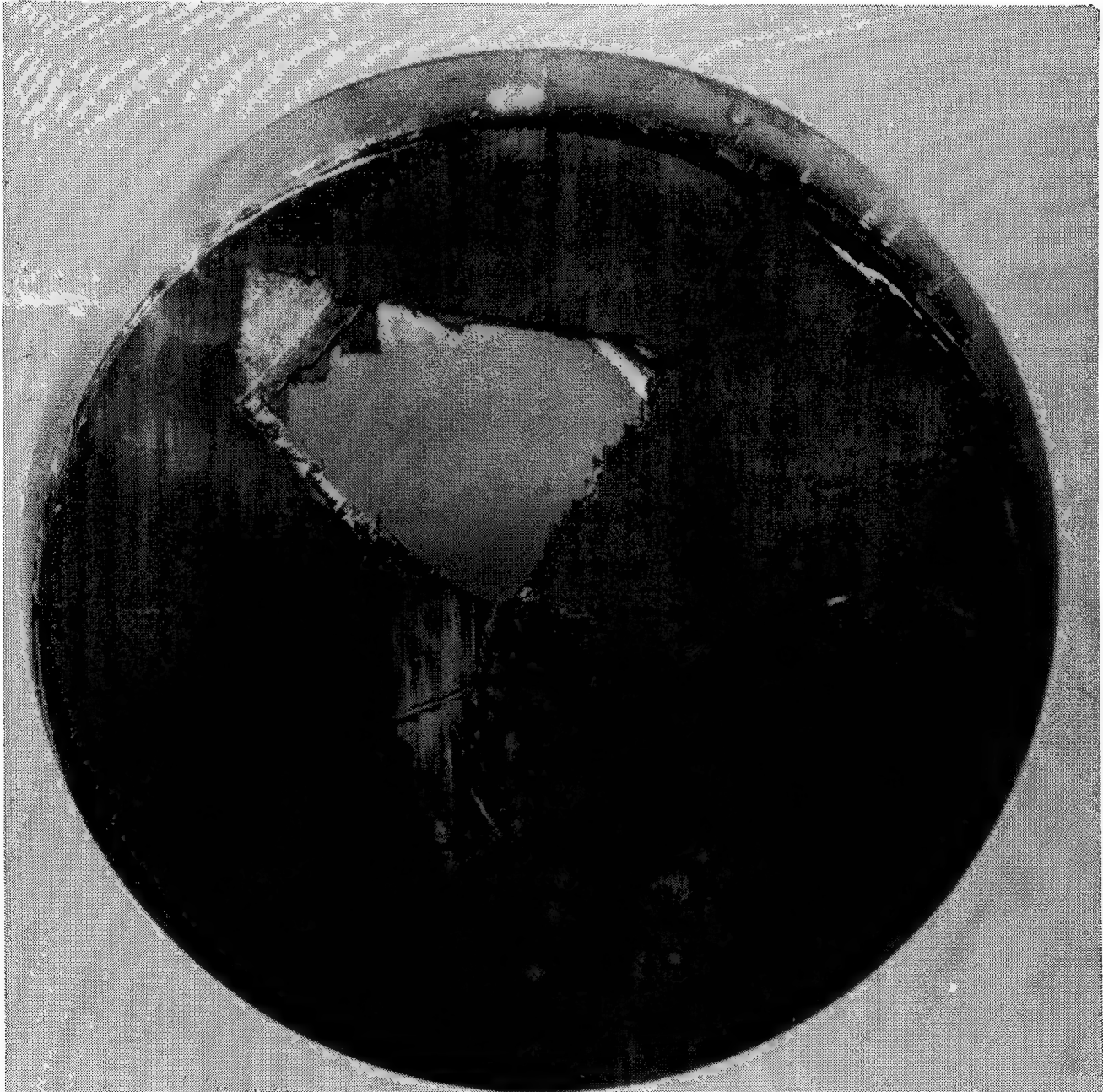


Figure 4

STATIC/IMPACT COMPARISON

Impact tests often result in local contact force histories including very high modes of vibration. Shown in figure 5 are the load-displacement relations for an impact test and for an equivalent static indentation test. In spite of the high noise spikes, the mean of the impact load-displacement curve follows approximately the curve for the static test. The curve for the static test, in turn, is bounded by the analytical curves for a plate and for a pure membrane in the region in which delamination occurs.

When both load-displacement curves are integrated to obtain energy absorbed as a function of displacement, the impact behavior is virtually identical to the static behavior (fig. 6). That implies that rate effects do not appear to affect the energy absorption and damage process, and also indicates that the high spike loads observed do not cause appropriate additional damage.

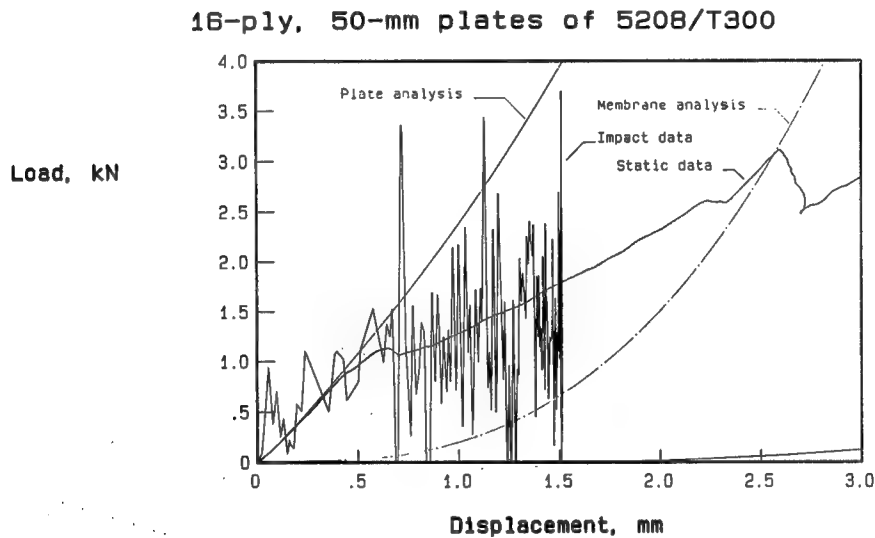


Figure 5

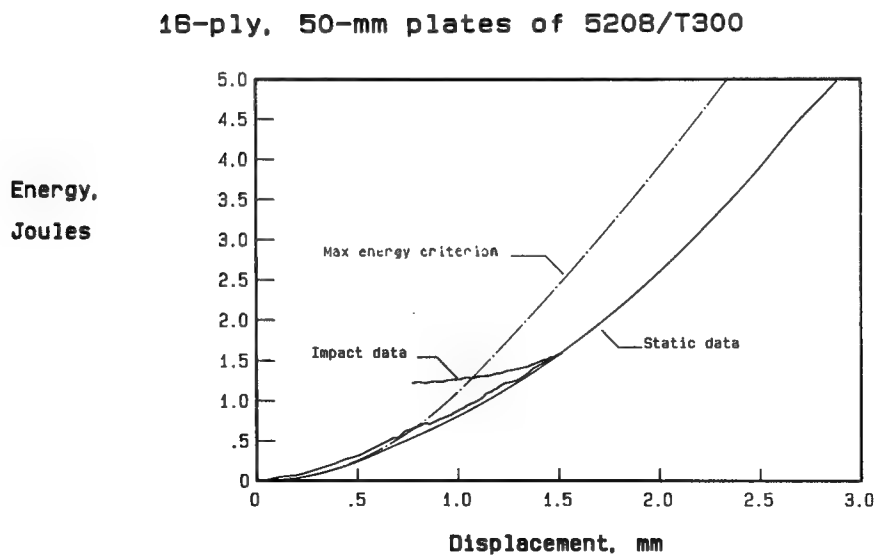
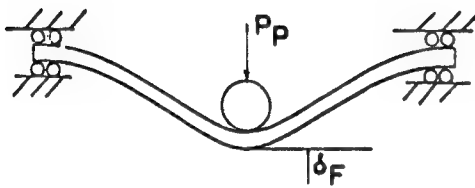


Figure 6

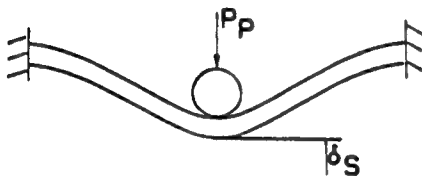
THIN PLATE ANALYSIS

Simple strength of materials formulations were found adequate to describe the deformation behavior of thin plates up to 32 plies (ref. 1). Figure 7 shows the superposition scheme for obtaining a total load displacement relation. First the flexural and shear displacements for a point-loaded plate are summed. For that summed midplane displacement, the large deformation membrane load term is obtained. The plate load and membrane reaction are summed to obtain the total load. The indentation displacement for the total load is added to the midplane displacement to calculate the total displacement. For large delaminations, the plate carries no load so that only the large deformation membrane load displacement relation is appropriate.

Model Superposition

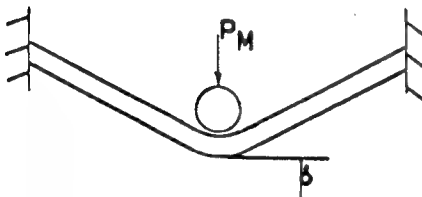


Flexural Deformation: $P_p = K_F \delta_F$



Shear Deformation: $P_p = K_S \delta_S$

$$\delta = \delta_S + \delta_F$$



Membrane Reaction: $P_M = K_M \delta^3$

$$P = P_p + P_M$$



Indentation Deformation: $P = K_I \delta_I^{3/2}$

$$\delta_T = \delta_I + \delta$$

Figure 7

TYPICAL LOAD-DISPLACEMENT RELATIONS

The load displacement relation, and hence the impact resistance, is a strong function of the boundary conditions. Figure 8 shows the static load displacement relation for an 8-ply laminate over a 1/2-inch-diameter hole and over a 3-inch-diameter hole. In both cases the load displacement relation initially follows the analytical plate solution and approaches the fully delaminated or membrane solution when the damage is extensive. The small diameter plate shows a larger stiffness loss due to delamination, as would be expected.

two 8-ply circular plates

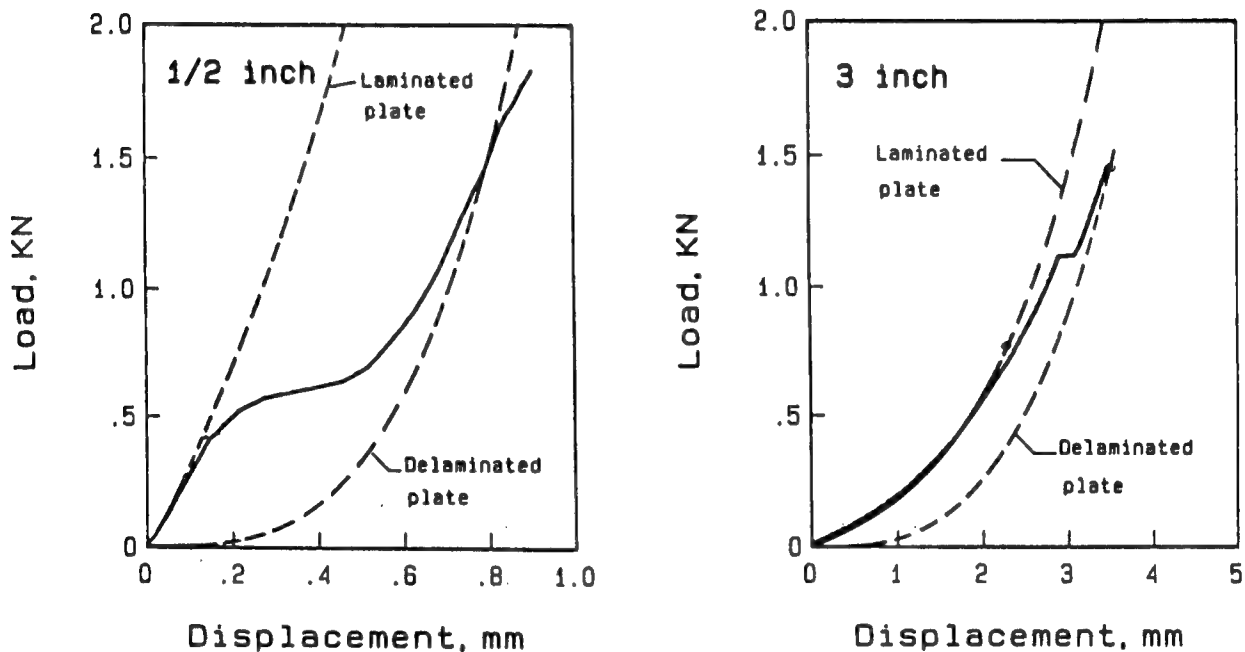


Figure 8

LOWER SURFACE FIBER STRAINS

The strength of materials models can also be used to calculate lower surface fiber strains, and figure 9 shows that the measured values of fiber strain basically agree with the calculations until splitting occurs in the lower ply.

clamped 2 inch diameter plate

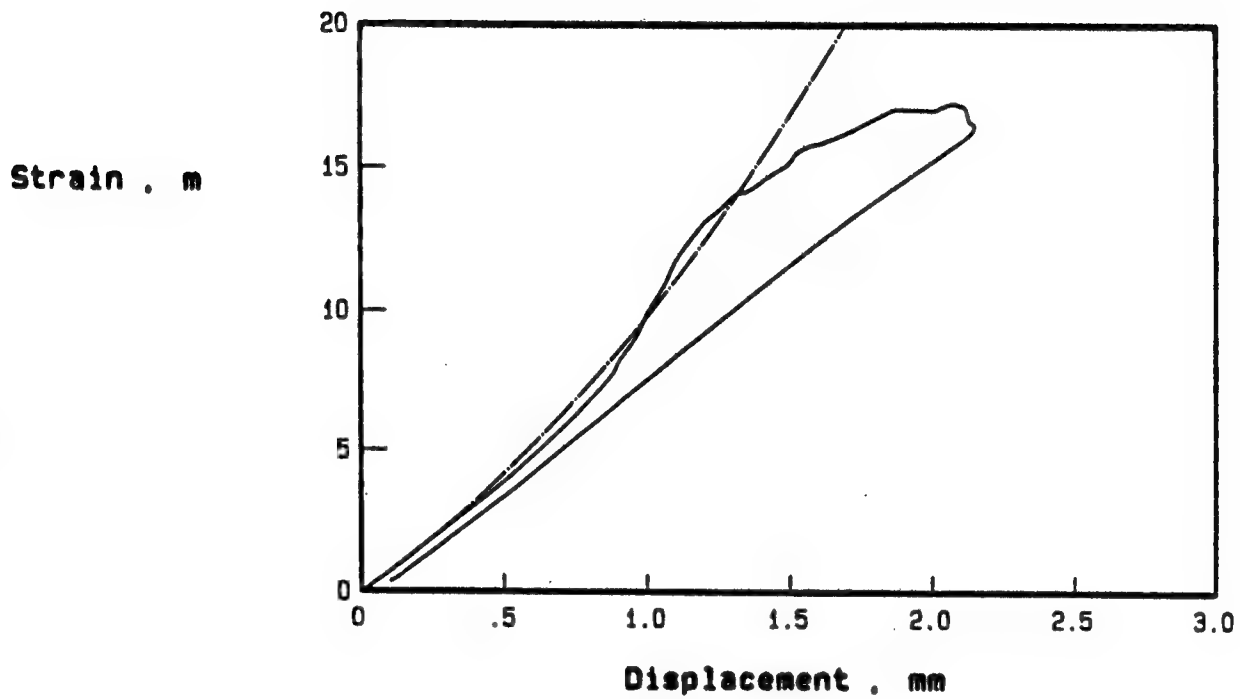


Figure 9

PLATE FAILURE CRITERIA

The strain expressions can be combined to calculate failure criteria as a function of plate size. If the plate is fully laminated, matrix shear failure must occur when the shear stress on the cylinder of the size of the indentation reaches a critical value. This is independent of plate size. As long as the plate is fully laminated, the strain in the bottom ply is a sum of the membrane and flexural strain. The middle curve in figure 10 describes the conditions when that strain reaches the fiber ultimate strain. But delamination starts at a lower load for this matrix (5208), so failure will occur when the membrane strain by itself reaches the fiber ultimate strain.

8-ply T300/5208 clamped plates

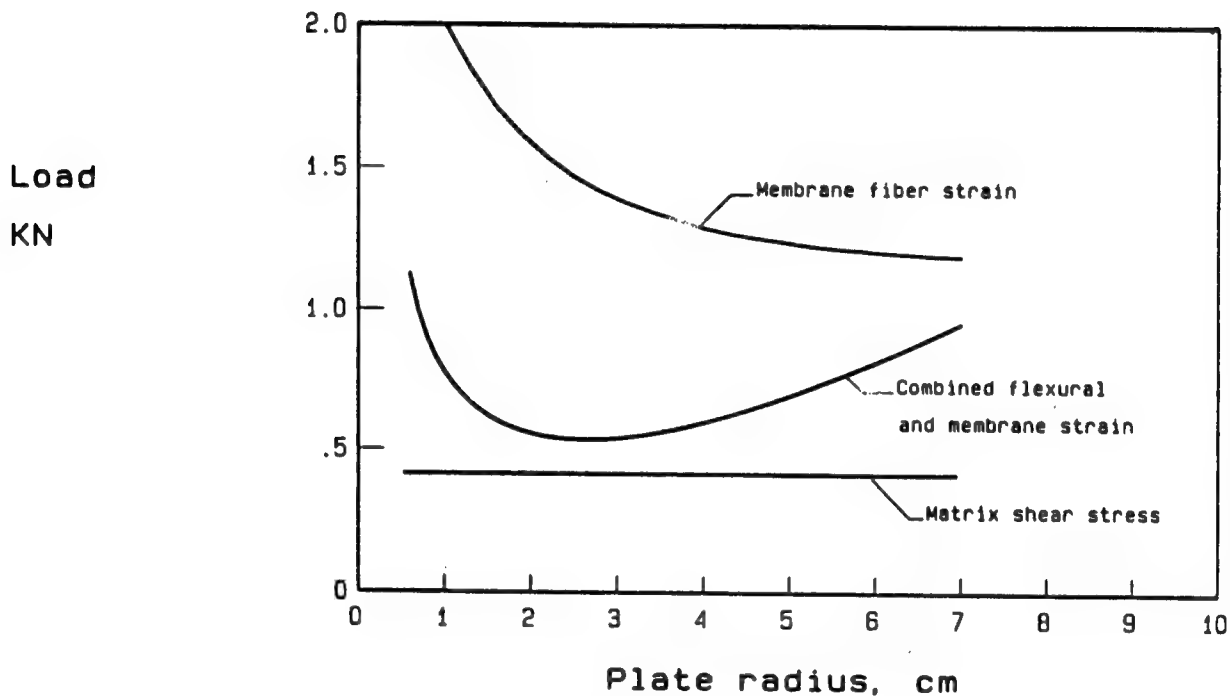


Figure 10

STATIC PENETRATION TESTS (I)

Figure 11 shows the load displacement relations obtained from static tests for 8-ply plates with three different support radii. The shear failure initiates at about 0.4 kN for all three plate sizes, but because these are thin plates, almost no stiffness is lost. In all cases the load displacement curves gradually approach the membrane state until fiber failures precipitate massive instabilities. In some cases the load may build up again until another ply (the bottom ply) fails.

8-PLY 5208/T300 LAMINATES

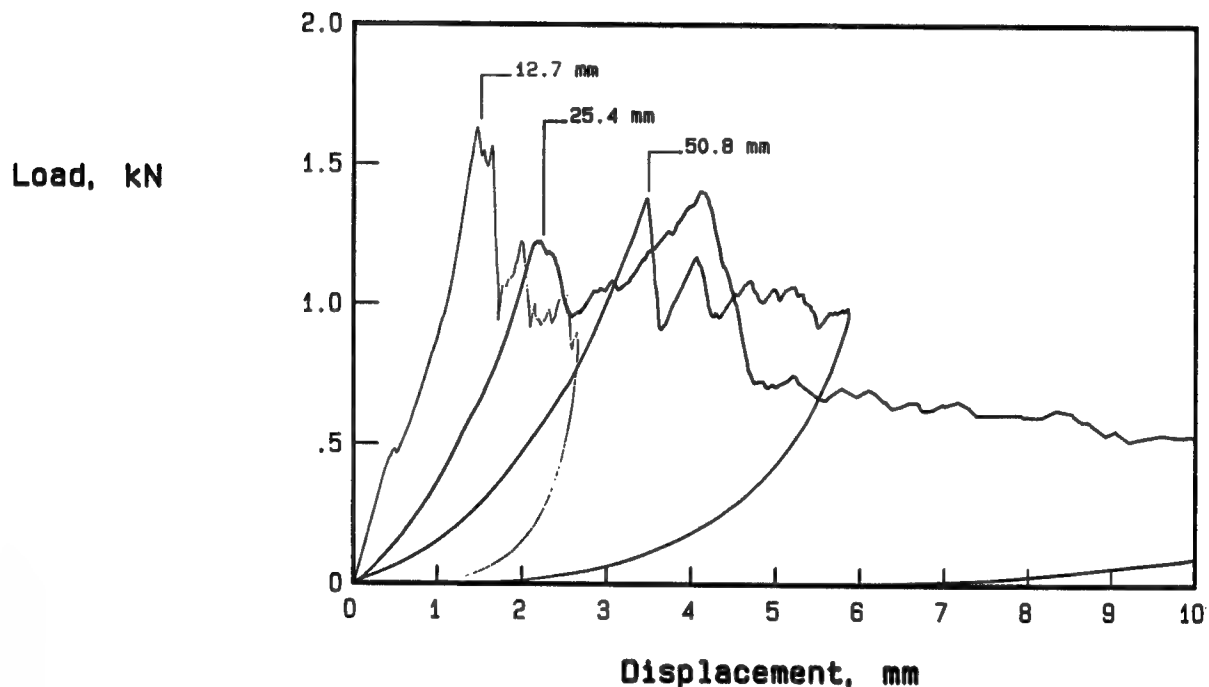


Figure 11

STATIC PENETRATION TESTS (II)

For the 16-ply plates shown in figure 12, shear stiffness is more significant and some stiffness loss is obvious at about 1.2 kN when the shear failures start in all three plate sizes. Again, the load displacement relations gradually become dominated by the membrane response and first-fiber failure is associated with significant stiffness loss.

16-PLY 5208/T300 LAMINATES

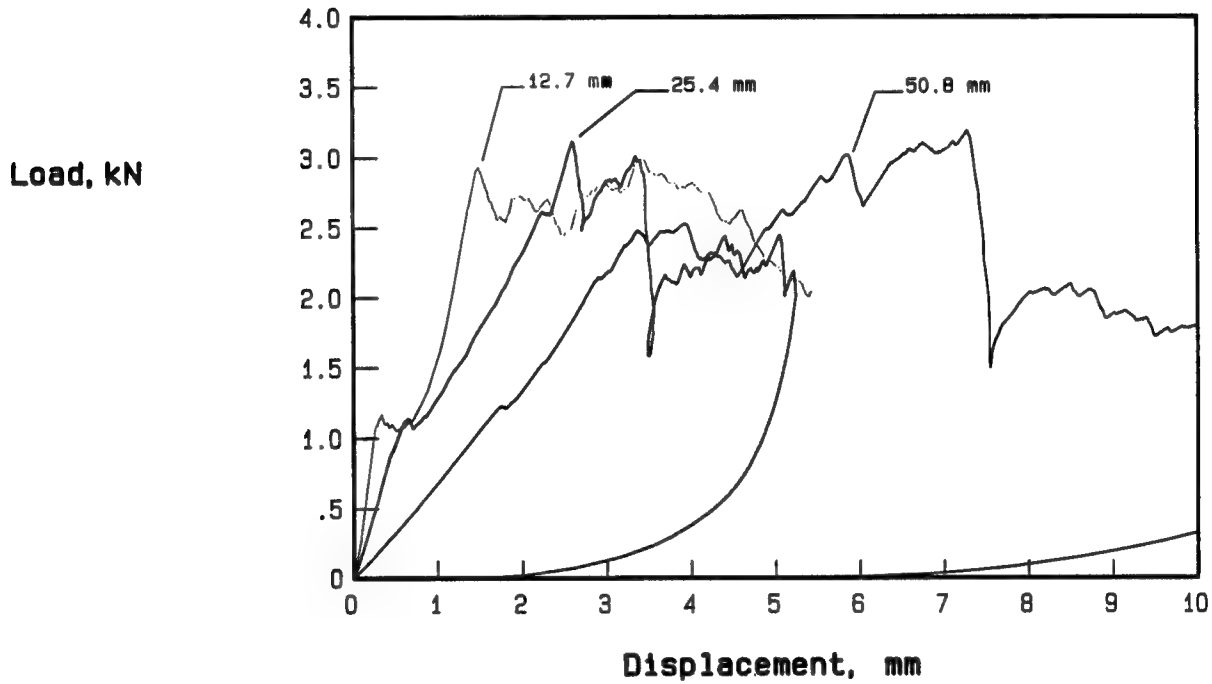


Figure 12

STATIC PENETRATION TESTS (III)

For the 32-ply data shown in figure 13, the shear failure instability is even more pronounced. Immediately after initiation, the delamination grows unstably to almost half of the plate diameter, with significant loss of stiffness. Further growth occurs as the displacement increases until the load-displacement relation is almost completely membrane dominated and fiber failure begins in the lower plies.

32-PLY 5208/T300 LAMINATES

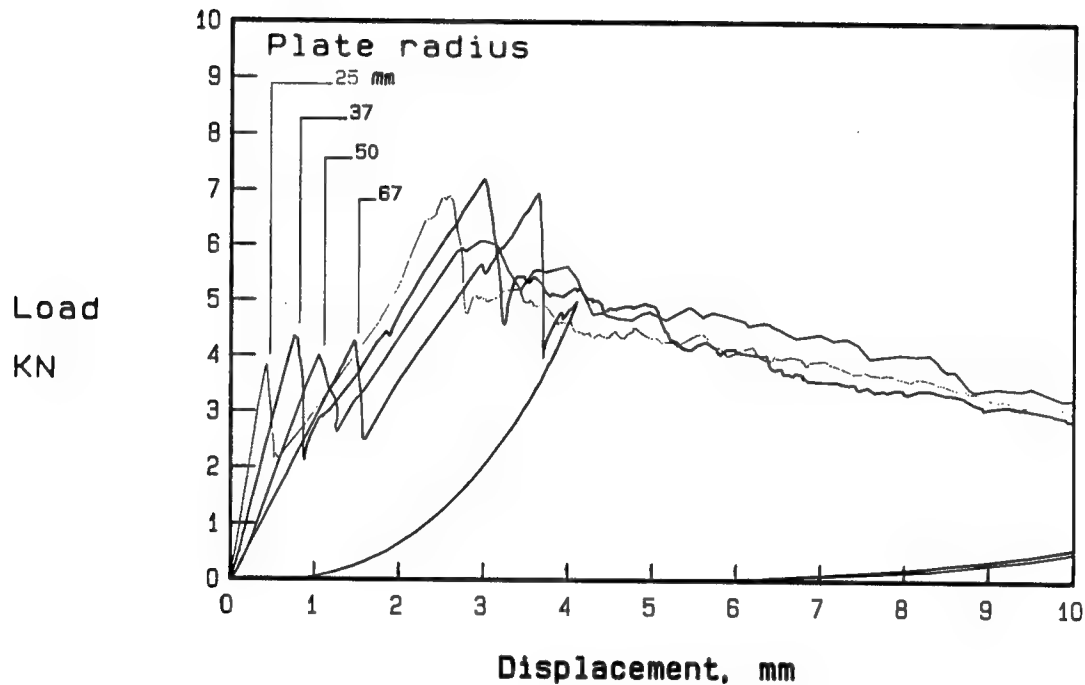


Figure 13

IMPACT FAILURE CRITERIA

The onset of delamination failure has been correlated with the punching shear stress on a cylinder of the diameter of the indentation circle. For the three thicknesses tested, a single critical shear strength describes the critical delamination load. This is shown in the left half of figure 14. The onset of membrane penetration by fiber failure has been correlated with the membrane tension strain under the load point. For the three thicknesses, a single value of ultimate strain described the critical displacements for both the first membrane instability point where one or more of the inner plies break and a second instability where the lower ply breaks. This is shown in the right half of figure 14.

5208/T300 GRAPHITE EPOXY LAMINATES

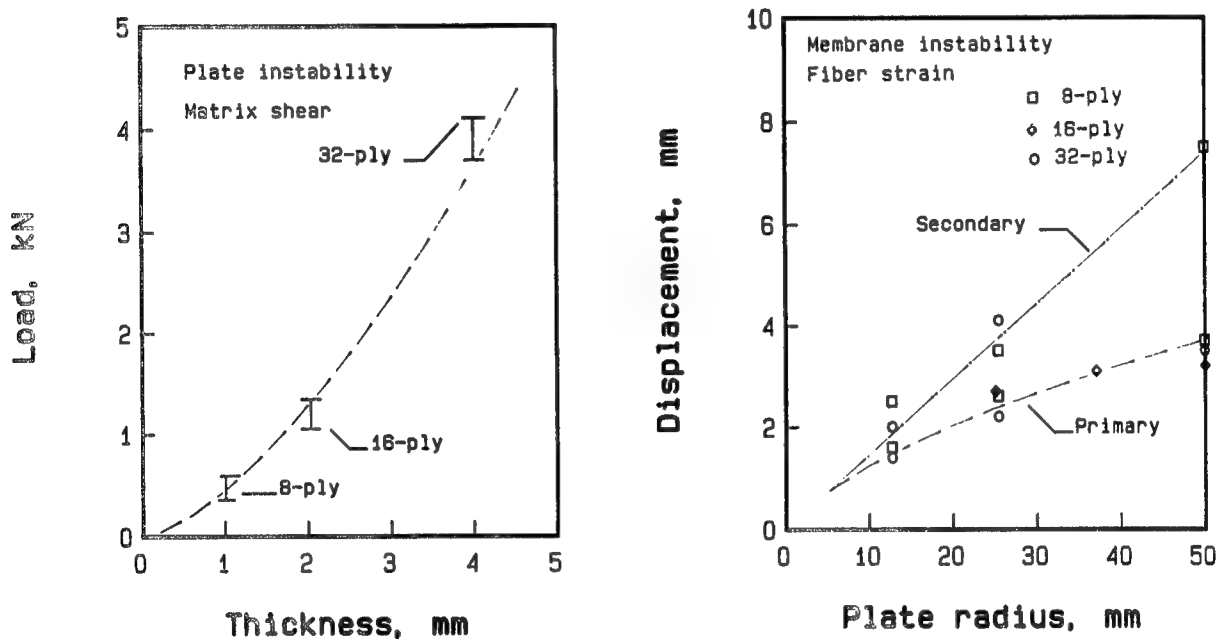


Figure 14

ENERGY LIMITS

Although generally the matrix properties are assumed to limit the impact resistance of composite laminates, improvements in matrix properties will result in fiber-initiated impact failures. In the left half of figure 15, the shaded area represents an upper bound on the impact energy up to the onset of penetration, based on the assumption that the matrix will not fail before fiber failure. In the right half of figure 15, this upper bound energy has been plotted against the support conditions for two types of fibers. The data from T300/5208 show that for the larger 8-ply plates, the impact resistance is essentially at the fiber limit.

8-ply T300/5208 clamped plates

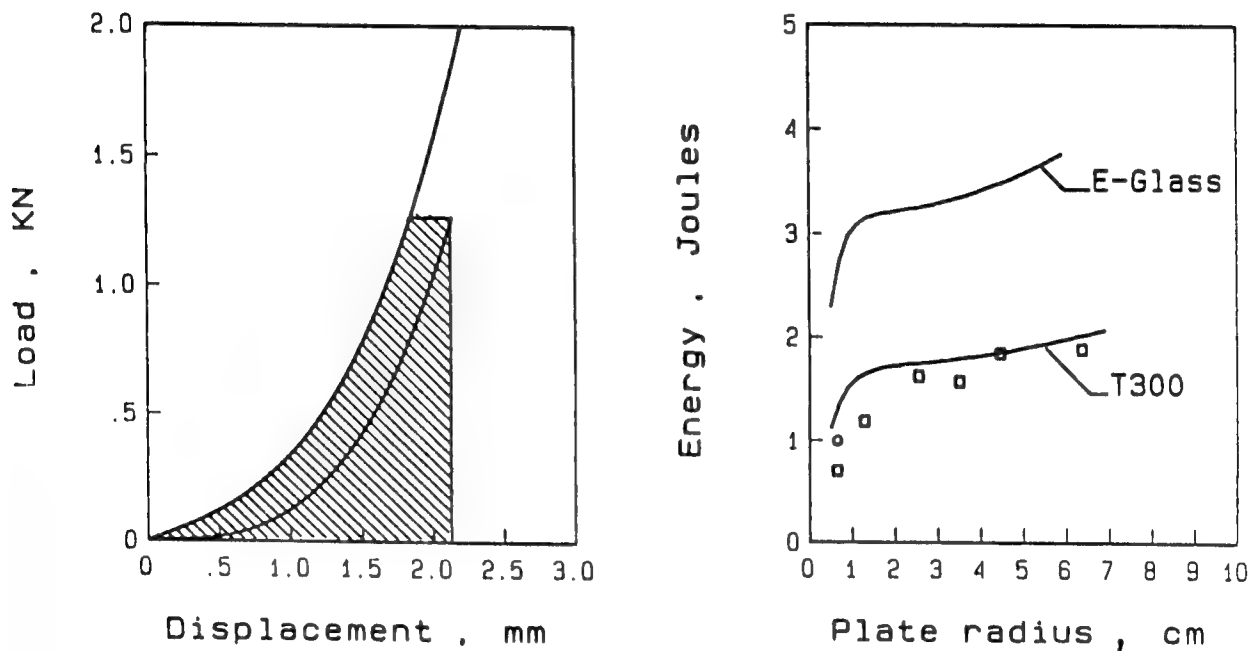


Figure 15

EFFECT OF MATRIX TOUGHNESS (I)

The polysulfone matrix P1700 is significantly tougher than the epoxy 5208. But, as expected, the load displacement plots in figure 16 for the two materials based on 8-ply 4-inch-diameter specimens do not show a difference because the failure is essentially fiber controlled.

8-ply, 100mm plates of 5208/T300 and P1700/C6000

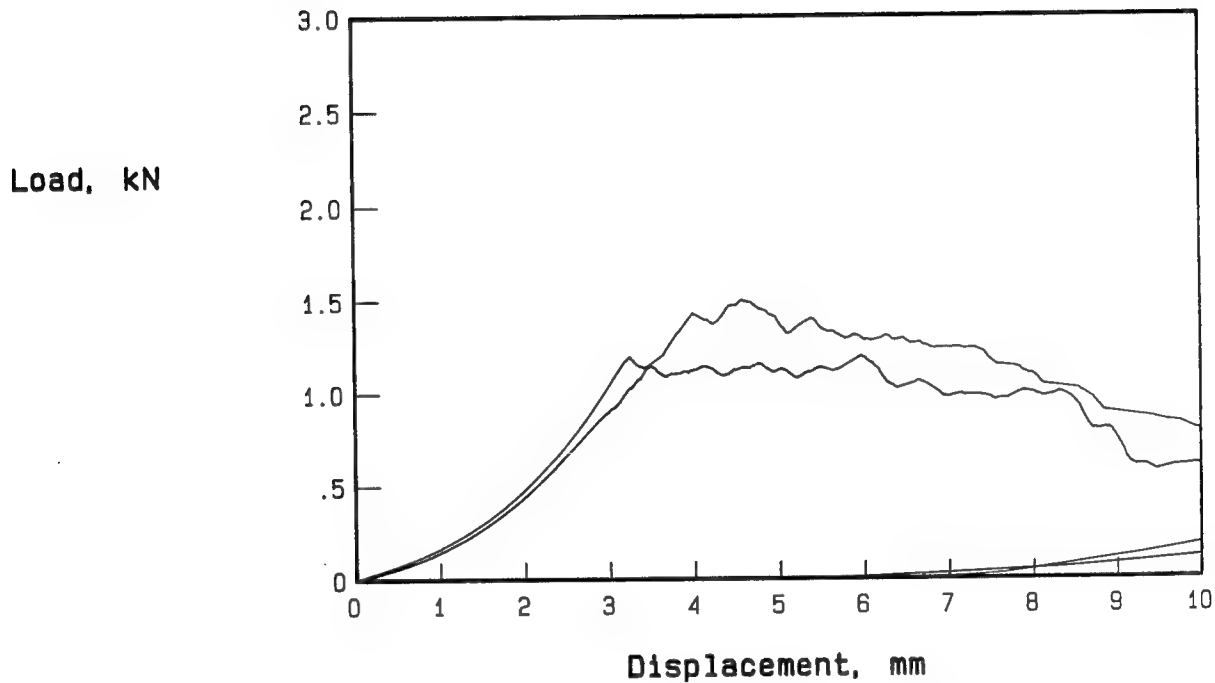


Figure 16

EFFECT OF MATRIX TOUGHNESS (II)

For smaller diameter plates, a small difference in load displacement relations in figure 17 is apparent. As in the 4-inch plate, fiber failure starts at smaller displacements than for the 5208 matrix because the stronger matrix retains much of the flexural stresses. The increased energy absorption comes largely during the penetration phase.

8-ply, 50-mm plates of 5208/T300 and P1700/C6000

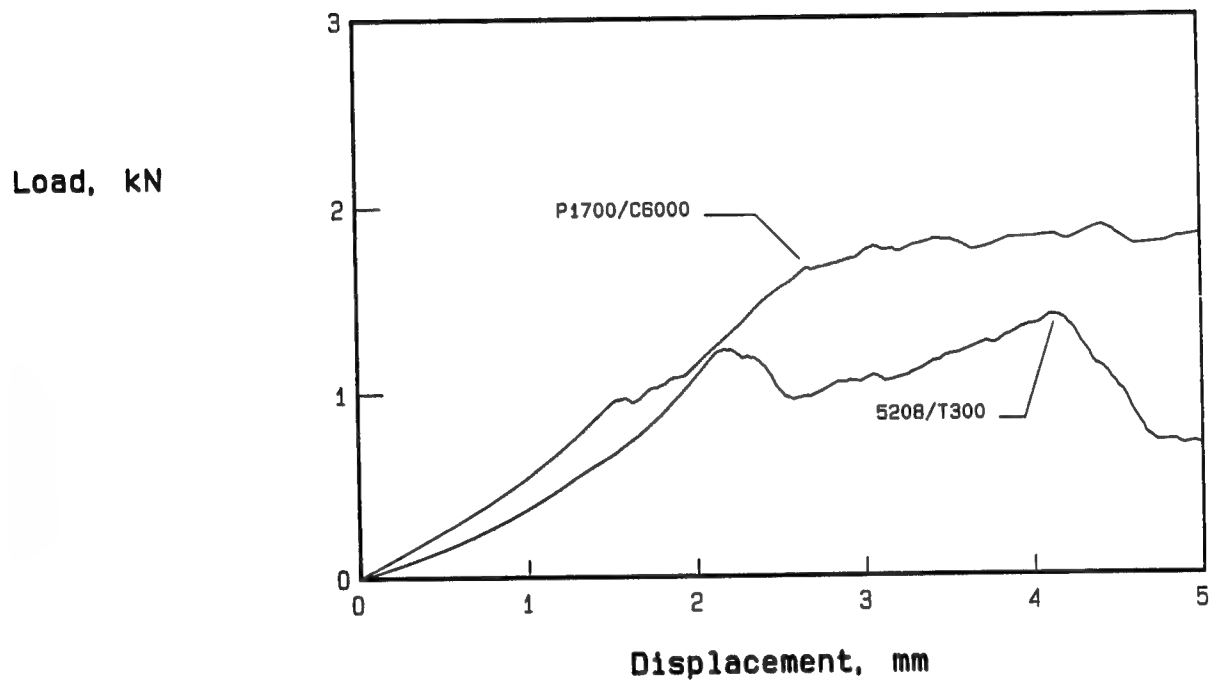


Figure 17

EFFECT OF MATRIX TOUGHNESS (III)

For the 1/2-inch-diameter support condition, the effect of matrix toughness becomes apparent before the onset of penetration, as shown in figure 18. Here the shear load on the matrix is high enough that matrix toughness contributes significantly to the energy absorption before the onset of fiber failure. In testing for impact resistance, it is therefore important to select the support conditions to reveal the effect of matrix properties.

8-ply, 13-mm plates of 5208/T300 and P1700/C6000

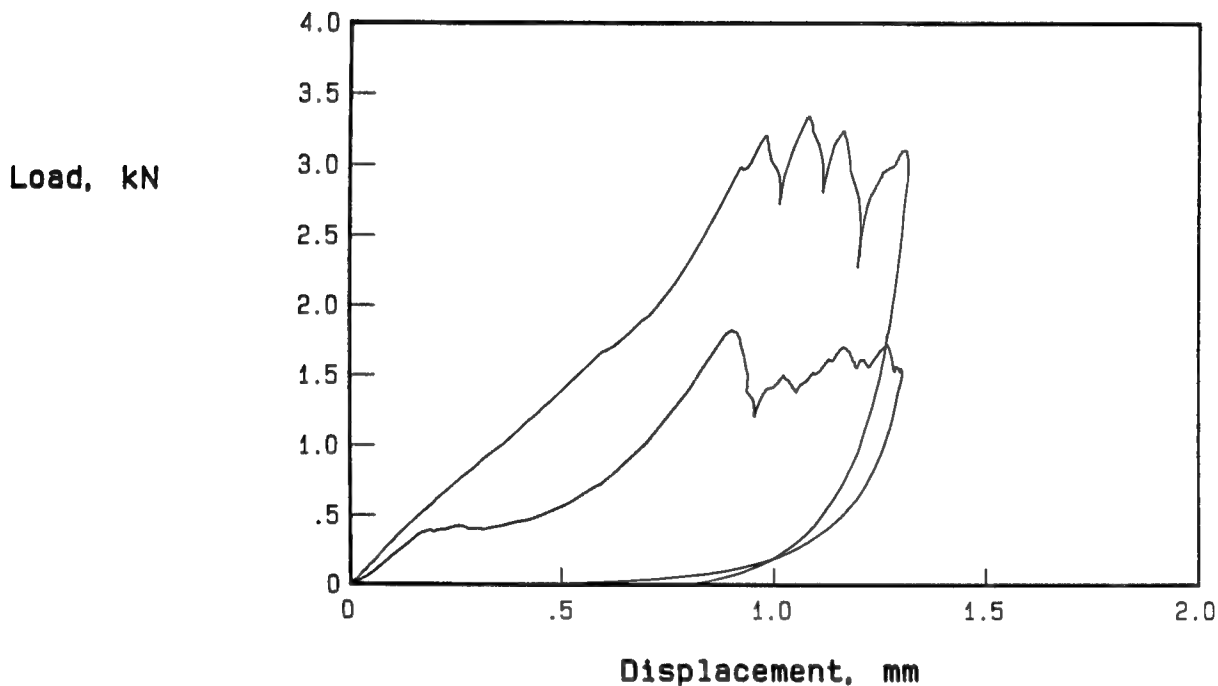


Figure 18

DELAMINATION ANALYSIS

The size of the delaminated area is a significant parameter in determining the residual compressive strength of impacted plates. Figure 19 shows that our static tests produce essentially the same delamination as impact tests taken to the same load or energy.

50 mm diameter 8-ply plates (T300/5208) .

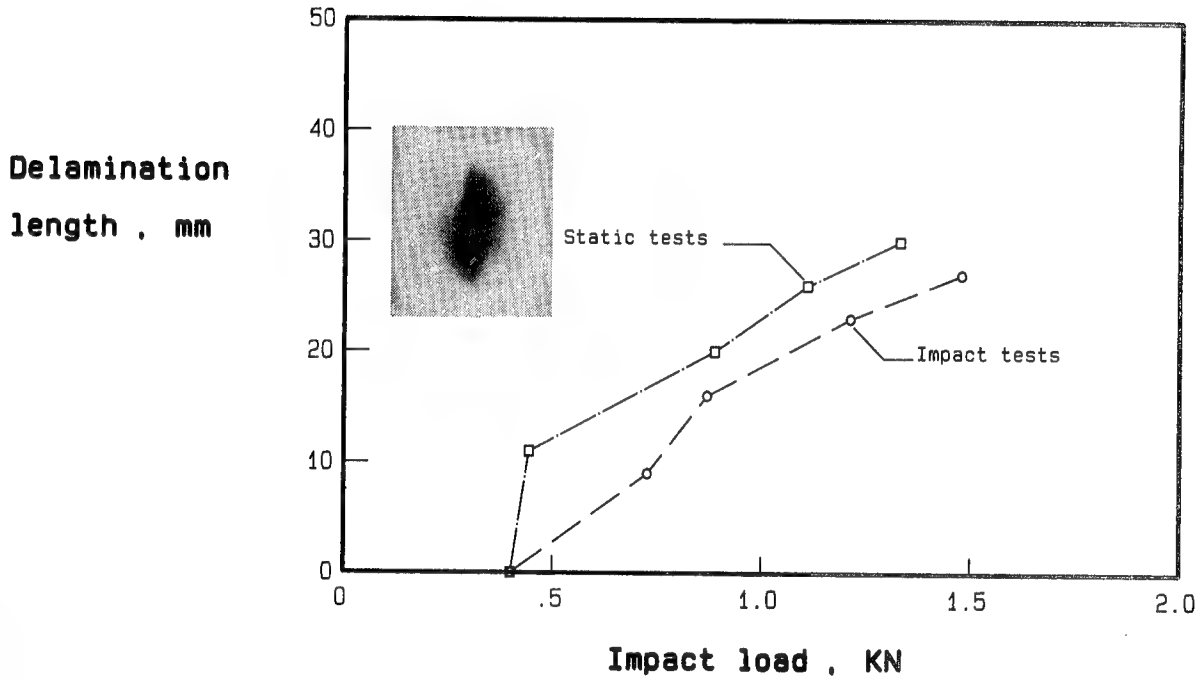


Figure 19

IMPACT FIBER DAMAGE

To reveal the amount of fiber damage and the sequence of damage, some impacted laminates were thermally deplied, separated into individual layers, and then divided into narrow fiber bundles representing essentially the original fiber tows. This process is shown in figure 20. These tows were then tension tested to establish the fiber damage from their residual strength (ref. 2).

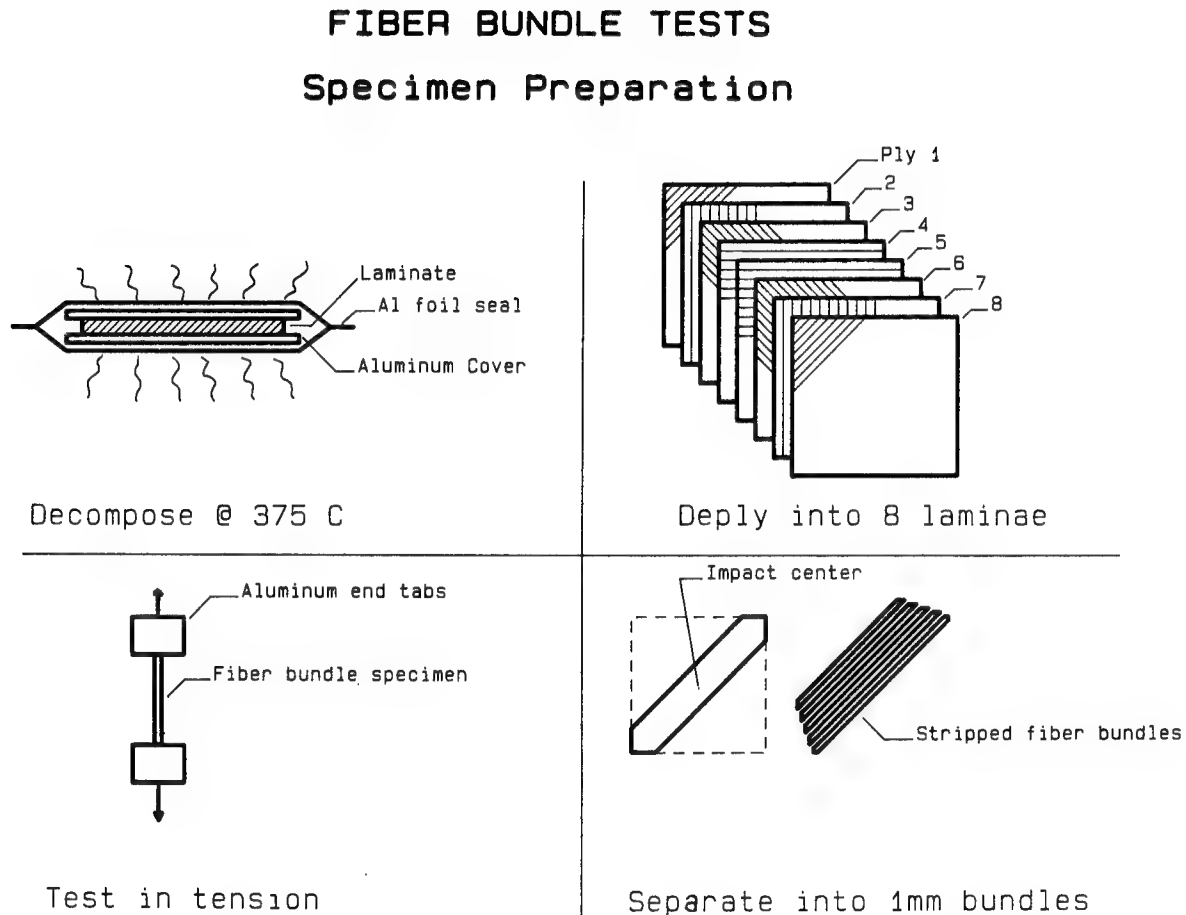


Figure 20

FIBER DAMAGE ANALYSIS

Figure 21 represents a scan of the residual tow strength in the vicinity of the impact center for an 8-ply plate tested to beyond the fiber damage onset. The most significant damage is found in the seventh ply (one layer from the back face). The eighth ply shows some damage, but no tow was completely broken. In the upper four plies (not shown), there was essentially no fiber damage.

Impact test to 1.04 Joules

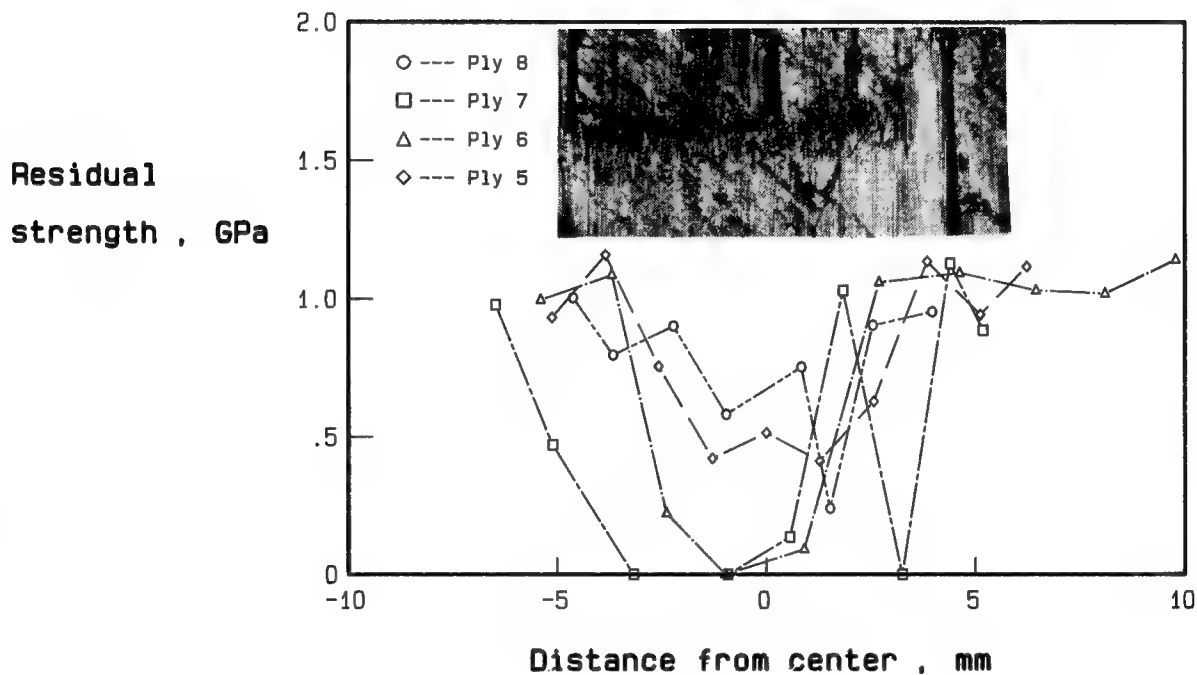


Figure 21

SUMMARY

Static indentation tests can provide better information about failure processes than impact tests, and they are simpler to conduct. In thin and thick laminates, we found that the matrix shear strength controls the onset of delamination damage and that the fiber strength controlled the penetration phase. In thin laminates, tough matrices do little to enhance impact resistance. Higher strain fibers would be required (fig. 22).

- * Matrix shear strength dominates the damage threshold especially in thick laminates.**
- * Matrix toughness dominates the type and extent of impact damage.**
- * Fiber ultimate strain dominates the membrane penetration energy.**
- * Tough composites require both tougher matrices and tougher fibers.**
- * Excessively strong matrix materials can result in brittle composites.**

Figure 22

REFERENCES

1. Bostaph, G. M.; and Elber, W.: Static Indentation Tests on Composite Plates for Impact Susceptibility. Proceedings of the Army Symposium on Solid Mechanics, 1982--Critical Mechanics Problems in Systems Design, AMMRC-MS-82-4, Sept. 1982, pp. 288-317.
2. Elber, W.: Failure Mechanics in Low-Velocity Impacts on Thin Composite Plates. NASA TP-2152, May 1983.

SESSION II

CONSTITUENT PROPERTIES AND INTERRELATIONSHIPS

CHAIRMAN: R. F. LANDEL

FUNDAMENTAL STUDIES OF COMPOSITE TOUGHNESS

Kenneth J. Bowles
NASA Lewis Research Center
Cleveland, Ohio

INTRODUCTION

As a part of our work in the area of tougher composites at the Lewis Research Center, we are conducting fundamental studies of composite toughness. In this study, it is expected that relationships between neat resin matrix properties and composite toughness characteristics can be established. We can then use these relationships to either specify or evaluate candidate tougher composite matrices. It is also expected that the results from this study will contribute to the ongoing effort to better understand composite toughness.

The overall approach in this research program is presented in Figure 1. The first five steps have been completed and work to complete step six is now in progress. Two of these steps merit special discussion. The first is step one. Four resins with a wide range of mechanical properties were selected as matrix materials to highlight any subtle relationships which might exist between resin properties and composite toughness. In the selection process, special consideration was given to tensile modulus, tensile strength and strain to yield or failure. Step five, the evaluation of impact behavior and measurement of interlaminar fracture toughness, was the key step in which composite toughness was evaluated. These two tests were chosen to assess damage threshold and damage propagation characteristics of the composites. Only the impact test results have been analyzed and will be discussed in this presentation.

OBJECTIVE: ESTABLISH RELATIONSHIPS BETWEEN BULK RESIN PROPERTIES
AND COMPOSITE TOUGHNESS

- APPROACH:**
1. SELECT FOUR RESINS WITH A WIDE RANGE OF MECHANICAL PROPERTIES.
 2. CHARACTERIZE EACH OF THE FOUR RESINS AS COMPLETELY AS POSSIBLE.
 3. FABRICATE COMPOSITES WITH THE SELECTED RESINS AS MATRICES.
 4. MEASURE MECHANICAL PROPERTIES OF THE PROCESSED COMPOSITES.
 5. EVALUATE IMPACT BEHAVIOR AND MEASURE INTERLAMINAR FRACTURE TOUGHNESS OF THE PROCESSED COMPOSITES.
 6. DETERMINE VALID RELATIONSHIPS BETWEEN RESIN PROPERTIES AND COMPOSITE TOUGHNESS.

Figure 1

MATERIALS

The materials that were used in this study are shown in Figure 2. The fiber is unsized Celion 6000 graphite fiber. The four resins are also listed along with general statements on the magnitude of the strength properties which were pre-determined to be most important in this study. Three of these resins are epoxies and one is a polysulfone. The first two resins were used in the as-received state. The last two are mixtures of Ciba-Geigy 6010 and Ciba-Geigy 508, a flexibilized resin. The flexibilized 508 resin is a mixture of the 6010 resin and a polyol. Figure 3 presents the designation of the matrix resins, the type of polymer along with the applicable mixing ratio and the type of hardener for each of the four resins. In Figure 4 the general chemical structures are presented.

FIBER: CELION 6000.

RESINS:

- ***FIBERITE 930 EPOXY. HIGH T.S. LOW STRAIN TO FAILURE. HIGH MODULUS.***
- ***UNION CARBIDE P-1700 POLYSULFONE. HIGH T.S. HIGH STRAIN TO FAILURE. MEDIUM MODULUS.***
- ***CIBA-GEIGY 6010-508-840 EPOXY. LOW T.S. HIGH STRAIN TO FAILURE. LOW MODULUS.***
- ***CIBA-GEIGY 6010-508-956 EPOXY. LOW T.S. VERY HIGH STRAIN TO FAILURE. VERY LOW MODULUS.***

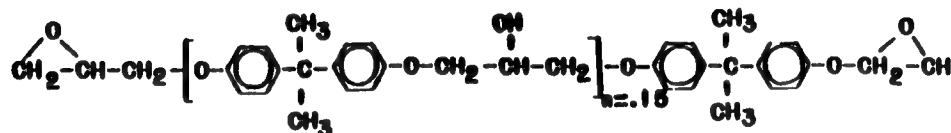
Figure 2

RESIN SYSTEMS

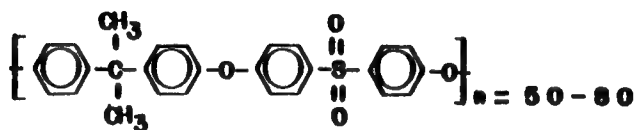
DESIGNATION	RESIN	HARDENER
930	DGEBA	DIAMINE
P1700	POLYSULFONE	
840	DGEBA:DGEBA + PO = 1:1	POLYAMIDE
956	DGEBA:DGEBA + PO = 2:3	TETRAMINE

Figure 3

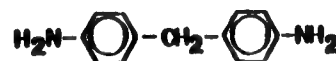
RESINS AND HARDENERS STUDIED



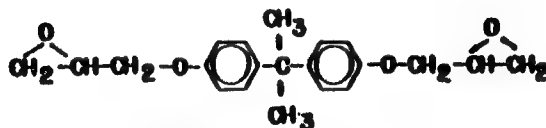
FIBERITE 930



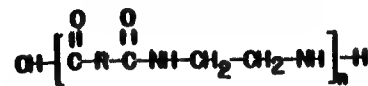
UNION CARBIDE P 1700



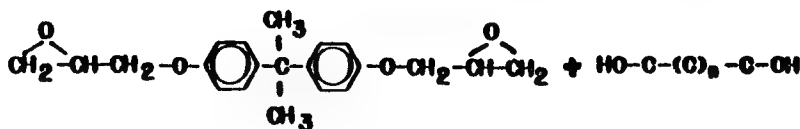
FIBERITE HARDENER



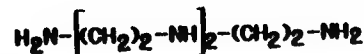
CIBA-GEIGY 6010



CIBA-GEIGY 840 HARDENER



CIBA-GEIGY 508



CIBA-GEIGY 956 HARDENER

Figure 4

RESULTS

A listing of the more significant resin properties measured is shown in Figure 5. Most of the properties were measured using standard test methods except for the fracture toughness, impact and dynamic moduli. Fracture toughness testing was done using compact tensile specimens. The impact testing was done on six inch square plates, clamped along all four edges, with an instrumented drop-weight impact tester, and dynamic shear moduli were measured using a commercially available dynamic mechanical spectrometer. The resin mechanical and physical properties, with the exception of compression and relaxation data, are presented in Figure 6. The data shown in Figure 6 clearly show the wide range in tensile properties of the resins. Strain to failure was not measured for the P-1700 polysulfone because at a strain of about 10-15 percent, the specimens sustained severe necking in the gage section. The strain to failure was calculated from the reduction in area, but there was much scatter in the data.

The manufacturers mechanical properties data for the graphite fiber are presented in Figure 7. The values listed for Poisson's ratio and the longitudinal thermal expansion are best estimates provided by the vendor.

RESIN PROPERTIES

- **TENSILE PROPERTIES.**
- **COMPRESSIVE PROPERTIES.**
- **FRACTURE TOUGHNESS.**
- **INSTRUMENTED IMPACT.**
- **DYNAMIC MODULI.**
- **RELAXATION.**
- **DENSITY.**

Figure 5

BULK PROPERTIES OF MATRIX RESINS

RESIN	E(KSI)	σ_y (KSI)	ϵ_y	ϵ_f	ν	G(KSI)	SPECIF. GRAVITY	α ($\text{MM/MM}^\circ\text{F}$) ⁺⁺	T_g ($^\circ\text{F}$) ⁺⁺
930	657	12.9	- -	0.019	0.36	236.4	1.335	29.5×10^{-6}	250
P-1700	344.6	11.9	.057	0.50 ⁺	0.37	134.6	1.240	31.5×10^{-6}	369
840	255	4.9	.03	0.35	0.44	82.6	1.146	64.7×10^{-6}	137
956	160	3.2	.05	0.50	0.365	52.2	1.179	38.8×10^{-6}	109

E = TENSILE MODULUS
 G = SHEAR MODULUS
 ν = POISSON'S RATIO
 σ_y = YIELD STRENGTH
 ϵ_y = YIELD STRAIN
 ϵ_f = ULTIMATE ELONGATION

α = COEFFICIENT OF
 THERMAL EXPANSION
 T_g = GLASS TRANSITION
 TEMPERATURE

⁺LOCAL NECKING PRECEDES FRACTURE

⁺⁺TMA MEASUREMENT

Figure 6

CELION 6000 PROPERTIES

LOT	1231	2531
TENSILE MODULUS	34.4 MSI	34.7 MSI
TENSILE STRENGTH	513 KSI	533 KSI
ULTIMATE ELONGATION	1.49 %	1.54 %
POISSON'S RATIO	0.3	0.3
SPECIFIC GRAVITY	1.77	1.77
COEFF. OF THERMAL EXP. (LONG.)	$-0.3 \times 10^{-6}/^\circ\text{F}$	$-0.3 \times 10^{-6}/^\circ\text{F}$

Figure 7

NEAT RESIN IMPACT RESISTANCE

Figure 8 shows some of the results of the neat resin impact tests. The left ordinate is the amount of energy absorbed at failure. The right ordinate is the scale for the load at failure as measured by the instrumented tup of the tester. The ranking of toughness for the four resins is the same regardless of which of the two quantities is used as a basis for ranking ($P-1700 > 956 > 840 > 930$). If the load at failure were chosen as the basis for comparison, the resin toughness would be a function of the strain at failure or yield. When one evaluates resin toughness on the basis of energy absorbed up to failure, one finds that the toughness is a function of the fraction of the load carried by the diaphragm action of the resin plate. This in turn is a function of yield strength and tensile modulus. From the results of this study, the toughness of neat resin materials, as assessed using the drop weight impact test, can be ranked using the resin stress-strain diagram.

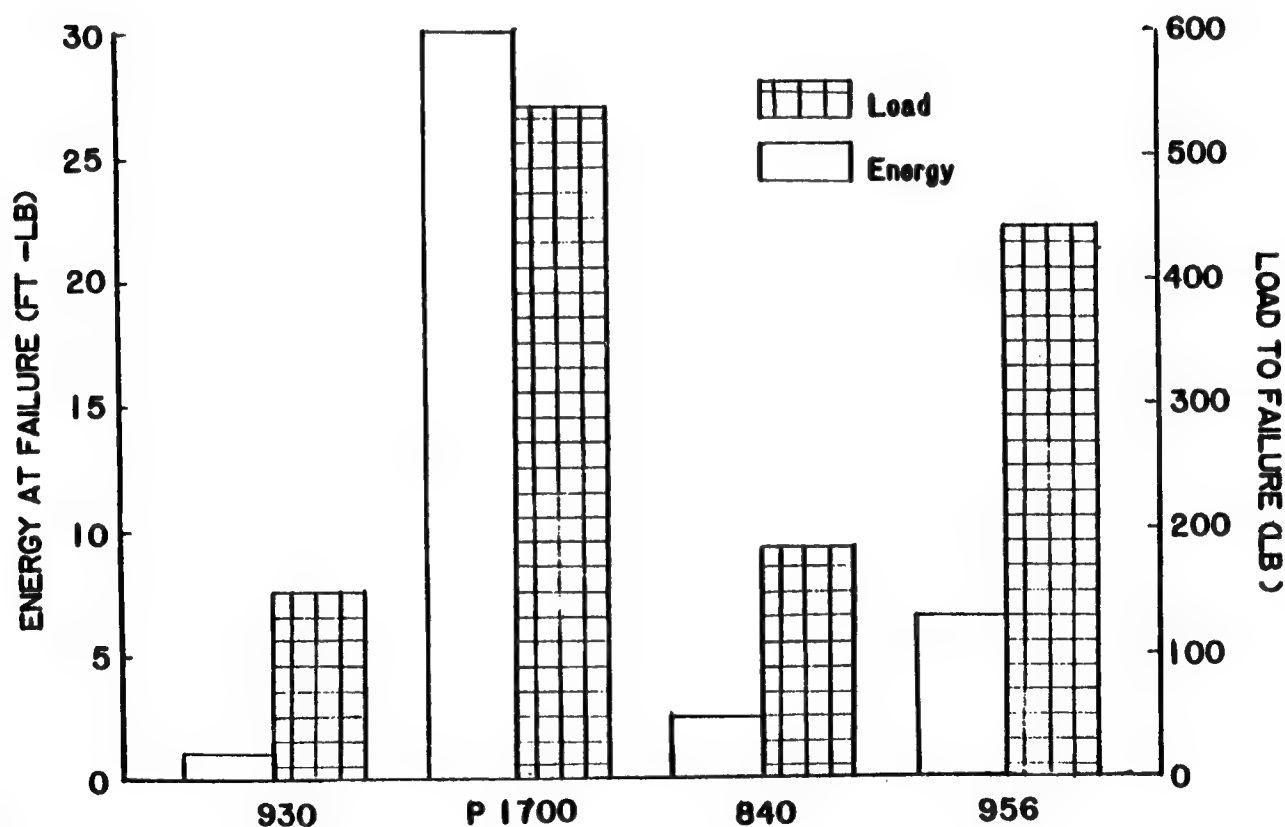


Figure 8

LOAD DEFLECTION CURVES

The instrumentation associated with the drop weight impact tester actually measures three variables. These variables are time, load and tup speed. The energy and displacement values are calculated from the last two of these measured values. In order to check the validity of these calculations, static load deflection tests were run on both resin and cross-ply composite plates. Figure 9 shows the results of these tests for a 956 resin plate. The solid line represents the load deflection curve from the impact tests. The open circles are data from the static tests. Disregarding the initial 0.08 inch deflection of the statically loaded specimen, the final portion of this curve is somewhat similar to the curve from the impact test. If the slopes of these two curves are considered as moduli, the modulus of the impacted specimen appears to be slightly greater than that of the statically loaded specimen after 0.08 inches of deflection. The same type of data are presented for a crossplyed composite in Figure 10. There is very close agreement between the results of the two types of tests. From the results of this work, one can be assured that the data generated by the drop weight impact tester are valid data. Also, it is evident that plate displacement reactions to low velocity impact can be simulated by static testing methods.

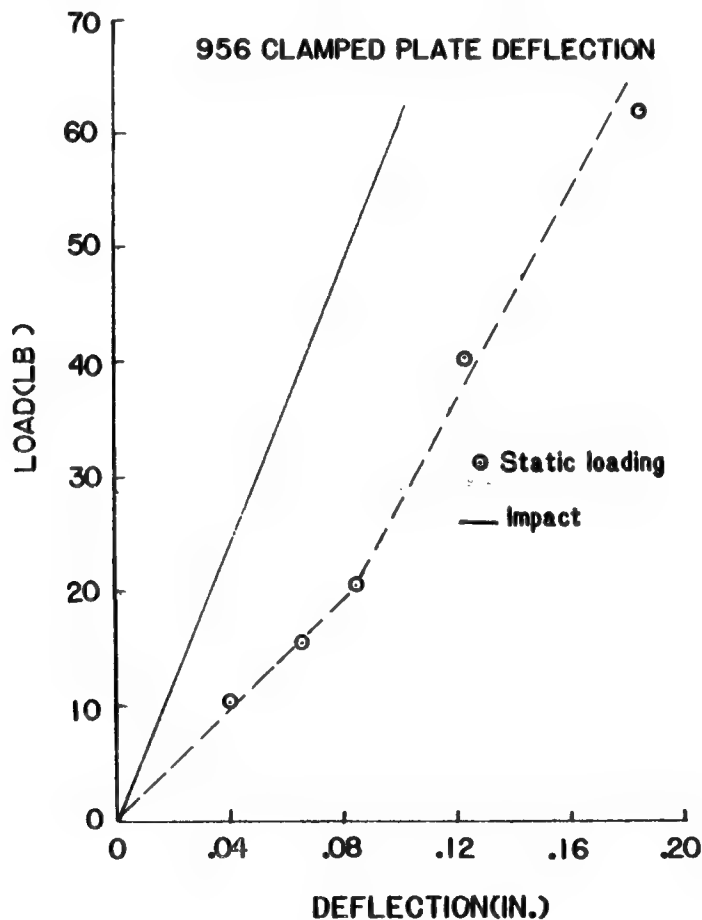


Figure 9

840/CELION 6000 PLATE DEFLECTIONS

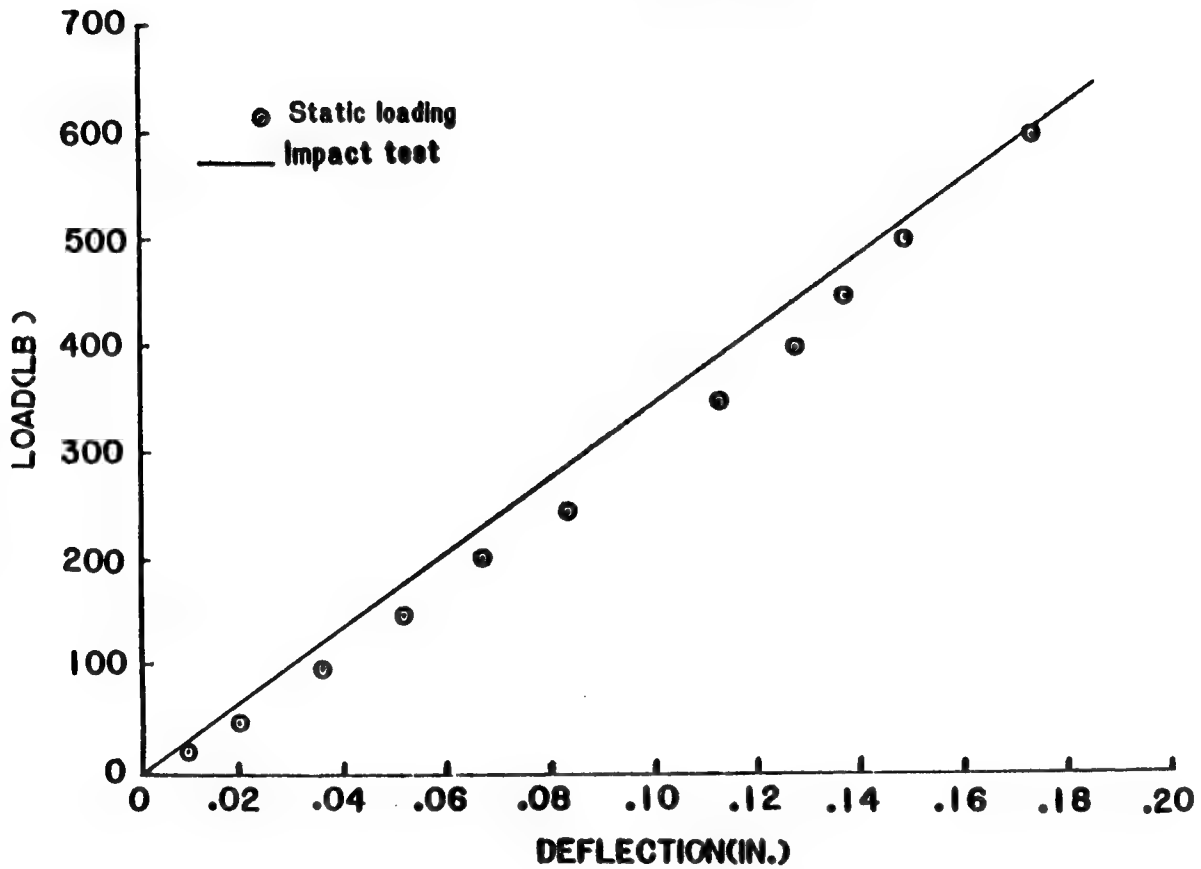


Figure 10

COMPOSITE PROPERTIES TESTS

Listed in Figure 11 are the tests that were used to generate the broad range of composite properties that are being studied for potential correlation with neat resin data. In this presentation only the results from the instrumented impact tests of crossplied composites will be discussed. The dynamic moduli and instrumented impact tests were conducted using the same equipment that was used for similar neat resin tests. The fracture toughness testing was done using double cantilever beam specimens. The impact tests utilized crossplied specimens having a thickness of 0.1 or 0.2 inches and unidirectional specimens having a thickness of 0.1 inch. Four specimens were tested for the 0.1 inch composites; two specimens were tested for the 0.2 inch composites; four specimens were tested for the unidirectional composites. The 0.2 inch thick specimens were subjected to an impact energy of 31 foot-pounds which was enough to initiate damage but not to cause thorough penetration. The 0.1 inch thick specimens were subjected to full penetration.

- **LONGITUDINAL TENSILE.**
- **TRANSVERSE TENSILE.**
- **10 DEGREE OFF AXIS.**
- **INTERLAMINAR FRACTURE TOUGHNESS (MODE I).**
- **BENDING MODULUS.**
- **INSTRUMENTED IMPACT.**
- **DYNAMIC MODULI.**

Figure 11

COMPOSITE DROP WEIGHT IMPACT TEST TRACES

Load deflection traces are shown for each of the four types of thin, crossplied specimens in Figure 12. These traces show two different types of reaction to impact. The upper two traces for the 930 and P-1700 matrix composites show a linear increase in load to failure. After failure initiates, the load either drops off or maintains an approximately constant value. Traces of the 840 and 956 matrix specimens show a linear increase in load up to the point where some damage initiates. After damage initiation, the slope of the load deflection curve then decreases, but still remains linear up to the point of full failure where the load then drops abruptly. When one examines the energy curves (the lower curves in each plot), one can see that at full failure both the 930 composite and the P-1700 composite have absorbed only 6 foot-pounds of energy. In comparison, the 840 and 956 composites have absorbed 15 and 13 foot-pounds respectively. Any energy absorbed by the specimen after full failure is not useful energy. Visual examination of 840 and 956 composite specimens which were not fully penetrated indicated compressive failure at the point of incipient damage in the traces for the 840 and 956 composites in Figure 12. Even for an apparently fiber dominated test such as this, resin properties do appear to have an effect on the initiation of damage and possibly the propagation of damage through the composites.

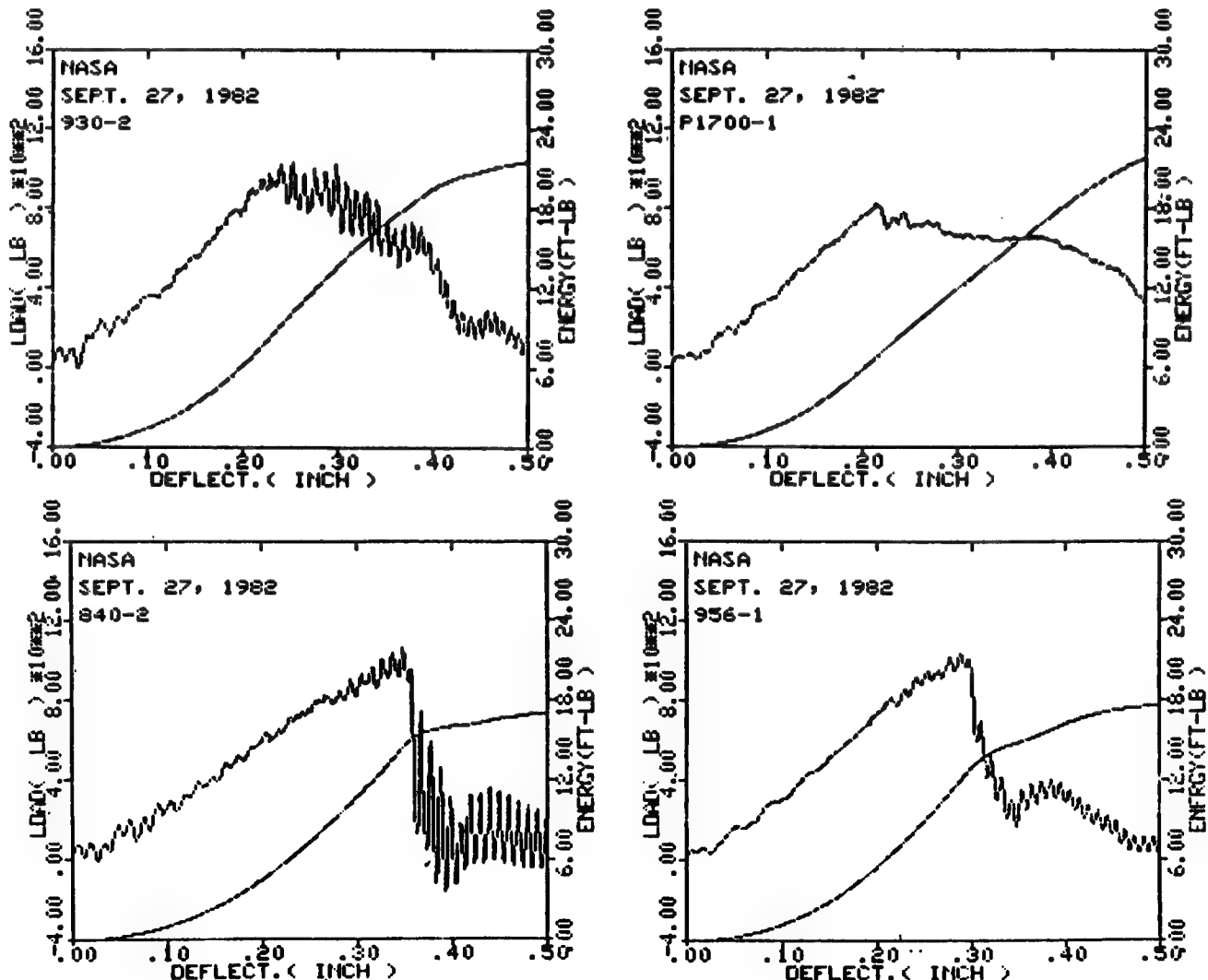


Figure 12

CONCLUDING REMARKS

Evaluation of drop weight impact testing of neat resin and crossplied graphite fiber reinforced composites has resulted in the development of three conclusions (Figure 13). Both geometric and composite constituent materials properties influence the drop weight impact resistance of crossplied composite plates. The matrix influence appears to be reflected in the incipient damage mechanism and the propagation of damage.

The future work in the area of tougher composites at the Lewis Research Center will be directed toward tougher, higher temperature composites. As a propulsion laboratory, we are interested in materials for aircraft engines. We propose to establish a data base for PMR-15 polyimide composites which are finding increased use in aircraft engine structures. This data base will be used as a reference against which we can evaluate the performance of newly developed, tougher, higher temperature composites.

1. DURING IMPACT OF CROSS-PLY LAMINATES, RESIN PROPERTIES APPEAR TO INFLUENCE THE EXTENT AND MECHANISM OF DAMAGE PROPOGATION.
2. BY ITSELF, NEAT RESIN STRAIN TO FRACTURE IS NOT A CONTROLLING INFLUENCE ON RESIN OR COMPOSITE FRACTURE TOUGHNESS.
3. IMPACT FAILURE ENERGY OF NEAT RESIN PLATES CAN GIVE A MISLEADING INDICATION OF THE RESIN CONTRIBUTION TO COMPOSITE IMPACT BEHAVIOR BECAUSE OF DIFFERENCES IN THE MAGNITUDE OF DIAPHRAGM ACTION IN THE TWO SYSTEMS.

Figure 13

INVESTIGATION OF TOUGHENED NEAT RESINS AND THEIR RELATIONS
TO ADVANCED COMPOSITE MECHANICAL PROPERTIES

R.S. Zimmerman
University of Wyoming
Composite Materials Research Group

INTRODUCTION

Our program with NASA Langley at the University of Wyoming has been to evaluate four polymer matrix systems chosen for the ACEE technology program. We evaluated four epoxies, Hercules 3502, Hercules 2220-1, and 2220-3, and Ciba-Geigy Fibredux 914 epoxy, to judge their merits within the ACEE program and also to provide material property input for our micromechanics finite element program. During the first year we accomplished a number of tasks: we developed a casting procedure for the four matrix systems mentioned, generated mechanical properties at three test temperatures and two moisture contents and also performed a scanning electron microscope study to catalogue fracture surfaces for the unreinforced (neat) epoxies. We performed tension testing, shear testing, a limited amount of fracture toughness testing, and thermal expansion coefficient and moisture expansion coefficient testing. Mechanical material properties were generated for input into our micromechanics program and to characterize these four matrix systems.

TENSION SPECIMEN CONFIGURATION

The top specimen is the Hercules 3502 epoxy baseline system. This epoxy was chosen as the baseline since it is an untoughened epoxy. The second specimen is the Fibredux 914 epoxy from Ciba-Geigy. The third and fourth systems are the 2220-1 and 2220-3 epoxy systems. The specimens are 6 inches long and 1/10 inch thick. We used these dogbone specimens for all tension testing. They were fabricated using a steel box mold with metal dividers and cast as rectangular pieces. The specimens were then configured into the dogbone shape using a high speed router. (See fig. 1.)

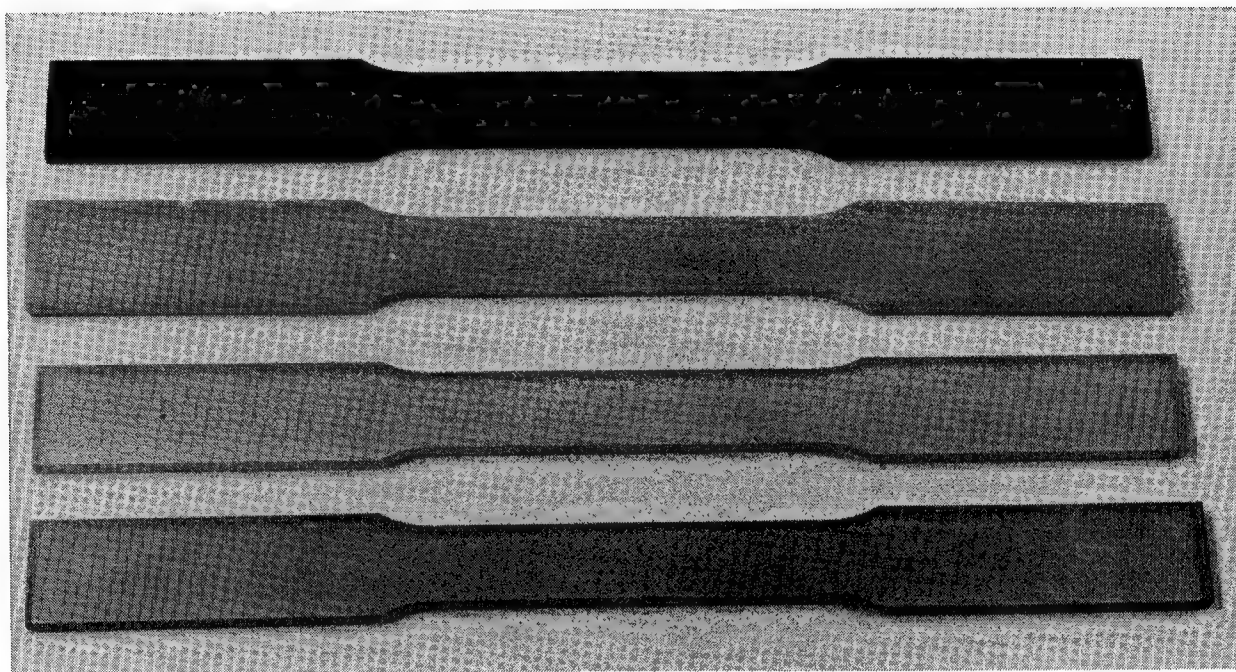


Figure 1

TORSION SPECIMEN

From top to bottom (fig. 2) the specimens are Hercules 3502 epoxy, Ciba-Geigy Fibredux 914, Hercules 2220-1 and 2220-3 epoxies. These were cast using two different methods. The three Hercules thermoset epoxies were easily cast using a steel mold. The Fibredux 914 epoxy from Ciba-Geigy was more difficult to cast. It had a much higher thermal expansion factor than the three systems from Hercules and was cast using a silicone rubber mold.

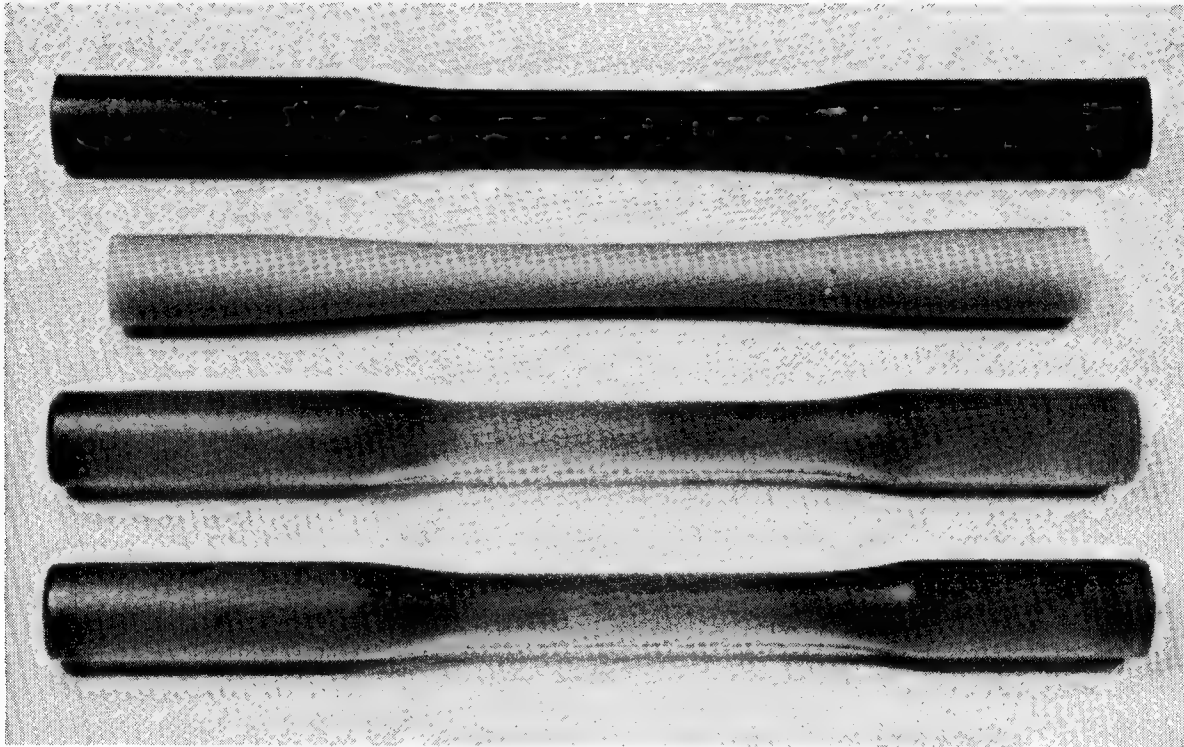


Figure 2

SQUARE STEEL MOLD WITH DIVIDERS AND SPACERS USED TO CAST FLAT TENSILE SPECIMENS

The steel mold in figure 3 was used to cast the 3502, 914 and 2220 epoxy systems. They were then machined into the dogbone shape, as seen in figure 1, using a high speed router.

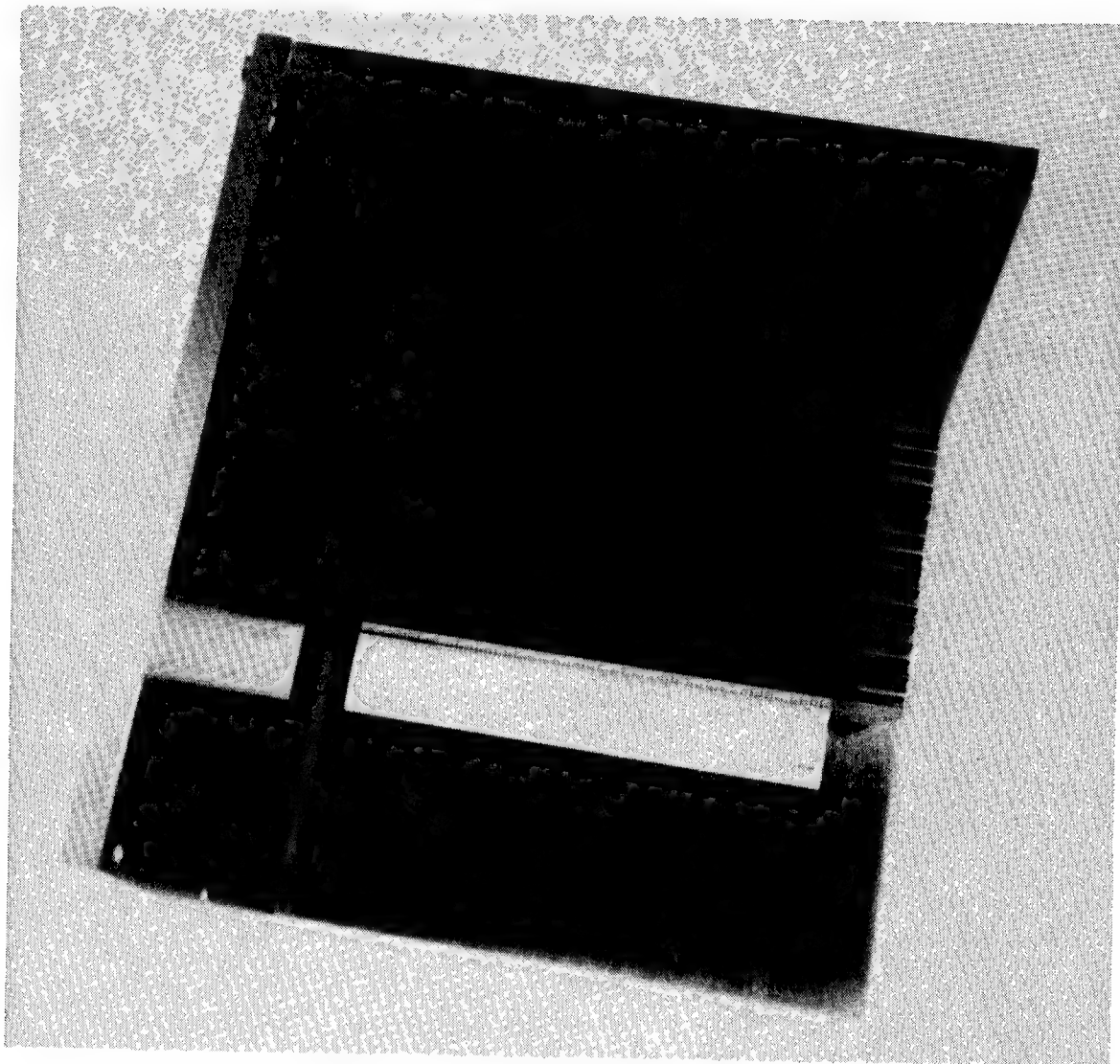


Figure 3

STEEL MOLD AND RUBBER FUNNEL USED TO CAST ROUND DOGBONE TORSION SPECIMENS

The torsion specimens were cast into the dogbone shape directly, as shown in figure 4.

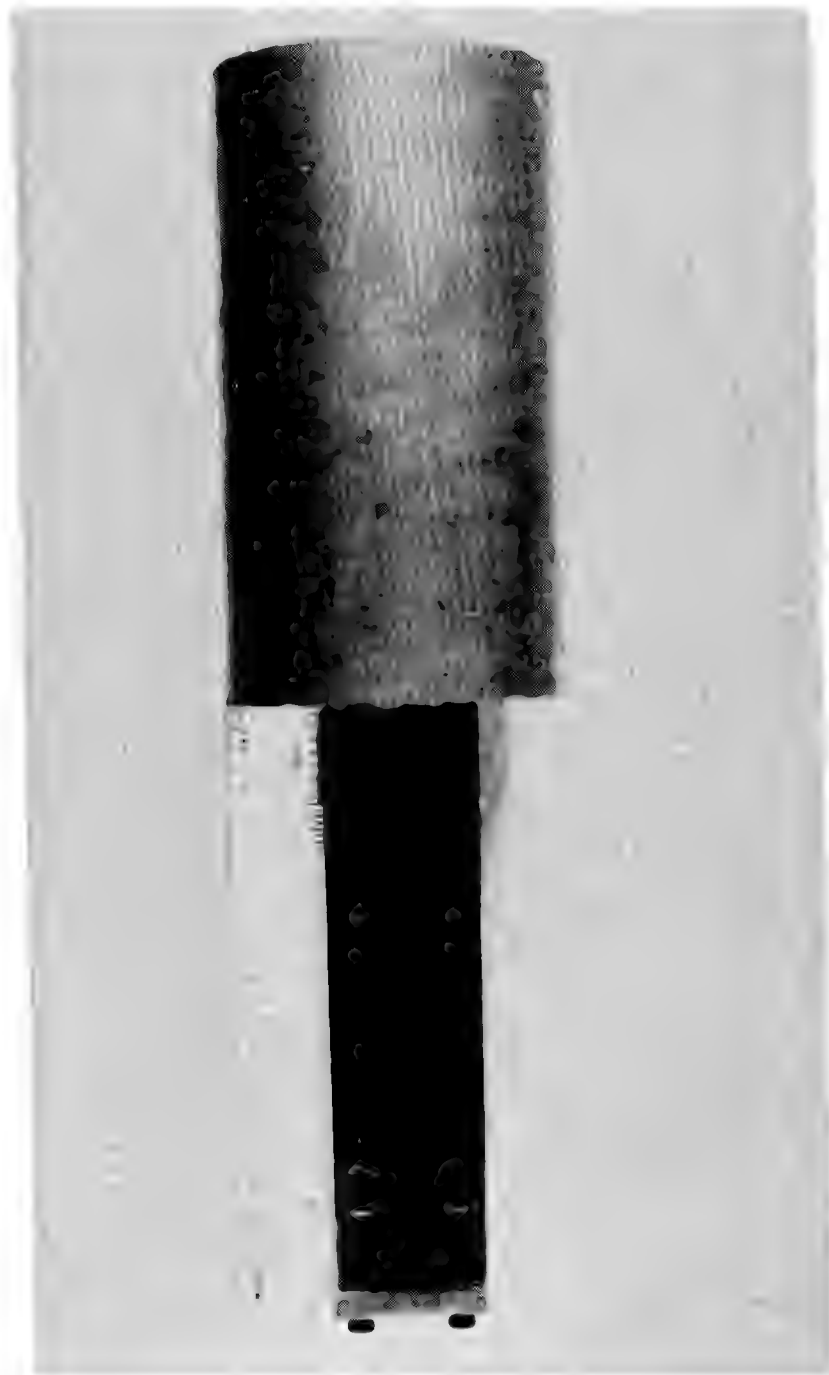


Figure 4

SILICONE RUBBER MOLD USED TO CAST THE CIBA-GEIGY FIBREDUX 914
IN THE ROUND DOGBONE SHAPE

The Fibredux 914 epoxy system was cast using the silicone rubber mold shown in figure 5 instead of the steel mold shown in figure 4 due to its slightly higher thermal expansion coefficient.

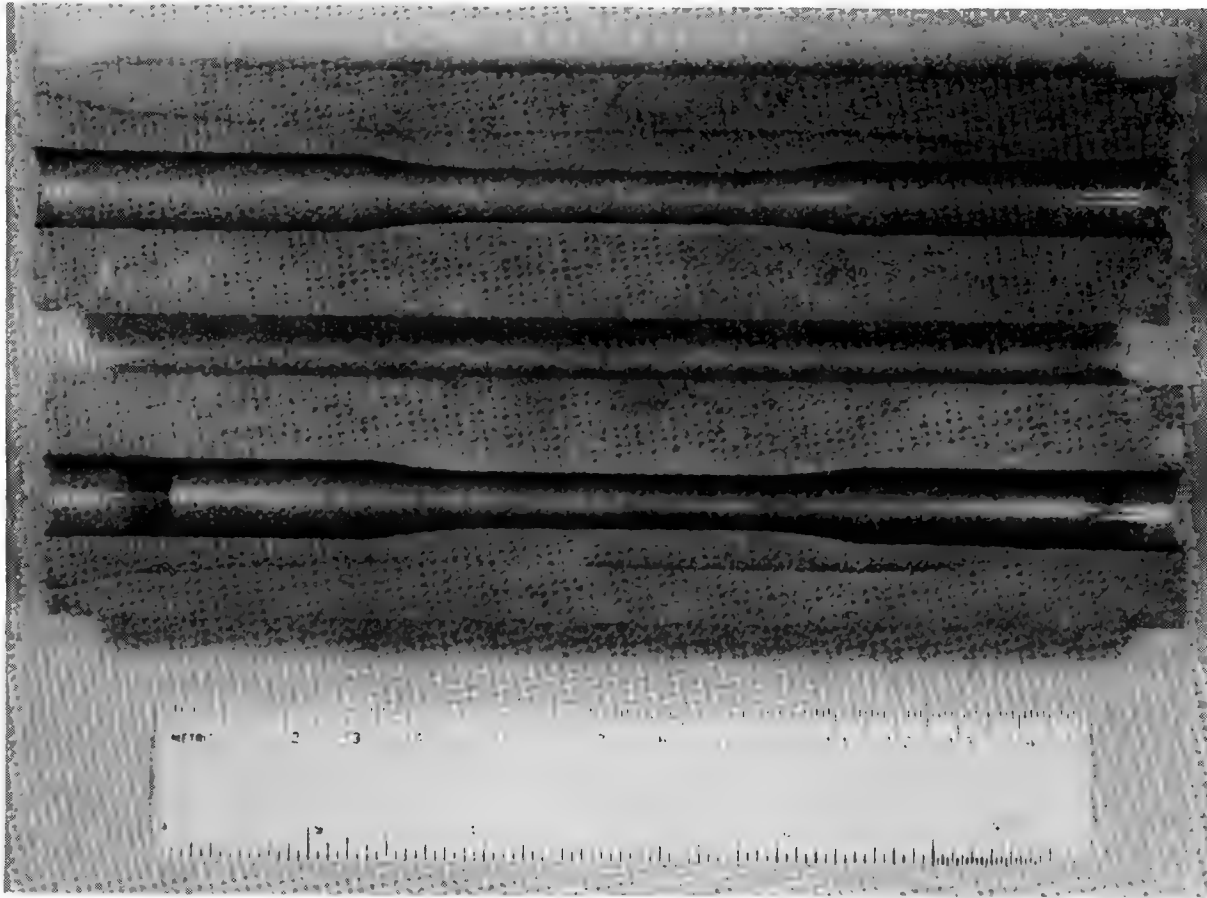


Figure 5

TYPICAL TENSION FAILURE FOR FLAT DOGBONE SPECIMENS

The important features in neat resin tensile failures were noted in a vast majority of the failures. (See fig. 6.) A flat section, at A, is probably the initiation point of the failure. After initiation, a crack propagates across the specimen and then splits as it crosses the specimen and ejects a piece out of one side of the specimen, at B. These features are noted in all but a very few of our tests performed during this program. Note the two-axis strain gage at C.

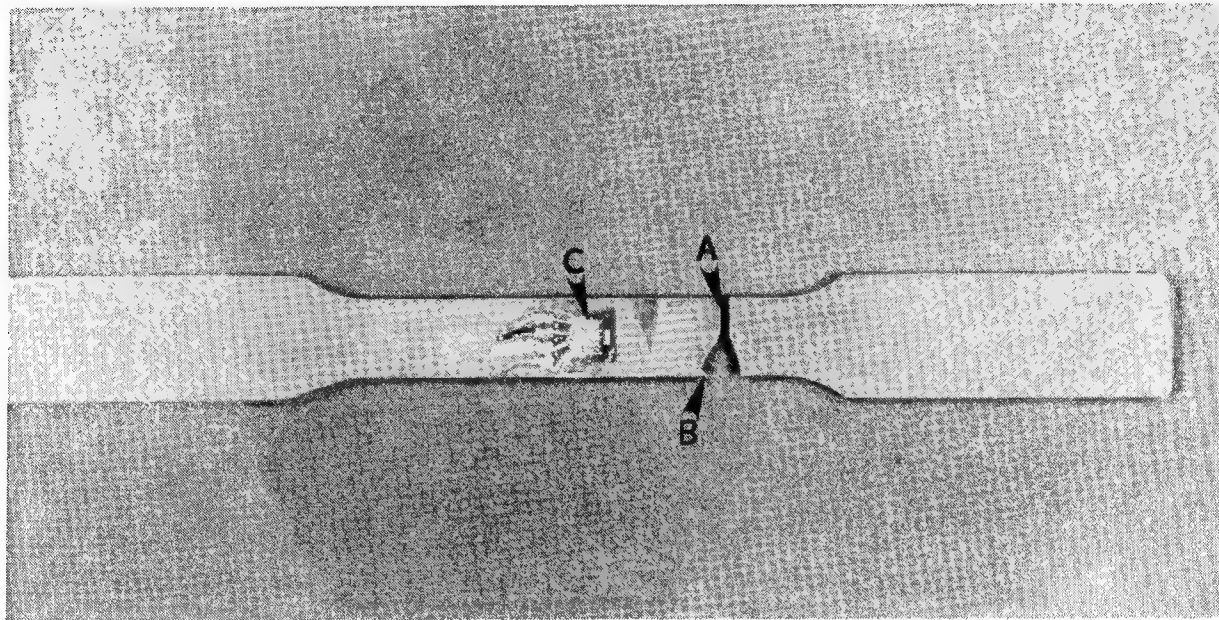


Figure 6

TYPICAL TENSION FAILURE SURFACE AS SEEN IN SCANNING ELECTRON MICROSCOPE (SEM)
(20X)

We have characterized four specific areas in neat resin tensile failure. The first area is an initiation point, A. (See fig. 7.) It is typically a void or a piece of dust or some other impurity in the neat epoxy. Surrounding the initiation site is a relatively smooth area, B. The third area, C, is a transition between the smooth and a very rough area, D. Referring back to figure 6, the initiation site was located in the flat section and transitioned into the coarse area, where the triangular piece was ejected.

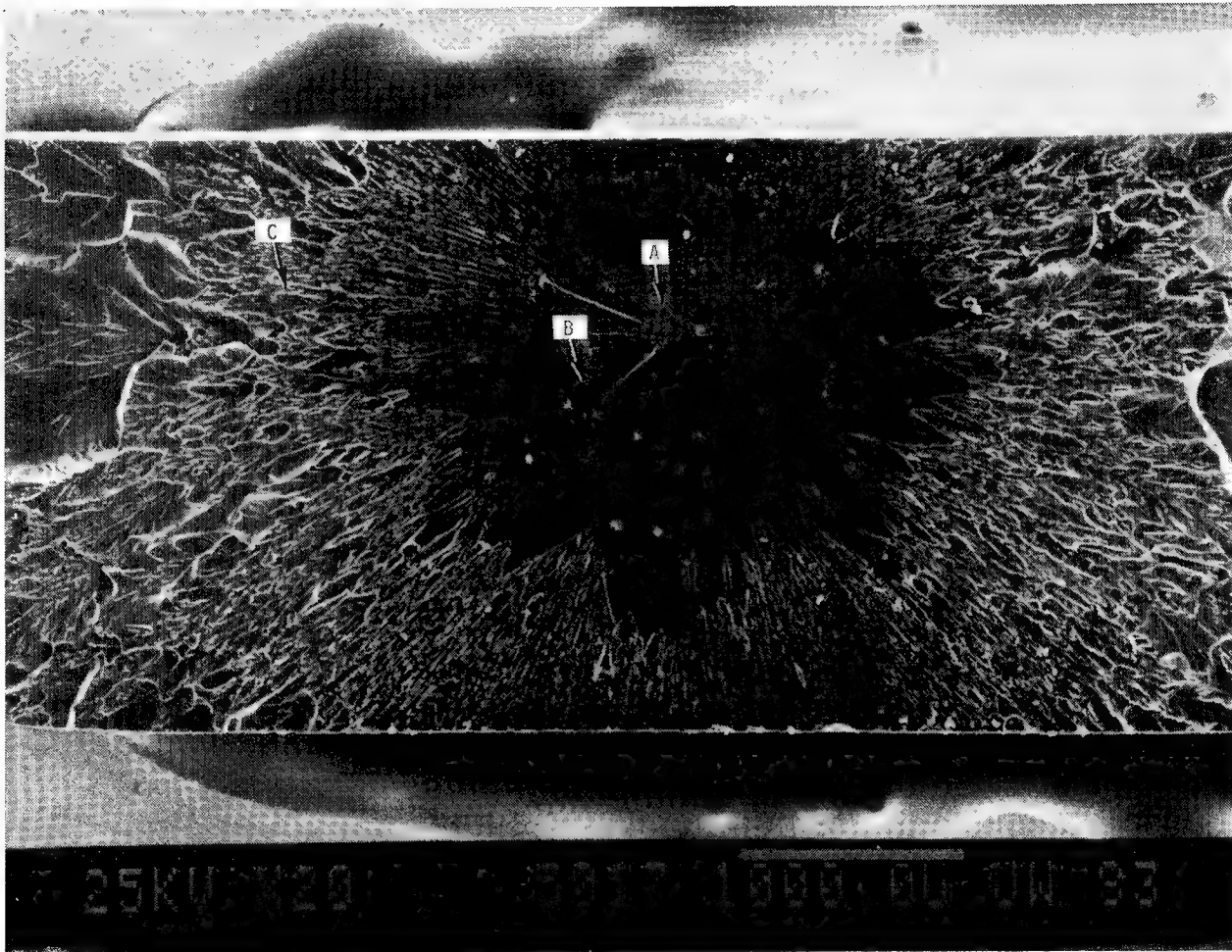


Figure 7

CLOSEUP OF TENSION FAILURE INITIATION SITE (100X)

This SEM closeup of figure 7 shows that this particular specimen had a small inclusion. One might note in this 100X magnification that the inclusion itself is somewhere around 100 μm in size. (See fig. 8.)

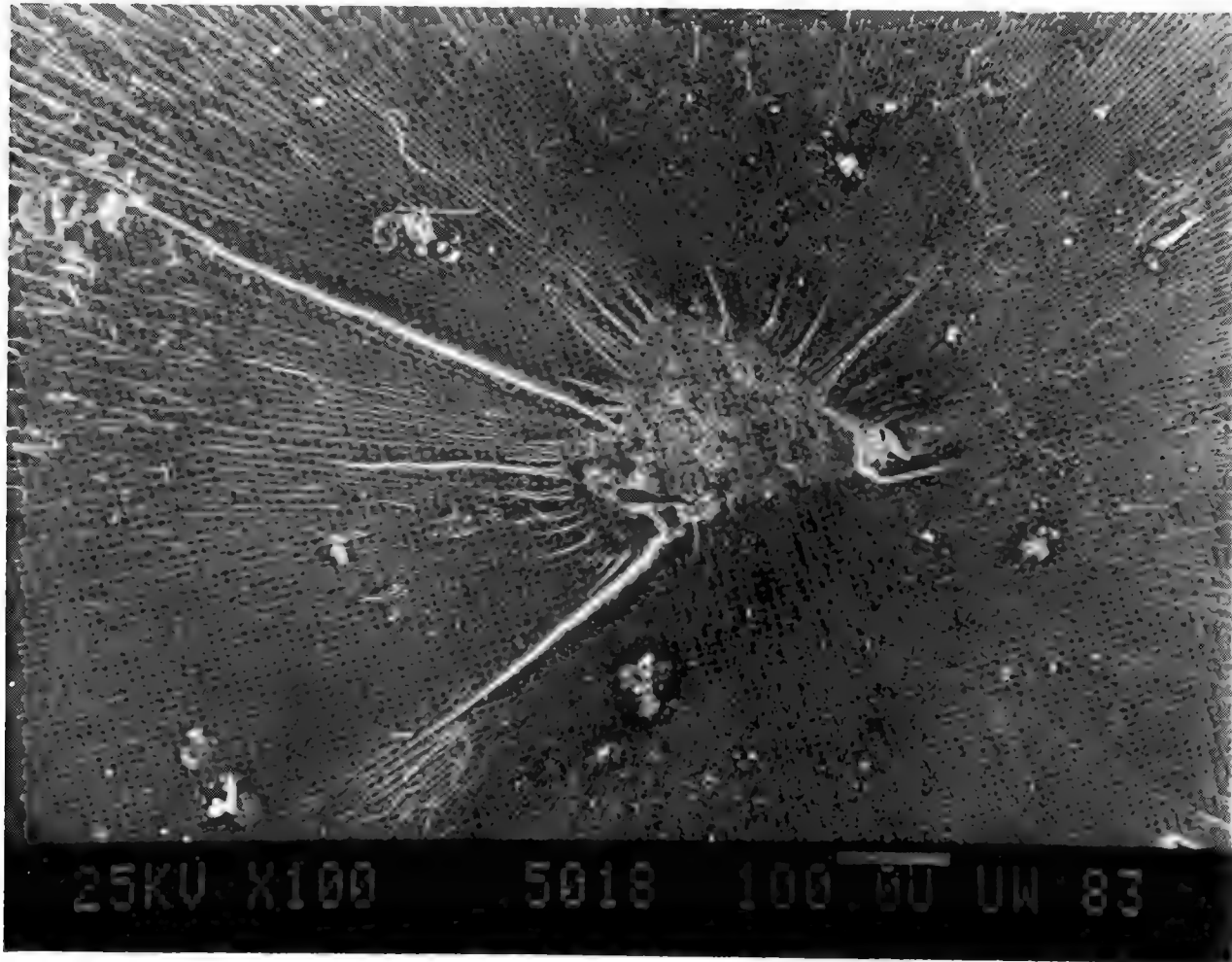


Figure 8

ATYPICAL FAILED TORSION SPECIMEN

Failures during shear testing can be demonstrated with this one-of-a-kind specimen (fig. 9). It failed at a relatively low strain compared to the other specimens, which helped preserve part of the failure process in the epoxy. The specimen is a 2220-1 tested at moisture saturation at 54°C. There is an internal 45° helix crack within this specimen. It is easy to visualize how the specimen basically unwinds and destroys itself as it fails. The vast majority of specimens shattered upon failure and were reduced to very small chips in the gage section. Although it is difficult to see in the figure, the feature to note is that the failure is at a 45° angle or on the tensile plane.

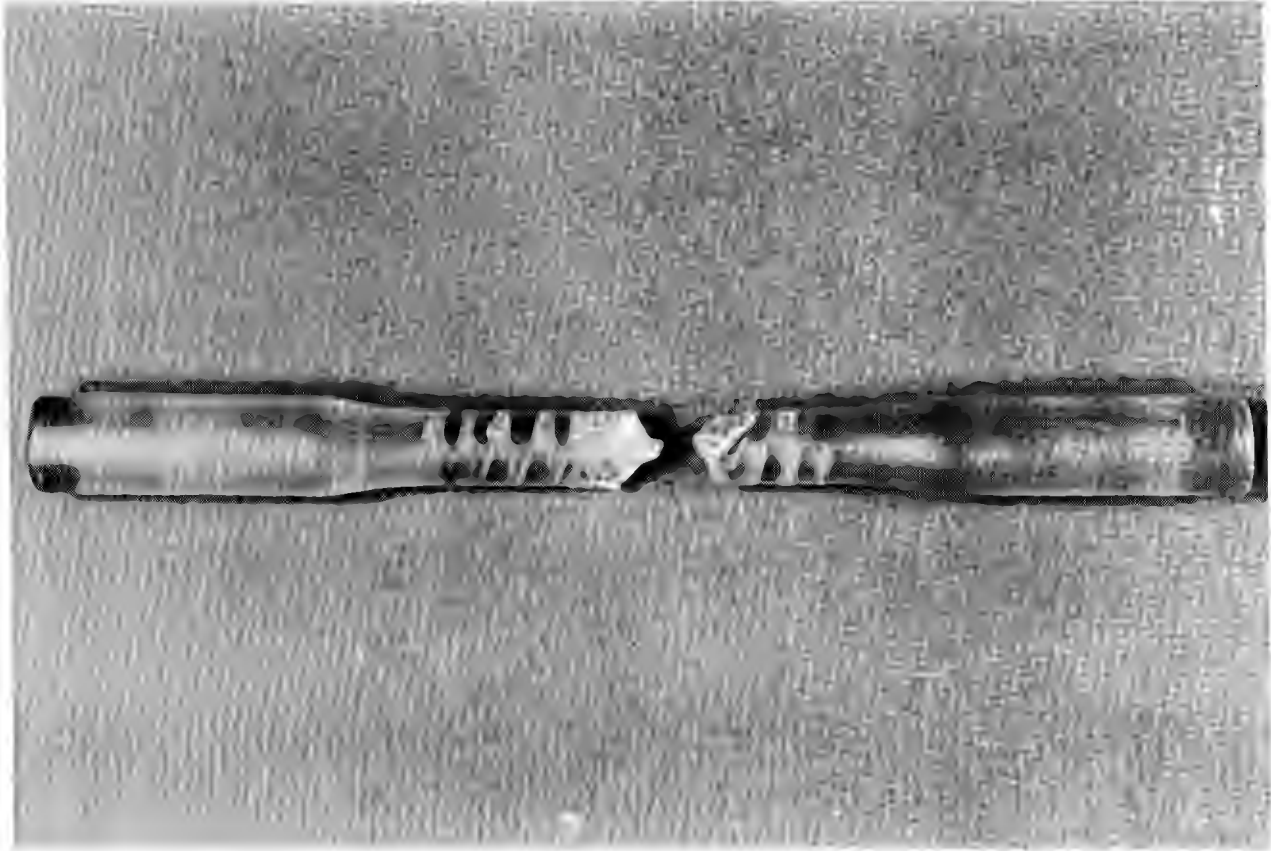


Figure 9

TORSION FAILURE SURFACE SHOWING AREAS OF FAILURE (10X)

In the torsion failure SEM photographs, we note the same four areas we saw in the tension failures. We have the initiation point either close to or on the surface as seen at A. It is surrounded by a fairly small smooth area at B with a transition area, C, into a rough area, D. (See fig. 10.)

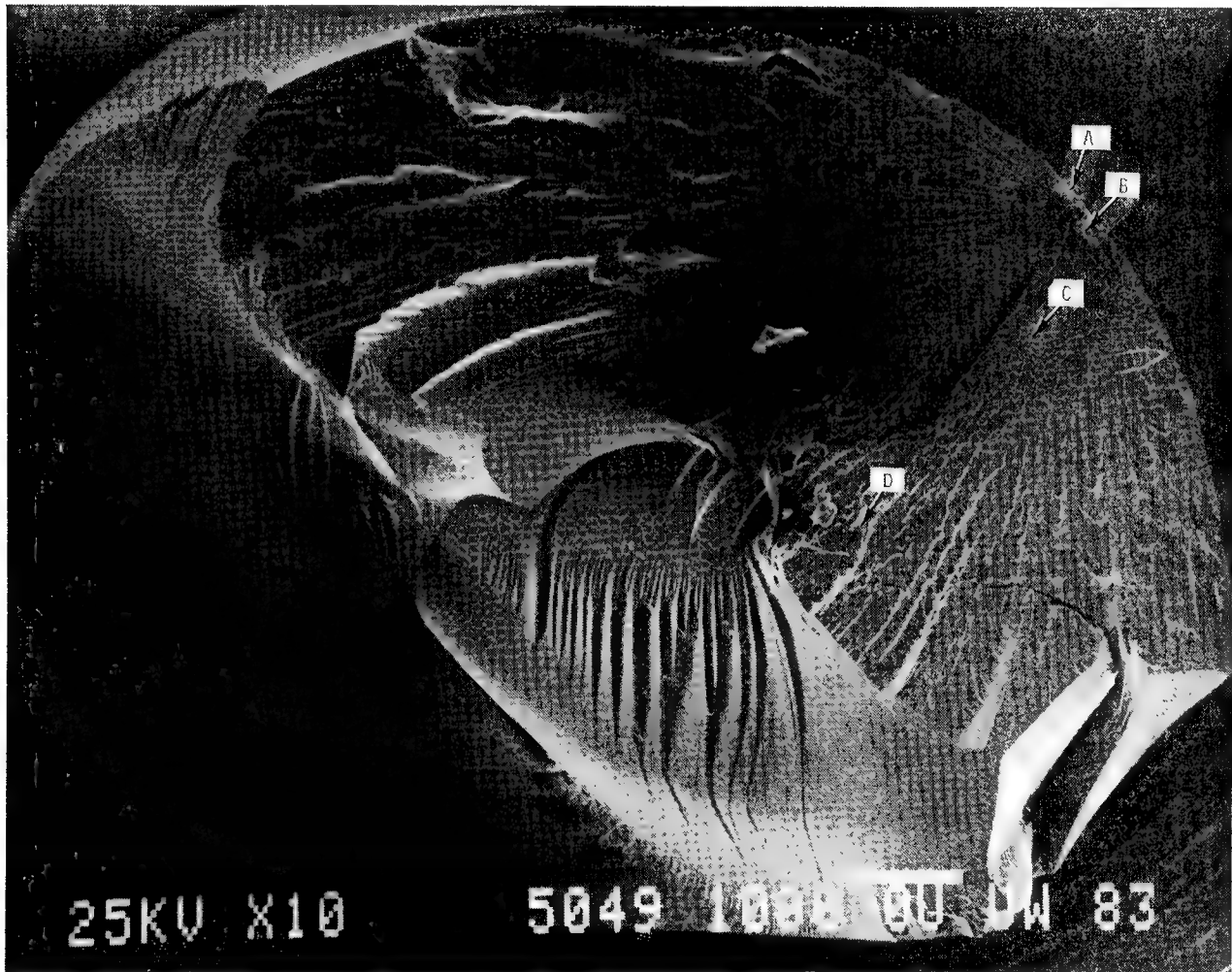


Figure 10

CLOSEUP OF TORSION FAILURE INITIATION SITE (50X)

This closeup of figure 10 shows the void just beneath the surface and affords a good view of the smooth area and the transition into the coarse areas of the failure. (See fig. 11.)

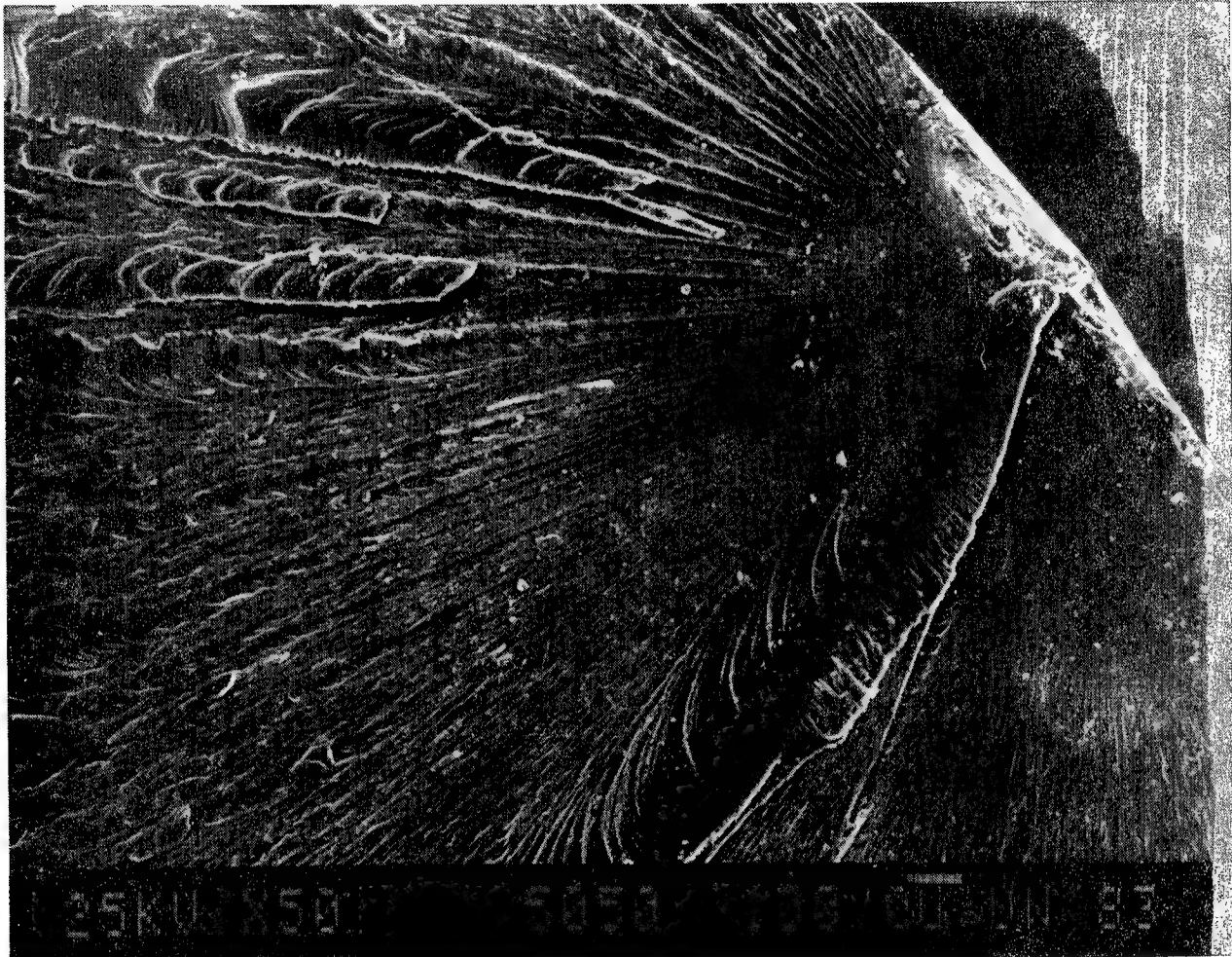
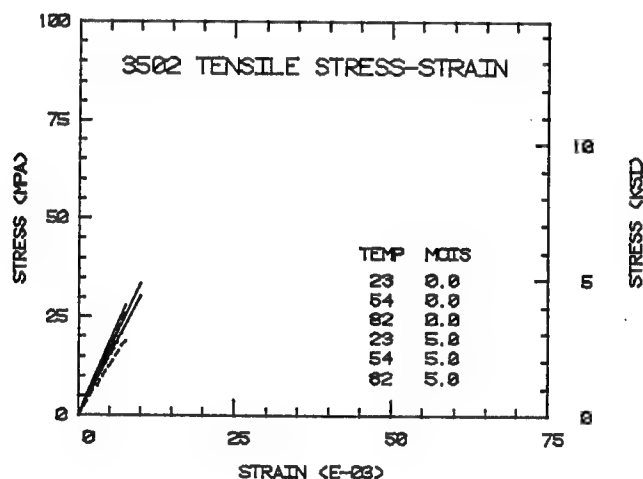


Figure 11

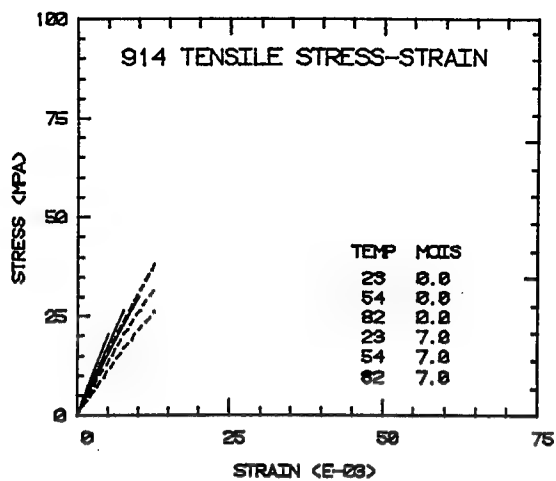
EPOXY STRESS-STRAIN DATA PLOTTED AT SIX DIFFERENT TEMPERATURE AND MOISTURE CONDITIONS FOR HERCULES 3502, FIBREDUX 914, 2220-1, AND 2220-3

These data, taken on our computer data acquisition system, allowed us to plot the stress-strain curves to failure (fig. 12). These are actual data and these four figures are all plotted to the same scale to give a better idea of the representative strengths, strains-to-failure, and moduli of the four epoxies studied. Note on these four figures that the solid lines (dry test results) show a slight increase in strength with increasing temperature. They also show an increase in strain with increasing temperature and a slight decrease in modulus with increasing temperature. The dashed lines (moisture-saturated test results) appear in the same order (i.e., room temperature, 54°C, and then 82°C) and show a decrease in strength with increasing temperature and a decrease in modulus and a slight increase in strain values with increasing temperature. It should be noted that on the four systems studied, the moisture content was slightly different, with the 2220 systems showing lower moisture absorption. The moisture contents were as follows: 3.8% for 2220-1, 4% for 2220-3, about 5% for 3502, and 7% for 914.

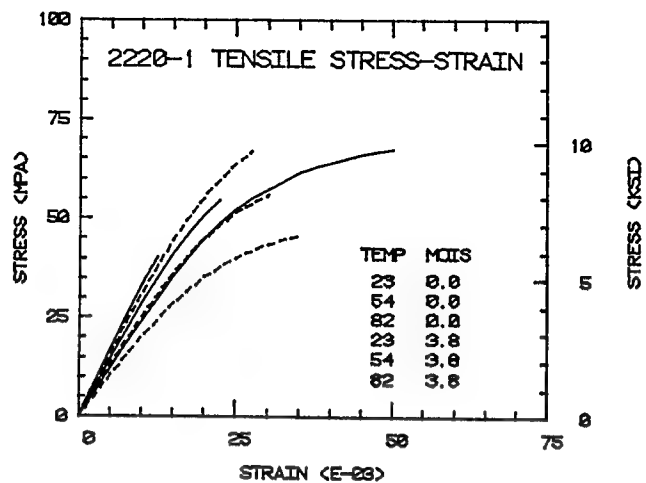


(a)

Figure 12

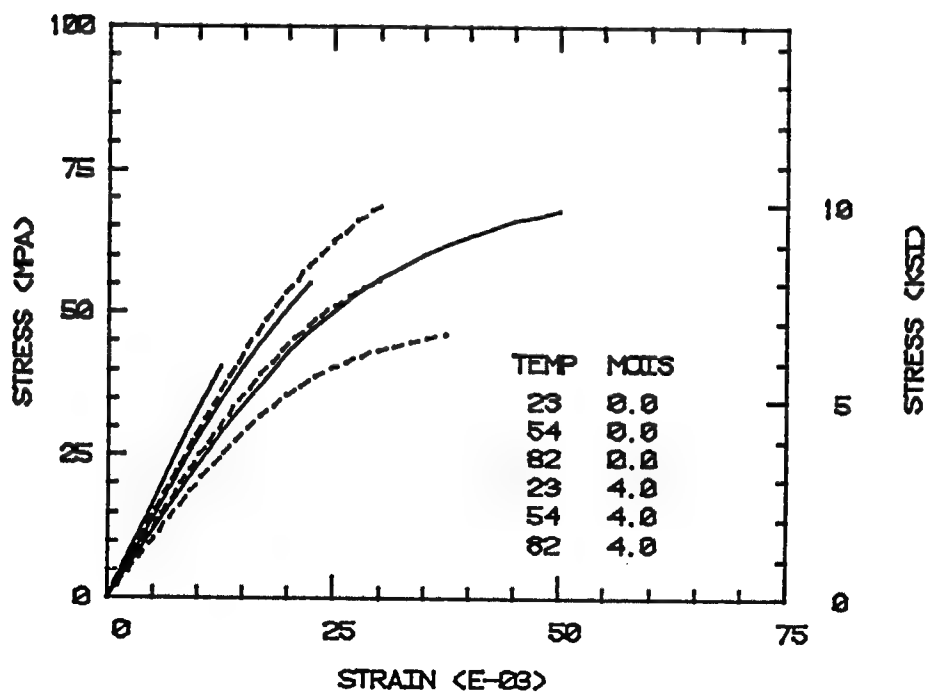


(b)



(c)

2220-3 TENSILE STRESS-STRAIN PLOT



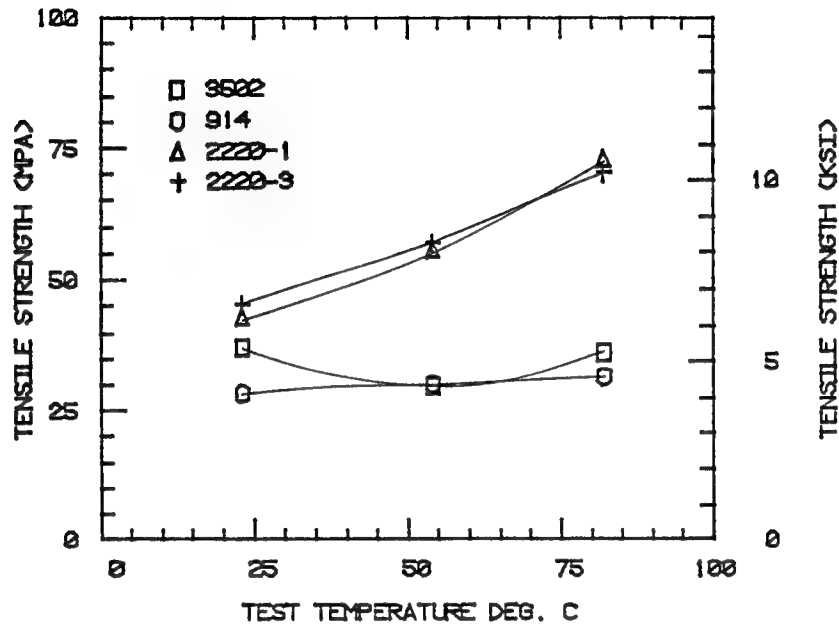
(d)

Figure 12.- Concluded.

AVERAGE VALUES FOR DRY AND MOISTURE-SATURATED TENSILE STRENGTHS FOR FOUR EPOXIES

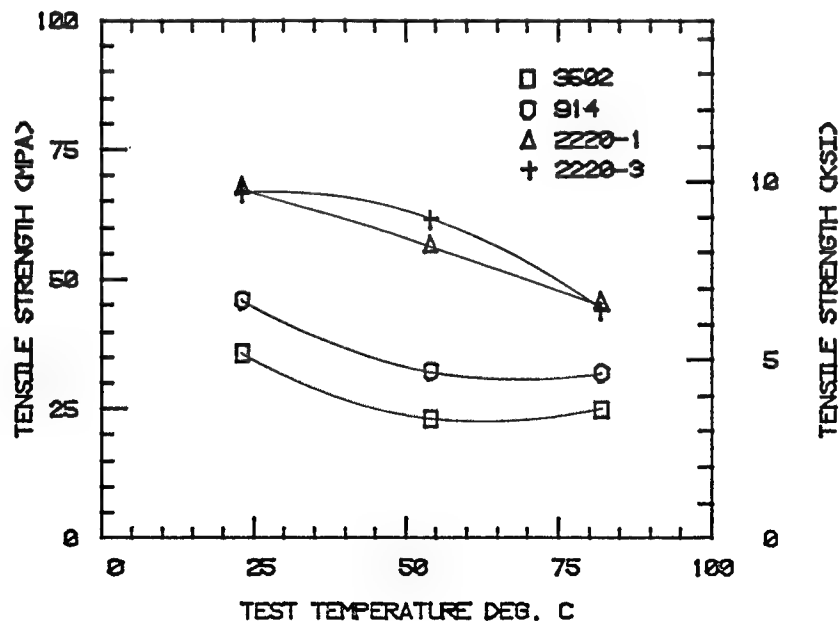
Dry tensile strengths increase with test temperature, as shown in figure 13. The strengths for the 2220 systems are much greater than those for the 3502 or 914 systems in the dry state. Strengths decrease as temperature increases in all four moisture saturated resins.

DRY EPOXY TENSILE STRENGTHS



(a)

MOIST. SAT. EPOXY TENSILE STRENGTHS



(b)

Figure 13

AS4/2220-1 GRAPHITE/EPOXY UNIDIRECTIONAL COMPOSITE LONGITUDINAL TENSILE
STRESS-STRAIN RESPONSE AS PREDICTED USING MICROMECHANICS

Using the stress-strain curves of the neat resin for the matrix and an AS4 fiber for input, the longitudinal stress-strain response of the unidirectional graphite/epoxy composite was predicted using a micromechanics computer program developed at the University of Wyoming. (See fig. 14.) Note that the stress-strain response of the composite is highly linear to failure, as expected.

AS4/2220-1 LONGITUDINAL TENSION

3.8% MOISTURE 100 DEG. C

FIBER VOLUME 60%

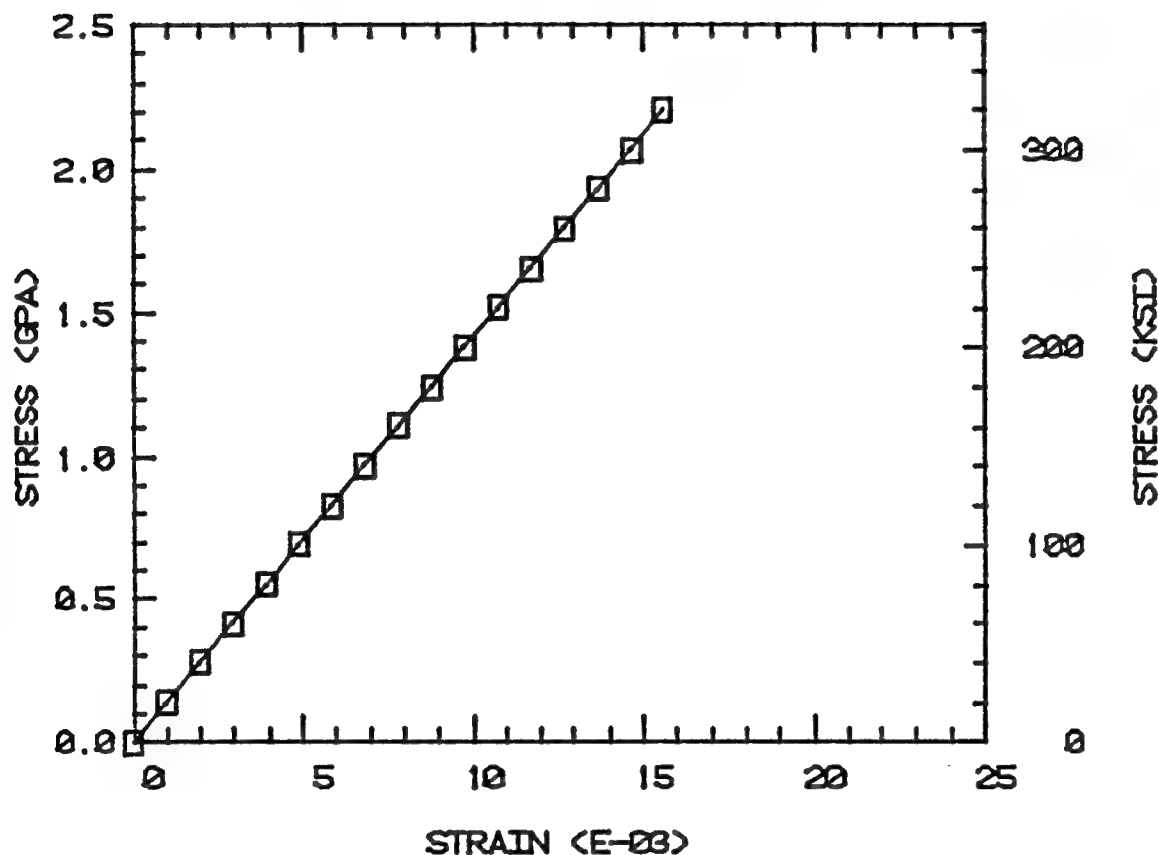


Figure 14

AS4/2220-1 GRAPHITE/EPOXY UNIDIRECTIONAL COMPOSITE TRANSVERSE
STRESS-STRAIN RESPONSE AS PREDICTED USING MICROMECHANICS

This micromechanics prediction plot starts out very linear but near the end there is a slight amount of nonlinearity in the stress-strain curve. (See fig. 15.)

AS4/2220-1 TRANSVERSE TENSION
3.8% MOISTURE 100 DEG. C
FIBER VOLUME 60%

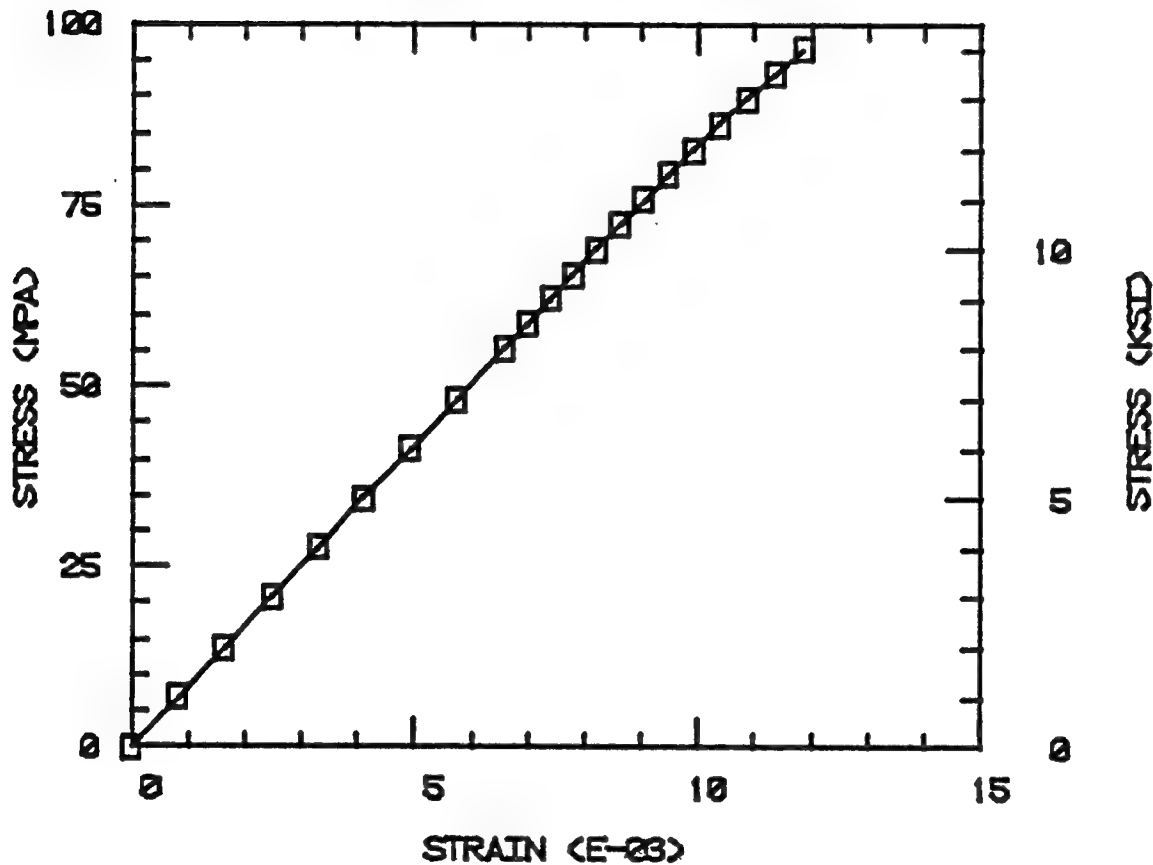


Figure 15

AS4/2220-1 GRAPHITE/EPOXY UNIDIRECTIONAL COMPOSITE LONGITUDINAL SHEAR
STRESS-STRAIN RESPONSE AS PREDICTED USING MICROMECHANICS

Our micromechanics program has a nonlinear analysis capability. Figure 16 shows the shear stress-strain curve to have a high degree of nonlinearity.

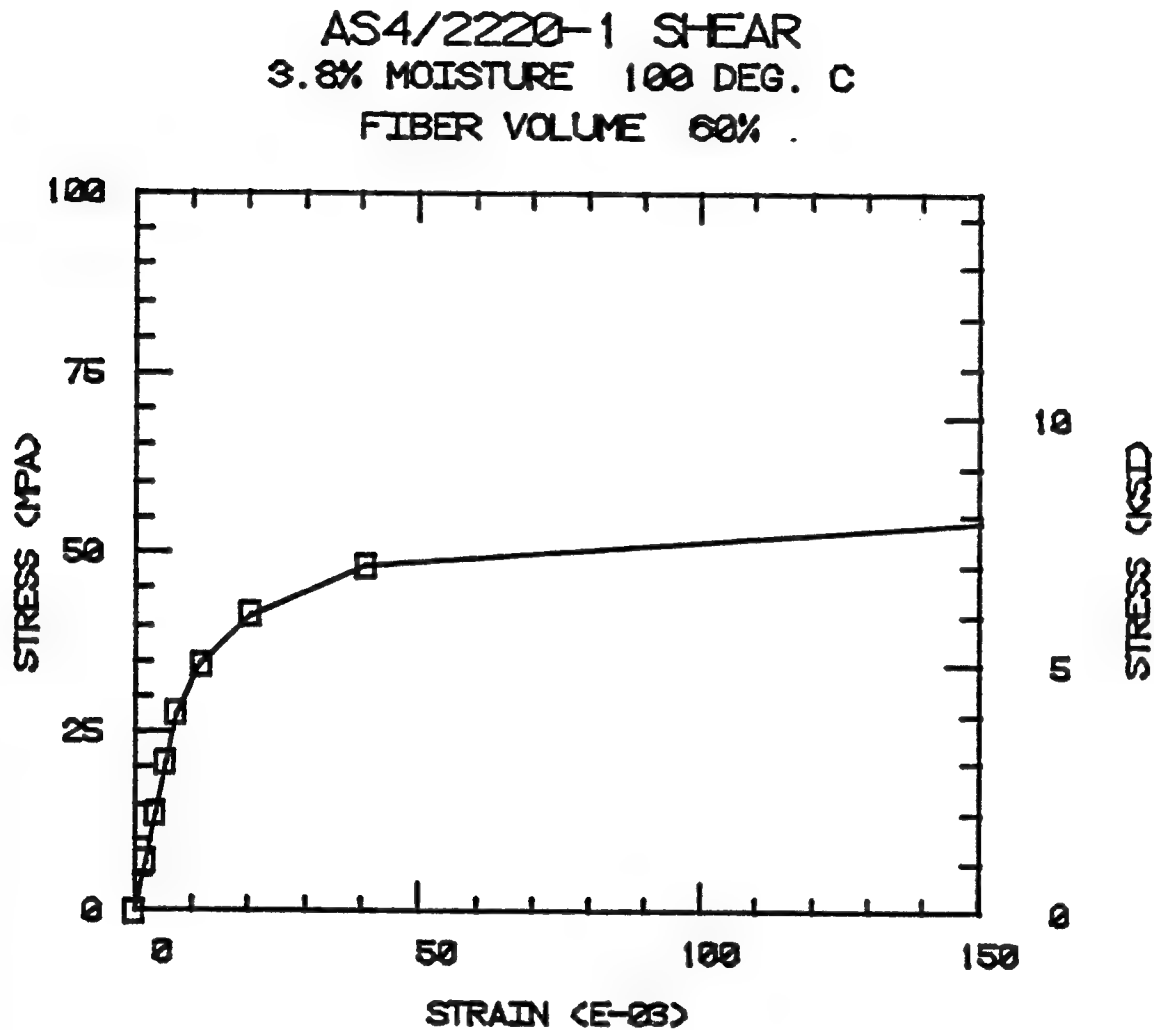
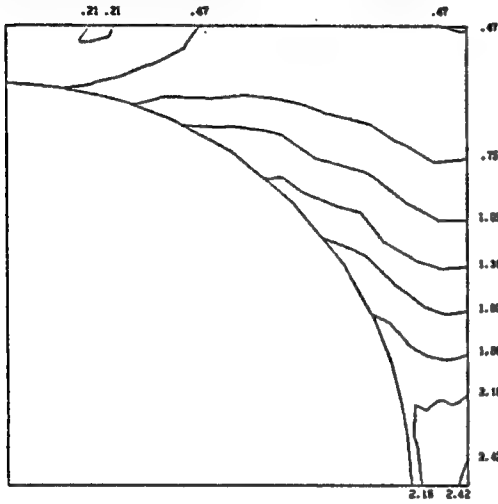


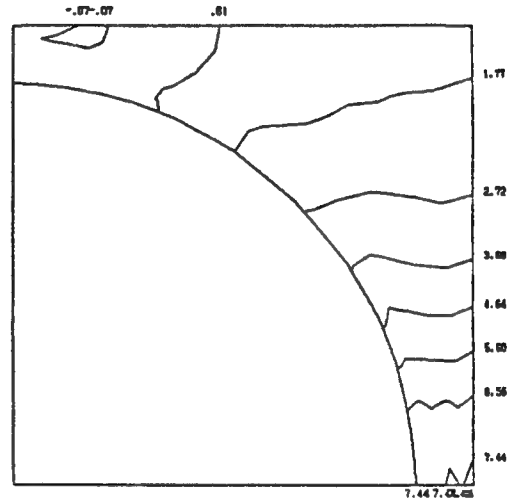
Figure 16

AS4/2220-1 GRAPHITE/EPOXY UNIDIRECTIONAL COMPOSITE, 100°C, 3.9 PERCENT
MOISTURE (ETW), 27.6 MPA (4 KSI) TRANSVERSE TENSILE APPLIED STRESS

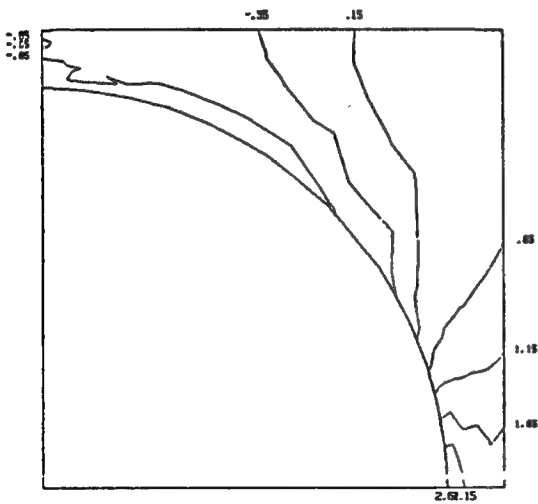
A wealth of information is available from the micromechanical analysis. Figure 17 shows a typical example of the output. The grid assumes a square array of packing of the fibers. No stress contours are plotted within a fiber because they tend to clutter up the plot. The stress contours plotted in the matrix are octahedral shear, maximum principal stress. Almost any stress can be obtained from the analysis. Many input parameters can be varied, such as magnitude of applied stress, temperature, or moisture content in the matrix.



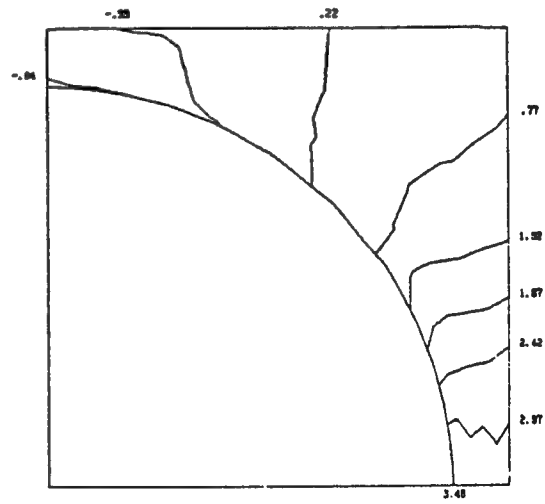
(a) Octahedral shear stress (ksi).



(b) Maximum principal stress (ksi).



(c) Minimum principal stress (ksi).



(d) Intermediate principal stress (ksi).

Figure 17

SUMMARY

Four neat resin systems were cast and their mechanical properties were generated. SEM photographs were analyzed and four specific areas common to all the specimens were identified on the fracture surfaces. The mechanical and physical properties were input into a micromechanics analysis and composite response was predicted for four different environmental conditions.

CONSTITUENT PROPERTY - COMPOSITE PROPERTY RELATIONSHIPS
IN THERMOSET MATRICES

J. Diamant and R. J. Moulton
Hexcel Corporation
Dublin, California

Hexcel is committed to development of resins for aerospace structures and advanced composites. To execute this task effectively, a screening and evaluation methodology needs to be developed. Our procedure is depicted schematically in figure 1.

This entire procedure requires less than 300 grams of neat resin. Learning as much as possible from small amounts is especially important where long and costly synthesis routes are involved.

After a resin is formulated and compounded, it is necessary to establish the correct cure time-temperature relationship. The cure viscosity is conveniently measured with a Rheometrics Dynamic Spectrometer (RDS), thus establishing the gel time and temperature. Following cure, dynamic mechanical data of the cured resin are taken with the RDS. Thereby modulus (G') versus temperature behavior and T_g are established. Likewise it is easy to find out whether and/or how much postcure is needed above T_g . Loss mechanisms are apparent from the G'' curve and in some cases may be related to mechanical and fracture behavior.

Tensile stress-strain measurements are performed on test specimens cast in dumbbell shape with a cylindrical cross section 3/16" in diameter and 1" long. Neat resin tensile modulus has been traditionally considered as a primary factor in matrix selection for primary composites (1).

High neat resin ultimate strain capability is needed for achieving high strain translation into composites, especially those made with high strain fibers. Laminate off-axis ultimate strain is reduced by a strain magnification of 5 to 10 times (2) and could be further complicated by different failure mechanisms in composites (3) compared to neat resins. Neat resin ultimate strain is one of several empirically known important parameters which has not been quantified. Compressive yield may be related to damage tolerance.

For G_{IC} measurements, 1 1/4" square coupons were cut from a 1/4" thick plate; compact double cantilever beam (CDCB) specimens were machined and tested according to ASTM E399 procedures (4).

Presently, mechanical tests are conducted under static conditions at 0.05 in/mi crosshead speed. Influence of testing rate, fatigue, and temperature will be investigated in the future. Instrumentation is being built now to investigate effects of moisture and measure accurately T_g at precisely known relative humidity. Neat resin physical properties, such as the coefficient of thermal expansion (CTE) and shrinkage in cure, are routinely measured for developmental resins. These properties may significantly affect mechanical and fracture behavior of composites, especially if the resin is brittle.

The purpose of the screening is to identify at an early stage matrices that will not have a chance of succeeding. But if a neat resin "passes," its laminate properties still may not be passable. A composite must be prepared at this step, and such variables as flow, fracture mechanisms, fiber-matrix interface, and translations of properties must be studied. Direct microscopic observation of load transfer from single fiber into matrix must be investigated. Longitudinal properties of unidirectional laminates are monitored and compared with predicted properties. This entire procedure serves as a semi-empirical method of scaling up the screening process from neat resin to composites.

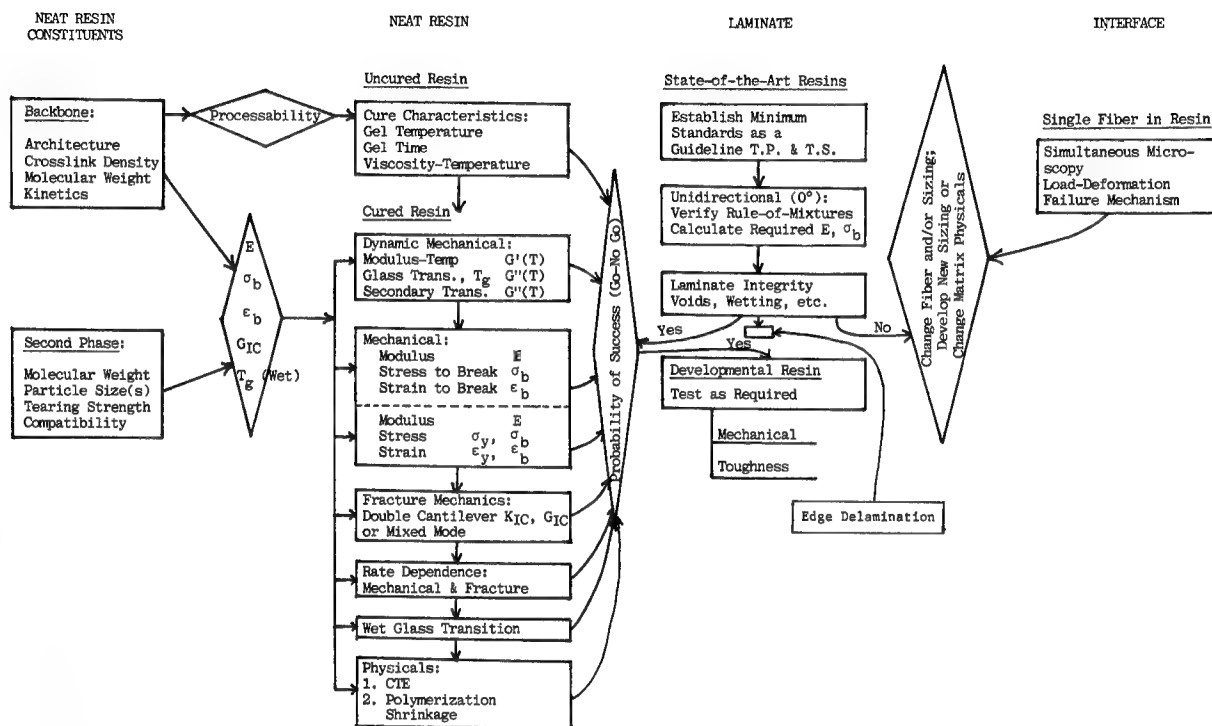


Figure 1. Resin screening and evaluation flowchart.

The desired architecture of the polymer backbone and neat resin morphology are dictated by the major requirements of the finished composite. One of the principal current requirements is to improve damage tolerance without sacrificing service temperature and stiffness. On the polymer level, this means improved fracture toughness without lowering the wet modulus and wet T_g . One of the most accepted tests for damage tolerance is compression after impact. Evaluation of laminates with different Hexcel resins showed that the plot of compressive strength after impact versus the logarithm of G_{IC} followed a straight line (see fig. 2).

Hexcel resin F-185 has unacceptably low, dry, and wet T_g . On the other hand, F-263, a TGDDM/DDS type resin, complies with the stiffness and service temperature requirements, but because of its brittleness, its damage tolerance is unacceptably low. To comply with the Boeing standard, it appears that the G_{IC} of F-263 has to be increased by a factor of 40.

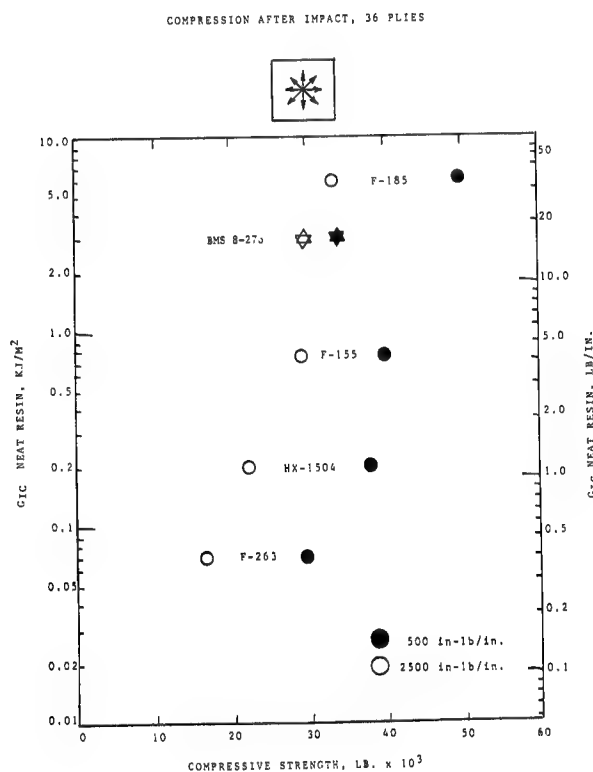


Figure 2. Neat resin G_{IC} versus laminate compression after impact.

The immediate question that arises is whether highly crosslinked resins can be made sufficiently tough. As a model, the TGDDM/DDS system was chosen because it is a state-of-the-art industry standard. To begin, toughening with carboxyl-terminated butadiene-nitrile (CTBN) rubbers was examined. Since toughening of highly cross-linked resins has not been thoroughly investigated, a more systematic view of the problem was taken. First the influence of rubber-resin compatibility was examined. Compatibility increases with increasing solubility parameter, which is directly related to the nitrile content. Second, the influence of rubber molecular weight was investigated. Third, the effects of rubber particle size were of interest. However, we do not have a way to control or regulate the rubber particle size, therefore it remains a dependent variable.

Figure 3 shows the chemical analysis, mechanical, fracture mechanics, and dynamic mechanical data of a TGDDM/DDS resin modified with 5% of different CTBNs. Chemical analysis of the pure CTBNs was performed. Titrations for epoxy and carboxyl were carried out and reported as equivalents per hundred (EPHR) and also converted to molecular weights using functionalities reported by the manufacturer. Molecular weights determined by GPC are approximately twice as high as those from titration. Below, $\bar{M}_n = 20,000$ for all \bar{M}_n values, but those measured by GPC agreed well. The GPC values were higher by a factor of 1.7. With increasing nitrile content a consistent increase in G_{IC} can be noted, while mechanical properties are unaffected. Low nitrile CTBNs produce G_{IC} values lower than those of the unmodified resin. Glass transition temperature is the same for all resins, including unmodified TGDDM/DDS, indicating good phase separation of the rubber.

	RESIN	DJ17 49-1	EB3-98A	EB3-98B	EB3-98D	EB4-28
TOUGHENING AGENT PROPERTIES	Toughening Agent(s) Type	None	CTBN 1300x31	CTBN 1300x8	CTBN 1300x13	Pre-reacted CTBN 1300x13
	Toughener Wt. %	↓	5	5	5	5
	Epoxy EPHR		-	-	-	-
	Carboxyl EPHR		0.052	0.054	0.060	0.060
	Titration \bar{M}_n		3,654	3,333	3,000	3,000
	GPC \bar{M}_n		6,792	7,419	6,571	6,571
	GPC \bar{M}_w		13,556	15,220	12,864	12,864
	Acrylonitrile % Solub. Parameter $\sqrt{\text{cal/cm}^3}$	↓	10 8.45	18 8.77	26 9.14	26 9.14
MECHANICAL PROPERTIES TENSILE	Modulus E msi	0.65	0.56	0.59	0.56	0.56
	Strength σ ksi	11	8.4	9.1	8.2	9.6
	Ult. Strain ϵ %	~2	1.75	1.40	1.3	4.5
	Modulus E msi	0.65	0.60	0.60	0.60	0.56
	Yield Stress σ_y ksi	24	20.9	18.7	20.5	18.2
MECHANICAL PROPERTIES COMPRESSIVE	Yield Strain ϵ_y %	7	7.5	6	7	7
	Break. Stress σ_b ksi	23	20.3	16.3	19.2	16
	Break. Strain ϵ_b %	10	16	11	15	11.3
	Pract. Tough. K_{IC} ksi $\sqrt{\text{in}}$	0.58	0.33	0.40	0.53	0.57
FRACTURE MECHANICS	Strain Energy Release Rate G_{IC} lb./in.	0.45	0.17	0.24	0.44	0.51
	G_{IC} KJ/m ²	0.079	0.030	0.042	0.078	0.089
DYNAMIC MECH.	Storage Mod. G' dyne/cm ²	1.70×10^{10}	1.48×10^{10}	1.53×10^{10}	1.48×10^{10}	1.46×10^{10}
	Loss Mod. G'' dyne/cm ²	3.95×10^8	3.30×10^8	4.09×10^8	5.31×10^8	4.04×10^8
	Glass Trans. Temp. T_g °C	243	242	242	242	243

Figure 3. The TGDDM/DDS resins modified with low \bar{M}_n CTBNs (liquid rubbers).

In figure 4 are shown TGDDM/DDS resins modified with medium and high \bar{M}_n rubbers. The former was synthesized by copolymerizing low \bar{M}_n CTBNs with a difunctional linear epoxy. Carboxyl titration indicates the extent of reaction whereas epoxy titration shows excess epoxy. The true \bar{M}_n may be regarded as approximately half the GPC value. G_{IC} values are higher than those obtained from epoxies containing the corresponding liquid rubbers, and increase with increasing nitrile content. Specimen DJ17-116D is an exception in this trend because of the lower degree of polymerization (low \bar{M}_n) of the rubber.

High \bar{M}_n (solid) rubber Hycars 1472 and 1001CG are two very high \bar{M}_n butadiene-nitrile rubbers. Hycar 1472 has similar composition to 1300x13, but much higher \bar{M}_n and consequently numerous pendant carboxyl groups. Hycar 1001CG has no reactive groups. Because of the low solubility of these rubbers, GPC data reflect only the sol fraction. Both high \bar{M}_n rubbers give the highest G_{IC} values. However, the non-reactive Hycar 1001CG gives low tensile values, and so do the epoxy-CTBN copolymers, which have reduced reactivity due to greater chain length between the reactive ends. Hycar 1472 and prereacted CTBN 1300x13 give the highest tensile values. The conclusions from this series of experiments regarding toughening of TGDDM/DDS resins with elastomers are:

- G_{IC} increases with increasing rubber \bar{M}_n
- G_{IC} increases with increasing CTBN nitrile content probably due to better compatibility with and adhesion to the matrix
- Tensile ultimate properties are sensitive to the extent of reaction between rubber and matrix

Particle size is in the range of 0.5 to 1 micron for all \bar{M}_n values. Therefore, the \bar{M}_n effect is not due to difference in particle size. When rubber concentration is increased to 10%, a significant drop in modulus and T_g is registered. Therefore, addition of more than 5% rubber may not be desirable.

RESIN		DJ17 48B	DJ17 84C	DJ17 84D	DJ17 116D	DJ17 117A	DJ17 117B
TOUGHENING AGENT PROPERTIES	Toughening Agent(s) Type	CTBN 2000x162 & Epoxy 5	CTBN 1300x31 & Epoxy 5	CTBN 1300x8 & Epoxy 5	CTBN 1300x13 & Epoxy 5	Hycar 1472 5	Hycar 1001CG 5
	Toughener Wt. %	.025	.0074	.017	.049	None	None
	Epoxy EPRR	.0004	.0004	.007	.023	.06	None
	Carboxyl GPC	20 55	31 114	18 47	11 26	48 267	32 154
	Acrylonitrile Solid, Parameter	0 8.04	10 8.45	18 8.77	26 9.14	27	≥ 27
MECHANICAL PROPERTIES TENSILE	Modulus E, ksi	0.55	0.54	0.58	0.49	0.57	0.50
	Strength σ, ksi	7	7	7	7.5	13	4
	Ult. Strain ε, %		3.5	2.5	2	5.5	2.5
	Modulus E, ksi					0.55	0.50
MECHANICAL PROPERTIES COMPRESSIVE	Yield Stress σ _y , ksi	None	None	None	None	21	15
	Yield Strain ε _y , %					8	7
	Strength σ, ksi	18.5	22	21	21	16	14
	Ult. Strain ε, %	6	6.5	7.5	7.0	11	10
FRACTURE MECHANICS	Fract. Tough. K _{IC} , ksi √in.	0.48	0.57	0.72	0.60	0.87	0.89
	Strain Energy lb./in.	0.36	0.53	0.78	0.64	1.16	1.39
	Release Rate G _{IC} , KJ/m ²	0.064	0.094	0.138	0.11	0.20	0.25
DYNAMIC MECHANICAL	Storage Mod. G', dyne/cm ²	1.44x10 ¹⁰	1.40x10 ¹⁰	1.51x10 ¹⁰	1.28x10 ¹⁰	1.49x10 ¹⁰	1.28x10 ¹⁰
	Loss Mod. G'', dyne/cm ²	3.81x10 ⁸	3.30x10 ⁸	4.07x10 ⁸	5.02x10 ⁸	9.64x10 ⁸	5.60x10 ⁸
	Glass Trans. Temp. T _g , °C	244	245	244	242	240	243

Figure 4. The TGDDM/DDS resins modified with medium and high \bar{M}_n (solid) rubbers.

Toughening brittle plastics with rubber particles is the best known and oldest method, but not the only one. Another possibility is to use tough thermoplastics for modifying brittle thermosets. If G_{IC} can be significantly improved without loss of stiffness and T_g , then this could be a superior method. As a first try, ULTEM polyetherimide made by General Electric Company was used to verify the viability of this proposition (fig. 5). As shown, addition of 10% ULTEM does not significantly affect the dynamic shear and compressive moduli. Tensile data were scattered and therefore meaningful numbers could not be derived. The G_{IC} has doubled as compared to that observed for unmodified resin. Therefore, in principle, this method seems to work. The next question to address is to determine what thermoplastic is best to use and how much? Some additional insights and partial answers to these questions may be gained from dynamic mechanical data. However, before that subject is addressed, some additional possibilities for toughening are explored and compared in figure 5.

		TOUGHENING METHOD		LOW \bar{M}	HIGH \bar{M}	HIGH \bar{M}	ABS	TOUGH	ULTRA-	NONE
				ELASTOMER	INERT	REACTIVE			HIGH \bar{M}	
TOUGHENING AGENT PROPERTIES		Type	Wt. %	(Liquid Rubber)	(Solid Rub.)	(Solid Rub.)	COPOLYMER	THERMO-PLASTIC	GLASSY THERMOPL.	
				CTBN	Hycar	Hycar				
				1300x13	10010G	1472				
				5	5	5		10	3	
				EPHR	None	0.060		None	None	
				Titration	-	-		-	-	
				Mnx10 ³	32	48		-	5000	
				GPC	154	287		-	-	
MECHANICAL PROPERTIES		Acrylonitrile Solub. Parameter	%	9.14	-	-	-	-	-	
				cal/cm ³	-	-		-	-	
	TENSILE	Modulus	E msi	0.56	0.50	0.57				
				ksi	4	13		5.6	10.5	
				Ult. Strain	2.5	5.5		2.8	6	
	COMPRESSIVE	Modulus	E msi		0.50	0.55		0.63		
				Yield Stress	15	21		20		
				Yield Strain	7	8		5		
				Break. Stress	14	16		19.5		
				Break. Strain	10	11		7		
FRACTURE MECHANICS		Fract. Tough.	K _{IC} ksi√in.	0.57	0.89	0.87	0.62	1.09	0.57	0.58
				Strain Energy						
				Release Rate						
DYNAMIC MECH.		Storage Mod.	G' dyne/cm ²	1.46x10 ¹⁰	1.28x10 ¹⁰	1.49x10 ¹⁰		1.65x10 ¹⁰		1.70x10 ¹⁰
				Loss Mod.	5.60x10 ⁸	9.64x10 ⁸		5.51x10 ⁸		
		Glass Trans. Temp.	T _g °C							
				243	243	240		190 & 244		

Figure 5. Toughening of TGDDM/DDS with different modifiers.

An attempt was made to increase fracture toughness by addition of ABS copolymer, Blendex 311 (made by Borg-Warner), which is used routinely to toughen PVC. This material was found to be incompatible with the resin matrix and formed particles that could be seen with the optical microscope. There was no significant improvement in toughness and, therefore, mechanical testing was not completed. The addition of an ultrahigh Mn modifier, in this case polyethylene oxide (PEO) with $\bar{M}_n \approx 5 \times 10^6$, was also studied. It was found that the PEO was miscible with the cured matrix giving translucent specimens. But because of its high viscosity, only a small amount of modifier could be used. Again, G_{IC} has not improved, and elaborate mechanical testing was not justified.

The above experiments indicate that epoxy modification with glassy thermoplastics is a viable method which seems to be superior to elastomer toughening. In figure 6 mechanical, fracture toughness, and thermal data are shown of a number of commercial engineering thermoplastics which may be considered for toughening of thermoset matrices.

Commercial Name			LEXAN	UDEL	VICTREX	RADEL-A	PEEK	ULTEM
Generic Type			Poly-carbonate	P-1700 Poly-sulfone	100P Poly-ether-sulfone	Poly-aryl-sulfone	APC-1 Poly-ether-ether-ketone	Poly-ether-imide
Manufacturer			G.E.	UCC	ICI	UCC	ICI	G.E.
TENSILE	Modulus	E ksi	0.345	0.36		0.385	0.56	0.43
	Yield Stress	y ksi	9.00	10.20		12.00	13.20	15.20
	Yield Strain	y %	7	5-6		6.5		7-8
	Break. Stress	b ksi	9.50		12.20	40.0	10.15	
	Break. Strain	b %	110	20-100	40-80		150	60
COMPRESSIVE	Modulus	E ksi						0.42
	Yield Stress	y ksi	12.50	40.00				20.30
	Yield Strain	y %						
	Break. Stress	b ksi						
	Break. Strain	b %						
FLEX	Flex. Modulus	E ksi	0.340	0.39	0.380	0.399		0.480
FRACTURE	Izod, Notched	ft. lb/in. KJ/m	16.00 0.86	1.30 0.070	1.57 0.084	1.60 0.085		1.0 0.054
	Fract. Tough.	K_{IC} ksi in. MPa m	3.47±.46 3.17	3.07±.53 2.80	2.15±.13 1.96	3.28±.19 2.98	6.63±.41 6.03	3.05±.20 2.78
	Strain Energy	G_{IC} lb/in. KJ/m ²	32.45 5.67	22.97 4.01	10.70 1.87	24.25 4.25	68.25 11.92	18.98 2.21
	Release Rate							
THERMAL	Glass Trans. Temp.	T _g °L	145	195	203(HDT)	216(HDT)	143	217
	Melting Temp.	T _m °L					332	

Figure 6. Mechanical and fracture properties of some engineering thermoplastics.

Dynamic mechanical data shed additional light on the mechanisms of toughening. In figure 7 are shown dynamic storage and loss moduli, G' and G'' , respectively, of TGDDM/DDS modified with liquid CTBNs of different nitrile content. It can be seen that while G' is unaffected by nitrile content, G'' increases over the whole temperature range as nitrile is increased. This is a result of better resin-rubber mixing (or increased interphase) (5,6) and compatibility as nitrile content is increased. Simultaneously, there is a slight decrease in T_g as compatibility improves.

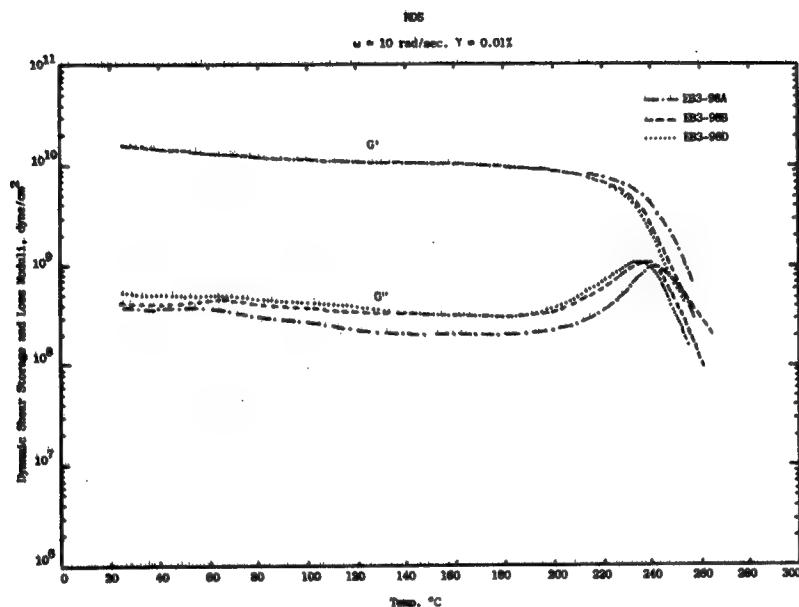


Figure 7. Dynamic moduli of TGDDM/DDS resins modified with low \bar{M}_n CTBNs containing 10% (---), 18% (----), and 26% (.....) nitrile.

Figure 8 shows G' and G'' curves of unmodified TGDDM/DDS and those modified with rubbers of different \bar{M}_n and reactivity but similar nitrile content. The former has the highest G' and lowest G'' , as expected. Highly reactive, high \bar{M}_n Hycar 1472 gives a lower G' because the rubber reduces stiffness. On the other hand, G'' is much higher as a result of a large particle-matrix interphase resulting from the extensive reaction between each molecule of this rubber and the epoxy matrix. The low \bar{M}_n rubber produces a G' slightly lower than the previous material. However, G'' is much lower due to smaller interphase. Apparently the reason is that each molecule has, at most, two reactive sites, but probably many of those are shielded by neighboring rubber molecules within the same particle, resulting in relatively low reactivity with the matrix. Still, G'' is higher than that of the unmodified material, indicating some interphase. The nonreactive high \bar{M}_n rubber gives G' similar to the previous material, with G'' slightly higher. This rubber has somewhat higher nitrile content and may interact with the matrix more extensively than the low \bar{M}_n rubber.

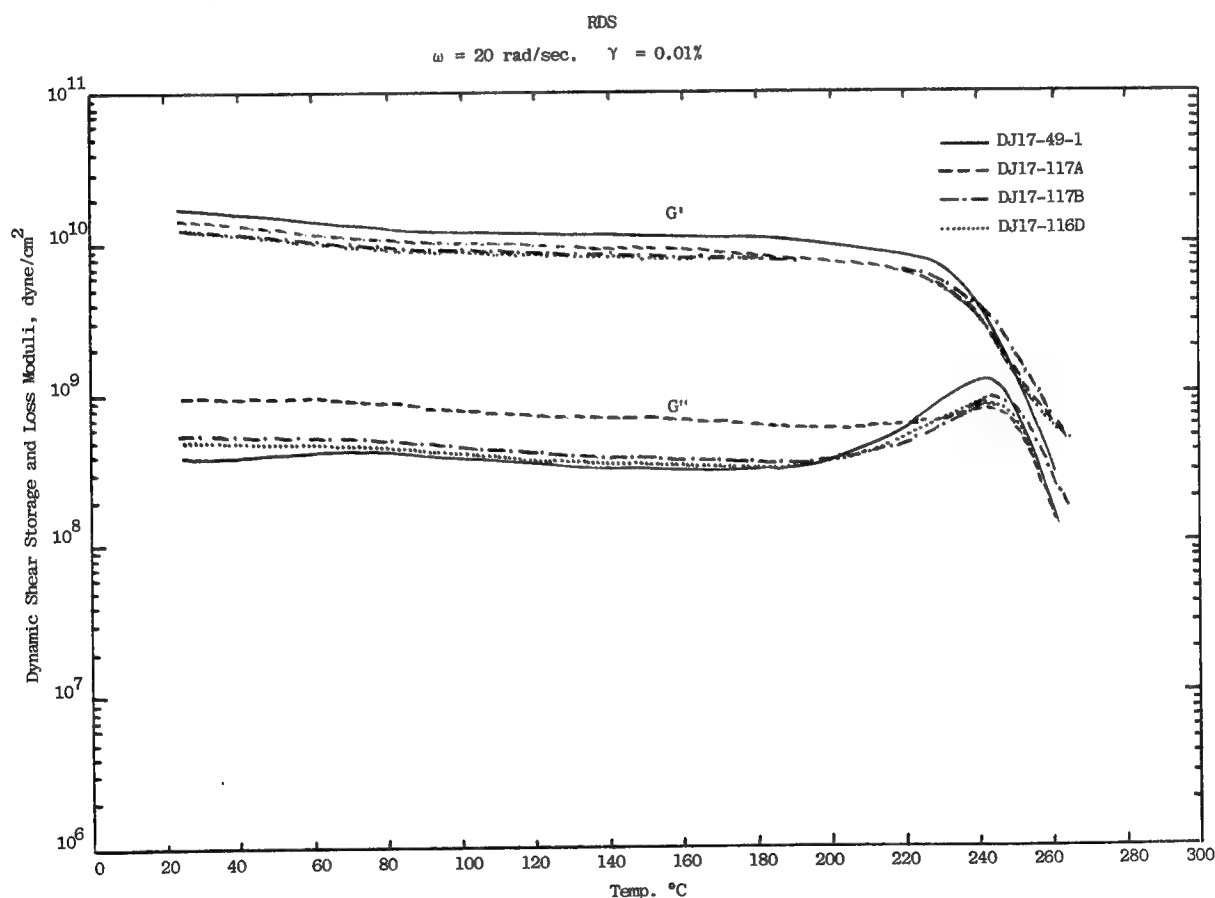


Figure 8. Dynamic moduli of TGDDM/DDS resins modified with different Hycar rubbers of high nitrile content: low \bar{M}_n CTBN (.....), high \bar{M}_n nonreactive rubber (-.-.-), high \bar{M}_n highly reactive rubber (----), and unmodified resin (—).

Dynamic mechanical data of TGDDM/DDS resins modified with 10% ULTEM are shown in figure 9. It shows that the modified material has two peaks in G'' , corresponding to the unmodified resin and ULTEM glass transitions, respectively. The ULTEM T_g in the modified resin is shifted to a lower temperature, apparently due to plasticization. The two T_g s clearly indicate that this is a two-phase material. Again, G'' is higher in the mixture than in either one of the ingredients, implying the presence of an interphase. Storage modulus, G' , is not diminished by the presence of ULTEM.

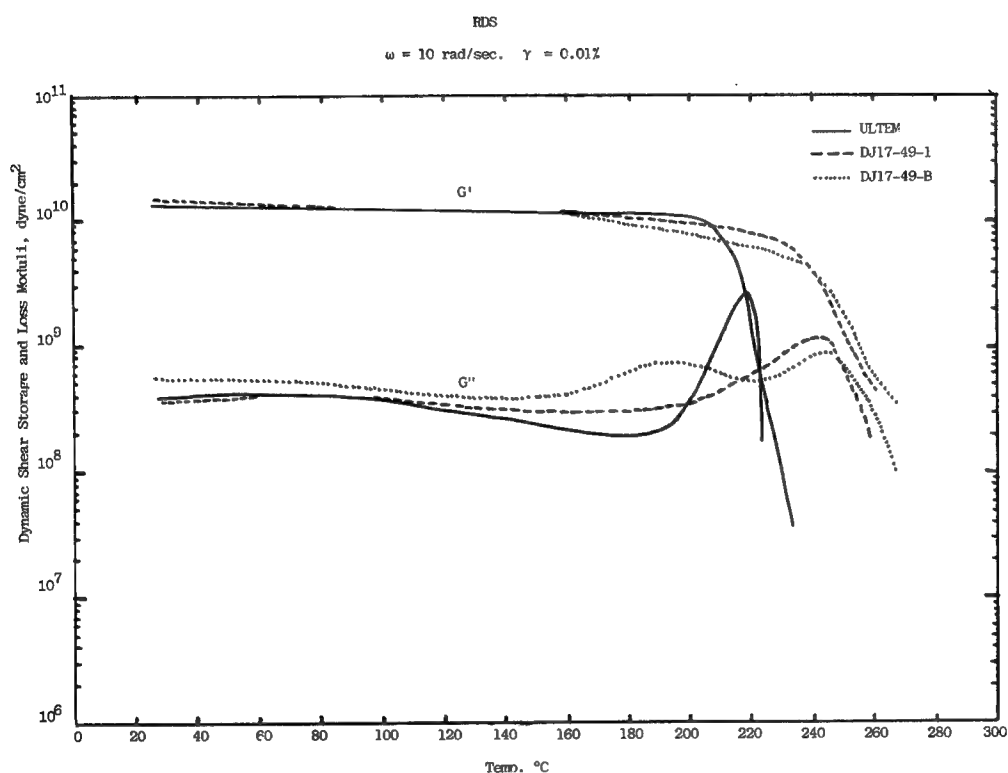


Figure 9. Dynamic moduli of TGDDM/DDS resin modified with 10% ULTEM (.....), unmodified resin (-----), and pure ULTEM (——).

CONCLUSIONS

The conclusions include:

1. Laminate damage tolerance correlates positively with neat resin G_{IC}
2. TGDDM/DDS resins can be toughened
3. Using butadiene-nitrile rubbers, neat resin G_{IC} and ultimate strain increase with increasing nitrile content, with the number of chemically reactive groups per molecule, and with increasing molecular weight
4. Better balance of properties combined with higher G_{IC} may be achieved by using tough glassy thermoplastics instead of rubbers to modify TGDDM/DDS resins
5. Both toughening mechanisms require good phase separation with an effective interphase
6. The kind and the amount of thermoplastic modifier remain to be selected
7. Presently only about a fourfold increase in G_{IC} was achieved, whereas a fortyfold increase is sought. Modification of the matrix backbone and of crosslinking is required

REFERENCES

1. Chamis, C. C., Hanson, M. P., and Serafini, T. T.: Modern Plastics, vol. 5, p. 90, 1973.
2. Christensen, R. M., and Wu, E. M.: Lawrence Livermore Laboratory Report UCRL-52169, November 1976.
3. Christensen, R. M., and Rinde, J. A.: Polymer Engrg. and Science, vol. 19, no. 7, May 1979.
4. ASTM E399 Standard. Standard Test Methods for Plane-Strain Fracture Toughness of Metallic Materials, 1981.
5. Diamant, J., Soong, D. S., and Williams, M. C.: Contemporary Topics in Polymer Science, vol. 4, 599-628, 1983.
6. Bates, F. S., Cohen, R. E., and Argon, A. S.: Macromolecules, vol. 16, no. 7, pp. 1108-1114, 1983.

THE EFFECT OF CROSS-LINK DENSITY ON THE TOUGHENING
MECHANISM OF ELASTOMER-MODIFIED EPOXIES

R.A. Pearson and A.F. Yee
General Electric Company
Corporate Research and Development Center
Schenectady, New York

PART I: SUMMARY

In Part I of our NASA contract, a DGEBA epoxide resin (EPON 828 from Shell Co.) was elastomer-modified by using three different carboxyl terminated butadiene-acrylonitrile copolymers of varying acrylonitrile content (HYCAR CTBN elastomers from B.F. Goodrich Co.). The acrylonitrile content (10-27 wt%) dictated the size of the precipitated rubber particles in the cured epoxy matrix (under identical cure conditions). The curing agent, piperidine, was added in the amount of 5 parts per hundred parts resin (phr). The curing schedule consisted of 16 hours at 120 deg C. Materials containing 5 to 30 phr elastomer were investigated. The fracture toughness of these elastomer-modified epoxies was measured in terms of the critical strain energy release rate, G_{IC} , using a three-point-bend geometry. The

toughening mechanism was elucidated using a tensile dilatometry technique that directly measures the longitudinal and transverse strains, thus enabling the calculation of volume strain. A plot of volume strain versus longitudinal strain often readily reveals the types of micromechanical deformations occurring in the uniaxial tensile specimen up to yield. Several microscopy techniques were employed to corroborate the tensile dilatometry results (see Figure 1).

BACKGROUND

REVIEW OF LAST YEAR'S WORK:

TOUGHNESS RESULTS— Toughness enhancement more a function of rubber content than rubber particle diameter

ELUCIDATION OF TOUGHENING MECHANISM—

Volume dilation of toughened materials indicate shear deformation & void growth

Microscopy— shear & voiding deformations

CONCLUSION— Rubber particles cavitate which dissipates bulk strain energy. The particles or cavities enhance shear band formation, which dissipates shear strain energy.

Figure 1

PART I: THE EFFECT OF RUBBER CONTENT

Epoxies composed of EPON 828/piperidine(5phr)/HYCAR CTBN 1300X8(varying content) are two phase materials consisting of an epoxy matrix with monodispersed one micron diameter rubber particles (abbreviated 828-pip-8). Epoxies composed of EPON 828/piperidine/HYCAR CTBN 1300X15(varying content) are two phase materials consisting of polydispersed 5-10 micron diameter rubber particles (abbreviated 828-pip-15). It was found that fracture toughness was more a function of rubber content than rubber particle size, for the 1-10 micron diameter range(see Figure 2). Also, it is important to note that Epoxy 828-pip-13 (13 is short for HYCAR CTBN 1300X13) did not contain a separate rubbery phase and exhibited little improvement in fracture toughness; thus the formation of a discrete rubbery phase seems to be essential to the rubber toughening of epoxies.

The addition of bisphenol "A" (BPA) to 828-pip-8 reduces the average particle diameter to ca. 5 microns at the 5 and 10 phr elastomer levels and induces a bimodal distribution of particle sizes (ten- and sub-micron) at 15 phr elastomer. Figure 2 also shows that the G_{IC} values of the 828-BPA-pip-8 epoxies are greater than those of

the 828-pip-8 epoxies. It is tempting to attribute the increased toughness enhancement to rubber particle size or size distribution. However, it will be shown later that this toughness enhancement is most likely due to the increased ductility of the epoxy matrix.

Note: it was observed that as the fracture toughness of these elastomer-modified epoxies increases, the size of the stress-whitened zone on the fracture surface of the 3PB specimens also increases; i.e., fracture toughness is directly related to the size of the stress-whitened or damaged zone.

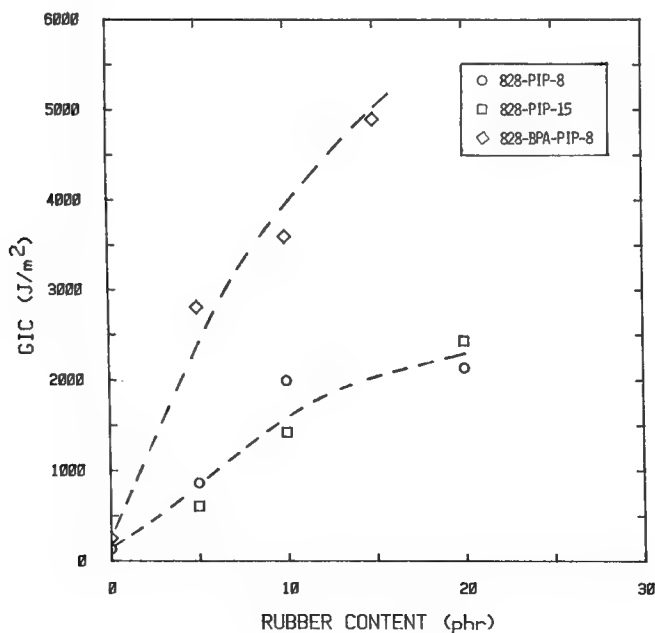


Figure 2

PART I: TENSILE DILATOMETRY DATA FOR BASELINE EPOXY

As mentioned previously, the toughening mechanism of these elastomer-modified epoxies was elucidated using tensile dilatometry. A servo-hydraulic testing machine was used to perform these experiments at several strain rates. Stress versus strain behavior as well as volume strain versus elongational strain behavior is monitored using this technique.

Figure 3 shows an engineering stress-strain curve and several volume strain curves taken at several strain rates for a neat epoxy. These curves are the results of an average of three tensile specimens tested for each strain rate reported. The stress-strain curve exhibits a yield stress and a reduction of stress after yield. This strain softening effect is indicative of shear band formation. Indeed, shear bands are easily detected with the naked eye on the surface of fractured tensile specimens. The interpretation of the volume strain curves is as follows: the initial increasing portion of the curve is simply due to the Poisson Effect; the curve then goes to a maximum volume strain, then to a slight decrease in volume strain which is indicative of shear deformation. Note that as the strain rate is increased the maximum in the volume strain increases and occurs at a larger elongational strain in a manner similar to that of the yield stress (not shown).

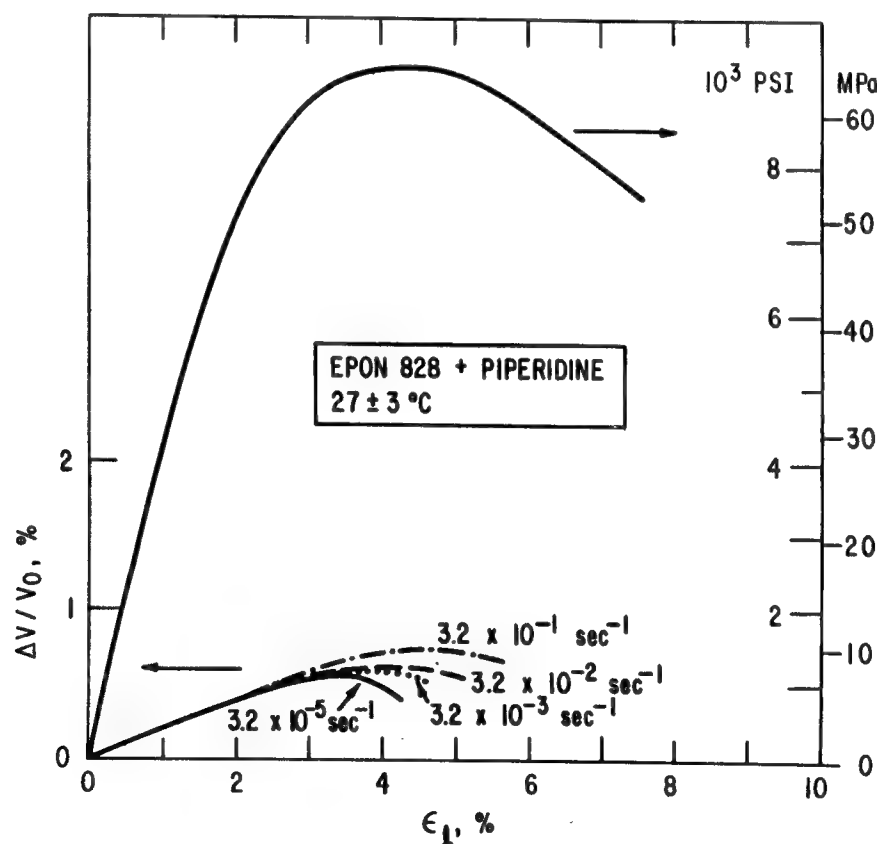


Figure 3

PART I: TENSILE DILATOMETRY DATA FOR ELASTOMER-MODIFIED EPOXY

Figure 4 contains the tensile dilatometry results of one of the elastomer-modified epoxies containing 20 phr HYCAR CTBN 1300X8. The set of stress-strain curves for this material clearly shows the increase of yield stress with increasing strain rate. At the lower strain rates the shape of the volume strain curves of these elastomer-modified epoxies is almost identical to that of the neat epoxy. However, at higher strain rates the volume strain curves are significantly different than those of the neat epoxy. At these high strain rates a process that causes an additional increase in volume strain occurs. This process is now known to be the voiding of the rubber particles. Also, a close examination of the volume strain curve taken at the highest strain rate reveals that enhanced shear deformation also occurs.

It is reasoned that these higher tensile strain rate results are more representative of the strain rates occurring at the crack tip. Thus, from the complete set of volume strain results (not all of the results are shown) the following toughening mechanism is proposed: the rubber particles, which are under a hydrostatic tensile stress at the crack tip, cavitate, which dissipates bulk strain energy. Furthermore, these cavitated particles promote the formation of shear bands which also dissipates bulk strain energy. It is the build-up of bulk strain energy that results in brittle fracture. In summary, cavitation and enhanced shear band formation are the micromechanical deformation mechanisms that occur ahead of the crack tip and produce a stress-whitened zone that effectively blunts the sharp crack, thus producing the fracture toughness enhancement.

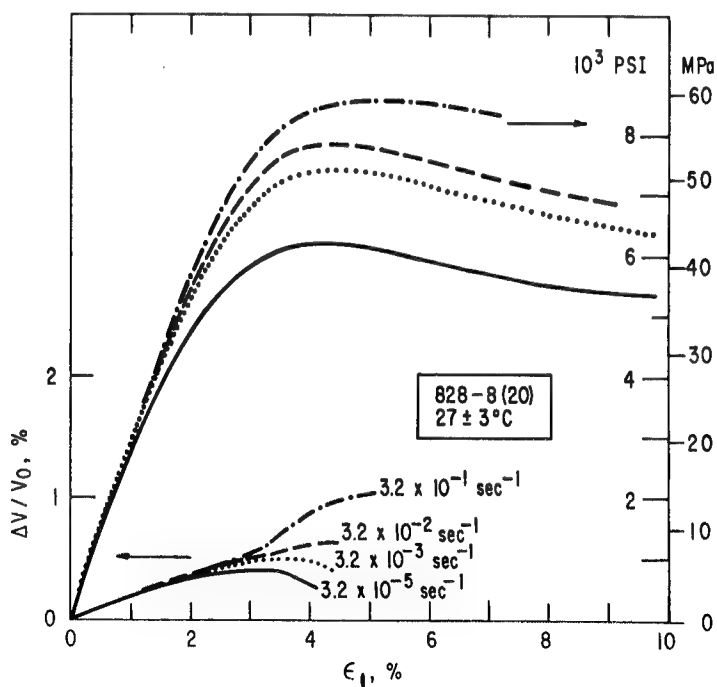


Figure 4

PART I: SCHEMATIC OF FRACTURE SPECIMENS

Scanning Electron Microscopy (SEM) and Transmission Optical Microscopy (OM) techniques were employed to corroborate the toughening mechanism elucidated using our uniaxial tensile dilatometry technique. Figure 5 is a schematic of the two types of fractured specimens used in this investigation. For brevity, let us concentrate on the stress-whitened region on the fracture surface of a SEN-3PB fracture toughness specimen, since the size of this region is related to fracture toughness.

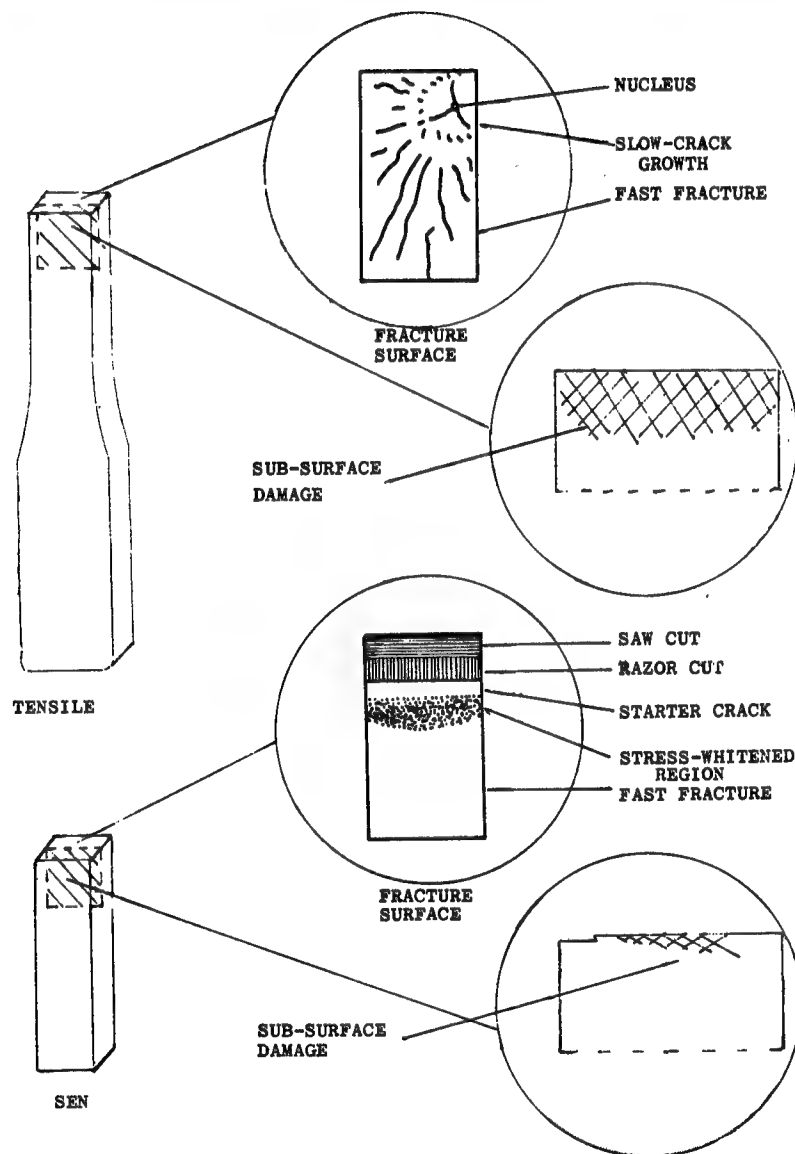


Figure 5

PART I: SEM MICROGRAPHS OF STRESS-WHITENED REGION AND FRACTURE SURFACE OF ELASTOMER-MODIFIED EPOXY

Figure 6 is an SEM micrograph of the stress-whitened region of 828-pip-15(30) that readily shows cavitation of the matrix and also signs of particle-particle interaction as evidenced by the non-hemispherical shape of the voids.

A SEM back-scattered electron imaging technique was employed on osmium tetroxide (OsO_4) stained fracture surfaces to prove conclusively

that the "missing rubber particles" do not simply "pop out" but instead cohesively fail and are actually lining the walls of the cavitated matrix. Figure 7 is such a SEM micrograph. Note that the regions which contain OsO_4 appear white. This micrograph shows that

the elastomer is in fact lining the walls of the cavities and the rubber particles are not "missing".

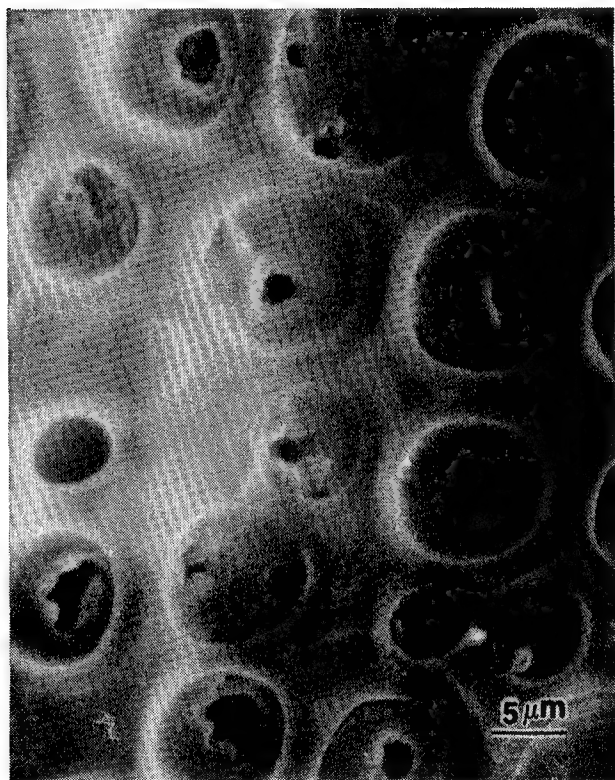


Figure 6



Figure 7

PART I: OPTICAL MICROGRAPH (OM) OF A FRACTURED ELASTOMER-MODIFIED EPOXY

OM is a useful technique for examining subsurface deformations which scatter light or induce birefringence. In order to view the damage below the fracture surface, a thin section perpendicular to the fracture surface was obtained by metallographic polishing techniques. Figure 8 is an optical micrograph of the subsurface damage in a SEN-3PB 828-pip-15(10) specimen which contains rubber particles greater than five microns in diameter, which are readily seen using this technique. In this micrograph, the thin section is viewed under bright field. The cavitated rubber particles appear dark since they scatter transmitted light. It is important to note that the oriented material composing the shear bands is more readily observed under crossed-polarized light.

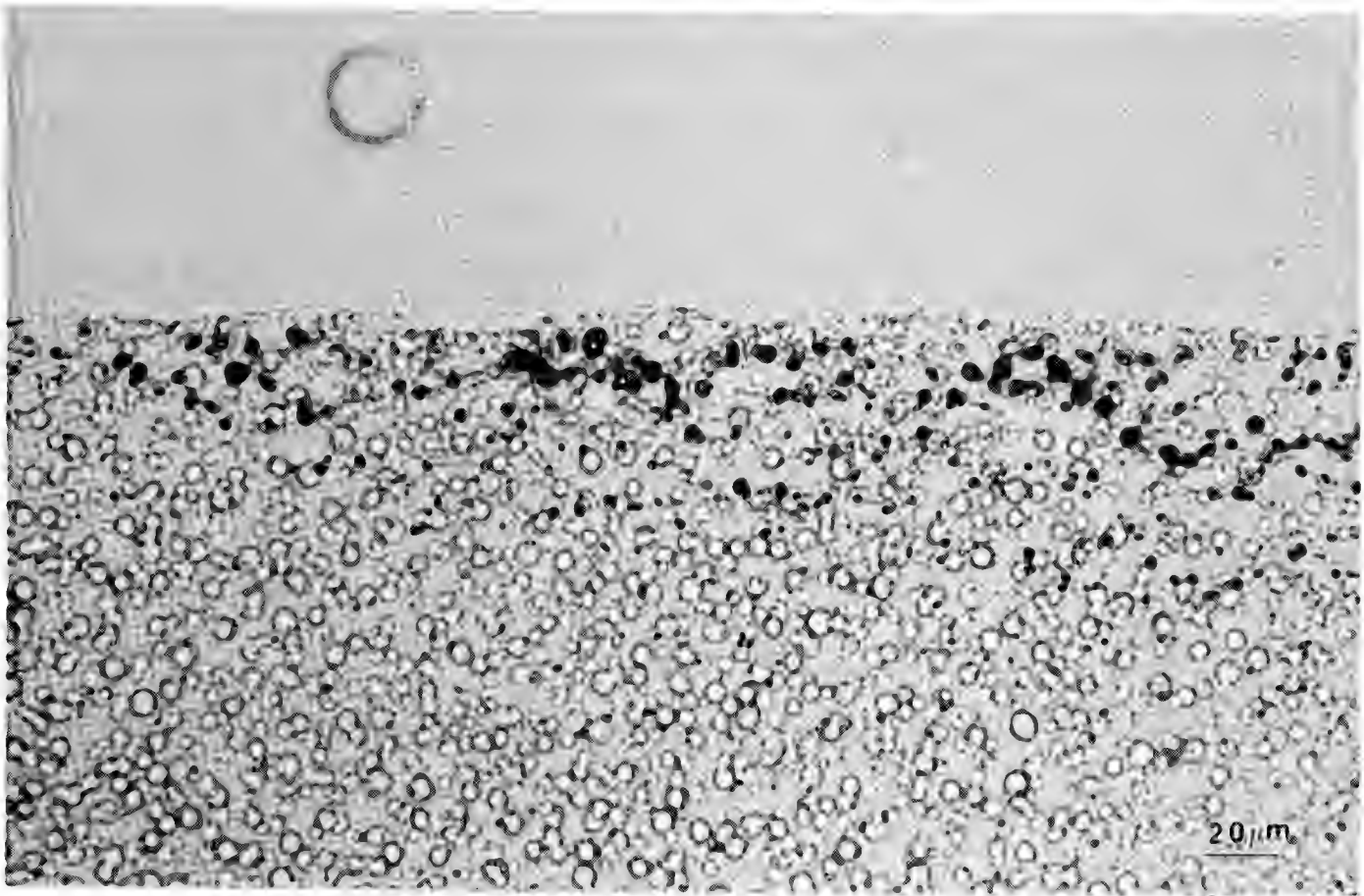


Figure 8

PART I: OPTICAL MICROGRAPH OF FRACTURED ELASTOMER-MODIFIED EPOXY UNDER CROSS-POLARIZED LIGHT

Figure 9 is an optical micrograph of the same thin section viewed between crossed polarizers. The birefringent regions which appear white are actually shear bands which connect the voided rubber particles. Shear banding and voided rubber particles are also seen in optical micrographs of thin sections of fractured tensile specimens (not shown).

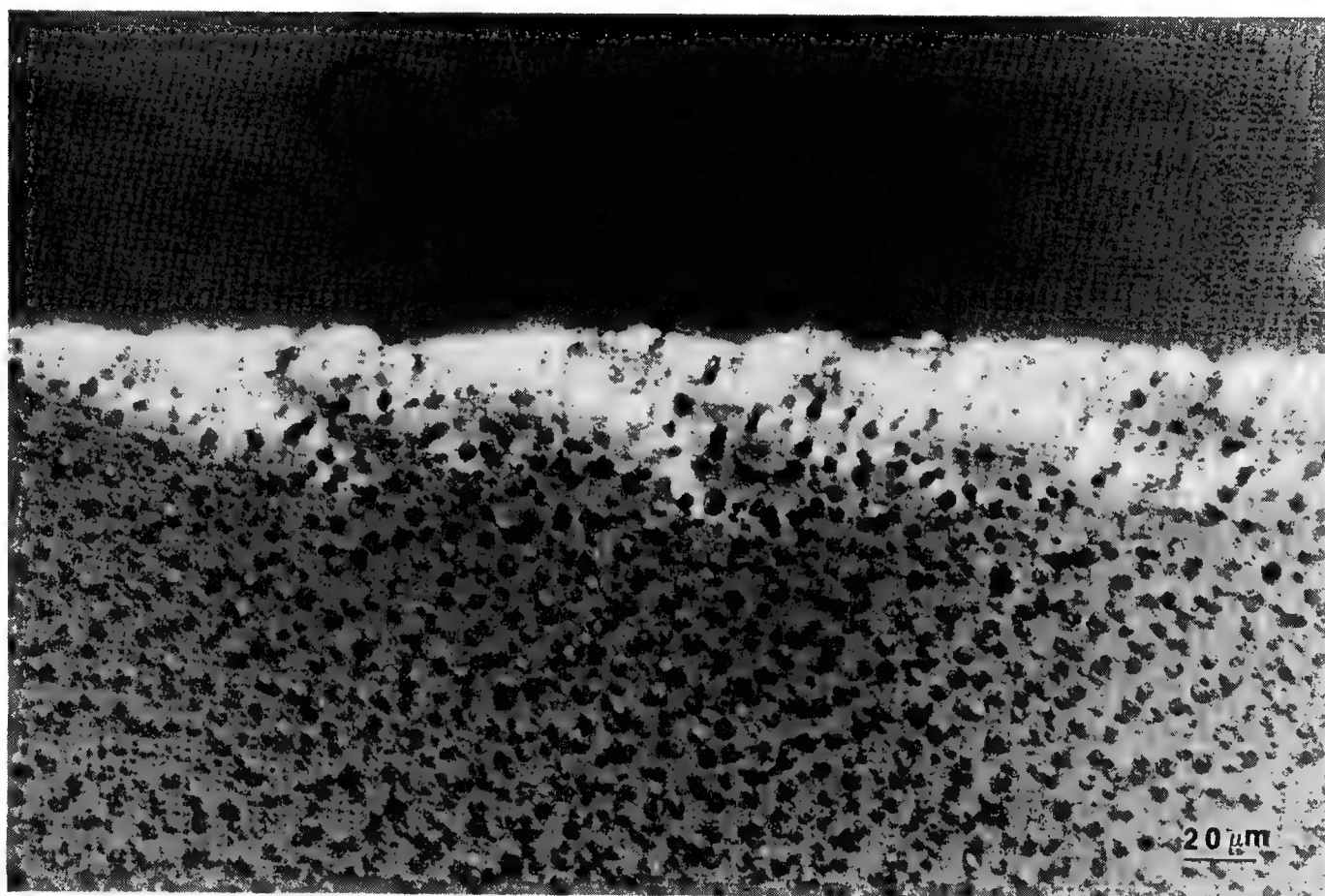


Figure 9

PART I: CONCLUSIONS

In summary, the types of deformations seen by the various microscopy techniques employed are completely consistent with our interpretation of the uniaxial tensile dilatometry data. It is important to note that Transmission Electron Microscopy (TEM) did not yield any evidence of even a single craze in these elastomer-modified epoxies and the tensile dilatometry results did not contain any evidence for the occurrence of a large dilatational process; hence massive crazing as an energy dissipating or toughening mechanism is unlikely. We have presented evidence that these elastomer-modified epoxies are toughened by the formation of a plastic zone ahead of the crack tip. This plastic zone consists of cavitated rubber particles and shear bands whose formation effectively dissipates bulk strain energy thus inhibiting brittle fracture. Since most of the energy dissipation is due to the deformation of the epoxy matrix, then it seems reasonable to assume that enhanced matrix ductility should produce an even more pronounced toughening effect (see Figure 10).

PREDICTION:

Since most of the energy dissipation was due to matrix deformation then enhanced matrix ductility should produce an even more pronounced effect

Figure 10

PART II: OBJECTIVES AND APPROACH

OBJECTIVE:

The Part II objective was to determine the role of matrix ductility on the toughening mechanism of elastomer-modified epoxies.

APPROACH:

Our approach was to reduce cross-link density (hence increasing ductility) by using various equivalent-weight epoxide resins. Fracture toughness was again measured in terms of G_{IC} . The characterization of the toughening mechanism was again performed using our uniaxial tensile dilatometry technique and corroborated using various microscopy techniques (see Figure 11).

2nd PHASE OBJECTIVE:

To determine the role of the matrix ductility on the toughenability and the toughening mechanism of elastomer-modified epoxies.

APPROACH:

Reduction of cross-link density by using epoxy resins of varying epoxide equivalent weights

Evaluation of fracture toughness by measuring G_{IC} in 3PB

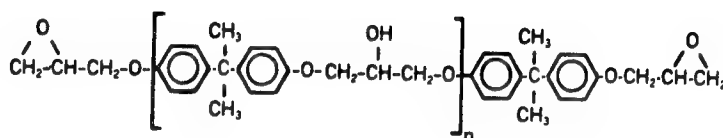
Characterization of toughening mechanism by tensile dilatometry and microscopy

Figure 11

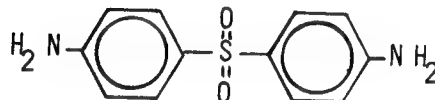
PART II: LIST OF MATERIALS

Figure 12 lists the materials used in this investigation. Several DGEBA epoxide resins where $n=0$ to 10 were used. These epoxide resin were cured with a stoichiometric amount of diaminodiphenyl sulfone (DDS). DDS was chosen due to its importance in aerospace applications. These epoxies were modified with a carboxyl terminated butadiene-acrylonitrile copolymer, a liquid elastomer commercially available from B.F. Goodrich (HYCAR CTBN 1300X13).

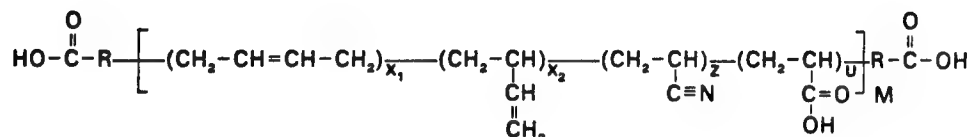
LIST OF MATERIALS



DGEBA Resin



DDS (curing agent)



LIQUID ELASTOMER (HYCAR CTBN 1300x13)

Figure 12

PART II: FRACTURE TOUGHNESS RESULTS

Figure 13 is a plot of G_{IC} versus epoxide monomer molecular weight.

For the neat resins there is little dependence of G_{IC} on monomer molecular weight. In fact all of these neat epoxies fail in a brittle manner when a sharp crack is present. As each of these epoxies is modified with 10% by volume elastomer an interesting effect is seen: the G_{IC} becomes very dependent upon the epoxide monomer molecular

weight. The highly cross-linked epoxies (low epoxide monomer molecular weight) are not toughened by the addition of the elastomeric phase. However, as the cross-link density is decreased the fracture toughness of the elastomer-modified epoxies increases; i.e., the toughenability increases.

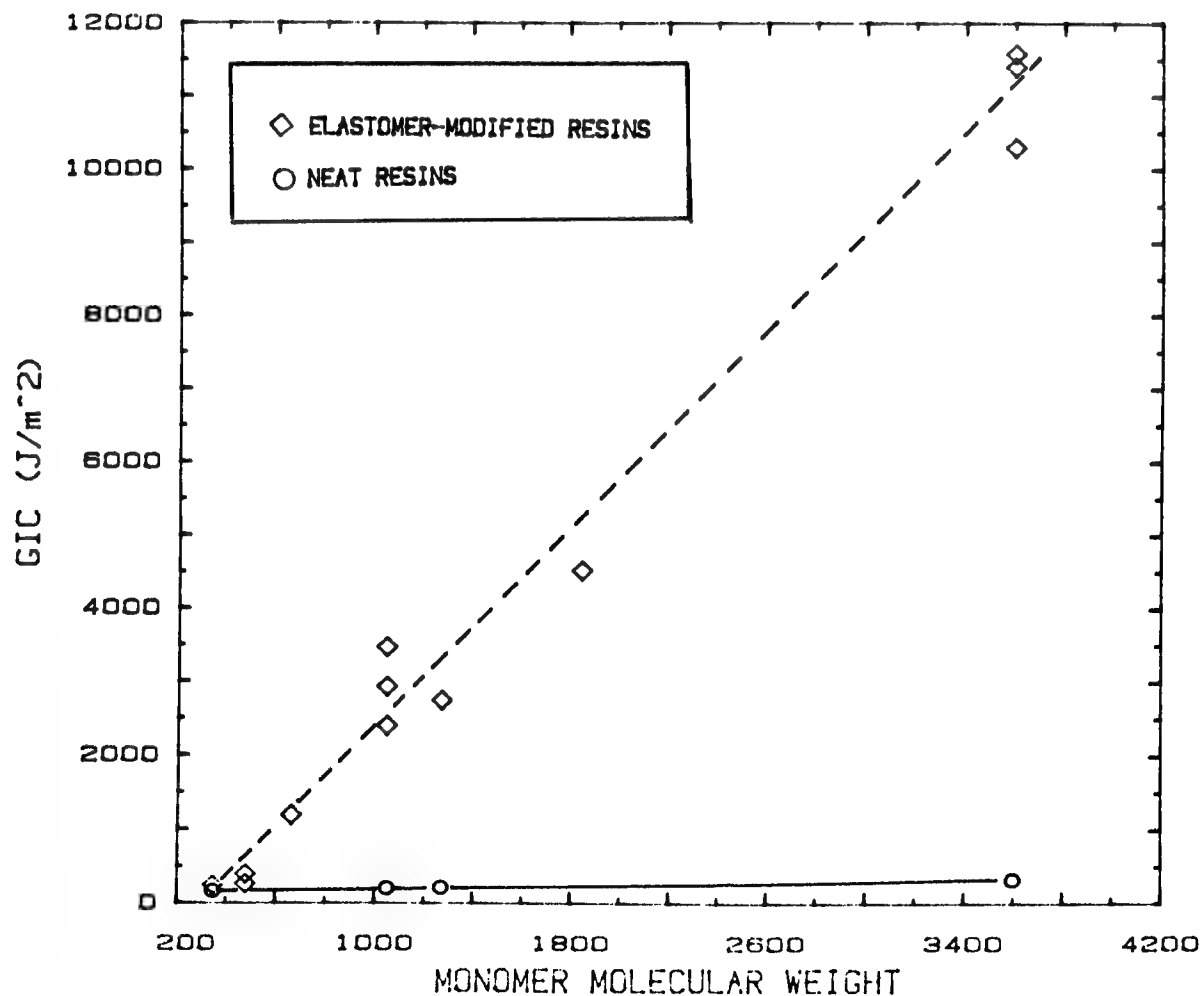


Figure 13

PART II: VOLUME STRAIN RESULTS

To elucidate the micromechanical mechanisms responsible for the enhanced toughness, volume strain measurements were again performed. However, only the highest strain rate was necessary. For the epoxy with the highest cross-link density, the volume strain data could not be measured since this material was very brittle even in uniaxial tension and fractured at less than 1% strain.

Figure 14 shows the tensile dilatometry results for an epoxy with a lower cross-link density. The solid lines are the results for the neat epoxy and the dot-dash lines correspond to the elastomer-modified epoxy. The reduction in the yield stress and tensile modulus upon elastomer modification is readily apparent in the stress strain curves. The volume strain curves exhibit the now familiar increase in volume strain due to the Poisson Effect. The slope of the volume strain curve decreases prior to yield, which indicates that a shear process has occurred. The slope of the volume strain curve of the elastomer-modified epoxy increases prior to yield, which indicates a voiding process has occurred.

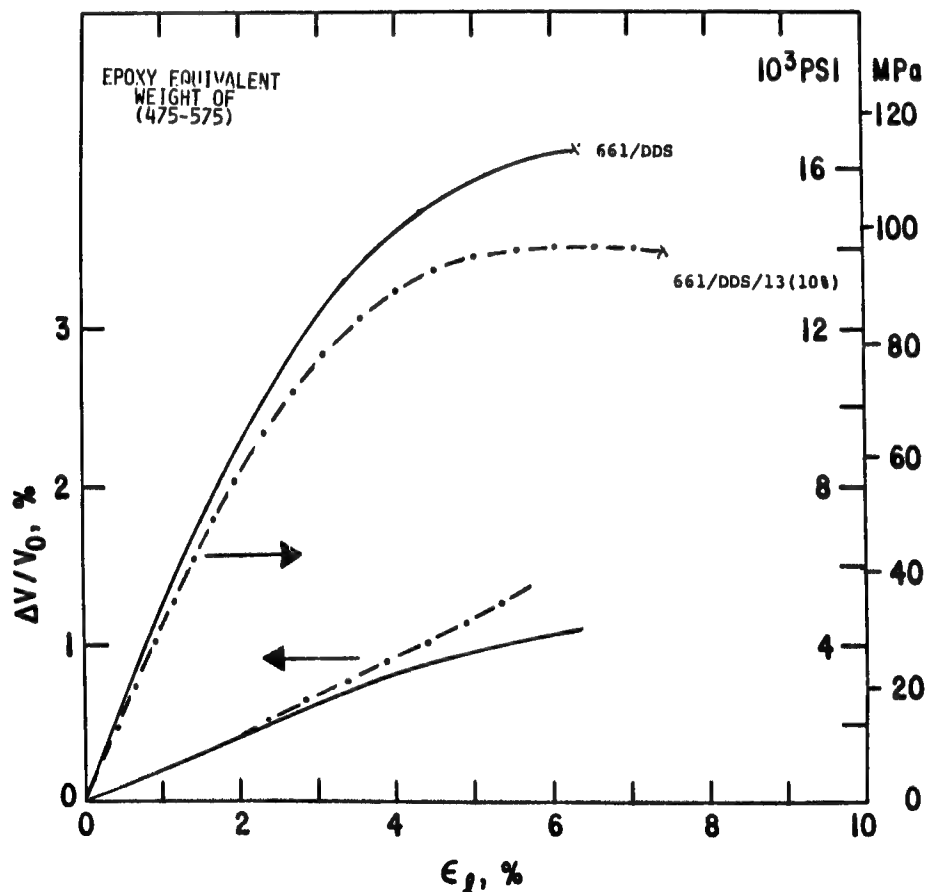


Figure 14

PART II: VOLUME STRAIN RESULTS

Figure 15 presents the uniaxial tensile data for the epoxy with the lowest cross-link density studied in this investigation. Note that in the stress-strain curves of both the neat and elastomer-modified epoxies there exists much extension after yield even at this high strain rate. These materials are very ductile compared to the epoxies with the highest cross-link density which are very brittle. The micro-mechanical deformation mechanisms are the same as in the other epoxies tested as evidenced by the volume strain curves. The neat resins tend to deform simply by shearing, while the elastomer-modified epoxies deform by voiding and shearing.

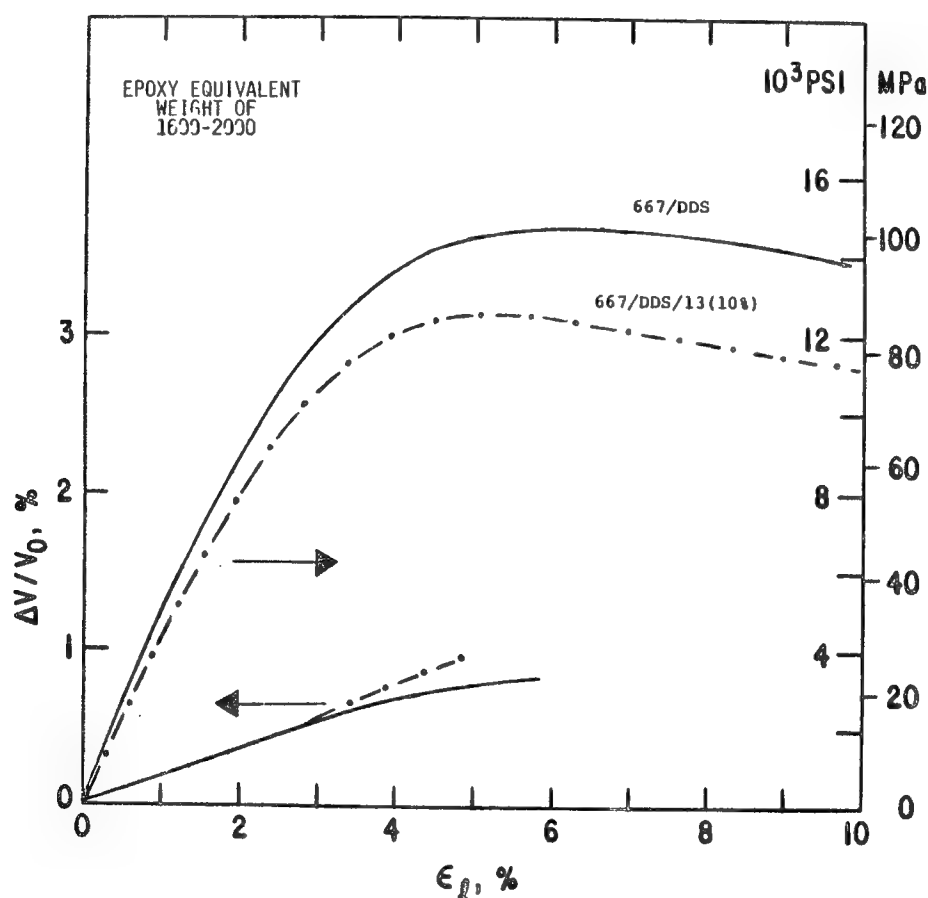


Figure 15

PART II: SEM ANALYSIS OF SEN-3PB FRACTURE SURFACES

SEM analysis of the fracture surface of the SEN-3PB specimens was again performed to corroborate our uniaxial tensile dilatometry results. Figure 16 is a SEM micrograph of the fracture surface of the elastomer-modified epoxy with the highest cross-link density. The crack had travelled from left to right and the area of interest is the small plastic zone which had formed prior to the propagation of the crack. Note that no stress-whitened zone can be detected with the naked eye since the small plastic zone was not sufficiently thick to scatter light. Also note that the shape of the fractured rubber particles are very hemispherical and are very shallow. The lack of shear deformation and cavitation of the matrix corresponds well to the lack of toughness enhancement seen.

Figure 17 is a SEM micrograph of the fracture surface of a SEN-3PB specimen of an elastomer-modified epoxy with a reduced cross-link density (monomer equivalent weight of 475-575 was used). For this specimen a stress-whitened zone is easily observed with the naked eye. The area of interest is again at the beginning of the plastic zone. The region before the plastic zone is of the precracked region and contains shallow cavities from fractured rubber particles. Note that in the plastic zone there exists evidence for localized shear deformation and the cavities appear to be much larger and deeper. The existence of the plastic zone corresponds well to the toughness enhancement.

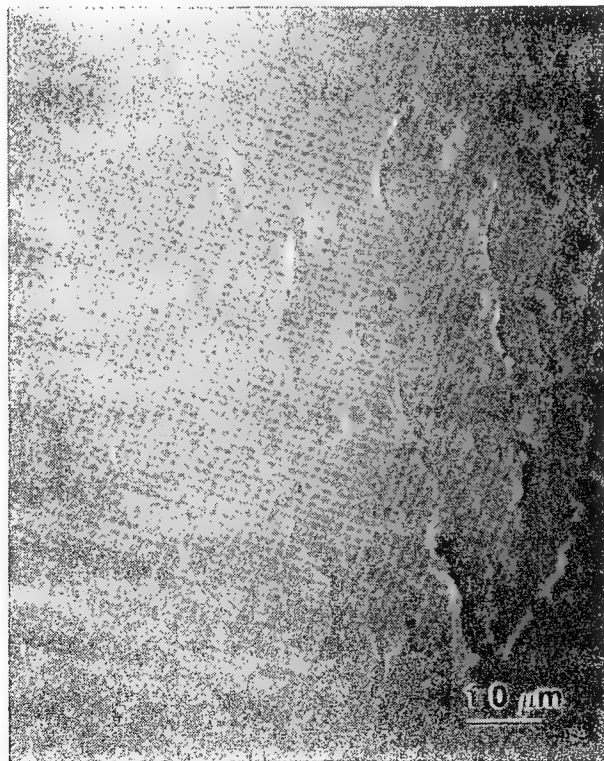


Figure 16

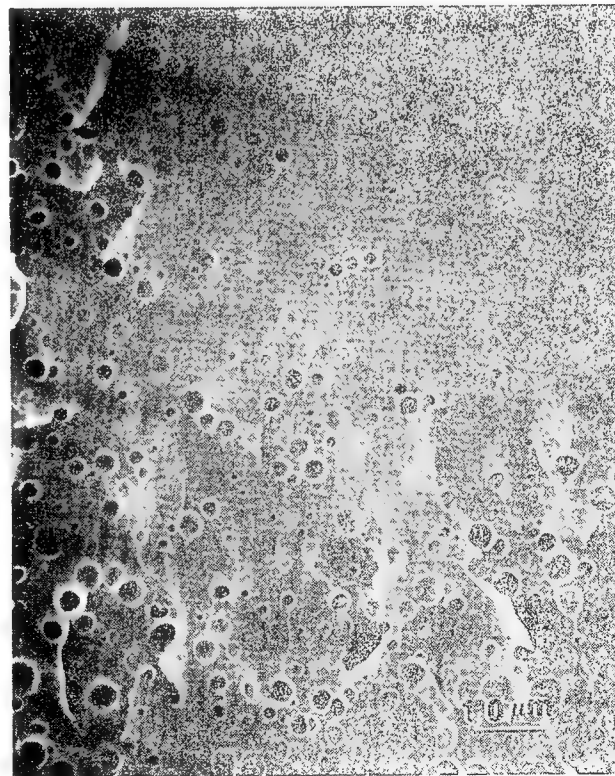


Figure 17

PART II: SEM ANALYSIS OF SEN-3PB FRACTURE SURFACES

Figure 18 is a SEM micrograph of the fracture surface of a SEN-3PB specimen of an elastomer-modified epoxy with the least cross-link density (monomer equivalent weight of 1600-2000 was used). The stress-whitened zone of this specimen spans the region where the starter crack had arrested to the edge of the specimen where the striker had made contact. This SEM micrograph shows that a stark contrast exists between the region of fast crack growth and the region of slow crack growth (the plastic zone). The plastic zone consists of rubber particles that have been sheared and cavitated to an extent much greater than in any of the other epoxies we have studied. The size of this plastic zone corresponds well to the increase in toughness enhancement.

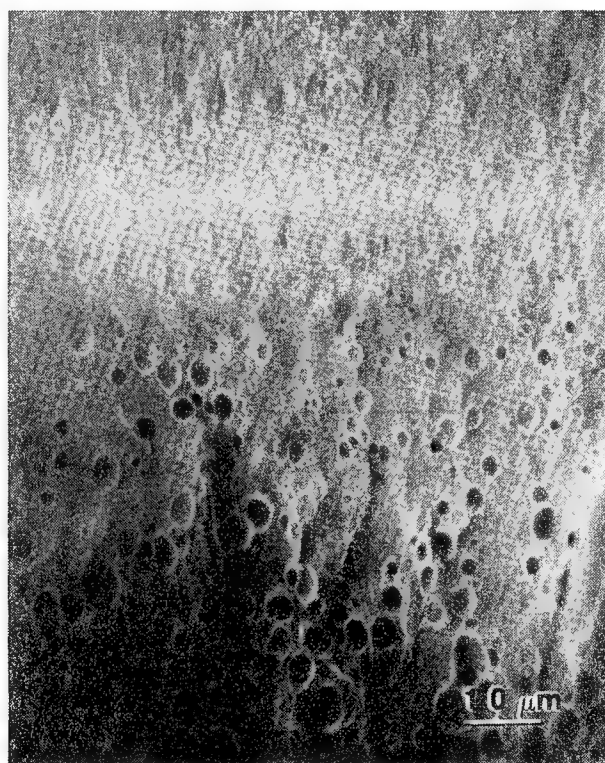


Figure 18

PART II: OPTICAL MICROSCOPY OF SUBSURFACE DAMAGE

Optical Microscopy (OM) was used to observe the sub-surface microdeformations that had occurred in the SEN-3PB specimens.

Figure 19 is an optical micrograph of the plane perpendicular to the fracture surface (see figure 5) of a SEN-3PB specimen composed of an elastomer-modified highly cross-linked epoxy. The thin specimen was viewed between crossed polarizers. There exists a shear zone of about three microns in thickness just below the fracture surface. Note that none of the particles appears dark; thus they did not cavitate. Also note the absence of shear bands. Since this plastic zone is relatively small, it is not surprising that no fracture toughness enhancement was seen.

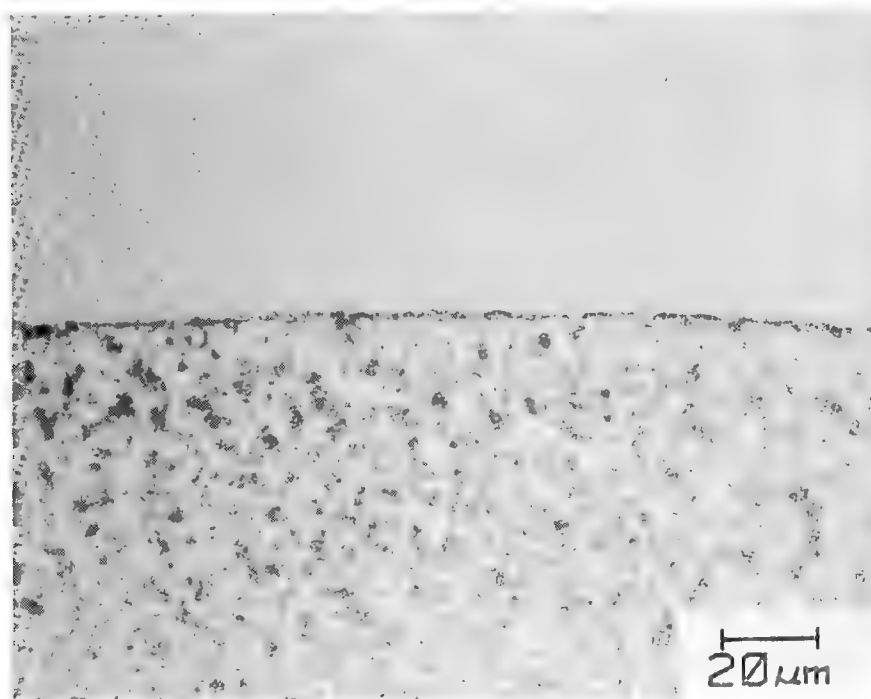


Figure 19

PART II: OPTICAL MICROSCOPY OF SUBSURFACE DAMAGE

However, as the cross-link density of the epoxy matrix is reduced or the elastomer-modified systems, the size of the stress-whitened zone and the value of G_{IC} increase.

Figure 20 is an optical micrograph, again taken in polarized light and in the same plane as the previous micrograph. But in this specimen the cross-link density of the matrix was reduced by using an epoxide monomer of 475-575 g/eq-wt. The particles which appear dark have cavitated and thus scatter light. Close examination reveals that birefringent bands - shear bands - connect the cavitated rubber particles. It seems more than reasonable to attribute the enhanced energy dissipation to the formation of shear bands and voids which comprise the plastic zone.

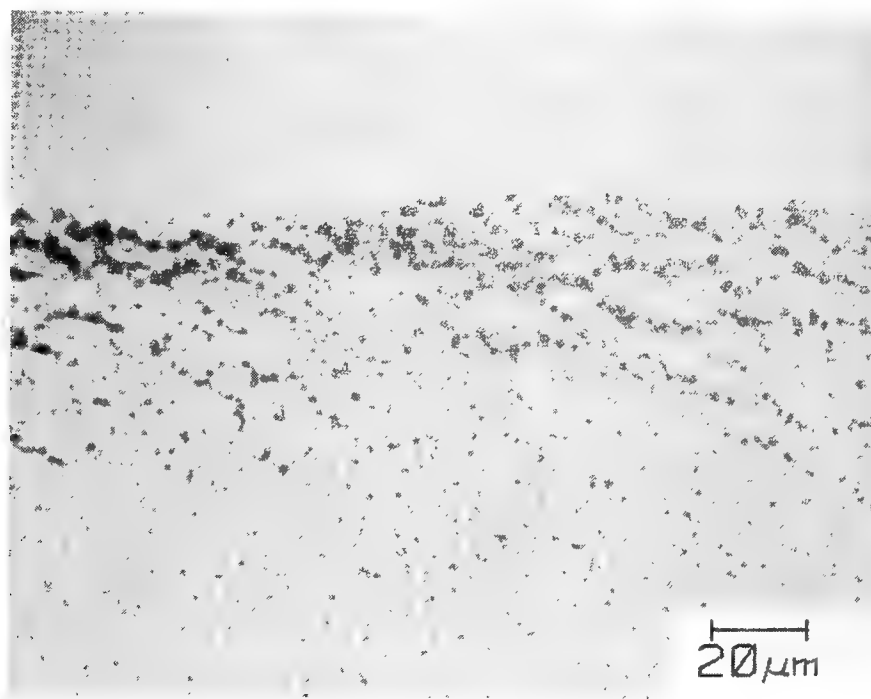


Figure 20

PART II: OPTICAL MICROSCOPY OF SUBSURFACE DAMAGE

In this case figure 21 is an optical micrograph taken under identical conditons of a SEN-3PB in which the cross-link density was reduced by using an epoxide monomer of 1600-1800 g/eq-wt. The damage zone is much larger than those seen in the previously examined elastomer-modified epoxies. There is evidence for much cavitation and shear banding. As previously mentioned, the size of the plastic zone corresponds well to the increase in fracture toughness.

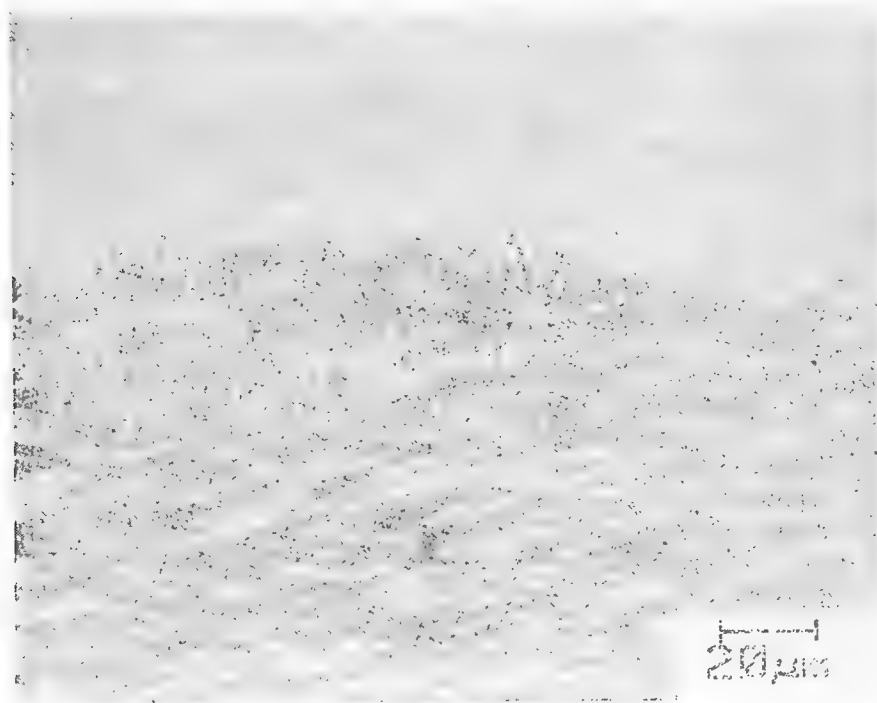


Figure 21

PART II: OPTICAL MICROSCOPY OF SUBSURFACE DAMAGE

Figure 22 is an optical micrograph of the same specimen but taken in the region where the specimen was subjected to a compressive stress due to the contact with the striker. This micrograph is important since it shows that these rubber particles can sustain large shear strains when subjected to a compressive stress.

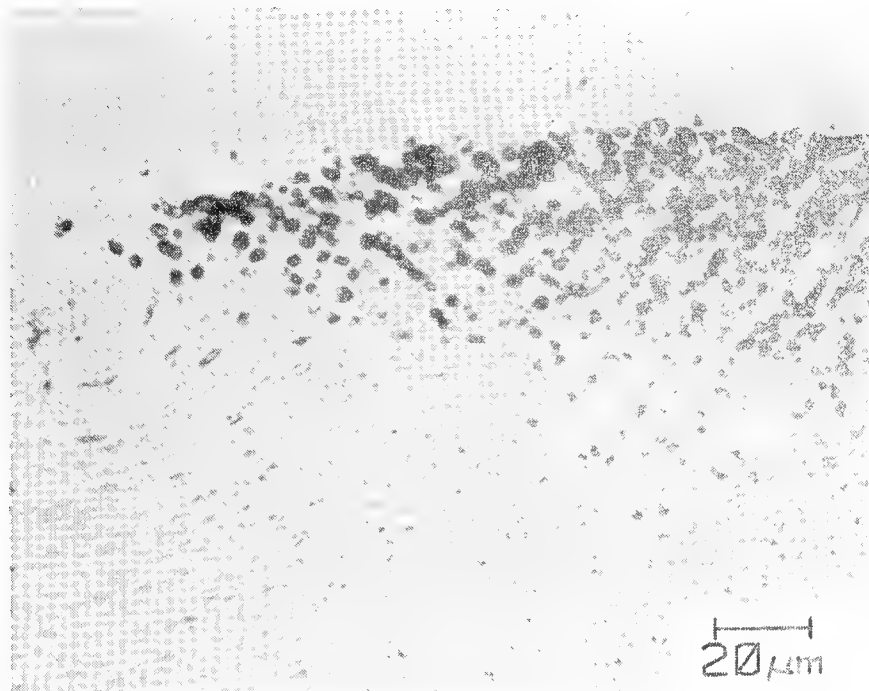


Figure 22

PART II: CONCLUSIONS

In conclusion, two points should be emphasized. First, the toughening mechanism of elastomer-modified epoxies consists of the formation of a plastic zone by voiding and shear banding. Second, increasing the ductility of the epoxy matrix enhances the toughenability of the matrix upon the addition of a second, rubbery phase. Therefore, as the cross-link density of the epoxy matrix decreases the fracture toughness of the elastomer-modified version increases. Figure 23 summarizes these conclusions.

CONCLUSIONS:

TOUGHENING MECHANISM— *When present, similar to piperidine cured systems => rubber particles cavitate and promote shear band formation*

EFFECT OF MATRIX DUCTILITY—

Lowering cross-link density enhances ductility

Increasing ductility enhances toughenability!

Figure 23

FREE VOLUME CONSIDERATIONS IN THERMOPLASTIC AND THERMOSETTING RESINS

Robert F. Landel, A. Gupta, J. Moacanin,
D. Hong, F. D. Tsay, S. Chen, S. Chung,
R. Fedors, and M. Cigmecioglu
Jet Propulsion Laboratory
Pasadena, California

This paper describes some of the work which has been done at JPL on the direct measurement of physical ageing and of the volume changes which go on during the course of this ageing. I particularly want to stress the need for concomitant stress-strain and volume-strain measurements. We first present some data on PMMA showing its physical ageing as measured by its stress relaxation response and the accompanying volume changes; we follow with an indication of how one can measure the free volume both directly from the volume change itself and (we think) relatively directly via a new and independent technique; and finally we show the application of this new technique -- electron spin resonance spectroscopy -- to other polymer systems.

Figure 1 is a reminder of the course of stress relaxation in PMMA for samples which have been aged at room temperature for various lengths of time, after cooling from the molten state, before starting the experiment (Cizmecioglu et al.).

For each ageing time the modulus is higher, although (in these experiments) the rate of stress relaxation remains constant. Hence the data are superposable to a single master curve by a translation in the direction shown by the arrow.

This ageing process occurs because the material is in the glassy state and hence is not at volumetric equilibrium.

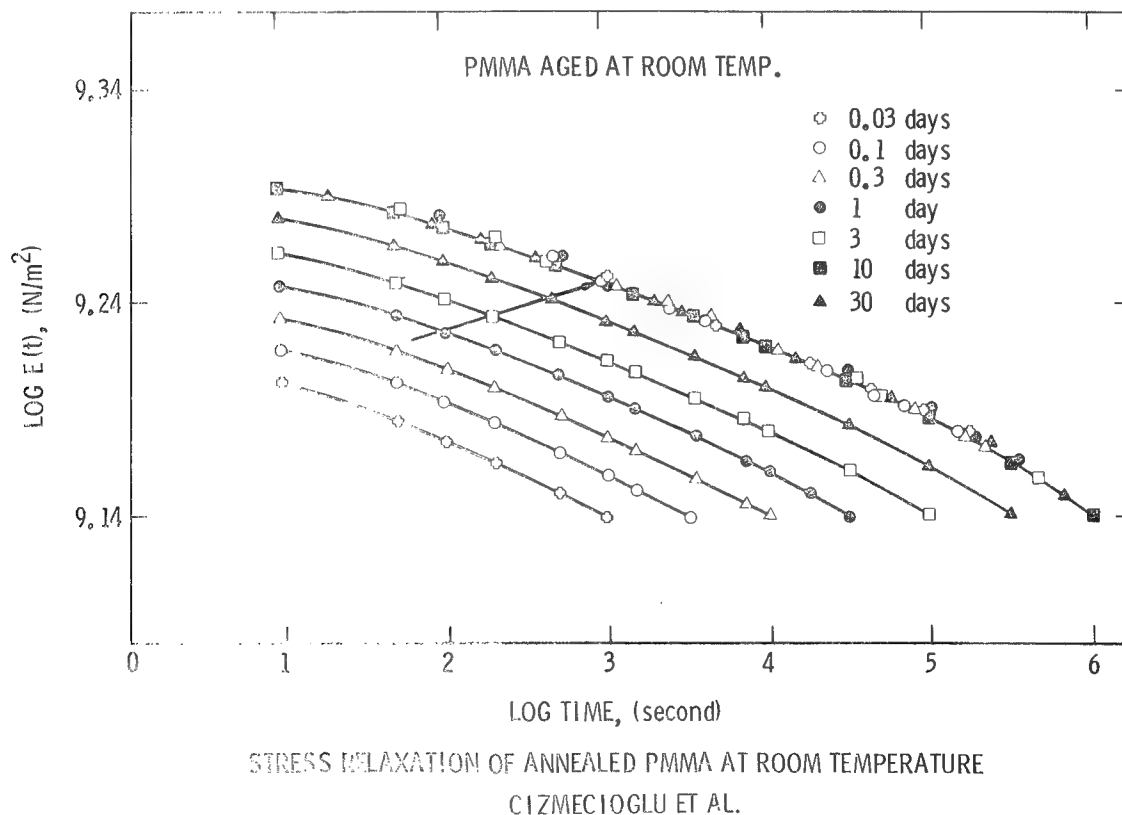


Figure 1

To examine the consequences of not being at equilibrium, consider the volume-temperature-time response. On cooling a glass-forming liquid, the volume follows the liquidus line, shown in figure 2. At the glass temperature T_g , the expansion coefficient changes and the volume follows the path containing point A. If the cooling rate is reduced, the volume proceeds farther along the liquidus line to a lower T_g , and then follows the path containing point B. If the sample is taken to point A and held at that temperature, the volume will slowly contract toward B, or even past it, as the volume drifts toward the equilibrium state denoted by point C. This state is a hypothetical one for temperatures much below T_g as conventionally measured (i.e., cooling rates of a few tenths of a degree Kelvin per minute).

The fact that the glass is not at equilibrium raises some interesting questions in trying to describe its mechanical properties in terms of elasticity theory, because the latter assumes that a material is being deformed from a fixed reference state, i.e., that it is at equilibrium. In glasses, the reference state is steadily changing with time even in the absence of additional load or deformation.

Setting this point aside, the question is: how could one follow the change in volume from point A to point B and what is the effect of this densification on the physical properties?

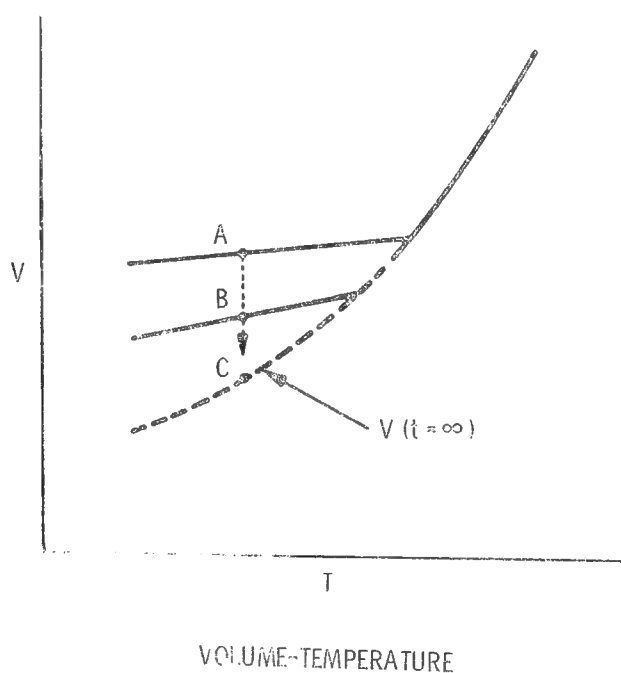


Figure 2

From the WLF treatment of time scaling in polymer relaxation processes, it is known that anything which affects the fractional free volume f of a material leads automatically to a change in the time response through a change in the time-scaling parameter or time shift factor a , as shown by the second bullet in figure 3. Here B is the Doolittle constant and f_0 is f measured at a reference state. Thus if f changes with temperature as: $f_0 = f_0 + \alpha_f (T - T_0)$, where T_0 is a reference temperature, one obtains the WLF equation at the right.

The volume shrinkage from A-->B-->C is almost solely a reflection of the loss in f , which is related to the difference in the volume at some time V (e.g. point A of Fig. 2) and the volume at equilibrium or infinite time V_∞ (e.g. point C in Fig. 2). The rate of volume shrinkage has been extensively studied by Kovacs and by Kovacs et al. Denoting the fractional change in volume as δ , Kovacs showed that the rate of change of δ with ageing time was approximately first order, with a time constant τ ; Kovacs et al. later showed that there is a spectrum of rates, so that $d\delta/dt$ is given by a summation over these rates. The problem then shifts to a need to calculate or measure δ .

• RATE OF APPROACH TO EQUILIBRIUM

$$\delta = \frac{V - V_\infty}{V_\infty}$$

$$\frac{d\delta}{dt} = \frac{\delta}{\tau_{\text{eff}}} \Rightarrow \sum^N \left. \frac{d\delta_i}{dt} \right|_T$$

HOW TO GET V_∞ IF $T \ll T_g$?

• SHIFT FACTORS

$$\ln a = B (f^{-1} - f_0^{-1}) \stackrel{\Delta T}{=} \frac{-(B/f_0)(T - T_0)}{(f_0/\alpha_f) + T - T_0}$$

KOVACS et al.

Figure 3

In order to calculate δ one needs first of all an analytic expression for the V-T response of the glass at the (hypothetical) equilibrium state (fig. 4). On the experimental side, one needs a direct measure of the volume state of the glass. This can be its time dependence during ageing/annealing as just described. Changes in volume can also arise with an applied strain and the magnitude of this change (and hence the magnitude of the change in physical properties) can also change with the strain field. That is, the value of δ for a given principal strain will depend on the degree of bi- and tri-axiality of the strain. Measurement of such volume changes accompanying the deformation should be made for a proper characterization of the response but unfortunately this is often done either crudely or not at all.

NEED:

1. V_{∞} -T IN GLASS STATE
2. DIRECT MEASURE OF VOLUME CHANGE WITH ANNEALING
3. DIRECT MEASURE OF VOLUME CHANGE WITH STRAIN AND STRAIN FIELD

Figure 4

The problem of defining an equilibrium volume temperature response and determining the resultant time scale parameter has been addressed recently by Curro, Lagasse and Simha. Simha and Somcynsky have developed an equation of state for liquids which are at equilibrium. It is based on a lattice model and relates reduced volume $\tilde{V} = V/V^*$, reduced temperature $\tilde{T} = T/T^*$ and reduced pressure $\tilde{P} = P/P^*$. The starred quantities are normalizing parameters which are material specific. At atmospheric pressure, a reduced equation of state results which relates V and T to the number of occupied lattice sites y . Empirically, it has been found that V^* and T^* can be determined by curve-fitting V - T data to the form $\ln \tilde{V} = A + B \tilde{T}^{3/2}$ and so the V - T curve in the liquid region can be described. This approach has been extended to liquids which are not at equilibrium, i.e. glasses, by Curro, Lagasse and Simha, who pointed out that an isothermal change in volume with time of ageing t_a , i.e., $V(T, t_a)$, is equivalent to a change in y . Taking the fractional free volume to be equal to $1-y$, they showed that it is possible to calculate V_{00} vs T . Then, using directly measured V - t_a data, one can calculate δ , thence f , and therefore a_{t_a} , i.e., the last equation in figure 5. The term t_{r_a} is a reference ageing time.

\tilde{V}, \tilde{T}, y RELATIONSHIP

$$\ln \tilde{V} = A + B \tilde{T}^{3/2}$$

GIVES T^*, V^* , THEREFORE y

$\tilde{V}, \tilde{T}, y_{\infty}$ RELATIONSHIP

CLS:

$$\tilde{V}(T, t_a) \Rightarrow y(T, t_a)$$

$$f(T, t_a) \equiv 1 - y(T, t_a)$$

$$f_{\infty} = 1 - y_{\infty}$$

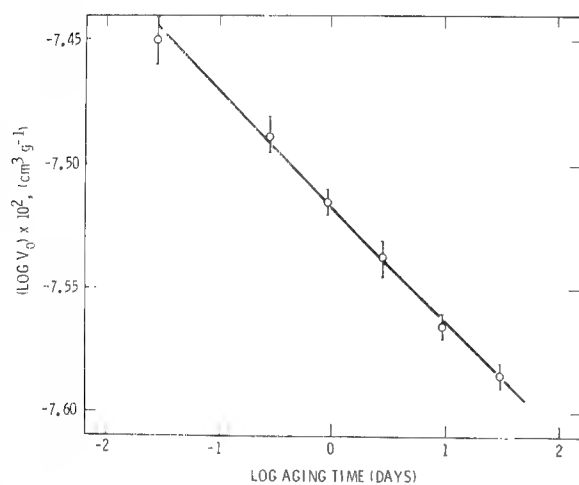
$$\text{LOG } a_T = \frac{B}{2.303} \left(\frac{1}{f(T)} - \frac{1}{f_{\infty}} \right), \text{ ABOVE } T_g, \text{ GIVES } B = 6.9$$

$$\text{LOG } a_{T, t_a} = \frac{B}{2.303} \left(\frac{1}{f(T, t_a)} - \frac{1}{f(T, t_a^*)} \right)$$

CURRO, LAGASSE, SIMHA

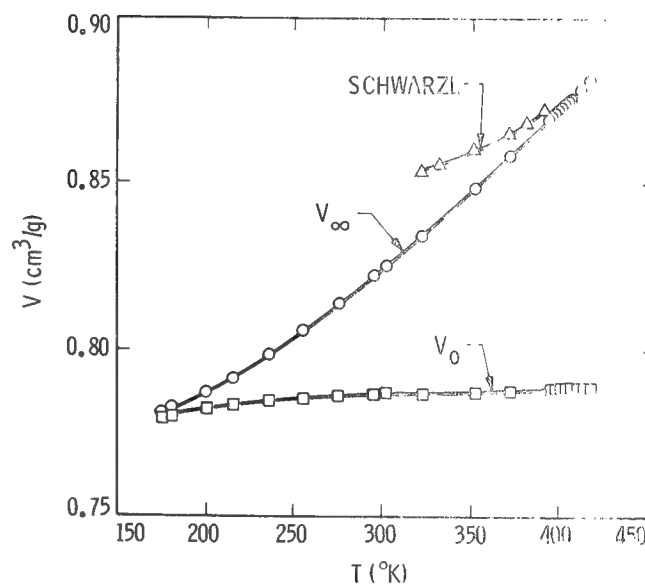
Figure 5

Using the JPL $V-t_a$ data of Hong et al. (fig. 6), they were able to determine the value of y as a function of T and hence calculate both the equilibrium volume V_∞ and the occupied volume V_0 as a function of temperature for PMMA (fig. 7). From these data and the value of B for PMMA in the glass transition region as found by Schwarzl and Zahradnik, they were then able to calculate a_{ta} .



MEASURED VOLUME VS. AGING TIME AT ROOM TEMPERATURE,
PMMA; CURRO, LAGASSE, SIMHA

Figure 6

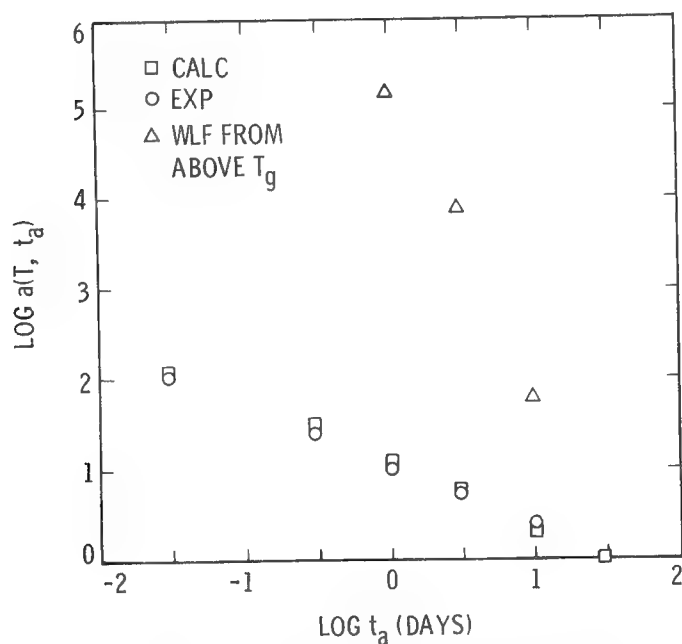


CALCULATED V, T RESPONSE; CURRO, LAGASSE, SIMHA

Figure 7

Figure 8 shows the excellent agreement obtained between the experimentally determined and calculated value of $\log a_{ta}$. Also shown (triangles) are the erroneous values of $\log a_{ta}$ which are calculated if parameters appropriate to the liquid state are used in the WLF equation to calculate the shift factor.

Hence it now appears to be possible to obtain the (hypothetical) equilibrium V-T response of a glass and from this to calculate both the rate of physical ageing and the consequences of ageing insofar as they affect the time scale of the physical property responses. Obtaining the requisite data can be a tedious task and so we are trying to establish independent means of assessing the free volume content, in order to both test the theory and reduce the labor involved.

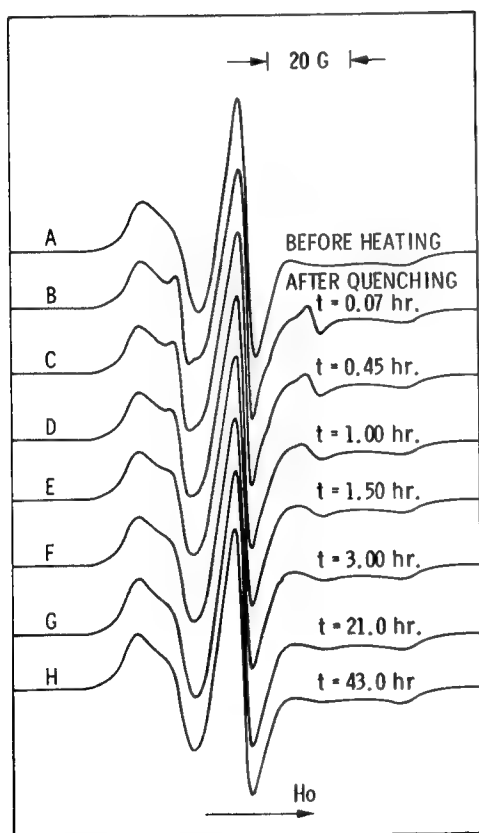


COMPARISON OF CALCULATED AND EXPERIMENTAL $\log a_{ta}$
SHIFT FACTORS; CURRO, LAGASSE, SIMHA

Figure 8

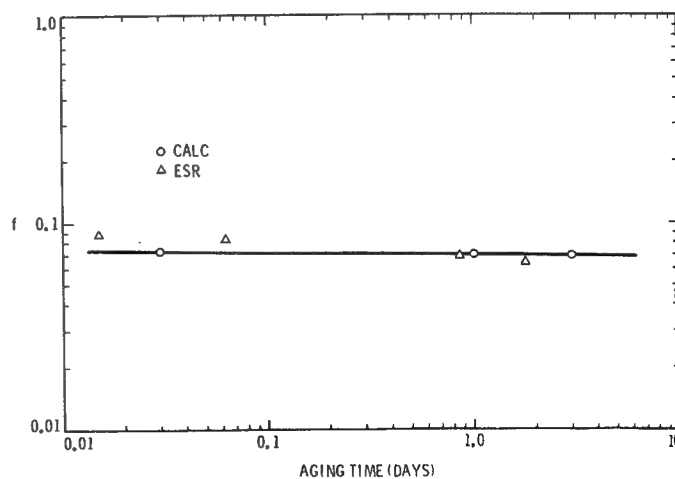
Tsay et al. (1982) at JPL have found that by introducing spin-active molecules into a polymer it appears to be possible to obtain a measure of the free volume. Figure 9 shows the electron spin resonance (esr) signal from the probe molecule TANOL (4-hydroxy-2, 2, 6, 6-tetramethyl-piperidine-1-oxyl) in PMMA. There is a broad assymmetric triplet, and on the high field side there can be a small narrow line component. The figure shows the decay of this narrow line component with ageing time, i.e., time after quenching the sample from the liquid state. This peak represents a fast, easy motion; the broad peak represents a retarded motion. We can separate out this narrow-line component by computer-assisted data reduction techniques and show that it corresponds exactly with the probe response when the PMMA is in the liquid state well above T_g .

Assuming that the existence and amplitude of the narrow line stem from the presence of the free volume and are a measure of their magnitude, then the ratio of the respective areas under these two peaks should be a direct measure of the free volume. If this is so, then one can calculate $\log a_{T_a}$ for the ageing PMMA. A comparison of the fractional free volume measured by this technique and calculated by Curro, Lagasse, and Simha in the manner just indicated shows that the agreement is excellent (fig. 10).



ESR DETECTION OF MOLECULAR RELAXATION IN QUENCHED PMMA SAMPLE (PROBE B)
TSAY, HONG, MOACAMIN, GUPTA (1982)

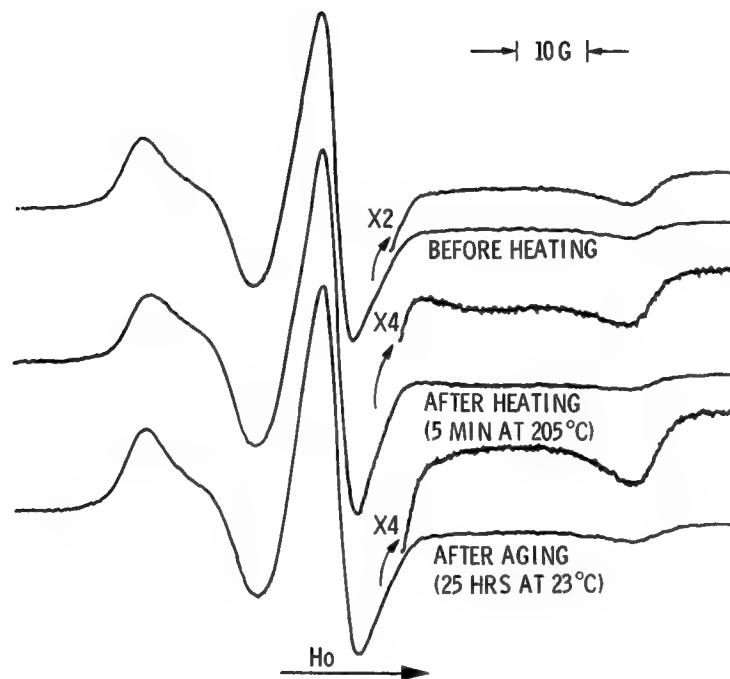
Figure 9



COMPARISON OF CALCULATED AND ESR-MEASURED FRACTIONAL FREE VOLUME IN PMMA AT 296°K

Figure 10

We are assessing this new technique for measuring fractional free volume in several ways. For example, esr can be used to follow the extent of cure as measured by a microviscosity or highly localized viscosity. Here, as the cure develops, one observes that the fast component decreases with cure time. Thus as the polymer passes from the mobile liquid state to the glassy state, the fractional free volume decreases. We are also using esr to probe the molecular mobility within polysulfone (Tsay, Hong, Moacanin, and Gupta, 1981). On ageing, one finds changes in line shape similar to these already shown for PMMA (fig. 11). Moreover, careful analysis of the line shape shows that four separate relaxation times can be identified.



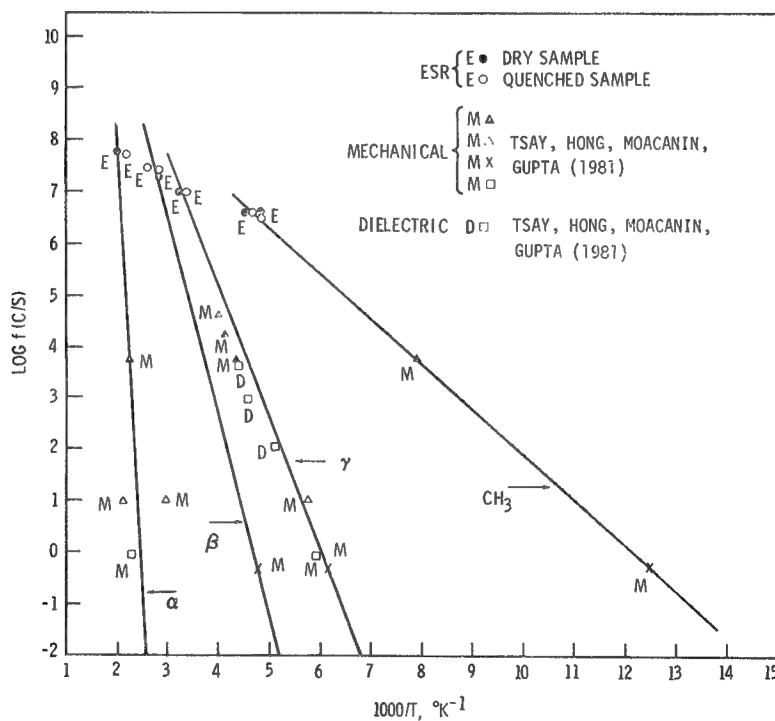
ESR DETECTION OF FREE VOLUME IN POLYSULFONE (TANOL PROBE)

Figure 11

We have been able to relate those relaxation times or their reciprocal (the frequencies of maximum absorption of energy) with the mechanical and dielectric relaxation peaks that one would conventionally measure using techniques such as the dynamic mechanical spectroscopy. We now plot each of these frequencies of the peak maximum against reciprocal temperature. Figure 12 shows the results for the dielectric data, other mechanical data, and the esr data. This plot is a typical way of comparing mechanical and other data. Clearly, the peaks we are picking up with the esr and their correlation times are exactly those which have previously been identified as the α , β , and γ and methyl rotation peaks in polysulfone.

Note that as the time scale of an experimental technique is changed, the peak maxima will occur at different temperatures. Thus an α peak measured at a time scale of, say, one second per cycle would represent what has been called the T_g of the material.

We feel that the gamma relaxation is related to the local reorientation of the phenyl ring, the β relaxation is the phenyl ring plus the sulfone and of course the α relaxation is always attributed to a large-scale segmental motion at T_g .



PLOT OF LOG F AGAINST $1/T$ FOR POLYSULFONE

Figure 12

We believe that it is the combined gamma and beta relaxations which are responsible, on a molecular scale, for the stress-strain response observed when a sample of polysulfone is deformed. These molecular rearrangements have very low activation energy, which would mean that they are able to respond very readily to deformations or loads on the sample. Figure 13 gives the transition temperature at the esr measured frequency for the four relaxation processes and their activation energies.

These measurements are being supplemented and expanded by Hong et al. at JPL, using birefringence measurements during the course of uniaxial tensile experiments. Such measurements can distinguish between a generalized lattice expansion, common to all solids, a local chain segment reorientation, and a full-scale chain reorganization and extension.

TRANSITION TEMPERATURES, ROTATIONAL FREQUENCIES,
AND ACTIVATION ENERGIES FOR MOLECULAR RELAXATION
PROCESSES IN POLYSULFONE

RELAXATION PROCESS	TRANSITION TEMPERATURE (°K)	ROTATIONAL FREQUENCY (MHz)	ACTIVATION ENERGY (KCAL/MOLE)
α	456	66	134
β	333	23	18.2
γ	294	12	12.1
CH ₃	200	3.6	4.1

Figure 13

One particular point that I want to make in summary (fig. 14) is that, first, glasses are not at equilibrium. This has different kinds of consequences, one of which is the question of how one would describe the material. It means in a pragmatic sense that the volume changes which occur during physical ageing or as a result of straining will lead to changes in the nature of the material, and its reference state; these are changes which have implications for the validity of the equations of mechanics currently in use to analyze the response of glassy systems. Secondly, it is clear that we need to measure such volume changes explicitly. On the theoretical side we need an expression for the equilibrium PVT response. Fortunately there is at least one expression in the literature for this, which gives us hope. Thirdly, we are introducing what one might call a new technique to probe molecular motions during aging --- esr. It is new in the sense of its use for this purpose. Finally, in one case at least, it appears that the esr technique can be used to estimate fractional free volume and the changes of fractional free volume with ageing. This novel development must now be tested, as one of our future activities.

- **GLASSES NOT AT EQUILIBRIUM**

CONSEQUENCES: PRAGMATIC

THEORETICAL DESCRIPTION

- **NEED EQM. PVT INFORMATION/EXPRESSION**
- **INTRODUCING "NEW" TECHNIQUE TO PROBE MOTIONS AND AGING . . . ESR**
- **(IN ONE CASE) FRACTIONAL FREE VOLUME**

SUMMARY

Figure 14

REFERENCES

1. Cizmecioglu, M., Fedors, R. F., Hong, S. D., and Moacanin, J., The Effect of Physical Ageing on Stress Relaxation of Poly (Methyl Methacrylate), *Polymer Eng. and Sci.*, 21, 942 (1981).
2. Kovacs, A. J., *Fortschr. Hochpolym. Forschung*, 3, 394 (1963) *Adv. Polymer Sci.*, 3, 394 (1964).
3. Kovacs, A. J., Aklonis, J. J., Hutchinson, J. M., and Ramos, A. R., *J. Polym. Sci. Polymer Phys. Ed.*, 17, 1097 (1979).
4. Curro, J. G., Lagasse, R. R., and Simha, R.; Use of a Theoretical Equation of State to Interpret Time-Dependent Free Volume in Polymer Glasses," *J. Appl. Phys.* 52, 5892 (1981).
5. Simha, R., and Somcynsky, T., *Statistical Thermodynamics of Spherical and Chain Molecule Fluids*, *Macromolecules*, 2, 342 (1969).
6. Hong, S. D., Chung, S. Y., and Fedors, R. F., Molecular Deformation and Stress-Strain Behavior of Diamino-diphenylsulfone-cured Tetraglycidyl-diamino-diphenyl Methane from Stress-Optical Studies. *Org. Coatings and Appl. Poly. Sci. Proc.*, 48, 586-587 (1983).
7. Schwarzl, F. R., and Zahradnik, F., The Time-Temperature position of the Glass-Rubber Transition of Amorphous Polymers and the Free Volume, *Rheol. Acta*, 19, 137 (1980).
8. Tsay, F. D., Hong, S. D., Moacanin, J., and Gupta, A. Studies of Magnetic Resonance Phenomena in Polymers. I. The Effects of Free Volume and Segmental Mobility on the Motion of Nitroxide Spin Probes and Labels in Poly (methyl Methacrylate), *J. Polymer Sci., Polymer Phys. Ed.*, 20, 763-772 (1982).
9. Tsay, F. D., Hong, S. D., Moacanin, J., and Gupta, A. Spin Trapping Studies of Tetraglycidyl-4,4'-diaminodiphenyl Methane (TGDDM) Cured with Diamino -diphenyl-sulfone (DDS), *Polymer Preprints*, 22, 231-232 (1981).

THE CHEMICAL NATURE OF THE FIBER/RESIN
INTERFACE IN COMPOSITE MATERIALS

R. Judd Diefendorf
Rensselaer Polytechnic Institute
Troy, NY

INTRODUCTION

The first high modulus carbon fiber/epoxy resin composites were found to have low interlaminar shear strengths¹. The question is where does the fracture occur, (Figure 1) and what factors affect the interlaminar strength. Carbon and aramide fibers are anisotropic and the properties transverse to the fiber axis are quite different than parallel to the axis². In some cases such as Kevlar aramide or pitch precursor carbon fiber, the fiber itself (Zone A) may fail transverse to the fiber axis in an interlaminar shear test. Furthermore, the fibers are not homogeneous and have a skin (Zone C) which is quite different from the core (Zone A)³⁻⁶. The skin (Zone C) is usually quite graphitic and weak in shear, and failure can occur in this skin adjacent to the interface. Also, the skin can be hard to bond to, which leads to interfacial failure, (Zone D). In all cases, failure must also run through the continuous phase matrix. The matrix properties also are known to be different close to the interface (Zone E) as compared to the bulk (Zone B). Residual stresses arising from curing and cool down from processing temperature places the matrix in hoop tension around the fiber. These stresses are modified in an opposite manner by water absorption. Hence, the system is complex, and although fracture may occur near the interface, it does not need to occur exactly at the interface. This paper will emphasize the nature of the fiber structure, and the interaction that occurs at the interface between fiber and matrix.

POSSIBLE FRACTURE ZONES

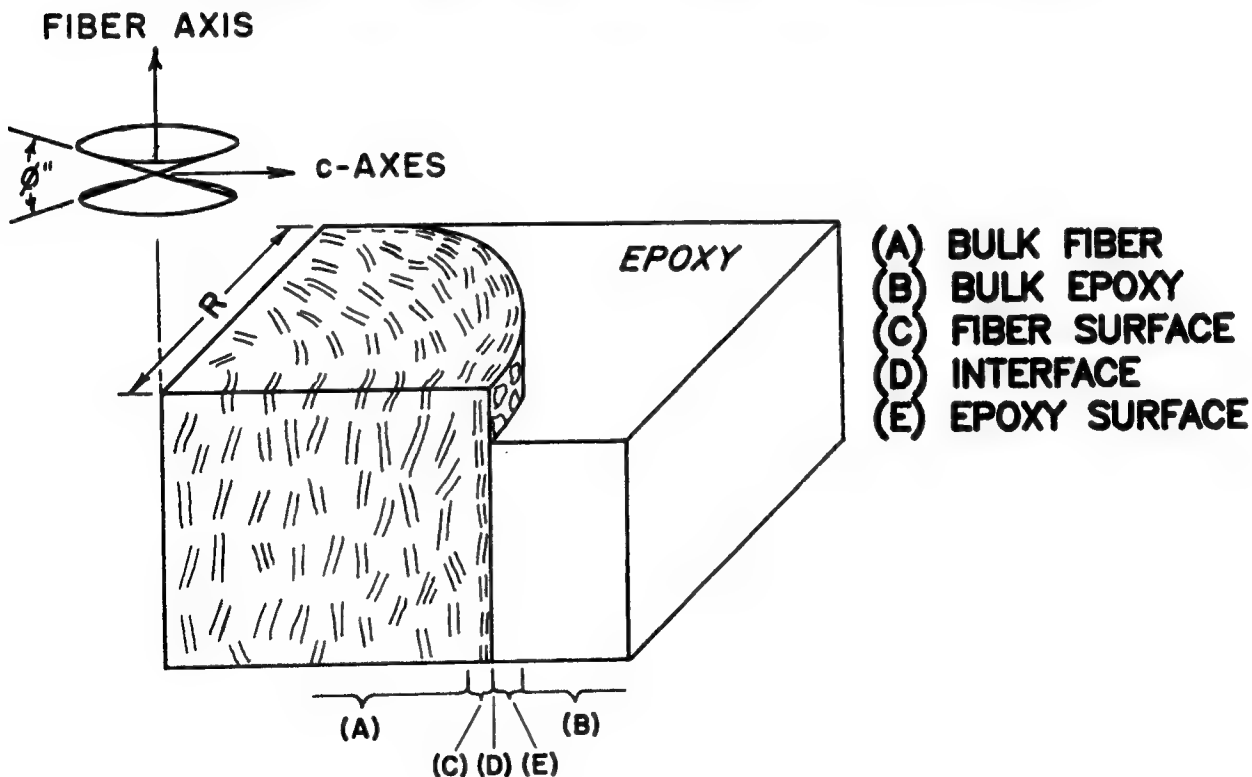
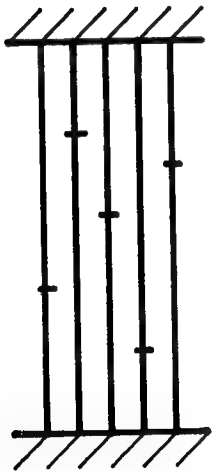


Figure 1

OPTIMUM INTERFACIAL BOND STRENGTH

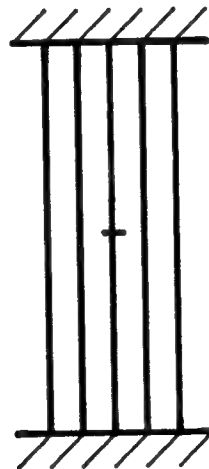
When carbon fibers first came out, it was difficult to make a strong interfacial bond with the matrix. The problem was solved by treating the carbon fiber surface. However, the increased bond strength produced more brittle composites. Figure 2 shows that a bundle of fibers with no resin (left) will have about 70% to 80% of the average tensile strength determined on the single fibers. With a very strong interface (right) between fiber and resin in a composite the whole composite can fail when the very weakest fiber in the composite fails⁷. Tensile strength will be low, and failure catastrophic. A proper interfacial strength as compared to fiber strength will have multiple filament fractures, and the tensile strength will equal or often exceed the average fiber tensile strength. Depending on the application, the fiber/matrix interfacial strength should be adjusted. Hence for pressure vessels with low shear stresses, the interfacial bond strength could be quite low. For a structural application with significant shear stresses, the interfacial bond strength must be higher even though the resulting composite may be more brittle. While in the past the cost of qualification prevented application-optimized surface treatments of fibers, better composites could be made with better control of the interfacial properties.

DRY STRAND



COMPOSITE INTERFACE

STRONG



WEAK

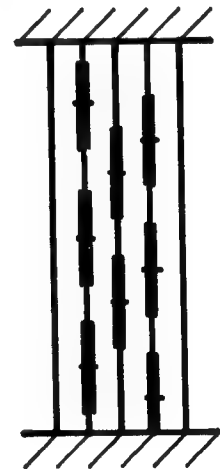
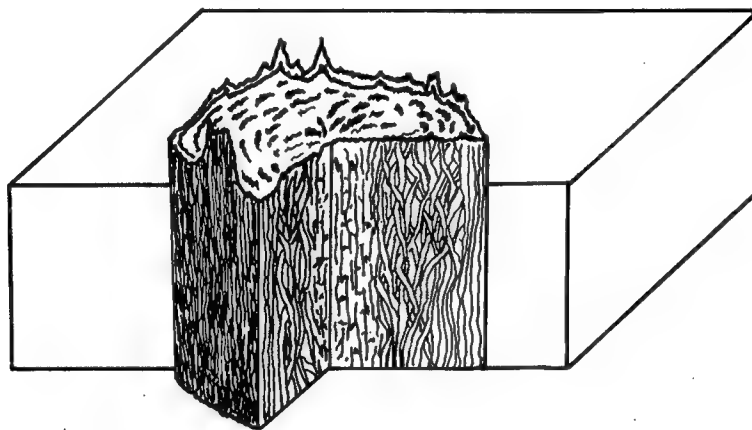


Figure 2

MICROSTRUCTURE OF CARBON FIBERS

The microstructure of carbon fibers (Figure 3a) is based on many people's work and especially some performed by my own students^{3,4,5,6,8}. The axial structure resembles groups of undulating ribbons of graphitic based planes, and the modulus of the fiber depends on the amplitude-to-wavelength ratio of the ribbon. (The lower the amplitude and the longer the wavelength, the higher the modulus of the fiber is). For the cases of PAN and pitch precursor carbon fibers, higher modulus was obtained by heat treating to higher and higher temperatures. A problem is that the heat treatment also improves the orientation radially as well and cool down from high temperature causes residual stress cracks parallel to the fiber axis⁸. Also, when a high modulus fiber is made, the undulating ribbons become straighter and tend to form an onion-skin layer of good graphite at the fiber surface. This layer is hard to bond to, and has poor shear and transverse tensile strength. Figure 3b illustrates the undulating ribbon structure in a higher modulus carbon fiber⁵. The $1/2$ wavelength is about 100\AA . Close to the surface of this fiber, the structure would be almost perfectly oriented.



(a)



(b)

Figure 3

INTERLAMINAR SHEAR STRENGTH

The interlaminar shear strength of carbon fiber/epoxy composites decreases with increasing fiber modulus¹. Even after surface treatment, the trend remains although the magnitudes are higher. The effect is not just a change in the mechanics of the problem caused by the increase in modulus, as the interlaminar shear strength for boron filament is high (Figure 4).

VARIATION OF COMPOSITE SHORT BEAM SHEAR STRENGTH WITH THE MODULUS OF CARBON FIBERS

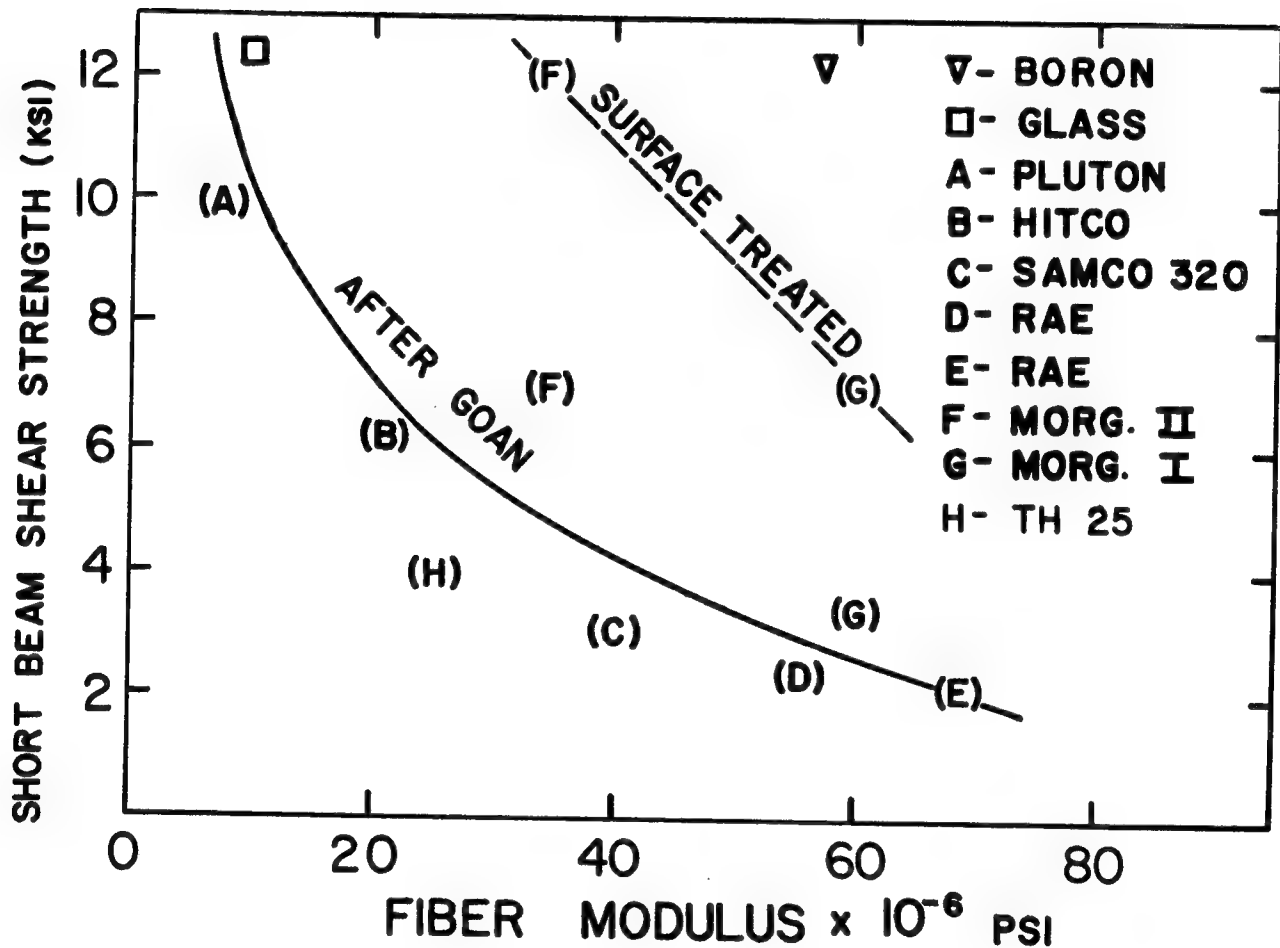
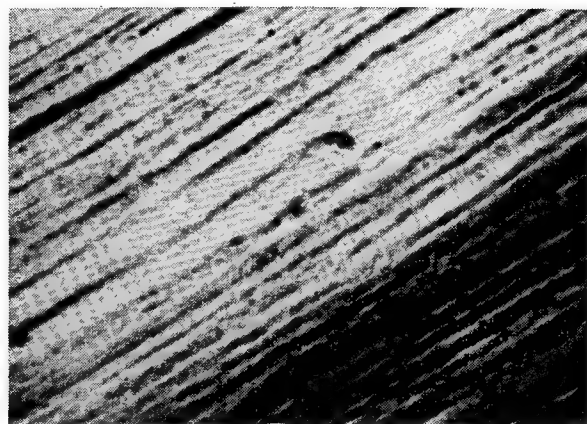


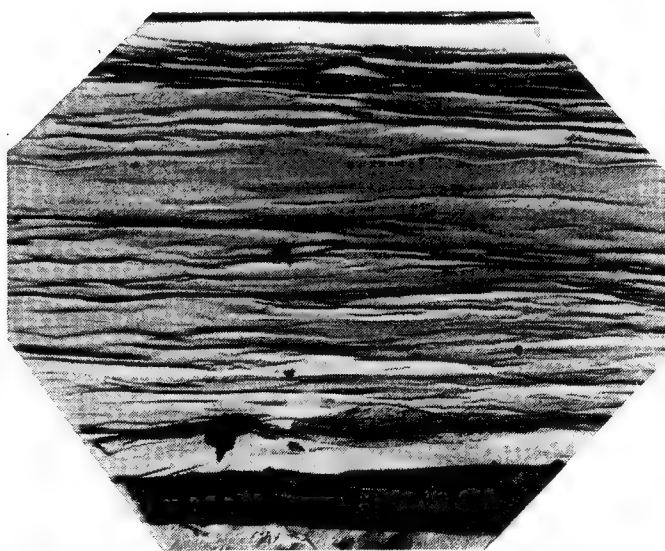
Figure 4

SURFACE ROUGHNESS EFFECTS ON INTERFACIAL BOND STRENGTH

The surface of carbon fibers does not significantly change with increasing fiber modulus at SEM magnifications ($\sim 10,000\times$). Surface treatment appears to smooth the surface. However, TEM of replicas at higher magnifications ($\sim 94,000\times$) shows quite different results⁵. Fiber surfaces get smoother with increasing modulus, and rougher with surface treatment. Figure 5a shows the pitted surface of a surface treated of a lower modulus fiber. By comparison, an unsurface-treated, very high modulus carbon fiber is quite smooth, Figure 5b. The shrinkage of the resin around the fiber upon processing would provide much better mechanical interlocking with the lower modulus/surface-treated fiber.



(a)

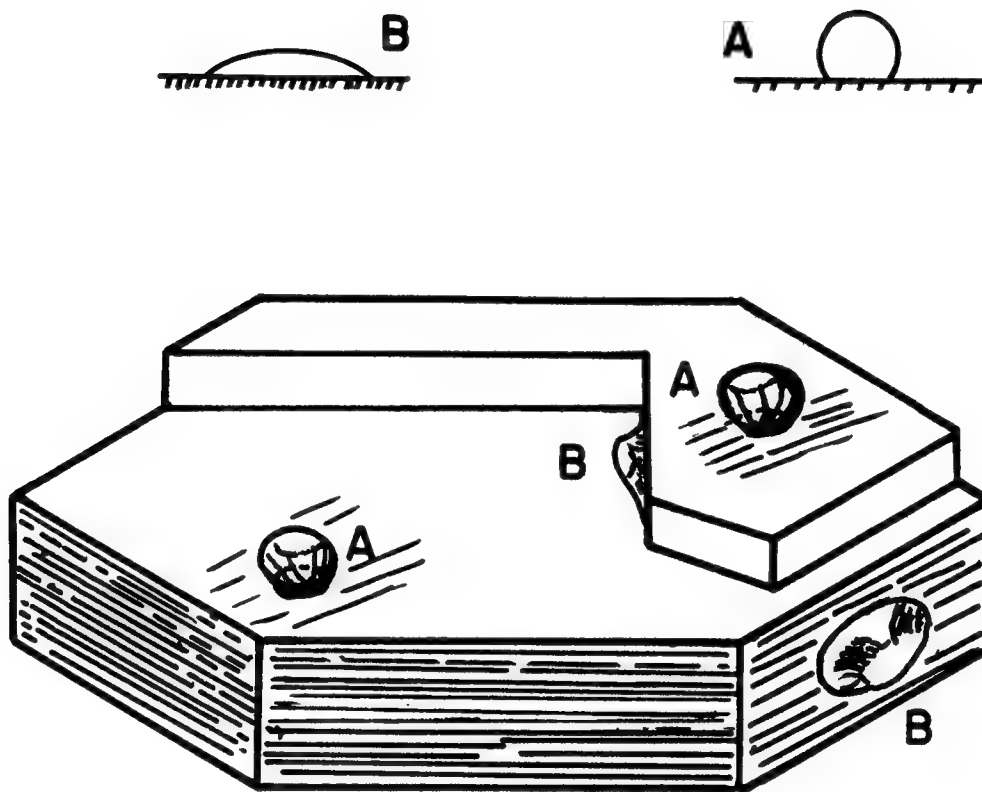


(b)

Figure 5

SURFACE ENERGY AND WETTING OF CARBON FIBERS

The difference in appearance of the surface of the carbon fibers with increasing modulus or after surface treatments indicates changes in the amount of graphitic basal plane and edge exposed on the surface. Figure 6 illustrates that the basal plane of graphite has a low surface energy and is hard to wet, while the edge has a high energy and is easy to wet (unless contaminated)³. The difficulty is that the surface is not monoenergetic, and the ease in wetting the surface will depend on the relative amount of edge and basal plane on the surface. Obviously, the higher modulus, unsurface-treated fiber would be harder to wet than the lower modulus surface-treated fiber.



Wetting of Single Crystal Graphite

Figure 6

BASAL PLANE AND EDGE TOPOGRAPHY

The wetting of the surface depends on more than just the ratio of basal plane to edge. For example, for the same ratio of basal plane to edge, the wetting characteristics of a pitted surface will be different from a stepped surface, Figure 7. In fact, the wetting behavior for the stepped surface would be different if the liquid was advancing from left to right versus bottom to top. Part of this problem can be relieved by studying both the advancement and retraction of the liquid on the surface. However, wetting is only properly defined for a monoenergetic surface. For a stepped graphite surface, the surface may appear to be wetted because of the high surface energy steps, but the basal plane areas may not really be wetted. While wetting is not a sufficient condition for a good interfacial bond, it is a necessary condition.

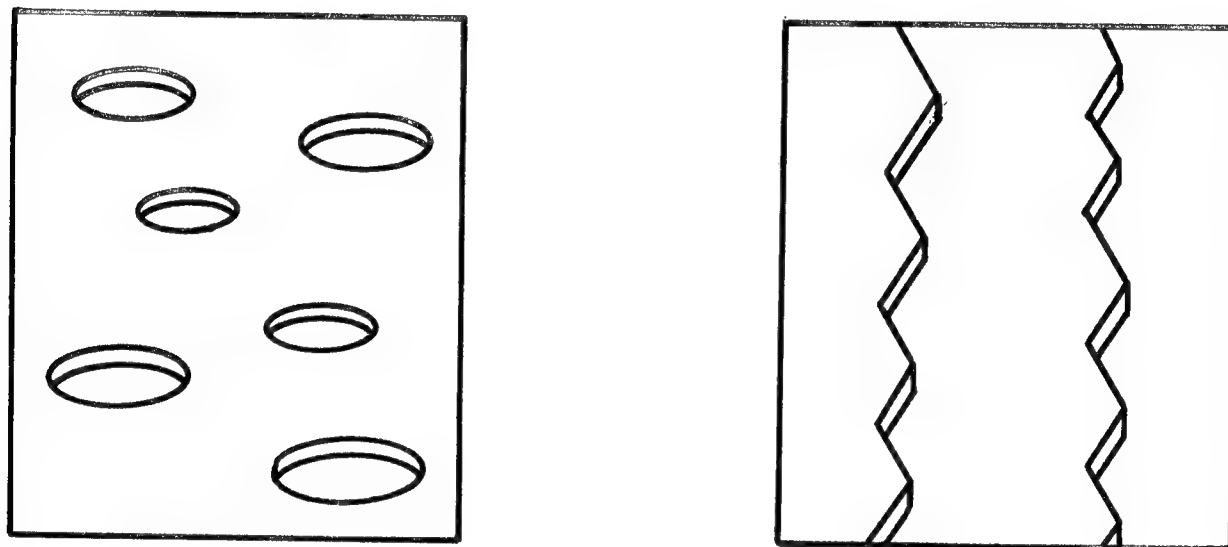
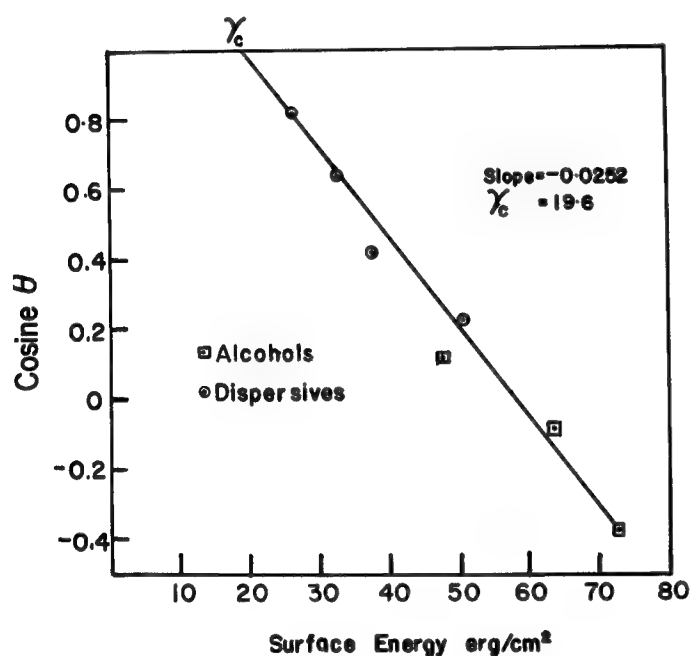


Figure 7

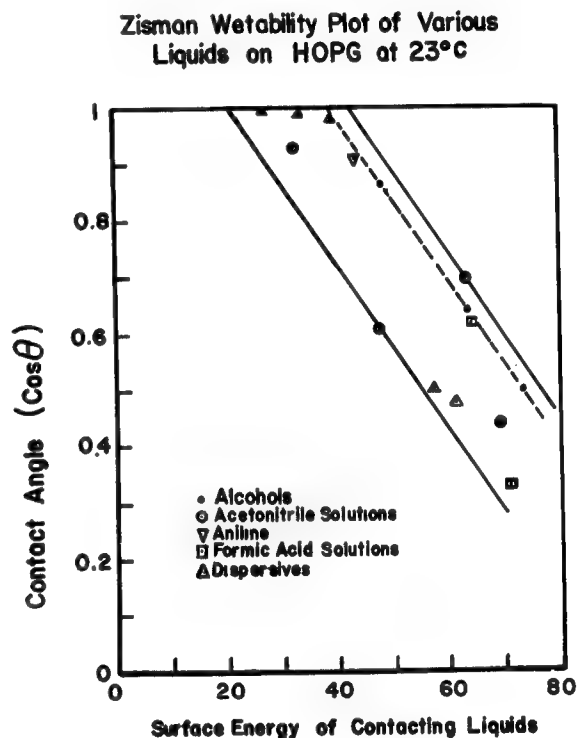
CRITICAL SURFACE ENERGY FOR WETTING

Zisman⁹ has shown for surfaces, which have predominantly dispersive-type surface energies, that the critical surface energy for wetting can be obtained by extrapolating the measured contact angles for various dispersive liquids to perfect wetting. Hence, a liquid will completely wet the solid if it has a lower surface energy than the critical surface energy for wetting of the solid. For predominantly dispersive surfaces such as PTFE, the extrapolation works well with dispersive liquids, although more polar liquids give more scatter (Figure 8a)^{10,11}. For a surface such as graphite with edges and basal planes, even more scatter should be expected. For highly perfect graphite surfaces prepared from highly annealed pyrolytic graphite, small variations in edge content can make significant differences, as can more polar liquids, Figure 8b^{10,11}. Working with just the dispersive liquids, the surface energy for the graphite basal plane is quite low and it is hard to wet. (Independent calculations, based on elastic constants, give a value of 39 erg/cm²)¹².



Zisman Wetability Plot of Various Liquids on Polytetrafluoroethylene at 20°C

(a)



(b)

Figure 8

WETTING OF SURFACES BY POLAR LIQUIDS

Zisman⁹ plots with slightly polar as well as dispersive liquids show more scatter. The polar liquids behave as if some of the surface energy doesn't count in terms of interacting with the surface to be wet. This could be explained by the polar part of the liquid molecule rotating away from the solid surface. By breaking the surface energy down into dispersive and polar components¹³, we have found that only one-half the polar component of the surface energy is effective for predicting the critical surface energy for wetting^{10,11}. Although this relation is not desirable from surface energy theories, the relation is so good (Figure 9) that there must be an underlying relationship.

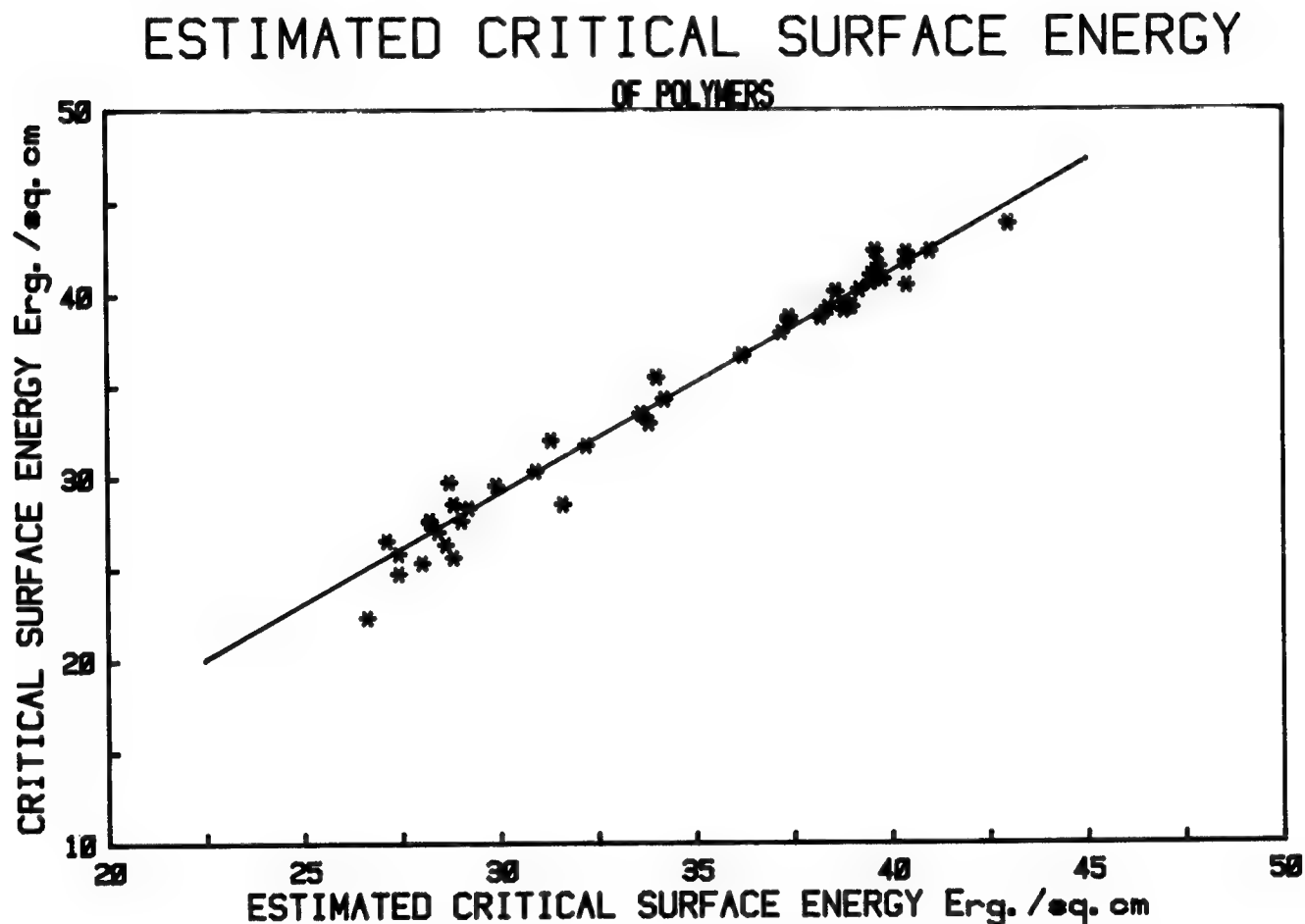


Figure 9

SURFACE ENERGY COMPONENTS

The idea of splitting the surface energy into dispersive and polar components has been effective in at least qualitatively explaining wetting behavior. This has been generalized to include a hydrogen bonding¹⁴ and an acid/base interaction component¹⁵. (Logically, the hydrogen bonding term commonly used is improper.) However the results to be presented are based just on the dispersive and polar components as shown in the bottom equation of Figure 10. The approach was to describe the dispersive and polar components of a number of solid surfaces such as graphite with known liquids. Then these surfaces were used to determine the dispersive and polar components of resin systems such that the work of adhesion might be calculated.

THE GIRIFALCO-GOOD-FOWKES- KAEBLE-YOUNG EQUATION

GEOMETRIC MEAN RULE OF INTERFACIAL ENERGY

$$\gamma_{AB} = \gamma_A + \gamma_B - 2(\gamma_A \gamma_B)^{1/2}$$

ONLY DISPERSIVE AND POLAR INTERACTIONS

$$\gamma_{AB} = \gamma_A + \gamma_B - 2(\gamma_A^d \gamma_B^d)^{1/2} - 2(\gamma_A^p \gamma_B^p)^{1/2}$$

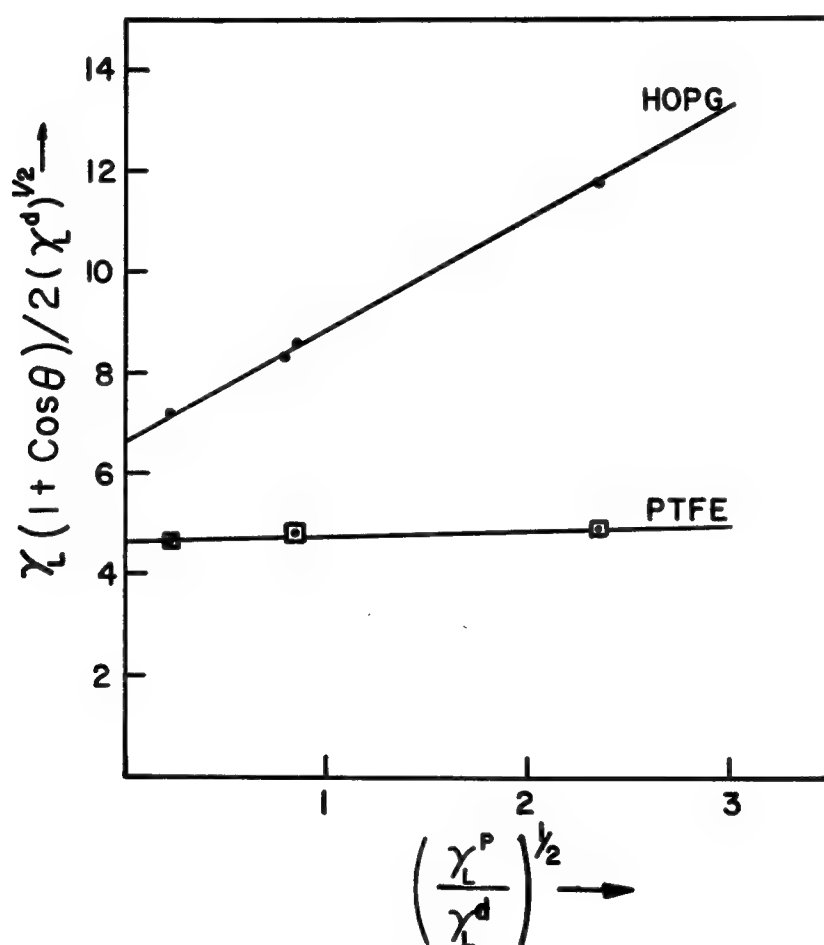
COMBINING THE YOUNG EQUATION

$$\cos \theta = -1 + \frac{2(\gamma_A^d \gamma_B^d)^{1/2}}{\gamma_L} + \frac{2(\gamma_A^p \gamma_B^p)^{1/2}}{\gamma_L} + \pi_e / \gamma_L$$

Figure 10

DETERMINATION OF DISPERSIVE AND POLAR SURFACE ENERGY COMPONENTS OF GRAPHITE AND PTFE

The contact angles for five liquids were measured on a freshly prepared highly oriented pyrolytic graphite (HOPG) surface and PTFE^{10,11}. From the known surface energy components of the liquids, the surface energy components of the solids can be determined (Fig. 11). The slope of the plot is proportional to the polar component and the intercept to the dispersive component. The zero slope for PTFE shows it to have no polar component, and to have only dispersive surface energy. The values agree with the literature¹⁶. The values for HOPG are very similar to those obtained by Drzal¹⁷ for HMU carbon fiber, which might be expected from microstructural results. In any case, the convenient flat HOPG surfaces appear to be useful for modeling carbon fiber surfaces.



Determination of the Surface Energy Components of
HOPG and PTFE at 20°C

Figure 11

CALIBRATED SOLID SURFACES FOR EPOXY RESIN STUDIES

The polar and dispersive surface energy components for a number of polymer and graphite surfaces were determined, Figure 12^{10,11}. This provided a calibrated set of surfaces with quite different surface energy components for studying with resins.

Comparison of the Surface Energy Components of HOPG and other Polymers.

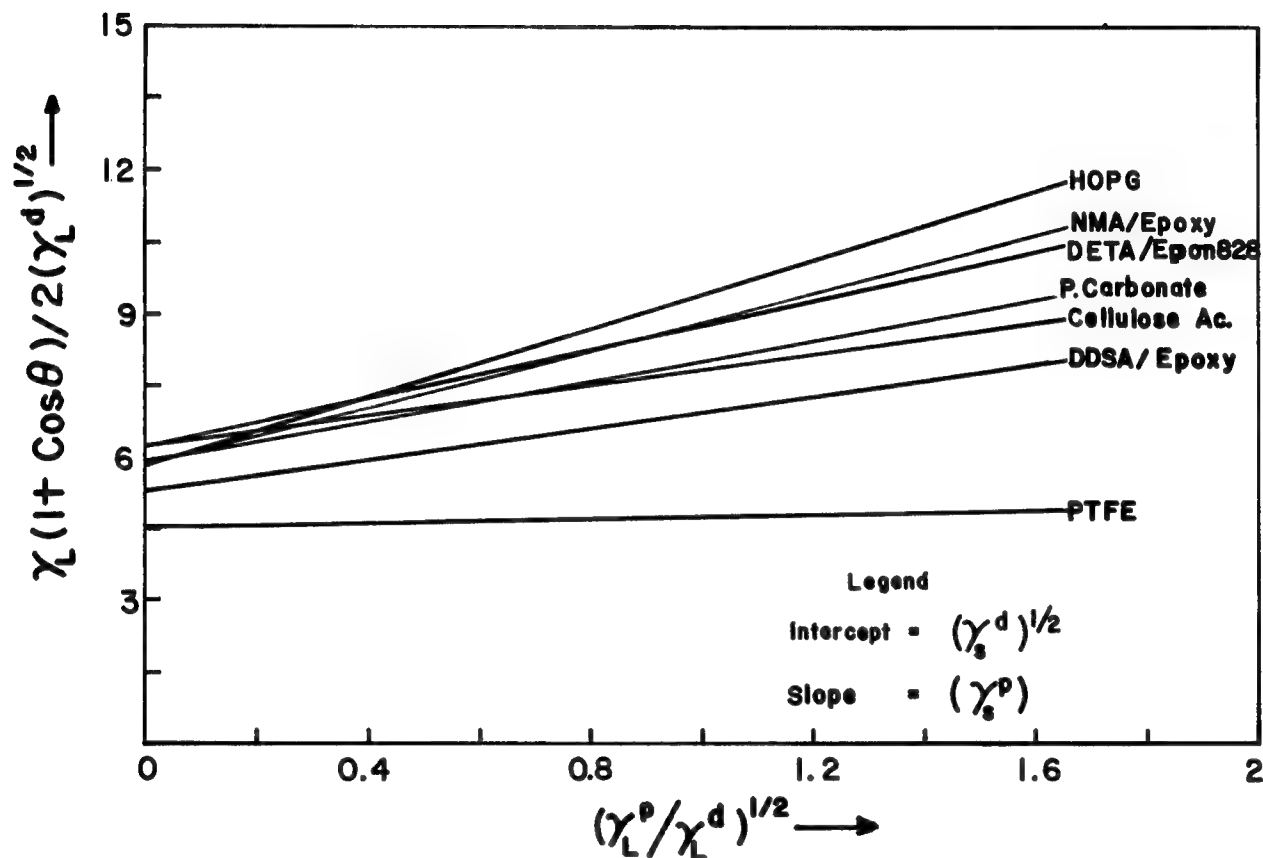


Figure 12

SURFACE ENERGY COMPONENTS OF EPOXY RESINS AND HARDNESS

The wetting of a number of epoxy resins and hardeners was studied on the calibrated surfaces. The corresponding surface energy components for resins and hardeners were calculated from these data. Some of the results are presented in Figure 13a^{10,11}. Hopefully, the wetting and interaction of an epoxy/hardener mixture with a substrate could be calculated from the constituents. Unfortunately, the hardener, particularly amines, tends to interact or adsorb on the graphite surface, Figure 13b, and the wetting is mainly determined by the hardener^{10,11}. While this makes the surface energy component approach of little value for direct calculation of wetting, it does point out when adsorption is occurring. It also provides information on how to maximize the surface interaction by acid/base phenomena.

SURFACE ENERGY COMPONENTS OF ANHYDRIDE CURED EPOXY RESINS

<u>SUBSTRATE</u>	<u>Dispersive Component</u>	<u>Polar Component</u>	<u>Total Surface Energy</u>
DDSA Cure:			
<u>CY-179</u>	29.2±0.6	2.9±0.7	32.1±1.4
<u>MY-720</u>	26.2±1.2	3.5±1.4	29.8±2.6
<u>Epon-828</u>	30.1±0.6	2.5±0.7	32.6±1.4
<u>Epon-152</u>	27.1±1.2	2.3±1.5	29.4±2.7
NMA. Cure:			
<u>CY-179</u>	34.3±1.2	10.2±1.4	44.4±2.6
<u>MY-720</u>	35.5±0.7	9.2±0.8	44.6±1.5
<u>Epon-152</u>	34.3±0.8	7.8±1.0	42.1±1.8

* All Values in Erg/sq.cm

Figure 13

SUMMARY OF COMPOSITE TOUGHNESS

Composite toughness can be improved by increased axial tensile and compressive strengths in the fibers (Fig. 14). Secondly, the structure of carbon fibers indicates that the fiber itself can fail transversely, and different transverse microstructures could provide better transverse strengths. The higher surface roughness of lower modulus and surface-treated carbon fibers provides better mechanical interlocking between the fiber and matrix. The physical chemical nature of the fiber surface has been determined, and adsorption of species on this surface can be used to promote wetting and adhesion. Finally, the magnitude of the interfacial bond strength should be controlled such that a range of composites can be made with properties varying from relatively brittle and high interlaminar shear strength to tougher but lower interlaminar shear strength. The selection would depend upon the application.

MATERIALS IMPROVEMENT

- * FIBER TENSILE AND COMPRESSIVE STRENGTH
- * INTERFACIAL BOND
 - FIBER SURFACE MORPHOLOGY AND CHEMISTRY
 - FIBER TRANSVERSE STRUCTURE
 - MATRIX CHEMISTRY
- * INTERPHASE
 - DUCTILE OR HIGH ELONGATION
 - INTERMEDIATE MODULUS
- * MATRIX

Figure 14

REFERENCES

1. Goan, J.C. and Prosen, S.P., "Interfacial Bonding in Graphite Fiber Composites Interfaces in Composites, ASTM-STP 422, ASTM 71st Session, San Francisco, CA, 1968, pp. 3-26.
2. Helmer, J.F., "Transverse Properties of Anisotropic Fibers and Their Composites", M.Sc. Thesis, Rensselaer Polytechnic Institute, Troy, NY, August 1983.
3. Butler, B.L., "The Effects of Carbon Fiber Microstructure on the Shear Strength of Carbon-Epoxy Composites", PhD Thesis, Rensselaer Polytechnic Institute, Troy, NY, September 1969.
4. Diefendorf, R.J. and Tokarsky, E.W., "High Performance Carbon Fibers", Polymer Engineering and Science, Vol. 15, No. 3, March 1975, pp. 150-159.
5. Diefendorf, R.J. and Tokarsky, E.W., "The Relationships of Structures to Properties in Graphite Fibers", AFML-TR-72-133, Parts I-IV, Oct. 1971 to Nov. 1971.
6. Johnson, D.J., Crawford, D., and Oates, C., "The Fine Structure of a Range of PAN-Based Carbon Fibers", Tenth Biennial Conf. on Carbon, Bethlehem, PA, June 1971.
7. Mullin, J., Berry, J.M., and Gatti, A., "Some Fundamental Fracture Mechanisms Applicable to Advance Filament Reinforced Composites", J. Composite Materials, Vol. 2, No. 1, June 1968, p. 82.
8. LeMaistre, C.W. and Diefendorf, R.J., "The Origin of Structure in Carbonized PAN Fibers", SAMPE Quarterly, Vol. 4, No. 4, 1973, pp. 1-6.
9. Zisman, W.A., "Constitutional Effects on Adhesion and Adhesions", in Symposium on "Adhesion and Cohesion", P. Weiss (Ed.), Elsevier, NY 1962.
10. Diefendorf, R.J. and Uzoh, C.E., "High Modulus Graphite Fiber Surface Modifications for Improved Interfacial Bonding with Materials", 39th Semi-Annual Progress Report May 1980 - Sept. 1980, NASA/AFOSR Composite Structural Programs, Rensselaer Polytechnic Institute, Troy, NY.
11. Diefendorf, R.J. and Uzoh, C.E., "The Surface Energy of Anhydride-Cured Epoxy Resins", 43rd Semi-Annual Report, Dec., 1982, NASA/AFOSR Composite Structural Program, Rensselaer Polytechnic Institute, Troy, NY.
12. Riggs, D.M. and Diefendorf, R.J., "The Solubility of Aromatic Compounds", Proceedings of 14th Biennial Conference on Carbon, American Carbon Society, 1979, p. 407.
13. Kaible, D.H., "Physical Chemistry of Adhesive", Wiley Interscience, NY, 1971, pp. 84-188.
14. Hansen, C.M. "Three Dimensional Solubility Parameter-Key to Paint Component Affinities: II and III, Dyes, Emulsifiers, Mutual Solubility and Compatibility and Pigments", J. Paint Tech., Vol. 39, No. 511, Aug. 1967, p. 505.
15. Fowkes, F.M. and Mostata, M.A., Ind. Eng. Chem. Prod., R&D, Vol. 17, No. 3, 1978

16. Wu, S., J. of Colloid and Interface Science, Vol. 17, No. 3, Oct. 1979, pp. 605-609.
17. Drzal, L.T., Mescher, J.A., Hall, D.A., "The Surface Composition and Energetics of Type HM Graphite Fibers", Carbon, Vol. 17, No. 5/A, 1979, pp. 375-382.

COMPOSITE PROPERTY DEPENDENCE ON THE
FIBER, MATRIX, AND THE INTERPHASE

Lawrence T. Drzal

Air Force Wright Aeronautical Laboratories
Nonmetallic Materials Division
Mechanics and Surface Interactions Branch
AFWAL/MLBM
Wright-Patterson Air Force Base, OH

I. BACKGROUND

Most of the material mentioned in this conference represented commercially available prepreg and composites where the properties of the resin are fixed and the properties of the fiber are fixed, and, therefore, intrinsically the properties of the interface are fixed. In other words, they are in a condition, a necessary condition for good composite performance, where the adhesion between the fiber and matrix is at least an acceptable level if not an optimum level. The purpose of this workshop and the task of our group in the Air Force is substituting materials in composites - either matrices or fibers. Then we are really faced with the task of relooking at the problem of the interface between the fiber and matrix where the normal additive relationships between fiber and matrix, which in many aspects describe composite behavior from the mechanic's point of view, don't hold anymore. So our view, as prejudiced as it is, is that we really have to understand the behavior of the interphase as the way to combine matrix and fiber properties into composite properties.

I. BACKGROUND - INTERPHASE CONCEPTUAL MODEL

Figure 1 [1] illustrates what might be included in an interphase. From the mechanic's point of view we consider that the interphase between fiber and matrix is continuous in terms of transferring stresses between the fiber and matrix. If we look at that area under a high-resolution microscope then we could resolve these properties. We define an interphase of some finite distance which, depending on the material system, could extend from a few to a few thousand angstroms. In that interphase region starting from the matrix side, it can be seen that there can be physical differences. From the matrix side as we go to the interphase, we can have adsorbed or unreacted species congregated in the interphase region. We may have unwetted areas or voids or impurities congregating there. We may have surface chemical groups which would be entirely different from the bulk chemical material present at the surface of the fiber. We could have morphological or structural changes in the fiber at its surface. Finally we get to some point in the fiber where the local properties are equal to the bulk properties.

That is what I'm calling the interphase region. We are trying then to analyze this interphase in an environment which may be a thermal, a mechanical, or a chemical environment and which can come to the interphase through the matrix, along the interphase itself, or through the fiber. So you see it is a complex task, one that does not lend itself to easy analysis of single parametric models of adhesion and requires a phenomenological approach.

What I would like to do in this paper is to relate to you the results of various efforts conducted in our laboratories. I'm going to try to keep a degree of commonality throughout the presentations by talking about work that has been done on the same fiber, with the same matrix, and with one type of test.

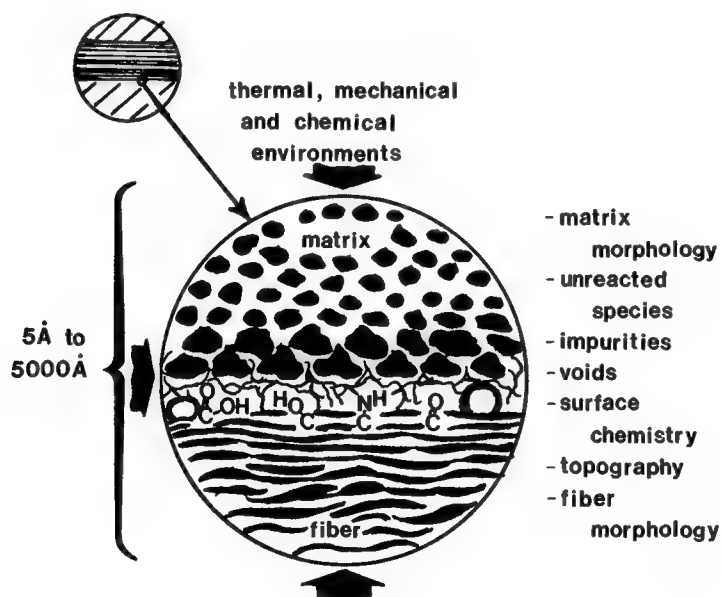


Figure 1.- Conceptual model of the fiber-matrix interphase in composite materials.

II. EXPERIMENTS

We have chosen, rather than to investigate a variety of different chemistries, to vary the matrix properties using one chemistry. The matrix chemistry we have chosen is an epoxy chemistry, in this case a difunctional epoxy, Epon 828, Shell Chemical Company, cured with meta-phenylene diamine. The cure cycle we have chosen is two hours at 75°C followed by two hours at 125°C. That gives us a matrix material that in the neat state has an initial modulus of around 500,000 psi with a strain to failure of around 6 to 7 percent and a fracture strength of around 12,000 to 13,000 psi. This matrix is intermediate in terms of properties between the brittle 5208 systems or 3501 systems and the rubber-toughened epoxy matrices.

Likewise for a fiber we have chosen to work with one fiber. It is the Hercules Type A fiber that has a 35 million modulus and a tensile strength of around 400,000 psi. We have obtained one large batch of the material, a portion of which was kept untreated. The rest of the material was surface treated with an oxidative surface treatment that was commercially available. Then we took a portion of the surface-treated material and had it finished, in other words we applied a thousand to two thousand angstroms of pure epoxy to the fiber surface in order to model an epoxy-compatible finished fiber. Those were the two components of our system.

Now depending on my outlook on a particular day, I could show you a composite fracture surface and I could pinpoint areas where you had interfacial fracture or had matrix fracture or had a combination of both. For an effort like this where an effort is being made to relate composite properties to the component material properties, composite testing is unsuitable. We have chosen to work with a single fiber test adapted from the metallurgists [2]. Advantage of the mismatch of strain properties between the fiber and the matrix is used to determine the interfacial shear strength.

A single graphite fiber is encapsulated in the matrix of interest, in this case our epoxy, in a tensile dogbone coupon specimen (Figure 2). That specimen is loaded in tension. Microscopically, in this sample at a low value of strain, the fiber will begin to break into fragments inside the matrix. As the strain on the sample is increased, the fiber in the sample will continue to break until you reach a point known as the critical transfer length where the shear stresses that build up on the fiber surface are no longer sufficient to break the fiber anymore. Extension of the matrix past this point causes no further breakage in the fiber. One can then by simple shear analysis relate critical transfer length, the fiber diameter and the fiber fracture strength at that length to an interfacial shear strength (Eqn. 1). In our experiments we usually use Weibull statistics. We just alter Eqn. 1 to reflect the Weibull statistics, and the calculation of the interfacial shear strength is made with the altered formula (Eqn. 2), which is our evaluation criteria for looking at interface properties.

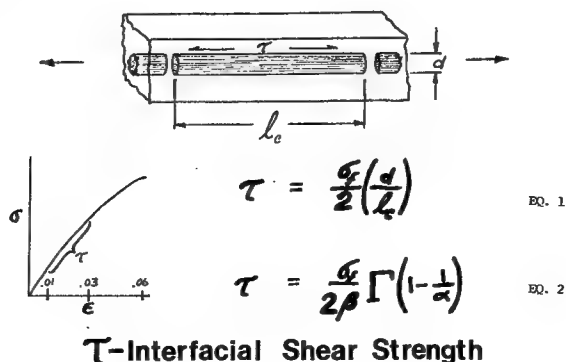


Figure 2.- The single-fiber interfacial shear strength test.

III. INTERPHASE: REINFORCEMENT SURFACE

The first part of our results will be looking at the fiber and the interface on the fiber side between fiber and matrix. For example if you analyze the fiber surface with some of the surface probes we have, the amount of oxygen on the surface undergoes about a twofold increase with surface treatment [3,4,5]. The surface oxygen seems to be of the carboxylic acid type. Likewise if you look at the total surface free energy, you see that it also goes up. The surface areas of the fibers do not change with surface treatment, at least not enough to reflect the doubling or tripling of interfacial properties that one would see with surface treatment. I would like to point out that when we expose the fiber to about 750°C in vacuum to a monolayer of hydrogen, we can remove all the oxygen down to about 3 percent. When we do that the polar component of the surface free energy and the total surface free energy of that fiber decrease without changing the fiber surface area.

The interfacial shear strength of those fiber specimens tabulated here shows that the untreated fiber gives a value around 4,000 psi. Surface treatment increases that to well over 10,000 psi. When we take those oxygen groups off the surface with the hydrogen treatment, the interfacial shear strength decreases. But it decreases to a level much higher than we get for the untreated fiber even though we remove oxygen groups to the point where we have 3 percent on the surface for this fiber and we have 9 percent for the untreated one.

That result puzzled us so we decided to look microscopically at the behavior of the fiber in the matrix. Figure 3 is just a collage of one particular fiber at its break in the matrix at about 400X with transmitted polarized light. After the fiber breaks, the matrix is placed under load and you see the stresses that develop with increasing strain. The fiber fragments tend to pull apart and immediately at very low levels of strain the entire fragment is in a state of stress. If you were to watch this in a dynamic sense, you could see the motion of alternating light and dark areas indicating that there is a nonsmooth progression of stresses as the fiber tends to move within the matrix. We have done some microtomy and ultrahigh resolution TEM work to look at the interface. We see for the untreated fiber that this material is entirely debonded from the matrix, and the fracture path goes between matrix and fiber interfacially but pulls apart fragments of the fiber surface from the untreated fiber.

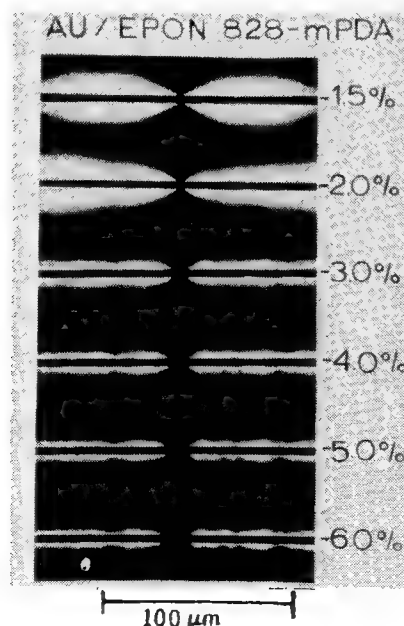


Figure 3.- Polarized transmitted light micrographs of an untreated (AU) fiber in the epoxy matrix with increasing strain.

III. INTERPHASE: REINFORCED SURFACE - MICROGRAPHS OF THE SINGLE-FIBER TEST

Now contrast those results with the surface-treated fiber and you get quite different results (Figure 4). Here again the fiber is broken with increasing strain. A highly stressed area moved away from the break. This is the tip of an interfacial crack. Growing from the break in the fiber behind the crack tip is an area where there are high frictional forces responsible for the narrow band of intense photo-elastic behavior. If we take this surface-treated fiber and remove those oxygen groups, although the interfacial strength drops, we still get the same type of interfacial crack growth where we now get complete separation between fiber and matrix with no evidence of the fiber breaking up in its outer layers.

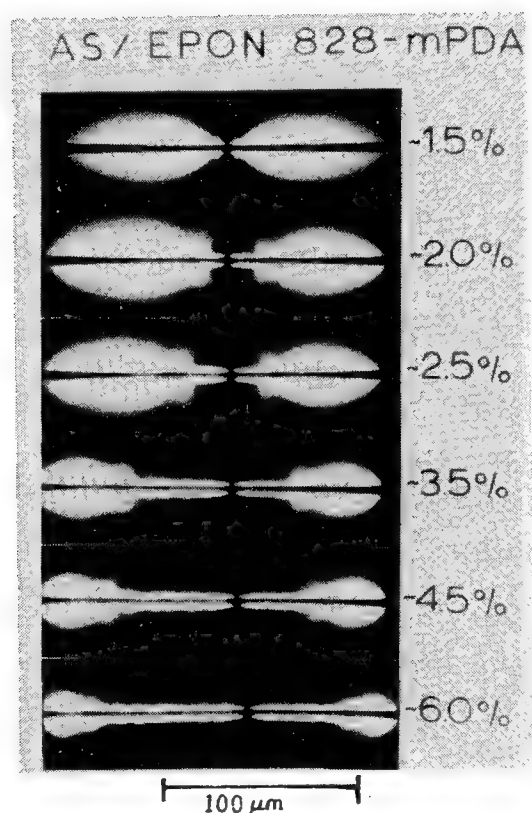


Figure 4.- Polarized transmitted light micrographs of a surface-treated (AS) fiber in the epoxy matrix with increasing strain.

III. INTERPHASE: REINFORCED SURFACE - SINGLE-FIBER INTERFACIAL SHEAR STRENGTHS

Interfacial shear strength is plotted as a function of surface oxygen in Figure 5. When we go from an untreated fiber to the surface-treated fiber, we get an improvement in interfacial shear strength. When we take the oxygen groups off the surface, we get a decrease, but the decrease still leaves us at a much higher value than we could get for the untreated fiber. Our explanation for this behavior is that two mechanisms are operating with these commercial oxidative surface treatments. The first part is the removal or etching away of the fiber surface, removing the weak boundary layer that is present on the fiber surface. The second step is the addition of the surface chemical groups. For this epoxy matrix we say that the surface treatment primarily creates a surface that can withstand higher shear loadings with the addition of surface chemical groups being a minor effect.

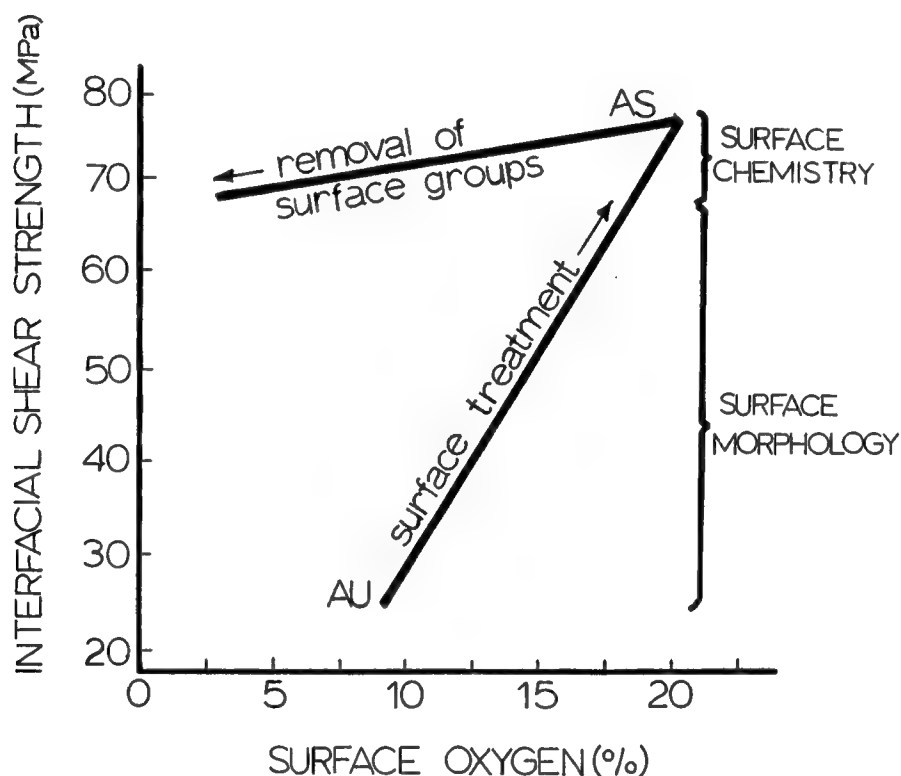


Figure 5.- Single-fiber interfacial shear strength plotted as a function of surface oxygen content.

IV. INTERPHASE: MATRIX

Let's look at the other side of the interface, and let's concentrate on the matrix side. The basic molecule we are working with is the DGEBA with N equal to about 0.1 which indicates we have some higher molecular weight species. The curing agent we are using is the meta-phenylene diamine. Its surface free energy is around 50 erg/cm² and the 828 surface free energy is around 42.3 erg/cm². Surface chemical effects for this particular system have been measured by using a pendant drop technique. By measuring the shape of the pendant drop of this material, one can determine if there is surface activity at the air-polymer surface. For this particular case as we increase the MPDA concentration, we have to go well beyond the stoichiometric point which is 14.5 phr before we start seeing any increase in surface free energy.

These epoxies are not homogeneous isotropic systems. They are quite inhomogeneous on a molecular scale. Figure 6 is a series of micrographs of epoxy samples at different amine-to-epoxy ratios [6,7]. The 14.5 phr is the ideal amount required to get complete reaction, 20 phr would be excess amine, and 10 phr would be a deficient amount of amine. The lower sample has been fractured in liquid nitrogen and then etched in a cold plasma. There are indications of heterogeneity indicated by the change in size and spacing with changing amine-to-epoxy ratio. The top specimens are microtomed samples which have been sliced into 600 angstrom thick sections. The shape of these osmium-stained dark areas and their concentration changes with the amine-to-epoxy ratio. This spherical morphology changes with composition.

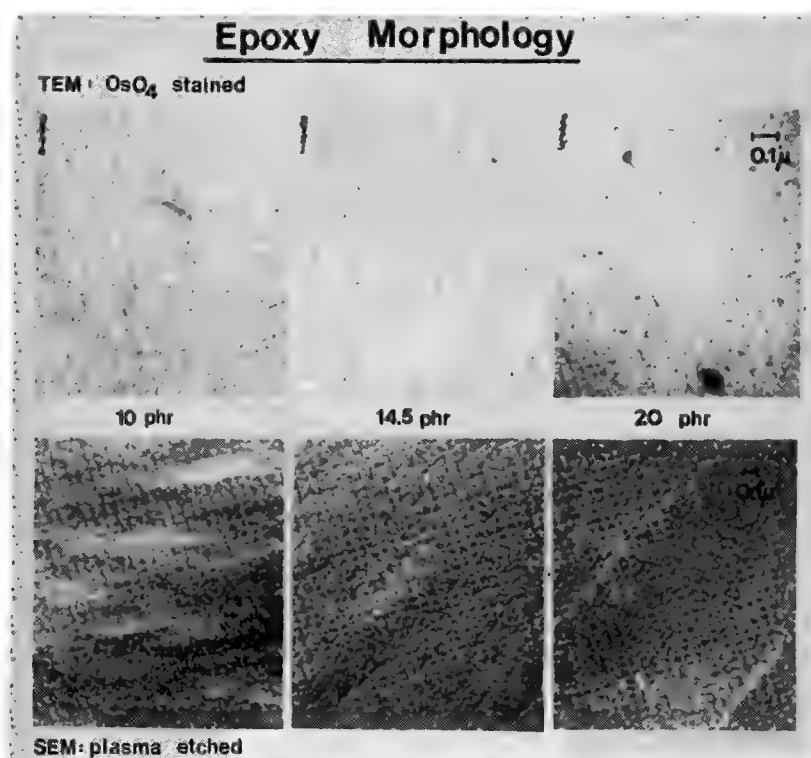


Figure 6.- Epoxy morphological changes occurring with alterations in amine-to-epoxy ratio. Top micrographs are ultramicrotomed sections which have been stained in osmium tetroxide. Bottom micrographs are epoxy samples fractured in liquid nitrogen.

IV. INTERPHASE: MATRIX - INTERFACIAL SHEAR STRENGTHS

We can alter the matrix side of the interface through the use of a finish. Graphite fibers are coated with about a thousand angstrom epoxy coating that is without the curing agent. When we compare just the surface-treated fiber with the surface-treated and finished fiber which only has a thousand angstroms of the pure epoxy resin, an improvement in interfacial shear strength is detected (Figure 7) [8].

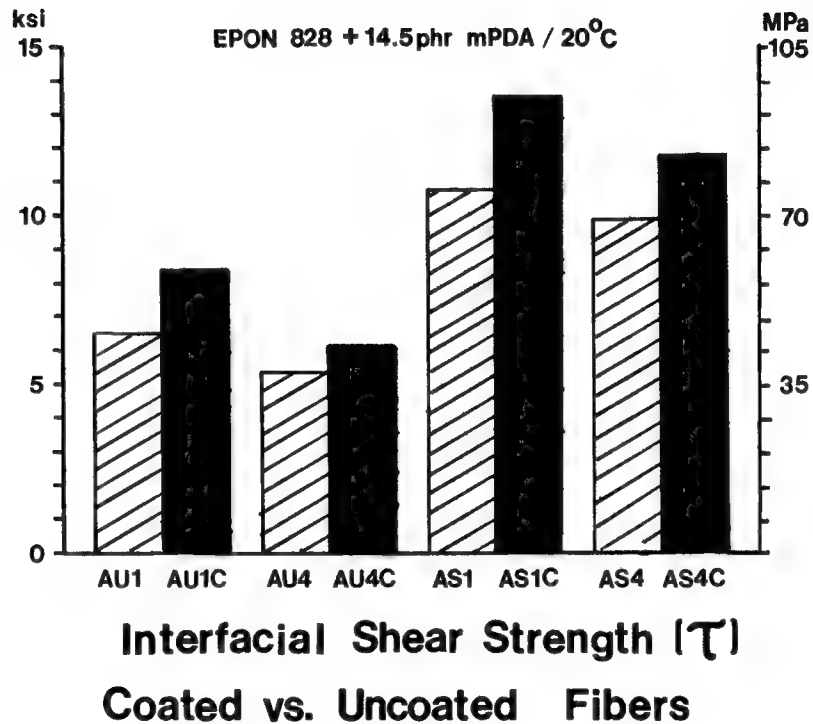


Figure 7.- Interfacial shear strength for carbon fibers with (C) and without epoxy finish.

IV. INTERPHASE: MATRIX - MICROGRAPHS OF THE CRITICAL-FIBER LENGTH TEST

Micrographs (Figure 8) of the fracture process that occurs show a third mode of failure. Whereas before we had an interfacial crack or actually frictional bonding now, with increasing strain after the fiber is broken, a matrix crack grows into the resin, not an interfacial crack.

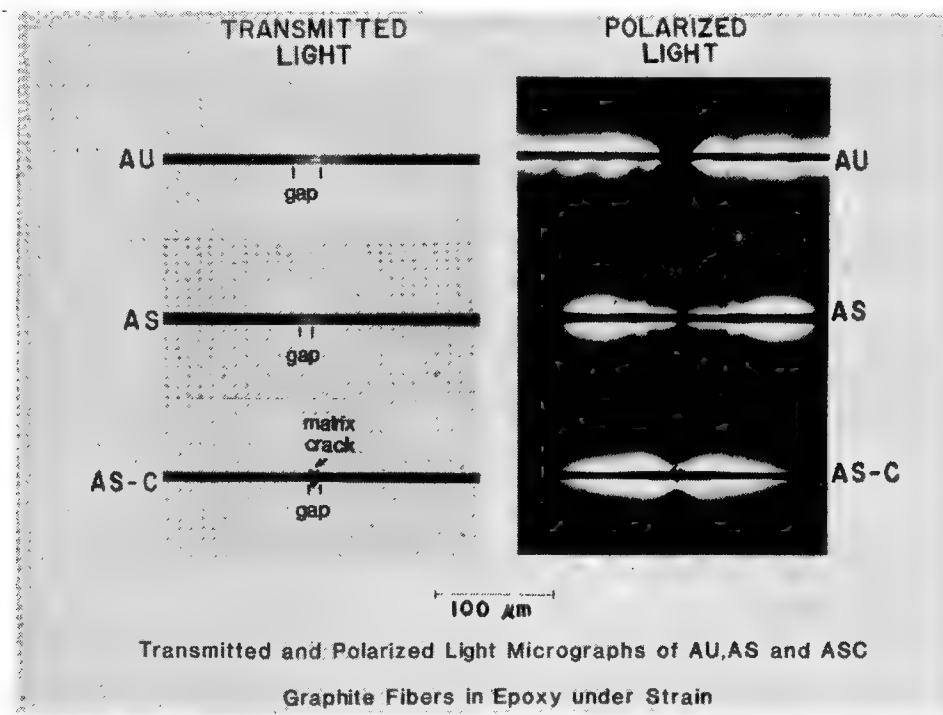
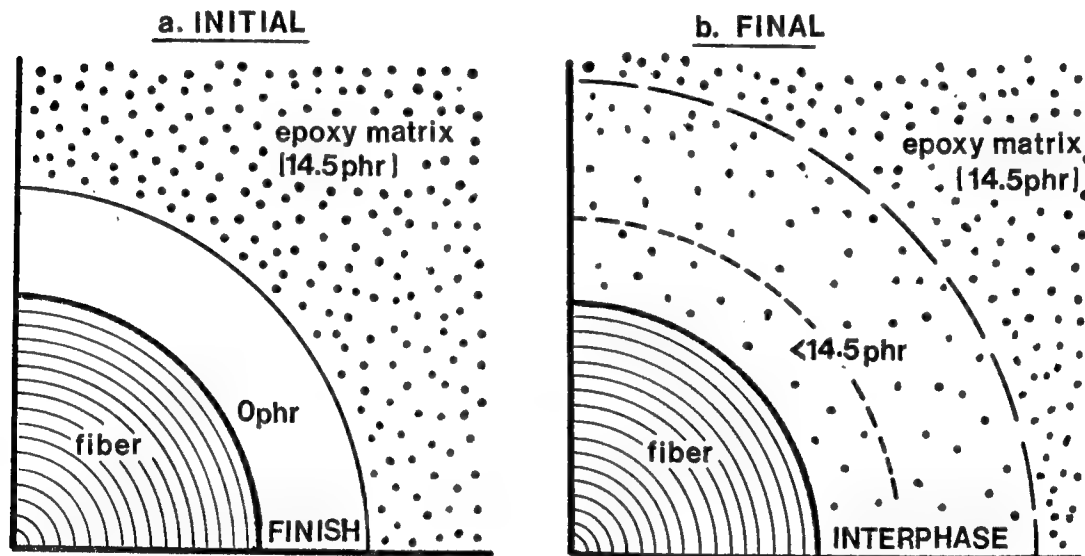


Figure 8.- Transmitted and polarized light micrographs of untreated (AU), surface-treated (AS), and surface-treated and finished (ASC) fibers under strain in an epoxy matrix.

IV. INTERPHASE: MATRIX - SCHEMATIC MODEL OF THE INTERPHASE

The explanation of what is happening here is the following (Figure 9). We are starting off with a fiber with a thin layer of finish at about 0 parts per hundred of amine. That fiber in turn is immersed in an epoxy matrix with 14.5 parts per hundred of amine. In our cure cycle it takes about 50 minutes for gelation to occur. During that period amine from the bulk matrix is diffusing into the finish layer and an interphase region of some thickness is formed. The properties of this interphase region are now changing from the fiber surface on out into the bulk. As the amine diffuses it also reacts so a gradient of amine is formed going from the bulk to the surface of the fiber.

Some studies on model compounds where the amine-to-epoxy ratio has been varied show that when the amine content is reduced, the epoxy material tends to go up in modulus, at the same time decreasing in both fracture strength and fracture strain. In this case we are creating a brittle interphase between fiber and matrix which promotes better stress transfer because it has a higher modulus but also has a lower toughness. This interphase therefore promotes matrix fracture as opposed to interfacial fracture.



Model of Interphase Development During Cure Cycle

Figure 9.- Schematic model of a single finished graphite fiber in quarter view showing the initial and final states of the interphase.

V. INTERPHASE: HYGROTHERMAL EFFECTS

We have been looking at the surface treated and finished fibers at 20°C. Figure 10 shows what happens with hygrothermal exposure [9]. The Tg of the matrix we are using is about 166°C. The Tg of the coating, if we assume it has less than the stoichiometric amount of amine, about 7.5 parts per hundred, is about 60°C to 70°C.

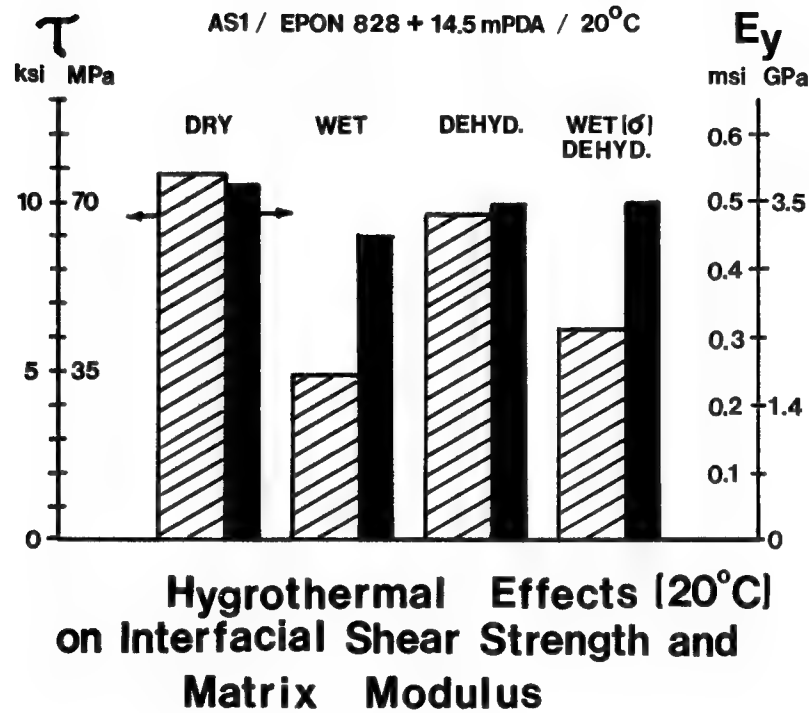


Figure 10.- Interfacial shear strength and matrix modulus for a surface-treated fiber after hygrothermal exposure at 20°C.

V. INTERPHASE: HYGROTHERMAL EFFECTS - 125°C EXPOSURE

If we do our hygrothermal exposure at elevated temperatures (Figure 11) at least above the transition temperature of the coating, the coating acts like a rubbery material and acts to protect the interface. In the dry condition where we expose the surface-treated but uncoated fiber to moisture and then bring it down to room temperature and test it, interfacial shear strength has been reduced. Interfacial shear strength after drying is recovered. Now contrast that to the same fiber with the same matrix in the presence of that 1,000-angstrom finish layer of pure epoxy. A high value of dry properties is available initially, but in the wet state some loss is experienced nearly to the level of the uncoated fiber. After drying, no recovery is observed, but the ultimate or residual level is much higher than the level that is obtainable for the untreated fiber.

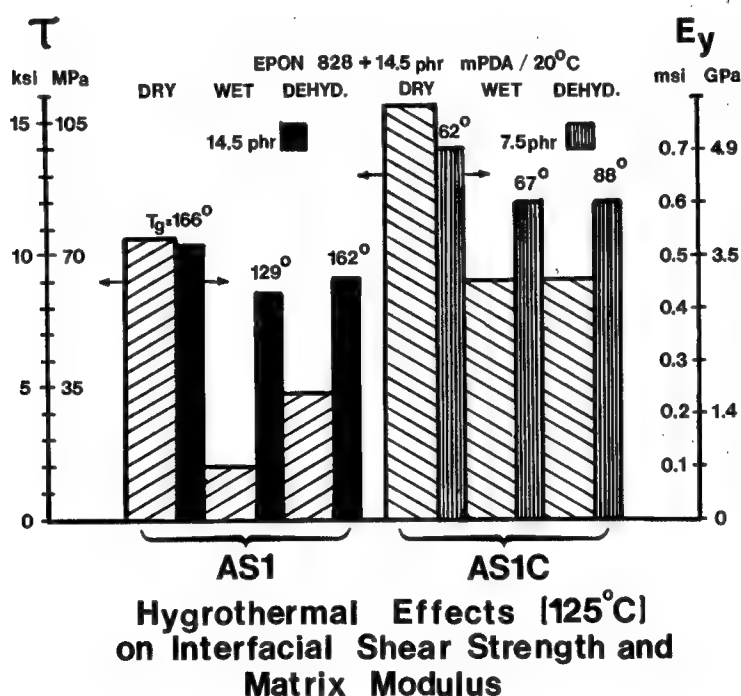


Figure 11.- Comparison of finished (AS1C) versus unfinished (AS1) fibers for interfacial shear strength and matrix and finish modulus after 125°C hygrothermal exposure.

V. INTERPHASE: HYGROTHERMAL EFFECTS - FRACTURED SURFACES PARALLEL TO FIBER AXIS

Finally let's look at how these interactions at the interface can affect the composite properties and how well the testing with a single filament test models composite properties. If you look at a composite in cross section, you see that the area where fibers come in contact is really a small proportion of the fiber diameter. Two thousand angstroms can be a significant portion of the interfiber distance in an actual composite. Composites were made from these three fibers: the untreated AU, the surface-treated AS, and the surface treated and coated ASC and at typical volume fractions with the same Epon 828-MPDA matrix system. Two different samples, both unidirectional about a tenth of an inch thick, were made. Compact tension specimens were fabricated with starter cracks in one case perpendicular to the fiber axis, in the other case parallel to the fiber axis [10]. The results are shown in Figure 12 for the untreated, surface treated, and surface treated and coated fibers. For the untreated fiber which had the lowest value of interfacial shear strength, the micrograph shows a lot of interfacial separation, clean fibers, and matrix without fibers in it. The intermediate surface treatment shows both situations, matrix failure as well as bridging in some areas of interfacial failure. Finally for the surface-treated and coated fiber, which had the highest degree of interfacial adhesion, there are no bare fibers. Every fiber that is there is coated with some degree of matrix.

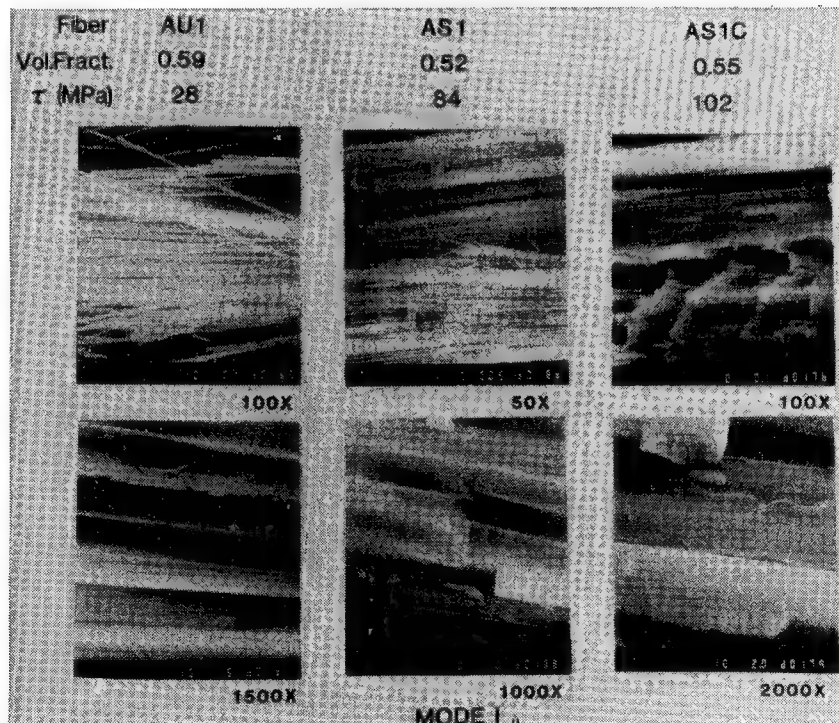


Figure 12.- Fracture surfaces of unidirectional composites with varying levels of adhesion parallel to the fiber axis.

V. INTERPHASE: HYGROTHERMAL EFFECTS - FRACTURED SURFACES PERPENDICULAR TO FIBER AXIS

Contrast the preceding results with fracture perpendicular to the fibers (Figure 13). The untreated fiber shows a very large degree of pull-out, where the pull-out lengths are on the order of half of what we measure in our single filament test. With surface treatment the pull-out length decreases. A very high degree of bonding gives almost planar fracture. The end of the fiber and the matrix surface are planar all along the entire fracture surface.

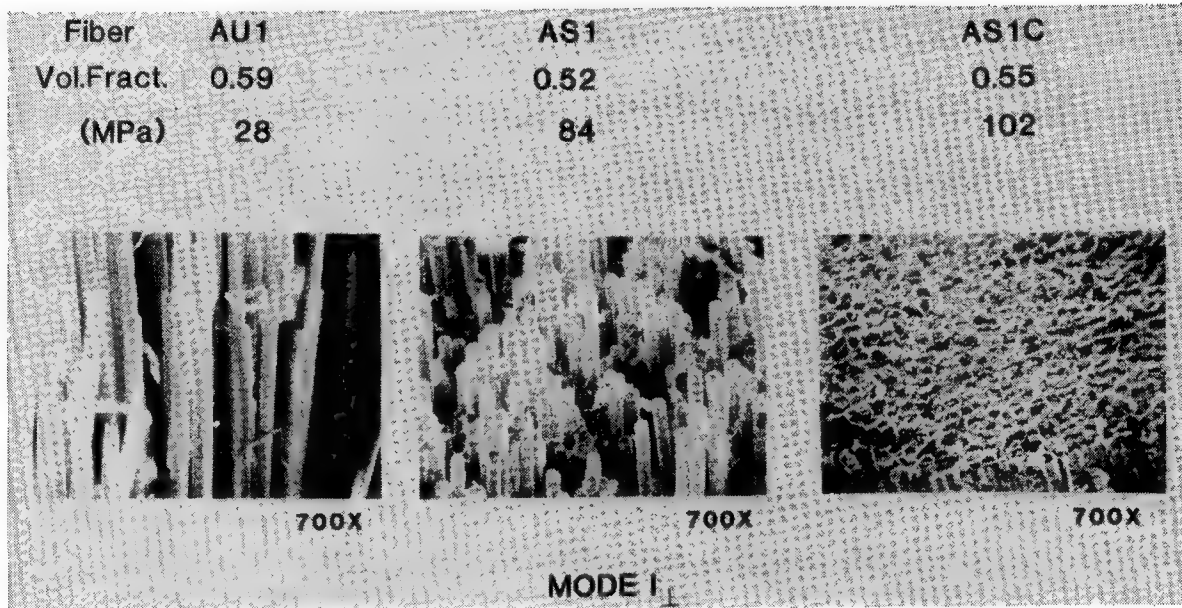


Figure 13.- Fracture surfaces of unidirectional composites with varying levels of adhesion perpendicular to the fiber axis.

VI. SUMMARY

In summary, I have tried to show that if one is going to consider altering the composite properties, for example, changing the toughness of the composite, one has to consider not only the matrix and the fiber but also the interface as well. What we would like to do ultimately is change the rule of mixtures from being purely additive between fiber and matrix properties to include the interface also as a design variable.

REFERENCES

- [1] "Adhesion of Graphite Fibers to Epoxy Matrices. I. The Role of Fiber Surface Treatment," L. T. Drzal, M. Rich, and P. Lloyd, J. Adhesion, 16, 1-30 (1983).
- [2] "A Single Filament Technique for Determining Interfacial Shear Strength and Failure Mode in Composite Materials," L. T. Drzal, et.al., Paper 20-C, 35th Annual Technical Conference, Reinforced Plastics/Composites Institute, SPI (1980).
- [3] "The Surface Composition and Energetics of Type A Graphite Fibers," L. T. Drzal, Carbon, 15, 129-138 (1977).
- [4] "The Surface Composition and Energetics of Type HM Graphite Fibers," L. T. Drzal, J. A. Mescher, and D. Hall, Carbon, 17, 375-382 (1979).
- [5] "Graphite Fiber Surface Analysis through XPS and Polar/Dispersion Free Energy Analysis," L. T. Drzal and G. Hammer, Appl. Surf. Sci., 4, 340-355 (1980).
- [6] "A Study of the Fracture Surface of Cured Epoxy Resin," L. T. Drzal, V. B. Gupta, and Y. L. Chen, Proceedings of the 41st Annual Meeting of the Electron Microscopy Society of America, 34-35, Phoenix, Arizona (1983).
- [7] "A Modified Replication Technique to Study the Morphology of Cured Epoxy Resin," L. T. Drzal, V. B. Gupta, and R. Omlor, Proceedings of the 41st Annual Meeting of the Electron Microscopy Society of America, 36-37, Phoenix, Arizona (1983).
- [8] "Adhesion of Graphite Fibers to Epoxy Matrices. II. The Effect of Fiber Finish," L. T. Drzal, M. Rich, M. Koenig, and P. Lloyd, J. Adhesion, 16, 133-152 (1983).
- [9] "Moisture Induced Interfacial Effects on Graphite Fiber-Epoxy Interfacial Shear Strength," L. T. Drzal, M. Rich, and M. Koenig, Paper 4-G, 38th Annual Technical Conference, Reinforced Plastics/Composites Institute, SPI (1983).
- [10] "Effect of Graphite Fiber-Epoxy Adhesion on Composite Fracture Behavior," L. T. Drzal, Proceedings of the 2nd U.S./Japan ASTM Conference on Composite Materials (1983).

NEWER CARBON FIBERS AND THEIR PROPERTIES

**Roger Bacon
Union Carbide Corporation
Parma Technical Center
Parma, Ohio**

INTRODUCTION

I will tell you about the newer carbon fibers that are either on the market or coming in the near future. Then I will discuss the structure of carbon fibers and describe how their properties depend on structure. Finally, I will describe how we get different types of structure by control of process parameters.

MATERIALS DEVELOPMENT GOALS

Some of the goals of composite materials development at Union Carbide are to achieve higher strength and stiffness, better damage tolerance, and better retention of properties at high temperatures. For some applications, dimensional stability of composites under rapid changes in temperature is required; here, modulus, thermal conductivity, and thermal expansion coefficient are important.

Better Composite Properties

- Strength
- Stiffness
- Damage Tolerance
- High Temperature
Properties Retention
- Dimensional Stability
(E , K_T , α_T)

KEY COMPOSITE PROPERTIES

Some key properties of composites are divided into fiber-dominated and resin-dominated properties. The fiber-dominated properties are mostly those measured in the 0 degree direction in a unidirectional composite. They include tensile strength, tensile modulus, compressive strength, thermal conductivity, and electrical conductivity. Shear strength is partly a fiber-dominated property (i.e., depends on the fiber surface) but it also is resin-dependent. Under resin-dominated properties, we include first the high temperature mechanical properties of the composite. Transverse strength, toughness, and (in part) longitudinal shear strength are resin-dominated properties.

Fiber-Dominated

- 0° Tensile Strength**
- 0° Tensile Modulus**
- 0° Compressive Strength**
- 0° Thermal Conductivity**
- 0° Electrical Conductivity**
- (Shear Strength)**

Resin-Dominated

- High Temp. Mechanical Properties**
- Transverse Strength**
- Toughness**
- (Shear Strength)**

NEWER CARBON FIBERS

The current state-of-the-art carbon fibers are listed below. Carbon fibers tend to be classified by their modulus. The so-called high-strength type of fiber possesses a 33 million psi Young's modulus. The higher modulus fibers possess moduli of 55 million psi and 75 million psi.

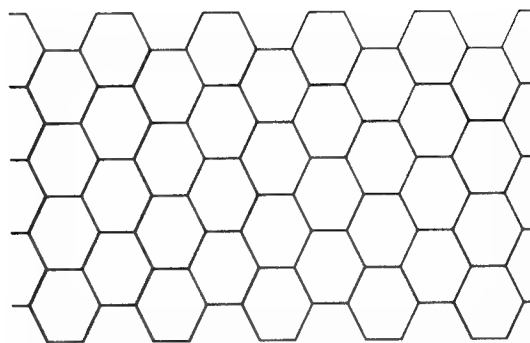
Under the heading of "Newer Fibers", we see that much higher strengths are currently being realized in fibers of 35-to-37 million psi modulus. Next, there is an "intermediate modulus" fiber with 41 million psi modulus and excellent tensile strength. Finally, for applications requiring extremely high stiffness and excellent thermal stability, we have the ultra-high modulus fibers with stiffnesses of 100-to-120 million psi.

Fiber Type	<u>State-Of-The-Art</u>		<u>Newer Fibers</u>	
	Modulus Strength		Modulus Strength	
High Strength	33 Msi	500 ksi	35 Msi	600 ksi
			37 Msi	750 ksi
Intermed. Modulus			41 Msi	700 ksi
High Modulus	55 Msi	350 ksi		
Very High Modulus	75 Msi	300 ksi		
Ultra High Modulus			100 Msi	325 ksi
			120 Msi	350 ksi

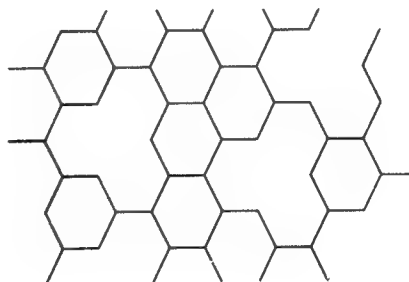
THE GRAPHITE LAYER PLANE

All carbon fibers are based on the graphite layer structure which is sometimes a very imperfect structure. The perfect graphite layer consists of a continuous "chicken-wire" network of carbon atoms. The layer planes are stacked together in a parallel arrangement. However, many carbon fibers, particularly the high strength varieties, have very small layer sizes and imperfect structures with missing carbon atom sites at which cross-linking can take place between the adjacent layers.

PERFECT

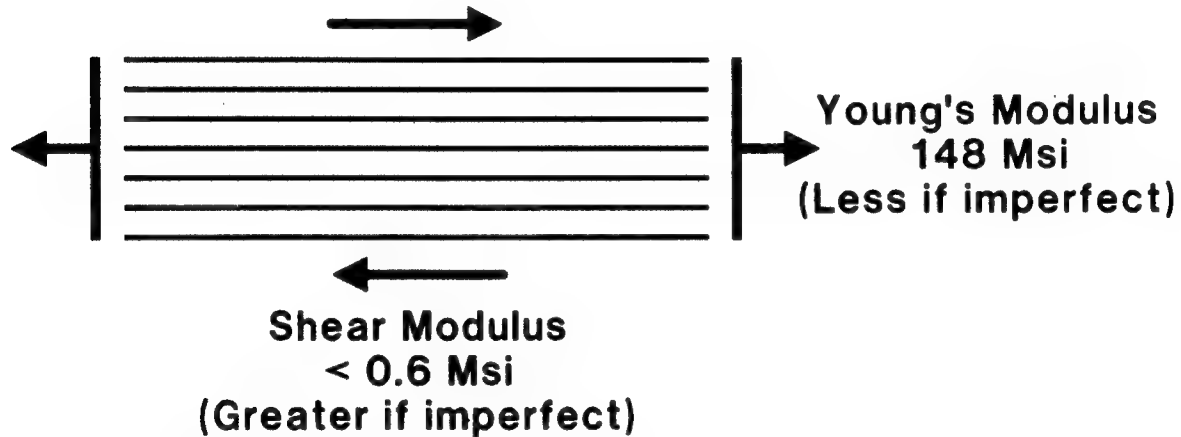


IMPERFECT



THE GRAPHITE CRYSTAL

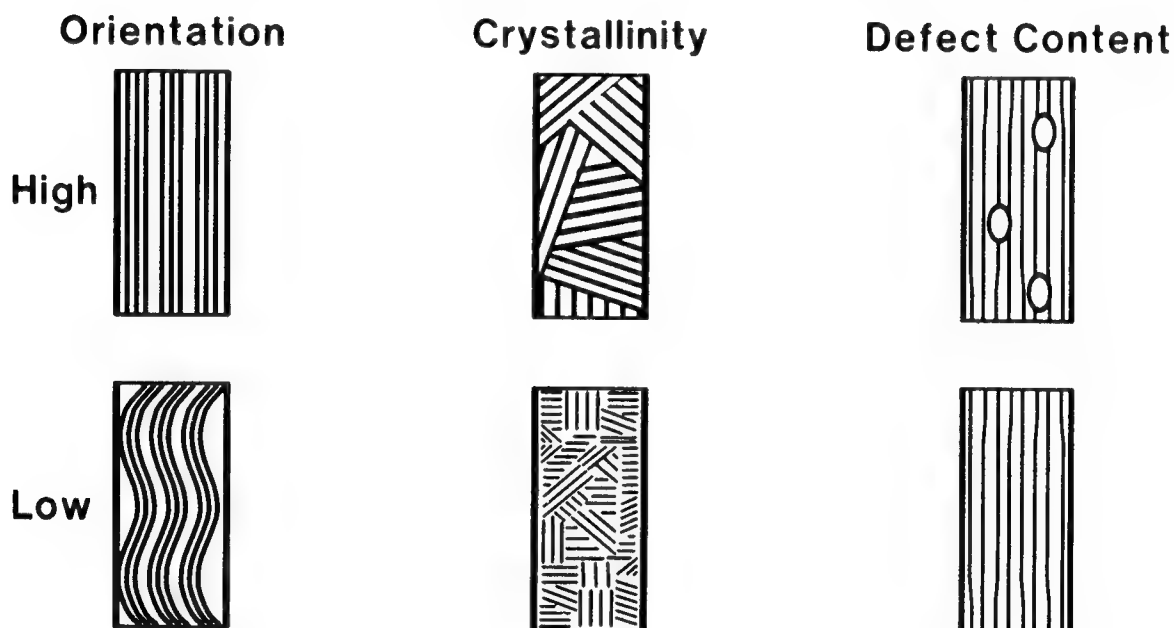
The figure below represents the graphite crystal edge-on, showing a parallel stacking of the graphite layers. For the perfect graphite crystal, the Young's modulus is 148 million pounds per square inch in the layer plane direction. If the layers are imperfect and hence distorted and cross-linked, the modulus is lower. The shear modulus, on the other hand, is extremely low: only six-tenths of a million psi or even less. If it is an imperfect structure with cross-linking, one can expect a higher shear modulus. To estimate tensile strengths of graphite structures one must take into account these same differences in structure: very high tensile strengths are realized for pure tension parallel to the basal plane (as high as 3 million psi has been measured in graphite whiskers) but if appreciable shear stress is introduced, the strength is very much lower, being limited by the weak bonding between graphite layers.



FIBER STRUCTURE

The main structural features of carbon fibers are indicated below. Orientation can be high or low depending upon whether the layers are straight and parallel to the fiber axis. Another important structural parameter is the crystallinity. If the linear dimensions of the perfect crystalline regions are large, the structure is said to possess a high degree of crystallinity; such regions tend to behave similarly to the perfect graphite crystal. Finally, defect content is very important, particularly with regard to fiber strength.

CARBON FIBER PROPERTIES ARE DETERMINED BY THEIR STRUCTURE:



EFFECTS OF ORIENTATION ON PROPERTIES

During more than two decades, many workers have related carbon fiber structure to properties. I will give a qualitative listing of those properties which increase and those which decrease as one changes the level of each of the major structural parameters. We list below the effects of increasing preferred orientation. The longitudinal tensile strength, the longitudinal tensile modulus, the thermal conductivity, and the electrical conductivity all increase with increased orientation. The longitudinal negative CTE also increases; in other words, the coefficient of thermal expansion becomes more negative in more highly oriented (higher modulus) fibers. Properties which decrease with improved orientation are the transverse tensile strength and the transverse elastic moduli.

AS ORIENTATION IS IMPROVED, THESE CARBON FIBER PROPERTIES

INCREASE

Longit. TENSILE STRENGTH
Longit. TENSILE MODULUS
THERMAL Conductivity
ELECTRICAL Conductivity
Longit. Neg. CTE

DECREASE

Transv. STRENGTH
Transv. MODULI

EFFECTS OF CRYSTALLINITY ON PROPERTIES

Crystallinity affects many properties. Those which increase with increasing crystallinity include thermal conductivity, electrical conductivity and negative CTE measured in the fiber direction. (The thermal expansion coefficient in the transverse direction is always positive.) Oxidation resistance improves in a more crystalline fiber. Properties which decrease with higher crystallinity include the tensile and compressive strengths (assuming that the degree of preferred orientation is fixed.) The transverse strength and stiffnesses decrease, as does the longitudinal shear modulus.

AS CRYSTALLINITY IS IMPROVED, THESE CARBON FIBER PROPERTIES

INCREASE

THERMAL Conductivity
ELECTRICAL Conductivity
Longit. Neg. CTE
OXIDATION RESISTANCE

DECREASE

Longit. TENSILE STRENGTH
Longit. COMPRESSIVE STRENGTH
Transv. STRENGTH & MODULI
Longit. SHEAR MODULUS

EFFECTS OF FIBER DEFECTS

As you remove defects you improve just about everything: most notably, tensile strength. Thermal conductivity and electrical conductivity (both transport properties) are affected by certain kinds of defects. Oxidation resistance is affected by the presence of catalyst impurities.

AS DEFECTS ARE REMOVED, THESE CARBON FIBER PROPERTIES IMPROVE:

**TENSILE STRENGTH
THERMAL Conductivity
ELECTRICAL Conductivity
OXIDATION RESISTANCE**

CARBON FIBER MANUFACTURING PROCESS

The carbon fiber manufacturing process is outlined below. The precursor polymers may be cellulose (rayon), polyacrylonitrile (PAN), or pitch. Today, rayon is used only for very low modulus fibers. The precursor polymer is converted into a fiber by an extrusion process which may be either wet spinning, dry spinning, or melt spinning. The originally coarse fibers are stretched or drawn into finer fibers. The next step is to stabilize the fiber by oxidation in air at a temperature of approximately 400°C. The fiber is next carbonized to drive off most of the volatiles, leaving only the carbon behind. The carbonization temperature is between 1000°C and 2000°C. It is carried out in inert atmosphere. A final heat treatment, to achieve higher modulus or higher crystallinity, is performed at temperatures above 2000°C and sometimes as high as 3000°C.

Precursor Polymer	Cellulose (Rayon) Polyacrylonitrile Pitch (Mesophase)
Fiberize	Wet-, Dry-, Melt-Spin Draw
Stabilize	Oxidize Heat to 400°C
Carbonize	To 1500°C ($\pm 500^\circ\text{C}$) Inert Atmosphere
Heat Treat	To 2500°C ($\pm 500^\circ\text{C}$)

CONTROL OF STRUCTURE

We can control carbon fiber structure as follows:

1) Orientation is improved by fiber drawing or by restraining the fiber so that it can't shrink during the heat treatments. The precursor fiber structure helps to determine the degree of orientation in the final carbon fiber; starting with an oriented fiber structure one tends to improve orientation still further by heat treatment.

2) Crystallinity is largely determined ahead of time by the precursor chemistry. It is also strongly affected by the heat treatment, that is, by the final processing temperature.

3) Defect content is controlled by the purity of the raw materials and by the mechanics of fiber handling.

Structural Parameter:

Orientation

Crystallinity

Defect Content

Controlled By:

1. Fiber Drawing
2. Precursor Fiber Structure
And Heat Treatment

1. Precursor Chemistry
2. Heat Treatment

1. Precursor Purity
2. Process Handling, Etc.

FUTURE CARBON FIBERS

Sometime in the future I think we will see, for the high strength variety of carbon fiber, a one million psi tensile strength. For tough composites, carbon fiber producers are already providing strains-to-failure approaching 2 percent, and we expect to exceed this number in the future. In the case of high modulus fibers (55 million psi Young's modulus), 600 ksi tensile strength should be achieved. The ultra high modulus fibers will have a similar tensile strength but a lower strain-to-failure.

Fiber Type	Modulus	Strength	Applications
High Strength	40 Msi	1000 ksi	Structural
High Modulus	55 Msi	600 ksi	Structural
Ultra High Modulus	140 Msi	600 ksi	Space, Electrical

SESSION III

MATRIX SYNTHESIS AND CHARACTERIZATION

CHAIRMAN: PAUL HERGENROTHER

DEVELOPMENT OF A HETEROGENEOUS
LAMINATING RESIN

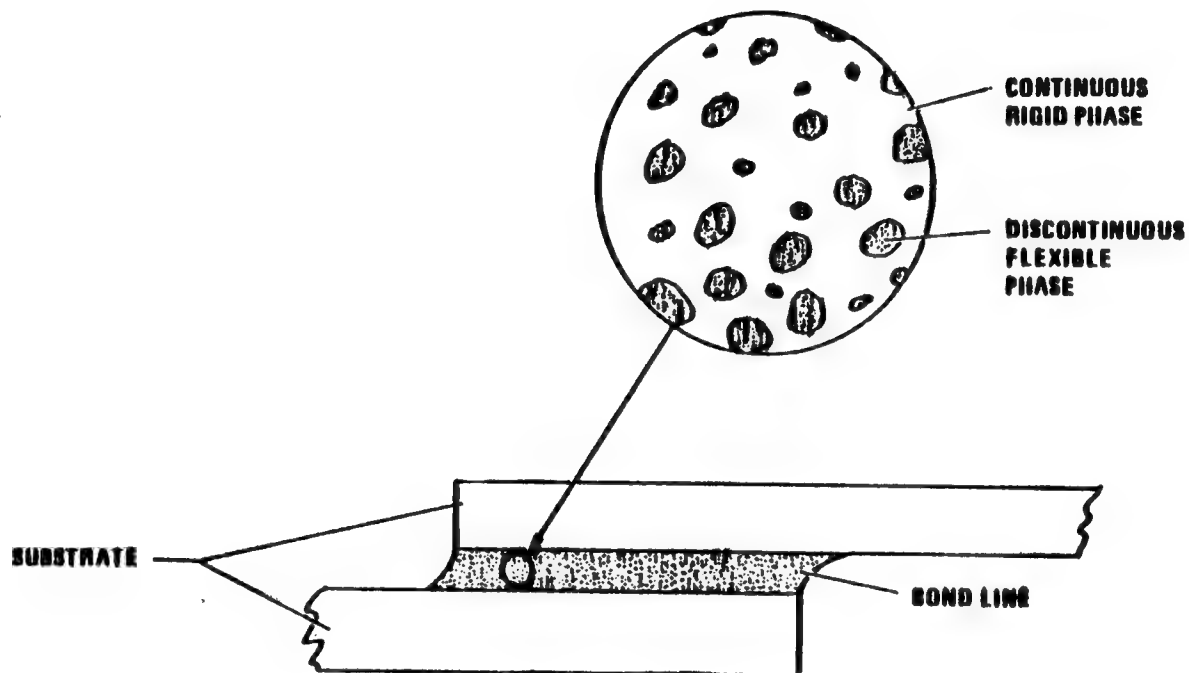
Rex Gosnell
Narmco Materials, Inc.
Anaheim, California

OBJECTIVE

The early part of this program was directed toward the feasibility of toughening the common types of matrix resins such as Narmco 5208 by utilizing a heterogeneous additive. The more significant latter part of the program evolved into a study of some basic concepts and principles in the toughening of matrix resins for advanced composites. An effort was made to determine the "why" and "how" of some approaches to toughening and to make an assessment of the sacrifices that must be made in the overall mechanical properties of a matrix resin.

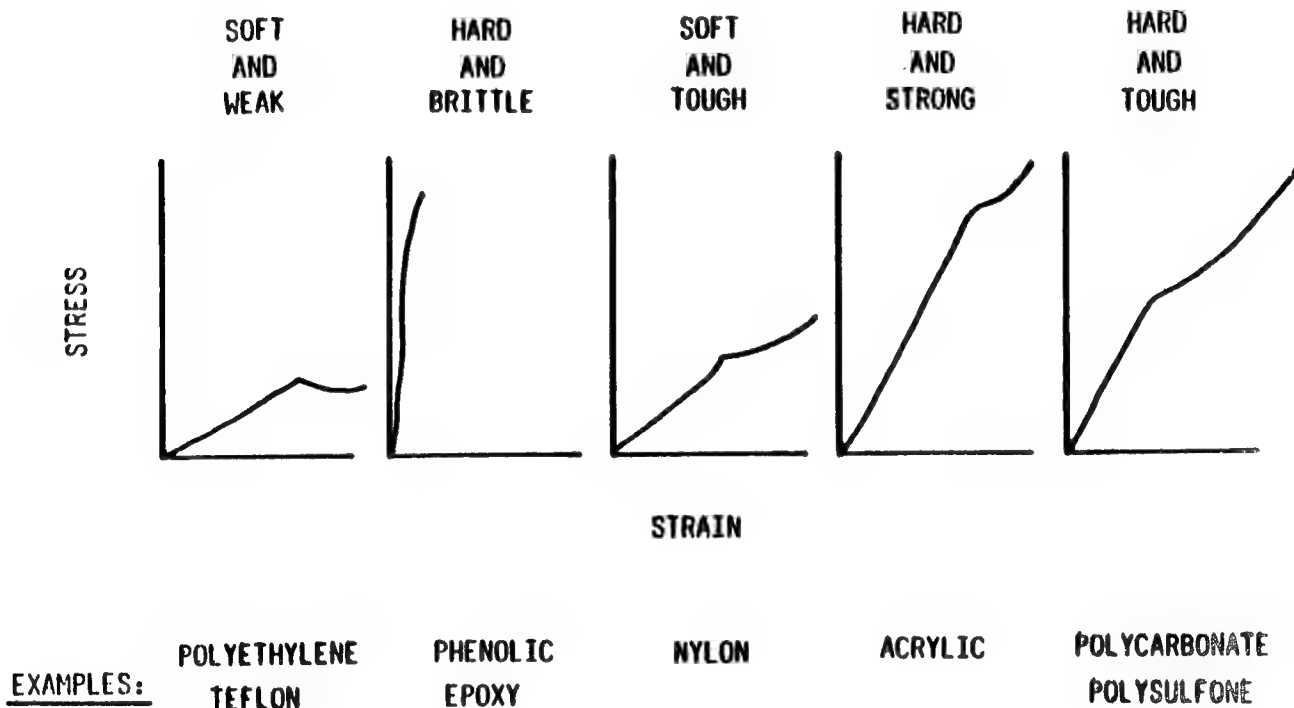
POLYBLEND EPOXY ADHESIVES

At the outset of this program, it was thought that the technology involving heterogeneous resins that have been successful with adhesives might be applicable to resin matrices. A number of commercial aircraft adhesives utilize a blend of a discontinuous dispersion of elastomer in a continuous phase of a cross-linked resin system. These polyblends were quite successful in some early adhesive systems such as nitrile-phenolics. The improvement in impact capability of such resins led to the thought that this might be a viable approach for composite matrix resins.



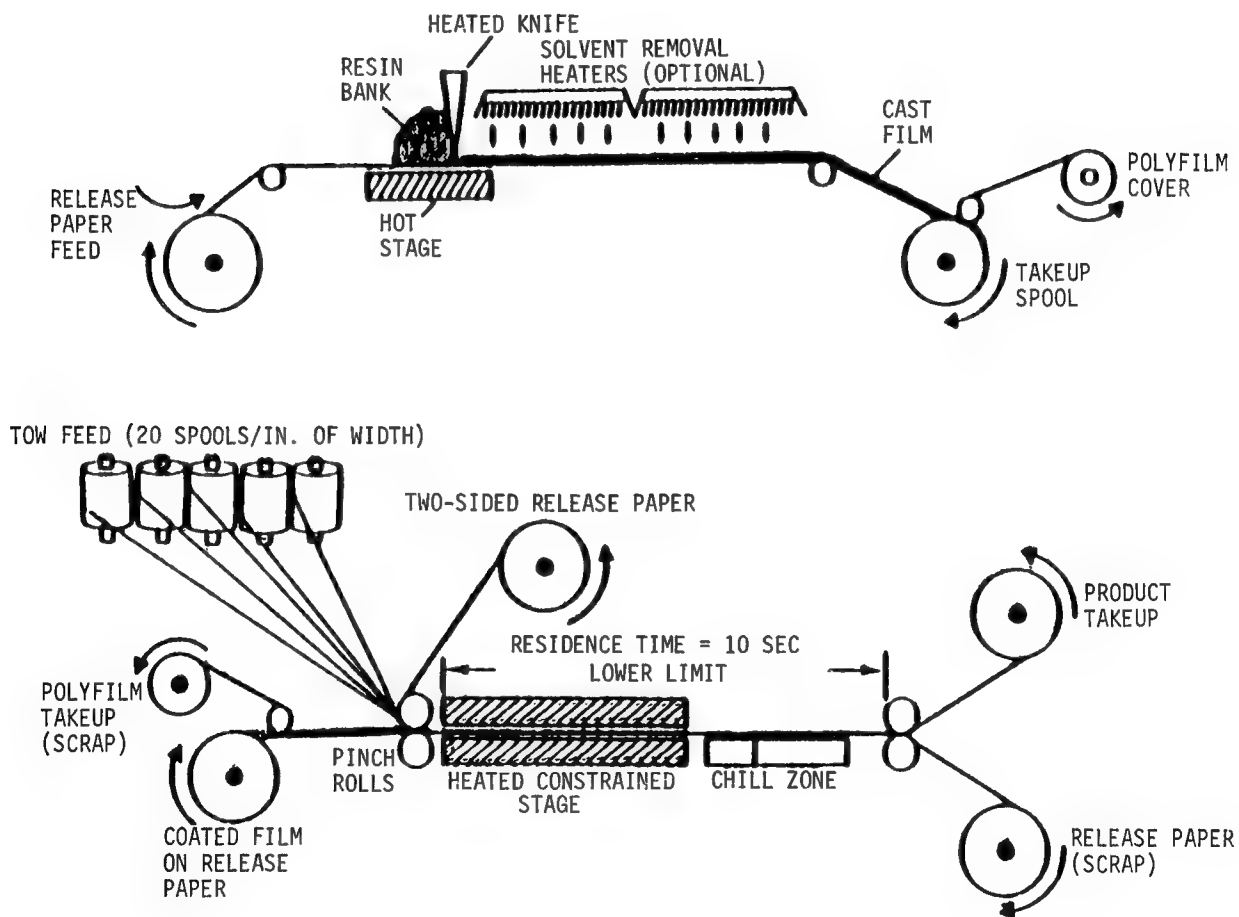
MECHANICAL BEHAVIOR OF POLYMERIC MATERIALS

Polymeric materials have a wide range of stress-strain behavior. Examples are shown. Of these, the last type seems to be the apparent need for improved tough resin matrix resins. As stated in the objective, the question is how you can improve this relationship of stress and strain in such a way that the overall performance of the composite will be attractive for advanced composites.



ELEMENTS OF MELT TRANSFER PROCESS FOR HIGH-MODULUS FIBER

Ideally, any modifications of resin systems would be compatible with existing prepreg processes, although this was not a primary consideration in this program. For example, some combinations of materials were very difficult to handle even in the laboratory, and would be totally unsuitable for existing prepregging methods. Information gained from these difficult systems might shed some light on other more viable approaches.



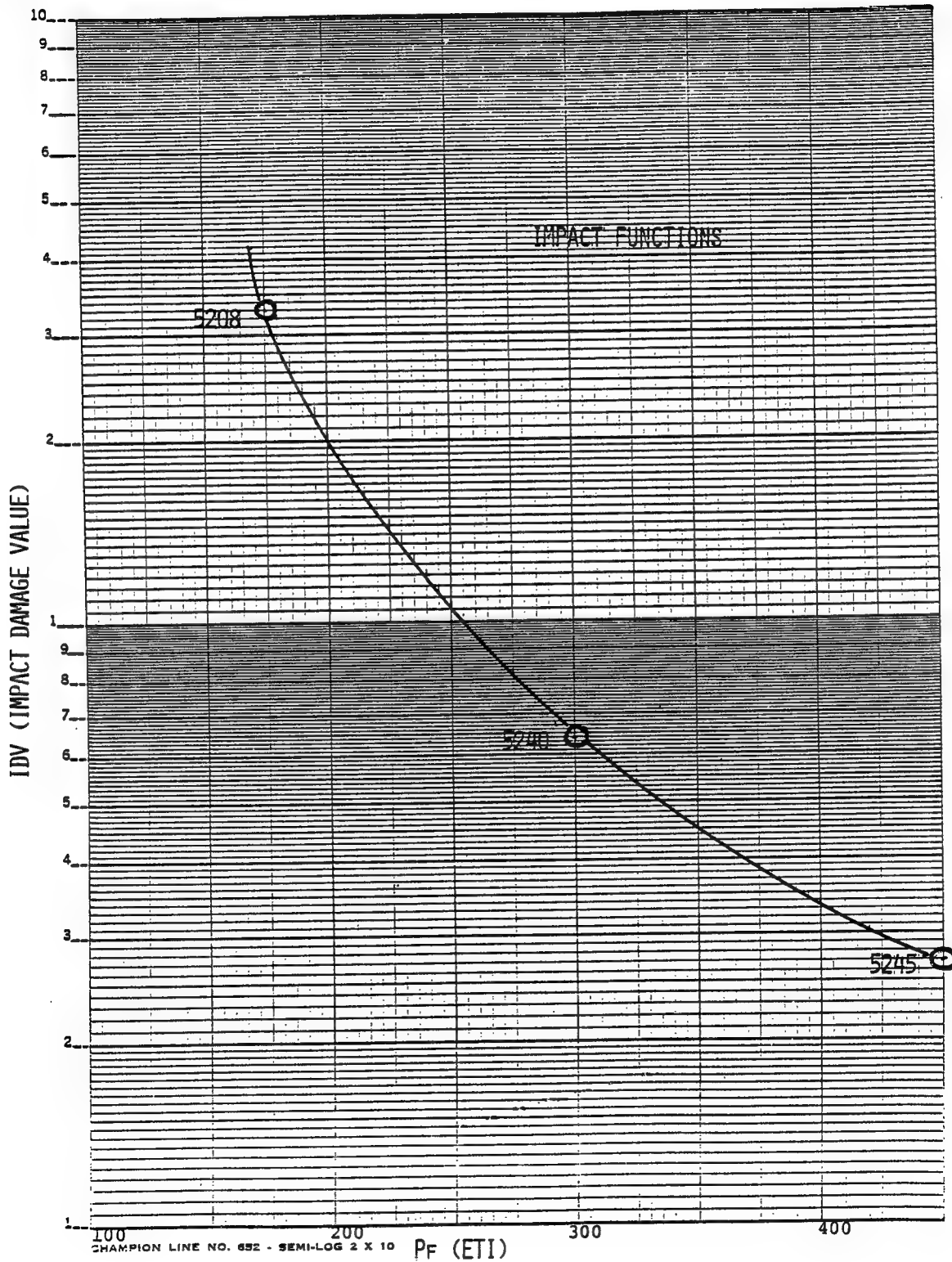
NARMCO COMPOSITE IMPACT SCREENING TEST

Narmco presently uses an impact screening test for assessment of the effectiveness of toughening of resin systems. This test was used in this program to determine relative toughening capability of the various approaches. The test is essentially a falling dart; the data treatment is discussed in the figure. A smaller number means less impact damage.

- 3K-70P/C-3000 FABRIC SOLUTION COATED
- 6" x 6" x 6 PLY LAMINATE
- DAMAGED AREA MEASURED AT 10, 20, 30 AND 40 IN. LB.
- GARDNER DAMAGED AREA FUNCTION QUANTITATIVELY DESCRIBES DAMAGE SUFFERED BY TEST LAMINATE AFTER IMPACT (REPRESENTING LOADINGS UP TO 900 IN. LB./IN. FOR NOMINAL .045" THICK LAMINATES)
 - REPORTED NUMBER IS WEIGHTED SUMMATION DERIVED BY INTEGRATING THE REGRESSION CURVE OVER THE SPECIFIED IMPACT ENERGY LEVELS
 - COMPUTED BY IN-HOUSE DEVELOPED EQUATION WHICH NORMALIZES THICKNESS AND REDUCES DATA SCATTER BY LEAST SQUARES LINE FIT

IMPACT DAMAGE VALUE

The value of this impact damage is correlated to ETI test values.



SHORT BEAM SHEAR

Retention of basic mechanical properties was monitored by using a standard short beam shear test. Early in the work, it was learned that this test gave reduced values when most of the toughening approaches were incorporated in the resin matrix resins.

12 PLY 4" x 6" LAMINATE

3K-70P/C-3000 FABRIC

SPAN/DEPTH = 4:1

WET TESTS AFTER 40 HOUR WATER BOIL

RT 200°F 270°F WET & DRY

PLASTIC FAILURES NOTED

"ALL-EPOXY" SYSTEMS

Using a simple epoxy formulation, several potential toughening agents were evaluated by the impact resistance and the short beam shear at RT, 200°F and 270°F, both dry and wet. Comparative data is also shown for Narmco 5208 and Narmco 5245C.

Hydroxyl-terminated polyethers, hydroxyl-terminated polyesters, ABS, and two CTBNs all produced improvement in impact value, but at a considerable sacrifice in 270°F wet short beam shear. Of all the material tested, the polycarbonate was the most effective in improving impact with the least sacrifice at the 270°F wet value. Note that Resicure #4 also improved impact strength with a similar reduction in 270°F wet short beam shear strength.

The polycarbonate was studied further in the program. It showed the most attractive improvement in impact value. (Smaller numbers are better.)

(2 Hrs. @350°F Cure)

<u>Ingredients</u>	<u>1</u>	<u>2</u>	<u>3</u>	<u>4</u>	<u>5</u>	<u>6</u>	<u>7</u>	<u>8</u>	<u>8A</u>	<u>5208</u>	<u>5245C</u>
<u>Epoxies</u>											
Den 439	11	11	11	11	11	11	11	11	11	-	-
RCI 98-180	4	4	4	4	4	4	4	4	4	-	-
Ciba MY-720	50	50	50	50	50	50	50	50	50	-	-
<u>Hardener</u>											
D.D.S.	21	21	21	21	21	21	21	21	21	-	-
<u>Catalyst</u>											
Resicure #4	.3	.3	.3	.3	.3	.3	.3	.3	-	-	-
<u>Filler</u>											
Cabosil	4.5	4.5	4.5	4.5	4.5	4.5	4.5	4.5	4.5	-	-
<u>Toughening Agent</u>											
Hydroxyl Containing Polyether (High M.W.)	5	-	5	-	-	-	-	-	-	-	-
Hydroxyl Terminated Polyester (Low M.W.)	8	10	-	-	-	-	-	-	-	-	-
Polycarbonate	-	-	-	4	-	-	-	-	-	-	-
ABS (K-2945)	-	-	-	-	5	-	-	-	-	-	-
CTBN (I)*	-	-	-	-	-	6	-	-	-	-	-
CTBN (II)*	-	-	-	-	-	-	6	-	-	-	-
<u>Laminate Mechanical</u> (3K70P)											
<u>Short Beam Shear (KSI):</u>											
RT. (Dry)	13.3	10.6	12.6	12.1	12.6	12.0	12.2	12.0	10.2	13.7	12.5
200°F (Dry)	10.2	7.7	9.6	10.2	9.3	9.5	9.1	9.9	9.8	10.7	11.2
270°F (Dry)	6.8	6.2	6.9	8.5	7.3	7.7	7.7	7.0	7.5	9.6	9.4
RT (Wet)**	10.0	9.8	11.3	10.0	10.6	10.0	10.1	10.6	10.3	12.1	12.0
200°F (Wet)	6.6	5.5	6.7	7.7	6.4	6.8	6.4	7.5	8.4	9.0	10.1
270°F (Wet)	2.7P	3.6P	3.7P	4.7P	3.8P	3.9P	3.6P	4.6P	6.2	7.5	8.6
<u>Impact Resistance</u>	415	600	1300	303	586	412	782	915	1964	3300	270

*CTBN (I) = CTBN 1300 prereacted with an epoxy novalac.

CTBN (II) = CTBN 1300 prereacted with Ciba MY-720.

**Wet = 40 hour water boil.

MORE "ALL-EPOXY" SYSTEMS

The effect of amine hardener on mechanical properties and impact resistance was studied, concentrating on the polycarbonate as the toughening agent. In example number 3, a very good impact number was observed, but a severe penalty was imposed on the mechanical properties. Anchor 1482 is a eutectic mixture of aromatic amines which showed some promise, but again, the poor 270°F wet strength is a sign that a heavy sacrifice is taken in composite mechanical properties to achieve the good impact value.

(2 Hrs. @350°F Cure)									
<u>Ingredients</u>	<u>1</u>	<u>2</u>	<u>3</u>	<u>4</u>	<u>5</u>	<u>6</u>	<u>7</u>	<u>5208</u>	<u>5245</u>
<u>Epoxyes</u>									
MY 720	-	-	50.0	51.0	51.0	51.0	51.0	-	-
ERL 0510	5.0	5.0	5.0	5.0	5.0	5.0	5.0	-	-
DEN 439	5.0	5.0	8.7	7.0	7.0	7.0	7.0	-	-
RCI 98-180	-	-	-	3.0	3.0	3.0	3.0	-	-
XU-276	67.7	57.0	-	-	-	-	-	-	-
<u>Hardeners</u>									
LSU-931	-	22.5	24.0	23.0	23.0	23.0	23.0	-	-
XU-205	-	-	-	7.0	7.0	7.0	7.0	-	-
DOS	16.0	-	-	-	-	-	-	-	-
Anchor 1482	-	3.2	5.0	-	-	-	-	-	-
<u>Catalyst</u>									
Resicure #4	0.3	0.3	0.3	0.3	0.3	0.3	0.3	-	-
<u>Filler</u>									
Cabosil M-5	3.5	3.5	3.5	3.0	3.0	3.0	3.0	-	-
<u>Toughening Agent</u>									
Lexan	4.0	4.0	4.0	-	4.0	4.0	4.0	-	-
DER 669	2.0	3.0	3.0	-	-	3.0	3.0	-	-
Photomer 4127	-	-	-	-	-	-	1.0	-	-
<u>Laminate Mechanical</u> (3K70P)									
<u>SBS</u>									
RT Dry	10.5	11.0	9.6	11.0	10.2	12.1	11.8 (12.0)	13.7	12.5
200°F Dry	7.5	6.5	8.0	9.1	9.1	9.4	9.4 (9.8)	10.7	11.6
270°F Dry	2.8	1.4	6.4	6.4	6.2	6.7	7.1 (8.1)	9.6	9.4
RT Wet	-	-	10.0	10.0	10.4	10.6	10.6 (10.6)	12.1	12.0
200°F Wet	-	-	6.8	6.5	6.3	6.9	6.7 (7.6)	9.0	10.1
270°F Wet	-	-	3.9	3.0	2.8	2.9	2.5 (5.6)	7.5	8.6
<u>Impact Resistance</u>	784	1084	144	1560	655 (624)	379 (562)	632	3300	270

Note: Values in parentheses obtained on post-cured samples (4 Hrs. @ 400°F)

BISMALEIMIDE/EPOXY SYSTEMS

The toughened bismaleimide/epoxy systems did not show the severe loss in hot-wet strength that was observed in the all-epoxy systems. Although room temperature values were somewhat lower than the epoxies, the temperature profile was more flat and the 270°F wet values were improved over straight epoxies. Impact values were respectable in the 300-700 range. (Lower values indicate less damage volume.)

(2 Hrs. @350°F Cure)

Ingredients	1	2	3	4	5	6	7	8	9	10	5208	5245C
Bismaleimide K-353	50	50	24	24	24	24	24	24	24	24	-	-
<u>Epoxies</u>												
Ciba MY 720	30	30	-	-	-	-	-	-	-	-	-	-
Ciba 0510	-	-	45	45	45	45	45	45	45	55	-	-
XU-276	-	-	-	-	-	-	-	-	-	14	-	-
<u>Hardeners</u>												
DDS	10	10	24	24	24	24	24	24	24	14	-	-
<u>Catalysts</u>												
Resicure #4	.3	.3	.3	.3	.3	.3	.3	.3	-	-	-	-
ETPI	-	-	-	-	-	-	-	-	.2	.3	-	-
<u>Filler</u>												
Cabosil	-	-	4.5	4.5	4.5	4.5	4.5	4.5	2	2	-	-
<u>Toughening Agent</u>												
Hydroxyl Containing Polyether (High M.W.)	8	5	-	-	-	-	-	-	-	-	-	-
Hydroxyl Terminated Polyester (Low M.W.)	2	-	-	-	-	-	8	-	-	-	-	-
ABS	-	-	-	5	-	-	-	4	6	6	-	-
Polycarbonate	-	5	-	-	-	-	-	2	-	-	-	-
CTBN/Epoxy I*	-	-	-	-	5	-	-	-	-	-	-	-
CTBN/Epoxy II**	-	-	-	-	-	6	-	-	-	-	-	-
<u>Laminate Mechanical (3K70P)</u>												
<u>SBS (KSI)</u>												
RT (Dry)	7.9	7.1	7.7	7.5	8.0	8.7	8.1	8.5	10.5	13.0	13.7	12.5
200°F (Dry)	7.2	6.1	8.1	8.2	8.2	8.7	7.9	8.3	9.5	11.5	10.7	11.2
270°F (Dry)	5.9	5.1	9.4	7.1	8.1	8.4	7.8	8.6	7.5	8.9	9.6	9.4
RT (Wet)***	6.7	8.9	8.5	9.0	8.7	8.3	8.6	9.4	9.5	13.6	12.1	12.0
200°F (Wet)	5.1	4.6	8.0	6.7	6.9	7.4	6.7	7.8	6.9	9.0	9.0	10.1
270°F (Wet)	3.7	2.9	6.9	4.6	5.5	5.2	4.5	5.3	-	5.7	7.5	8.6
<u>Impact Resistance</u>	261	305	738	706	832	679	622	641	678	790	3300	270

*CTBN 1300 prereacted with epoxy novalac.

**CTBN 1300 prereacted with MY-720

***40 Hr. water boil

CONCLUSIONS

1. The use of damage volume as a guide for measurement of impact resistance appears to be a valid determination.
2. Short beam shear is a good test to determine the effect of toughening agents on mechanical properties.
3. Rubber toughening results in improved laminate impact strength, but with substantial loss in high temperature dry and wet strength.
4. In the all-epoxy systems, the polycarbonate toughening agent seemed to be the most effective, although hot-wet strength is sacrificed. ABS was not as effective.
5. In general, the toughened all-epoxy systems showed better damage tolerance, but less hot-wet strength. Toughened bismaleimides had better hot-wet strength.

MODIFIED EPOXY COMPOSITES

W. J. Gilwee

NASA Ames Research Center
Moffett Field, CA

The potential use of graphite-fiber/resin matrix composites to achieve weight savings in aircraft and space applications is well documented (1). The design requirements for this type of composite include high strength, stiffness, impact resistance, and resistance to burning. The use of reactive liquid rubber to improve the toughness (impact resistance) of epoxy resin composites has been reported by a number of investigators (2-5). The two-phase system of a brittle epoxy resin phase and rubber phase is believed to increase the impact strength by means of a crack-terminating mechanism.

In this investigation, which is part of a screening program, we have studied the properties of a rubber-modified experimental epoxy resin as well as a standard epoxy as composite matrices. In addition, a brominated epoxy resin was used in varying quantities to improve the fire resistance of the composite.

OBJECTIVES

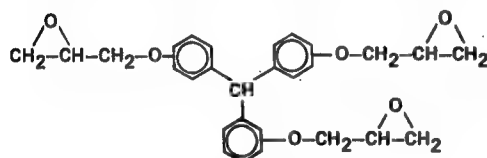
CARBON FIBER/RESIN COMPOSITES

- **350°F OR LOWER CURE TEMPERATURE**
- **HOT/WET PROPERTIES**
- **IMPROVED TOUGHNESS OVER CURRENT EPOXY RESIN**
- **LOW FLAME PROPAGATION**
- **LONG SHELF-LIFE PRE-PREG**

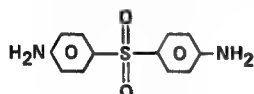
The experimental resin was tris-(hydroxyphenyl)methane triglycidyl ether, known as tris epoxy novolac (TEN). The standard epoxy resin used was tetraglycidyl 4,4'-diaminodiphenyl methane (TGDDM). The brominated epoxy was bisphenol A polymer with 50% by weight Br.

The above resins were modified with carboxyl-terminated butadiene acrylonitrile (CTBN) rubber. The rubber was added as a prereacted concentrate containing 50% CTBN rubber and 50% epoxy resin. Two different concentrates were used. For the nonbrominated formulation, the concentrate was prepared by reacting 50% CTBN rubber with TGDDM. For the brominated formulation, a prereacted concentrate of the brominated diglycidyl type with 50% Br was used. Both concentrates were synthesized by following recommended procedures (2). The chemical structures for the various resins are shown below.

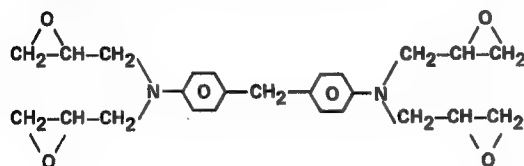
1. TRIS-(HYDROXYPHENYL) METHANE TRIGLYCIDYL ETHER



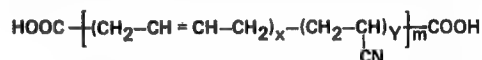
2. DIAMINO DIPHENYL SULFONE (DDS)



3. TETRAGLYCIDYL 4,4'-DIAMINO DIPHENYLMETHANE (TGDDM)



4. CARBOXYL-TERMINATED, LIQUID COPOLYMER OF BUTADIENE AND ACRYLONITRILE (CTBN)



5. BROMINATED POLYMERIC ADDITIVE (BPA)



6. BPA-CTBN PREREACTIONED CONCENTRATE



Materials Used: The graphite cloth used for reinforcement was a product of Hexcel: F3T-584-42, 300, 3K 8 Harness satin weave with an epoxy resin sizing. The resins used include the following: TEN, an experimental resin of Dow Chemical Co. called XD 7342.00L (6) with an epoxide equivalent weight (EEW) of 162; F2001P, a brominated bisphenol epoxy resin from Makhteshim Chemical Works, Israel, with an EEW of 545 and 50% Br; TGDDM, a commercial product of Ciba-Geigy (MY-720); CTBN rubber, a commercial product of B. F. Goodrich, called Hycar 1300x13; and diamino diphenyl sulfone (DDS), an epoxy hardener with a stoichiometric ratio of 80%. The table shows the components of the various resins used.

Modification of Epoxy Resin with CTBN Rubber: The epoxy resin and the CTBN rubber were placed in a resin kettle and heated to 353 K; mixing was effective at that temperature. Triphenylphosphine (0.15%) was added under N₂ atmosphere. The reaction continued for 2 hrs. at temperatures of 403 K to 423 K. The reaction advancement was monitored by 0.1 N KOH/EtOH titration to determine the equivalent per hundred grams (EPHR) of the carboxyl group. The reaction continued to 1% of the initial EPHR.

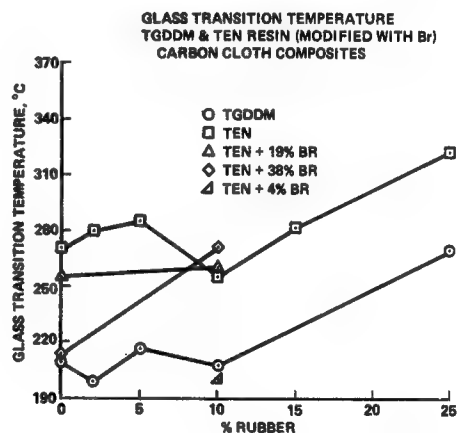
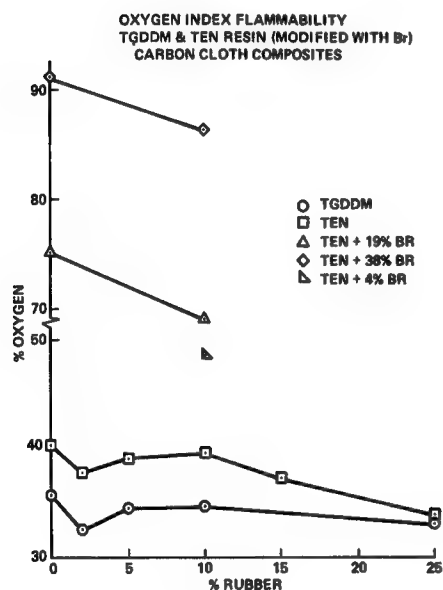
FORMULATIONS OF COMPOSITES

COMPONENT	TGDDM	TGDDM WITH RUBBER	TEN	TEN WITH RUBBER	TEN WITH Br	TEN WITH Br RUBBER
TETRAFUNCTIONAL EPOXY RESIN	X	X				
TRIFUNCTIONAL EPOXY			X	X	X	X
EPOXY-RUBBER* (50/50 PREREACTIONED)		X		X		
F2001P (BPA WITH 50% Br)					X	X
F2001P-CTBN (50/50 PREREACTIONED)						X
DIAMINODIPHENYL SULFONE - DDS	X	X	X	X	X	X
METHYLETHYLKETONE (MEK, ml)	X	X	X	X	X	X

*50/50 PREREACTIONED CTBN WITH TGDDM.

The LOI and the Tg are given below. The LOI for the modified TGDDM and TEN epoxy resins show a decrease (higher flammability) with an increase in rubber content, a result of the more aliphatic character of the rubber. Composites prepared with brominated resin had Higher LOI values than the nonbrominated composites. The LOI of rubber-modified TEN epoxy resin composites containing no bromine was 48.9%, with 19% Br the LOI was 69.3%, and with 38% Br the LOI was 86.6%. The composites with Br but no rubber gave even higher LOI values.

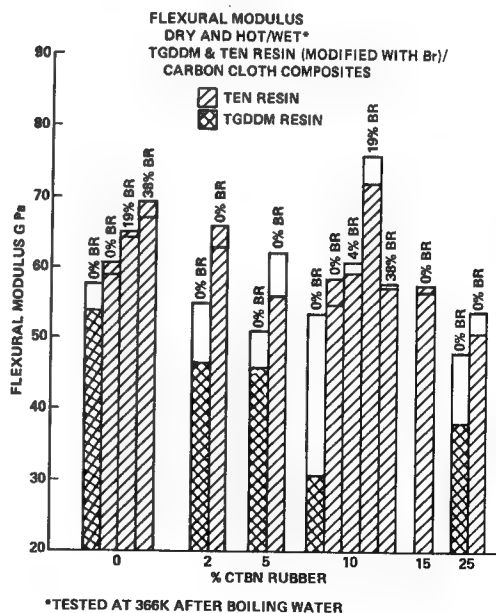
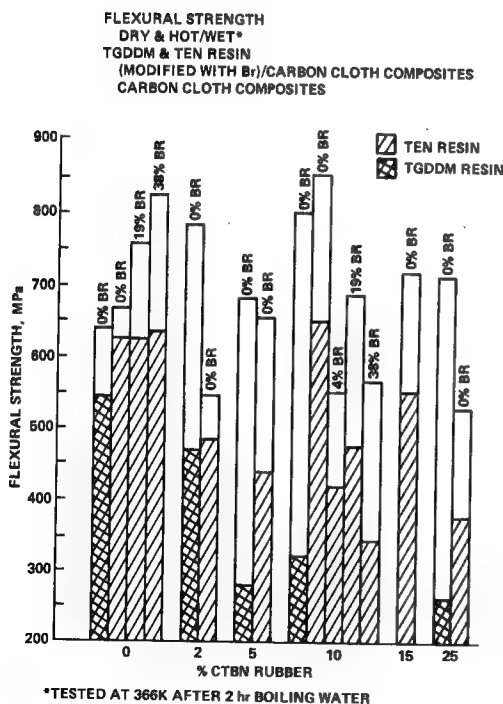
The modification of TGDDM and TEN epoxy resins with rubber and brominated resin does not have a deleterious effect on the Tg of the composites. This has been seen by other investigators (7) when working in the range of 5-10% rubber modification. The explanation of the increase in Tg is beyond the scope of this investigation. Since other investigators (8) have shown the additive effect of modification of epoxy resin, this area should be investigated in the future.



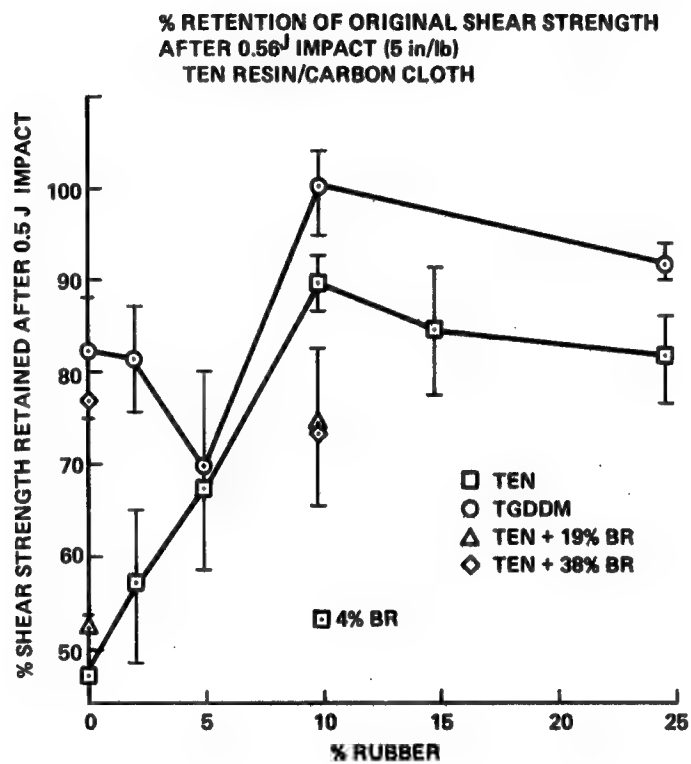
With two exceptions, the room-temperature flexural strengths of composites made with TGDDM and TEN epoxy resins increased with the addition of rubber. The flexural modulus was also closely retained or increased with the addition of rubber. Even with 25% rubber, the TGDDM and TEN epoxy resins retained 85% and 91%, respectively, of their original flexural modulus.

Samples modified with rubber and measured under hot/wet conditions showed more loss in flexural strength than did the TGDDM and TEN epoxy resin controls without rubber. However, the brominated and nonbrominated TEN epoxy resins were consistently higher than the modified TGDDM resin. For example, the TGDD resin with 10% rubber retained 84% and the brominated resin (19% Br) retained 62% of the original flexural strength when tested in hot/wet conditions.

The flexural modulus of the rubber-modified brominated and nonbrominated TEN epoxy resins measured in hot/wet conditions were uniformly higher than the modified TGDDM composites. In fact, they were equal to or better than the TGDDM control resin. For example, the hot/wet modulus of the TGDDM control resin was 54.8 GPa (96% retention) and the hot/wet TEN epoxy resin with 10% rubber was 59.2 GPa (108% retention).

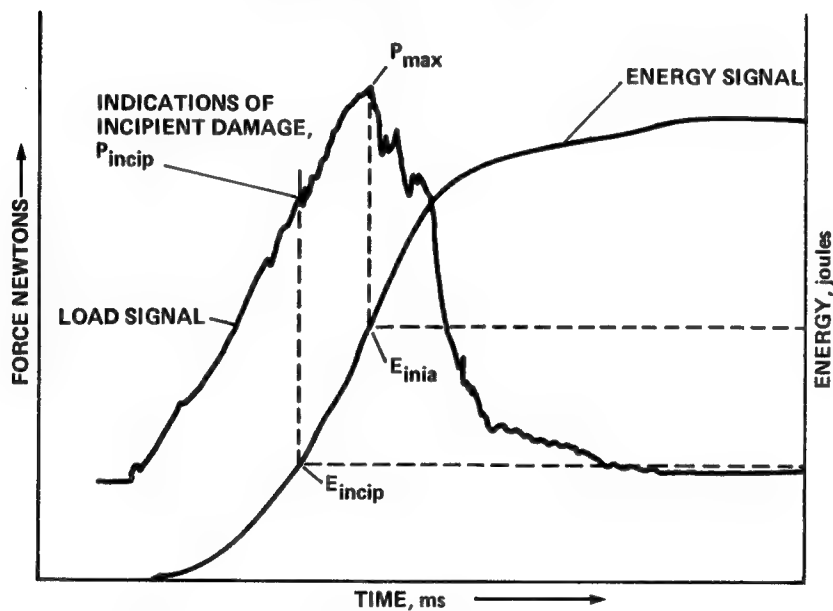


The maximum shear strength retention after impact was obtained on components made with 10 percent rubber modification. This was true for both the TEN and the TGDDM matrix resins as well as the two brominated TEN resins.



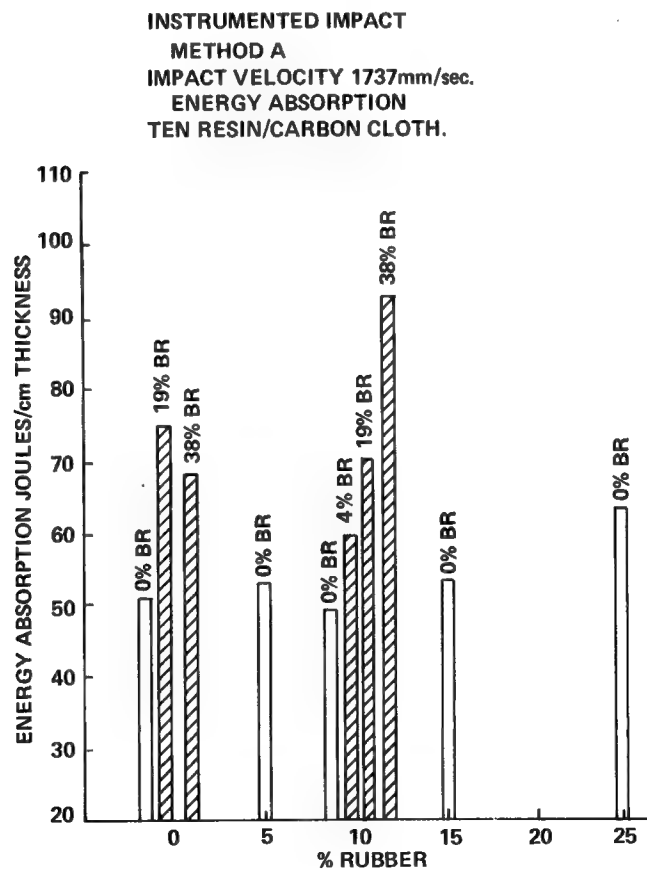
Instrumented Impact Tests: The instrumented impact testing was performed using two methods. The first method (A) used the General Research (formerly, Effects Technology) Dynatup Impact Tester (Model 8200). In this procedure a 16 mm hemispherical head impacts a test specimen at a constant velocity. This instrumented impact technique provides a complete record of the impact event. Automated data analysis provides a record of the applied load and energy absorbed during impact. The second method (B) used a Rheometrics Impact Tester. This method also uses a microprocessor to collect, calculate, and display impact data. In both cases the test specimen is supported by a metal frame. In method A the specimen is mounted horizontally, whereas in method B the specimen is mounted vertically. The use of both methods for testing the impact resistance of composites is well documented in the literature (7, 9, 10).

INSTRUMENTED IMPACT

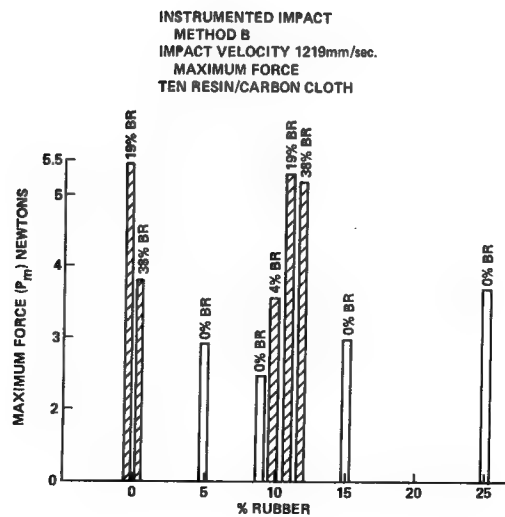
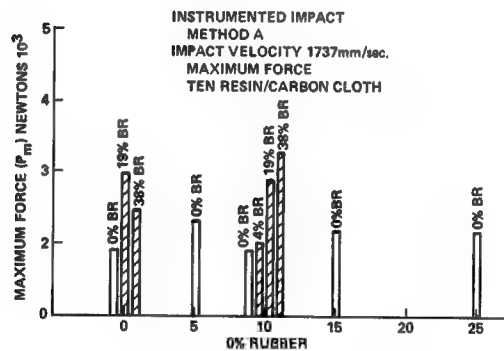
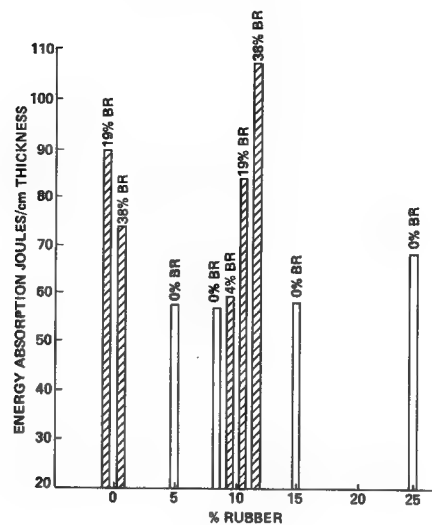


Instrumented Impact: The data for instrumented impact are given below. This test was performed only with composites made with the TEN epoxy resin. No instrumented impact was run on the TGDDM composites because of their low hot/wet flexural test values. The instrumented impact test specimens in all cases were 10.2 cm x 10.2 cm and thickness varied from 23 mm to 28 mm. The impact tests were run at room temperature.

Two values were reported for each test method. First is the maximum force (expressed in newtons) necessary for penetration of the test specimen. This is characterized as the delamination and fiber breaking of the composite specimen. The second value is the total energy absorbed during the impact event (expressed in J/cm thickness). The impact velocity of method A was 147 mm/sec and that of method B was 102 mm/sec. The maximum-force and energy-absorbed test results were higher for method B than for method A. However, the relative rankings of the samples by the two methods were, in general, in close agreement.



INSTRUMENTED IMPACT
METHOD B
IMPACT VELOCITY 1219mm/sec.
ENERGY ABSORPTION
TEN RESIN/CARBON CLOTH



CONCLUSIONS

- MODIFICATION OF TEN RESIN WITH BROMINE GIVES BETTER IMPACT RESISTANCE THAN RUBBER MODIFICATION ALONE.
- 25% RUBBER ADDITION IS NECESSARY TO OBTAIN SIGNIFICANT IMPROVEMENT IN IMPACT RESISTANCE.
- IMPACT RESISTANCE INCREASES WITH BROMINE CONTENT.
- IMPACT VELOCITY DOES NOT SIGNIFICANTLY AFFECT THE ENERGY ABSORBED BY THE TEST SAMPLE.
- T_g DID NOT DECLINE WITH RUBBER MODIFICATION.
- TEN RESIN HAD BETTER HOT/WET PROPERTIES THAN TGDDM RESIN.

REFERENCES

1. D. A. Kourtides, Proceedings of the 21st AIAA Structures, Structural Dynamics and Materials Conference, May 12-14, 1980.
2. H. Drake and R. A. Siebert, SAMPE Quarterly, 6, No. 4 (1975).
3. E. H. Rowe and R. A. Siebert, Advances in Chemistry Series 154, ACS, Washington, DC (1976), pp. 326-346.
4. B. L. Lee, C. M. Lizak, C. K. Riew, and R. J. Moulton, Proceedings of the 12th National SAMPE Technical Conference, Seattle, Washington, Oct. 7-9, 1980.
5. Z. Nir, W. J. Gilwee, D. A. Kourtides, and J. A. Parker, Proceedings of the 41st Annual Technical Meeting (ANTEC) of the SPE, Chicago, Illinois, May 2-5, 1983.
6. K. L. Hawthorne, F. C. Henson, and R. Pinzelli, Organic Coatings and Applied Polymer Science Proceedings, ACS, 46, Las Vegas, Nevada, March 25-April 2, 1982, pp. 493-497.
7. F. Harper-Trevet, Proceedings of the 27th National SAMPE Symposium, San Diego, California, May 4-6, 1982.
8. G. Lee and B. Hartman, Journal of Applied Polymer Science, 28, 823-830 (1983).
9. G. F. Sykes and D. M. Stoakley, Proceedings of the 12th National SAMPE Technical Conference, Seattle, Washington, Oct. 7-9, 1980.
10. A. G. Miller, P. E. Hertzberg, and V. W. Rantala, Proceedings of the 12th National SAMPE Technical Conference, Seattle, Washington, Oct. 7-9, 1980.

MORPHOLOGY AND DYNAMIC MECHANICAL PROPERTIES OF DIGLYCIDYL ETHER OF BISPHENOL-A
TOUGHENED WITH CARBOXYL-TERMINATED BUTADIENE-ACRYLONITRILE

Su-Don Hong, Shirley Y. Chung, Robert F. Fedors,
Jovan Moacanin and Amitava Gupta

Jet Propulsion Laboratory
California Institute of Technology
Pasadena, California

INTRODUCTION

The incorporation of a carboxyl-terminated butadiene acrylonitrile (CTBN) elastomer in diglycidyl ether bisphenol A (DGEBA) resin was reported to produce more than a 10-fold increase in the fracture toughness of the unmodified resin (1-9). The fracture toughness of fiber-reinforced composites containing such modified resins, however, has not always been reported to be increased (10-11). It was thought that these diverse results were at least in part due to the fact that the CTBN-modified DGEBA matrix had differing rubber particle size as well as size distribution which influenced the shape of the crack tip deformation zone (12) and hence the fracture toughness of the material. The particle sizes and size distribution of the rubber inclusions in a CTBN-modified epoxy can be affected by both the curing conditions and the chemistry and composition of the starting resin mixture (3,4,7,8,13,14). The presence of graphite fibers in the composite may further influence the morphology of the CTBN inclusions. Depending on the fiber surface treatment, the surfaces of graphite fibers may have reactive chemical groups (15,16) which will influence the cure kinetics of the resin and, consequently, possible change of the morphology of CTBN inclusions. Measurements of dynamic mechanical properties, scanning electron microscopy and small-angle x-ray scattering were carried out to characterize the state of cure, morphology and particle size and size distribution of the neat resins and their graphite fiber reinforced composites, as summarized in Figure 1.

CHARACTERIZATION OF STATE OF CURE, MORPHOLOGY AND PARTICLE SIZES AND PHASE SEPARATION

- DYNAMIC MECHANICAL PROPERTIES TESTING
 - STATE OF CURE
- SCANNING ELECTRON MICROSCOPY
 - MORPHOLOGY OF FRACTURED SURFACES
 - DOMAIN SIZES FROM SEVERAL HUNDRED ANGSTROMS UP TO MICRONS
- SMALL-ANGLE X-RAY SCATTERING
 - DOMAIN SIZES IN THE RANGE OF 50^oÅ TO 5000^oÅ
 - PHASE SEPARATION

Figure 1

COMPOSITIONS OF TESTING SPECIMEN

Table 1 summarizes the compositions of the unmodified DGEBA base epoxy resin, trade name Hexcel 205 (HX-205), and the CTBN-modified epoxy resin, trade name F-185. Two fiber-reinforced composites, designated GD-31 and GD-48, made from Celion 6000 graphite fiber were also used for the testing. The matrix corresponding to GD-31 is F-185 and that for GD-48 is HX-205. Both composites are 6-ply laminates with unidirectional fiber layup. The resin content in both composites is about 37% by weight. All neat resins were supplied by Hexcel Corporation; composites were made and supplied by NASA Langley Research Center.

TABLE 1. COMPOSITIONS OF HX-205 AND F-185 RESINS

HX-205		F-185	
COMPONENT	APPROXIMATE WEIGHT %	COMPONENT	APPROXIMATE WEIGHT %
EPOXIDES			
(DIGLYCIDYL ETHER OF BISPHENOL A)			
(EPOXIDIZED NOVOLAC, EPOX. EQ. WT 165)	73	HX-205	86.5
DIPHENOLS			
(BISPHENOL-A)			
(TETRABROMOBISPHENOL-A)	20	Hycar 1300 x 9	8.1
CATALYST			
(DICYANDIAMIDE)			
(SUBSTITUTED UREA)	7	Hycar 1472	5.4

CHARACTERIZATION OF THE STATE OF CURE OF NEAT RESINS

The comparison of the $\tan\delta$ versus temperature plots for HX-205 and F-185 are shown in Figure 2. F-185 shows an enhanced $\tan\delta$ at temperatures above -50°C ; at temperatures higher than about 25°C , $\tan\delta$ for F-185 starts to increase drastically even though HX-205 and F-185 appear to have the same glass transition temperature. The glass transition temperatures of CTBN components are; Hycar 1300x9, -49°C and Hycar 1472, -24°C , as reported by the manufacturer (A. Siehert, private communication). F-185 does not show the separate transition peaks corresponding individually to Hycar 1300x9 and Hycar 1472. It appears that the CTBN components in F-185 do not form a pure rubber phase; instead, the rubber phase is blended with the epoxy resin to form CTBN-rich domains.

TAN δ vs. TEMPERATURE FOR HX-205 AND F-185

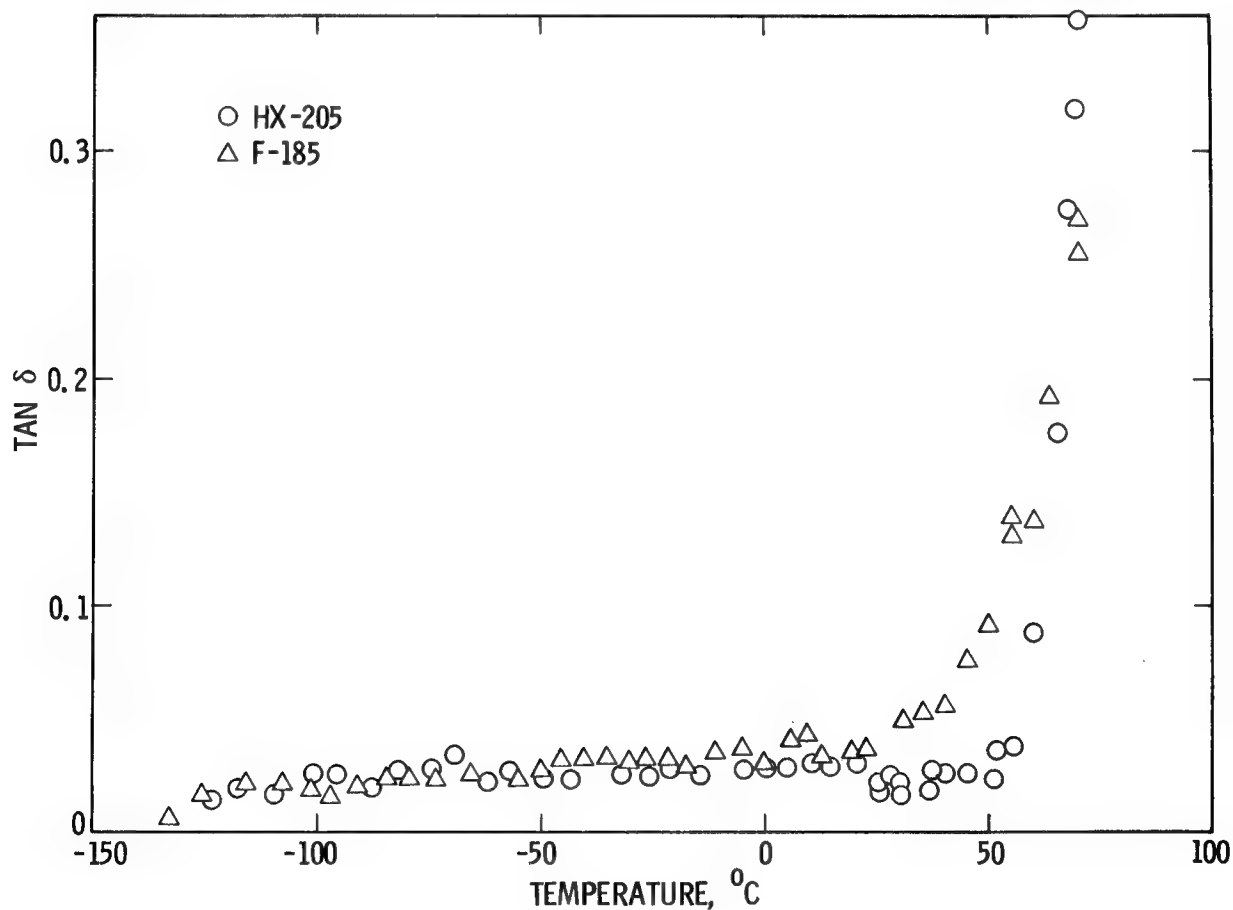


Figure 2

CHARACTERIZATION OF THE STATE OF CURE OF FIBER-REINFORCED COMPOSITES

The plots of $\tan\delta$ as a function of temperature for the composites GD-48 and GD-31, shown in Figure 3, are very similar to the corresponding plots for HX-205 and F-185 neat resins shown in Figure 2. Thus the dynamic mechanical property characterization indicates that HX-205 both as neat resin and matrix material in GD-48 composite and F-185 as neat resin and matrix in GD-31 composite have similar states of cure. For both F-185 neat resin and matrix, extensive mixing of CTBN rubber and epoxy resin occurs.

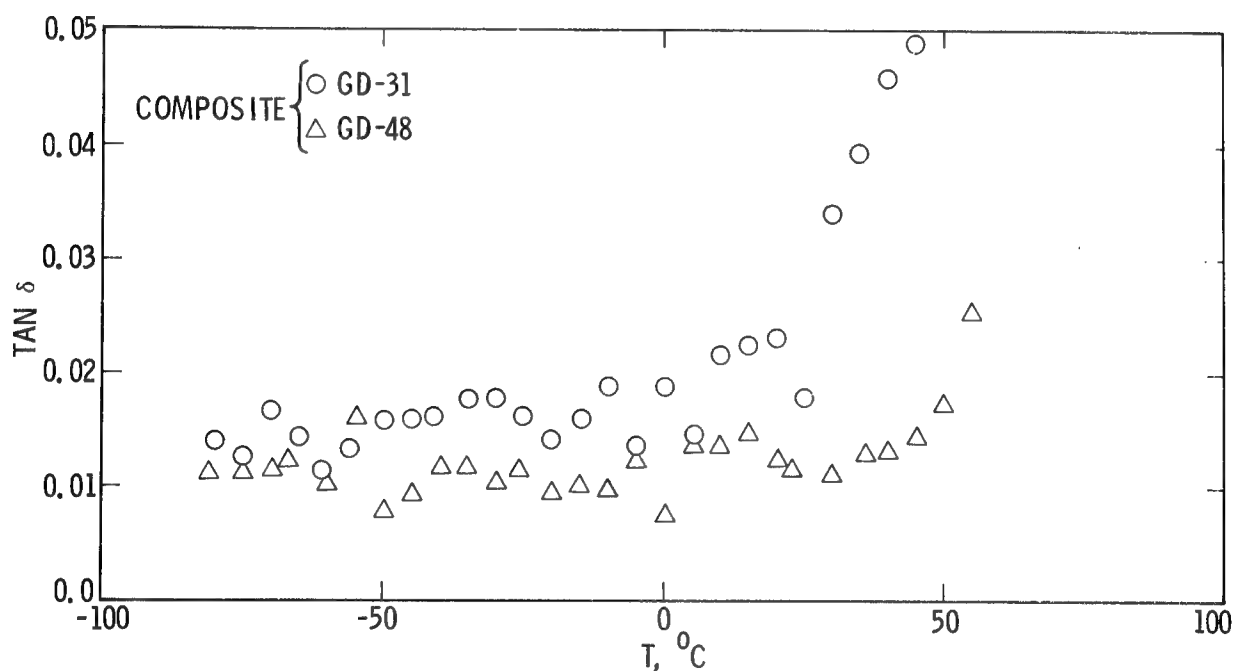
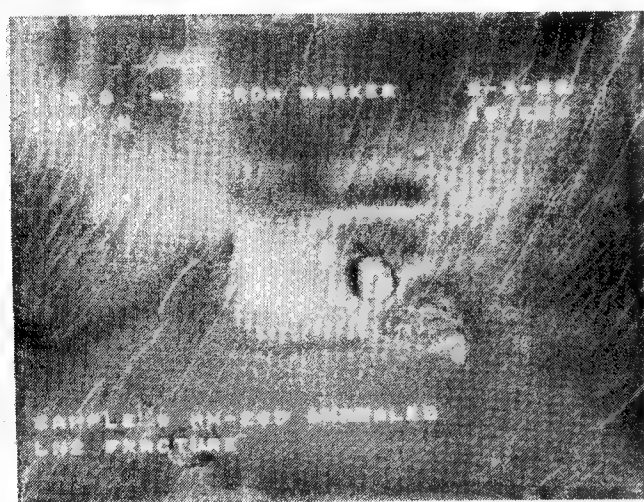


Figure 3

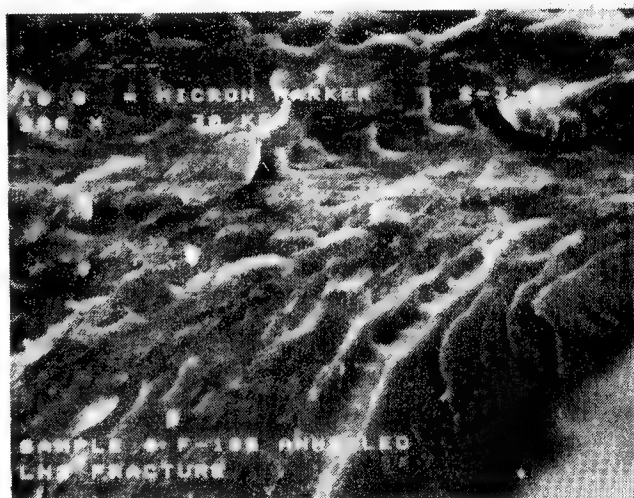
MONPHOLOGY OF FRACTURE SURFACES OF NEAT RESINS

The scanning electron micrographs of fracture surfaces of both HX-205 and F-185 neat resins are shown in Figure 4. The fracture surface of HX-205 is very smooth, indicative of typical brittle fracture behavior. On the other hand, F-185 has a very rough fracture surface, indicating that the resin was highly strained before fracture occurred. There are also craters which appear to represent the separation of spheroidal rubber domains from the matrix.

SEM MICROGRAPHS OF FRACTURE SURFACES OF HX-205 AND F-185 RESINS



HX-205



F-185

Figure 4

MORPHOLOGY OF FRACTURE SURFACES OF FIBER-REINFORCED COMPOSITES

The scanning electron micrographs of GD-31 (F-185 / graphite fiber composite) and GD-48 (HX-205/graphite fiber composite) are shown in Figure 5. The GD-48 laminate gave a relatively clean fracture with no sign of the resin being strained before fracture occurred. On the other hand, the GD-31 laminate exhibited a very rough fracture surface with indications that some regions of the matrix were highly strained before fracture.

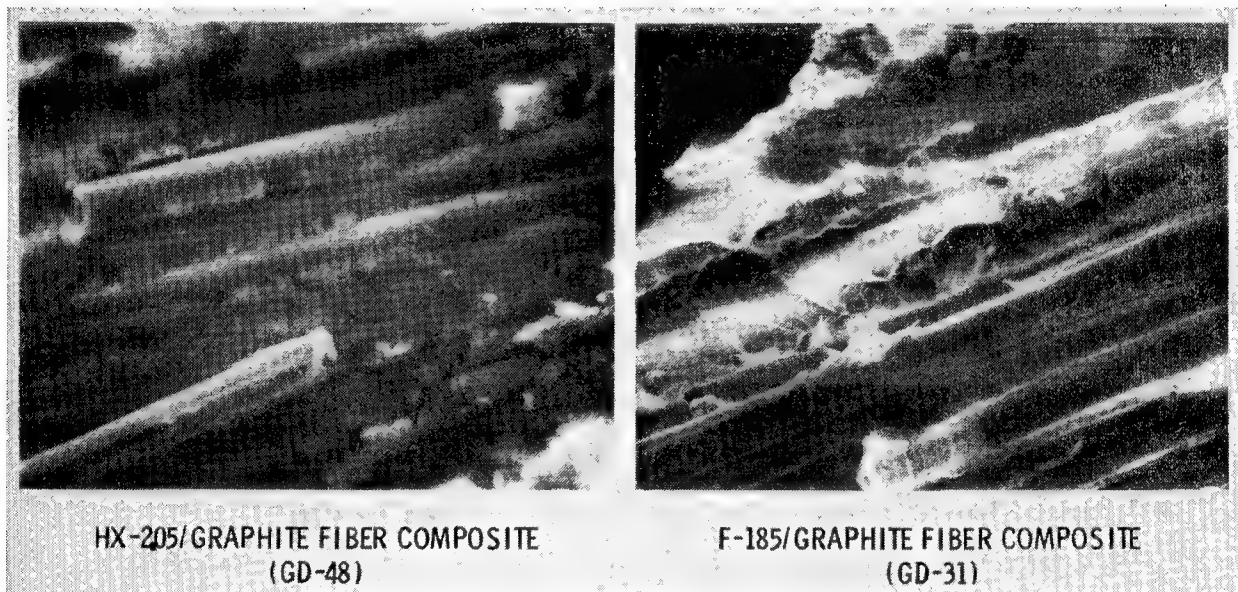


Figure 5

SAXS CHARACTERIZATION OF PARTICLE SIZE AND SIZE DISTRIBUTION

Small angle x-ray scattering was carried out to determine if the morphologies of the CTBN-rich domains in the neat resin and in the composite matrix are similar. Results for both HX-205 and F-185 neat resins as well as their corresponding composites are shown in Figure 6. In the scattering angle range 0.7×10^{-3} to 40×10^{-3} radians, the F-185 neat resin has a higher scattering intensity, by a factor of about 10 in the lower angle region, than does the HX-205 neat resin. This indicates that there are smaller rubber-rich domains having sizes of the order of 100\AA to several thousand angstroms present in the CTBN-toughened neat resin. A comparison of the scattering profiles for both the F-185 neat resin and the GD-31 composite indicates that both have nearly identical scattering intensities at scattering angles lower than 4×10^{-3} radians. The scattering intensity at larger angles for F-185 in the composite is much higher than that for the F-185 neat resin. Analysis of the data⁽¹⁷⁾ indicates that there is a larger fraction of smaller CTBN domains in the F-185 matrix of the composite than in the F-185 neat resin.

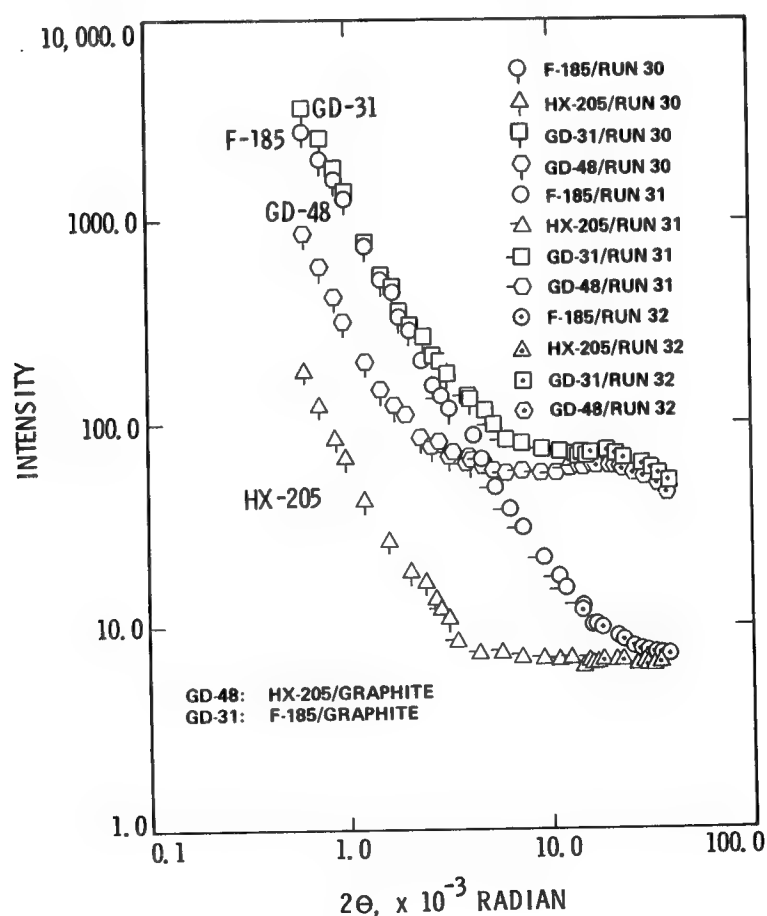


Figure 6

CONCLUSION

The HX-205 and F-185 neat resins and the corresponding composites appear to have the same state of cure as characterized by dynamic mechanical properties. The CTBN-rich domains in F-185 neat resin and F-185 composite resin have sizes ranging from 50 Å or smaller to 40 μm and larger. The F-185 material, both as neat resin and as matrix, shows a ductile fracture behavior, indicating a toughening effect due to incorporation of CTBN rubber. The morphology of the CTBN domains in the F-185 matrix, as determined by small-angle X-ray scattering, appears to be different from that in the neat resin. There is a larger fraction of smaller sizes of CTBN domains existing in the F-185 matrix as compared to the corresponding F-185 neat resin. Because CTBN domains in the size range of the order of several hundred angstroms are less effective in increasing fracture toughness, this fact may partially explain the reported observation that some composites made with the CTBN-modified DGEBA epoxy resins did not show significant improvement in fracture toughness. It is emphasized that the neat resin and the corresponding matrix prepared from the identical resin material may not have similar morphology even when prepared using the same curing procedure.

REFERENCES

1. W. D. Bascom, R. J. Moulton, E. H. Rowe and A. R. Siebert, Org. Coat. Plast., Preprint, 1978, 39, 164.
2. F. J. McGarry, Proc. Roy. Soc. London, 1970, A319, p. 59.
3. E. H. Rowe, A. R. Siebert and R. S. Drake, Mod. Plast., 1970, 417, 110.
4. J. N. Sultan, R. C. Laible and F. J. McGarry, Appl. Polymer Symp., 1971, 16, 127.
5. J. N. Sultan and F. J. McGarry, Polym. Eng. Sci., 1973, 13, 29.
6. W. D. Bascom, R. L. Cottingham, R. L. Jones and P. Peyser, J. Appl. Polymer Sci., 1975, 19, 2545.
7. C. K. Riew, E. H. Rowe, and A. R. Siebert, ACS ADVANCES IN CHEMISTRY, 1976, SERIES No. 154, p. 326.
8. C. B. Bucknall and T. Yoshii, Brit. Polym. J., 1978, 10, 53.
9. W. D. Bascom and D. L. Hunston, Plastic and Rubber Institute, London, Preprints, 1978, 1, p.22.
10. G. B. McKenna, J. F. Mendell and F. J. McGarry, Soc. Plastic Industry, Ann. Tech. Conf 1974, Section 13-C.
11. J. M. Scott and D. C. Phillips, J. Mat. Sci., 1975, 10, 551.
12. W. D. Bascom, J. L. Bitner, R. J. Moulton and A. R. Siebert, Composites, January 1980, 9.
13. A. C. Meeks, Polymer, 1974, 15, 675.
14. T. T. Wang and H. M. Zupko, J. Appl. Polym. Sci., 1981, 26, 2391.
15. F. Hopfgarten, Fiber Sci. Technol., 1978, 11, 67.
16. G. E. Hammer and L. T. Drzal, Applications of Surface Science, 1980, 4, 340.
17. S. D. Hong, S. Y. Chung, G. Neilson and R. F. Fedors, in "Characterization of Highly Cross-linked Polymers." ASC Symposium series 243, page 91-108, Ed. SS. Labana and R. A. Dickie, 1984.

MATRIX RESIN CHARACTERIZATION IN CURED GRAPHITE COMPOSITES
USING DIFFUSE REFLECTANCE-FTIR

Philip R. Young
NASA Langley Research Center
Hampton, VA

and

A. C. Chang
Kentron Technical Center
Hampton, VA

INTRODUCTION

The chemical characterization of cured graphite fiber reinforced polymer matrix composites is complicated by the fact that the resins are insoluble and the composites are opaque. Standard analyses which depend either on the ability to dissolve the sample or to detect transmitted radiation are impossible. As a result, data reported on environmentally exposed composites primarily concerns macroscopic information such as weight loss or changes in selected mechanical properties. The correlation of changes in resin molecular structure with this information could lead to a more fundamental understanding of why composite performance generally deteriorates with environmental aging.

The objective of the present research is to gain a basic chemical understanding of composite and adhesive behavior. Our approach has been to develop diffuse reflectance in combination with Fourier transform infrared spectroscopy to gain access to this information. Several composite and adhesive materials were characterized before and after environmental exposure. In each case significant changes in resin molecular structure were observed and correlated with changes in mechanical properties, providing new insights into material performance.

RESIN CHARACTERIZATION IN CURED GRAPHITE FIBER REINFORCED COMPOSITES USING DIFFUSE REFLECTANCE-FTIR

OBJECTIVE: GAIN A FUNDAMENTAL CHEMICAL UNDERSTANDING OF CURED COMPOSITE MATERIALS AND POLYMERIC ADHESIVES

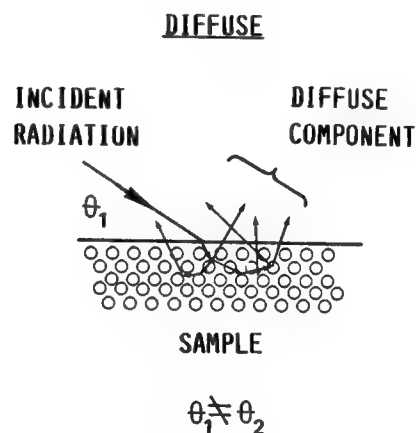
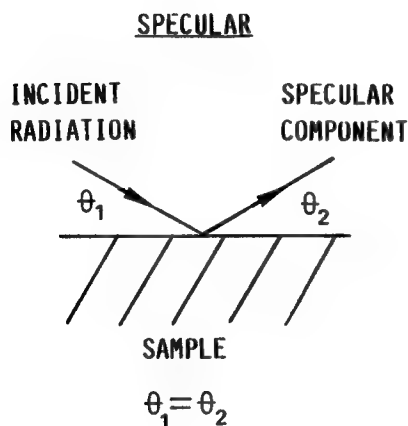
APPROACH: DEVELOP DIFFUSE REFLECTANCE-FTIR AS AN ANALYTICAL TECHNIQUE TO OBTAIN MOLECULAR LEVEL INFORMATION ON CURE AND ENVIRONMENTAL BEHAVIOR

REFLECTANCE TECHNIQUES

Diffuse reflectance infrared spectroscopy using dispersive monochromators has been used for a number of years to obtain optical information about opaque materials (ref. 1). However, the spectra obtained were not generally considered to be high quality, particularly where organic compounds were involved. Recent work (refs. 2 through 4) has shown that the combination of diffuse reflectance with Fourier transform infrared spectroscopy (DR-FTIR) can lead to high-quality spectra of a variety of samples. Our contribution has been to develop and demonstrate the applicability of the technique for high-performance composites and adhesives.

Reflected radiation is composed of specular and diffuse components. Specular reflection is mirror-like in that the angle of incidence is equal to the angle of reflection. Since selected wavelengths are absorbed upon surface reflection, this component contains optical information about the sample. Composites are not good specular reflectors in the infrared. However, they do exhibit a significant diffuse component.

Diffuse reflection arises from radiation penetrating into the interior of a sample and undergoing multiple reflections before reemerging. Selected wavelengths are again absorbed at each reflection. Thus, the diffuse component also contains valuable optical information.



APPLICATIONS:

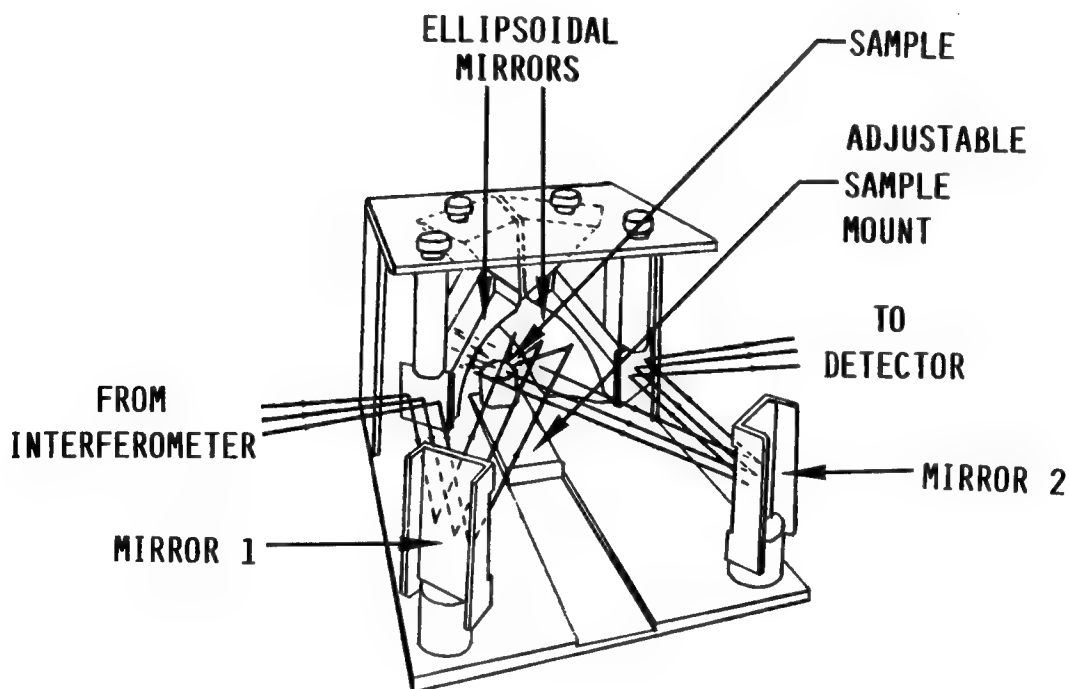
MIRRORS
METALS
CRYSTALLINE MATERIALS

POWDERS
OPAQUE AMORPHOUS MATERIALS
SCATTERING SURFACES

DIFFUSE REFLECTANCE OPTICS

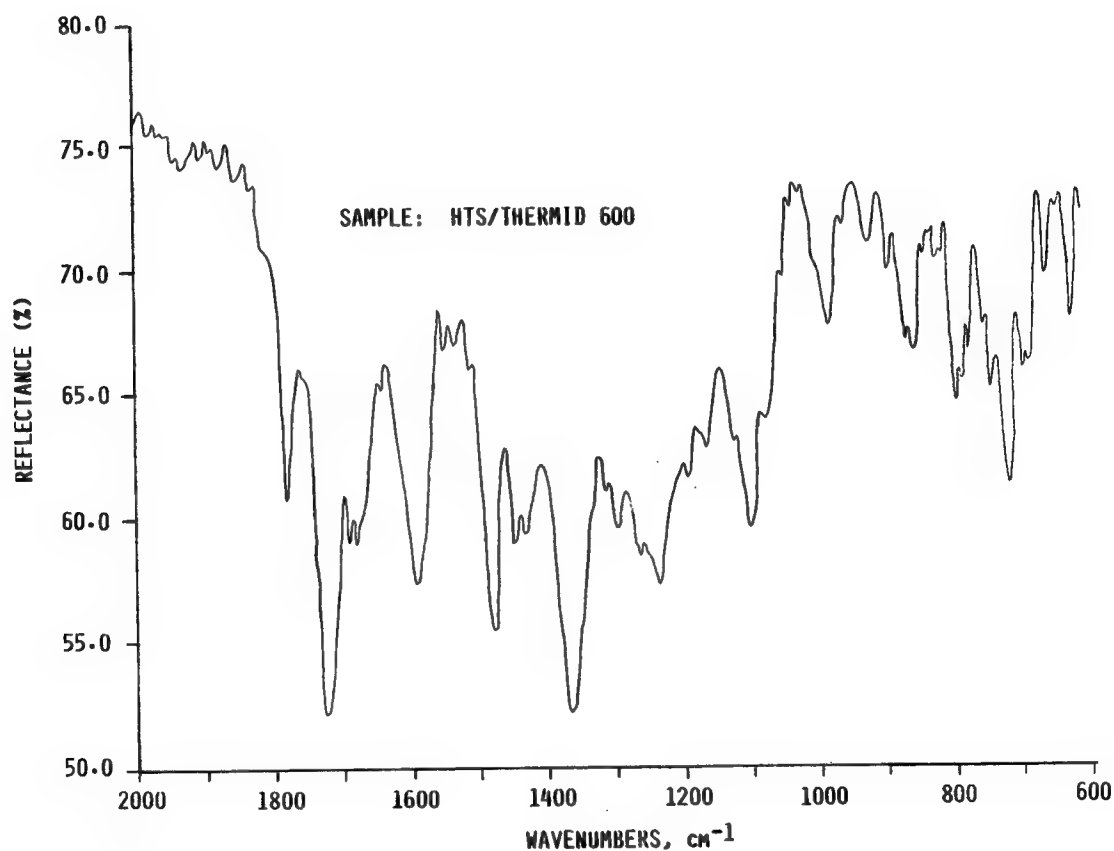
A schematic of the commercially available optics used to make this study is given below. The unit sits inside the sample compartment of the FTIR optical bench. Radiation from the interferometer eventually reflects from an off-axis ellipsoidal mirror onto the sample which is placed in a holder and adjusted to sit at the focal point of the mirror. A second ellipsoidal mirror collimates the diffusely reflected components and passes them to the detector.

Spectra may be obtained by reflecting radiation directly off the surface of a small (0.8 cm x 0.8 cm) piece of composite placed in the sample mount. More definitive spectra are usually obtained by filing into the composite and mixing the resulting powder at 3% by weight with potassium bromide (KBr). These two sampling techniques are discussed later in greater detail.



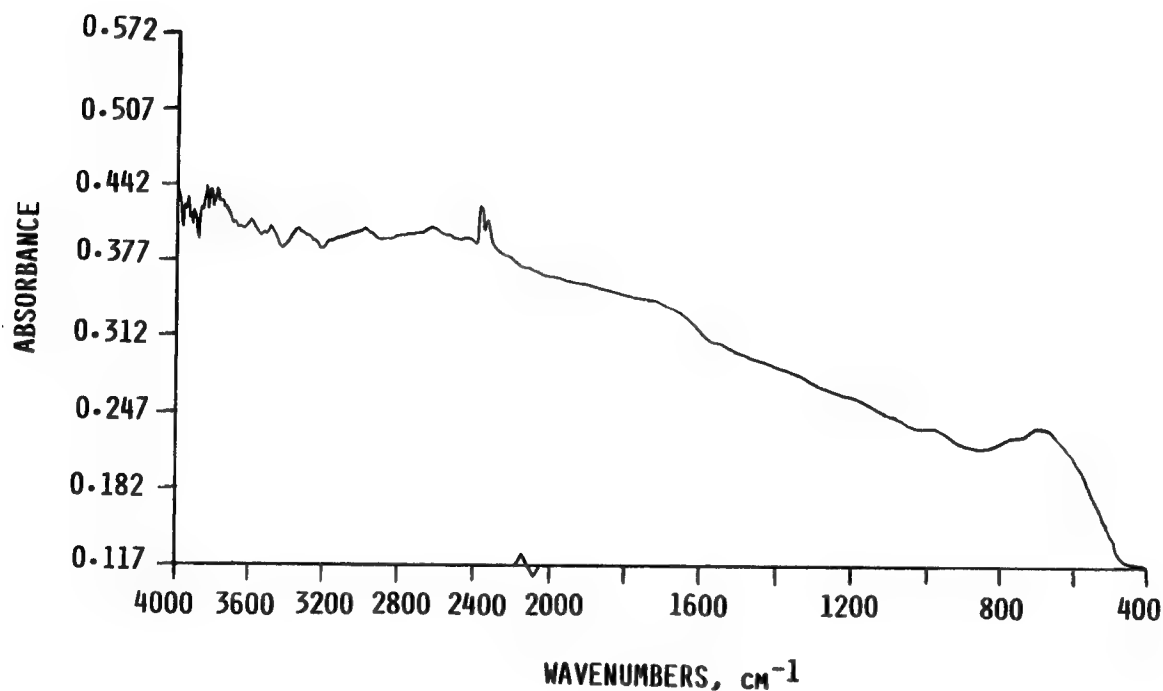
DR-FTIR SPECTRUM OF CURED GRAPHITE COMPOSITE

This figure shows the spectrum of a fully cured graphite/polyimide matrix resin composite and serves as an example of the quality of spectra that can be obtained. This spectrum, of a powdered sample mixed with KBr, is easily interpretable. The ordinate gives the percent reflectance, the ratio of the sample reflectance to that of a powdered KBr reference. This axis is converted to absorbance in spectra presented subsequently. Generally, 10 to 40 percent of the total energy available is retained by DR-FTIR. Thus, there is no need to expand very weak signals to yield an apparent enhanced spectrum. Typically, 512 scans are taken at 1.8 seconds per scan and 4 wavenumber resolution. Vendor-supplied software was quite adequate for mathematical computations and data manipulation.



DR-FTIR SPECTRUM OF CELION 6000 GRAPHITE FIBER

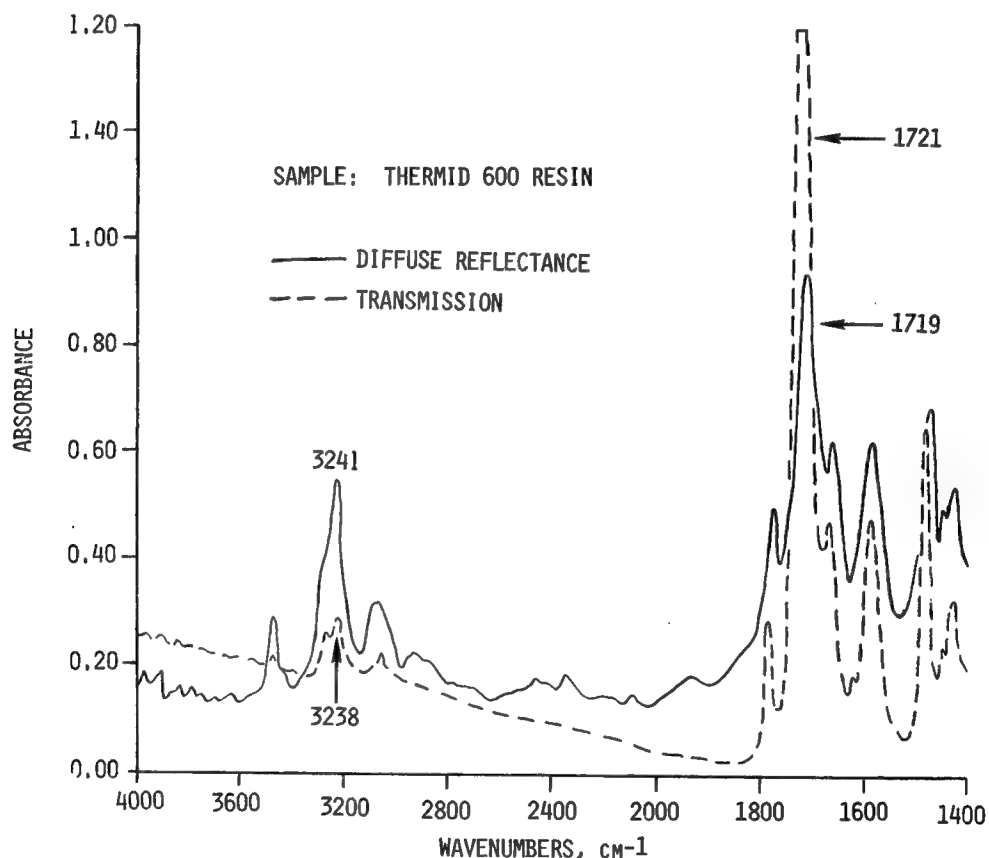
Several experimental aspects of DR-FTIR will be discussed before considering initial applications of the technique. The figure below gives the spectrum of Celion 6000 graphite fiber. A fairly flat baseline was obtained. The minor peak around 2400 wavenumbers (cm^{-1}) is due to carbon dioxide which was not completely purged from the sample compartment. Since no significant peaks are attributable to the graphite fiber, any peaks observed for a composite are assumed to be due only to the matrix resin. Attempts to record a spectrum of the sizing on commercial fibers have been unsuccessful.



COMPARISON OF SPECTRA OBTAINED BY DIFFUSE REFLECTANCE AND KBr TRANSMISSION

Diffuse reflectance can produce artifacts not normally encountered with transmission spectroscopy. The spectra below were determined on an uncured matrix resin with no graphite fiber present. The solid-line DR-FTIR spectrum was generated by mixing the resin at 4% by weight with KBr. The dashed-line spectrum was obtained by standard transmission techniques after pressing the above resin/KBr mix into a pellet. Thus, the figure compares diffuse reflectance with transmission on essentially the same sample.

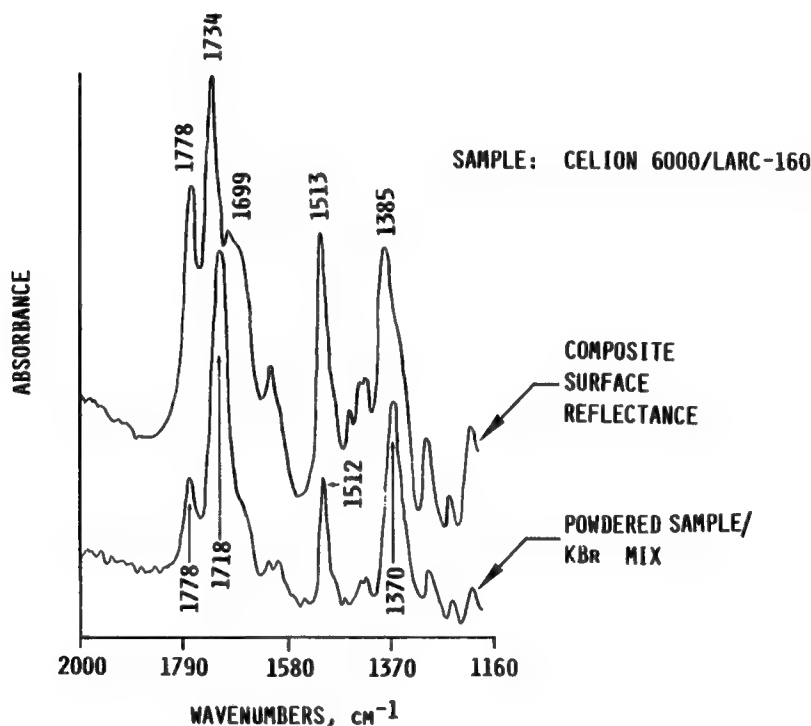
Diffuse reflectance tends to enhance weak bands and suppress strong ones. This enhancement may be an advantage, particularly if the weak bands have significance. In this figure, the band at 3241 cm^{-1} is most likely due to unreacted acetylene groups and could be used to monitor cure. Further analysis of the figure reveals that wavelengths of peaks obtained by reflectance and transmission are not always the same.



COMPARISON OF SPECTRA OBTAINED BY SURFACE REFLECTANCE AND POWDERED SAMPLE TECHNIQUES

Very strong bands may be distorted when spectra are determined using the composite surface rather than by mixing a small amount of powdered composite with KBr. This is illustrated in the figure for a cured polyimide matrix resin composite. The spectra are separated for clarity and absorbance values are not given on the ordinate.

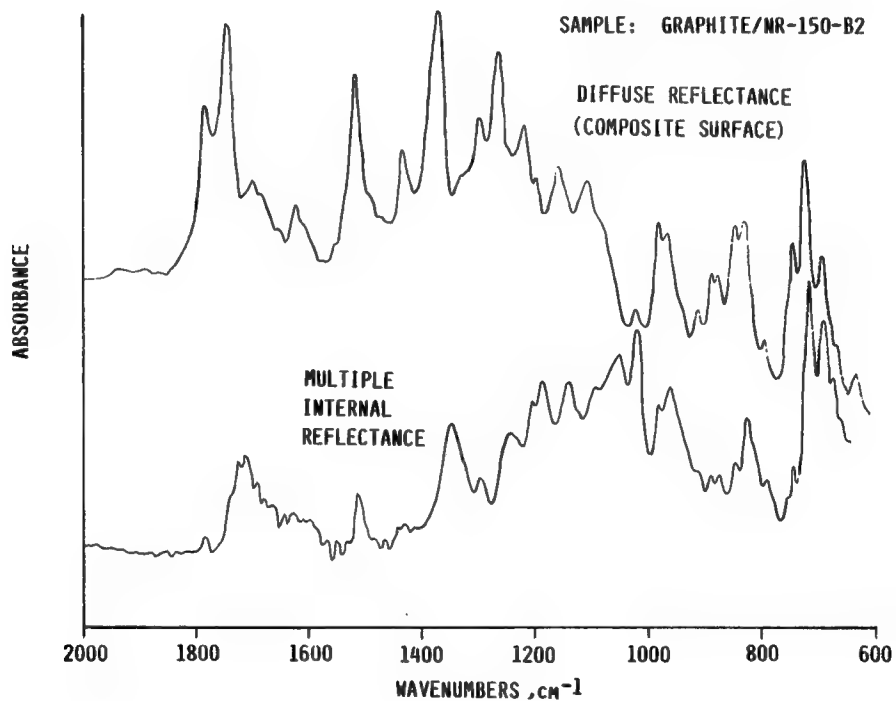
A normal appearing imide carbonyl at 1718 cm^{-1} is obtained by the powdered sample/KBr mix technique. This carbonyl is distorted when the unaltered composite surface is analyzed directly. This artifact initially created confusion and almost led to the erroneous conclusion that the chemistry of the resin on the surface of the composite was different from that beneath the surface. This behavior has since been identified as due to interference by a specular component in regions where distortion occurs (ref. 5).



COMPARISON OF INFRARED SAMPLING TECHNIQUES

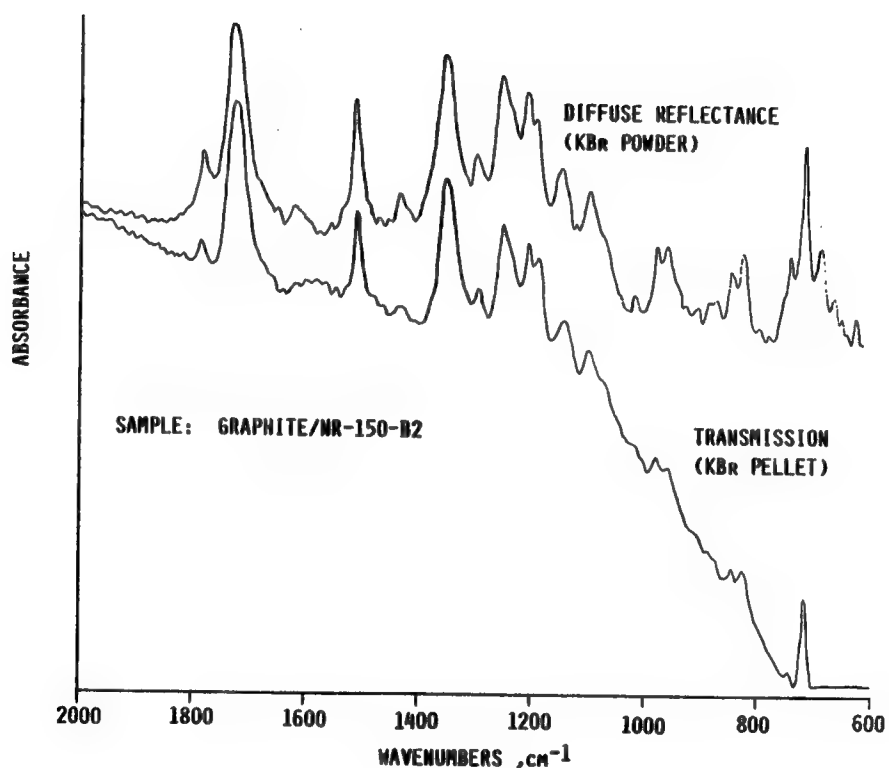
The next two figures compare diffuse reflectance spectra with spectra obtained by more conventional techniques. Diffuse reflectance is compared with multiple internal reflectance or attenuated total reflectance (ATR) in this figure, where spectra for a polyimide matrix resin composite are given. As previously discussed, the imide carbonyl around 1700 cm^{-1} is distorted by DR-FTIR. However, the diffuse spectrum obviously contains more information. This laboratory has not had success obtaining quality spectra of cured composites by ATR.

As a sampling note, the top spectrum was recorded on a $0.8\text{ cm} \times 0.8\text{ cm}$ piece of composite. ATR generally requires a much larger sample. In addition, the sample surface must be smooth to provide good contact and avoid scratching the ATR optical crystal.



COMPARISON OF INFRARED SAMPLING TECHNIQUES (CONTINUED)

Diffuse reflectance and KBr transmission spectra are compared in this figure for the same polyimide matrix resin composite analyzed in the preceding figure. transmission spectrum, the best of several attempts, contained more information than anticipated. If enough FTIR scans are made and the data are optimized, surprisingly good KBr pellet spectra of these materials can be generated. However, the transmission of KBr increases around 1000 cm^{-1} . This results in a baseline inflection, a problem not encountered with diffuse reflectance where the baseline remains relatively flat. The reflectance spectrum is deemed to be superior since it is more informative.



DIFFUSE REFLECTANCE ARTIFACTS

This figure summarizes several experimental aspects of diffuse reflectance spectroscopy. Although supportive spectra are not presented in this report, particle size can also affect the quality of spectra when analyzing by the powdered sample technique. The procedure used in this research of filing into the composite with a jeweler's file provided an approximately constant 100 μm particle size.

- ENHANCEMENT OF WEAK BANDS
- SUPPRESSION OF STRONG BANDS
- λ BY % R MAY DIFFER FROM λ BY % T
- PARTICLE SIZE MAY AFFECT SPECTRUM QUALITY
(POWDERED SAMPLE TECHNIQUE)
- POSSIBLE DISTORTION OF STRONG BANDS
(SPECIMEN REFLECTANCE)

INITIAL APPLICATIONS OF DR-FTIR

Several different materials have been examined by DR-FTIR to demonstrate the usefulness of the technique for the analysis of high-performance composites and adhesives. These materials are summarized below. Whenever possible, samples were failed mechanical test specimens which other researchers had exposed to various environments, tested, and then reported. Details of these earlier studies are found in references 6-9.

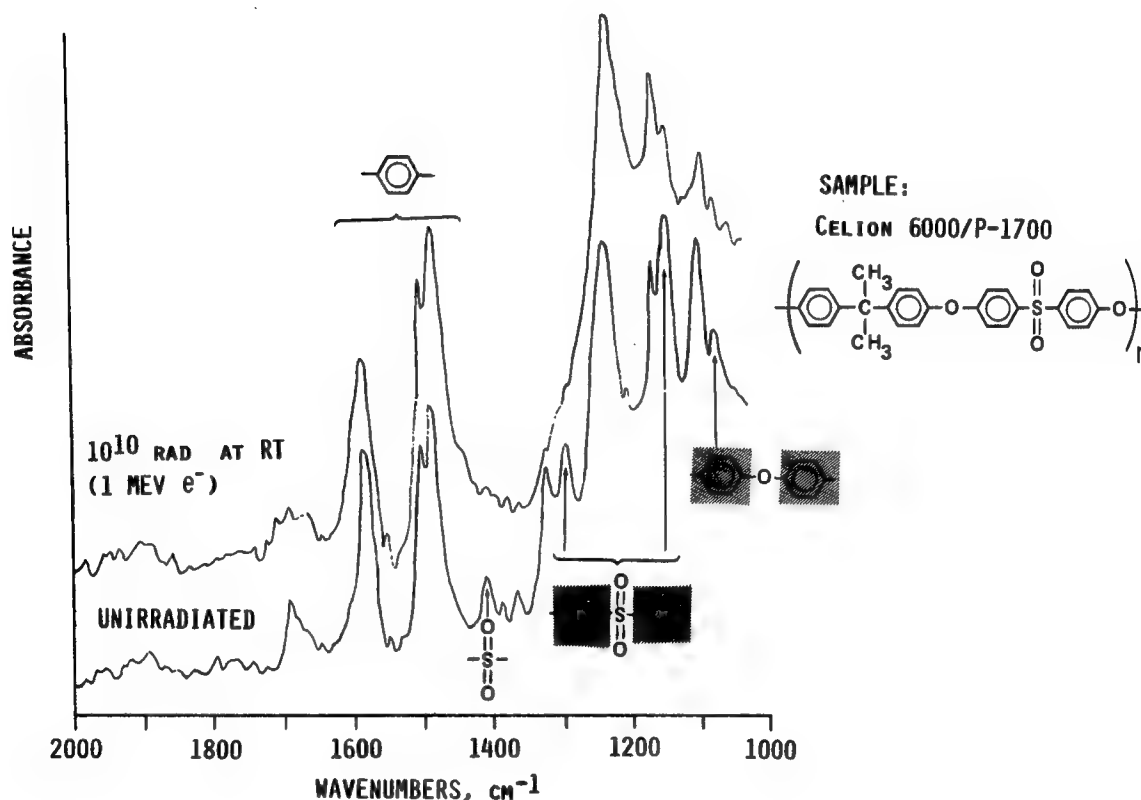
Note that the reported property changes are macroscopic in nature, such as a change in tensile strength or a weight loss. The ultimate goal of the present research is to provide a molecular level understanding of these changes. This level of information has not been available in the past due to the intractable nature of the materials undergoing analysis.

MATERIAL	ENVIRONMENTAL EFFECT	SIGNIFICANT PROPERTY CHANGE
GR/POLYSULFONE: CELION 6000/P-1700	ELECTRON RADIATION 10 ¹⁰ RAD	25° INCREASE IN T _G 24% DECREASE IN OXYGEN 1- CONTENT
GR/EPOXY: AS/3501-5	THERMAL AGING 250°F/50,000 HRS	NO DECREASE IN TENSILE STRENGTH
GR/POLYIMIDE: A. HTS/SKYBOND 710	THERMAL AGING 450°F/25,000 HRS 550°F/25,000 HRS	NO CHANGE IN TENSILE STRENGTH AT 450°F; 80% DECREASE AT 550°F
B. CELION 6000/LARC-160	THERMAL AGING 450°F/15,000 HRS	13° INCREASE IN T _G 8% WEIGHT LOSS
ADHESIVE: EXPTL. POLYIMIDE- SULFONE	CURE	IMIDIZATION LOSS OF VOLATILES

1. THIN-FILM DATA

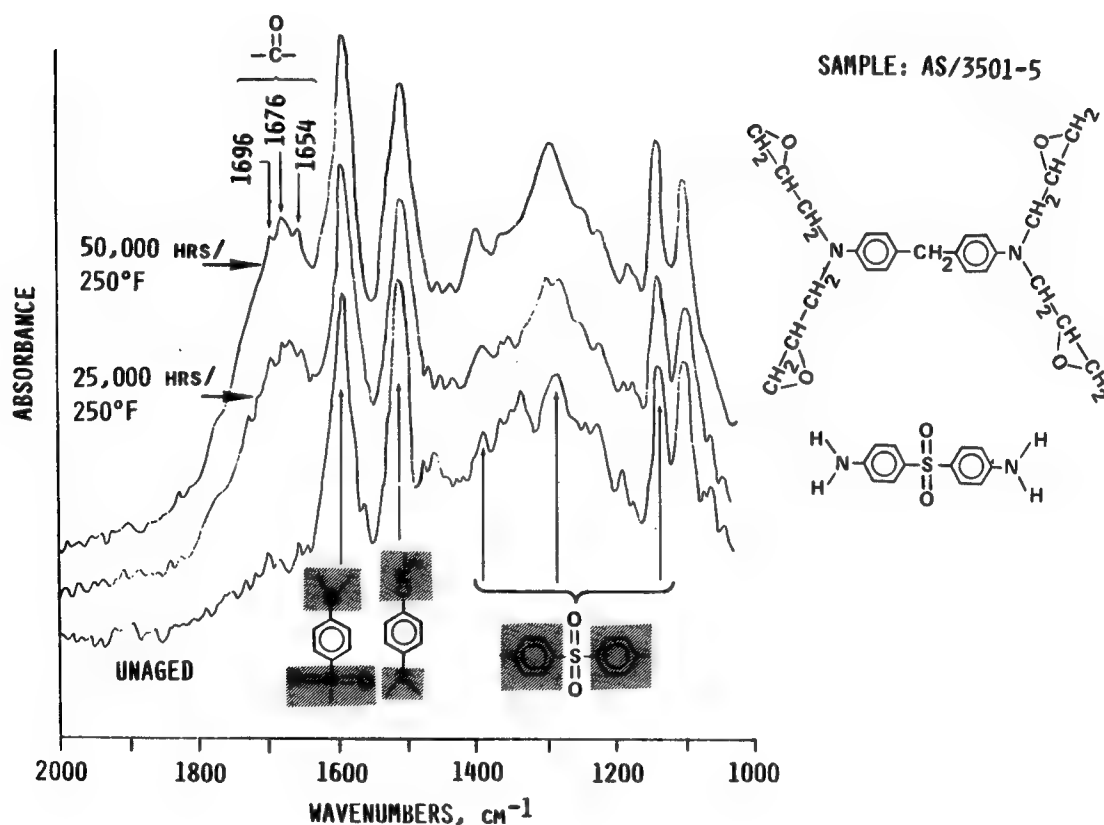
DR-FTIR SPECTRA OF GRAPHITE/POLYSULFONE COMPOSITE BEFORE AND AFTER RADIATION EXPOSURE

This figure shows a portion of the spectrum of a graphite/polysulfone composite before and after receiving 10^{10} rad of electron radiation. The polymer repeat unit is included in the figure. Degradation is apparent; bands associated with the $-\text{SiO}_2$ -group (1409 , 1294 , and 1150 cm^{-1}) have disappeared or decreased in intensity as the result of exposure. As noted in the preceding figure, a loss of oxygen was reported for polysulfone films irradiated under the same conditions (ref. 6). Apparently, additional cross-linking also occurred to increase the T_g of this material. The aromatic rings do not appear to be affected by radiation since no decrease in intensity or change in band shape is observed in the spectrum for those groups.



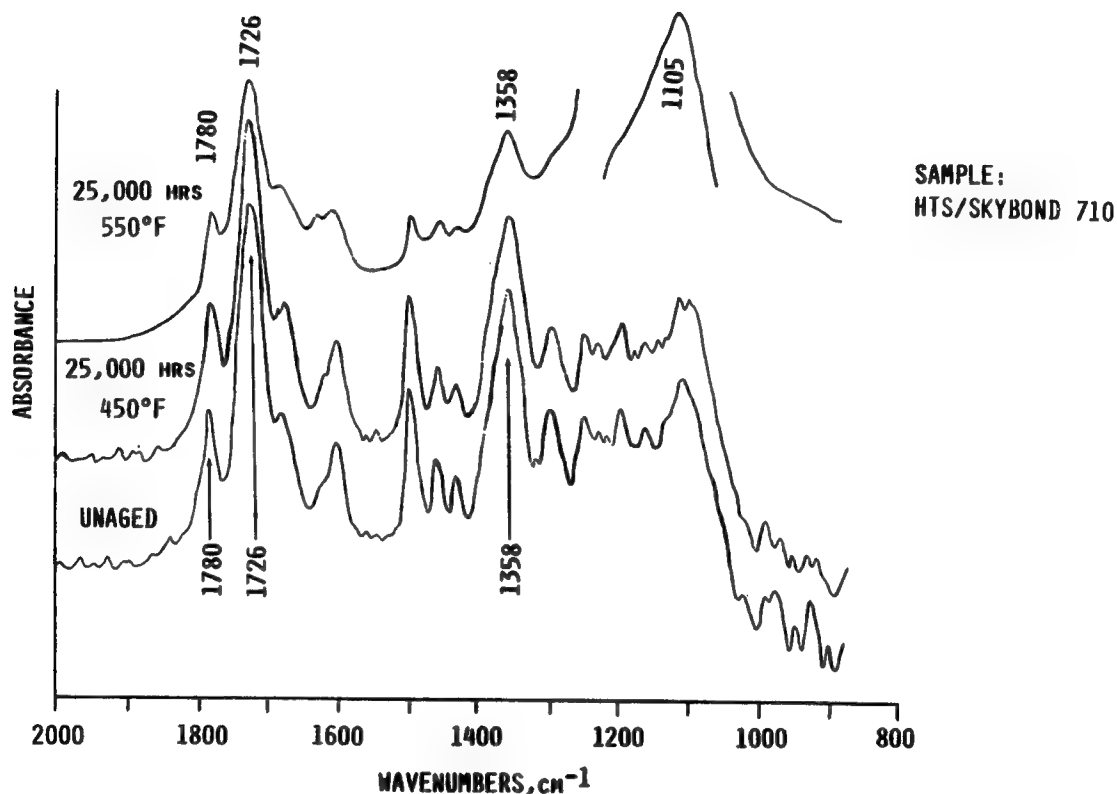
DR-FTIR SPECTRA OF GRAPHITE/EPOXY COMPOSITE BEFORE AND AFTER THERMAL AGING

Spectra of graphite/epoxy composites thermally aged at 250°F are given below along with monomer unit structures. Phenyl bands (1594 and 1512 cm^{-1}) and sulfone bands (1389, 1287, and 1143 cm^{-1}) have not changed significantly, indicating that these portions of the polymer backbone are not adversely affected by extended exposure at 250°F. However, new bands did develop between 1700 and 1650 cm^{-1} . This is apparently due to >C=O which resulted from the oxidation of $\text{-CH}_2\text{-}$ or residual -OH groups in the epoxy resin. This oxidation was not reflected in longitudinal tensile strength measurements (refs. 7, 8) for these specimens. Spectra of composites aged at 350°F showed extensive oxidation to >C=O above 1700 cm^{-1} . A decrease in tensile strength reported for specimens aged at this temperature may reflect a loss of resin in the aliphatic portions of the matrix resin.



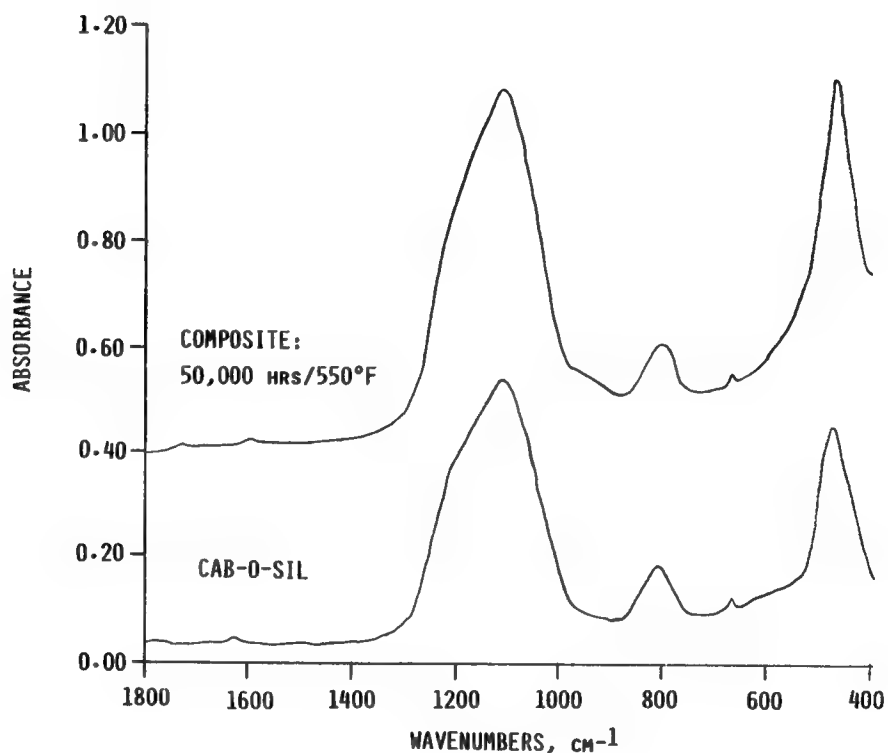
DR-FTIR SPECTRA OF GRAPHITE/POLYIMIDE COMPOSITE
BEFORE AND AFTER THERMAL AGING

This figure gives spectra of a thermally aged linear polyimide matrix resin composite. No shift in frequency or change in band intensity is noted after 25,000 hours at 450°F. No change in tensile strength was reported for this exposure (refs. 7, 8). However, band intensity had decreased markedly after 25,000 hours at 550°F, suggesting resin loss. A very intense band centered at 1105 cm^{-1} is apparent after 25,000 hours at the higher temperature. This was initially thought to be due to the formation of carbon-oxygen ether linkages. However, further study proved this to be due to silicon-oxygen vibrations.



SPECTRA OF THERMALLY AGED SKYBOND 710 COMPOSITE AND CAB-O-SIL

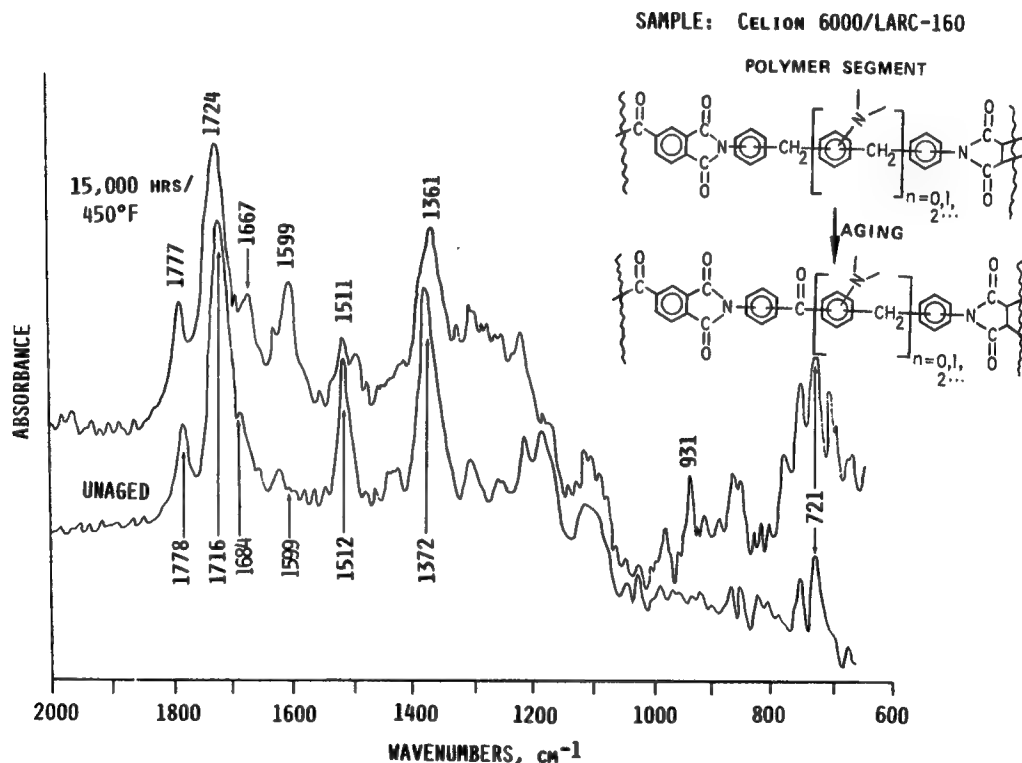
The spectrum of the residue remaining after 50,000 hours at 550°F is given below. The spectrum of CAB-O-SIL is included in the figure, leaving little doubt as to the identity of the residue observed in the thermally aged composite. Apparently, a vendor added CAB-O-SIL to the resin to adjust the viscosity during the prepregging operation. This event did not become apparent until after the material had been processed into composites and then aged for a considerable period of time.



DR-FTIR SPECTRA OF GRAPHITE/ADDITION POLYIMIDE COMPOSITE BEFORE AND AFTER THERMAL AGING

An addition polyimide matrix resin composite showed significant changes as the result of thermal aging. New bands at 1667 and 931 cm^{-1} are apparent in the 15,000 hr/450°F spectrum. This is due to $-\text{CH}_2-$ groups having been oxidized to $>\text{C}=\text{O}$ groups. When this occurred, phenyl bands at 1599 and 1512 cm^{-1} switched in intensity due to conjugation with the new carbonyl group.

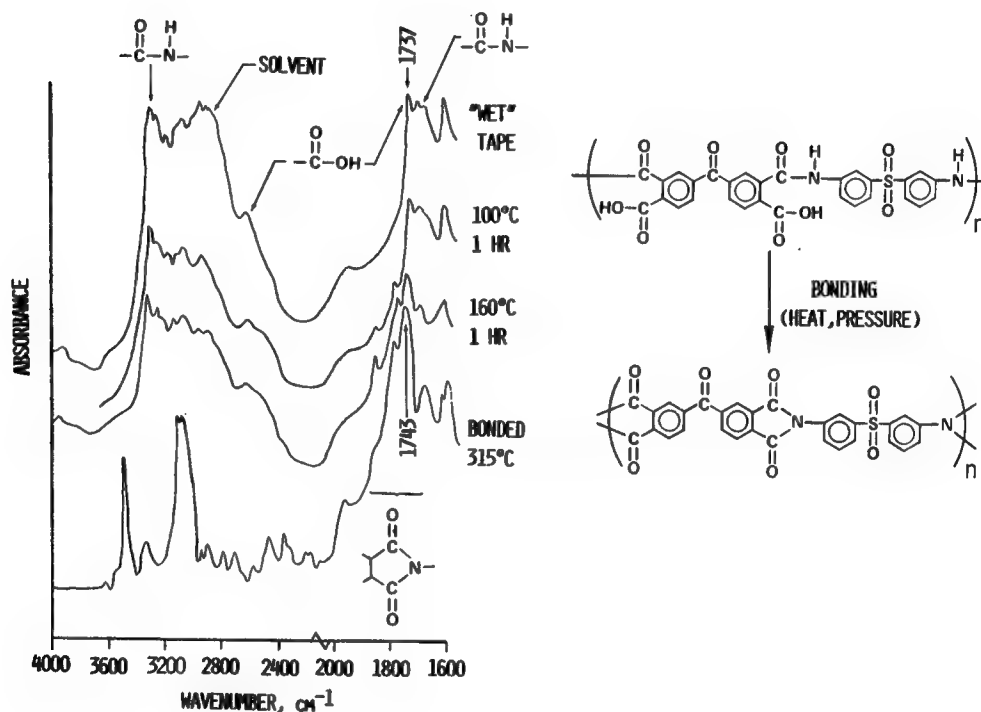
Shifts in the position of two bands associated with imide vibrations are also noted. Bands at 1716 and 1372 cm^{-1} for the unaged composite shifted to 1724 and 1361 cm^{-1} , respectively, after aging. These bands did not move for the linear polyimide matrix resin composite after aging for 25,000 hours at 550°F. A detailed DR-FTIR study involving both model compounds and sets of isothermally aged composites (ref. 9) strongly suggested that this movement was indicative of additional cure and/or crosslinking which constrained the vibration of the imide rings.



DR-FTIR SPECTRA OF POLYIMIDE-SULFONE ADHESIVE DURING CURE

DR-FTIR appears promising as a technique for studying the cure of adhesive systems. The figure shows spectra at various stages during the cure of an experimental polyimide-sulfone adhesive being developed at NASA Langley Research Center. The spectra were obtained on a piece of glass tape coated with the adhesive.

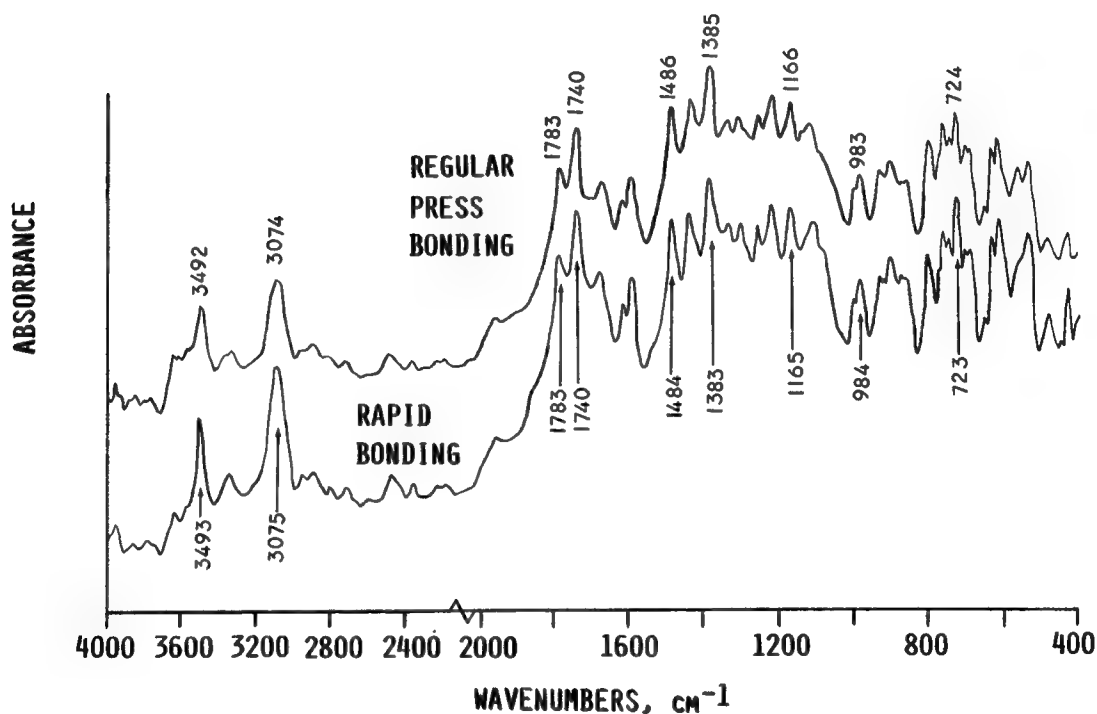
Bands due to amide and acid portions of the adhesive are apparent in the spectrum of the wet tape. Aliphatic solvent is also present. Progressive staging at 100°C and 160°C removed some solvent and slightly imidized the resin. Bonding appears to completely imidize the material. Bands associated with the pre-polymer are now gone and a strong imide carbonyl dominates the spectrum. Aromatic protons, previously hidden, are now apparent by the absorption slightly above 3000 cm^{-1} . A weak imide overtone appears around 3500 cm^{-1} .



COMPARISON OF REGULAR PRESS AND RAPID BONDING OF POLYIMIDE-SULFONE ADHESIVE ON TITANIUM

NASA Langley is developing a rapid method for bonding joints. With this method, the specimen is taken through a two-minute cure cycle as opposed to the standard cycle of placing the specimen in a press, bringing the press to temperature, and applying pressure. The latter procedure can take up to two hours. The question was raised as to whether the resin chemistry was the same for the two cure cycles.

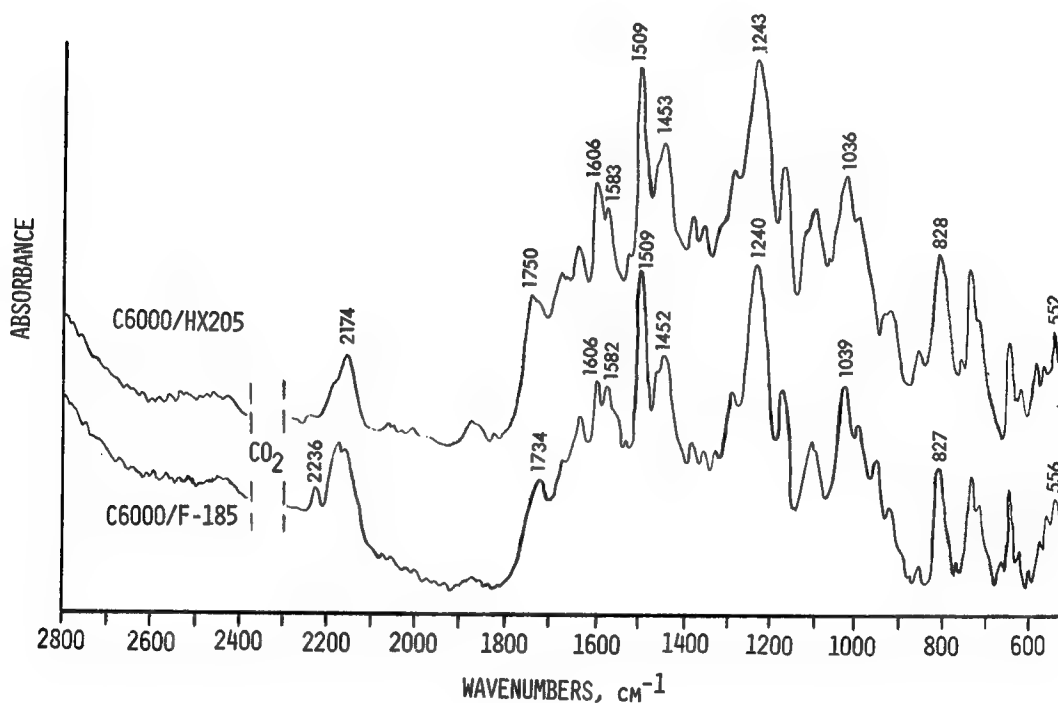
The figure shows spectra of failed titanium lap shear specimens bonded by the two methods. The polyimide-sulfone adhesive shown in the preceding figure was used for bonding. Small portions (0.8 cm x 0.8 cm) of the titanium adherend containing the adhesive were analyzed directly. The two spectra are virtually superimposable, leading to the conclusion that the resin chemistry has not been altered by the rapid bonding procedure.



DR-FTIR SPECTRA OF TOUGHENED EPOXY COMPOSITE

DR-FTIR was also demonstrated to provide information on toughened materials. The top spectrum (C6000/HX205) was determined on a standard graphite/epoxy resin composite. The bottom spectrum (C6000/F185) is for the same epoxy resin modified by the addition of about 8% of a liquid carboxy-terminated butadiene-acrylonitrile (CTBN) and 5.4% of a solid CTBN.

The spectra are interpretable; phenyl bands (~ 1600 , 1580 , 1500 , and 1450 cm^{-1}) and an ether band (~ 1240 cm^{-1}) are readily apparent. Both resins were cured with dicyanodiamide (DICY). Absorption around 2175 cm^{-1} is due to $\text{C}\equiv\text{N}$ in the curing agent. The small band at 2236 cm^{-1} for the toughened composition is apparently due to nitrile in the CTBN. The carboxy-terminated portion of the toughener can be observed using FTIR subtractive techniques.



SUMMARY

The combination of diffuse reflectance with Fourier transform infrared spectroscopy has been demonstrated as an effective technique for gaining molecular level information on advanced materials. Several different graphite fiber reinforced polymeric matrix resin composites exposed to various environmental conditions were examined. In each case, significant changes in resin molecular structure were observed. These changes provided insights into previously reported changes in composite weight or mechanical properties. The technique was also shown to be applicable to adhesives and toughened systems. DR-FTIR is anticipated to play an increasingly important role in the characterization of advanced composites and adhesives, pointing towards new directions for the analysis of environmentally stable and processable polymers for efficient aerospace structures.

DIFFUSE REFLECTANCE-FTIR SPECTROSCOPY PROVIDES

- ACCESS TO PREVIOUSLY INACCESSIBLE MOLECULAR INFORMATION
- PRECISION AND REPEATABILITY
- FUNDAMENTAL INSIGHTS INTO COMPOSITE BEHAVIOR
- CONCEPTS FOR IMPROVED RESIN SYSTEMS

REFERENCES

1. Wendlandt, W. W., editor: Modern Aspects of Reflectance Spectroscopy, Plenum Press, New York (1968).
2. Fuller, M. P. and Griffins, P. R.: Anal. Chem., 50, 1906 (1978).
3. Fuller, M. P. and Griffins, P. R.: Appl. Spectrosc., 34, 533 (1980).
4. Maulhardt, H. and Kunath, D.: Appl. Spectrosc., 34, 383 (1980).
5. Smyrl, N. R., Fuller, E. L., and Powell, G. L.: Appl. Spectrosc., 37, 38 (1983).
6. Santos, B. and Sykes, G. F.: Radiation Effects on Four Polysulfone Films, SAMPE Preprints, 13, 256 (1981).
7. Kerr, J. R. and Haskins, J. F.: Time-Temperature Stress Capabilities of Composite Materials for Advanced Supersonic Technology Applications. NASA CR-159267, April 1980.
8. Kerr, J. R. and Haskins, J. F.: Effects of 50,000 Hours of Thermal Aging on Graphite/Epoxy and Graphite/Polyimide Composites. Paper presented at the AIAA/ASME/ASCE/AHS 23rd Structures, Structural Dynamics, and Materials Conference, New Orleans, LA, May 1982.
9. Nelson, J. B.: Thermal Aging of Graphite/Polyimide Composites. Long-Term Behavior of Composites, ASTM STP 813, O'Brien, T. K., Ed., American Society for Testing and Materials, Philadelphia, 206 (1983).

SOLVENT RESISTANT THERMOPLASTIC COMPOSITE MATRICES

P. M. Hergenrother and B. J. Jensen
NASA Langley Research Center
Hampton, VA

S. J. Havens
Kentron International, Inc.
Hampton, VA

INTRODUCTION

More extensive use of resin matrix/fiber reinforced composites in commercial aircraft has been identified as a viable means of reducing the weight and thereby increasing the fuel efficiency and payload. Although major improvements in composite properties (e.g. better damage tolerance and moisture resistance) have been made by improving the resin matrix (e.g. rubber and thermoplastic toughened epoxies, epoxy/bismaleimide and cyanate/bismaleimide blends), these new systems still exhibit shortcomings such as limited prepreg shelflife, unforgiving and long cure cycles, and cocuring problems. Another approach to better resin matrices involves the modification of thermoplastics. Commercial thermoplastics such as UDEL® polysulfone and Victrex® polyethersulfone are excellent engineering materials with good toughness and thermoformability but poor solvent resistance. The latter feature is an important requirement in composite structures on commercial airplanes which demand ~50,000 hours of service at temperatures from -54°C to 93°C in an environment which includes exposure to moisture and aircraft fluids (e.g. hydraulic fluid and paint strippers) while under load. The problem, objective and technical approach of this research are summarized in Figure 1.

Problem

Thermoplastics (e.g. polysulfones) as structural resins (e.g. adhesives and composite matrices) are sensitive to aircraft fluids (e.g. hydraulic fluid and paint stripper) and, upon exposure, undergo a loss of mechanical properties, especially in a stressed condition.

Objective

The objective is to develop new concepts and technology that improve the solvent resistance of thermoplastics without severely compromising the attractive features such as toughness and thermoformability.

Approach

The approach is to modify thermoplastics with ethynyl (acetylenic) groups which undergo thermally induced addition reactions (no volatiles) to improve the solvent resistance.

Figure 1

MODIFIED POLYSULFONES WITH IMPROVED SOLVENT RESISTANCE

Previous attempts to modify polysulfones to primarily improve the solvent resistance are listed in Figure 2. In the mid-1970's, Union Carbide Corporation introduced RADEL®, a sulfone polymer containing biphenyl moieties, which exhibited better solvent resistance than UDEL®. However, RADEL® was more difficult to process than UDEL® and still did not have the solvent resistance required for composite application on commercial aircraft. An experimental material from Union Carbide Corporation, PKXA (sulfone polymer end-capped with trimethoxysilyl groups which underwent hydrolysis and subsequent reaction to yield siloxane moieties), also failed to exhibit the required solvent resistance. Work at AFWAL involved the blending of a reactive plasticizer, bis[4-(3-ethynylphenoxy)phenyl]-sulfone, with UDEL® which, upon curing, exhibited improved solvent resistance (1). Sulfone block copolymers containing crystalline regions were reported to exhibit improved solvent resistance (2). Cured nadimide-terminated polysulfone, designated NTS-20, was initially reported to have good resistance to methylene chloride, exhibiting only slight swelling in composite form after 2 months immersion (3). Later work revealed severe loss of mechanical properties after 28 days exposure to methylene chloride (4). Cured ethynyl (acetylenic)-terminated sulfone oligomers exhibited good resistance to hydraulic fluid and chloroform when the linear sulfone segment was relatively short [number average molecular weight (\bar{M}_n) ~3000 g/mole] (5).

- o RADEL® and PKXA, Union Carbide Corp., Mid-1970's
- o Blend of reactive plasticizer with UDEL®, AFWAL, 1978
- o Semi-Crystalline Sulfone Block Copolymers, VPI&SU, 1979
- o Nadimide-Terminated Polysulfone (NTS-20), Boeing Aerospace Co., 1980
- o Ethynyl-Terminated Sulfone Oligomers (ETS), NASA Langley, 1982

Figure 2

APPROACHES INVESTIGATED

Various approaches were investigated to improve the solvent resistance of thermoplastics and are listed in Figure 3. Ethynyl groups were placed on the ends of sulfone oligomers as discussed in subsequent figures. Ethynyl groups were incorporated pendent along the backbone of sulfone/ester polymers as presented later in this paper. Ester oligomers were also end-capped with ethynyl groups. To further investigate the effect of pendent ethynyl groups on the properties of cured resins, phenoxy resins containing pendent ethynyl groups were prepared and characterized. The last approach involved the use of a coreactant which was blended with a phenoxy resin containing pendent ethynyl groups.

- o Ethynyl groups on the ends of sulfone oligomers
- o Ethynyl groups pendent on sulfone/ester polymer
- o Ethynyl groups on the ends of ester oligomers
- o Ethynyl groups pendent on phenoxy resins
- o Coreactant blended with phenoxy resins containing pendent ethynyl groups

Figure 3

SYNTHESIS OF HYDROXY-TERMINATED SULFONE OLIGOMERS

Hydroxy-terminated sulfone oligomers of different molecular weights were synthesized according to a known procedure (6) from the reaction of 2,2-bis(4-hydroxyphenyl)propane (bis-phenol A) and 4,4'-dichlorodiphenylsulfone using potassium carbonate in N,N-dimethylacetamide as depicted in Figure 4. The hydroxy-terminated sulfone oligomers were characterized by titration to determine hydroxyl end-groups (7) and accordingly \bar{M}_n , size exclusion chromatography, differential scanning calorimetry to obtain the glass transition temperature (T_g) and inherent viscosity as presented in table 1. Two hydroxy-terminated sulfone oligomers are of particular interest in this paper: one with a \bar{M}_n up ~ 12000 g/mole employed in the synthesis of the ethynyl-terminated sulfone oligomer and the other with a \bar{M}_n of ~ 4000 g/mole used to prepare the sulfone/ester polymer containing pendent ethynyl groups. Characterization data on these two oligomers are presented below.

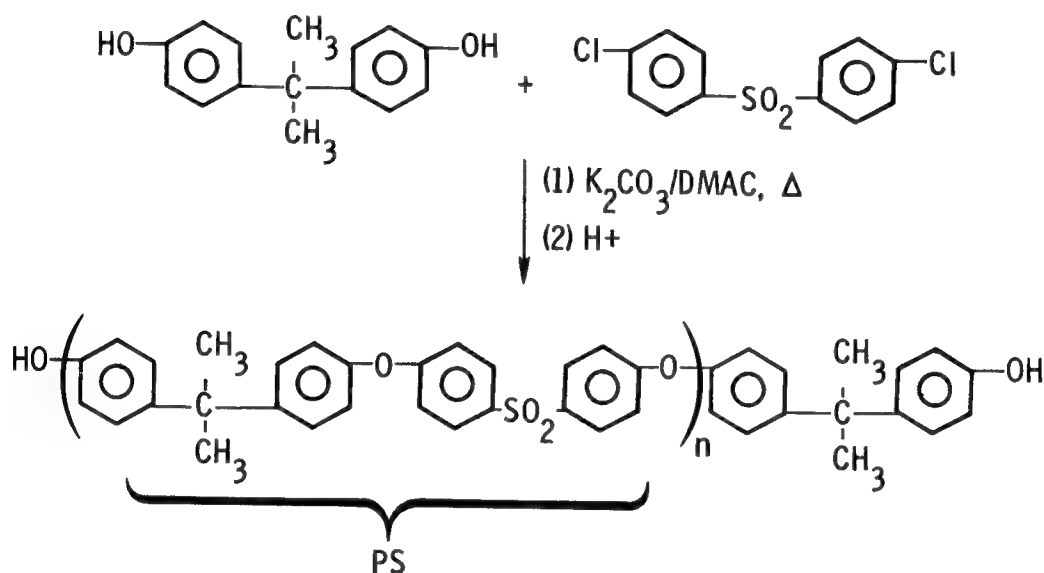


Figure 4

TABLE 1

\bar{M}_n g/mole	η_{inh} , dl/g ¹	SEC Peak Retention Time, min ²	T_g , °C ³
4,000	0.09	18.90	167
12,000	0.38	17.65	183

¹Inherent viscosity determined on 0.5% solution in chloroform at 25°C

²Size exclusion chromatography determined using a bank of μ -Styragel columns (10^6 , 10^5 , 10^4 and 10^3 Å) and chloroform as solvent

³Glass transition determined by differential scanning calorimetry (DSC) at a heating rate of 20°C/min

SYNTHESIS OF 4-ETHYNYLBENZOYL CHLORIDE

The 4-ethynylbenzoyl chloride was prepared as shown in Figure 5 according to a known procedure (8). The acid chloride was obtained as a yellow crystalline solid, melting point (mp), 75°C to 76°C, after recrystallization from hexane. A lower cost route to 4-ethynylbenzoyl chloride has since been developed which utilizes 2-methyl-3-butyn-2-ol in place of trimethylsilylacetylene. Early work with the 2-methyl-3-butyn-2-ol route resulted in incomplete cleavage of the 2-hydroxypropyl group (acetone as a by-product) from an intermediate using sodium hydroxide. Recent work using a catalytic amount of sodium hydride resulted in near-quantitative cleavage of the 2-hydroxypropyl group (9).

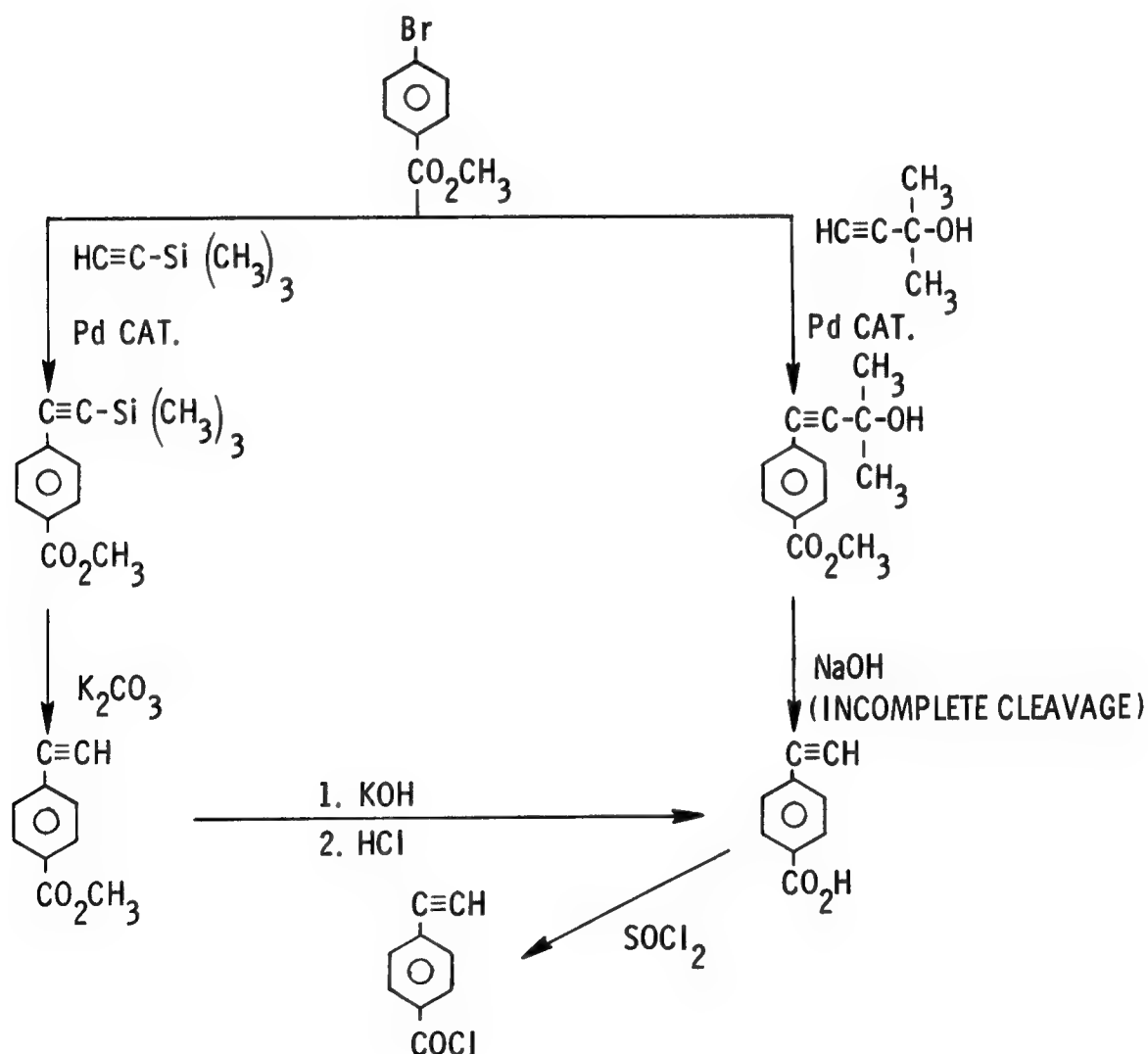


Figure 5

SYNTHESIS OF ETHYNYL-TERMINATED SULFONE (ETS)

An ethynyl-terminated sulfone (ETS) was prepared as shown in Figure 6 from the reaction of a hydroxy-terminated sulfone oligomer of \bar{M}_n of ~12000 g/mole with a slight stoichiometric excess of 4-ethynylbenzoyl chloride as previously reported (5). Characterization of the ETS, the cured resin therefrom and UDEL® are presented in table 2. The 250°C cured ETS exhibited a higher Tg and better resistance to chloroform than UDEL®. This was due to the thermally induced reaction of the ethynyl group which caused some crosslinking. The swelling of the cured ETS in chloroform was expected since the linear sulfone portion of the molecule is relatively long and prone to attack by chloroform, an extremely aggressive solvent for polysulfones.

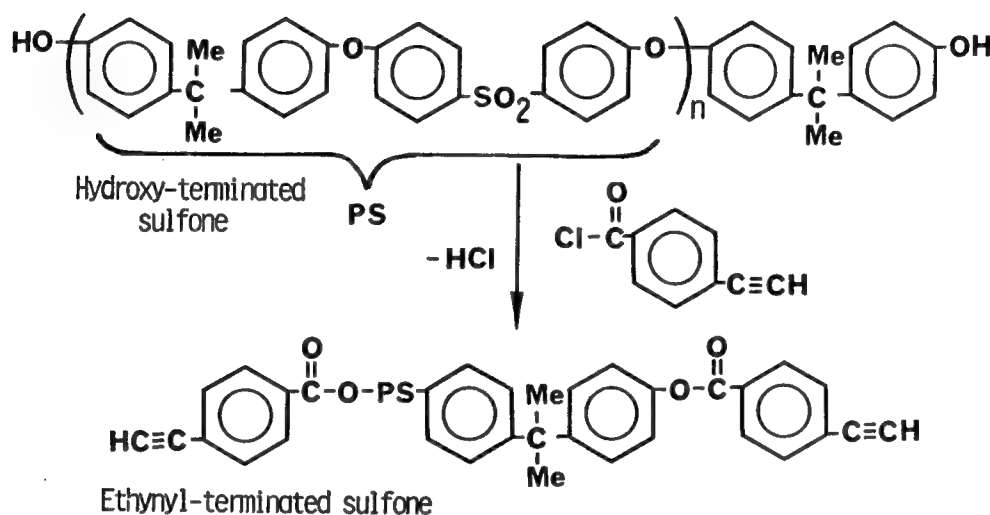


Figure 6

TABLE 2

Polymer	\bar{M}_n , g/mole	η_{inh} , dl/g	SEC Peak Retention Time, min	Tg, °C ¹	Solubility in Chloroform
ETS	~12,000	0.39	17.54	198	Soluble uncured, Swells when cured ¹
UDEL®	~25,000	0.44	17.14	192	Soluble

¹ After curing for 0.5 hr at 250°C in air

ISOTHERMAL AGING PERFORMANCE OF 250°C CURED FILMS

The thermooxidative stability of cured films (~0.002 in. thick) of UDEL® and two ETS of $\bar{M}_n = \sim 12,000$ g/mole containing 20 and 80 ppm of palladium are shown in Figure 7. The effect of residual palladium which enhances the thermooxidative degradation is readily evident. The ETS with 20 and 80 ppm of palladium exhibited weight losses of 11.5 and 69.1 respectively after 90 hours at 250°C and 26.2 and 98.2 respectively after 64 hours at 288°C. The ETS exhibited relatively low weight losses at 177°C. UDEL® exhibited excellent stability at 177, 250 and 288°C. At 250°C, the UDEL® film melted to form a clump whereas the ETS films retained their form. Palladium was introduced during the preparation of 4-ethynylbenzoyl chloride. Recent work has involved the removal of the palladium from 4-ethynylbenzoyl chloride by the purification of one of the intermediates (9).

Aging Temp, °C (circulating air)	Time, hr	Weight Loss, %		
		UDEL®	ETS (20 ppm Pd)	ETS (80 ppm Pd)
177	1200	1.1	1.3	2.0
250	90	0.6	11.5	69.1
288	64	1.0	26.2	98.2

Figure 7

THIN-FILM PROPERTIES

The mechanical properties of thin films (~0.002 in. thick) of UDEL® and ETS prepared by solution casting onto plate glass and stage curing in air to a final temperature of 250°C and at 250°C for 0.5 hr are presented in Figure 8. Tensile strengths and moduli for the ETS film are higher than those of UDEL®, especially at 93°C. The UDEL® film was of better quality where elongation at 25° of 14% was obtained. The ETS film exhibited failure before it could elongate appreciably due to the poorer quality of the film. The UDEL® film was easily removed from the glass whereas severe problems were encountered in removing the ETS film from the glass. The ETS film could not be removed without tearing the glass, even upon soaking in water overnight. As a result, the ETS film had stress areas which served as points of weakness, causing premature failure, before the film could elongate appreciably. It was expected, however, that the elongation of the ETS film would be less than that of UDEL®.

Material	UDEL®		ETS ($\bar{M}_n = 12,000$)	
	25	93	25	93
Test temp., °C	25	93	25	93
Tensile strength, ksi	10.8 (10.6) ¹	8.2	12.1	9.6
Tensile modulus, ksi	320 (286) ¹	282	356	336
Elongation (break), %	14.1 (110) ¹	17.3	4.3	5.3

¹ Lit. (ref. 10) values for unoriented slot-cast thin film

Figure 8

PRELIMINARY UNIDIRECTIONAL CELION-6000 LAMINATE PROPERTIES

Unidirectional ETS and UDEL® preregs were made by solution coating drum-wound Celion-6000 carbon/graphite fiber. The prepreg was vacuum dried at 100°C for 18 hours to reduce the volatile content to ~2%. Unidirectional laminates (3 in. x 7 in. x 0.060 and 0.110 in.) were fabricated in a stainless steel mold in a press starting at ambient temperature under 100 psi for UDEL® and 300 psi for ETS, heating under pressure to 316°C during ~45 minutes and maintaining at 316°C under pressure for 0.5 hour. Preliminary laminate properties are reported in Figure 9. The ETS laminate displayed slightly higher properties than UDEL® which may be attributed to better wetting of the filaments since the viscosity of the ETS solution used in prepreg preparation was lower than that of UDEL®. The flexural strengths of ETS at 177°C were higher than those of UDEL® although both systems exhibited thermoplastic failure at 177°C.

Test Conditions	Flexural st., psi x 10 ³		Flexural mod., psi x 10 ⁶		Short beam shear st., psi x 10 ³	
	UDEL®	ETS	UDEL®	ETS	UDEL®	ETS
RT	189	197	18.6	19.4	8.5	9.3
93°C, 10 min.	177	192	17.1	18.9	8.1	8.9
177°C, 10 min.*	121	153	13.4	15.5	4.1	5.3
177°C, 1200 hr @ 177°C*	--	--	--	--	4.3	5.4

Resin Content: ~34%
*Thermoplastic failure

Figure 9

SOLVENT RESISTANCE (24-Hour SOAK)

The solvent resistances of various specimen forms of UDEL® and ETS after a 24-hour soak in different solvents are presented in Figure 10. UDEL® specimens exhibited sensitivity towards all the solvents whereas ETS was relatively unaffected by the solvents except for chloroform. Chloroform, like methylene chloride which is present in most paint strippers, is an aggressive solvent towards sulfone polymers. In chloroform, the area of the ETS film increased by ~55% due to swelling. Swelling is unacceptable for a composite matrix because this is obviously accompanied by severe strength loss.

Specimen Form	Solvent	Results	
		UDEL®	ETS (Cured)
Stressed film	JP-4 Jet Fuel	Sl. Crazed	Unaffected
	Ethylene Glycol	Crazed	Unaffected
	Chevron Hyjet IV*	Badly Crazed	Unaffected
	Chloroform	Dissolved	Swelled
Hanging lap shear	Chevron Hyjet IV	~50% RT Strength Loss	~10% RT Strength Loss
	Chloroform	Dissolved	
Composite SBS	Chevron Hyjet IV	~20% RT Strength Loss	No RT Strength Loss
	Chloroform	Dissolved	Badly Swelled

*Hydraulic Fluid

Figure 10

FRACTURE ENERGY OF VARIOUS POLYMERS

The fracture energies of UDEL®, ETS, and various other polymers included for comparison are listed in Figure 11. Composite interlaminar fracture properties cannot be predicted based upon neat resin and fiber properties. High fracture energy of a neat resin does not necessarily mean a high interlaminar fracture energy in composite form. The ability of the resin to translate good composite properties must be determined. Several factors are important such as fiber/resin interface and residual stresses. As a result, it would be improper to predict the interlaminar fracture energy of an ETS composite based upon neat resin fracture energy. The cured ETS had a modest fracture energy of 1700 J/M², half the value of UDEL®.

<u>POLYMER</u>	<u>FRACTURE ENERGY, J/M²¹</u>
UDEL® (UC Polysulfone)	3400 ²
ETS (\bar{M}_n = 12,000 g/mole)	1700 ²
ULTEM® (GE Polyimide)	3700 ²
121°C Cure Rubber Toughened Epoxy (Hexcel F-185)	5100 ³
121°C Cure Epoxy (Hexcel 205)	270 ³
177°C Cure Epoxy (Narmco 5208)	76 ²

¹ Compact Tension Specimens.

² Courtesy of D. Hunston, National Bureau of Standards, private communication.

³ Taken from reference 11.

Figure 11

SULFONE/ESTER POLYMER CONTAINING PENDENT ETHYNYL GROUPS

A hydroxy-terminated sulfone oligomer ($\bar{M}_n = \sim 4000$ g/mole) was reacted with 5-(4-ethynylphenoxy)isophthaloyl chloride to yield a sulfone/ester polymer containing pendent ethynyl groups as shown in Figure 12. The physical properties of the sulfone/ester polymer and that of UDEL®, included for comparison, are presented in table 3. The cured sulfone/ester polymer exhibited better solvent resistance than UDEL® but not as good as anticipated. The crosslink density of the cured sulfone/ester polymer was not high enough to provide the degree of solvent resistance towards chloroform as observed for an ETS with a linear sulfone segment of ~ 3000 g/mole (5). The cured sulfone/ester polymer has a T_g higher than that of UDEL® presumably due to higher intermolecular association and not solely crosslinking.

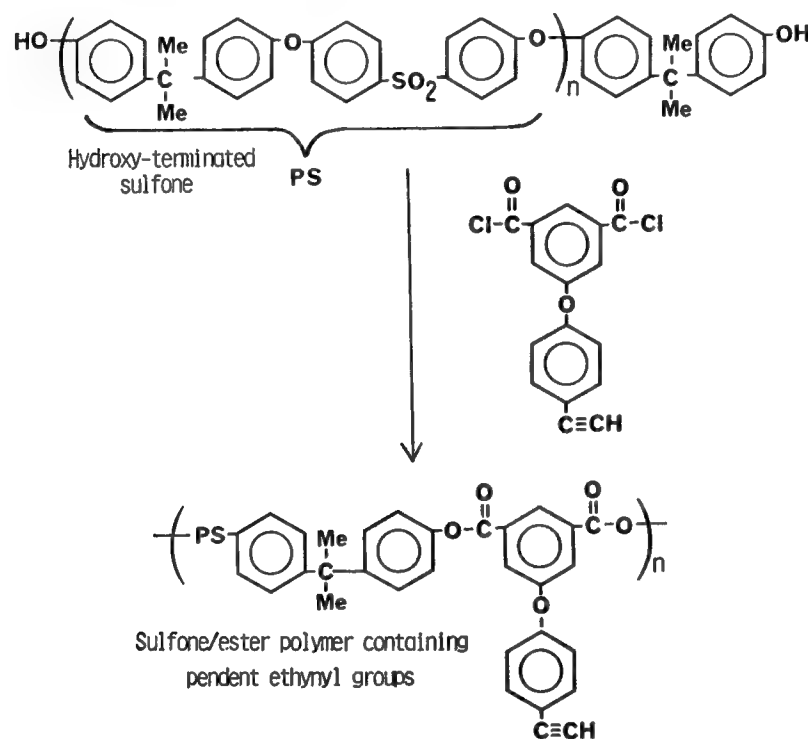


Figure 12

TABLE 3

Polymer	η_{inh}^1 dl/g ¹	SEC Peak Retention Time, min ¹	T_g of Cured Polymer, °C ¹	Chloroform Solu- bility of Cured Polymer Film ²
Sulfone/Ester with Pendent Ethynyl Groups	0.34	17.55	204	Pronounced Swelling
UDEL®	0.44	17.14	192	Soluble

¹See Figure 4.

²Cured 0.5 hour at 250°C in air.

FILM PROPERTIES OF SULFONE/ESTER POLYMER AND UDEL®

Preliminary mechanical properties of 250°C cured thin films (0.002 in. thick) of a sulfone/ester polymer containing pendent ethynyl groups and UDEL® are reported in Figure 13. The properties are essentially identical except that the sulfone/ester polymer showed no loss in tensile modulus at 93°C. The low elongation of the sulfone/ester polymer is not due solely to cross-linking but attributed to the poor quality of the film specimens. The films were cast on plate glass. The sulfone/ester polymer film tore the glass surface which caused stress areas in the film.

Polymer	UDEL®		Sulfone/Ester With Ethynyl Groups	
	25	93	25	93
Test Temp, °C	25	93	25	93
Tensile Strength, ksi	10.8 (10.6) ¹	8.2	11.0	8.4
Tensile Modulus, ksi	320 (286) ¹	282	318.5	319.7
Elongation (Break), %	14.1 (110) ¹	17.3	4.6	3.3

¹Taken from reference 10.

Figure 13

ETHYNYL-TERMINATED POLYARYLATES

Similar to the synthesis of ETS, ethynyl-terminated polyarylates (aromatic polyesters) were prepared from the reaction of hydroxy-terminated polyarylates of different M_n with 4-ethynylbenzoyl chloride (8) as shown in Figure 14. Characterization of the various ethynyl-terminated polyarylates and ARDEL® (a commercial aromatic polyester from Union Carbide Corporation) is presented in table 4. As the length of the linear ester segment increased in the cured polymers, the T_g decreased and the chloroform sensitivity increased due to lower crosslink density.

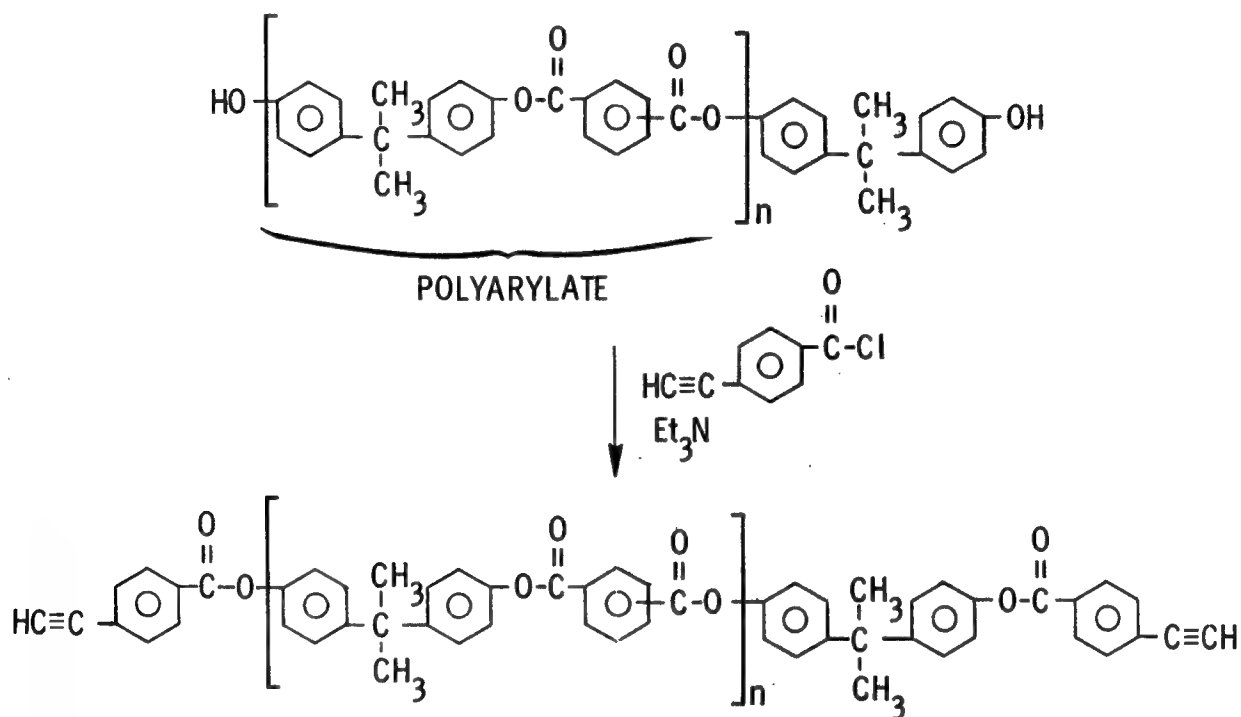


Figure 14

TABLE 4				
\bar{M}_n , g/mole	η_{inh} , dl/g	GPC Peak Retention Time, min	T_g of Cured Polymer, °C	$CHCl_3$ Solubility of Cured Polymer
2,500	0.30	18.53	218	Very Sl. Swelling
5,000	0.34	18.23	215	Sl. Swelling
7,500	0.42	17.86	207	Swelling
10,000	0.47	17.45	203	Swelling
24,000 (ARDEL®)	0.59	17.21	197	Soluble

PHENOXY RESINS CONTAINING PENDENT ETHYNYL GROUPS

A commercial phenoxy resin (PKHH, Union Carbide Corp.) was systematically modified (12) by introducing different amounts of pendent ethynyl groups by reaction of the pendent hydroxy group on the phenoxy resin with 4-ethynylbenzoyl chloride and benzoyl chloride as shown in Figure 15. Characterization of the various compositions is presented in table 5. As the amount of pendent ethynyl groups in the phenoxy and accordingly crosslink density in the cured resin increased, the Tg and the resistance to chloroform also increased but the flexibility of films decreased.

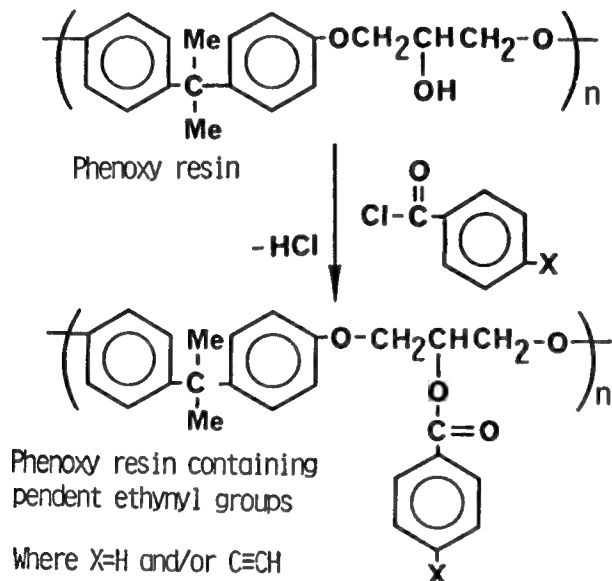


Figure 15

TABLE 5

Composition of Phenoxy		η _{inh} , dl/g	GPC Peak Retention Time, min	Tg of Cured Resin, °C	Film Flexibility	Chloroform Solu- bility of Cured Film (% increase in area)
Mole % benzoyloxy	Mole % ethynyl- benzoyloxy					
100	0	0.40	17.31	87	Very Flexible	Soluble
90	10	0.46	17.33	91	Very Flexible	>100% Swelling
66	34	0.48	17.25	110	Flexible	~50% Swelling
66	34	--	--	145	Brittle	<10% Swelling
34	66	0.47	17.30	150	Moderately Flexible	~30% Swelling
0	100	0.52	17.34	235	Brittle	Insoluble
PKHH	--	0.40	17.48	101	Very Flexible	Soluble

USE OF A COREACTANT TO INCREASE CROSSLINK DENSITY

The chemical structure and the DSC curve of a coreactant are shown in Figure 16. This coreactant was prepared from the reaction of bis-phenol A and 4-ethynylbenzoyl chloride. The DSC curve shows a melting endotherm peaking at 189°C and an exothermic peak at 219°C due to reaction of the ethynyl groups. Ten and thirty weight percents of the coreactant were blended with a phenoxy resin where 34% of the pendent hydroxyl groups had been converted to ethynylbenzoxymethoxy group and the remaining 66% to benzoyloxy groups. The properties of the modified phenoxy resin without the coreactant and the blends are reported in table 6. As the amount of coreactant is increased, the cured blends showed an increase in the Tg, less flexibility in the film and better resistance to chloroform. The changes are attributed to higher crosslink density.

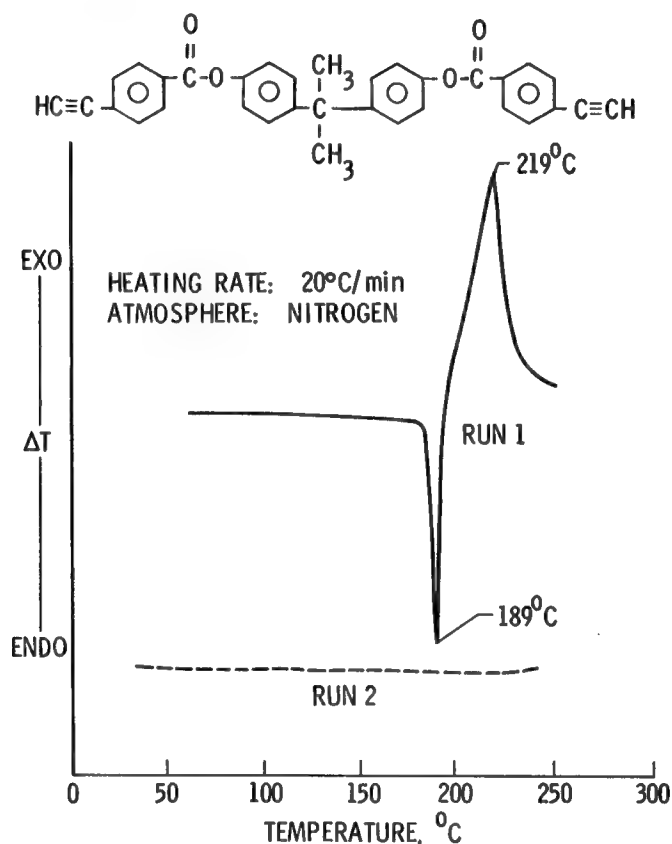


Figure 16

TABLE 6

Weight % of Coreactant	Tg of Cured Resin, °C	Film Flexibility	Chloroform Solubility of Cured Film (% Increase in Area)
0	110	Flexible	~50% Swelling
10	114	Moderately Flexible	~20% Swelling
30	145	Brittle	~ < 10% Swelling

CONCLUSIONS

- o The following approaches improved the solvent resistance and raised the T_g of thermoplastics:
 - o End-capping oligomers with ethynyl groups
 - o Incorporating ethynyl groups pendent along the polymer chain
 - o Coreacting polymers containing pendent ethynyl groups with a low molecular weight diethynyl compound
- o Film and composite properties of an ethynyl-terminated sulfone were better than those of UDEL®
- o Fracture energy of an ethynyl-terminated sulfone was lower than that of UDEL®
- o Residual palladium in the cured ethynyl-terminated sulfone lowered the thermooxidative stability of the cured resin
- o The properties of a phenoxy resin were altered considerably by placing pendent ethynyl groups along the polymer chain
- o Property trade-offs must be considered when thermoplastics are modified via reactant groups

REFERENCES

1. G. A. Loughran, A. Wereta and F. E. Arnold, U. S. Pat. 4,108,926 (1978).
2. R. Vismanathan and J. E. McGrath, Polym. Prepr. 20 (2), 365 (1979).
3. C. H. Sheppard, E. E. House and M. Stander, Soc. Plast. Ind. Inc., 36th Ann. Conf. Prepr., Session 17-B, page 1 (1980).
4. C. H. Sheppard, E. E. House and M. Stander, Nat'l SAMPE Conf. Ser. 14, 70 (1982).
5. P. M. Hergenrother, J. Polym. Sci. Polym. Chem. Ed. 20, 3131 (1982).
6. J. E. McGrath, T. C. Ward, E. Shchori and A. J. Wnuk, Polym. Eng. Sci. 17, 647 (1977).
7. A. J. Wnuk, T. F. Davidson and J. E. McGrath, Polym. Prepr. 19 (1), 506 (1978).
8. S. J. Havens and P. M. Hergenrother, Polym. Prepr. 24 (2), 16 (1983).
9. S. J. Havens and P. M. Hergenrother, submitted to J. Org. Chem., August 1984.
10. R. N. Johnson in Encycl. Polym. Sci. and Tech. (H. F. Mark, N. G. Gaylord and N. M. Bikales, eds.) Vol. 11, Wiley-Interscience, New York, 1969, p. 447.
11. W. D. Bascom, J. L. Bitner and A. R. Siebert, Composites, 11, (9), 1980.
12. P. M. Hergenrother, B. J. Jensen, and S. J. Havens, Phenoxyl Resins Containing Pendent Ethynyl Groups, NASA TM-85747, January 1984.

THERMOPLASTIC/MELT-PROCESSABLE POLYIMIDES

T. L. St. Clair and H. D. Burks
NASA Langley Research Center
Hampton, Virginia

INTRODUCTION

Linear aromatic polyimides since their inception in the 1960's have been regarded as difficult materials to process into useable shapes. During the last 15 years many significant advances have been made in the processing of these materials. One particular advance that holds promise for the structural materials field has been the synthesis of polyimides that can be processed as thermoplastics. The initial materials that were processable in this manner required very high temperatures and pressures for proper consolidation. This paper describes some of the advancements that have been made at NASA Langley in developing aromatic polyimides that are facile to process. The primary objective has been to lower processing temperatures and/or pressures through the synthesis of polyimides with diluted imide content and/or with greater chain flexibility.

OBJECTIVE: TO LOWER THE PROCESSING TEMPERATURE OF
LINEAR AROMATIC POLYIMIDES

APPROACH: A SYNTHESIS PROGRAM WHEREBY THE IMIDE CONTENT IS
DILUTED & THE CHAIN FLEXIBILITY IS INCREASED

LARC TPI

A linear thermoplastic polyimide, LARC TPI, has been synthesized, characterized and developed for a variety of high-temperature applications. In its fully imidized form this material can be used as an adhesive for bonding metals such as titanium, aluminum, copper, brass, and stainless steel. LARC TPI is being evaluated as a thermoplastic adhesive for bonding titanium (6-aluminum-4-vanadium alloy) and to-date has shown no loss in properties after 25,000 hours of air-aging at 450°F. It is also being developed commercially as a laminating agent for bonding large pieces of polyimide film to metals to produce 100% void-free flexible circuits. This polymer has also been evaluated as a molding powder, composite matrix resin, high-temperature film, and fiber (ref. 1).

A MULTI-PURPOSE THERMOPLASTIC POLYIMIDE

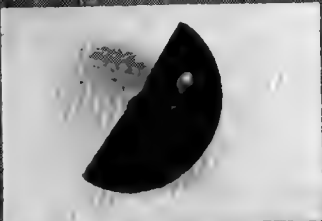
$$\left[\text{HN} \begin{array}{c} \text{O} \\ \parallel \\ \text{C} \end{array} \text{C}_6\text{H}_2 \begin{array}{c} \text{O} \\ \parallel \\ \text{C} \end{array} \text{NH} - \text{Ar} \right]_n$$

**SOLAR SAIL ADHESIVE
(POLYAMIC ACID)**

$\xrightarrow[\text{-H}_2\text{O}]{\Delta}$


$$\left[\text{N} \begin{array}{c} \text{O} \\ \parallel \\ \text{C} \end{array} \text{C}_6\text{H}_2 \begin{array}{c} \text{O} \\ \parallel \\ \text{C} \end{array} \text{N} - \text{Ar} \right]_n$$

**LARC-TPI
(THERMOPLASTIC POLYIMIDE)**




LARC-TPI MOLDING

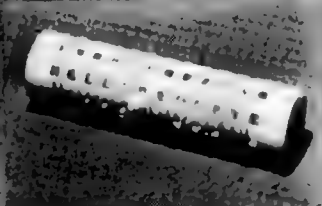
- (1) STRUCTURAL ADHESIVE
(FOR METALS OR COMPOSITES)
- (2) PI FILM LAMINATING ADHESIVE
- (3) MOLDING POWDER
- (4) COMPOSITE MATRIX RESIN
- (5) HIGH-TEMP FILM
- (6) HIGH-TEMP FIBER



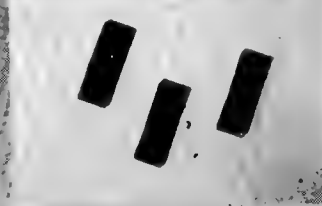
LARC-TPI FILM



**LARC-TPI/KAPTON[®]
LAMINATE**



LARC-TPI FIBERS



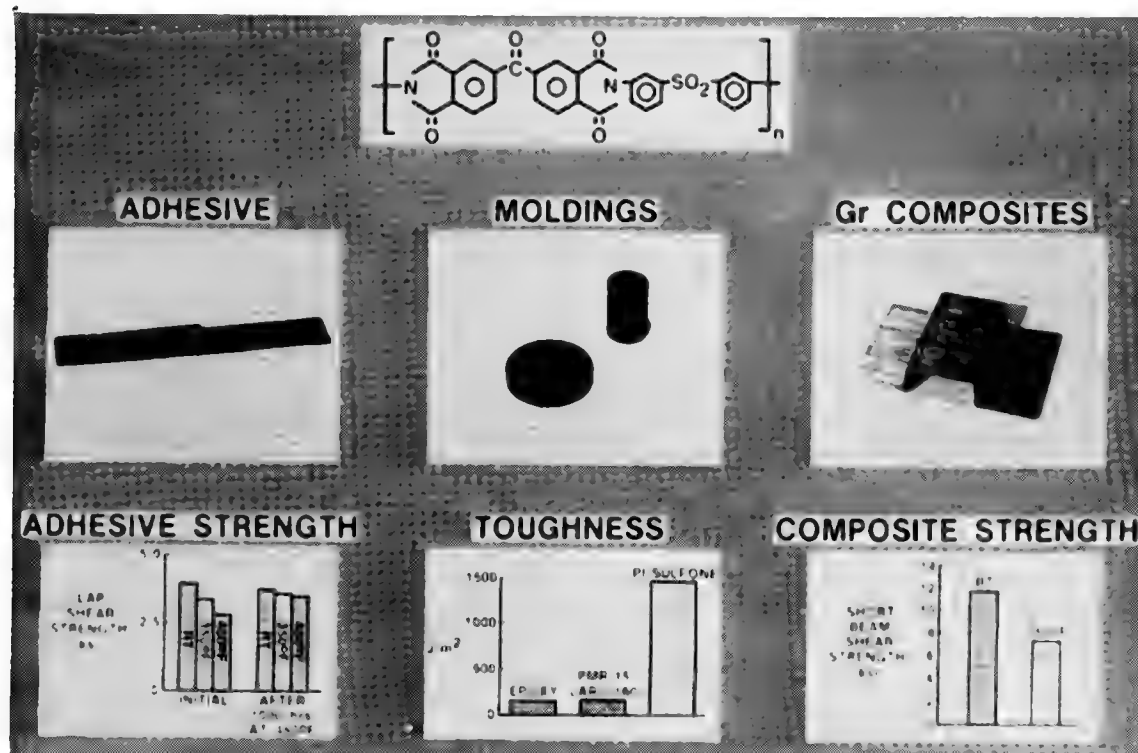
**LARC-TPI/CELION[®] 6000
COMPOSITES**

THERMOPLASTIC POLYIMIDESULFONE

Aromatic polysulfones, a class of high-temperature engineering thermoplastics, have a major deficiency in their tendency to swell and dissolve in many common solvents. This solvation can cause structural components which are fabricated from these polymers to be susceptible to damage by these solvents and thereby lose their structural integrity.

Aromatic polyimides, conversely, are a class of polymers which are known to be resistant to solvents, but they are generally not processable via thermoplastic means. These polyimides are known to be exceptionally thermally stable and like polysulfones and other thermoplastics their use temperature is governed by the softening temperature of each system.

A novel polymer system that possesses the processability of the polysulfones and the solvent resistance of the polyimides has been synthesized and characterized as a film, unfilled molding, and adhesive. The structure of this polyimidesulfone is shown below along with some adhesive and molding data (ref. 2).



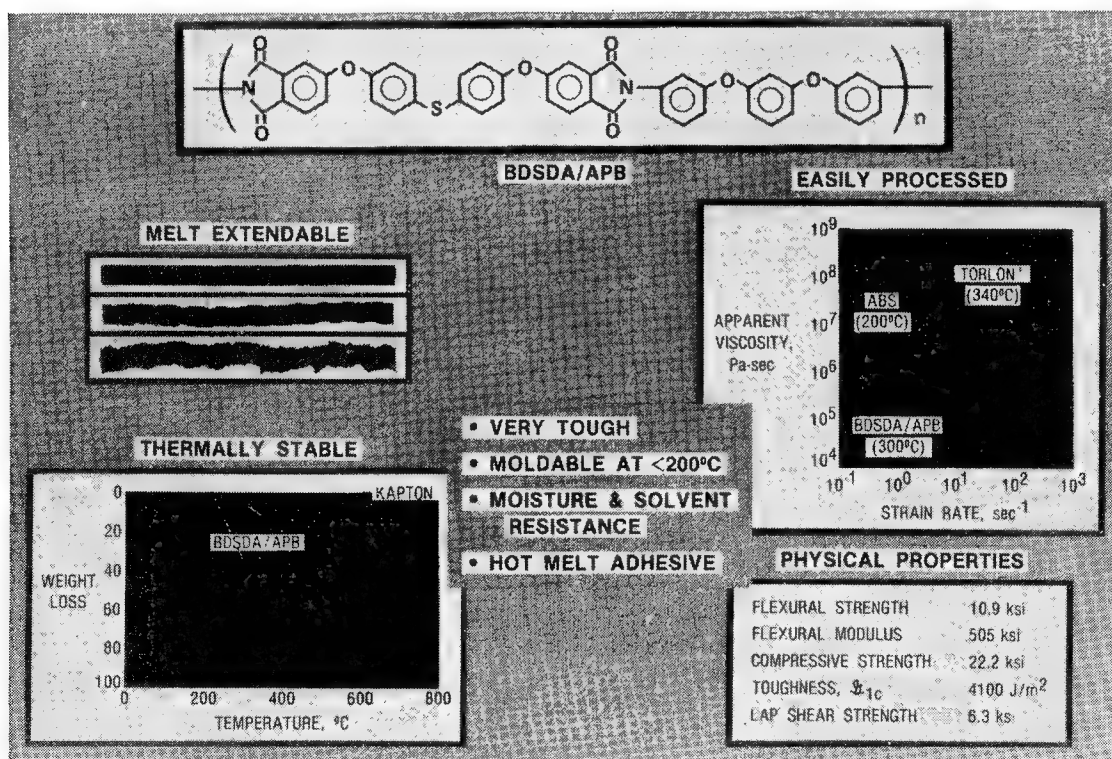
HOT-MELT PROCESSABLE POLYIMIDE

Linear aromatic polyimides are a class of polymers which are generally not processable via conventional thermoplastic or hot-melt techniques. This class of polymer is, however, exceptionally thermally stable and has high glass transition temperatures. It is also resistant to attack by common organic solvents.

Linear aromatic polyphenylene oxides and sulfides, on the other hand, are more easily processed than the polyimides, generally exhibit lower glass transition temperatures, and still have relatively good thermal stability, although not equal to the polyimides. These systems also do not possess solvent resistance equal to the polyimides.

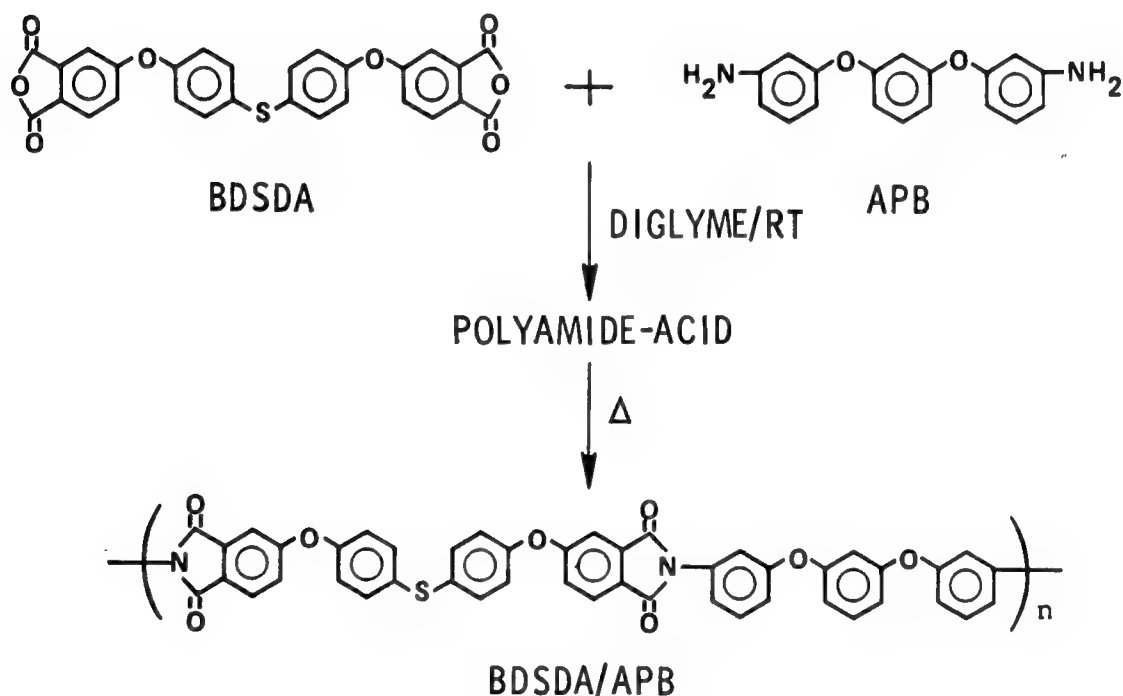
A novel linear aromatic polyphenylene ethersulfideimide (PPX-PI) has been synthesized which has some of the favorable characteristics of each parent system. The polymer has been molded, used as a resin, and cast into thin films. A limited characterization indicates this system can be processed via conventional thermoplastic techniques and may have a wide variety of applications (ref. 3).

The synthesis and characterization of this novel system is the primary subject for the remainder of this paper. The overall characteristics of this polymer system make it very attractive for use as a composite matrix resin.



POLYMER SYNTHESIS SCHEME

The PPX-PI system has been prepared via the scheme shown below. The reaction of the monomers is carried out at room temperature in the solvent diglyme. The resulting polyamide-acid is soluble in this solvent, but when it is converted to the imide the polymer becomes insoluble. This phenomenon allows the polymer to be handled in solution form if this is desirable (prepregging) and after conversion to the imide form the polymer no longer has affinity for the solvent. This is in sharp contrast to other thermoplastics because they tend to tenaciously hold onto the solvent in which they were dissolved. The key point that must be emphasized is the subject PPX-PI system is one class of polymer in solution that becomes another class of polymer when the solvent is thermally removed. Both systems are thermoplastic.



MECHANICAL PROPERTIES UNFILLED BDSDA/APB

The properties of the unfilled polymer are shown below. The flexural strength of 10.9 ksi is typical of thermoplastic polymers. The flexural modulus of this material is quite high when compared to conventional thermoplastics. In fact this modulus is more characteristic of thermoset systems. In contrast is the G_{IC} value for this material. The value of 4100 J/m^2 is exceptionally high compared to these thermoset systems ($< 100 \text{ J/m}^2$). Because of the combination of high modulus and high G_{IC} (toughness indicator) this system should be attractive for the fabrication of impact-resistant structures.

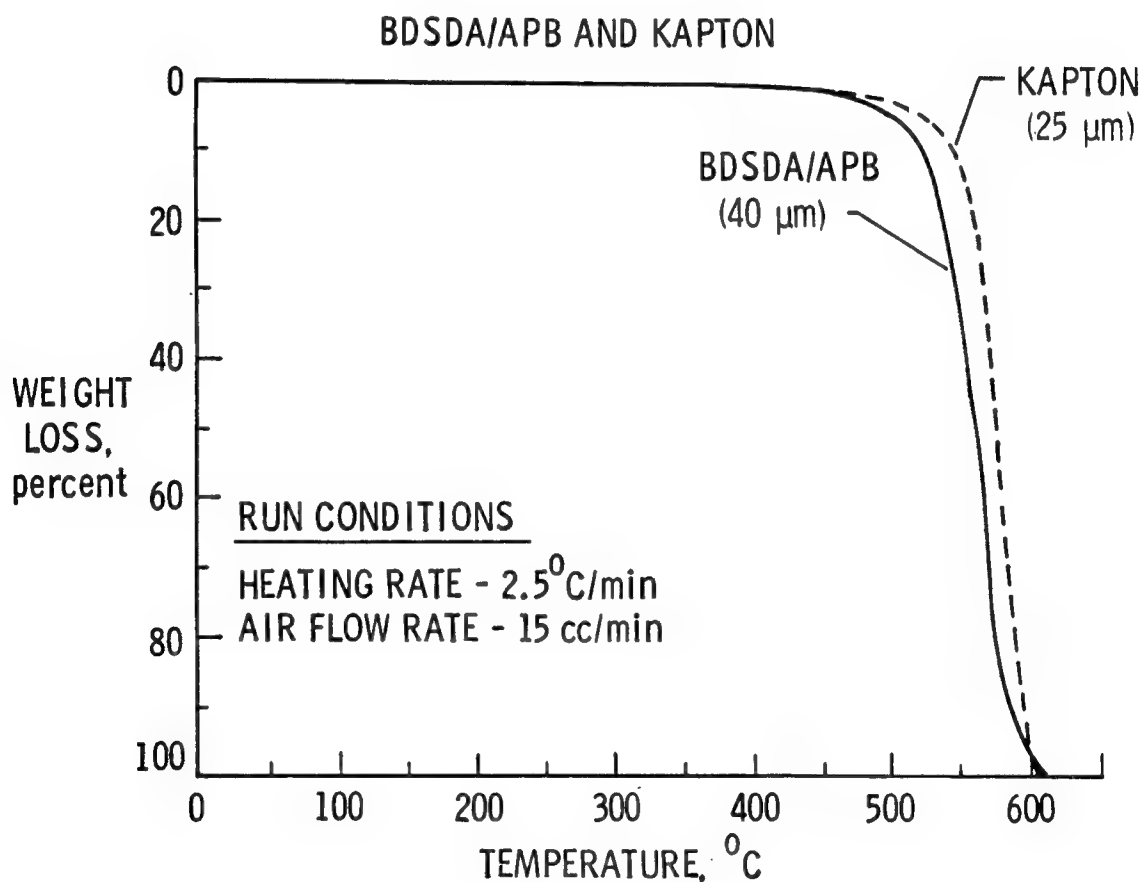
FLEXURAL STRENGTH	75.1 MPa (10.9 ksi)
FLEXURAL MODULUS	3.48 GPa (505 ksi)
COMPRESSIVE STRENGTH	153 MPa (22.2 ksi)
CRITICAL RATE OF RELEASE OF STRAIN ENERGY, G_{IC}	4100 J/m^2
LAP SHEAR STRENGTH (Ti/Ti)*	
LOW HEATING RATE (5°C/min)	40.3 MPa (5.85 ksi)
HIGH HEATING RATE (22°C/min)	43.4 MPa (6.30 ksi)

* BONDED AND TESTED ACCORDING TO ASTM STANDARD D 1002-72
(REF. 4)

THERMOOXIDATIVE STABILITY COMPARISON

The PPX-PI (BDSDA/APB) system has very good thermooxidative stability. When a 40- μm thick piece of this material was subjected to a dynamic thermogravimetric weight analysis at a standard 2.5°C/minute heating rate, the subject material had a weight loss profile similar to a 25- μm thick Kapton® standard that is used for instrument calibration. The approximate 10-20°C difference in decomposition temperature is significant and indicates that this material would not withstand elevated temperature (> 200°C) exposures as well as Kapton®*.

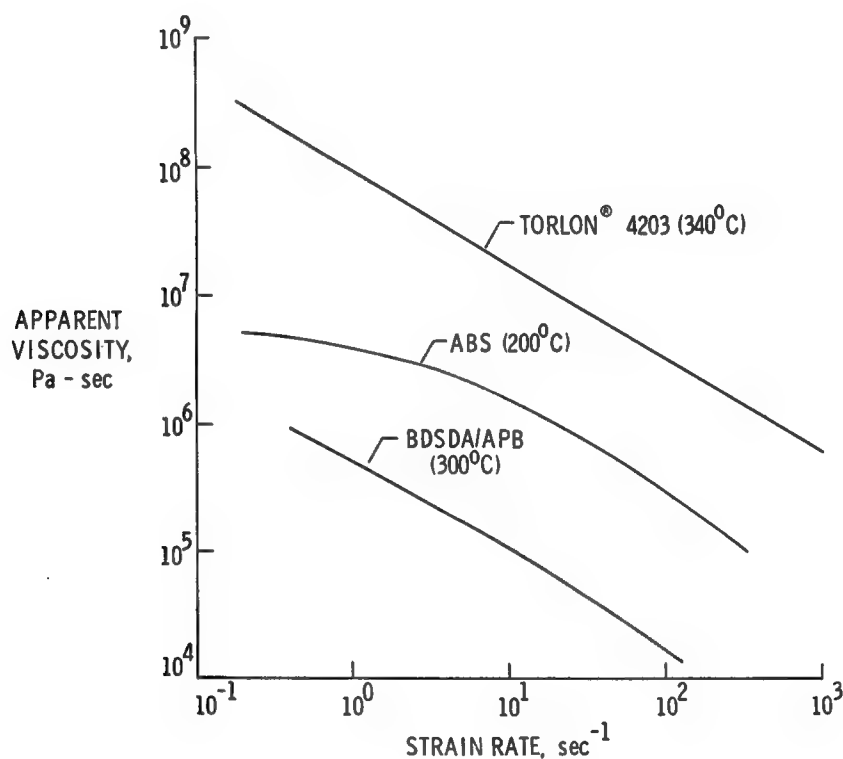
* Kapton is a registered trademark for a DuPont polyimide film.



VISCOSITY AT MIDRANGE PROCESSING TEMPERATURE

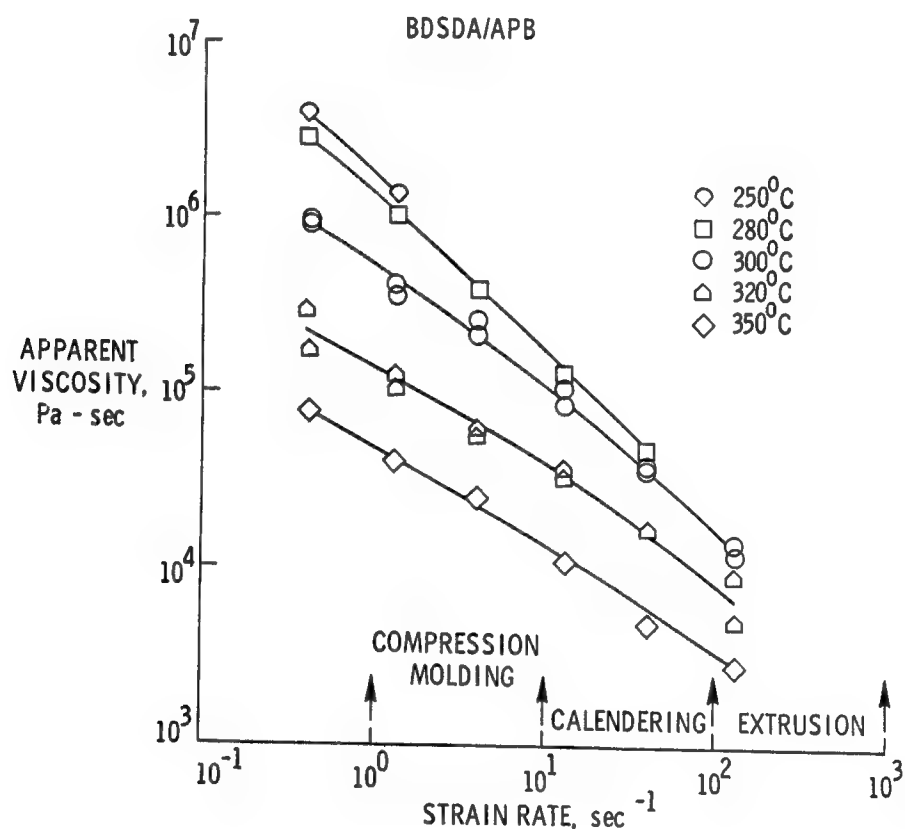
This figure compares the change in apparent viscosity with strain rate at the midrange processing temperature for the subject polymer (BDSDA/APB), commercially available Torlon*, and a typical widely used ABS resin (ref. 5). This comparison is made because no data have been generated on a linear aromatic polyimide system prior to this BDSDA/APB study. At low strain rates the BDSDA/APB exhibits a considerably lower melt viscosity (i.e., lower processing pressure) than Torlon or ABS resin and maintains this relationship even at the higher strain rates. This would indicate it to be a somewhat more easily processable material.

*Torlon is the registered trademark of an Amoco poly(amide-imide).



APPARENT VISCOSITY FOR PROCESSING PARAMETERS

The apparent viscosity as a function of strain rate at various temperatures is shown for the strain rates encountered in different industrial processes. The apparent viscosity was calculated by dividing the flow stress by the strain rate. As the strain rate was calculated from the volumetric flow data and was not corrected to obtain the wall rate, the viscosity is an apparent rather than a true viscosity (ref. 6). The BDSDA/APB polymer should be processable via compression molding and calendering techniques. However, no conclusions can be drawn concerning the extrudability of the polymer above a strain rate of 135 sec^{-1} due to the stress and strain rate limitations of our rheometer in its present configuration.



CHEMICAL RESISTANCE

The chemical resistance of BDSDA/APB thin film (40 μ m thick) to six common solvents was determined and the results listed in this figure. Methylene ketone, cyclohexanone, xylene, and tricresylphosphate had no visible effect on the film and there was no change in T_g (apparent). Methylene chloride and cresol caused severe swelling and T_g measurements were not possible, although the methylene chloride-soaked film did maintain sufficient integrity as a film to allow mounting in the T_g fixture.

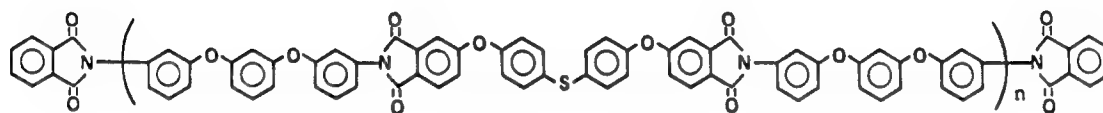
BDSDA/APB FILM		
<u>SOLVENT</u>	<u>EFFECT</u>	<u>CHANGE IN T_g, (APPARENT), $^{\circ}\text{C}^*$</u>
METHYLETHYL KETONE	NONE	NONE
CYCLOHEXANONE	NONE	NONE
XYLENE	NONE	NONE
TRICRESYLPHOSPHATE	NONE	NONE
METHYLENE CHLORIDE	SWELLED	NOT DETERMINED
CRESOL	SWELLED	NOT DETERMINED

40- μ m THICK FILM

* THERMOMECHANICAL ANALYSIS OF SOLVENT-LADEN FILMS
SOAKED 72 hrs AT ROOM TEMPERATURE AND BLOTTED DRY

ENDCAPPED PROCESSABLE POLYIMIDE

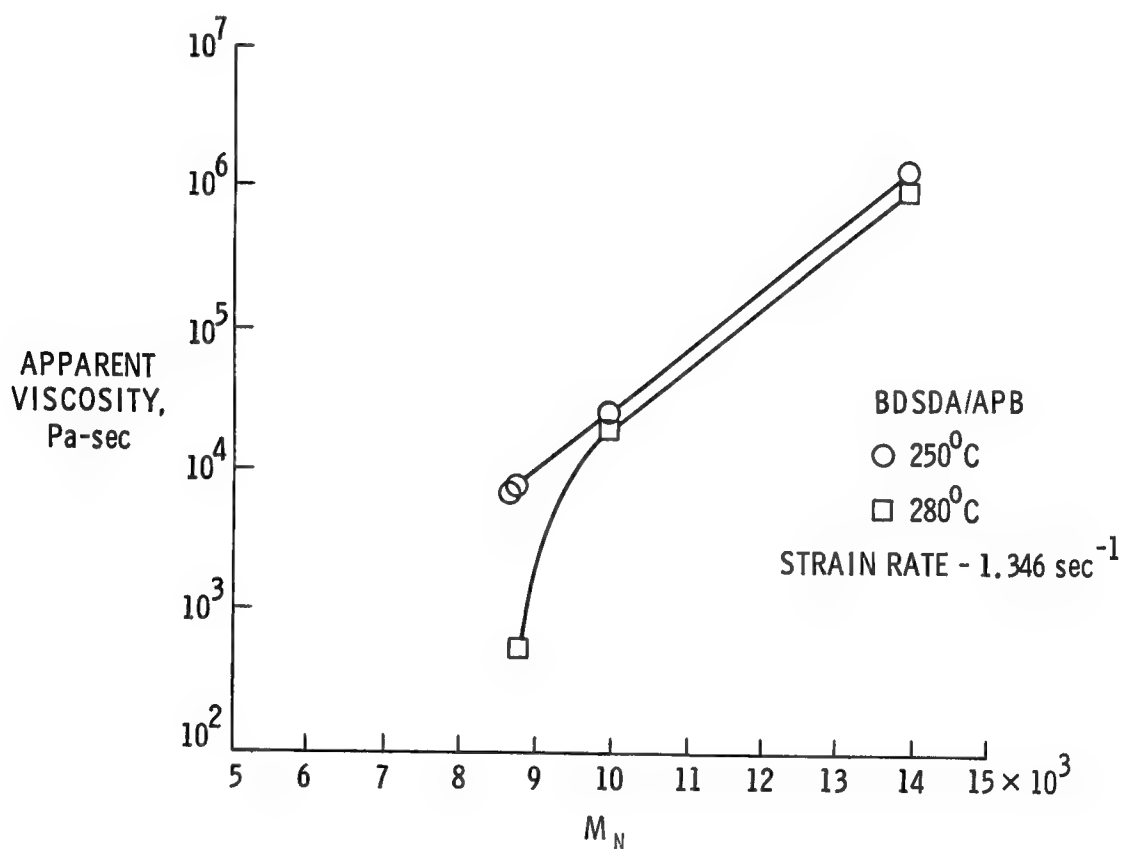
In an attempt to improve the processability of the BDSDA/APB polyimide system a series of endcapped analogues were prepared. These were accomplished by substituting the monofunctional phthalic anhydride for some of the BDSDA. The general synthesis scheme used was to decrease the difunctional BDSDA by one mole percent and add the phthalic anhydride at a two-mole percent level. A two-for-one substitution is used because the anhydride molar equivalence must be held equal to the amine molar equivalence. In subsequent figures the 1%, 2%, and 4% endcapped systems refer to the molar amount of phthalic anhydride (ref. 7).



BDSDA/APB

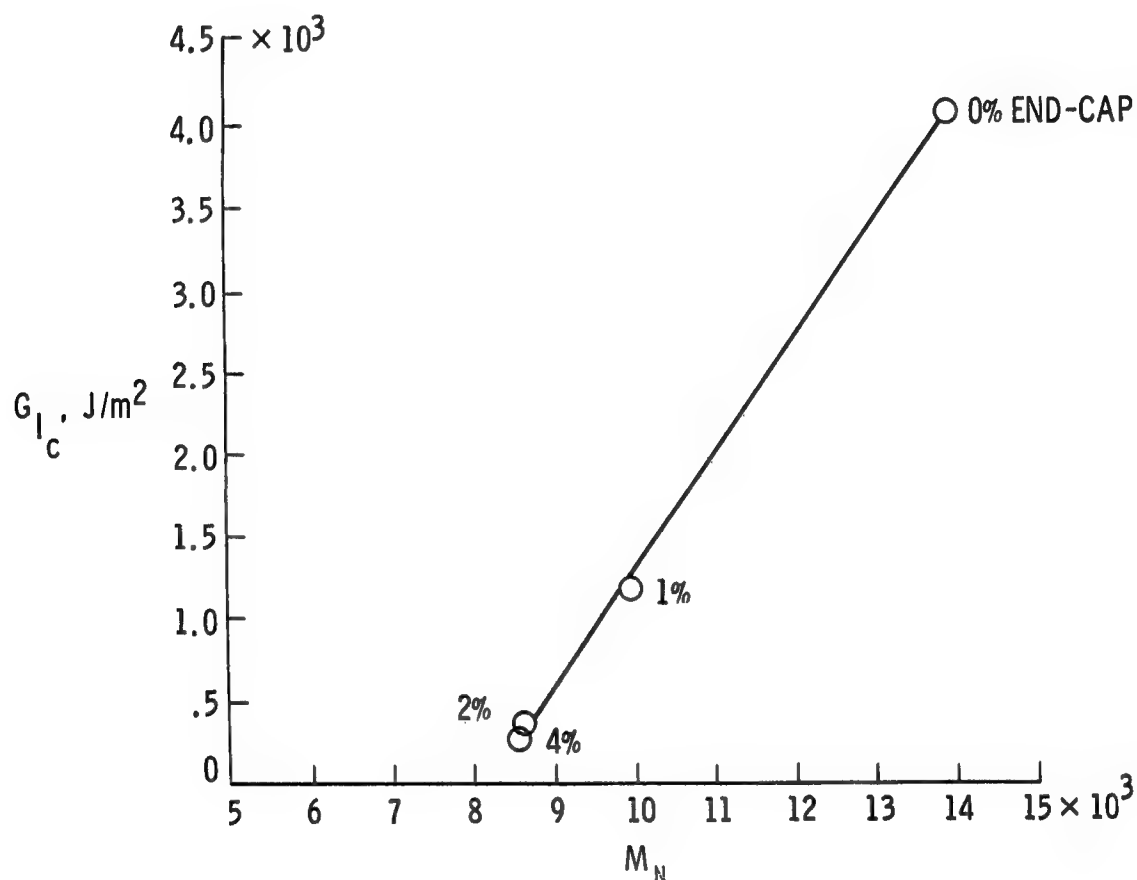
EFFECT OF MOLECULAR WEIGHT ON VISCOSITY

An objective of this research was to determine the effect of M_n on melt-flow properties of this polymer (BDSDA/APB). Based on the work of Fox and Flory (ref. 8) it was expected that as the M_n decreased the melt-flow would increase. However, their work was on another polymer and the degree of change must be determined for each individual polymer system. In the endcapped polyimide study there was a direct relationship between M_n and apparent viscosity as shown in the figure. At 250°C there was no deviation from linearity, but at the higher extrusion temperature of 280°C the viscosity dropped precipitously for the systems with an M_n below 10,000. The apparent viscosity of the 4% endcapped material was too low at 280°C for the capillary rheometer to measure. Particularly noteworthy was the drop of two orders in magnitude for the apparent viscosity at 250°C when the M_n changed from approximately 14,000 to 8,700 amu. This information should be valuable in optimizing processability.



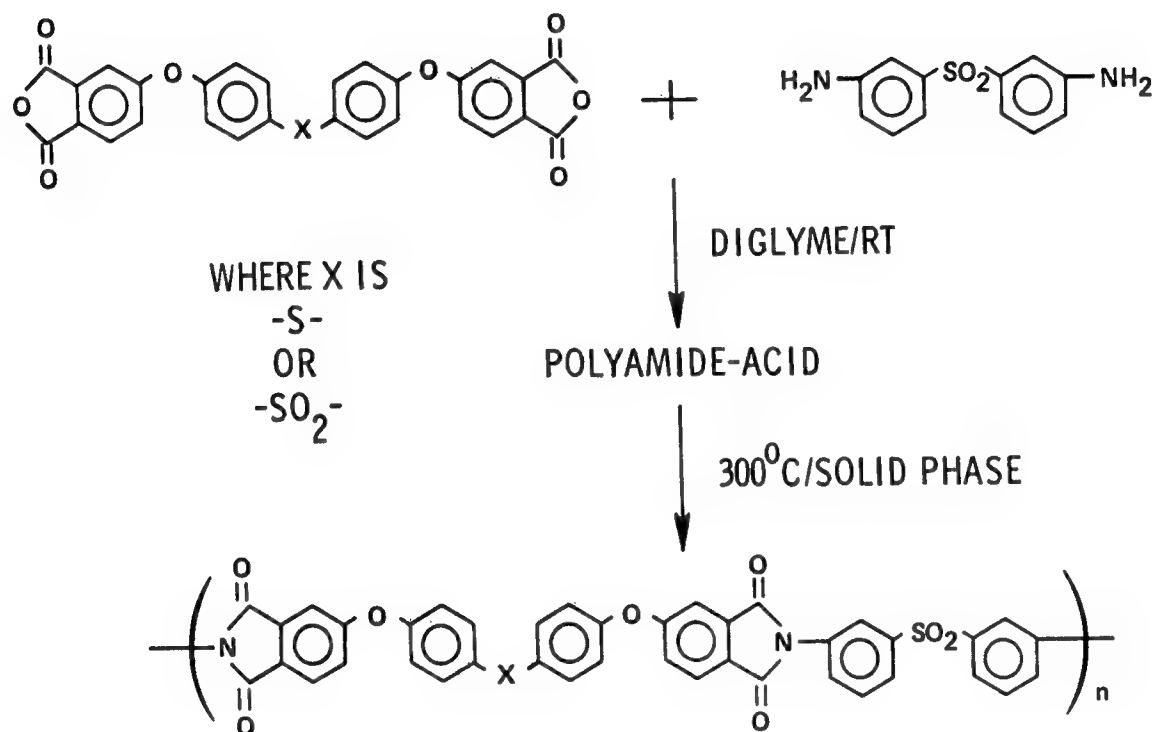
EFFECT OF MOLECULAR WEIGHT ON TOUGHNESS

When moldings were prepared from the different molecular weight polymers, it was obvious that the higher M_n systems resisted cracking more than the lower M_n systems. The G_{IC} data proved that a considerable loss in fracture resistance does occur as the molecular weight decreases. This relationship is shown in the figure. Of particular interest was that over the range tested the G_{IC} value was linearly related to the number-average molecular weight. The steep slope of this relationship was quite surprising. A change in M_n from 14,000 to 10,000 amu resulted in nearly a 3000 J/m² loss in G_{IC} .



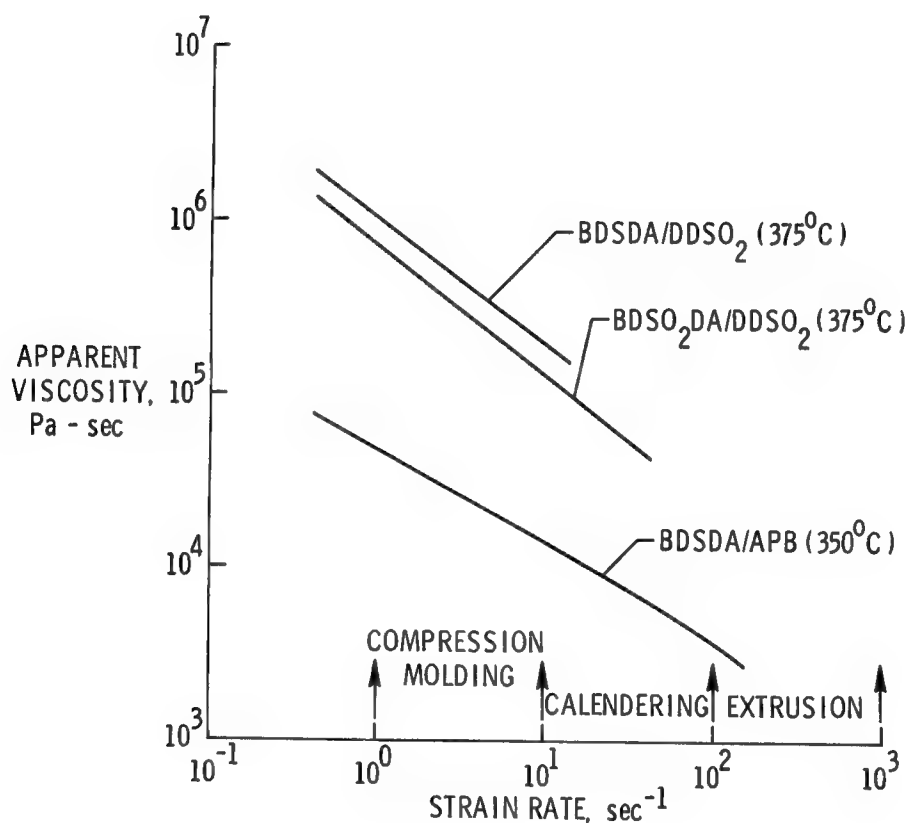
SYNTHESIS OF TWO PROCESSABLE POLYIMIDES

In an effort to further research the area two additional hot-melt processable polyimides have been prepared (ref. 9). These materials have oxygen, sulfur and bridges which link the aromatic rings through both the para and meta positions. The synthesis of the amide-acid polymer was accomplished at room temperature in diglyme as the solvent. These polymers were precipitated in water and after air-drying overnight they were imidized in a forced-air oven at 300°C.



VISCOSITY/STRAIN RATE DATA

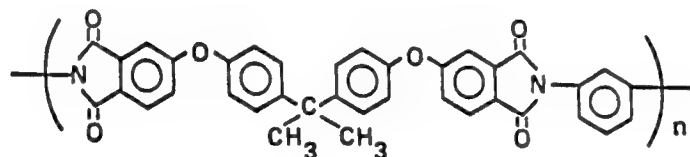
The apparent viscosity as a function of strain rate is shown in the figure for the two new polyimides. The BDSDA/APB viscosity/strain rate characteristics are shown for comparison. The new materials exhibited continuous flow over the strain rate regime indicated. However, this flow is not continuous to the higher strain rate levels as it was for the BDSDA/APB. Both of the new materials required a higher processing temperature and exhibited higher viscosity values. Nevertheless, both materials show promise for hot-melt processing.



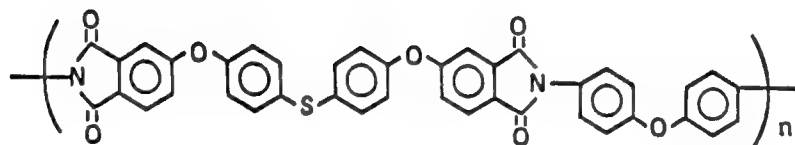
COMMERCIALLY PROMISING PROCESSABLE POLYIMIDES

Presently there are two polyimides that are available and attractive for hot-melt processing into fiber-reinforced laminates. These are Ultem® from General Electric and the NASA Langley BDSDA/ODA (LARC-ODA). The LARC-ODA is available in experimental quantities from M&T Chemicals (Rahway, NJ). This material has also been prepregged onto woven graphite by American Cyanamid (Hayre de Grace, MD). Both systems exhibit very high G_{IC} values, 3700 J/m² for Ultem and 5400 J/m² for LARC-ODA.

Unfortunately, the Ultem is only available in the imidized form which causes difficulty in the preparation of composites for two reasons. First, when attempts have been made to hot melt impregnate fiber, poor wet-out of the fiber occurs. Second, any solvent used to dissolve the Ultem for solvent impregnation is tenaciously held by the polymer during the entire fabrication operation. Since the LARC-ODA is made as an amide acid it is soluble in solvents that are easily excluded when the material converts to the insoluble imide.



ULTEM - GENERAL ELECTRIC



BDSDA-ODA LaRC

SUMMARY

Several polyimides have been prepared which show promise for aircraft composite applications. This has been achieved through a systematic polymer synthesis program where the glass transition temperatures have been greatly lowered when compared to the older polyimide systems. Several of the materials have been shown to be hot-melt processable and are attractive matrix resin candidates especially in light of their high G_{IC} values. At least two of these polyimides are available for evaluation and others are on the research horizon.

- o SEVERAL PROCESSABLE PIs HAVE BEEN PREPARED
- o A SYSTEMATIC DECREASE IN PROCESSING TEMPERATURE HAS BEEN ACHIEVED
- o PROMISING COMMERCIAL CANDIDATES HAVE BEEN IDENTIFIED
- o SCALE-UP OF SEVERAL POLYMERS HAS BEEN ACCOMPLISHED

REFERENCES

1. St. Clair, A. K. and St. Clair, T. L.: A Multi-Purpose Thermoplastic Polyimide. Material and Process Applications: Land, Sea, Air, and Space, 26th National SAMPE Symposium and Exhibition 26, pp. 165-173, 1981.
2. St. Clair, T. L. and Yamaki, D. A.: A Thermoplastic Polyimidesulfone. NASA TM 84574, November 1982.
3. Burks, H. D. and St. Clair, T. L.: Synthesis and Characterization of a Melt Processable Polyimide. NASA TM 84494, May 1982.
4. Standard Test Method for Strength Properties of Adhesives in Shear by Tension Loading (Metal-to-Metal), ASTM Standard D 1002-72, 1982 Annual Book of ASTM Standards, Part 10, 1982.
5. Torlon Applications Guide, Amoco Chemical Corp., p. 11, Feb. 1979.
6. VanWazer, J. R.; Lyons, L. W.; Kim, K. Y.; and Colwell, R. E.: Viscosity and Flow Measurements, Interscience Publishers, New York, NY, p. 193, 1963.
7. Burks, H. D. and St. Clair, T. L.: The Effect of Molecular Weight on the Melt Viscosity and Fracture Energy of BDSDA/APB. J. of Applied Polymer Science, vol. 29, pp. 1027-1030, March 1984.
8. Fox, T. G. and Flory, P. J.: Second-Order Transition Temperatures and Related Properties of Polystyrene. J. of Applied Physics, 21, p. 581, 1950.
9. Burks, H. D. and St. Clair, T. L.: Synthesis and Characterization of a Polyethersulfoneimide. NASA TM 84621, April 1983.

ALIPHATIC-AROMATIC HETEROCYCLICS AS POTENTIAL
THERMOPLASTICS FOR COMPOSITE MATRICES

Chad B. Delano and Charles J. Kiskiras
Acurex Corporation
Aerotherm Division
Mountain View, California

INTRODUCTION

The successful development of impact- and solvent-resistant thermoplastic systems for glass and graphite composites is particularly attractive because of the demonstrated streamlined manufacturability of such composites. Hypothetically, thermoplastics only require simple heating and cooling cycles for component manufacture, whereas thermosets require precise, and possibly extended heating schedules which must be consistent with the cure chemistry. The sensitivity of the majority of existing thermoplastics to aircraft fluids and other solvents preempts their serious consideration in aircraft components. This is the basic reason that Acurex proposed insolubility in common solvents as the starting point for this NASA Langley sponsored program. The target properties for the new thermoplastic resin are summarized in Figure 1.

- PREPREG PROPERTIES
 - USE OF CONVENTIONAL PREPREGGING EQUIPMENT
 - 6+ MONTHS SHELF STABILITY
 - PROCESSABILITY: 316°C, 0.69 MPa (600°C, 100 PSI)
 - THERMOFORMABILITY
- COMPOSITE PROPERTIES
 - -54°C TO 93°C CAPABILITY
 - GOOD MECHANICAL PROPERTIES
 - GOOD ENVIRONMENTAL PROPERTIES (UNDER STRESS)
 - IMPACT RESISTANCE

*IN PROGRESS NAS1-16808 -- DEVELOPMENT OF AN IMPACT AND SOLVENT RESISTANT COMPOSITE MATRIX

Figure 1

PBI-8

Several aliphatic-aromatic heterocyclic polymers have been reported in the literature; however, systematic studies of their properties as thermoplastics are not readily available. Acurex was attracted to this class of polymers for the excellent solvent resistance demonstrated by the polybenzimidazole from 3,3',4',4'-tetraaminobiphenyl with sebacic acid (PBI-8). Its solvent resistance is compared to the solvent resistance of polysulfone and polyphenylene oxide (PPO) in Figure 2.

Property	PBI-8 ^a	Polysulfone	PPO
Heat deflection temperature, °F	420	345	375
Thermal coefficient of expansion in./in./°F	4.1 x 10 ⁻⁵	3.1 x 10 ⁻⁵	2.9 x 10 ⁻⁵
Specific gravity	1.17	1.24	1.06
Water absorption, percent (24 hr)	0.28	0.22	0.06
Tensile strength, psi at 72°F at 275°F	11,000 4,500	10,200	11,000
Tensile elongation, percent at 72°F	5	50 to 100	50 to 80
Modulus, psi at 72°C	3.4 x 10 ⁵	3.9 x 10 ⁵	3.7 x 10 ⁵
Solvent resistance ^b			
Aliphatic hydrocarbons	N	N	N
Aromatic hydrocarbons	N	P	S
Chlorinated hydrocarbons	N	S	S
Ketones	N	S	P

^aPBI-8 = Acurex's melt processible PBI

^bN = no effect; P = partially soluble; S = soluble

Figure 2

APPROACH

The Acurex approach included selection of several flexible and rigid segments for two classes of polymers as outlined in Figure 3.

- SOFT (FLEXIBLE) SEGMENT-RIGID SEGMENT POLYMERS
- ALIPHATIC-AROMATIC HETEROCYCLIC POLYMERS
 - ALIPHATIC POLYIMIDES
 - ALIPHATIC POLYBENZIMIDAZOLES

Figure 3

POLYIMIDE STRUCTURES

The flexible and rigid segments selected for investigation of polyimides are indicated in Figure 4. The dianhydrides investigated were pyromellitic dianhydride (PMDA), 3,3',4,4'-benzophenonetetracarboxylic dianhydride (BTDA) and 5-(2,5-diketotetrahydrofuryl)-3-methyl-3-cyclohexene-1,2-dicarboxylic dianhydride (MCTC). The diamines investigated were 1,6-hexanediamine, 1,8-octanediamine (ODA) and 1,12-dodecanediamine.

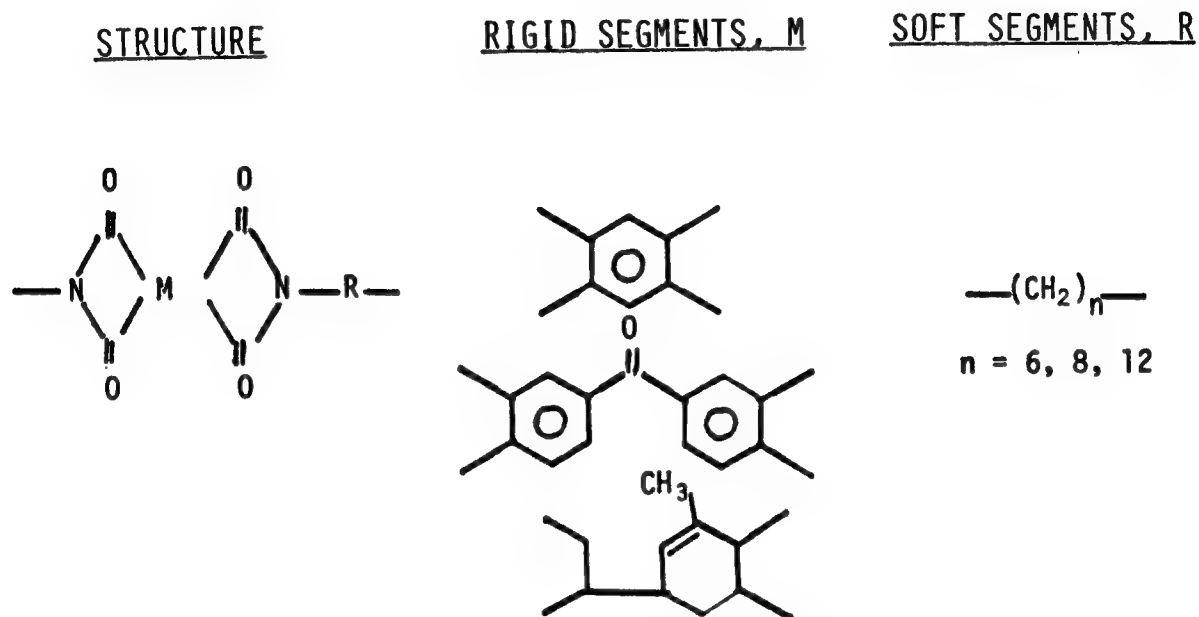


Figure 4

LINEAR ALIPHATIC POLYIMIDES FROM CONDENSATION IN CRESOL

We succeeded in polymerizing most of the monomer combinations indicated in Figure 4 by condensation in cresol solution. The inherent viscosities obtained on the polymers are indicated in Figure 5. The crystalline polyimide from PMDA with 1,8-octanediamine routinely provides very high inherent viscosities.

	<u>REACTANTS</u>	<u>VISCOSITY, DL/GM IN H₂SO₄</u>
PMDA	1,6-HEXANEDIAMINE	1.05
	1,8-OCTANEDIAMINE	3.32
	1,12-DODECANEDIAMINE	1.16
BTDA	1,6-HEXANEDIAMINE	1.70
	1,8-OCTANEDIAMINE	1.66, 1.54 (<1 PERCENT INSOLUBLES)
	1,12-DODECANEDIAMINE	1.00 (24 PERCENT INSOLUBLES)
MCTC	1,8-OCTANEDIAMINE	0.84

- INSOLUBLES CAUSED BY CONDENSATION AT HIGH TEMPERATURES (E.G., MELT CONDENSATION)
- PMDA POLYMERS ARE CRYSTALLINE
- HIGH MOLECULAR WEIGHT POLYMERS ARE ACHIEVED WITH SOLUTION CONDENSATION

Figure 5

POLYBENZIMIDAZOLE STRUCTURES

Flexible and rigid segments selected for investigation of polybenzimidazoles are indicated in Figure 6. The tetraamines investigated were 3,3',4,4'-tetraaminobiphenyl (TAB) and 4,4'-bis(o-aminoanilino)biphenyl. The aliphatic diacids investigated were suberic, sebacic, and 1,12-dodecanedicarboxylic acids.

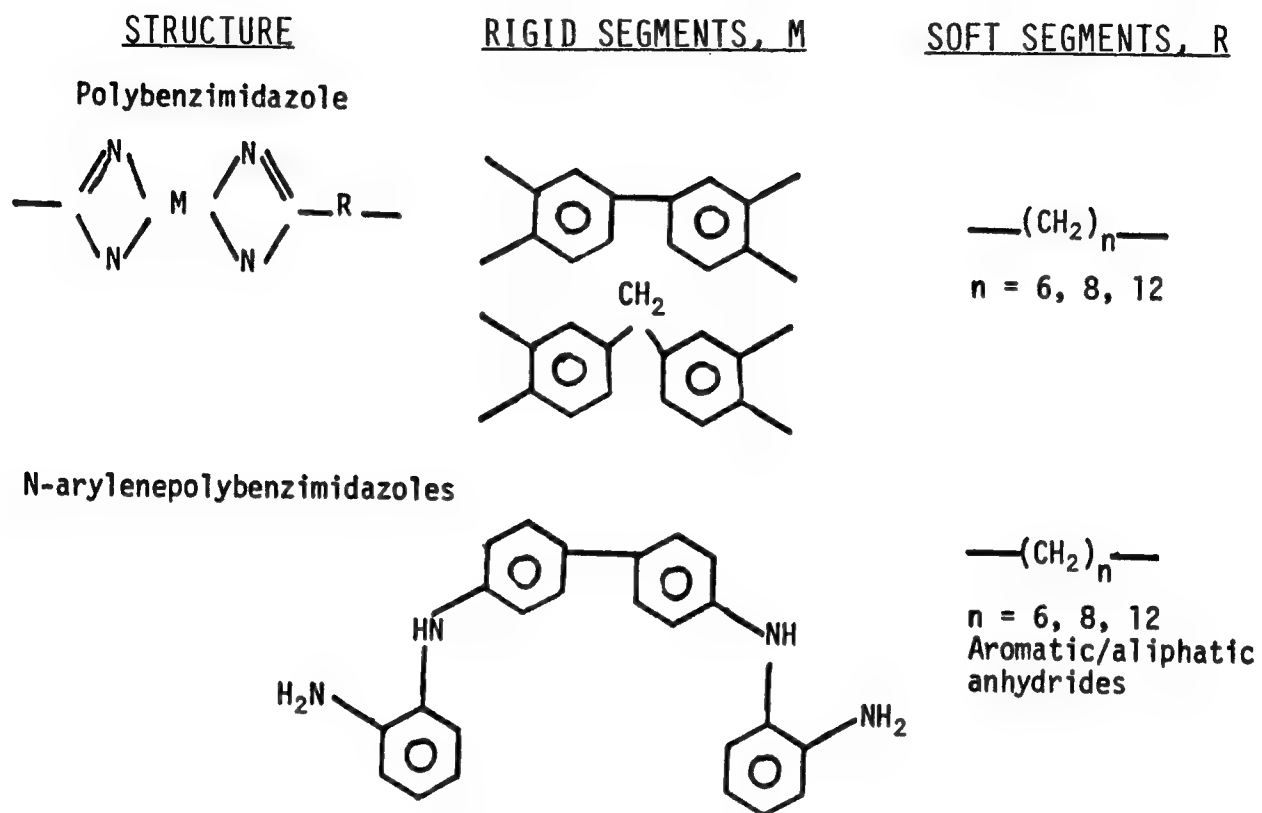


Figure 6

LINEAR ALIPHATIC POLYBENZIMIDAZOLES

We were successful in melt polymerizing several polybenzimidazoles which were subsequently characterized for both Tg and solvent resistance. Inherent viscosities of the polymers from the two types of polybenzimidazoles are indicated in Figure 7.

<u>REACTANTS</u>	<u>VISCOSITY, DL/GM</u>
3,3',4,4'-TETRAAMINOBIPHENYL	
SUBERIC ACID	1.59 (H ₂ SO ₄ -- 33% INSOLUBLES)
SEBACIC ACID	2.69 " 22% "
1,12-DODECANEDICARBOXYLIC ACID	2.31 " 7.2% "
4,4'-BIS(O-AMINOANILINO) BIPHENYL	
SUBERIC ACID	1.10 (H ₂ SO ₄)
SEBACIC ACID	0.88 (CRESOL)
1,12-DODECANEDICARBOXYLIC ACID	0.68 (H ₂ SO ₄ -- 3.5% INSOLUBLES)
METHYLHEXAHYDROPHthalic ANHYDRIDE	CLEAR 1.10; OPAQUE 1.62 (CRESOL)
PHTHALIC ANHYDRIDE	0.92 (H ₂ SO ₄)

- MELT CONDENSATION PRODUCES TOUGH POLYMERS

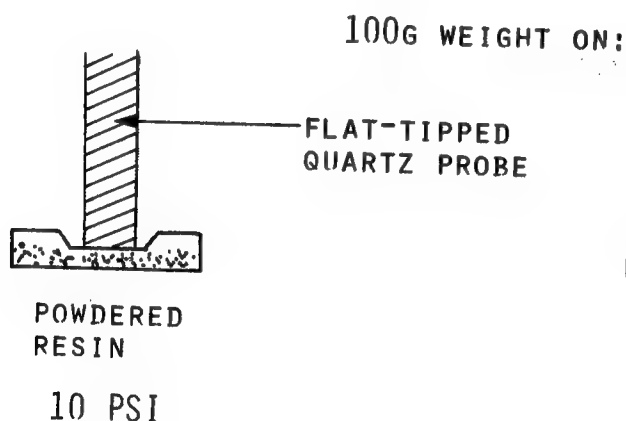
Figure 7

FLOW BY TMA

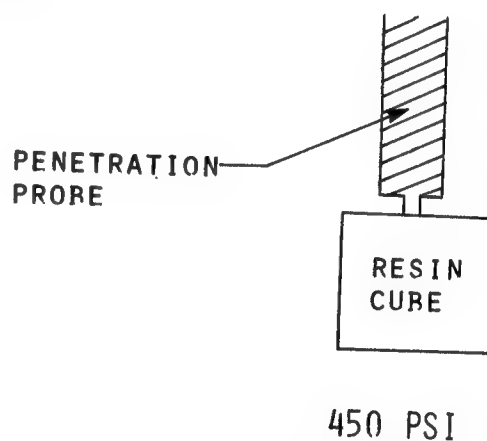
We found that the flow properties of powdered resin samples could be determined conveniently in the laboratory by placing the powder between two DSC cups* as sketched in Figure 8 and generating the familiar TMA† curves. Initial trial molding temperatures for each polymer were selected from such curves and after obtaining molded resin specimens TMA curves were conducted at higher penetration pressures for heat distortion temperature simulation to provide indication of upper use temperatures for each polymer composition. This latter test procedure is also sketched in Figure 8.

*Small thin metal dishes used in differential scanning calorimetry (DSC)
†Thermomechanical analysis (TMA)

MELT FLOW BY TMA



DISTORTION TEMPERATURE UNDER LOAD



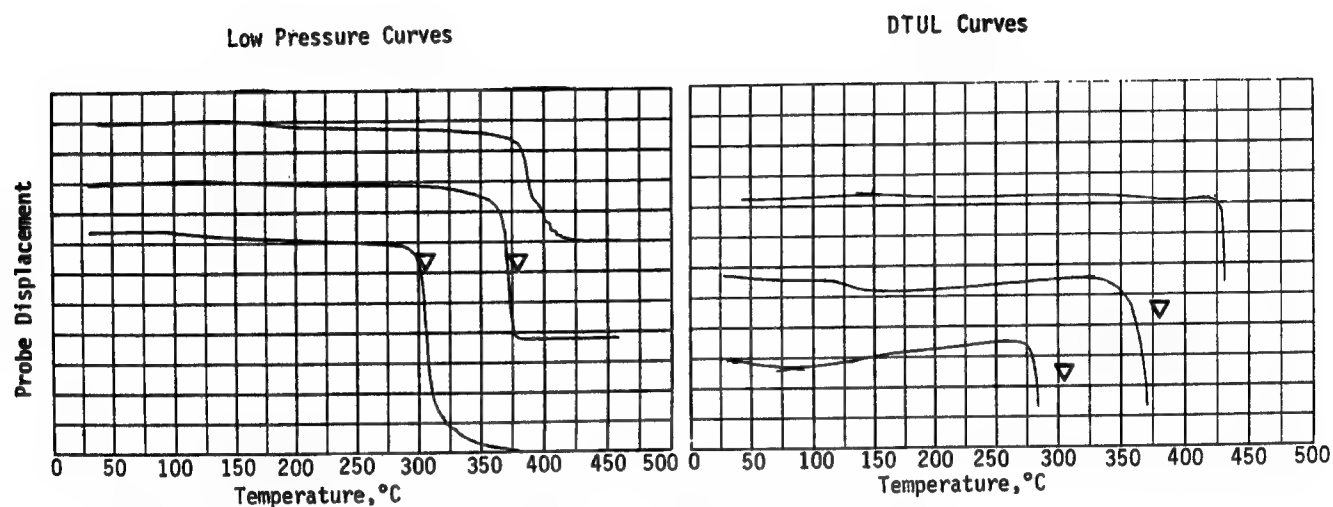
- PROCEDURES EMPLOYED FOR DETERMINING MOLDING CONDITIONS AND UPPER USE TEMPERATURES

Figure 8

FLOW CURVES FOR ALIPHATIC POLYIMIDES

Low pressure and distortion temperature under load (DTUL) curves for the PMDA-based polyimides are indicated in Figure 9. DSC analysis showed these polyimides to be crystalline. The T_m^* is indicated on the diagram by the triangle and is seen to control the flow properties of the polymer.

* T_m = crystalline melting temperature



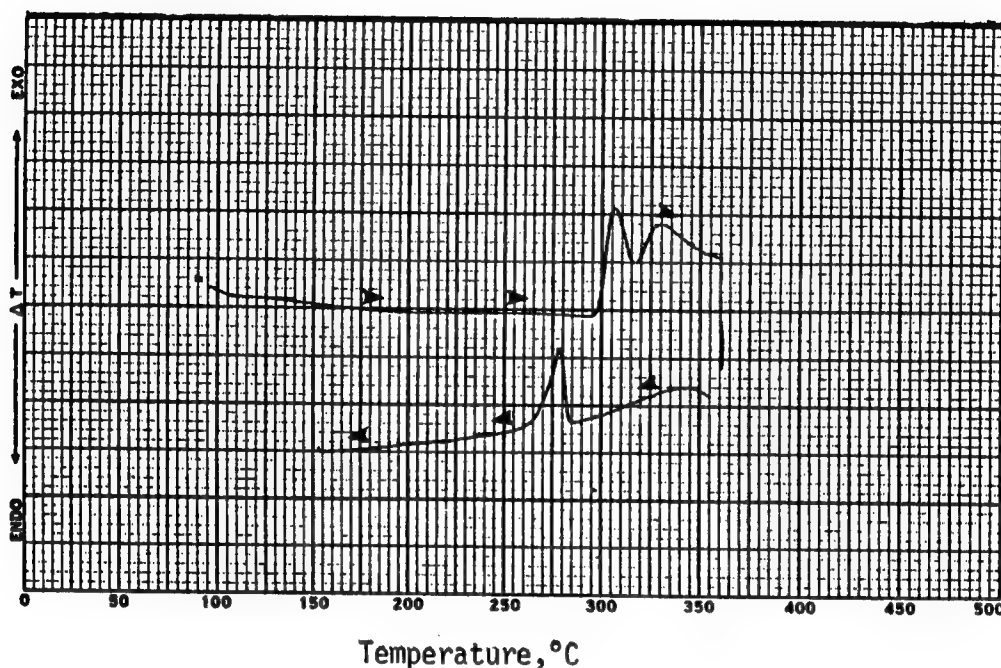
PMDA with C_6 , C_8 , and C_{12} diamines (top to bottom curves respectively)

- INVERSE RELATIONSHIP BETWEEN T_m AND DIAMINE LENGTH EXISTS
- 450 PSI COMPRESSIVE LOAD DID NOT PENETRATE UNTIL T_m REACHED

Figure 9

DSC CURVES FOR PMDA/1,12-DODECANEDIAMINE POLYIMIDE

The heating curve shown in Figure 10 shows an endotherm close to 315°C and an exotherm upon cooldown close to 230°C for this polyimide. Its crystallinity was confirmed by X-ray analysis. As indicated in the previous figure the degree of crystallinity is high enough to control its flow properties and support the 450 psi compressive load (DTUL measurement) to very high temperatures.

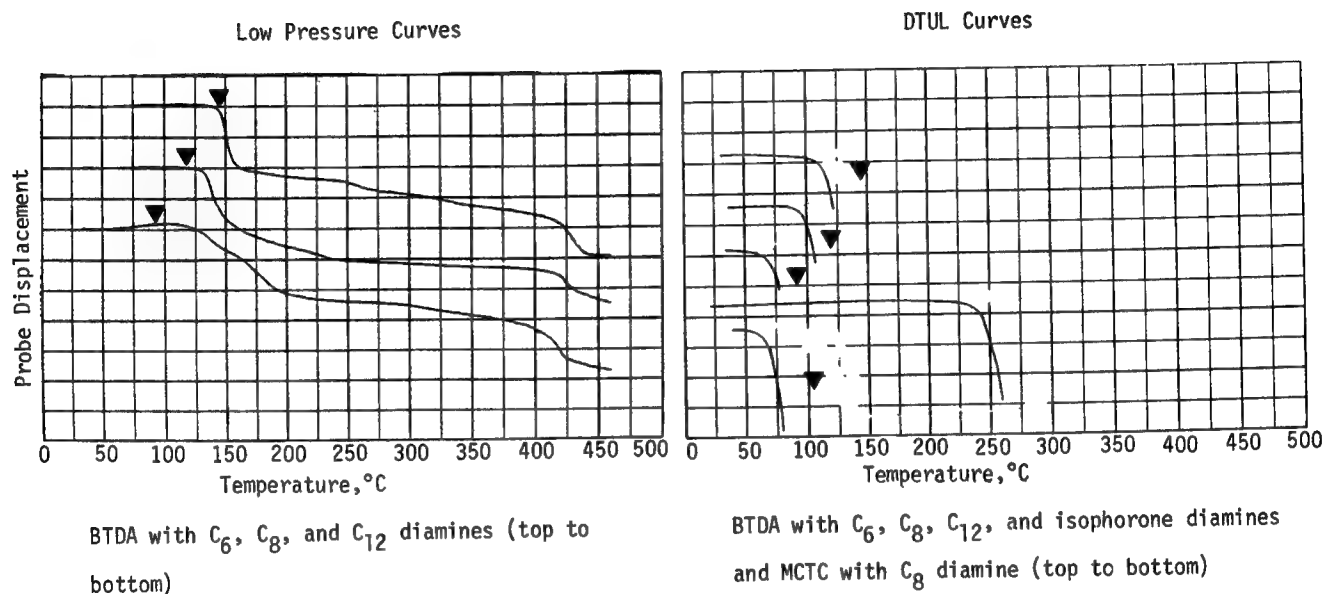


• THERMAL CRYSTALLIZATION

Figure 10

FLOW CURVES FOR ALIPHATIC POLYIMIDES

Low pressure flow and DTUL curves for the BTDA- and MCTC-based polyimides are provided in Figure 11. DSC analysis of these polymers provided T_g which is indicated on the diagrams. The T_g of these noncrystalline systems clearly controls their flow properties.

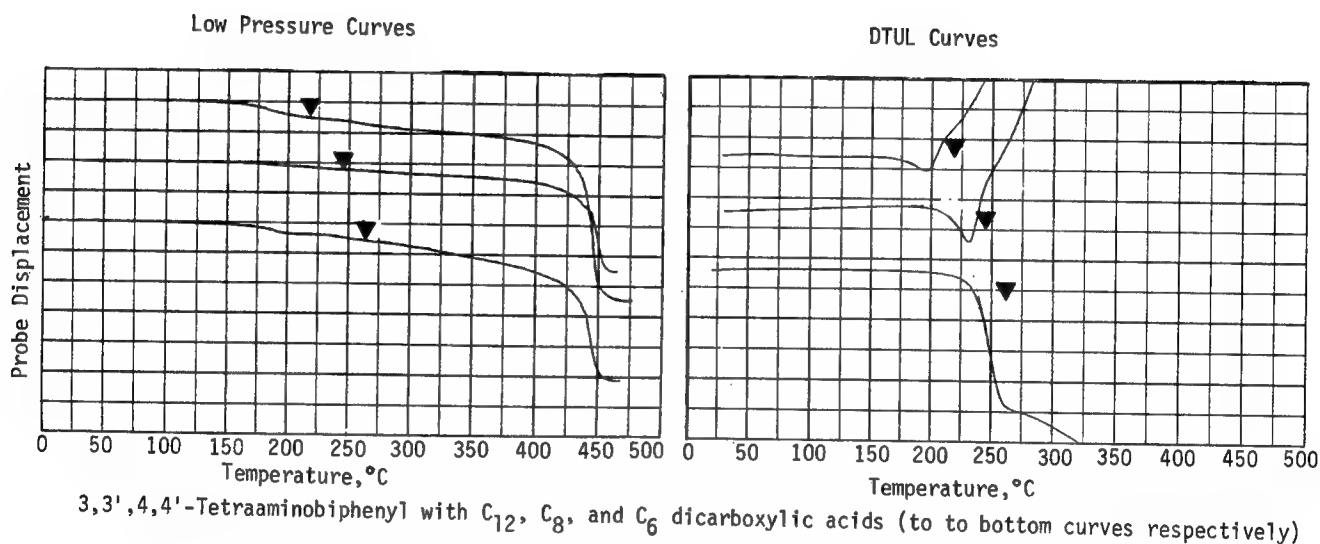


- BTDA POLYMERS DID NOT SHOW CRYSTALLINITY
- EXPECTED HIGH T_g OBTAINED WITH CYCLOALIPHATIC COMPARED TO LINEAR ALIPHATIC DIAMINE

Figure 11

FLOW CURVES FOR ALIPHATIC POLYBENZIMIDAZOLE

Low pressure flow and DTUL curves for the aliphatic polybenzimidazoles are shown in Figure 12. Unlike the flow curves for the polyimides shown in Figures 9 and 11 where low pressure and 450 psi pressure produce approximately the same flow properties, significant differences exist between the flow properties of the aliphatic polybenzimidazole under the two conditions. Lower molecular weight polymers frequently do flow under low pressure testing at lower temperatures. Thermal history of the polymers prior to flow testing appears to play an important role in the flow properties of these systems.



- HIGH MOLECULAR WEIGHT POLYMERS DO NOT FLOW AT LOW PRESSURES UNTIL FAR ABOVE T_G
- 450 PSI COMPRESSIVE LOAD PENETRATED POLYMERS AT MUCH LOWER TEMPERATURES

Figure 12

FLOW CURVES FOR N-ARYLENEPOLYBENZIMIDZOLES

Figure 13 provide the low pressure and DTUL curves of the aliphatic N-arylenepolybenzimidazoles. The T_g indicated on the diagrams appears to control the flow properties of these polymers except for the low pressure curve for the polymer from suberic acid which as prepared was crystalline. The molded polymer was not crystalline.

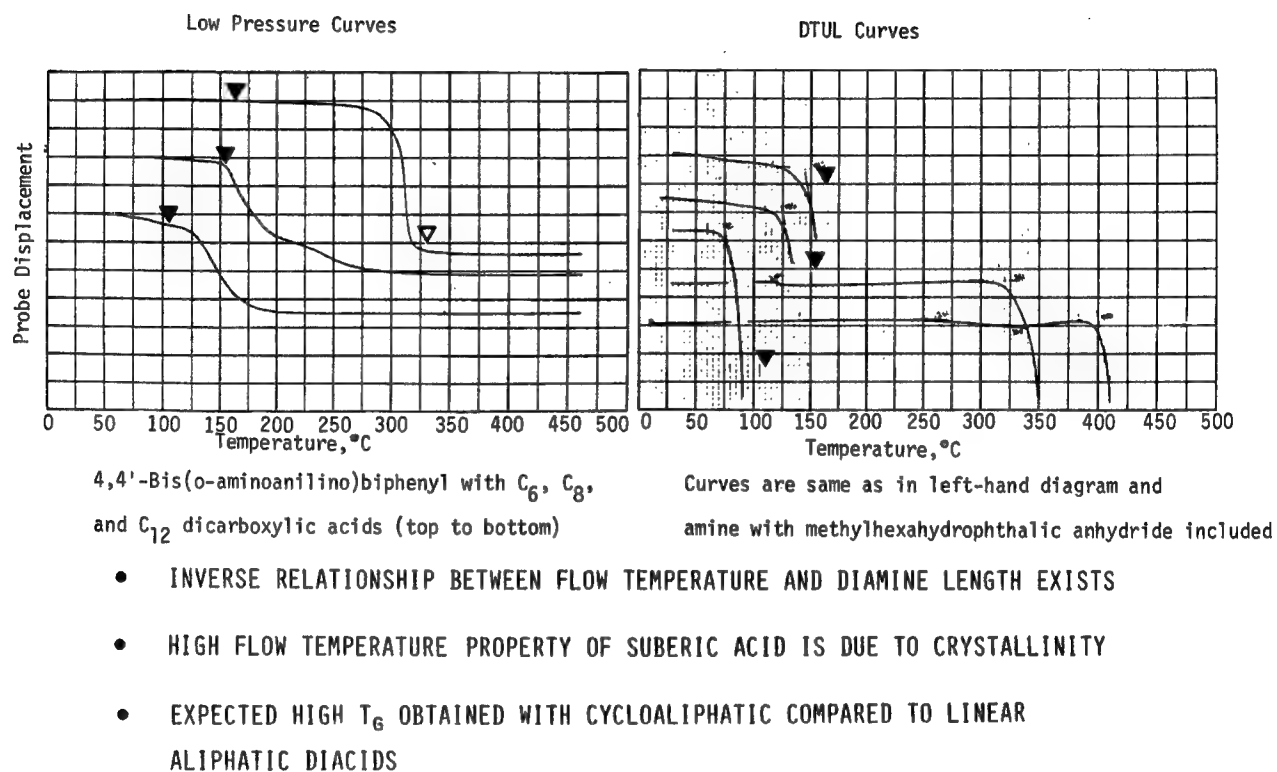


Figure 13

DRY AND WET POLYMER PROPERTIES OF POLYIMIDES

Twenty-four hour water boil properties of epoxy resins show weight gains of approximately 5 percent. The weight gains of most of the polyimide moldings are much lower than epoxy resins and the environmental moisture durability of these systems would be predicted to be superior to epoxy resins. These values are indicated in Figure 14. One usually associates high barcol hardness values with composite matrix resins and most of the aliphatic polyimides investigated do not give high hardness values.

POLYMER	SPECIFIC GRAVITY (g/cc)	HARDNESS OF MOLDING		DTUL MEASUREMENTS (°C)				SAMPLE WEIGHT GAIN DUE TO 24-HR WATER BOIL (PERCENT)
				INITIAL DRY		24-HR WATER BOILED	INTERCEPT SHIFT DUE TO MOISTURE (°C)	
		BARCOL	SHORE D	INTERCEPT				
POLYIMIDES								
PMDA, C ₆ DIAMINE	1.38	a	a	148	428	278	-150	0.9
PMDA, C ₈ DIAMINE	1.28	6-10	--	108	353	350	-3	0.2
PMDA, C ₁₂ DIAMINE	1.20	0	65	NOT CLEAR	278	282	+4	0.0
BTDA, C ₆ DIAMINE	1.32	20	--	98	113	102	-11	3.9
BTDA, C ₈ DIAMINE	1.28	0	65	79	98	85	-13	1.6
BTDA, C ₁₂ DIAMINE	1.21	0	45	59	72	63	-19	0.9
BTDA, ISOPHORONEDIAMINE	1.14	a	a	222	242	130	-112	3.6
BTDA, C ₈ DIAMINE AND M-PHENYLENEDIAMINE		40	--	155	187	180	-7	0.9
MCTC, C ₈ DIAMINE	1.12	0	60	48	67	62	-5	9.2

*SAMPLE BREAKS DURING HARDNESS TESTING

MOISTURE WEIGHT GAIN OF PMDA POLYMERS IS REMARKABLY LOW
 MARKED IMPROVEMENT IN BARCOL HARDNESS OCCURS WITH M-PHENYLENEDIAMINE
 COREACTANT

Figure 14

DRY AND WET POLYMER PROPERTIES OF POLYBENZIMIDAZOLES

Twenty-four hour water boil of the aliphatic polybenzimidazoles does not appear to offer much improvement over incumbent epoxy resins except with the 1,12-dodecanedicarboxylic acid system. The N-arylenepolyimidazoles appear to offer improved moisture resistance over the classical polybenzimidazoles (Figure 15).

POLYMER	SPECIFIC GRAVITY (g/cc)	HARDNESS OF MOLDING		DTUL MEASUREMENTS (°C)				SAMPLE WEIGHT GAIN DUE TO 24-HR WATER BOIL (PERCENT)
				INITIAL DRY		24-HR WATER BOILED	INTERCEPT SHIFT DUE TO MOISTURE (°C)	
		BARCOL	SHORE D	DEVIATION FROM LINEARITY	INTERCEPT	INTERCEPT		
<u>PBIs</u>								
FROM C ₆ DICARBOXYLIC ACID	1.14	45	--	197	235	126	-109	7.9
FROM C ₈ DICARBOXYLIC ACID	1.12	30	--	185	207	127	-80	5.6
FROM C ₁₂ DICARBOXYLIC ACID	1.08	18	--	160	175	134	-41	4.3
<u>N-ARYLENE PBIs</u>								
FROM C ₆ DICARBOXYLIC ACID	1.17	15	--	115	143	118	-25	3.1
FROM C ₈ DICARBOXYLIC ACID	1.13	10	--	108	125	102	-23	3.6
FROM C ₁₂ DICARBOXYLIC ACID	1.12	a	75	58	75	63	-12	2.9
FROM PHTHALIC ANHYDRIDE	--	a	a	300	321	319	-2	1.2
FROM METHYLHEXAHYDROPHTHALIC ANHYDRIDE	1.10	a	a	260	400	407	+7	1.1

*SAMPLE BREAKS DURING HARDNESS TESTING

ALIPHATIC POLYBENZIMIDAZOLES HAVE GOOD BARCOL HARDNESSES

T_G LOSS DUE TO WATER BOIL IS NOT AS GOOD AS THE ALIPHATIC POLYIMIDES

Figure 15

SOLVENT SCREENING OF MOLDED SPECIMENS

As indicated in Figure 16 the unstressed solvent resistance of most of the polyimides is excellent when acetone or tricresylphosphate is the test solvent. Upon exposure to chloroform, however, only three polymers show good resistance to this solvent. Chloroform is considered to be very aggressive in comparison to other organic solvents in its ability to soften plastics. It is related to chlorinated paint strippers which must not degrade the composite.

POLYMER	SOLVENT, EXPOSURE TIME, PERCENT WEIGHT GAIN								
	ACETONE			CHLOROFORM			TCP		
	1 DAY	7 DAYS	50 DAYS	1 DAY	7 DAYS	50 DAYS	1 DAY	7 DAYS	50 DAYS
<u>POLYIMIDES</u>									
PMDA, C ₆ DIAMINE	0	0	0	0	0	--	1	2	0
PMDA, C ₈ DIAMINE	0	0	a	3	5	a	1	0	a
PMDA, C ₁₂ DIAMINE	1	1	3	12	30	29	0	0	0
BTDA, C ₆ DIAMINE	0	0	2	SWELLS			1	0	0
BTDA, C ₈ DIAMINE	2	6	11	SWELLS			0	0	0
BTDA, C ₁₂ DIAMINE	7	9	9	SWELLS			1	1	0
BTDA, ISOPHORONEDIAMINE	0	0	6	SWELLS			a	1	0
BTDA, C ₈ DIAMINE AND M-PHENYLENE DIAMINE	1	--	1	2	--	6	0	--	0
MCTC, C ₈ DIAMINE	SWELLS			DISSOLVED			SWELLS	DISSOLVED	

*SAMPLE USED FOR DTUL MEASUREMENT

COMMON SOLVENT RESISTANCE OF PMDA/ODA AND BTDA/ODA-MPDA POLYIMIDES
IS EXCELLENT

Figure 16

SOLVENT SCREENING OF MOLDED POLYBENZIMIDAZOLES

As indicated in Figure 17 the two classes of aliphatic polybenzimidazoles showed completely different responses to chloroform exposure. The unmodified N-arylenepolybenzimidazoles do not appear as a class to be suitable for use in composites where exposure to paint strippers can occur compared to the classical polybenzimidazoles which are excellent in this regard.

POLYMER	SOLVENT, EXPOSURE TIME, PERCENT WEIGHT GAIN								
	ACETONE			CHLOROFORM			TCP		
	1 DAY	7 DAYS	50 DAYS	1 DAY	7 DAYS	50 DAYS	1 DAY	7 DAYS	50 DAYS
<u>PBIs</u>									
FROM C ₆ DICARBOXYLIC ACID	0	0	0	0	0	--	4	4	5
FROM C ₈ DICARBOXYLIC ACID	0	0	a	0(0)	0(0)	a	1(0)	2(0)	a(0)
FROM C ₁₂ DICARBOXYLIC ACID	0	0	a	2	4	a	1	1	a
<u>N-ARYLENE PBIs</u>									
FROM C ₆ DICARBOXYLIC ACID	4	14	14	SWELLS			0	0	0
FROM C ₈ DICARBOXYLIC ACID	11	18	16	DISSOLVED			-2	-1	0
FROM C ₁₂ DICARBOXYLIC ACID	23	14	-2	DISSOLVED			-2	-5	HALF DISSOLVED
FROM PHTHALIC ANHYDRIDE	6	--	--	SWELLS			--	--	--
FROM METHYLHEXAHYDROPHthalic ANHYDRIDE	15	15	2	DISSOLVED			3	4	4

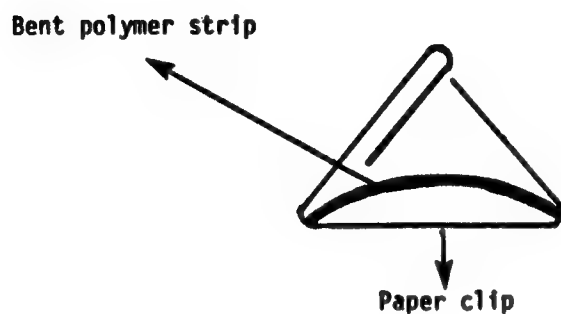
*SAMPLE USED FOR DTUL MEASUREMENT

COMMON SOLVENT RESISTANCE OF PBI'S IS EXCELLENT
COMMON SOLVENT RESISTANCE OF N-ARYLENE PBI'S IS POOR

Figure 17

STRESSED SOLVENT RESISTANCE OF SELECTED POLYMERS

Three aliphatic-aromatic heterocyclic thermoplastic composites were selected for stressed solvent resistance testing. The composition of these polymers and the test method are indicated in Figure 18.



500 HR EXPOSURE TO ACETONE, CHLOROFORM AND TCP GAVE NO EVIDENCE OF FAILURE

- POLYIMIDES FROM PMDA/1,8-OCTANE DIAMINE AND BTDA/1,8-OCTANE DIAMINE-M-PHENYLENE DIAMINE
- POLYBENZIMIDAZOLE FROM 3,3',4,4'-TETRAAMINOBIIPHENYL/SEBACIC ACID

Figure 18

POLYMER SELECTIONS

The properties of the three selected polymers which showed no effect under stressed solvent testing are summarized in Figure 19. Tensile properties of the systems are also indicated. The low tensile strength of the polyimide from PMDA with 1,8-octanediamine needs comment. The first molding of this system was very tough and nearly clear. The second molding was opaque and fracture sensitive. The latter molding was used in the tensile testing and gave premature failure. The modulus of this system needs to be redetermined. The polyimide from BTDA with 1,8-octanediamine and m-phenylene diamine was selected for further investigation.

	MOLD TEMP., °C	BARCOL HARDNESS	DRY ^a DTUL, °C	WET ^a DTUL, °C	TENSILE PROPERTIES
<u>POLYIMIDES</u>					STRENGTH, PSI/ELONGATION, %/MODULUS, PSI ^b
PMDA WITH C ₈ DIAMINE	725	10	108 (353)	95 (350)	4,400/3/166,000
BTDA WITH C ₈ DIAMINE AND M-PHENYLENE DIAMINE	510	40	155 (187)	148 (180)	17,000/14/177,000
<u>POLYBENZIMIDAZOLES</u>					
TAB WITH SEBACIC ACID	725	25	185 (207)	120 (126)	14,700/10/166,000

^aDEVIATION FROM LINEARITY VALUES; INTERCEPT VALUES ARE IN PARENTHESIS
^bTANGENT MODULUS, NOT INITIAL MODULUS

Figure 19

FIRST YEAR'S KEY PROGRAM RESULTS

The results of the first year's investigation on the aliphatic-aromatic heterocycle thermoplastics are summarized in Figure 20. The program results suggest that a number of these types of systems could be devised; for example, a benzoxazole rigid segment might be a candidate.

- DEVELOPED POLYMERIZATION FOR POLYIMIDES WHICH PRODUCES VERY HIGH MOLECULAR WEIGHT POLYMERS
- DEVELOPED POLYMERS WHICH OBTAIN COMMON SOLVENT INSENSITIVITY BY THREE MECHANISMS
 1. CRYSTALLINE POLYMERS
 2. INSOLUBLE SEGMENT COPOLYMERS
 3. HYDROGEN BONDED POLYMERS
- MILESTONE OF MOLDABLE, COMMON SOLVENT INSENSITIVITY ACHIEVED
- PROGRAM RESULTS SUGGEST THAT MANY SOLVENT RESISTANT, HIGH TENSILE ELONGATION RESINS CAN BE DEVELOPED

Figure 20

WORKING GROUP SUMMARIES

SESSION I: COMPOSITE FRACTURE TOUGHNESS AND
IMPACT CHARACTERIZATION

T. K. O'Brien, Chairman

The basic threat to the more widespread use of composites in aircraft primary structure is the problem of residual strength in the presence of damage. Specific problem areas that need to be addressed include the following:

1. Modeling/understanding composite failure
 - a. Impact: relate strain energy release rate (G_{Ic}) to strain-to-failure
 - b. Open hole compression: relate shear crippling to strain-to-failure
 - c. Account for variables such as thickness and stacking sequence
2. Micromechanics models: develop a pragmatic model to serve as a "useful guide"
3. Consider the use of hybrid combinations, both interply and intraply, using graphite, Kevlar, and glass
4. Modeling/understanding the role of the interface

The chemists envision a strong need for an "all-inclusive" micromechanics model that will allow them to measure neat resin (and interface) properties and estimate their influence on composite properties. This need is especially strong in relating neat resin fracture toughness to composite interlaminar fracture toughness. Chemists continue to emphasize that specimen size should be "small."

The mechanics and material science community has many reservations about committing large amounts of dollars and resources to developing a single, all-inclusive micromechanics model. They point out that over the past 20 years micromechanics has been reasonably useful for predicting bulk properties (modulus) but has not been useful for predicting damage and ultimate failures (strength). Since toughness falls into the latter category, the mechanics community is very skeptical of the possibility of a successful micromechanics bridge of the gap between neat resin fracture toughness (and some interface property measurement) and composite interlaminar fracture toughness. The attempt to bridge this gap should be pragmatic. It would be best to identify those who have sound ideas for attempting to bridge the toughness gap and establish a small concentrated effort to develop, if not an all-inclusive model or strong predictive tool, at least a useful guide.

One concern about the development of micromechanics models to predict ultimate properties (toughness) was the fear that the major result would be a lot of solutions to boundary value problems. It was stated that what is needed instead is a multidisciplinary approach involving new physics, new concepts, and a lot of new material inputs to get a very realistic appraisal of how the constituents behave and how they interact together.

Concern was expressed that the bulk properties of matrix materials are not those that should be used in micromechanics models. The bulk properties we measure come from relatively large samples. In the composite, the bulk of the resin occupies 5 to 10 μm , and the resin properties at that scale may have only a limited relationship to those measured from large specimens. It was strongly suggested that this is a first-order effect and should be addressed soon, especially in view of the long-range program NASA has established.

Only the mechanics group focused on the gap between composite material and structural laminate properties. The group agreed that the most important and most urgent tasks were in this area. Although what needs to be done in this area is a little more clear cut, the problems are not simple or solvable in the near future. Further, solving these problems involves a multidisciplinary approach including dynamics, structural stability, composite mechanics, and fracture mechanics.

SESSION II: CONSTITUENT PROPERTIES AND INTERRELATIONSHIPS

R. F. Landel, Chairman

This session expressed considerable unease with the topic of toughness. The concept clearly has different meanings for different applications and different disciplines. A repeated call for guidance was made.

The framework for the session was set by noting the role of people working in this area relative to the hierarchy of activities from the end user back to the organic chemist. Thus, the structural engineering community defines the (generalized) loads which must be withstood; the composites designer/fabricator defines layups, the method of fabrication and the engineering material properties. The materials group, represented by those in Session II, then had the dual job of defining local response and failure (i.e., the micromechanics analysis of single and simple multiply systems) and translating the parameters or functions of micromechanics to molecular parameters of the matrix polymer chain (e.g., chemical units, chain topology, crosslink density) or to chain mobility, system morphology, or other structural features. The chemist then defines and creates appropriate molecular structures to accomplish the desired connectivity and morphology.

Of course this is a two-way street, at least up to the composites engineer. However, it is a vastly imperfect one. At each level there is a clear need for an input/output handoff of information. In particular, the resin chemist and materials property communities are clamoring for more explicit guidance from the next level up.

Session II therefore adopted a conceptual framework of considering the extent to which (or ease by which) one might be able to interpret or predict response. That is, assume one has a stated problem area and ask: What would you expect? How could it be analyzed? Do we have the appropriate tools and data? What characterizing parameters or functions appear, or have been omitted.

As an illustration, one currently assesses dry ply properties from, say, the fiber longitudinal and transverse moduli and strength, the matrix tensile and shear moduli and strength, and Poisson's ratio. These can be taken as input data to calculate stiffness but the prediction of strength can be far off the mark, and especially so with more ductile systems. Why? What is missing such that even a qualitative estimate cannot be made?

The resulting discussion led to the development of statements of problems which prevent us from carrying out such an analysis and translation, and also to comments that much relevant information was already available in each case but was not being used effectively. Clearly the widely varying disciplines involved in developing composites are not yet as successful as desired in communicating their needs and knowledge to each other.

Table I summarizes the requirements identified to address these problems. These are therefore recommendations for action. A discussion of each follows. Note that fibers were not discussed per se, and that processing was alluded to several times but not addressed explicitly in this session.

TABLE I

CONSTITUENT PROPERTIES AND RELATIONSHIPS:
REQUIREMENTS AND RECOMMENDATIONS

1. Need a program goals/requirements statement
2. Need a better definition of toughness: application, test mode, test commonality
3. Assess limitations of current micromechanics models/procedures
4. Assess currently known resin toughening mechanisms and determine their relative importance to matrix resins
5. Need methods to define, in situ, the properties of the interphase region
6. Assess thermodynamic compatibility of any new resin with the fiber
7. Study model polymer matrices, including ideal as well as simplified/practical systems

1. Goals/requirements statement: Concern was expressed over the need for a clearer statement of the goals of the program and the real requirements of the airframe. More directly pertinent to the session was a perceived lack of direction or lack of targets to aim for from the fracture community.

2. Better operational definition of toughness: This requirement was in part a more explicit statement of previous requirement. The quantitative meaning of toughness and damage tolerance seems to shift from application to application. Considerable and repeated concern was expressed over the apparently evanescent nature of these targets. The opinion was strongly voiced that the search for a universally applicable answer should be replaced with a series of more narrowly defined targets and that Session I should translate such targets into clearer statements of requirements for Session II. For example, impact resistance on thick and thin sections and the potentials for crack propagation represent four different situations. Separate solutions to the problems may be easier to attain.

In addition to the need for operational definitions, there is a need to assess which of the various fracture toughness tests ought to be employed for resins and composites and then to adopt appropriate ones.

When reporting program results, contractors should use some consistent set of tests to define the properties or changes in properties with formulation, such that there would be at least some common means of comparing results.

3. Assess limitations of current micromechanics models/procedures: Most numerical models take the matrix material response as linear elastic. As such, they can predict small deformation response (e.g. modulus and expansion coefficients), but they cannot predict failure. What is needed is to incorporate the ability to handle viscoelasticity, nonlinear multiaxial response, and better failure criteria. Various ways of accomplishing the first two have been developed, and failure criteria represent in principle merely some predefined cap on the response. Two elements are missing, however.

First, there is a need to employ existing procedures (codes) to analyze various test geometries or damage situations and do a parametric study or sensitivity analysis to assess the importance of various assumed but realistic material behaviors. In this connection, the reminder was made that crack tip processes occur on very short time scales, on the order of microseconds, and this should be factored into input data or interpretation.

Second, there is, or appears to be, an almost total dearth of experimental data on nonlinear multiaxial behavior of matrix materials and failure behavior under multiaxial loads. Hence, analyses of their response at conditions approaching rupture or crack initiation cannot be carried out at this time, even where the numerical techniques are said to exist.

4. Explicitly assess currently known resin toughening mechanisms and determine their relative importance to matrix resins: At least five means of toughening resins and several for composites are known. The relative importance of these to a composite matrix is not known. Thus, certain amorphous thermoplastics craze or can be induced to craze (e.g., with the addition of rubber particles). But it is not clear that thermosets craze, or, should they be shown to craze, that the extent of crazing would be significant enough to impact the resistance to crack propagation. Similarly, rubber toughening is accompanied by a large deformation zone ahead of a crack tip, but the constraints of the fiber will restrict the size of the disturbed zone and reduce the in situ effectiveness. Correspondingly, crystalline polymers can be tough, but will the presence of the fiber or the bonding layer induce an unfavorable size or orientation of the crystalline region, destroying the toughness? In short, studies are needed on the extent to which toughening mechanisms useful in bulk resins will carry over to the in situ matrix resin.

One suggested characterization technique was that of determining the biaxial stress-strain response up to failure.

5. Method to define the interphase region in situ: There is no accepted technique for characterizing the polymer in the interphase region for graphite fiber systems. Without this the physical properties of the region cannot be interpreted in terms of molecular origin, even if they could be measured, and with neither available there are no real or assumed-but-reasonable input data for use in micromechanical models.

6. Assess thermodynamic compatibility of any new resin with the fiber: When new resin systems are being investigated their thermodynamic ability to interact effectively with the fiber surface or surface coating should be determined, lest promising candidates be unnecessarily discarded.

7. Model polymer systems - idealized, simplified real: Just as micromechanics models need careful assessment and employment, it was felt that the study of model matrix materials such as polymethyl methacrylate or polyethylene terephthalate would fulfill a real need in helping to distinguish the roles of molecularly related parameters such as backbone moieties or network topology. The time dependence, nonlinearity, failure behavior (e.g., brittle-ductile transition), and other such properties are well characterized and the molecular origins of the responses are reasonably well understood. Thus, there exists a precalibrated tool, as it were, to examine the effects of such parameters on composite behavior rather more closely than has been possible to date. Similarly, with such well-characterized polymers, one has hard input data to use in exercising the micromechanics models and checking the extent to which they can predict the response of real materials.

SESSION III: MATRIX SYNTHESIS AND CHARACTERIZATION

P. M. Hergenrother, Chairman

The discussion in the synthesis section of the tough composite matrix workshop was extremely candid and open, with the majority of the 35 or so attendees actively participating. A list of questions had been compiled prior to the meeting to aid in the discussion. These questions, however, initiated a particular criticism of the workshop, namely, that no detailed resources or roadmap were presented and no objective was defined. In essence, the audience interested in synthesis wanted more specifics on where the NASA effort is headed, how NASA hopes to get there, and, when they arrive, what NASA is going to do with the technology.

Early in the discussion, the NASA position on exclusive licensing was explained. A detailed plan must be submitted which indicates how the invention will be developed to commercial application. Nonexclusive licenses are also available.

The following ten questions were addressed. The answers represent a consensus of the workshop participants.

1. Did the workshop provide an adequate overall review of the synthetic work? No, because the audience was not informed of the details of the overall effort, such as objective, resources, and how the program was tied together.
2. Is NASA addressing the proper subjects in its synthetic work? Yes, even though this response may appear to contradict the answer to the first question. The synthetic effort involves thermosets, including rubber and thermoplastic toughened systems, and thermoplastics, encompassing linear, lightly crosslinked, and semicrystalline types. It was generally expressed that the NASA synthetic effort serves a very useful purpose to industry and should be continued. Some minor changes will be forthcoming as a result of recommendations from the audience. These are discussed in answer to some of the following questions.
3. Is the synthetic effort too broad? The audience felt that NASA should continue to maintain a broad synthetic effort, performing scouting expeditions in an attempt to uncover new concepts and technology. It was emphasized that NASA is not developing products but is directing the effort toward developing fundamental information that can be used by industry, if desired, to develop products.
4. Should the synthetic effort concentrate on one area more than another? A broad synthetic effort should be maintained, but it was recommended that work on epoxies be de-emphasized. It was generally thought that epoxy work was adequately covered by industry. Another recommendation was that more fundamental work on crystalline polymers be done by NASA.
5. What will be the biggest advance in the synthesis of composite materials over the next 10 years? The answer was computer modeling and fiber interface improvement. Advances in computer modeling will assist the synthetic chemist in the design and preparation of a toughened composite matrix with the best overall combination of properties. Improvement at the fiber interface, primarily through new surface treatments, will help maximize the mechanical properties of the composite system.

6. Concerning thermoplastics, what is the maximum acceptable processing temperature and pressure? The answer was that any conditions that would be cost effective in reproducibly fabricating quality composites could be used. No restrictions were placed upon either temperature or pressure. However, the temperature must obviously be controlled to avoid thermal degradation of the thermoplastic.

7. Is resistance to paint strippers an absolute requirement of composite matrices? Yes; although there are other means of removing paint, paint stripping solvents will continue to find widespread use. Composite matrices under stress are prone to attack by aggressive liquids such as paint strippers. Even epoxies will swell under these conditions. Semicrystalline materials such as PEEK (crystalline polyetheretherketone) were reported to be unaffected by paint strippers.

8. Is crystallinity in a polymer an acceptable approach to a solvent-resistant tough composite matrix? The answer was a resounding yes, if the crystallinity can be controlled. This question was proposed because of conflicting views on crystalline polymers. Some researchers feel that the same degree and type of crystallinity cannot be uniformly obtained in a composite structure which varies in thickness because heat transfer and controlled cool-down rate are problems. Others feel that the degree of crystallinity in a matrix will change as a function of environmental exposure, particularly when under stress to hydraulic fluid at elevated temperatures. If the degree of crystallinity changes, the physical and mechanical properties can change accordingly. Although these are only a few of the unknowns of crystalline materials, it was felt that these questions would be answered in the future and also that crystalline polymers offer an extremely good potential as a tough solvent-resistant composite matrix.

9. Is there a need to predict neat resin properties from base polymer molecular structure? Yes, if neat resin properties can be correlated with composite matrix properties.

10. What evaluation techniques are needed to guide the synthetic effort? Standard tests are needed using small amounts of material to evaluate toughness and solvent and moisture resistance under stress, as well as other physical and mechanical properties. It was recommended that the synthetic chemist have a series of standard screening tests that can be used to help ascertain the potential of a new polymer. If a new polymer exhibits good performance in these initial screening tests, then costly scale-up work can be conducted to obtain larger quantities for more comprehensive evaluation. Unfortunately, as implied in question 9, currently no real correlations exist between neat resin properties and composite properties. Work at NASA as well as elsewhere is under way in an attempt to develop pertinent tests than can be used to determine if such a correlation is possible. Although it was agreed that standard screening tests are needed, no action was recommended to develop a series of such tests.

1. Report No. NASA CP-2334		2. Government Accession No.		3. Recipient's Catalog No.	
4. Title and Subtitle TOUGH COMPOSITE MATERIALS				5. Report Date December 1984	
				6. Performing Organization Code 505-33-33	
7. Author(s) Louis F. Vosteen, Norman J. Johnston, and Louis A. Teichman, Compilers				8. Performing Organization Report No. L-15857	
9. Performing Organization Name and Address NASA Langley Research Center Hampton, VA 23665				10. Work Unit No.	
				11. Contract or Grant No.	
				13. Type of Report and Period Covered Conference Publication	
12. Sponsoring Agency Name and Address National Aeronautics and Space Administration Washington, DC 20546				14. Sponsoring Agency Code	
15. Supplementary Notes					
16. Abstract This publication is a compilation of papers and working group summaries presented at the Tough Composite Materials Workshop, held at NASA Langley Research Center, May 24-26, 1983. Presentations were made by selected speakers conducting research aimed at improving composite material performance and improving our understanding of composite material behavior. The papers were divided into three sessions: Session I: Composite Fracture Toughness and Impact Characterization Session II: Constituent Properties and Interrelationships Session III: Matrix Synthesis and Characterization The workshop also provided a forum for more in-depth discussions through separate panel meetings on the three disciplinary areas listed above. A summary of these discussions, including conclusions and selected recommendations, is included in this publication.					
17. Key Words (Suggested by Author(s)) Composites Fracture toughness Tough composites Impact Resins Compression Polymers Synthesis Characterization Graphite fiber				18. Distribution Statement Unclassified - Unlimited Subject Category 24	
19. Security Classif. (of this report) Unclassified		20. Security Classif. (of this page) Unclassified		21. No. of Pages 396	
				22. Price* A17	

* For sale by the National Technical Information Service, Springfield, Virginia 22161